Increasing structural diversity by prenylation-based modifications

Erhöhung der strukturellen Vielfalt durch prenylierungsbasierte Modifikationen

Dissertation

zur Erlangung des Doktorgrades

der Naturwissenschaften

(Dr. rer. nat.)

dem Fachbereich Pharmazie

der Philipps-Universität Marburg

vorgelegt von

Huomiao Ran

aus Jiyuan, China

Marburg an der Lahn, 2020

Erstgutachter: **Prof. Dr. Shu-Ming Li**

Zweitgutachter: **Prof. Dr. Michael Keusgen**

Eingereicht am 12. August 2020

Tag der mündlichen Prüfung: 25. September 2020

Hochschulkennziffer: 1180

Dedicated to my family

Table of contents

List of publications

1. **<u>Huomiao Ran</u>**, Viola Wohlgemuth, Xiulan Xie and Shu-Ming Li (2018). A nonheme Fe^{II}/2-oxoglutarate-dependent oxygenase catalyzes a double bond migration within a dimethylallyl moiety accompanied by hydroxylation. *ACS Chemical Biology*, 13 (10), 2949–2955, DOI: 10.1021/acschembio.8b00588.

2. Jinglin Wang,* **<u>Huomiao Ran</u>**,* Xiulan Xie, Kaiping Wang, and Shu-Ming Li (2020). Spontaneous oxidative cyclisations of 1,3-dihydroxy-4-dimethylallylnaphthalene to tricyclic derivatives. *Organic and Biomolecular Chemistry*, 18 (14), 2646–2649, DOI: 10.1039/d0ob00354a (*equal contribution)

3. Jonas Nies,* **<u>Huomiao Ran</u>**,* Viola Wohlgemuth, Wen-Bing Yin and Shu-Ming Li (2020). Biosynthesis of the prenylated salicylaldehyde flavoglaucin requires temporary reduction to salicyl alcohol for decoration before reoxidation to final product. *Organic Letters*, 22 (6), 2256–2260, DOI: 10.1021/acs.orglett.0c00440. (*equal contribution)

4. **<u>Huomiao Ran</u>** and Shu-Ming Li (2020). Fungal benzene carbaldehydes: occurrence, structural diversity, activities and biosynthesis. *Natural Product Reports*. DOI: 10.1039/d0np00026d.

Erklärung zum Eigenanteil

Titel der Publikation und Journal incl. Jahr, Heft, Seitzahl + doi O: Originalarbeit Ü: Übersichtartikel/Review	Autoren	geschätzter Eigenanteil in %	Bitte angeben: angenommen/eingereicht
A nonheme Fe^{II}/2-oxoglutarate-dependent oxygenase catalyzes a double bond migration within a dimethylallyl moiety accompanied by hydroxylation. *ACS Chemical Biology*, 2018, 13 (10), 2949–2955 DOI: 10.1021/acschembio.8b00588 Originalarbeit	**Huomiao Ran**, Viola Wohlgemuth, Xiulan Xie Shu-Ming Li	60	angenommen
Spontaneous oxidative cyclisations of 1,3-dihydroxy-4-dimethylallylnaphthalene to tricyclic derivatives. *Organic & Biomolecular Chemistry*, 2020, 18 (14), 2646–2649 DOI: 10.1039/d0ob00354a Originalarbeit	Jinglin Wang,* **Huomiao Ran**,* Xiulan Xie, Kaiping Wang, Shu-Ming Li	35	angenommen
Biosynthesis of the prenylated salicylaldehyde flavoglaucin requires temporary reduction to salicyl alcohol for decoration before reoxidation to final product. *Organic Letters*, 2020, 22 (6), 2256–2260 DOI: 10.1021/acs.orglett.0c00440 Originalarbeit	Jonas Nies,* **Huomiao Ran**,* Viola Wohlgemuth, Wen-Bing Yin Shu-Ming Li	35	angenommen
Fungal benzene carbaldehydes: occurrence, structural diversity, activities and biosynthesis. *Natural Product Reports*, 2020 DOI: 10.1039/d0np00026d Übersichtartikel/Review	**Huomiao Ran**, Shu-Ming Li	65	angenommen

*: These authors contributed equally to this work.

Kandidat(in)

Unterschrift Betreuer(in)

Abbreviations

The international system of units and units derived thereof has been used.

$[M+H]^+$	molecular ion plus proton
$[M-H]^-$	molecular ion minus proton
× *g*	gravitational acceleration
A domain	adenylation domain
AA	ascorbic acid
ACP domain	acyl carrier protein domain
AT domain	acyltransferase domain
BGC	biosynthetic gene cluster
bp	base pair
br	broad (NMR signal)
C domain	condensation domain
CD_3OD	deuterated methanol
$CDCl_3$	deuterated chloroform
CoA	coenzyme A
COSY	correlation spectroscopy
cyclo-L-Trp-L-Trp	*cyclo*-L-tryptophan-L-tryptophan
cyclo- L-Trp- L-Ala	*cyclo*-L-tryptophan-L-alanine
cyclo- L-Trp- L-His	*cyclo*-L- tryptophan-L-histidine
cyclo- L-Trp- L-Pro	*cyclo*-L- tryptophan-L-proline
d	doublet
D_2O	deuterium oxide
Da	dalton
dd	double doublet
ddd	double double doublet
DH domain	dehydratase domain
DMAPP	dimethylallyl diphosphate
DMAT	dimethylallyltryptophan
DMATS	dimethylallyltryptophan synthase
DMSO-*d_6*	deuterated dimethyl sulfoxide

ABBREVIATIONS

DNA	deoxyribonucleic acid
dq	double quartet
dt	double triplet
E. coli	*Escherichia coli*
e.g.	exempli gratia
EIC	extracted ion chromatogram
E domain	epimerization
ER domain	enoyl reductase domain
ESI	electrospray ionization
FPP	farnesyl diphosphate
gDNA	genomic DNA
GMM	glucose minimal medium
GPP	geranyl diphosphate
His_6	hexahistidine
HMBC	heteronuclear multiple bond correlation
HPLC	high performance liquid chromatography
HRMS	high resolution mass spectrometry
HR-PKS	highly reducing-polyketide synthase
HSQC	heteronuclear single quantum coherence
Hz	hertz
i.e.	id est
IPP	isopentenyl diphosphate
J	coupling constant
kbp	kilo base pairs
kcat	turnover number
kDa	kilodaltons
K_M	Michaelis-Menten constant
KR domain	ketoreductase domain
KS domain	β-ketoacyl synthase domain
LC-MS	liquid chromatography–mass spectrometry
m	multiplet
m/z	mass-to-charge ratio

mAU	milliabsorbance unit
Mb	mega base pairs
mRNA	messenger ribonucleic acid
MT domain	methyl transferase domain
multi	multiplicity
NADH	nicotinamide adenine dinucleotide
NADPH	nicotinamide adenine dinucleotide phosphate
NMR	nuclear magnetic resonance
NP	natural product
nonheme Fe^{II}-2OG	nonheme Fe^{II} 2-oxoglutarate
NOESY	nuclear overhauser effect spectroscopy
NRPS	nonribosomal peptide synthetase
NR-PKS	non-reducing-polyketide synthase
P450	cytochrome P450
PCP domain	peptidyl carrier protein domain
PCR	polymerase chain reaction
PD	potato dextrose
PDB	potato dextrose broth
PEG	polyethylene glycol
PKS	polyketide synthase
PPi	inorganic pyrophosphate
ppm	parts per million
PR-PKS	partially reducing-polyketide synthase
PT	prenyltransferase
PT domain	product template domain
q	quartet
R domain	reductase domain
RBS	ribosome binding site
RNA	ribonucleic acid
rpm	revolutions per minute
s	singlet
SDS-PAGE	sodium dodecyl sulfate polyacrylamide gel electrophoresis

SM	secondary metabolite
t	triplet
T domain	thiolation domain
TB	terrific broth
td	triple doublet
TE domain	thioesterase domain
THN	tetrahydroxynaphthalene
Tris	tris(hydroxymethyl)aminomethane
UV	ultraviolet
v/v	volume per volume
w/v	weight per volume
WT	wild type
δ_C	chemical shift of ^{13}C
δ_H	chemical shift of ^{1}H

Summary

Fungi have the ability to generate tremendously complex and diverse natural products. Fungal secondary metabolites are highly relevant in mankind's daily life by playing an important role in medicine, agriculture and manufacturing industries. Since the discovery of antibiotics in the first half of the last century, an enormous variety of natural products has been discovered in different fungi. With the advent of the genomics revolution, scientists have realized that the remarkable chemical space of fungal secondary metabolites has resulted from the diversification of biosynthetic gene clusters (BGC). Enzymes as efficient catalysts are the bridge between these biosynthetic genes and the resulting small molecules. The initial chemical scaffolds are assembled by backbone enzyme(s) and undergo decorations catalysed by a set of tailoring enzymes to mature the products. Prenyltransferases are one representative family of these tailoring enzymes. "Aromatic" prenyltransferases accept a broad spectrum of substrates including, but no limited to, indole derivatives, benzene carbaldehydes and naphthalenes. Prenylated metabolites can be further modified by enzymatic or nonenzymatic reactions to facilitate the functional group density. Thus, understanding the complexity and diversity of natural product scaffolds requires investigation of whole biosynthetic assembly lines *in vivo* as well as the participating enzymes and their mechanisms.

There are substantial studies demonstrating the diversification of enzymatic post-modifications on prenyl moieties. For example, the nonheme Fe^{II}/2-oxoglutarate (2-OG)-dependent oxygenase FtmOx1 from *Aspergillus fumigatus* is involved in the biosynthesis of fumitremorgin-type mycotoxins and catalyses an endoperoxide formation by insertion of an oxygen molecule into two prenyl moieties. Following this work, we cloned and overexpressed its homologous gene NFIA_045530 from *Neosartorya fischeri*. The recombinant protein EAW25734 encoded by NFIA_045530 was purified to apparent homogeneity and incubated with intermediates of the fumitremorgin biosynthetic pathway. LC-MS analysis revealed no consumption of fumitremorgin B, the natural substrate of FtmOx1, but good conversion with its biosynthetic precursor tryprostatin B in the presence of Fe^{II} and 2-OG. Structure elucidation confirmed the three products as 22-hydroxylisotryprostatin B, 14α-hydroxylisotryprostatin B and 14α, 22-dihydroxylisotryprostatin B. Further detailed biochemical characterization proved EAW25734 to be a nonheme Fe^{II}/2-OG-dependent oxygenase, which catalyses a double bond migration within the dimethylallyl moiety accompanied by hydroxylation. We proposed that the reaction mechanism for this transformation is a radical rearrangement prior to accepting a hydroxyl radical from Fe^{III}. The major origin of the hydroxyl groups at $C14\alpha$ and C22 was confirmed to be O_2 by labelling experiments. Solvent exchange was also observed for that at C22. LC-MS analysis of the fungal culture revealed the presence of 22-hydroxylisotryprostatin B, indicating the hijacking of tryprostatin B by EAW25734 from the fumitremorgin pathway. Our study demonstrates a notable oxidative modification of prenyl moieties.

SUMMARY

In cooperation with Dr. Jinglin Wang, we investigated spontaneous rearrangements of 4-dimethylallyl-1,3-dihydroxynaphthalene to two tetrahydrobenzofuran and one bicyclo[3.3.1]nonane derivatives. Incubations of FgaPT2, 1,3-dihydroxynaphthalene and DMAPP under $^{18}O_2$-enriched atmosphere and with ^{18}O-enriched water confirmed that the two additional hydroxyl groups were originated from one molecule of O_2. Thus, a radical-involved mechanism was proposed starting with a reactive C4-peroxyl intermediate, which led to radical shifts and the formation of tricyclic products. These results provide one additional example for the nonenzymatic oxidative cyclisation and give valuable insights into the structural diversification by spontaneous reactions.

In cooperation with Jonas Nies, a nine-gene *fog* cluster was identified in *Aspergillus ruber*. Genome mining revealed the presence of a prenyltransferase gene *fogH* in the *fog* cluster. The involvement of the *fog* cluster in the biosynthesis of the prenylated salicylaldehyde flavoglaucin and congeners was confirmed by heterologous expression of the whole cluster in *Aspergillus nidulans*. The highly-reducing polyketide synthase FogA, together with three additional enzymes, was proven to be responsible for the formation of the benzyl alcohol intermediates. Deletion of *fogH* led to the accumulation of C5-hydroxylated hydroquinones, which were unstable and partially oxidised to their benzoquinone forms. Biochemical characterization revealed that the prenyltransferase FogH can accept both hydroquinone and benzoquinone forms as substrates. Consecutively, the alcohols were oxidized to the final aldehyde products by an oxidase, which only accepts prenylated derivatives as substrates. Meanwhile, the spontaneous oxidoreduction from prenylated benzoquinone alcohols to final hydroquinone aldehydes was observed as a minor side reaction during isolation. Therefore, this study demonstrated a highly efficient and programmed biosynthetic machinery for the flavoglaucin formation and highlighted the importance of the prenyltransferase FogH in the assembly line.

In the review on fungal benzene carbaldehydes, we summarised their structural features, distribution, biological activities and biosynthesis with focus on alkylated derivatives and meroterpenoids. The first group carries different alkyl chains (C_3, C_5, C_7, C_9 or C_{11}) at the *ortho*-position to the aldehyde group and the second group contains structural features derived from a C_5, C_{10} or C_{15} prenyl moiety. In addition, simple benzaldehydes, benzophenones, spirocyclic and other benzene carbaldehydes were also included. Most of the reviewed compounds are salicylaldehyde derivatives, which are assembled by polyketide synthases from ascomycetes and released directly as aldehydes or afterwards oxidised/reduced by tailoring enzymes.

Zusammenfassung

Pilze besitzen die Fähigkeit hoch komplexe und diverse Naturstoffe zu produzieren. Pilzliche Sekundärmetabolite sind von hoher Relevanz im täglichen Leben von Menschen und spielen eine wichtige Rolle in Medizin, Landwirtschaft und Industrie. Seit der Entdeckung der Antibiotika in der ersten Hälfte des letzten Jahrhunderts wurde eine Vielzahl von verschiedenen Naturstoffen aus Pilzen isoliert. Mit dem Aufkommen der genomischen Revolution wurde es für Wissenschaftler deutlich, dass die bemerkenswerte Varianz und Vielfalt der pilzlichen Sekundärmetabolite aus der Diversifizierung von biosynthetischen Genclustern (BGCs) resultiert. Enzyme, als effiziente Katalysatoren, bilden die Brücke zwischen diesen Genen und den resultierenden niedermolekularen Verbindungen. Die anfänglichen Grundgerüste werden durch sogenannte „Backbone"-Enzyme konstruiert und durch weitere Enzyme zu den jeweiligen Endprodukten modifiziert. Ein Vertreter dieser modifizierenden Enzyme ist die Prenyltransferase. „Aromatische" Prenyltransferasen akzeptieren diverse Substrate, einschließlich, aber nicht beschränkt auf Indolderivate, Benzaldehyde und Naphthaline. Prenylierte Metabolite können durch enzymatische oder nichtenzymatische Reaktionen weiter modifiziert werden, um die Vielfalt der funktionellen Gruppen zu erhöhen. Um die Komplexität und strukturelle Vielfalt von Naturstoffen zu verstehen, sind daher Untersuchungen der gesamten Biosynthesewege, sowie der beteiligten Enzyme und ihrer Mechanismen erforderlich.

Es gibt umfangreiche Studien, die die Diversifizierung enzymatischer Postmodifikationen an Prenyleinheiten demonstrieren. Die nicht-Häm-Fe^{II} / 2-Oxoglutarat (2-OG) abhängige Oxygenase FtmOx1 aus *Aspergillus fumigatus* ist, z.B. an der Biosynthese der Mykotoxine vom Fumitremorgin-Typ beteiligt und katalysiert die Bildung eines Endoperoxids durch Insertion eines Sauerstoffmoleküls zwischen zwei Prenylresten. Darauf aufbauend haben wir ein homologes Gen NFIA_045530 aus *Neosartorya fischeri* kloniert und überexprimiert. Das von NFIA_045530 kodierte rekombinante Protein EAW25734 wurde zur Homogenität gereinigt und mit den Intermediaten des Fumitremorgin-Biosynthesewegs inkubiert. Die LC-MS Analyse zeigte keinen Umsatz von Fumitremorgin B, dem natürlichen Substrat von FtmOx1, allerdings aber einen guten Umsatz mit seinem Vorstufe Tryprostatin B in Anwesenheit von Fe^{II} und 2-OG. Die Strukturaufklärung bestätigte die drei Produkte als 22-Hydroxylisotryprostatin B, 14- Hydroxylisotryprostatin B und 14,22-Dihydroxylisotryprostatin B. Detaillierte biochemische Untersuchungen zeigten, dass die nicht-Häm-Fe^{II} / 2-Oxoglutarat abhängige Oxygenase EAW25734 die Doppelbindungsverschiebung innerhalb der Dimethylallyl-Einheit und gleichzeitige Hydroxylierung katalysiert. Als Reaktionsmechanismus haben wir eine radikale Umlagerung vorgeschlagen, bevor ein an das Fe^{III} gebundene Hydroxylradikal übertragen wird. Durch Markierungsexperimente wurde bestätigt, dass der Sauerstoff an C14α und C22 hauptsächlich aus O_2 stammt. Für C22-OH wurde ein Austausch des Sauerstoffs mit H_2O nachgewiesen. LC-MS Analyse der Pilzkultur bestätigte das Vorhandensein von 22-Hydroxylisotryprostatin B, was darauf schließen ließ, dass EAW25734 Tryprostatin B aus der Fumitremorgin-Biosynthese abzweigt.

ZUSAMMENFASSUNG

In einer Kooperationsstudie mit Dr. Jinglin Wang haben wir eine spontane Umlagerung von 4-Dimethylallyl-1,3-Dihydroxynaphthalin zu zwei Tetrahydrobenzofuran- und einem Bicyclo[3.3.1]nonan-Derivat untersucht. Inkubation von FgaPT2, 1,3-Dihydroxynaphthalin und DMAPP unter $^{18}O_2$-angereicherter Atmosphäre und mit ^{18}O-angereichertem Wasser bestätigten, dass die beiden zusätzlichen Hydroxylgruppen von einem O_2-Molekül stammten. Daher wurde ein Mechanismus vorgeschlagen, der mit einem reaktiven C4-Peroxyl-Zwischenprodukt beginnt, zu Radikalverschiebungen und zur Bildung trizyklischer Produkte führt. Diese Ergebnisse liefern ein weiteres Beispiel für die nichtenzymatische oxidative Zyklisierung und geben wertvolle Einblicke in die strukturelle Diversifizierung durch spontane Reaktionen.

In Kooperation mit Jonas Nies wurde das *fog*-Gencluster in *Aspergillus ruber* entdeckt, das insgesamt neun Gene umfasst. Durch Genome-mining wurde darin auch das Prenyltransferasengen *fogH* identifiziert. Durch heterologe Expression in *Aspergillus nidulans* konnte gezeigt werden, dass das *fog*-cluster für die Biosynthese von dem prenylierten Salicylaldehyd Flavoglaucin und Analoga verantwortlich ist. Gendeletionsexperimente im heterologen Expressionsstamm deuteten darauf hin, dass die hoch-reduzierende Polyketidsynthase FogA zusammen mit drei zusätzlichen Enzymen für die Bildung der Benzylalkohol-Zwischenprodukte verantwortlich ist. Die Deletion von *fogH* führte zur Akkumulation von instabilen C5-hydroxylierten Hydrochinonen, die teilweise zu ihren Benzochinonformen oxidierten. Die biochemischen Untersuchungen zur Prenyltransferase FogH ergab, dass diese sowohl die Hydrochinon- als auch die Benzochinonform als Substrate akzeptieren kann. Anschließend wurden die Alkohole durch eine Oxidase, die nur prenylierte Intermediate als Substrate akzeptiert, zu den endgültigen Aldehydprodukten oxidiert. Des Weiteren konnte während der Isolierung in geringer Menge die spontane Oxidoreduktion von prenylierten Benzochinonalkoholen zu endgültigen Hydrochinonaldehyden beobachtet werden. Diese Studie zeigt die hocheffiziente und programmierte Maschinerie zur Biosynthese von Flavoglaucin und Analoga und hebt vor allem die Bedeutung der Prenyltransferase FogH im gesamten Kontext hervor.

In dem Übersichtsartikel haben wir die strukturellen Besonderheiten, Verbreitung, biologische Aktivitäten und Biosynthese pilzlicher Benzaldehyde zusammengefasst. Der Schwerpunkt lag auf alkylierten Derivaten mit unterschiedlichen Alkylketten (C_3, C_5, C_7, C_9 oder C_{11}) an der *ortho*-Position zur Aldehydgruppe und Meroterpenoiden mit Strukturelementen aus einem C_5-, C_{10}- oder C_{15}-Prenylrest. Einfache Benzaldehyde, Benzophenonaldehyde und spirozyklische Benzaldehyde wurden ebenfalls behandelt. Die meisten der besprochenen Substanzen sind Salicylaldegydderivate, die von Polyketidsynthasen aus Schlauchpilzen synthetisiert werden. Diese werden entweder direkt als Aldehyde freigesetzt oder durch Modifikationsenzyme nachträglich oxidiert/reduziert.

1 Introduction

1.1 Fungi as source of natural products

Together with plants and animals, fungi represent one of the three major eukaryotic lineages of the terrestrial ecosystems (Heitman et al. 2017). They originated as a distinctive group of unicellular eukaryotes in the Precambrian about 760 million to 1.06 billion years ago (Watkinson et al. 2015). After million years of diversification and adaption, fungi are present all over the planet earth in different habitats ranging from aquatic to terrestrial ecosystems. With persistent evolution and long-distance dispersal, approximately 80,000 to 120,000 fungal species have been described so far. The total number of species is estimated at least to be 5.1 million (Blackwell 2011). In the most recent phylogenetic classification scheme, the true fungi (or Eumycota), which make up this monophyletic clade called Kingdom Fungi, comprise the seven phyla: Chytridiomycota, Blastocladiomycota, Neocallimastigomycota, Microsporidia, Glomeromycota, Basidiomycota and Ascomycota. (Hibbett et al. 2007; Moore et al. 2020) The majority of the described fungal species belong to the Ascomycota and the Basidiomycota (Kavanagh 2017).

It is well known that fungi can bring disaster but also blessing to humankind. Fungi act as harmful entities which spoil our foods and food grains, blight cultivated plants and cause health hazards. On the other side, fungi are commonly used in food production, weaving, chemical and pharmaceutical industries. Most of the drastically different impacts of fungi are related to their secondary (or specialized) metabolites (SMs), also known as natural products (NPs). In general, SMs are small molecules produced late in the growth cycle. They are not essential for basic growth, development or reproduction, but involved in ecological or environmental interactions (Mérillon and Ramawat 2016), *e.g.*, for self-protection against predators, inhibition of competing microorganisms (Calvo and Cary 2015; Schrettl et al. 2010), communication purposes (Dufour and Rao 2011; Tsitsigiannis and Keller 2007) and establishing interactions with their biotic environment (Brakhage 2013; Rohlfs and Churchill 2011). The fungal dependence on SMs to conquer diverse habitats and promote their development is proven for most species.

Since the discovery of the first broad-spectrum antibiotic penicillin G by Alexander Fleming in 1928 and proof of its importance in World War II, significant progress has been achieved not only in medical use but also in screening for other bioactive SMs from fungi (Fleming 1929). To date, over 250,000 NPs were discovered in total *via* various strategies (**Figure 1**) (Wilson et al. 2020), about 45 % of them originated from fungi (Bérdy 2012). Historically, chemists focused on the characterisation of the expressed metabolome, which was achieved by detection of unidentified structures in fungal crude extracts or bio-guided fractionation for bioactive metabolites. To meet the growing demand on bioactive compounds, new fungal resources from marine and extreme environments were taken into consideration. Furthermore, a so-called OSMAC (One Strain - Many Compounds) approach was

suggested to discover a broader array of compounds , which is based on alteration of culture conditions *e.g.* light, pH value, nutrients and co-cultivation with different microorganisms (Ariantari et al. 2019; Bode et al. 2002; Selegato et al. 2019). However, the OSMAC-based fermentation approach has failed to access all of the potential compounds from one organism due to the far greater number of hypothetical BGCs in its genome. In the last decade, advances in sequencing technologies and molecular biology gave rise to the idea that genome manipulation is a successful strategy in fungal NP identification. Bioinformatics analysis of available fungal genome sequences revealed that approximately 80 % of their secondary metabolome remains unidentified, indicating the plethora of compounds waiting to be discovered (Heitman et al. 2017). To activate the silent/lowly expressed biosynthetic gene clusters (BGCs), strategies such as epigenetic regulation, global regulator (de)activation and specific transcription factor stimulation have been applied to influence the production of SMs (Keller 2019; Lyu et al. 2020). For example, the 'Velvet Complex' composing VelB, VeA and LaeA is associated with global positive regulation of many BGCs in filamentous fungi (Amare and Keller 2014; Bok et al. 2005; Bok and Keller 2004; Kumar et al. 2017), while McrA acts as a global negative regulator in *Aspergillus* and *Penicillium* species (Oakley et al. 2017). Bioinformatics analysis of interesting active clusters provides the basis for gene deletion or overexpression experiments in the native strain (Matsuda and Abe 2016; Sanchez et al. 2012a). Furthermore, for slow-growing and genetically difficult to be manipulated fungi, heterologous expression in surrogate hosts represents another way for discovery of novel NPs (Lazarus et al. 2014; Zhang et al. 2019a).

Based on their biosynthetic origin, well-studied fungal NPs mainly belong to polyketides, peptides, terpenoids and alkaloids (**Figure 1**). Most of these molecules exhibit an enormous range of biological activities, *e.g.* antibacterial, antifungal and antitumor activities or even toxicity, hence representing both positive and negative effects of fungal SMs.

Polyketides are the most abundant and sophisticated fungal SMs, which are generally synthesized by polyketide synthases (PKSs). The fungal polyketide metabolite lovastatin from *Aspergillus terreus* is known as the first cholesterol-lowering statin approved by the Food and Drug Administration (Alberts et al. 1980; Golomb and Evans 2008). Griseofulvin from *Penicillium griseofulvum* serves as the earliest antifungal agent against dermatophyts (Develoux 2001; Oxford et al. 1939). Another representative is aflatoxin B_1 produced by *Aspergillus flavus* with a highly hepatotoxic activity (Hesseltine et al. 1966; Li et al. 2001). Moreover, peptides also play an important role in fungal natural product diversity and are mostly produced by nonribosomal peptide synthetases (NRPSs). Typical examples of NRPS-produced peptides include penicillin G and cyclosporine A. Penicillin G, as mentioned above, is one of the most famous antibiotics (Houbraken et al. 2011; Sika-Paotonu and Liligeto 2019; Smith et al. 1990). Cyclosporine A is another clinically used cyclic undecapeptide from the fungus *Tolypocladium inflatum* with immunosuppressive and antifungal properties (Bolton et al. 1982; Borel and Wiesinger 1979). An isocyanide-NRPS hybrid antibiotic xanthocillin was isolated from *Penicillium notatum* in 1950 (Lim et al. 2018; Rothe 1954). The presence of the isonitrile moiety usually exhibits unique

biological and chemical properties and has enabled synthetic and biochemical applications (Garson and Simpson 2004; Wilson et al. 2012).

Terpenoids, also known as isoprenoids, comprise the structurally diverse family of fungal NPs. They are synthesized from the 5-carbon precursors (dimethylallyl diphosphate (DMAPP) and isopentenyl diphosphate (IPP)), elongating with C_{5n} IPP (n = 1, 2, 3, etc.) by head-to-tail coupling reactions (Kellogg and Poulter 1997; Poulter and Rilling 1978). The subsequent cyclisation reactions yield a myriad of products typically containing multiple fused rings and stereo centres (Gao et al. 2012b; Lesburg et al. 1998; Quin et al. 2014). For example, a highly oxygenated tetracyclic diterpenoid, gibberellin A3, contains seven stereo centres in the 20-carbon skeleton. It has positive effects on plant development, such as stimulation of rapid stem and root growth (Bomke and Tudzynski 2009). In
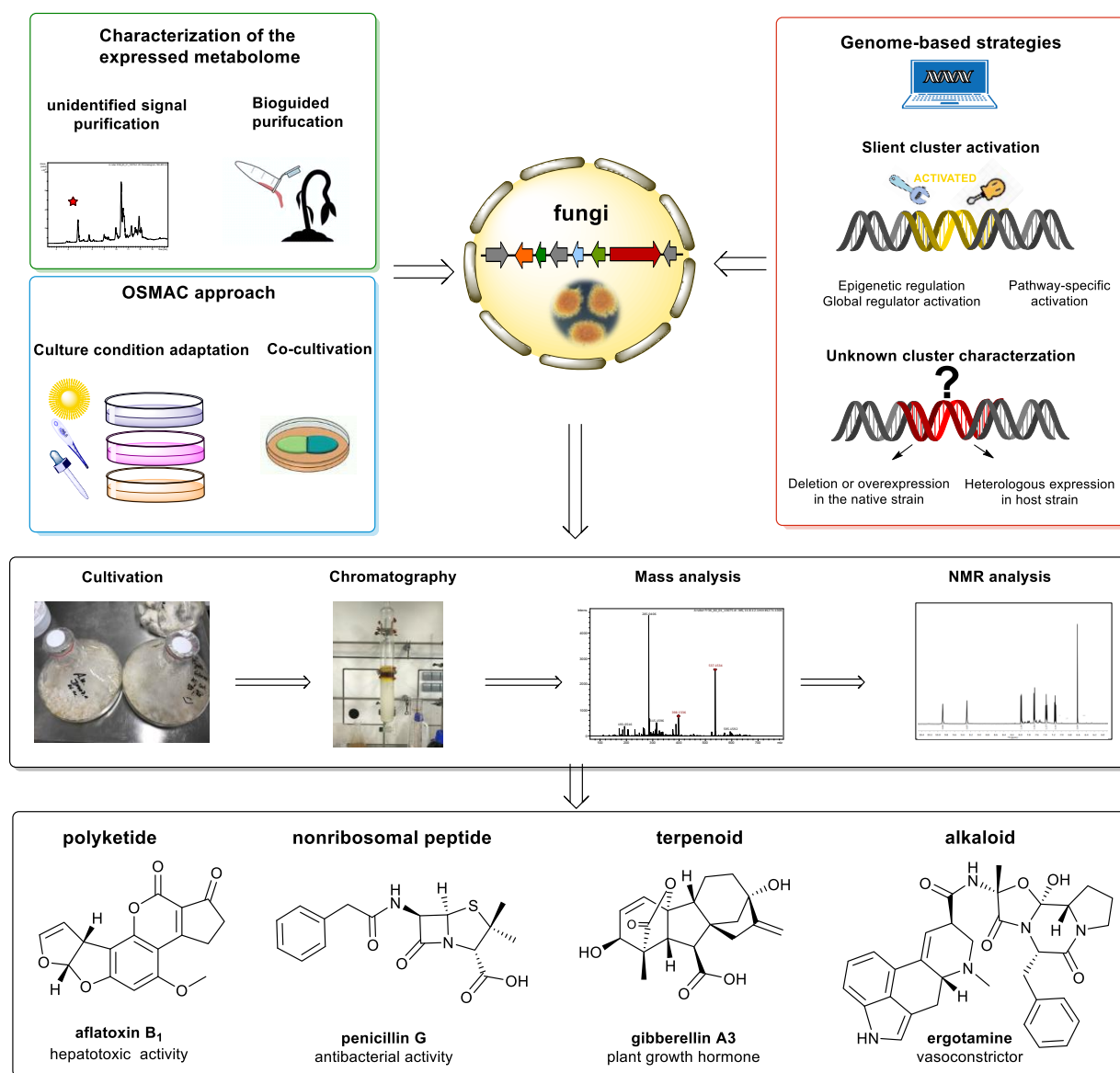
Figure 1 Application of multiple strategies for the discovery of abundant fungal natural products

addition, alkaloids are one of the largest classes of nitrogen-containing fungal SMs. Most of them present attractive bioactivities, such as ergotamine from *Claviceps purpurea* as a vasoconstrictor and paxilline from *Penicillium paxilli* as a mycotoxin (Rowan 1993; Silberstein 1997).

Humanity's fascination with the Fungal Kingdom is a natural and ancient one. It is probably based on the countless natural products which bring humankind food and famine, drugs and diseases. Today, we are familiar with the importance of SMs in pharmaceuticals, agrochemicals, food additives and cosmetics. Advances in microbiology, biochemistry, genome sequencing and bioinformatics provide unlimited possibilities to enrich the natural product library and expand the pharmaceutical repertoire.

1.2 Prenylated aromatic natural products

As aforementioned, natural products are widely distributed in terrestrial and marine organisms with a great structural diversity. These include prenylated natural containing aromatic scaffolds and one or more prenyl moieties, *e.g.* prenylated indole alkaloids, naphthalenes, benzene carbaldehydes, flavonoids, xanthones and quinones (**Figure 2A**). They exhibit an extensive range of biological and pharmacological activities such as cytotoxic (Li et al. 2014), antioxidant (Sunassee and Davies-Coleman 2012), antimicrobial (Liu et al. 2013; Oya et al. 2015), antiviral (Sanna et al. 2018) activities, which are often distinct from their non-prenylated precursors. The distinctive prenyl moieties play an important role in the structural diversity of these natural products, due to various backbones, assorted prenylation positions and different prenyl donors as well as different patterns (regular or reverse) (**Figure 2**). In general, prenyl donors can be classified into DMAPP (C_5), geranyl (GPP, C_{10}), farnesyl (FPP, C_{15}) and geranylgeranyl (GGPP, C_{20}) diphosphate. They can be attached onto the scaffold in regular or reverse manners. The regular prenylation implies the connection of the prenyl moieties *via* their C-1' to an acceptor and the reverse prenylation *via* their C-3' atoms (Winkelblech et al. 2015). In addition, the prenylated compounds can be further modified by rearrangement, cyclisation, oxidation and hydroxylation.
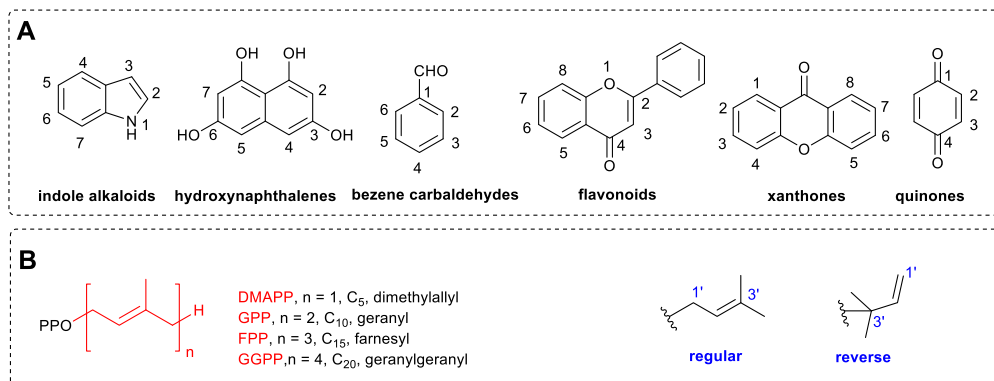

Figure 2 Representatives of common numbering of aromatic scaffolds (A); prenyl donors and their connection patterns (B)

1.2.1 Prenylated indole alkaloids

Fungal prenylated indole alkaloids are hybrid natural products containing indole/indoline and isoprenoid moieties or structures derived thereof (Li 2010). They are mainly produced by the genera *Penicillium* and *Aspergillus* of the Ascomycota. The majority of the prenylated indole alkaloids are L-tryptophan-containing compounds derive from NRPS-related biosynthetic pathways with diketopiperazine or benzodiazepindinone skeletons. Representatives of the prenylated cyclic dipeptides are brevianamide F and its derivatives consisting of L-tryptophan and L-proline (**Figure 3A**). The formation of brevianamide F is catalysed by the synthetase FtmPS also termed FtmA, which was proven by heterologous overexpression of the NRPS gene *ftmA* in *Aspergillus nidulans* (Maiya et al. 2006). It can be further converted to tryprostatin B with a regular C2-prenylation or deoxybrevianamide E with a reverse C2-prenylation. Tryprostatin B acts as a key intermediate in the biosynthesis of diverse metabolites such as tryprostatin A, demethoxyfumitremorgin C and fumitremorgin C or its N1-prenylated derivatives verruculogen and fumitremorgin B in *Aspergillus fumigatus* (Li 2011). Spirotryprostatins A and B with unique spiro ring systems have been frequently chosen as a target of chemical synthesis due to their structural complexity and important pharmaceutical activities (Cui et al. 1996). Meanwhile, deoxybrevianamide E serves as the precursor of brevianamide A and austamide as well as notoamides B and E (Grundmann and Li 2005; Kato et al. 2007; Tsukamoto et al. 2008; Williams et al. 2000).
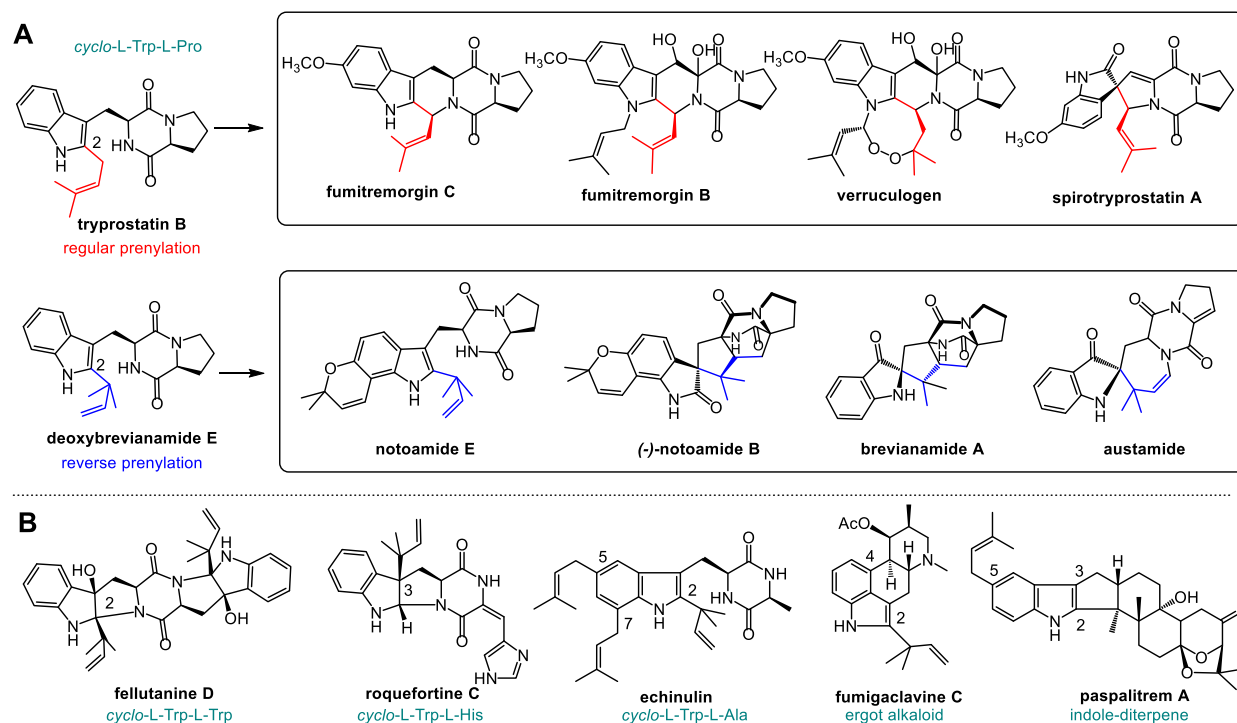
Figure 3 structures of prenylated indole alkaloids derived from *cyclo*-L-Trp-L-Pro and their biosynthetic relationship (A); examples of other L-tryptophan-containing natural products (B)

Besides *cyclo*-L-Trp-L-Pro, L-tryptophan-containing natural products can also comprise other amino acid such as a second L-tryptophan, L-histidine or L-alanine (**Figure 3B**). Fellutanine D from *Penicillium fellutanum* is diprenylated *cyclo*-L-Trp-L-Trp with a fused ring system and exhibits cytotoxic activity against several cell lines (Kozlovsky et al. 2000). Prenylated *cyclo*-L-Trp-L-His derivative roquefortine C with a reverse prenylation at C3 was firstly isolated from *Penicillium roqueforti* (Scott and Kennedy 1976) and identified later in a quantity of *Penicillium* strains as the precursor of several prenylated indole alkaloids such as roquefortine E, glandicoline B, meleagrin and oxaline (Overy et al. 2005; Reshetilova et al. 1995; Steyn and Vleggaar 1983). A prominent example of muti-prenylated *cyclo*-L-Trp-L-Ala is echinulin initially isolated from *Aspergillus amstelodami* (Birch et al. 1961) and later, together with congeners, from assorted *Aspergillus* strains (Cardani et al. 1959; Du et al. 2012; Ma et al. 2016). Apart from cyclic dipeptides, ergot alkaloids are another complex family with diverse structures and biological activities (Flieger et al. 1997; Schardl et al. 2006). Biogenetically, the ergoline ring in ergot alkaloids such as fumigaclavine C is derived from the C4-prenylated tryptophan (**Figure 3B**). In addition, the indole-diterpene hybrid compounds produced by filamentous fungi are composed of an indole residue and a cyclic geranylgeranyl moiety as shown in **Figure 3B** (Cole et al. 1977; Sings and Singh 2003).

1.2.2. Prenylated benzene carbaldehydes

Prenylated benzene carbaldehydes are a group of compounds consisting of dimethylallyl, geranyl or farnesyl moieties on benzaldehyde skeleton and are widely distributed in ascomycetes and basidiomycetes. The prenyl moieties are usually attached on *meta*-position (C3) of the aldehyde group as shown in **Figure 4**. An example is cristaldehyde A from the marine-derived fungus *Eurotium cristatum* as a prenylated chromene-5-carbaldehyde (Zhang et al. 2019b). It displays a significant anti-inflammatory effect on the LPS-stimulated RAW 264.7 cells (Zhang et al. 2019b). Other well-known prenylated benzaldehydes are flavoglaucin and its congeners, which were obtained from different *Aspergillus*/*Eurotium* strains with antibacterial (Fathallah et al. 2019; Shi et al. 2019), antioxidant (Huang et al. 2012; Miyake et al. 2014), anti-inflammatory (Shi et al. 2019; Wu et al. 2014a) and cytotoxic (Wang et al. 2006) activities. Annullatin A with a benzofuran ring derived from the dimethylallyl group was isolated from the entomopathogen *Cordyceps annullata* (Asai et al. 2012). It exhibits potent agonistic activity towards the cannabinoid receptors CB1 and CB2 (Asai et al. 2012). A representative geranylated benzene carbaldehyde is ilicicolin E was obtain from pathogenic fungus *Verticillium hemipterigenum* with a substituted cyclohexone ring by cyclisation within a modified farnesyl chain (Seephonkai et al. 2004).
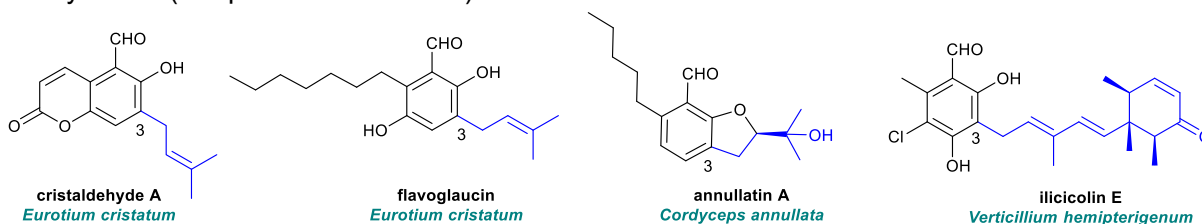

cristaldehyde A
Eurotium cristatum

flavoglaucin
Eurotium cristatum

annullatin A
Cordyceps annullata

ilicicolin E
Verticillium hemipterigenum

Figure 4 Examples of prenylated benzene carbaldehydes

1.2.3. Prenylated naphthalenes

Prenylated naphthalenes are a less abundant class of prenylated secondary metabolites, which are mainly derived from a tetrahydroxynaphthalene (THN) precursor formed through the action of a polyketide synthase (Funayama et al. 1990). Single or multiple prenylation events with further cyclisation *via* enzymatic or nonenzymatic reactions decorate the THN precursor and form complex natural products. Various prenyl donors, including dimethylallyl, geranyl and farnesyl diphosphates, are initially appended to the nucleophilic C-2 and C-4 positions of THN *via* electrophilic aromatic substitution reactions catalysed by aromatic PTs (Murray et al. 2020). The non-nucleophilic C3-prenyl moiety originates from a C4-prenylated intermediate *via* oxidative dearomatisation and a halogenation-induced α-hydroxyketone rearrangement of the prenyl moiety from C4 to C3 (Murray et al. 2018). Based on C2 or C3/C4 prenylation patterns, most prenylated naphthalenes can be divided in two classes (**Figure 5**). Furanonaphthoquinone I (Haagen et al. 2006), adenaflorins A and D (Hussein et al. 2004) and vismione E (Laphookhieo et al. 2009) belong to the first group. They exhibit antimicrobial, (Nagata et al. 1998) cytotoxic (Hussein et al. 2004) and antimalarial (Laphookhieo et al. 2009) activities, respectively. Examples for the second group of prenylated naphthalenes are the cytotoxic tri-prenylated adenaflorin C from *Adenaria floribunda* (Hussein et al. 2004), antibiotic merochlorin B from *Streptomyces* sp. strain CNH-189 (Kaysser et al. 2012), 7-demethylnaphterpin from *Streptomyces prunicolor* (Shin-ya et al. 1992) as well as the antibiotic debromomarinone from a marine actinomycete (Pathirana et al. 1992).
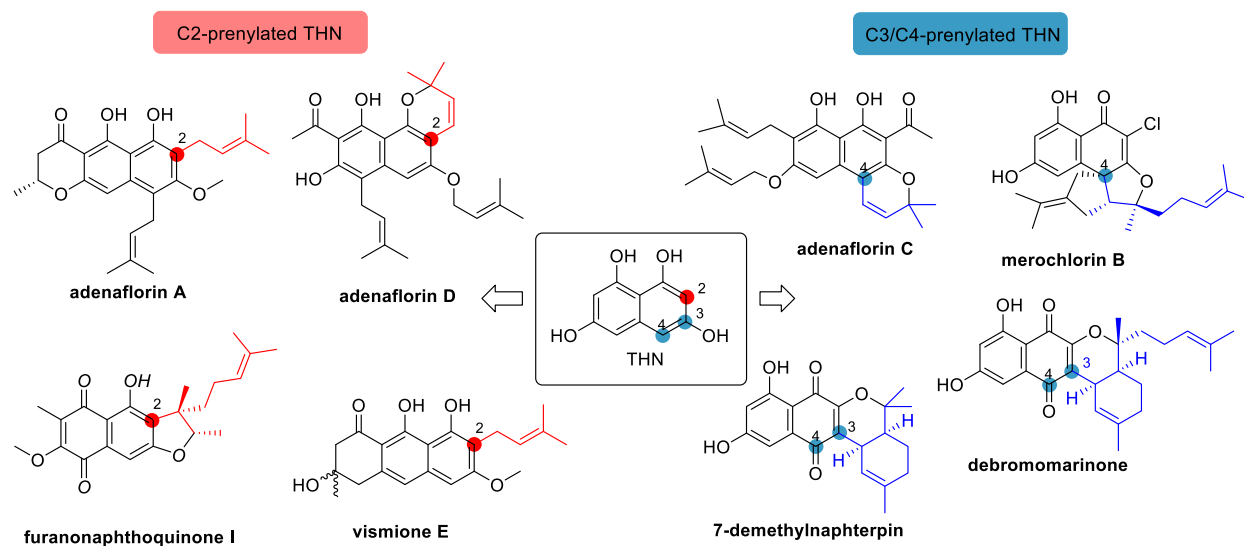
Figure 5 Examples of prenylated naphthalenes

1.3. Backbone enzymes in microbial natural product biosynthesis

In contrast to the primary metabolites synthesized by genes distributed through the genome, secondary metabolites are general encoded by genes arranged in a contiguous fashion as a

biosynthetic gene cluster (Keller 2019). A typical BGC contains one or more major genes responsible for the backbone formation of the metabolite, *e.g.* PKS, NRPS and terpene synthase, and one or more genes in charge of structural modification, metabolite transport or expression regulation (Rokas et al. 2020).

Within the wide variety of the natural product library, polyketides and peptides are the prolific origin of bioactive natural products such as the cholesterol-lowering lovastatin and the antibiotic penicillin G. They share a similar chemical logic and enzymatic machinery of biosynthetic assembly lines: starting with the recruitment of monomer units, followed by extension of the ketidyl/peptidyl chains that are transiently bound as covalent thioester intermediates to carrier protein domains, which can undergo - modifications and will be released from the synthetase after the formation of the initial backbone (Rokas et al. 2020; Walsh and Tang 2017).

1.3.1 Polyketide synthase

PKS is the core enzyme in the biosynthesis of the carbon backbone for polyketides *via* repetitive decarboxylative Claisen condensation. The common logic and enzymatic machinery for polyketides is mimicked from fatty acid synthesis, *i.e.* initiation, elongation, process and termination. Generally for minimal assemblage, a PKS requires an acyltransferase (AT) to transfer a start unit onto an acyl carrier protein (ACP) and then a β-ketoacyl synthase (KS) to introduce an extender unit for the chain elongation which will be repeated until product release. In some cases, during each extension cycle, three processing enzyme components, *i.e.* β-ketoacyl reductase (KR), dehydratase (DH), enoyl reductase (ER), can catalyse the conversion of the β-C=O to the β-CH$_2$. In addition, methyltransferase (MT), product template (PT), thioesterase (TE), as well as reductase (R) domain may also act as accessory domains for the construction and modification of polyketide products.

Based on the domain architecture, the PKSs can generally be categorized into three types: (i) type I PKSs are huge proteins with multiple autonomously functional domains found in fungi and bacteria (Keatinge-Clay 2012); (ii) type II PKSs are a set of separate individual proteins that interact only transiently and are mainly found in gram-positive actinomycetes (Hertweck et al. 2007); (iii) type III PKSs consist of very simple ketosynthases which use one or more malonyl-CoA molecules as extender units and are mostly found in plants but also in fungi and bacteria (Abe and Morita 2010; Funa et al. 1999; Hashimoto et al. 2014). Among the three distinct classes, type I PKSs can be subclassified in modular and iterative groups. Modular type I PKSs possess a multitude of domains and each of them is used once. They are the producers of linear or macrocyclic and reduced polyketides. In comparison, iterative type I PKSs, commonly found in fungi, only have one copy of each catalytic and carrier protein domain, the functional domains are used repetitively (Walsh and Tang 2017). It is now well-accepted that the nonreducing (NR), the highly reducing (HR), and the partial reducing (PR) PKSs are three major classes of iterative type I PKSs with different degrees of reductive behaviour (Cox 2007).

Obviously, the variable domain constructions as well as various starter and extender molecules lead to the structural diversity and complexity of polyketides. As shown in **Figures 6** and **7**, the rounds of chain extension influence the number of aromatic rings and the different oxidative rearrangement reactions lead to various ring topologies. The released product can be further decorated by tailoring enzymes to afford the bioactive secondary metabolites.

Fungal aromatic polyketides are mainly synthesized by NR-PKSs in which no reductive domain is employed during the elongation steps of the polyketide chain. Cyclisation reactions are generally catalysed by the PT domain with a poly-β-ketone backbone as the substrate. In the case of citrinin biosynthesis, after four rounds of chain elongation and two times of *C*-methylation, the linear poly-β-ketone intermediate is accepted by the PT domain for the C2–C7 aldol condensation to afford the aromatic ring. Afterwards, the R domain is proposed to catalyse reductive release of the polyketide, which morphs into citrinin (**Figure 6A**). In contrast, the tricyclic norsolorinic acid anthrone, represented by aflatoxin B$_1$, reflects a distinct cyclisation regioselectivity that starts the first ring with a C4–C9 bond formation and then the second with C2–C11 (**Figure 6B**). Moreover, the third pattern with C6–C11 first-ring cyclisation is involved in the biosynthesis of tetracyclic fungal metabolite such as viridicatumtoxin (**Figure 6C**).
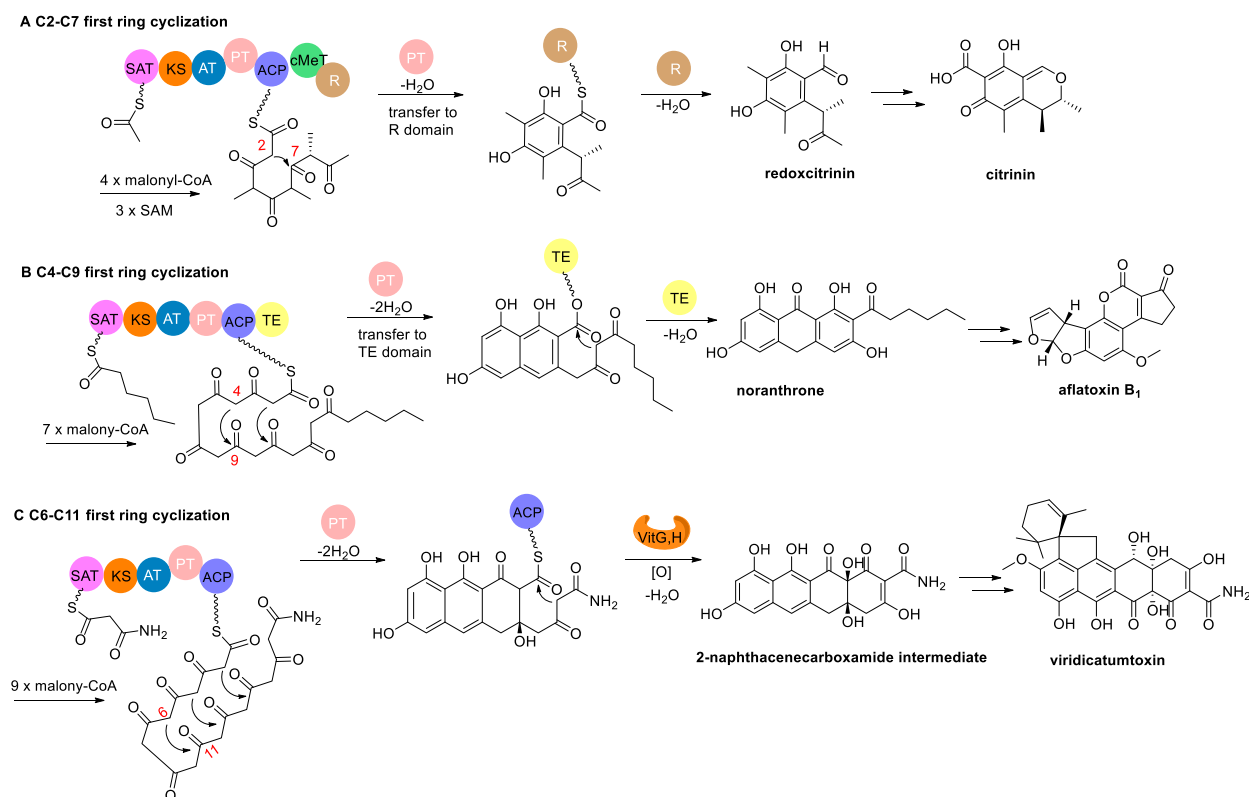
Figure 6 Biosynthesis of aromatic polyketides by various NR-PKSs. PT domain mediated cyclisation reactions are classified by three distinct regioselectivities

Besides the specific PT domain mediated cyclisation products made by NR-PKSs, aromatic products can also be produced by PR- and HR-PKSs. Unlike the NR-PKSs, the domain architecture of most PR-PKSs does not include a PT-similar domain but is still able to form the aromatic skeleton, *e.g.* 6-methylsalicylic acid synthase (MSAS) (**Figure 7A**). The HR-PKSs exhibit more complex biosynthetic programming. Some of them contain additional processing domains to achieve a β-keto reduction. For example, a recent study from Yi Tang's group showed another aromatisation mechanism: two individual short-chain dehydrogenases/reductases, Vir B and Vir C, selectively reoxidized β-hydroxyl groups to β-ketones in the linear HR-PKS product, which enabled further intramolecular aldol condensation between C2 and C7 (**Figure 7B**).

The highly programmed PKS assembly lines offer a large group of structural diverse and bioactive natural products, which fascinates many biochemists and biomolecular engineers. On one hand, sustained exploration of natural PKS holds the potential for discovering new natural bioactive polyketides. On the other hand, a better understanding of mechanisms could promote the evolution of PKS engineering, thus enabling us to effectively expand the polyketide chemical space artificially.
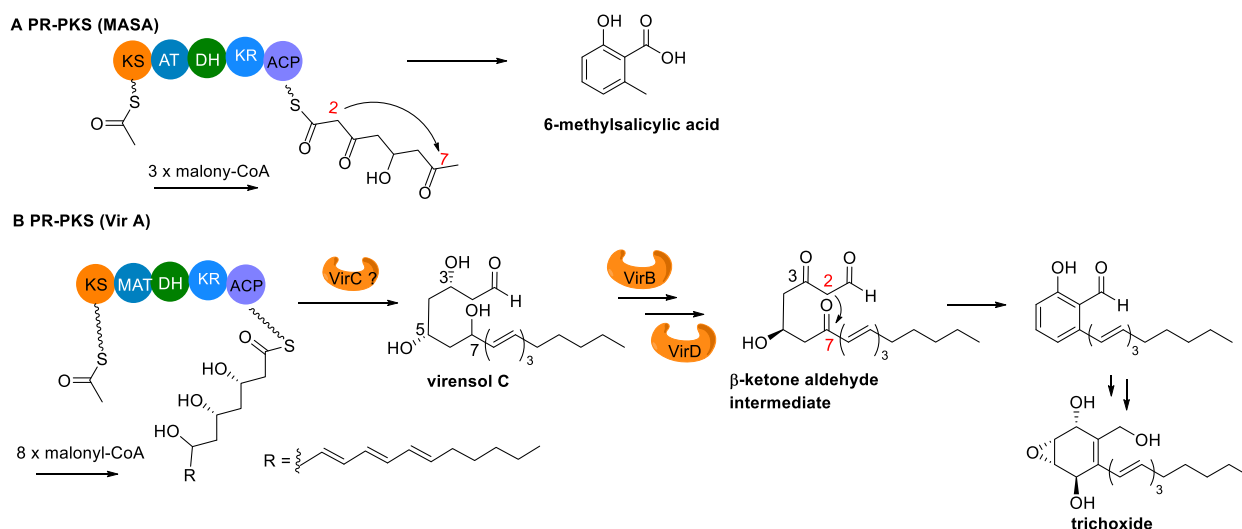
Figure 7 Biosynthesis of aromatic polyketides by PR- (A) and HR-PKSs (B)

1.3.2 Nonribosomal peptide synthetase

Similarly, NRPSs serve as templates to program the assembly of amino acids by forming C-N bond linkages in a parallel chemical logic to PKSs (Walsh and Tang 2017). In analogy to the minimal domain architecture (KS-AT-ACP) of a PKS module, there are three core domains in a minimal NRPS module, *i.e.* condensation (C), adenylation (A) and thiolation (T) domains (Sieber and Marahiel 2005). The A domain is responsible for recognition and activation the amino or aryl acid monomer as well as transfer to the adjacent T domain, also referred to as peptidyl carrier protein (PCP). The C domain is responsible for the peptide chain extension *via* C-N bond formation between the electrophilic upstream

peptidyl-S-T_1 and the nucleophilic downstream aminoacyl-S-T_2. The typical order of domains for elongation is C-A-T. While the extending intermediate is covalently tethered onto the T domain, several specialized domains can carry out further modifications to increase the diversity and complexity of the final products. For example, the epimerization (E) domain can epimerize and incorporate L-amino acid monomers to their D-form (Süssmuth and Mainz 2017). Methyltransferase (MT) domains can transfer a -CH_3 group onto the amino group of the aminoacyl-S-T intermediate with an N-methylation. The Cy (cyclisation) domain as a subset of a C domain exhibits a heterocyclization activity. Like type I PKSs, the termination modules of NRPS assembly lines usually have a C-A-T-TE organization to release the product by hydrolysis or cyclisation. In fungal systems, a terminal C domain may perform the cyclisation reaction for termination as shown in **Figure 8** (Gao et al. 2012a).

The nonribosomally produced peptides reflect the complexity and abundance of structural classes, from simple indole alkaloids to 20-mer peptides. Among them, the indole-containing nonribosomal peptides are produced when an NRPS module incorporates an L-tryptophan as start monomer. A representative is the biosynthesis of verruculogen in *Aspergillus fumigatus* (**Figure 8**) (Maiya et al. 2006). The prototypic fungal dipeptide synthetase FtmA was identified by deletion and overexpression in the native host as well as heterologous expression in *Aspergillus nidulans*. Theoretically, the A_1 domain in FtmA recognizes L-tryptophan, activates the carboxylated group which is then installed as an aminoacyl thioester on the neighboring T_1 domain. The next module C-A_2-T_2 extends the chain by adding a prolinyl group. Then the dipeptide brevianamide F is released and post-modified to various products such as tryprostatins, spirotryprostatins and fumitremorgins (Li 2011).
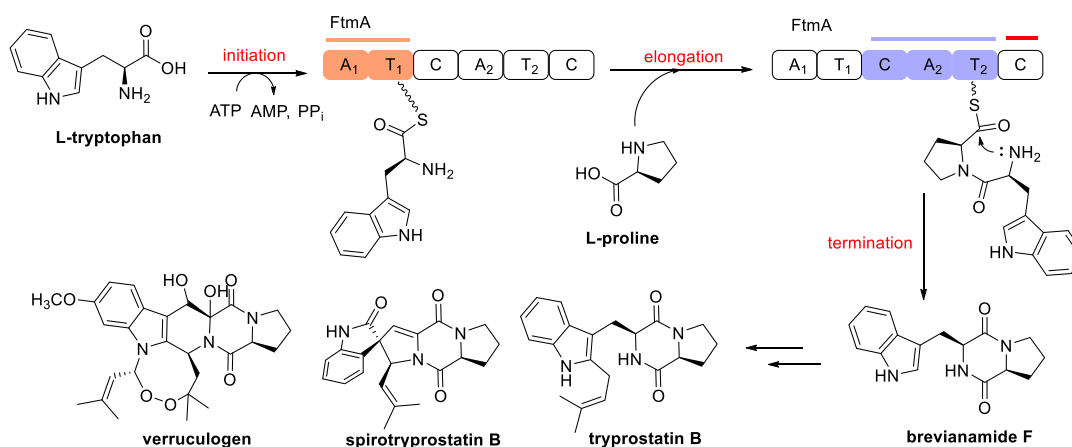
Figure 8 The biosynthesis of verruculogen in *Aspergillus fumigatus*

The number of genes known to code for PKSs and NRPSs has increased rapidly because of development in genome sequencing over the past decade. A fundamental understanding of the underlying biosynthetic logic would facilitate the elucidation of the structural diversification of polyketides, nonribosomal peptides and their hybrids. Advances of biosynthesis-inspired chemical

synthesis and combinatorial biosynthesis suggest new methods for enhancing structural diversity and drug discovery and allow reprogramming of new assembly lines for effective chemical production.

1.4. Aromatic prenyltransferases as modification enzymes

As aforementioned, the released products of PKS and NRPS are in many cases not the final metabolic products. They are often modified by various specialized enzymes, termed as post-assembly or tailoring enzymes, contributing to the diverse and sophisticated structural modifications of NPs (Li 2009; Sattely et al. 2008; Walsh 2008). A notable set of decorating enzymes are prenyltransferases (PTs) which catalyse the transfer of different prenyl moieties onto numerous acceptor molecules (Winkelblech et al. 2015). Aromatic PTs are generally classified into the UbiA-type, the CloQ/NphB-type, and the dimethylallyltryptophan synthase (DMATS)-type (Winkelblech et al. 2015).

The PTs of the UbiA superfamily are membrane-bound proteins and their reactions are dependent on the presence of divalent ions (Young et al. 1972). They are not only involved in secondary but also in primary metabolism and use diverse aromatic compounds as substrates (Li 2016). LaPT1 (Shen et al. 2012) and SfG6DT (Sasaki et al. 2011) from this family catalyse the prenylation of flavonoids, while UbiA and its homolog MenA play important roles in the biosynthesis of menaquinone (vitamin K2) and ubiquinone (coenzyme Q) (Meganathan and Kwon 2009). In contrast to the membrane-bound PTs, the members from the CloQ/NphB and DMATS superfamilies are soluble proteins containing no aspartate-rich motif, *e.g.* NDxxDxxxD, in their sequences (Bonitz et al. 2011; Heide 2009; Winkelblech et al. 2015). Known CloQ/NphB-like PTs are mainly found in *Streptomyces* and use aromatic compounds such as hydroxynaphthalenes, phenazines, quinones and phenolic compounds as substrates (Heide 2009; Winkelblech et al. 2015). NphB was proven to be involved in the biosynthesis of naphterpin and derivatives (Kuzuyama et al. 2005). Its crystal structure contains the typical $\alpha\beta\beta\alpha$ barrel fold with antiparallel strands (Kuzuyama et al. 2005).

The DMATS superfamily is the most investigated subgroup among the aromatic prenyltransferases. They are metal-independent enzymes, but addition of metal ions such as Ca^{2+} and Mg^{2+} strongly enhance their activities in some cases (Li 2009; Pockrandt et al. 2012; Yu et al. 2012). Structural analysis of DMATS enzymes reveals a common $\alpha\beta\beta\alpha$ PT fold (Metzger et al. 2009; Pojer et al. 2003; Saleh et al. 2009). The first member of this family is the tryptophan C4-prenyltransferase DmaW in the biosynthesis of ergot alkaloids in *Claviceps fusiformis* (Gebler and Poulter 1992; Tsai et al. 1995). The PTs of the DMATS superfamily are involved in the biosynthesis of diverse microbial secondary metabolites, especially prenylated indole alkaloids (Li 2010). In the biosynthesis of the ergot alkaloid fumigaclavine C, FgaPT2 catalyses the first pathway-specific step, *i.e.* the C4-prenylation of L-tryptophan, resulting in the formation of 4-dimethylallyl-L-tryptophan as the key intermediate (Unsöld and Li 2005). In the case of the fumitremorgin/verruculogen biosynthetic pathway, FtmPT1 catalyses a C2-regular prenylation of brevianamide F at an early stage (Grundmann and Li 2005) and FtmPT2

carries out an N1-prenylation (Grundmann et al. 2008). The final product fumitremorgin A with an additional *O*-prenyl moiety is formed by prenylation with FtmPT3 (Mundt et al. 2012). In most cases, one PT only catalyses one specific transfer reaction, but there are also rare multifunctional PTs involved in more than one prenylation steps. The remarkable examples are EchPTs in the echinulin biosynthesis in *Aspergillus ruber*. EchPT1 catalyses the first prenylation step, leading to preechinulin. The unique EchPT2 attaches, in a consecutive prenylation cascade, up to three dimethylallyl moieties to preechinulin and its dehydro forms neoechinulins A and B, resulting in the formation of echinulin and congeners (Wohlgemuth et al. 2017).

More interestingly, members of the DMATS superfamily demonstrate an intriguing substrate flexibility and catalytic promiscuity (Fan et al. 2015). They accept not only natural substrates but also molecules with different scaffolds. Several studies have proven that bacterial metabolites such as flavonoids, hydroxynaphthalenes and indolocarbazoles as well as plant metabolites like flavonoids and acylphloroglucinols can also be accepted by fungal DMATS enzymes (Yu et al. 2012; Yu et al. 2011; Yu and Li 2011; Zhou et al. 2015). The high substrate plasticity of the DMATSs facilitated an enzyme-driven regiospecific production of various prenylated products. In a previous study, one-step reactions were performed for the production of seven monoprenylated products from one unnatural substrate,
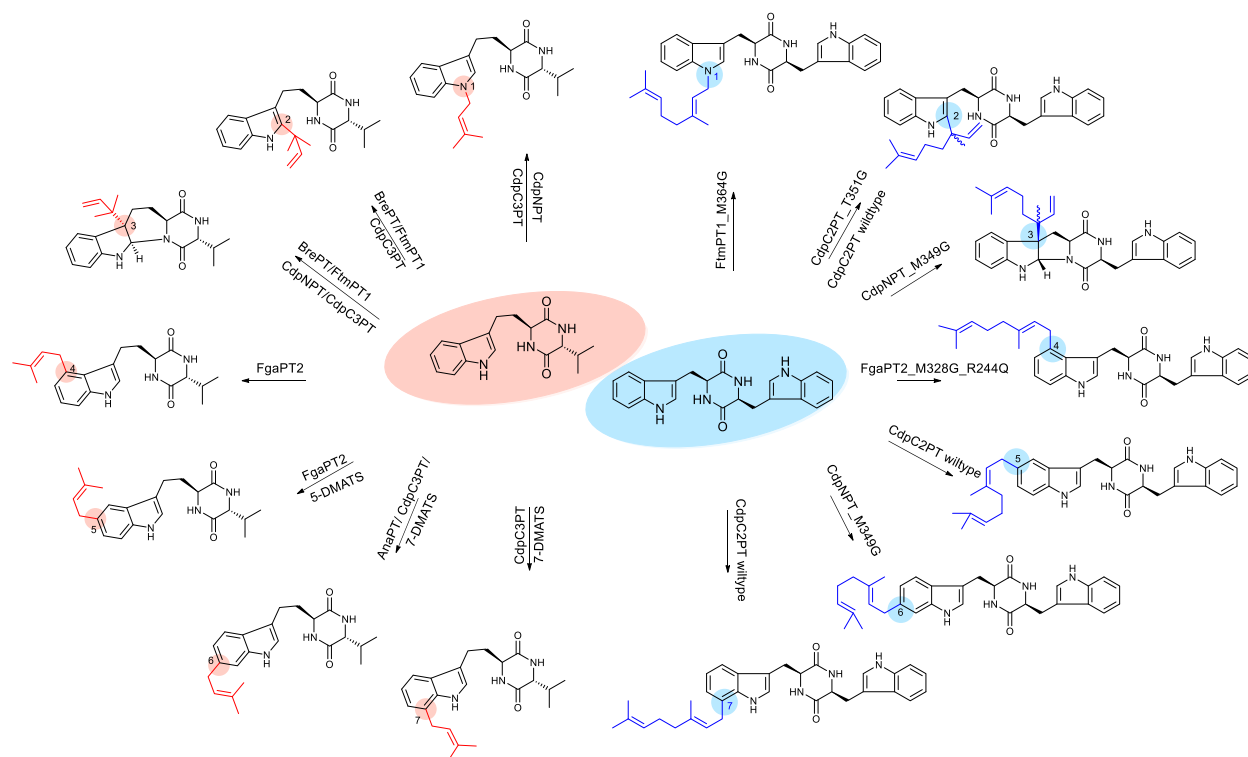
Figure 9 Overview of one-step reactions achieving the attachment of prenyl moieties to all nucleophilic reactive positions of the indole nucleus *via* chemoenzymatic synthesis (modified after (Fan and Li 2013; Liao et al. 2018))

cyclo-L-homotryptophan-D-valine, by eight PTs (**Figure 9**). (Fan and Li 2013) This study expands significantly the potential usage of prenyltransferases as biocatalysts for Friedel–Crafts alkylation. However, one bottleneck for the use of DMATS enzymes in biotechnology is their high specificity toward DMAPP as the prenyl donor (Fan et al. 2015). Advances in enzyme crystal structure analysis provide a better understanding of reaction mechanisms and basis for protein engineering. Structure-guided molecular modelling and site-directed mutagenesis on FgaPT2 led to the creation of GPP- and FPP-accepting enzymes (Mai et al. 2018). Mutation of the gatekeeping residues in six PTs turned on or improved the acceptance of GPP for cyclo-L-Trp-L-Trp prenylation to generate nine products with different prenylation positions or patterns (Liao et al. 2018). These efficient biochemical approaches tremendously enrich the biocatalyst toolboxes.

PTs serve as remarkable decoration enzymes during numerous metabolite post-assembly lines to produce key intermediates or final products. Further investigation on their characteristics will benefit their potential application in chemoenzymatic synthesis and synthetic biology to increase structural diversity.

1.5. Post-modifications on the prenyl moieties

The attached prenyl moiety can undergo significant structural diversification to yield the final bioactive compounds. Prenylated pathway intermediates can be further modified by a variety of chemical transformants such as cyclisation, halogenation, alkynylation dehydrogenation and rearrangements (**Figures 10 − 12**). Once the prenyl group is attached on the nascent intermediate, enzymatic or nonenzymatic reactions can take place to diversify chemical structures and enhance the bioactivity of the resulting products.

1.5.1. Post-modifications by enzymatic reactions

An example for enzymatic post-modification of a prenylated intermediate can be found in the penigequinolone biosynthesis in *Penicillium thymicola*. The *pen* cluster contains an assortment of genes for redox enzymes, PTs and methyltransferases (**Figure 10**) (Zou et al. 2015). Genome mining showed that this BGC was putatively responsible for the productions of penigequinolone and yaequinolone C with a highly modified C_{10} isoprenoid chain. The backbone synthase PenN and associating enzymes catalyse the formation of a 6,6-bicyclic core skeleton (**1**). The first prenyltransferase PenI carries out the attachment of only one dimethylallyl group (C_5) which undergoes a dehydrogenation to generate the aryl diene quinolone **3**. The terminal $\Delta 3'$ double bond in **3** affords the electron-rich position C4' for the subsequent "head to tail" prenyl-prenyl elongation by the second prenyltransferase PenG to the C3'-prenylated "pseudo-geranyl" intermediate **4**. After the epoxidation of compound **4**, two distinct biosynthetic routes are performed *via* cationic epoxide rearrangements to build the cyclopropane-tetrahydrofuran or -tetrahydropyran ring systems, respectively (Zou et al. 2017). Generally, the prenyl moiety is transferred onto the electron-rich

substrate with the designated size (dimethylallyl, geranyl, farnesyl, etc.) in natural product biosynthesis. Nevertheless, Zou et al. published an unprecedented prenyl chain extension mechanism *via* "prenyl-prenylation" (Zou et al. 2015).
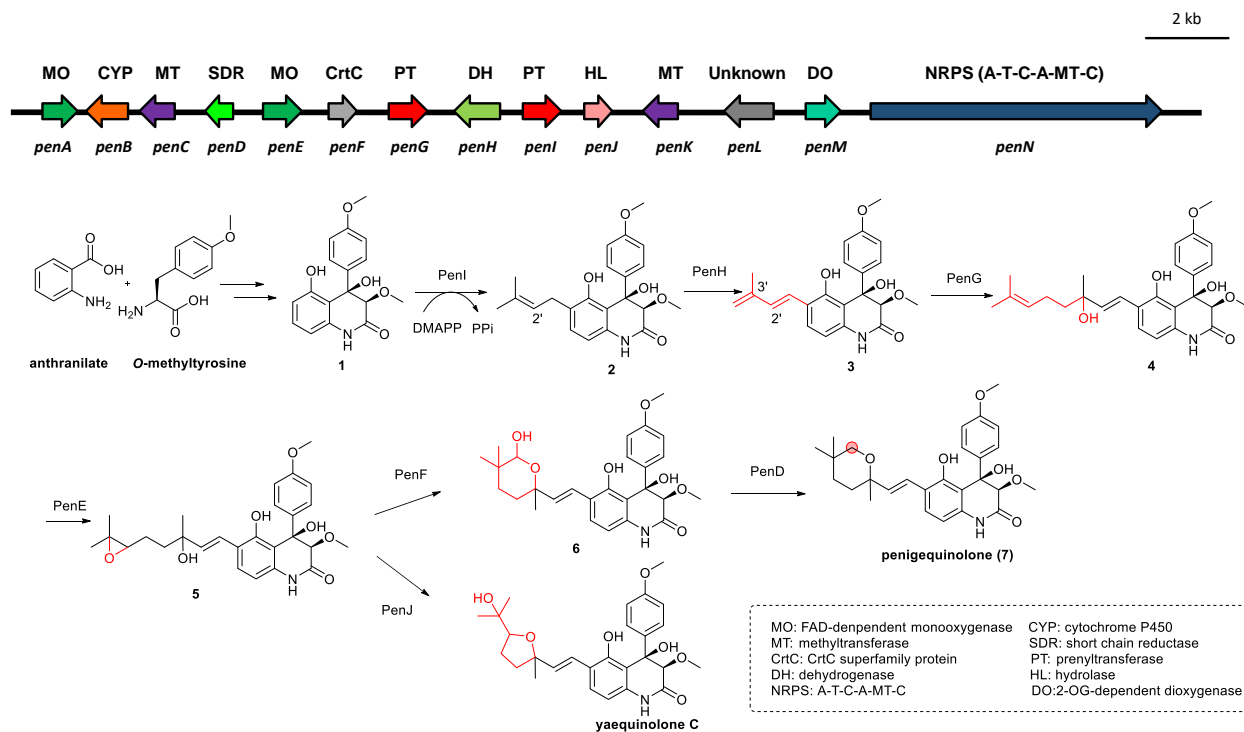
Figure 10 Genetic organisation of the *pen* gene cluster in *Penicillium thymicola* and the simplified biosynthetic pathways of penigequinolone and yaequinolone C

In addition to dehydrogenation, iterative prenylation, epoxidation and consequent rearrangement as in the penigequinolone biosynthesis, there are also other post-modifications on prenyl moieties. The notable set is cyclisation *via* C-N, C-O or C-C bond to afford morphed scaffolds and structural rigidity (**Figure 11**). For example, the cytochrome P450 FtmE and FAD-binding oxidoreductase CnsA catalyse the oxidative C-N bond formation between the C2' of the indole prenyl group and the nearby N atom to form six or seven number rings (Chen et al. 2020; Kato et al. 2009). Another cyclisation type is the endoperoxide formation catalysed by the nonheme Fe^{II}/2-oxoglutarate (Fe^{II}/2-OG)-dependent oxygenase FtmOx1 (Steffan et al. 2009). This intriguing enzyme converts fumitremorgin B to verruculogen by introducing one molecule of O_2 to assemble the O-O bond. Furthermore, a uniquely fused spirobicyclisation on the geranyl moiety is carried out by the cytochrome P450 VrtK *via* two C-C coupling steps (Chooi et al. 2013). The cyclisation most likely starts with an initial oxidation of C17 to an allylic carbocation resulting in the first C15-C19 cyclisation, which can undergo concerted 1,2-alkyl shift/1,3-hydride shift to yield a new C15 tertiary carbocation, following by C7 Friedel−Crafts alkylation to afford the second C7-C15 cyclisation. The bicyclo[2.2.2]diazaoctane nucleus is widely distributed among natural products such as notoamides and brevianamides. This core framework was

proven to be biosynthesized by a reductase MalC *via* an intramolecular [4+2] hetero-Diels–Alder cyclisation (Dan et al. 2019).

Recent studies of the enzymatic post-modifications on prenyl moieties revealed the biosynthetic bases for two decade-old problems. One is for the formation of the tetracyclic ergoline core *via* initial
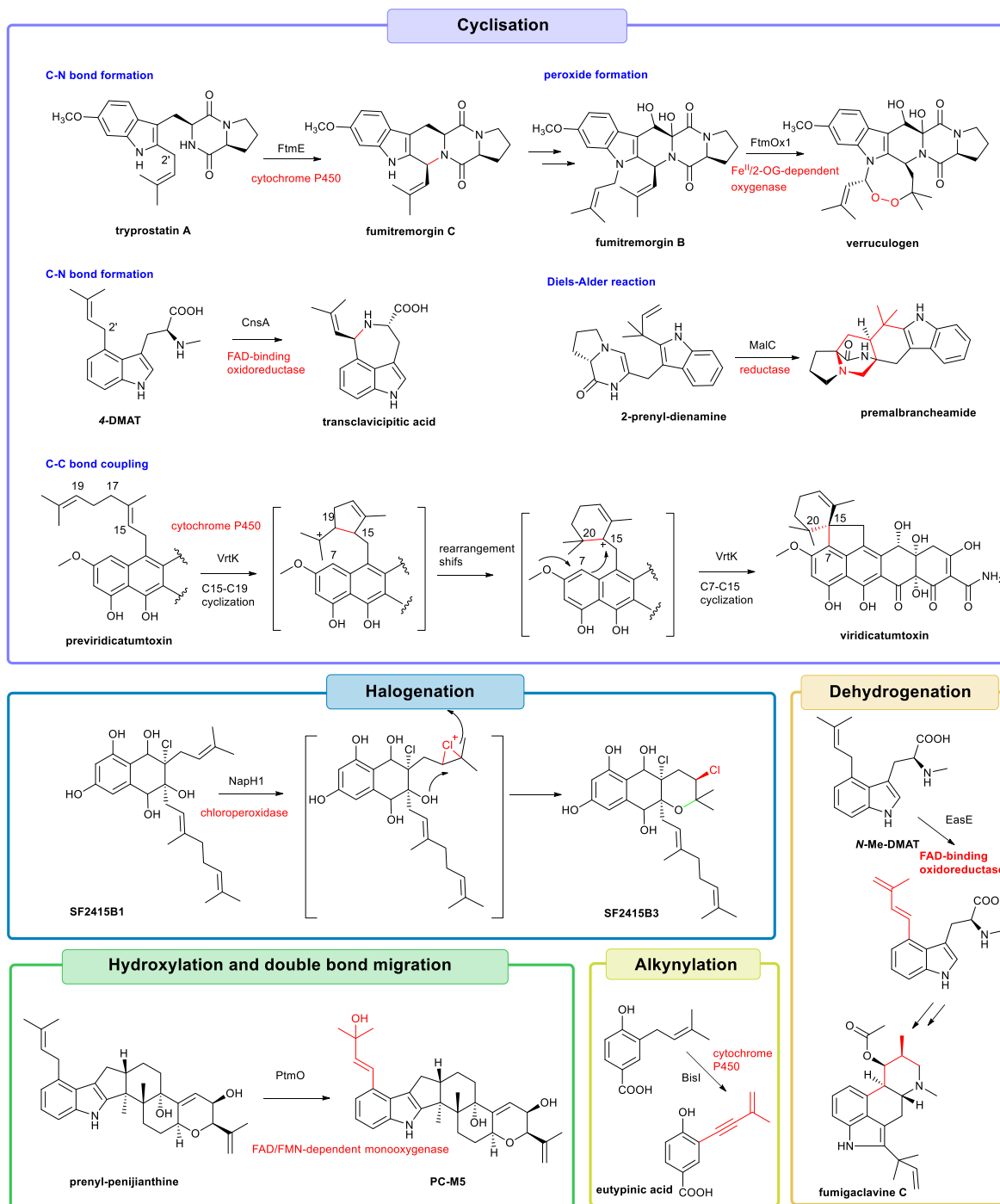
Figure 11 Enzymatic reactions on the prenyl moieties

oxidoreductase (EasE) catalysed dehydrogenation (**Figure 11**) (Yao et al. 2019). Another is for the construction of an alkyne group by an unprecedented cytochrome P450 enzyme BisI (**Figure 11**) (Lv et al. 2020). Moreover, the chloroperoxidase NpaH1 was identified to introduce a Cl^+ leading to a spontaneous C-O coupling cyclisation to the tetrahydropyran ring (**Figure 11**) (Bernhardt et al. 2011). The hydroxylation and double bond migration was performed by a FAD/FMN-dependent monooxygenase to generate an active intermediate PC-M5 for the construction of the characteristic bicyclo[4.2.0]octane system (**Figure 11**) (Liu et al. 2015).

1.5.2. Post-modifications by nonenzymatic reactions

Alternatively to the enzymatic modifications mentioned above, the diversity of prenylated secondary metabolites can also be increased by the assistance of nonenzymatic reactions. During natural product formation, enzymatic and nonenzymatic reactions generally unfold in a cooperative manner, since in some cases the enzymatic products are chemically unstable and tend to convert to chemically more stable forms.

Investigations of prenylation mechanisms revealed the unique tandem enzymatic/nonenzymatic sequence *via* post-rearrangements in some biosynthetic pathways (Tanner 2015). Based on the *C*- or *O*-prenylation, the pericyclic reactions can be classified into Claisen rearrangement and Cope rearrangement (**Figure 12A and B**). Biochemical study of the tyrosine prenyltransferase LynF demonstrated an O to C Claisen rearrangement at 'physiological' temperature in aqueous buffers, which occurred nonenzymatically after nascent *C*-prenylated product release (McIntosh et al. 2011). This example provides another mechanism for aromatic prenylation, which is not through an electrophilic aromatic substitution, but as a result of the Claisen rearrangement. Similarly, the generation of 4-DMAT, the early-stage product of ergot alkaloid biosynthesis, was speculated to be derived from a C3-reversed prenyl adduct that undergoes the Cope rearrangement following by deprotonation on the aromatic ring (Luk et al. 2011). Apart from 4-DMAT, the subsequent rearrangements after nucleophilic C3-prenylation can most likely occur in many fungal indole alkaloid biosynthetic pathways, like N-DMAT (Qian et al. 2012), tryprostatin B (Cardoso et al. 2006) and paxilline (Tagami et al. 2013).

In addition to the rearranged intermediates, environmental stimuli can also initiate the chemical conversions. These include pH- or temperature-mediated, light- or oxygen-induced, or even organic solvent catalysed reactions (Capon 2020). Phenols with a prenyl substituent on the *ortho*-position are prone to acid-mediated cyclisation or hydroxylation during isolation and handling (**Figure 12C**). The enzymatic or nonenzymatic epoxidation on the isoprenyl side chain most likely leads to the spontaneous cyclisation (**Figure 12C**). A series of butenolides were isolated from three marine-derived *Aspergillus terreus* species treated with chlorinated solvents, *i.e.*, acidic conditions (**Figure 12D**) (Parvatkar et al. 2009; Sun et al. 2018; Wang et al. 2011). The chemical cyclisation of prenylated products was observed under 2 % conc. aqueous sulphuric acid or 2 % conc. HCl in methanol

(Parvatkar et al. 2009). The spontaneous 5-*exo* and 6-*endo* cyclisation was detected with an epoxide as the intermediate to form tetrahydrofuran and tetrahydropyran (43:1) products *in vitro* (He et al. 2019).
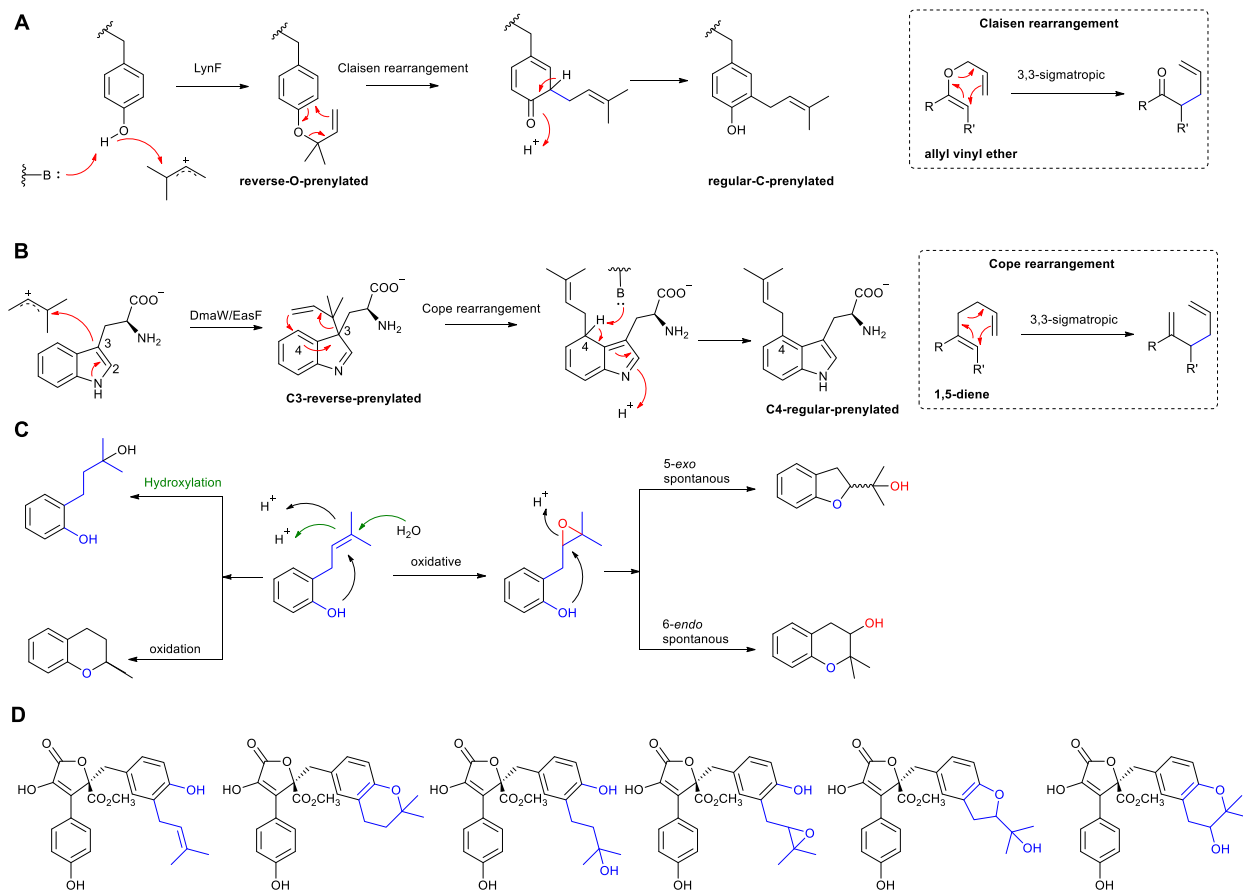
Figure 12 Examples of non-enzymatic reactions: the Claisen rearrangement during tyrosine prenylation (A); the Cope rearrangement during indole alkaloid prenylation (B); pH-mediated phenol rearrangements (C); examples of rearranged artifacts from the prenylated precursor (D)

In summary, the diversity of prenylated aromatic products is expanded by the combination of various core scaffolds derived from diverse backbones and variable prenyl moieties with enzymatic or nonenzymatic modifications. How nature assembles these hybrid structures raises a number of intriguing points: i) The exploration of related synthetic mechanisms has been used for the design and development of novel chemical entities by combinatorial biosynthesis; ii) Commitment identification of the chemical and biological properties of artifacts provides new insights into the natural product chemical space; iii) Further development of genetic manipulation, chemoenzymatic synthesis and analytical instrumentation will enhance future prospects for exciting new discoveries of natural products.

1.6. Isotopic labelling experiments in the elucidation of reaction mechanisms

Biosynthetic studies have established themselves to be one of the most exciting areas of natural product research and have become an important part of modern drug discovery and development efforts. Isotopic labelling experiments have been commonly applied to confirm the biosynthetic origin and identity the enzymatic logic with simple precursors, *e.g.* acetate, glucose, O_2, CO_2, H_2O, and methionine (**Figure 13A**) (Schor and Cox 2018a; Walsh and Tang 2017). However, more elaborated studies are needed in some cases, *e.g.* for more complex biosynthetic intermediates that often are result of a complicated synthetic mechanism (Bloomer et al. 1968; O'Brien et al. 2003).

Feeding experiments with isotopic building blocks remain crucial in order to determine the origin and their connectivity before generating to the end products. Through isotope tracer studies, several previously unrecognized biosynthetic pathways have now become obvious. One of the remarkable examples is the discovery of the emodin and ravenelin pathways (**Figure 13B**). Emodin has been served as a well-studied anthraquinone since 1924 (Dong et al. 2016; Jacobson and Adams 1924). Later, ravenelin was identified as the first fungal xanthone from *Helminthosporium ravenelii* (Raistrick et al. 1936). Feeding experiments with [1-^{13}C]-, [1,2-^{13}C$_2$]- and [1-^{13}C, ^{18}O$_2$]-acetate led to the generation of the tricyclic ring system in emodin (Birch et al. 1975; Hill et al. 1982). The results proved acetate as the origin of the methyl group on the aromatic C ring and the presence of the symmetrical benzophenone intermediate. Furthermore, the oxidative removal of the C-10 in emodin is most likely *via* a Baeyer-Villiger-like reaction, thereby introducing the atmospheric 4- and 8/10a- oxygen prior to ring closure to the xanthone skeleton (Schor and Cox 2018b).

Moreover, the mechanism of enzymatic or nonenzymatic post-assembly lines can also be clarified by isotopic studies. Treatment with an ^{18}O$_2$-enriched atmosphere during the FtmOx1 reaction led to the incorporation of one molecule labelled ^{18}O$_2$ (Steffan et al. 2009). This demonstrated that the Fe^{II}/2-OG-dependent oxygenase captured both oxygen atoms to form the endoperoxide bond (**Figure 13C**). Incubation of hydroxyclavatol in H$_2$^{18}O at 25 °C for 16 h resulted in the incorporation of ^{18}O into hydroxyclavatol, which therefore indirectly evidenced the existence of chemically reactive intermediate *ortho*-quinone methide and subsequent nonenzymatic 1,4-Michael additions (**Figure 13D**) (Fan et al. 2019).

Overall, classical isotope tracer experiments remain an important role in understanding how and from what precursors a specific natural product is constructed. This in turn provides meaningful information for further investigation using genetic and enzymatic approaches. Thus, using a combination of genome manipulation, enzymology and chemistry, coupled with mass and NMR spectroscopy, it is now possible to dissect mechanisms and processes involved in the natural product biosynthesis at the molecular level.
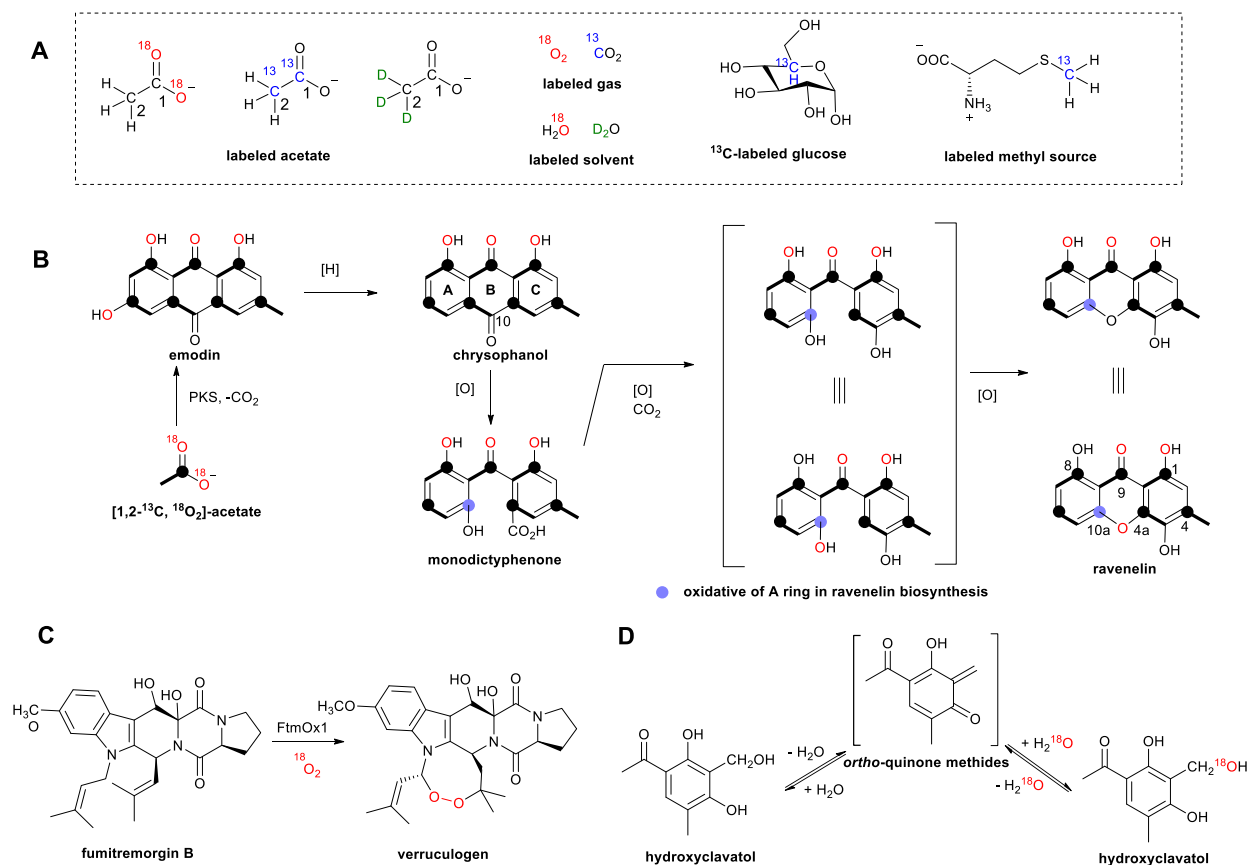
Figure 13 Examples of labelling experiments: commonly used isotopomers in natural product labelling experiments (A); labelling pattern in ravenelin biosynthesis revealed from isotopic feeding experiments (B), modified after (Schor and Cox 2018b); oxidative labelling pattern for peroxide formation (C), modified after (Steffan et al. 2009); confirmation of reactive intermediate by ^{18}O-isotopic water (D), modified after (Fan et al. 2019)

2 Aims of this thesis

The following issues have been addressed in this thesis:

Double bond migration and hydroxylation within a dimethylallyl moiety catalysed by a nonheme Fe^{II}/2-oxoglutarate-dependent oxygenase

Prenylated products represent a large group of SMs and are widely distributed across bacteria, fungi, and plants. Prenylation contributes significantly to the structural diversity of natural products. They often can be further modified *via* hydroxylation, cyclisation, epoxidation and double bond migration by various tailoring enzymes. Among them, Fe^{II}/2-OG-dependent oxygenases as unique oxidative enzymes catalyse a remarkably wide array of biochemical transformations such as the peroxide formation by FtmOx1. These oxidative transformations play critical roles in biochemical processes and highlight their importance in nature. Inspired by the notable Fe^{II}/2-OG-dependent oxygenase FtmOx1, a homologue enzyme EAW25734 from the fungus *Neosartorya fischeri* was identified and characterized biochemically. The following experiments were carried out:

- Sequence alignments of the nonheme Fe^{II}/2-oxoglutarate-dependent oxygenases FtmOx1$_{Af}$, FtmOx1$_{Nf}$ and EAW25734. This part was carried out by Viola Wohlgemuth.
- Overproduction and *in vitro* investigation of EAW25734 with verruculogen and its biosynthetic intermediates as substrates
- Isolation and structure elucidation of the enzyme products by LC-HR-MS and NMR analyses
- Biochemical characterization of the recombinant protein EAW25734
- The natural role of EAW25734 in *Neosartorya fischeri*
- Elucidation of the reaction mechanism by ^{18}O labelling experiments

Tricyclic derivative formation *via* spontaneous oxidative cyclisations of 1,3-dihydroxy-4-dimethylallylnaphthalene

Prenylated naphthalene derivatives exhibit intriguing structure diversity and a whole array of biological activities. Our recent study demonstrated the acceptance of hydroxynaphthalenes by eight members of the DMATS superfamily, *i.e.* FgaPT2, 7-DMATS, FtmPT1, AnaPT, CdpC3PT, CdpNPT, CTrpPT and SirD (Yu et al. 2011). Twelve prenylated naphthalenes were isolated and identified. None of them underwent spontaneous rearrangement. In this project the rearrangements of the C4-prenylated 1,3-dihydroxynaphthalene were investigated. The following experiments were carried out in cooperation with Dr. Jinglin Wang.

- Overproduction and purification of the recombinant prenyltransferases FgaPT2, CdpNPT, FtmPT1 and AnaPT
- Testing their activities with 1,3-dihydroxynaphthalene in the presence of DMAPP
- Testing the stability of 1,3-dihydroxy-4-dimethylallylnaphthalene
- LC-MS analysis of the incubation mixtures
- Isolation and structure elucidation of the rearrangement products
- Proof of the spontaneous oxidative cyclisations of 1,3-dihydroxy-4-dimethylallylnaphthalene *via* the isotopic labelling experiments

Biosynthesis of the prenylated benzene carbaldehyde flavoglaucin and its congeners requires prenylation as a key biosynthetic step

Flavoglaucin and congeners are prenylated benzene carbaldehyde derivatives carrying a C_7 side chain without/with one to three double bonds or with a furan ring. They were isolated from different microbes and exhibit a whole array of different biological activities. Moreover, they are also proposed to be precursors of interesting complex molecules. Their biosynthetic origin was still unknown prior to this study. The aim of this project is to identify the biosynthetic pathway of flavoglaucin in *Aspergillus ruber* by genome mining-based molecular biological and biochemical strategy as well as by feeding experiments. The following experiments were carried out in cooperation with Jonas Nies.

- Genome mining for flavoglaucin biosynthetic gene cluster in *Aspergillus ruber*
- Heterologous expression of the whole *fog* cluster in *Aspergillus nidulans* LO8030 under the control of their native promoters
- Verifying the role of *fog* cluster in the flavoglaucin biosynthesis by LC-MS and NMR analyses of the pathway products
- Functional proof of the genes from the *fog* cluster by gene deletion, heterologous expression and pathway intermediate analysis
- Characterisation of the prenyltransferase FogH by *in vitro* investigation with recombinant protein. *FogH* was cloned by Viola Wohlgemuth in the expression vector pVW84.
- Verification of the *fogF* function by heterologous expression and feeding experiment

Jonas Nies carried out genetic experiments, while the PhD candidate carried out the isolation and structure elucidation as well as biochemical characterisation.

3 Results and discussion

3.1 Double bond migration and hydroxylation within a dimethylallyl moiety catalyzed by a nonheme Fe^{II}/2-oxoglutarate-dependent oxygenase

Prenylations fulfil an important function in the biosynthesis of secondary metabolites. Attachment of one or more prenyl moieties from different donors with C_{5n} (n=1, 2, 3…) units to a wide range of prenyl acceptors contributes substantially to natural product diversity. In most cases, prenylated molecules serve as intermediates for further conversion by tailoring enzymes. Therefore, enzymatic post-modification on the prenyl moiety is an attractive research field. *In vivo* biosynthetic experiments can be extremely challenging due to multiple complex interactions and parameters that cannot be controlled. Therefore, design and optimization of biocatalysts *in vitro* is an effective approach to address this challenge.

In a previous study, the Fe^{II}/2-OG-dependent oxygenase FtmOx1$_{Af}$ from *Aspergillus fumigatus* was reported to catalyse an endoperoxide formation between two prenyl moieties (Steffan et al. 2009). Later gene sequencing of the close relative *Neosartorya fischeri* NRRL181 resulted in the identification of a very similar fumitremorgin gene cluster containing the homologue FtmOx1$_{Nf}$ with an identity of 95 % on the amino acid level and one additional *O*-prenyltransferase (Mundt et al. 2012). Further genome mining in *Neosartorya fischeri* led to the identification of another homologous protein EAW25734 in the same fungi with a sequence identity of 48 % with both FtmOx1$_{Af}$ and FtmOx1$_{Nf}$. Sequence alignments of EAW25734 with FtmOx1$_{Af}$ (Steffan et al. 2009; Yan et al. 2015), FtmOx1$_{Nf}$ (Mundt et al. 2012) and other two known Fe^{II}/2-OG-dependent oxygenases PrhA (Nakashima et al. 2018) and AusE (Nakashima et al. 2018) indicated the presence of typical conserved 2-His-1-Asp ion-binding triad in the potential nonheme iron enzyme EAW25734 (**Figure 14**).
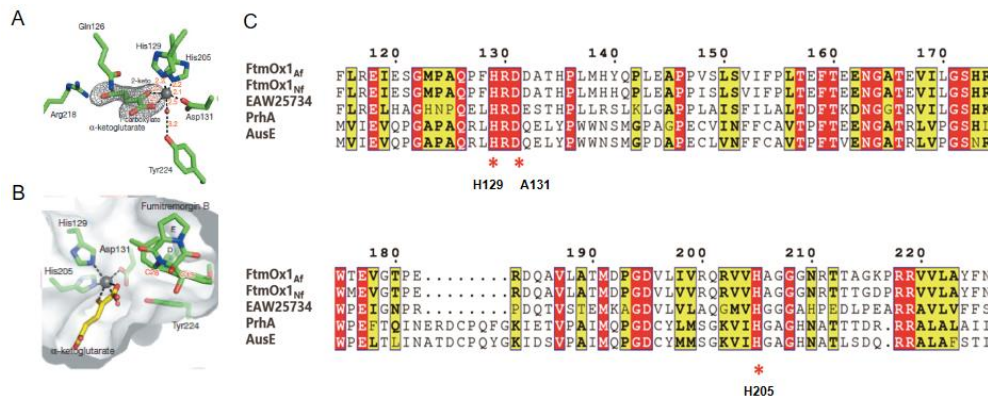
Figure 14 Sequence analysis of EAW25734 and homologue: Mode of FtmOx1-Fe^{II}-2-OG binary complex (A), modified after (Yan et al. 2015); Structure of the FtmOx1-Fe^{II}-2-OG-fumitremorgin B tertiary complex (B), modified after (Yan et al. 2015); Sequence alignments of nonheme Fe^{II}/2-OG-dependent oxygenases (C)

For biochemical characterization, the coding sequence of EAW25734 was cloned into pQE-70 and overexpressed in *E. coli* by Viola Wohlgemuth. The PhD candidate was handed over this project and purified the recombinant N-terminally His$_6$-tagged protein to near homogeneity as confirmed on SDS-PAGE, yielding 7.6 mg per litre of bacterial culture (**Figure 15A**). The high homology with both FtmOx1 proteins encouraged us firstly to test its activity with fumitremorgin B as substrate. However, EAW25734 did not replicate the function of FtmOx1 to form an endoperoxide bond in the presence of ascorbic acid (AA), Fe[(NH$_4$)$_2$(SO$_4$)$_2$] (Fe^{II}) and 2-OG at 37 °C for 16 h (**Figure 15B**). This inspired us to examine other intermediates in the fumitremorgin biosynthetic pathway as potential substrates. LC-MS analysis revealed the acceptance of tryprostatin B (**8**) by EAW25734. Three products **9**, **10** and **11** were clearly detected with conversions of 50.5 %, 3.8 % and 26.9 %, respectively.

These products were afterward isolated for structure elucidation by MS and NMR analyses. HRMS analysis gave [M-H]$^-$ ions at *m/z* 366.1830 ± 0.005 for **9** and **10** and *m/z* 382.1773 ± 0.005 for **11**, *i.e.* 16, 16 and 32 Dalton larger than that of **8** at *m/z* 350.1876 ± 0.005. This indicated the insertion of one or two oxygen atoms into the product structures. Inspection of the ^{1}H NMR spectrum of the major product **9** revealed the formation of a hydroxyl group appearing as a singlet at 4.70 ppm and a new double bond with two doublets between 6.4−6.7 ppm. The ^{13}C and relevant 2D NMR spectra confirmed that the double bond shifted from C21/C22 to C20/C21 and the hydroxyl group was introduced at C22.
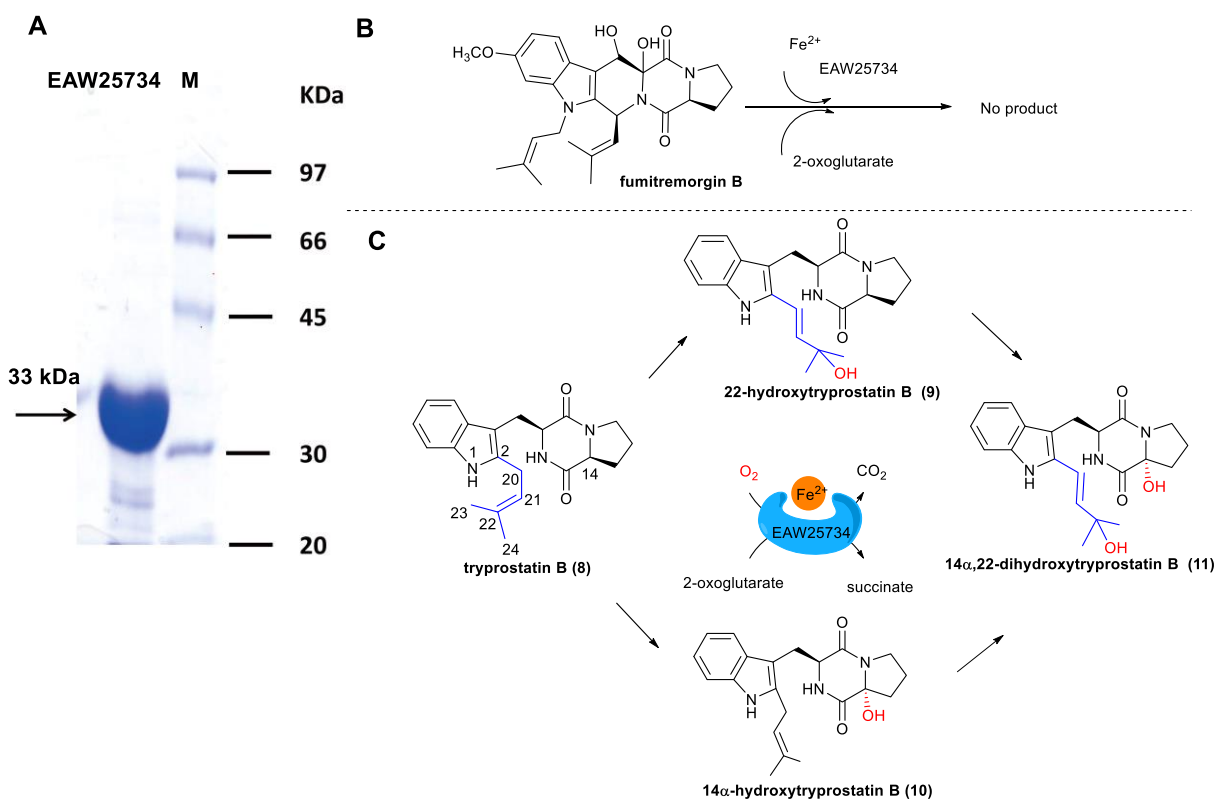
Figure 15 SDS-PAGE analysis of the recombinant EAW25734 (A) and its enzymatic reactions with fumitremorgin B (B) and tryprostatin B (C) as substrates, respectively

Similarly, the structures of the other two products were proven to be 14α-hydroxylisotryprostatin B (**10**) and 14α,22-dihydroxylisotryprostatin B (**11**) by MS and NMR analyses, respectively. The stereochemistry of the hydroxyl group at C14 in **10** was assigned after interpretation of the NOESY correlations.

Further experiments with **9** and **10** as substrates demonstrated that EAW25734 converted both compounds to **11**, but preferred **10** than **9**, explaining the conversion ratio and relationship among the three enzymatic products (**Figure 15C**). Furthermore, we tried to address the biosynthetic role of EAW25734 in the native strain. Cultivation of the fungus *Neosartorya fischeri* NRRL 181 in mCDY medium led to the detection of **9** by LC-MS, indicating that tryprostatin B could be hijacked by EAW25734 from the fumitremorgin pathway and launches a shunt route.

To investigate EAW25734 biochemically, time and co-factor dependencies were tested. Time dependent experiments also confirmed double bond migration accompanied by the hydroxylation at the dimethylallyl moiety as the main reaction and the α-hydroxylation at C14 as a side reaction of EAW25734. Incubation without exogenous 2-OG and Fe^{II} led to nearly no consumption of **8**, while the absence of AA resulted in a slight decrease of enzyme activity from 81.2 % to 51.8 %. These results proved unequivocally EAW25734 as a nonheme Fe^{II}/2-OG-dependent oxygenase.

Inspired by the biochemical study of 2-OG-dependent oxygenases (Schofield and Hausinger 2015), we postulated a reaction mechanism as shown in **Figure 16**. The important aspect in this mechanism is the abstraction of the hydrogen atom from C20 on the prenyl moiety by the Fe^{IV}=O species (stage E, **Figure 16**), followed by radical rearrangement and hydroxyl group attachment to form the 3-hydroxyl-3-methyl-1-butenyl moiety in **9**. To further investigate the origin of oxygen in the hydroxyl groups, ^{18}O labelling experiments were performed. In the incubation mixture under $^{18}O_2$-enriched atmosphere, incorporation of ^{18}O into the hydroxyl group at C22 and C14 was calculated to 35 % and 95 %, respectively. These results suggested that O_2 supplies the majority of the installed hydroxyl groups. Consistently, incorporation of one ^{18}O atom into the hydroxyl group at C22, but not into that at C14, was detected in the incubation mixture in ^{18}O-enriched water. The different oxygen origins at C22 could arise from solvent exchange (Schofield and Hausinger 2015) or two distinct reaction mechanisms.

As mentioned above, prenylated products could be further modified to expand the structural diversity and biological activities. Exploration of related decoration enzymes gave researchers a clue for better understanding of the assembly line to create efficient approaches for novel and bioactive compounds. However, one challenge in elucidating biosynthetic pathways comes from the extremely low production of natural products in the producing strain such as compound **9** in *Neosartorya fischeri*. Here, investigation on the involved enzymes *in vitro* could be an effective method to define the catalysts and intermediates that constitute the biosynthetic pathway of interest.
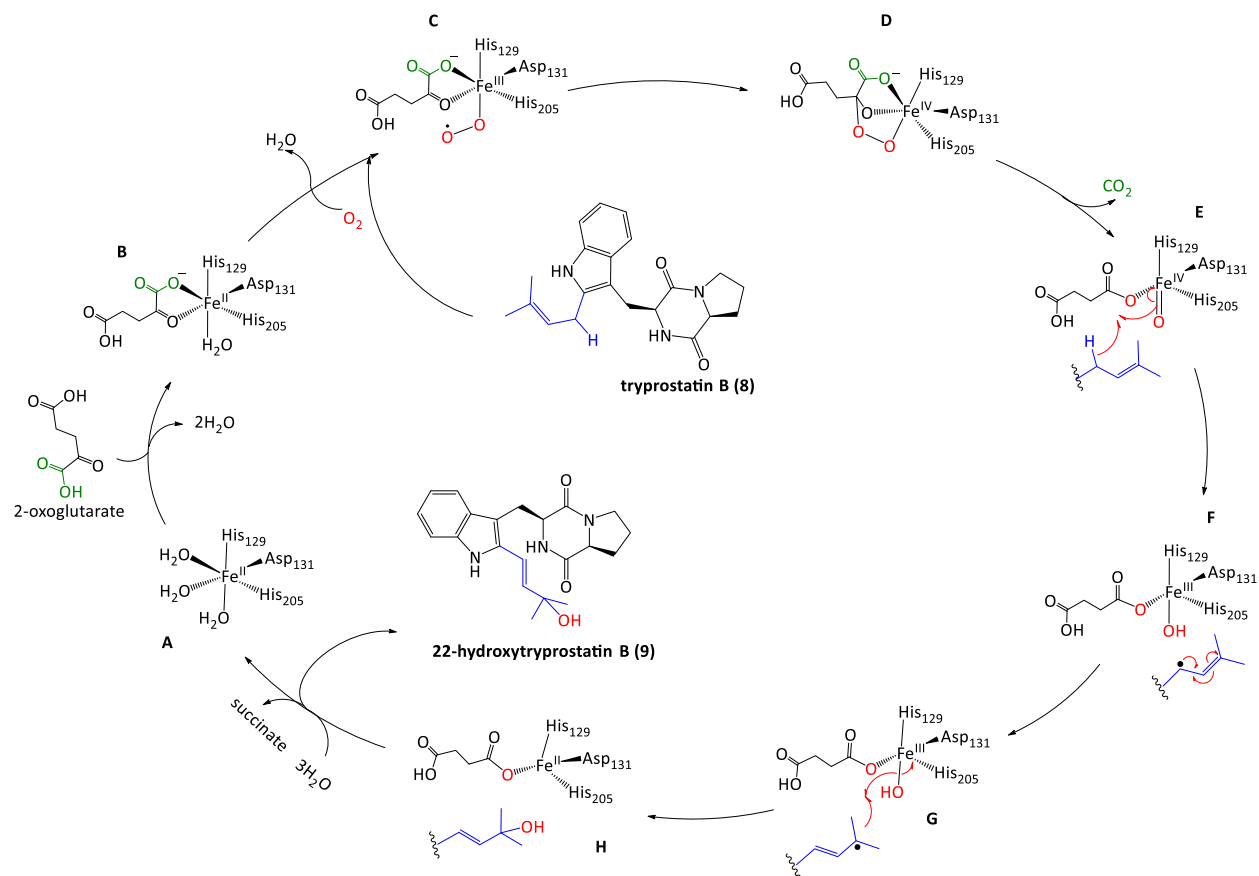
Figure 16 Proposed mechanism of EAW25734-mediated double bond migration accompanied by hydroxylation

For details on this work, please see the publication (section 4.1)

3.2 Tricyclic derivative formation *via* spontaneous oxidative cyclisations of 1,3-dihydroxy-4-dimethylallylnaphthalene

Prenylated naphthalenes are polyketide-isoprenoid hybrid molecules with a wide range of biological and pharmacological activities, *e.g.* antitumor (Komiyama et al. 1990), antagonistic (Shiomi et al. 1986) and antioxidant (Shin-ya et al. 1990) potentials. Many of these natural products have been discovered from terrestrial and marine *Streptomyces* during past decades. Advances in biosynthetic research and ^{13}C-labelling studies confirm that hydroxynaphthalene serves as the key aromatic polyketide framework, which can undergo prenylation with various prenyl donors catalysed by CloQ/NphB-type PTs. Interestingly, fungal PTs from DMATS superfamily share no significant sequence homology, but structure similarity with the CloQ/NphB-type PTs.

In a previous study, eight members of the DMATS superfamily were tested for the acceptance of different hydroxynaphthalenes (Yu et al. 2011). The products were isolated and identified as regularly *C*-prenylated derivatives without further modification on the prenyl moieties. However, benzofuran or benzopyran ring systems are found in natural products with a 1,3-dihydroxynaphthalene (**12**) core scaffold (**Figure 5**). It seems that the prenylation on an electron-rich aromatic nucleophile facilitates the subsequent enzymatic conversion or chemical rearrangement. Therefore, it would be interesting to investigate the behaviour of prenylated 1,3-dihydroxynaphthalenes.

Dr. Jinglin Wang used the available expression construct for *fgaPT2* expression, overproduced and purified the recombinant FgaPT2 to near homogeneity as described previously (Steffan et al. 2007) (**Figure 17A**). The recombinant protein was then incubated with **12** in the presence of DMAPP and $CaCl_2$ at 37 °C for 30 min in 100 µL Tris-HCl buffer (pH 7.5). After addition of 100 µL acetonitrile and centrifuging at 13,000 rpm for 30 min, 10 µL of supernatant were subjected to LC-MS analysis, which revealed the presence of four product peaks. LC-HR-MS data proved that one product (**13**) bared a molecular weight of 228.115, 68 Da larger than that of **12**, indicating a monoprenylated derivative. Other three products share the same $[M + H]^+$ at *m/z* 261.112 ± 0.005, being 100 Da larger than that of **12.** This suggests the addition of one prenyl moiety and two oxygen atoms. Interpretation of the HMBC spectrum of **13** proved its structure as C4-dimethylallylated derivative. In the ^{1}H NMR spectra of **14**, **15** and **16**, four coupling protons at H5−H8 for the phenyl ring can be easily recognized by the presence of typical signals between 7.0 to 8.0 ppm. Furthermore, signals of two alcoholic hydroxyl groups were detected at δH 4.7−7.0. Correspondingly, signals in the spectrum of **13** for H-1' and 2' of the prenyl moiety and for two phenolic protons were disappeared. Similar ^{1}H and ^{13}C spectra of **14** and **15** indicated their isomeric feature. HMBC correlations proved their structures as tetrahydrobenzofuran derivatives. Interpretation of the ^{13}C spectrum of **16** revealed the presence of two ketone carbons and the absence of olefinic carbons of the dimethylallyl moiety in **13**. Comprehensive analysis of the HSQC and HMBC data confirmed **16** to be a bicyclo[3.3.1]nonane

derivative. The relative configurations of **14**, **15** and **16** were elucidated by NOESY experiments (**Figure 17B**).
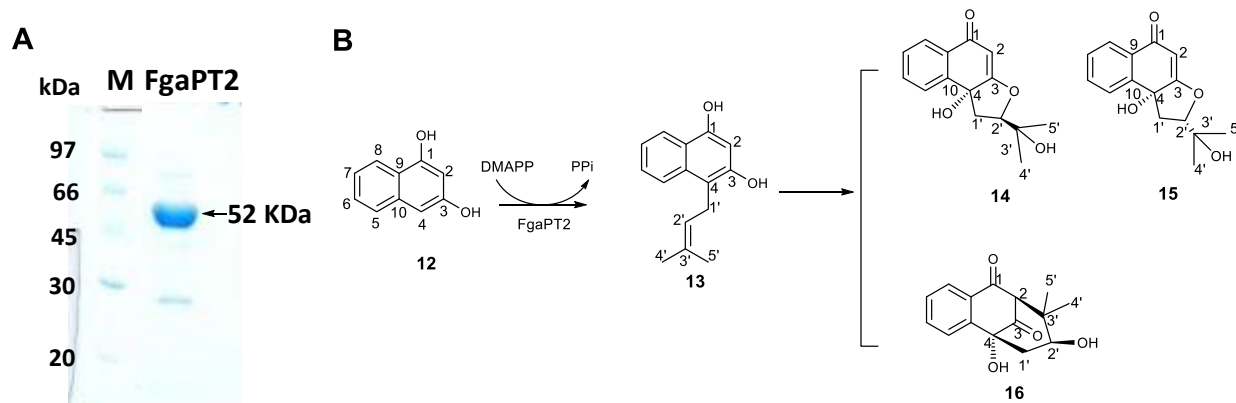
Figure 17 SDS-PAGE analysis of the recombinant FgaPT2 (A); structures of compounds **12−16** (B)

Identification of the three tricyclic products raised the question on their formation. Firstly, we wondered whether the cyclisation is specific for the FgaPT2 reaction. Three prenyltransferases, CdpNPT, FtmPT1 and AnaPT, were then incubated with **12** in the presence of DMAPP and $CaCl_2$ at 37 °C for 16 h. The three tricyclic products **14−16** were also clearly detected in all the reaction mixtures.

To investigate that **14**, **15** and **16** are enzymatic or nonenzymatic products, we incubated the prenylated product **13** with the heat-inactivated FgaPT2 in the presence of DMAPP and $CaCl_2$ at 37 °C for 30 min, 4h and 24h, respectively. HPLC analysis showed approx. 22 % of **13** was already converted to **14**, **15** and **16** after dissolving in solvent (**Figure 18**). The conversion was calculated to be approx. 46 % and 86 % after incubation for 0.5 and 4 h, respectively (**Figure 18**). The total consumption of **13** was detected in the 24h incubation mixture. These results proved the nonenzymatic oxidative cyclisation of **13** to **14**, **15** and **16** (**Figure 18**).

To provide more evidence for the relationship among **13**, **14**, **15** and **16**, pH-dependent assays were carried out for **13** at 37 °C for 1 h. After 1h incubation in phosphate buffer at pH 2.5, 6.0, 7.5, 8.5 and 10.0, the reaction mixtures were analysed by LC-MS The conversions under acidic conditions were clearly slower than those under neutral and basic conditions. 51.4 % and 75.6 % of **13** were converted to **14**, **15** and **16** at pH 2.5 and 6.0, respectively. In comparison, approx. 99 % were consumed in the buffer of pH 7.5 and higher pH values. Those data proved the spontaneous pH-dependent oxidative rearrangement from **13** to **14**, **15** and **16**.
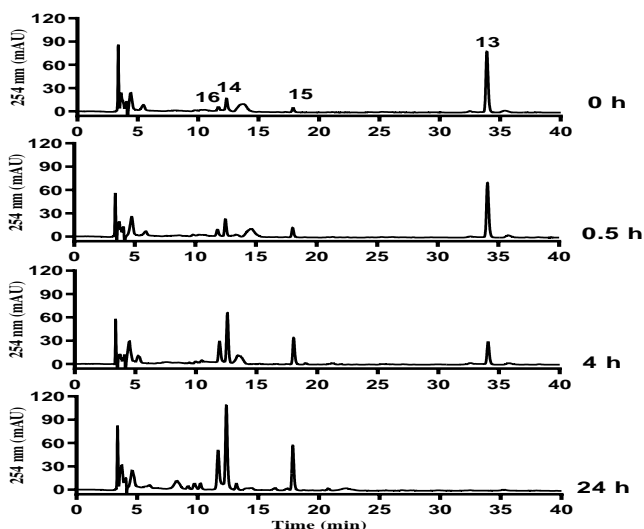
Figure 18 The reaction mixtures were incubated in Tris buffer (pH 7.5) at 37 °C for 0, 0.5, 4 and 24 h

To investigate the origin of the introduced oxygen atoms, FgaPT2 assays with **13** and DMAPP were carried out under $^{18}O_2$-enriched atmosphere and in ^{18}O-enriched water. The reaction mixtures were then analysed on LC-HR-MS. Under UV absorption at 254 nm, 100 % conversion of **13** to **14**, **15** and **16** was clearly observed in all reaction mixtures. Compounds **14**, **15** and **16** were detected in the incubation mixture under normal atmosphere with $[M + H]^+$ ions at m/z 261.1126, 261.1132 and 261.1127, respectively. In the incubation mixture under ^{18}O-enriched atmosphere, incorporation of two oxygen-18 atoms each in **14**, **15** and **16** was confirmed by detection of the isotope peaks of their $[M + H]^+$ ions at m/z 265.1189, 265.1200 and 265.1205, respectively. In contrast, no oxygen-18 insertion was observed in the incubation mixture in ^{18}O-enriched water. These results undoubtedly proved the involvement of O_2 during the oxidative rearrangement to form two hydroxyl groups in **14**, **15** and **16**.

Having proved the O_2-originated spontaneous reactions, we postulated the relative reaction mechanism in **Figure 19**. The cyclisation process starts by the attachment of one O_2 molecule on the prenylated position (C4). The reactive peroxyl radical **17** can undergo radical addition to both of the olefinic positions of the dimethylallyl moiety at C2' or C3', leading to the formation of two endoperoxide patterns in **18** and **21**. Subsequent radical transfer in **18** resulted in the cleavage of the O-O bond in **19**, which can be further oxidized to an active oxygen radical and subjected to an intramolecular nucleophilic attack to form the diastereomers **14** and **15**. In the other endoperoxide manner, the radical shift and endoperoxide cleavage enabled to generate the bi-radical intermediate **23**. Consequent radical cyclisation takes place *via* C-C coupling to form the bicyclo[3.3.1]nonane skeleton in **16**.
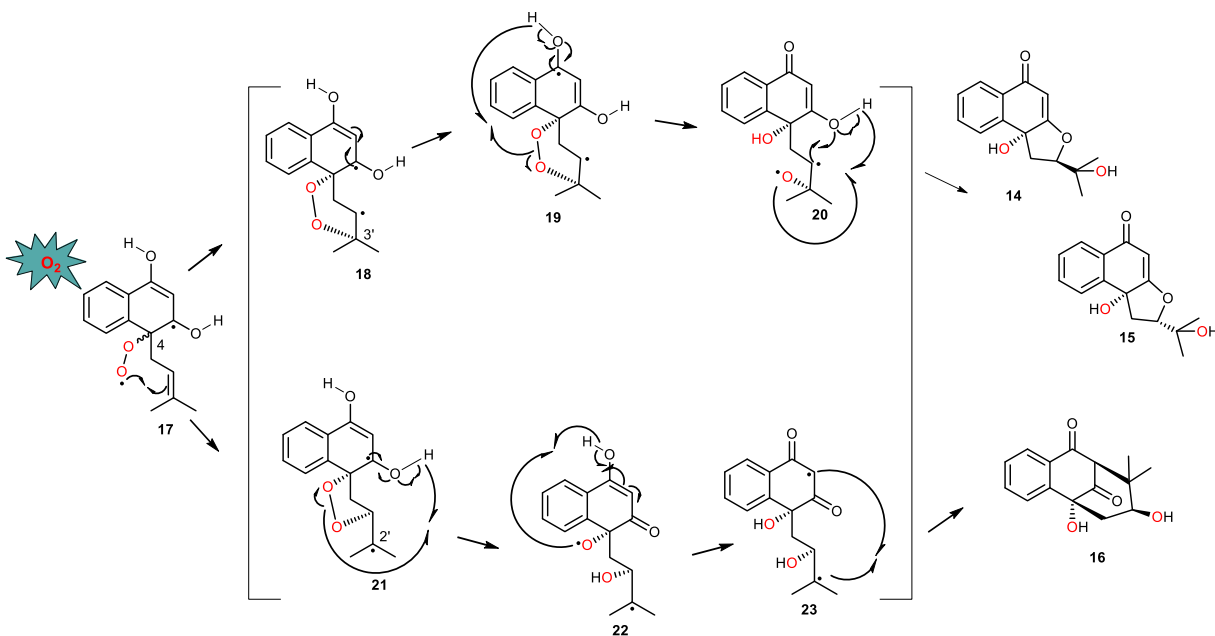
Figure 19 The proposed cyclisation mechanism

In summary, we identified three new rearranged prenylated naphthalene derivatives with tetrahydrobenzofuran (**14** and **15**) and bicyclo[3.3.1]nonane (**16**) cores. Detailed investigations including time- and pH-dependent assays proved that they are spontaneous oxidative cyclisation products of 1,3-dihydroxy-4-dimethylallylnaphthalene **13**. The incorporation of two labelled oxygen atoms in the product structures supports the peroxyl radical-mediated cyclisation mechanism. These results provide one additional example for the nonenzymatic oxidative cyclisation of enzyme products.

<u>For details on this work, please see the publication (section 4.2)</u>

Jinglin Wang,* **Huomiao Ran**,* Xiulan Xie, Kaiping Wang, and Shu-Ming Li. (2020). Spontaneous oxidative cyclisations of 1,3-dihydroxy-4-dimethylallylnaphthalene to tricyclic derivatives. *Organic and Biomolecular Chemistry*, 18 (14), 2646-2649, DOI: 10.1039/d0ob00354a (* equal contribution)

3.3 Biosynthesis of the prenylated benzene carbaldehyde flavoglaucin and its congeners requires prenylation as a key step

Flavoglaucin (**24a**) and congeners **24b−f** are prenylated benzene carbaldehyde derivatives carrying a saturated or an unsaturated C_7 side chain and with an additional dimethylallyl (C_5) moiety at C3 position (**Figure 20**) (Hamasaki et al. 1980; Huang et al. 2012; Li et al. 2008a). They show interesting biological activities such as antioxidant (Huang et al. 2012; Miyake et al. 2014; Sun et al. 2013), antibacterial (Fathallah et al. 2019) and anti-inflammatory properties (Shi et al. 2019; Wu et al. 2014b). Their side chains can be further modified to a benzofuran system (**25b−d**) and spirocyclic compound (Li et al. 2008a; Li et al. 2008b). However, little is known about their biosynthesis and the involved enzymes prior to this study. Recently, Zhao et al reported on the biosynthesis of the alkylated salicylaldehyde derivative sordarial from *Neurospora crassa* by involvement of a HR-PKS containing cluster (*srd*) (Zhao et al. 2019). Lately, a homologous (*vir*) cluster was discovered for the trichoxide biosynthesis in *Trichoderma virens* (Liu et al. 2019). Those reports suggest that **24a−f** could also be biosynthesised by a HR-PKS containing cluster.
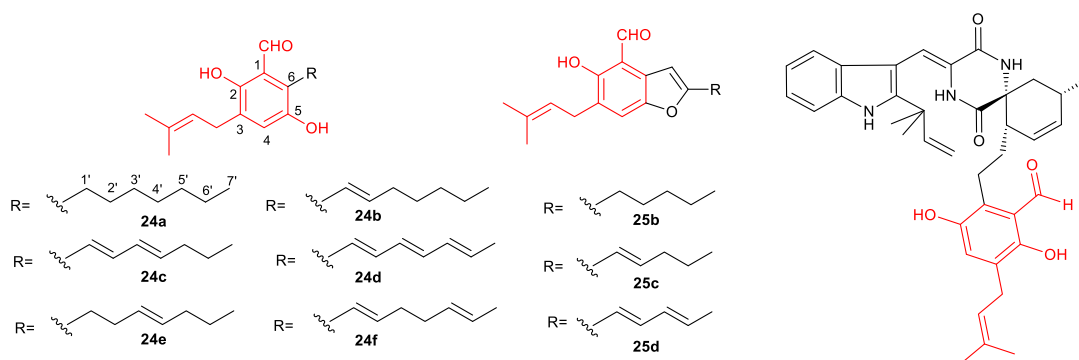
Figure 20 Structures of compounds isolated from *Aspergillus ruber*

To investigate the biosynthetic pathway, Jonas Nies carried out genome mining in *Aspergillus ruber* by using AntiSMASH (Weber et al. 2015) and by comparison with the members of the known *srd* and *vir* clusters, leading to the identification of the *fog* cluster containing nine genes (*fogA−I*). Heterologous expression of the identified *fog* cluster in *Aspergillus nidulans* LO8030, LC-MS analysis of the extracts from the transformants as well as isolation and structure elucidation proved the accumulation of **24a−f** and the involvement of *fogA-I* for their biosynthesis. Deletion of the putative transcription factor gene *fogI* in the heterologous expression strain completely abolished the production of **24a−f**, suggesting its role as a positive regulator for gene expression.

To elucidate the function of each gene, deletion and coexpression experiments in *Aspergillus nidulans* LO8030 were carried out. The HR-PKS FogA with a domain structure of KS-AT-ACP-DH-ER-KR was integrated into the host *Aspergillus nidulans* genome under the control of the constitutive *gpdA*-promoter. One major product **26** and three minor products **27−29** were detected by LC-HR-MS analysis of the rice culture extract. A spontaneous conversion of **26** to **27−29** was observed during the isolation process on a silica-gel column. LC-HR-MS data proved that **27−29** share a molecular formula of $C_{14}H_{22}O_5$, indicating the conversion of **26** ($C_{14}H_{24}O_5$) to **27−29** by elimination of one molecule water. NMR data, especially the HMBC correlations confirmed that **27**, **28** and **29** harboured δ-alerolactone, heptanolactone and tetrahydropyran core nuclei in their structures, respectively. This confirmed the linear trihydroxy **26** as their common precursor. The determination of ^{1}H-^{1}H coupling constants for the olefinic protons with 15 Hz proved the all-trans geometry of the double bonds on the side chain. The relative configuration in **27** and **28** were determined by interpretation of the NOESY correlations. (**Figure 21**).
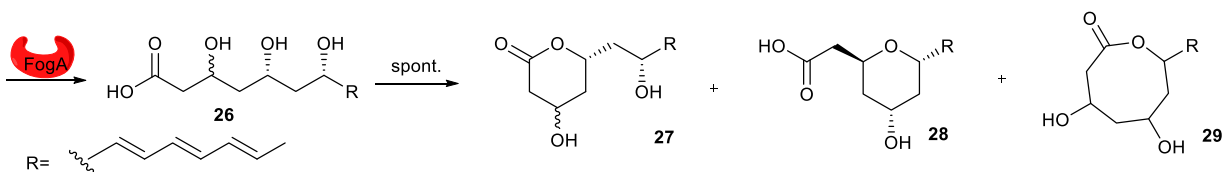
Figure 21 Nonenzymatic cyclisation from **26** to **27−29**

To identify the enzymes involved in the formation of aromatic products, Jonas Nies deleted *fogA*, *fogB*, *fogC* or *fogD* from the cluster. None of the resulted mutants was able to produce flavoglaucin and congeners. A small number of **26** was monitored in the Δ*fogB*, Δ*fogC* and Δ*fogD* mutant strains, indicating the slight accumulation of initial PKS product. We then constructed the coexpression strain of *fogABCDI* by removing genes *fogEFGH* from the whole cluster expression strain. The first aromatic pathway intermediates **30a−d** were identified and isolated as C6-alkyl salicyl alcohols with none, one, two, and three double bonds on the side chain, respectively (**Figure 24**). These results imply that the nascent polyketide is modified in FogA-bound form by FogBCD to generate the aromatic scaffold.

The cytochrome P450 FogE-catalysed hydroxylation on C5 position was confirmed by deletion of *fogE* and *fogH*. Benzyl alcohols **30a−d** and their hydroxylated derivatives, were detected in the extract of Δ*fogE* strain. The accumulation of unprenylated dihydroxybenzyl alcohols **31a** and **31b** in the *fogH* deletion transformants indicated that the FogE products are substrates of the PT FogH (**Figure 24**). To confirm this hypothesis, the recombinant FogH was overproduced in *E. coli* and purified to near homogeneity as confirmed on SDS-PAGE. Incubation of FogH with **31a** in the presence of DMAPP at 37 °C for 10 min resulted in the formation of a major product **32a** and a minor one **34a** with conversions of 77.7 % and 2.3 %, respectively. In the ^{1}H NMR spectra of both compounds, signals for a dimethylallyl moiety were clearly detected at approx. 3.2, 5.3 and 1.7 ppm, proving **32a** as a C3-

prenylated dihydroxybenzyl alcohol, as **34a** its dihydroquinone derivative. We have also observed that the dihydroquinone alcohol forms **31a** and **32a** were instable and can be easily oxidized to the benzoquinones **33a** and **34a** during the isolation. Both unprenylated hydroquinone **31a** and benzoquinone **33a** can be accepted by FogH as shown in **Figure 22A**.To provide evidence that the benzyl alcohol feature is really essential for the prenylation, this PhD candidate synthesized the corresponding aldehyde **35a** and tested with FogH. However, **35a** was not consumed by FogH at all, proving the alcohol group is a prerequisite for the acceptance by FogH. Determination of the kinetic parameters proved that both the hydroquinone **31a** and benzoquinone **33a** are natural substrates of FogH.

In addition, the spontaneous oxidoreduction was observed in the stability test of **31a−34a** in water at 25 °C. The benzoquinone alcohols **33a** and **34a** were reactive agents that slightly converted to the dihydroquinone alcohols **31a/32a** and the dihydroquinone aldehydes **35a/24a** in approx. equal amounts (**Figure 22A**). A proposed mechanism is given in **Figure 22B**. Two molecules **34a** can act as both oxidant and reductant to form **32a** and the instable benzoquinone aldehyde intermediate **36**, which reacts with a third molecule of **34a** to form the aldehyde **24a**.
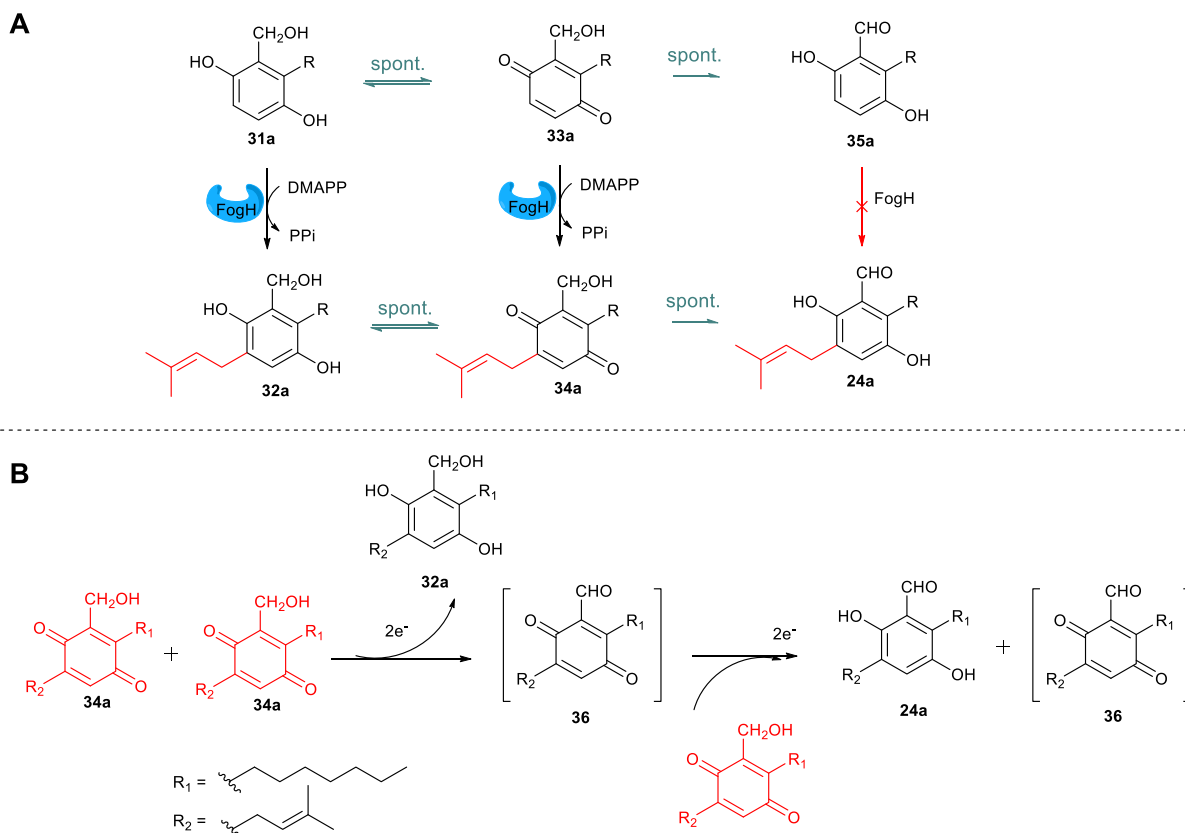
Figure 22 *In vitro* assays of FogH and spontaneous conversion between hydroquinones, benzoquinones and aldehyde (A), proposed mechanism of the spontaneous conversion (B)

Subsequently, the prenylated benzyl alcohols have to be finally oxidized to aldehydes. Deletion of FogF indeed led to the accumulation of **34a** and congeners **34b−d**. Feeding **34a** to the *fogF* overexpression *Aspergillus nidulans* strain led to the production of flavoglaucin **24a**, which proved FogF as an alcohol oxidase (**Figure 24**). No conversion was detected for the unprenylated **31a** by the same strain, indicating the importance of the prenyl moiety for the acceptance by FogF.

During the isolation from the extract of the Δ*fogF* mutant, **32a−d** were observed as instable metabolites and rapidly oxidized to their reactive benzoquinone form **34a−d**. In the presence of a double bond at C1' (**34b−d**), benzofuran derivatives were identified as compounds **37b−d**, very likely *via* spontaneous intramolecular cyclisation of the proposed benzoquinone (**Figure 23**). Feeding experiments of the benzofuran alcohol **37b** to the *fogF* expression strain did not lead to aldehyde formation, suggesting that the furan ring in some flavoglaucin derivatives, *e.g.* **25b−d**, was very likely formed after oxidation of the benzyl alcohol to aldehyde.
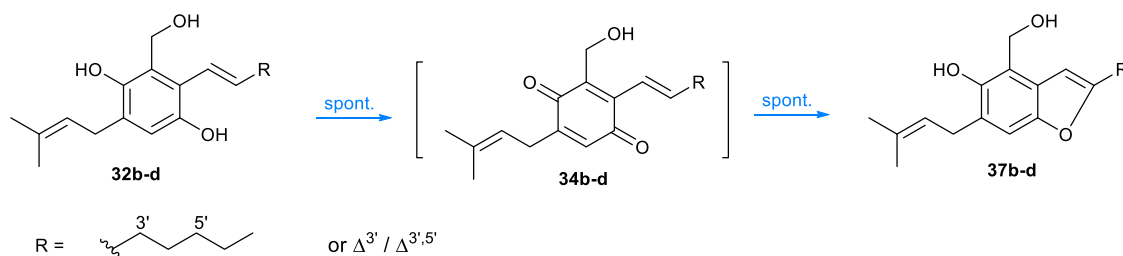
Figure 23 Spontaneous conversion to benzofuran derivatives

Taken together, we elucidated the biosynthesis of flavoglaucin and congeners by genome mining, heterologous expression, feeding experiments and biochemical characterisation (**Figure 24**). A HR-PKS and three tailoring enzymes are responsible for the formation and release of the salicyl alcohol
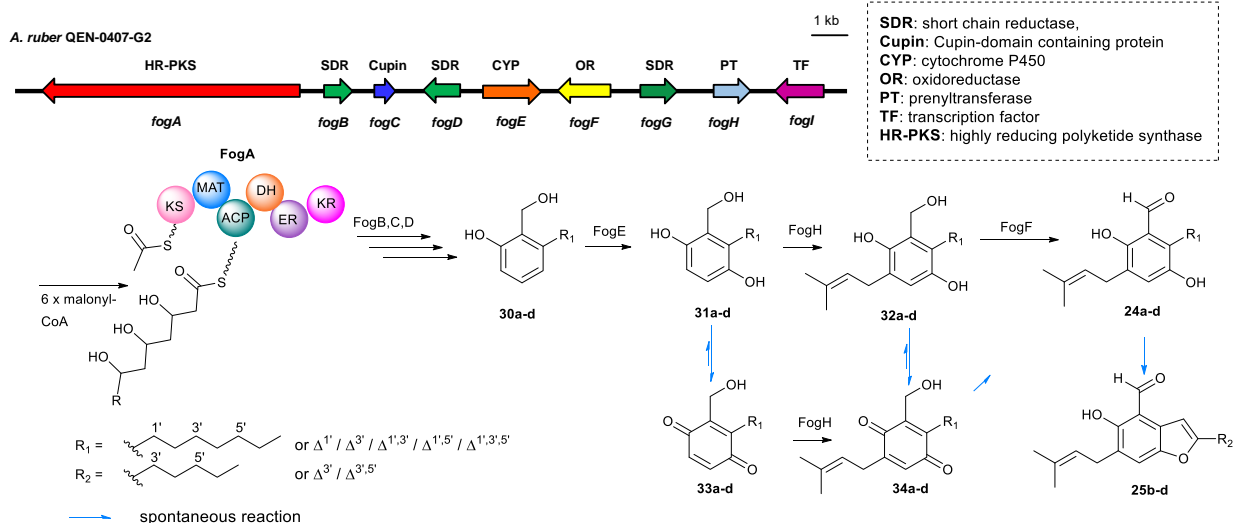
Figure 24 Proposed biosynthetic pathway of flavoglaucin and congeners

derivatives which is a prerequisite for subsequent hydroxylation and prenylation. The prenyltransferase FogH as a key enzyme in the biosynthesis accepts both hydroquinone and benzoquinone derivatives as substrates, but requires the presence of the alcohol character. Consecutively, the alcohol was oxidized to the final aldehydes by an oxidase, which only accepts prenylated derivatives as substrates. This cooperative and highly programmed machinery ensure the effective formation of the final pathway products.

<u>For details on this work, please see the publication (section 4.3)</u>

Jonas Nies,* **<u>Huomiao Ran</u>**,* Viola Wohlgemuth, Wen-Bing Yin and Shu-Ming Li (2020). Biosynthesis of the prenylated salicylaldehyde flavoglaucin requires temporary reduction to salicyl alcohol for decoration before reoxidation to final product. *Organic Letters*, 22 (6), 2256-2260, DOI: 10.1021/acs.orglett.0c00440. (* equal contribution)

3.4 The review of fungal benzene carbaldehydes on their structural features, distribution, biological activities and biosynthesis

In addition to my research work, the PhD candidate contributed, together with Prof. Dr. Shu-Ming Li, to a review article on fungal benzene carbaldehydes. This substance family with salicylaldehydes as predominant representatives carry usually hydroxyl, methyl and chloro groups, prenyl moieties or alkyl side chains. They are widely distributed from terrestrial to marine-derived, plant endophytic and pathogenic fungi, including both ascomycetes (79 %) and basidiomycetes (17 %). These natural products display a wide range of biological and pharmacological activities. Cytotoxic, antibacterial and antifungal activities were detected for a large number of benzene carbaldehydes, followed by anti-inflammatory and antioxidant activities. Since the first report on the family members, flavoglaucin and auroglaucin, in the fungus *Aspergillus glaucus* in 1934 (Gould and Raistrick 1934), at least 185 structures were identified in various fungi. They can be grouped into six categories based on skeleton substitutions: simple benzene carbaldehydes, alkylated benzene carbaldehydes, meroterpenoids, benzophenones, spirocyclic and miscellaneous benzene carbaldehydes (**Figure 25**).
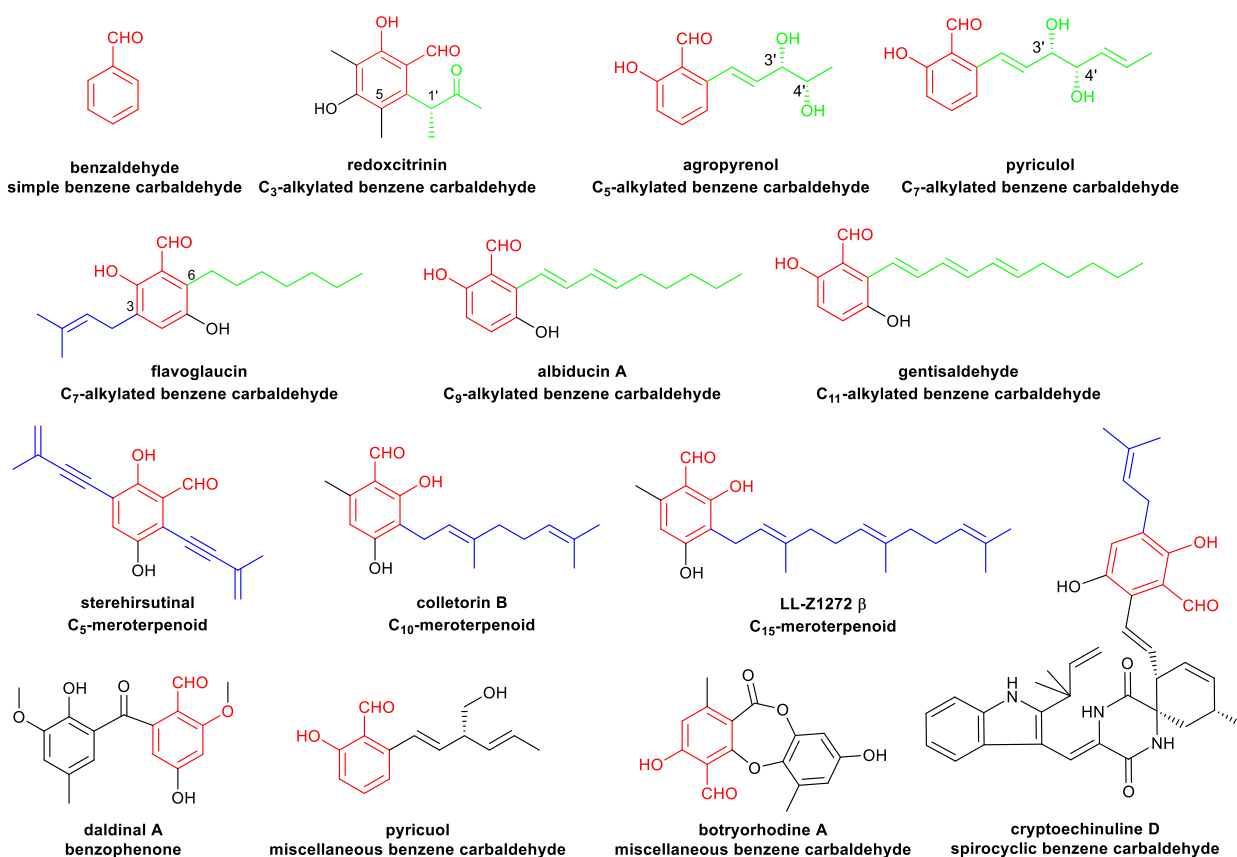
Figure 25 Representatives of fungal benzene carbaldehydes

Simple benzene carbaldehydes are a class of merely hydroxylated, halogenated, methylated and/or ethylated benzaldehydes with broad biological and pharmacological activities such as antifungal, antibacterial and cytotoxic activities. The majority of their producers are the genera of *Aspergillus*, *Penicillium* and *Bjerkandera*. Benzaldehyde is the simplest representative of benzene carbaldehydes (**Figure 25**) and one of the most industrial used chemicals in cosmetic and food industries. Furthermore, benzaldehyde shows antioxidant, anti-insect, antibacterial and antifungal potentials (Ullah et al. 2015).

Alkylated members constitute the largest class of benzene carbaldehydes with 66 structures. In comparison to the simple benzene carbaldehydes, most of them (94 %) share a modified or unmodified alkyl chain at the *ortho*-position to the formyl group. With one exception, all these natural products are salicylaldehyde congeners from ascomycetes. They also exhibit important biological activities like antibacterial, antifungal and cytotoxic potentials. Biosynthetically, alkylated benzene carbaldehydes are derivatives of aromatic polyketides extended with different numbers of malonyl-CoA units (Cox 2007; Staunton and Weissman 2001). Thus, the members of this group can be conveniently subdivided according to the length of the side chains, *i.e.* C_3-, C_5-, C_7-, C_9- and C_{11}-alkylated benzene carbaldehydes (**Figure 25**).

Meroterpenoids belong to another major benzene carbaldehyde class and contribute significantly to the structural diversity of these natural products. Meroterpenoids are hybrid natural products which mostly generated from polyketide and terpenoid pathways (Blunt et al. 2004; Geris and Simpson 2009; Matsuda and Abe 2016; Murray et al. 2020; Sunassee and Davies-Coleman 2012). The majority of the fungal meroterpenoids have a C_5, C_{10} or C_{15} terpenoid chain, which is usually connected to *meta*-position of the formyl group and *ortho*-position of at least one hydroxyl group or structural feature derived thereof (**Figure 25**). Similarly, they share interesting bioactivities, *e.g.* antiviral, antifungal, antibacterial, anti-inflammatory, phytotoxic and cytotoxic activities. The main producers with 66 % of the mentioned metabolites are from ascomycetes, while 30 % of them are from basidiomycetes.

In addition, benzophenones with a diarylketone skeleton and spirocyclic derivatives *via* [4+2] Diels-Alder reaction are all isolated from ascomycetes, which can be further modified by hydroxylation, methylation, methoxylation, halogenation, prenylation or cyclisation (**Figure 25**). Moreover, more than 20 fungal benzene carbaldehydes with naphthalene, chromanone or other skeletons are also discussed in this review (**Figure 25**).

The benzene carbaldehydes act as critical intermediates or end products of various biosynthetic pathways. Biosynthetically, benzene carbaldehydes are formed by direct releasing from NR-PKS, alcohol oxidation or acid reduction, which was intensively discussed and clearly exemplified in the review. Releasing from NR-PKSs is usually catalysed by a terminal R domain, while several other enzymes are involved by releasing form HR-PKS.

Up to April 2020, more than 140 publications deal with the structural features, distribution, biological activities and biosynthesis of fungal benzene carbaldehydes. However, it became a challenge to get new bioactive natural products under conventional laboratory culture conditions. One solution could be screening microorganisms from less explored or untapped sources such as extreme environments (Chávez et al. 2015; Ibrar et al. 2020; Matsuda and Abe 2016; Wilson and Brimble 2009; Wilson and Brimble 2020) and/or symbiotic systems (Adnani et al. 2017). Furthermore, metabolite dereplication (Covington et al. 2017; Mohimani et al. 2017; Nielsen and Larsen 2015), OSMAC approach (Ariantari et al. 2019; Bode et al. 2002; Selegato et al. 2019) and genetic manipulation as mentioned in **section 1.1** (Keller 2019; Lazarus et al. 2014; Lyu et al. 2020; Matsuda and Abe 2016; Sanchez et al. 2012b; Zhang et al. 2019a) became remarkable strategy for bioactive metabolite finding.

For details on this work, please see the publication (section 4.4)

Huomiao Ran and Shu-Ming Li (2020). Fungal benzene carbaldehydes: occurrence, structural diversity, activities and biosynthesis. *Natural Product Reports*, DOI: 10.1039/d0np00026d.

4 Publications

4.1 A nonheme Fe^{II}/2-oxoglutarate-dependent oxygenase catalyzes a double bond migration within a dimethylallyl moiety accompanied by hydroxylation

A Nonheme Fe^II/2-Oxoglutarate-Dependent Oxygenase Catalyzes a Double Bond Migration within a Dimethylallyl Moiety Accompanied by Hydroxylation

Huomiao Ran,[†] Viola Wohlgemuth,[†] Xiulan Xie,[‡] and Shu-Ming Li*,[†][ID]

[†]Institut für Pharmazeutische Biologie und Biotechnologie, Philipps-Universität Marburg, Robert-Koch-Straße 4, 35037 Marburg, Germany

[‡]Fachbereich Chemie, Philipps-Universität Marburg, Hans-Meerwein-Straße, 35032 Marburg, Germany

S *Supporting Information*

ABSTRACT: Prenylation of cyclodipeptides contributes largely to the structure diversification and biological activity. The prenylated products can be further metabolized by modifications like hydroxylation with cytochrome P450 enzymes or nonheme Fe^II/2-oxoglutarate-dependent oxygenases. Herein, we cloned and overexpressed *NFIA_045530* from *Neosartorya fischeri*, which shares high sequence similarity with the nonheme Fe^II/2-oxoglutarate-dependent oxygenase FtmOx1_Af from *Aspergillus fumigatus* on the amino acid level. FtmOx1_Af is a member of the biosynthetic enzymes for fumitremorgin-type mycotoxins and catalyzes the conversion of fumitremorgin B to verruculogen by insertion of an oxygen molecule into the two prenyl moieties. The recombinant protein EAW25734 encoded by *NFIA_045530* was purified to apparent homogeneity and then was used for incubation with intermediates of the fumitremorgin biosynthetic pathway. LC-MS analysis revealed no consumption of fumitremorgin B but good conversion with its biosynthetic precursor tryprostatin B in the presence of Fe^II and 2-oxoglutarate. Structure elucidation confirmed 22-hydroxylisotryprostatin B and 14α, 22-dihydroxylisotryprostatin B as the major enzyme products. Further detailed biochemical characterization led to the identification of a novel enzyme, which catalyzes a double bond migration within the dimethylallyl moiety of tryprostatin B with concomitant hydroxylation. Incubation with ^18O_2-enriched atmosphere confirmed O_2 as the major origin of the hydroxyl groups. Solvent exchange was also observed for that at C22. LC-MS analysis confirmed the presence of 22-hydroxylisotryprostatin B in a *Neosartorya fischeri* extract, highlighting the role of this enzyme in the metabolism of intermediates of the fumitremorgin/verruculogen pathway. A plausible reaction mechanism implementing a radical rearrangement prior to accepting a hydroxyl radical from Fe^III is discussed.
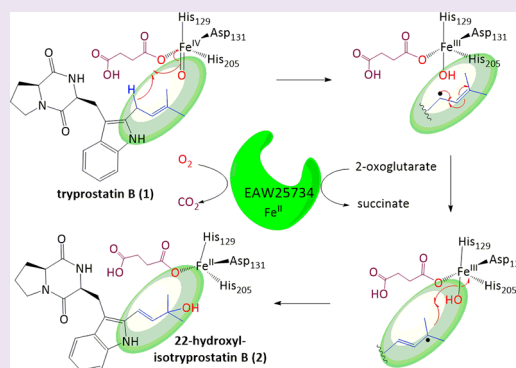
INTRODUCTION

Prenylated natural products have diverse important functions in living organisms.[1,2] These compounds can be further modified by hydroxylation,[3] epoxidation,[3] cyclization,[4] oxidation,[5] and double bond migration.[6] The 3-hydroxy-3-methyl-1-butenyl moieties, which are highlighted in the structures of Figure 1,[7−12] can be considered as modifications of dimethylallyl moieties. Liu et al. demonstrated that a FAD/FMN-dependent oxidase PtmO in the penitrem biosynthesis catalyzes the conversion of 20-prenylpenijanthine to PC-M5 by conversion of the dimethylallyl to a 3-hydroxy-3-methyl-1-butenyl moiety.[13]

Fe^II/2-oxoglutarate-dependent oxygenases belong to a unique, well-studied subfamily of oxidative enzymes. They are ubiquitously distributed in viruses,[14] bacteria,[15] fungi,[16] plants,[17] as well as animals,[18] and catalyze a remarkably wide array of biochemical transformations including hydroxylation, dealkylation, elimination, desaturation, epimerization, epoxidation, halogenation, cyclization, peroxide formation, and ring

rearrangement.[19−24] These oxidative transformations play crucial roles in biochemical processes and highlight their importance in nature. Therefore, extensive mechanistic investigations on Fe^II/2-oxoglutarate-dependent oxygenases have been reported.[25] Although radical rearrangement was proposed for the conversion of penicillin N to deacetoxycephalosporin C,[26−28] specific conversions catalyzed by nonheme Fe^II/2-oxoglutarate-dependent oxygenases have not been reported before.

In the course of our investigations on the biosynthesis of indole alkaloids, a biosynthetic gene cluster for verruculogen was identified from the opportunistic fungus *Aspergillus fumigatus* Af293.[29] One gene from this cluster, *ftmOx1_Af*, encodes a nonheme Fe^II and 2-oxoglutarate-dependent oxygenase and catalyzes the conversion of fumitremorgin B to
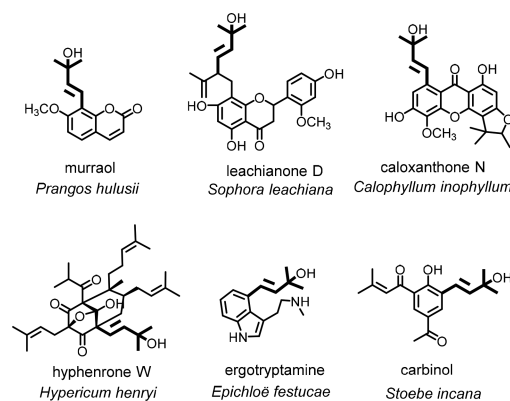
Figure 1. Natural product examples containing 3-hydroxy-3-methyl-1-butenyl residues.

verruculogen by installing an oxygen molecule into the two prenyl residues to form an endoperoxide bridge (Scheme 1).[30,31] The biosynthetic intermediates like tryprostatins A and B can also be metabolized to side products such as spirotryprostatins (Scheme 1).[32] Later, a similar cluster with one additional gene for the conversion of verruculogen to fumitremorgin A was identified in *Neosartorya fischeri* NRRL181.[33] The two proteins FtmOx1$_{Af}$ and FtmOx1$_{Nf}$ from both clusters share a sequence identity of 95%. In this study, we identified an additional homologue EAW25734 encoded by *NFIA_045530* in *N. fischeri* NRRL181, which is not located in the fumitremorgin gene cluster and has a protein sequence identity of 48% with both FtmOx1$_{Af}$ and FtmOx1$_{Nf}$. The conserved 2-His-1-Asp ion-binding triad was clearly identified in the EAW25734 sequence (Supplementary Figure 1). This high homology encouraged us to investigate its role in the fumitremorgin biosynthetic pathway or metabolism of its precursors.

RESULTS AND DISCUSSION

Overproduction and In Vitro Characterization of the Oxygenase EAW25734. To investigate its function, *NFIA_045530* comprising merely one exon of 894 bp was cloned from genomic DNA and overexpressed in *Escherichia*

coli XL1 Blue MRF' cells. The recombinant protein was purified with the aid of Ni-NTA agarose resin and confirmed on SDS-PAGE and LC-ESI-TOF-MS analyses (Supplementary Figure 2), yielding 7.6 mg of purified EAW25734 per liter of bacterial culture. Due to the high homology with FtmOx1$_{Af}$ and FtmOx1$_{Nf}$, we speculated that EAW25734 could be a nonheme Fe^{II}/2-oxoglutarate-dependent oxygenase also accepting fumitremorgin B as a substrate. The purified recombinant EAW25734 was therefore first incubated with fumitremorgin B in the presence of 2-oxoglutarate, ascorbic acid and Fe^{II}, as carried out for FtmOX1$_{Af}$ previously.[30] HPLC chromatogram of the reaction mixture did not show any product formation (Supplementary Figure 3).

Interestingly, in the LC-MS chromatogram of a reaction mixture containing the pathway precursor tryprostatin B (**1**) EAW25734, 2-oxoglutarate, ascorbic acid, and Fe^{II}, three products were clearly detected (Figure 2, i), which are absent
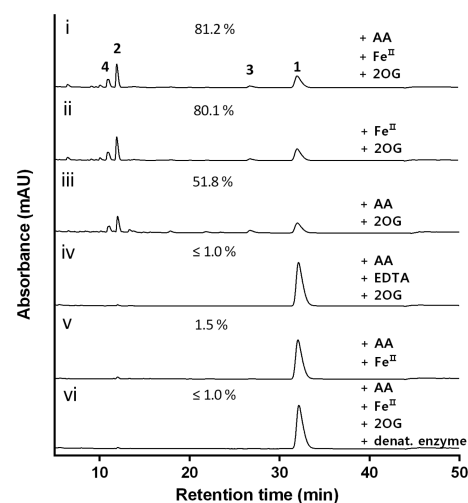
Figure 2. HPLC analysis of the incubation mixtures of **1** with EAW25734 in the full assay with native enzyme, ascorbic acid (AA), Fe^{II} and 2-oxoglutarate (2OG) (i); full assay without AA (ii); full assay without exogenous Fe^{II} (iii); full assay without exogenous Fe^{II}, but with EDTA (iv); full assay without 2OG (v); denatured enzyme with AA, Fe^{II} and 2OG (vi). Absorptions at 296 nm are illustrated.

Scheme 1. Proposed Metabolism of 1 in *N. fischeri*[a]
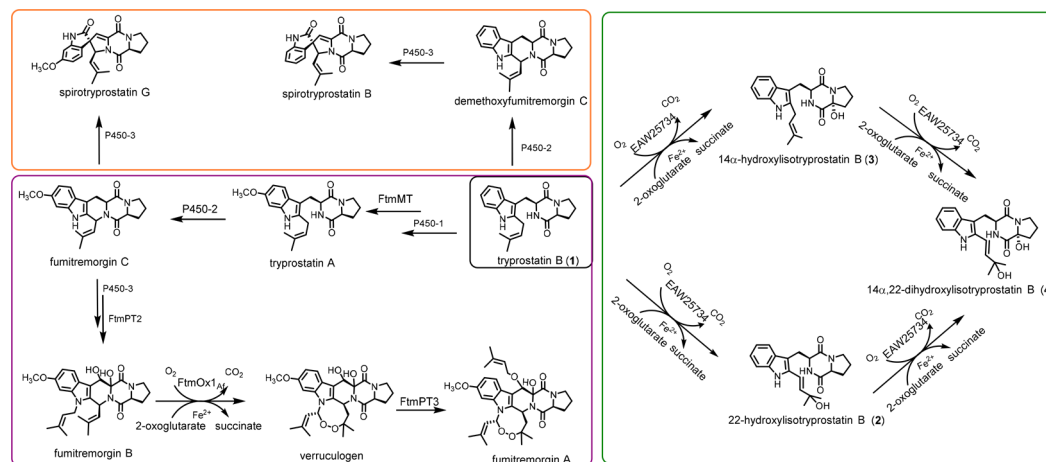
[a]The main biosynthetic pathway leading to the formation of fumitremorgins is highlighted with a purple,[29] the branch-pathway forming spirotryprostatins with an orange,[32] and the conversion by EAW25734 with a green frame.

in the assay with heat-inactivated enzyme (Figure 2, vi). Substrate consumption of 81.2% was calculated after incubation of 1 mM **1** with 15.6 μM EAW25734 at 37 °C for 16 h. Further investigations demonstrated that this enzyme requires Fe^{II} and 2-oxoglutarate but not ascorbic acid as cofactors. A slight decrease of enzyme activity was observed in the assay without ascorbic acid (Figure 2, ii). In contrast, nearly no consumption of **1** was detected in the assay without 2-oxoglutarate (Figure 2, v). In the assay without exogenous Fe^{II}, a conversion yield of 51.8% was observed and corresponds to a relative activity of 63.8%, in comparison to that of the full assay (Figure 2, i, iii). Addition of the chelating agent EDTA to the reaction mixture abolished the enzyme reaction completely (Figure 2, iv). These results proved that EAW25734 functions as a nonheme Fe^{II}/2-oxoglutarate-dependent enzyme.

Identification of the Enzyme Products. Detailed analysis of the HPLC chromatogram in Figure 2, i, revealed peak **2** as the major enzyme product with a conversion yield of 50.5% under the condition described above. High-resolution mass spectrometric analysis gave a $[M-H]^-$ ion at m/z 366.1830 (Supplementary Table 1), corresponding to the molecular formula of $C_{21}H_{25}N_3O_3$ and indicating incorporation of one oxygen atom into **1**. Interpretation of the ^1H NMR spectrum and data (Supplementary Table 2 and Supplementary Figure 4) revealed the presence of an *E*-configured double bond bearing two protons with signals at 6.69 (d, *J* = 16.2 Hz) and 6.40 (d, *J* = 16.2 Hz) ppm, respectively. Due to this double bond formation, the broad triplet signal of H-21 and the doublet of H-20 in **1** disappeared. This indicated that the double bond was very likely shifted from C21/C22 to C21/C20. The ^{13}C and relevant 2D NMR spectra (Supplementary Table 2 and Supplementary Figures 5−9) confirmed the double bond position and the introduction of the hydroxyl group at C22. This proved unequivocally the conversion of **1** to 22-hydroxylisotryprostatin B (**2**) by double bond migration and hydroxylation, as depicted in Scheme 1.

In analogy, products **3** and **4** with conversion yields of 3.8 and 26.9%, respectively, were also isolated and used for taking NMR and MS spectra (Supplementary Tables 3 and 4, Supplementary Figures 10−19). Interpretation of the spectroscopic data suggested the α-hydroxylation at C14 in **3** (14α-hydroxylisotryprostatin B). The stereochemistry of the hydroxyl group at C14 of **3** was assigned after interpretation of the NOESY correlations (Supplementary Figure 16) between OH-14 and H-19α, H-19β and H-17β as well as H-11α and H-17α (Scheme 1). The $[M-H]^-$ ion of the second major product **4** was observed at m/z 382.1773, that is, 32 Da larger than that of **1** at m/z 350.1876 ($[M-H]^-$), indicating insertion of two oxygen atoms into the structure. Interpretation of its NMR spectra and comparison with those of **2** and **3** confirmed the double bond migration from C21/C22 to C21/C20 and hydroxylation at C14 and C22.

Conversion of 2 and 3 by EAW25734 to 4. From their structures, it seems like **2** and **3** could serve as precursors of **4** in an enzyme or nonenzyme conversion. To prove this hypothesis, we assayed **2** and **3** with active or denatured EAW25734 as well as 2-oxoglutarate, ascorbic acid and Fe^{II}. LC-MS analysis confirmed the enzymatic conversion of **2** and **3** to **4** (Figure 3, i, (ii). Interestingly, **2** was lesser (approximately 17.7%) converted to **4** than **3** (approximately 61.0%). This is in line with the observed ratios of the three products in the assay with **1** (Figure 2, (i), which was also
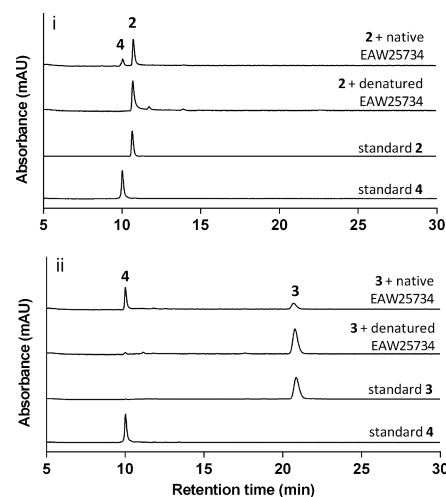
Figure 3. LC-MS analysis of the incubation mixtures of EAW25734 with **2** (i) and **3** (ii) as substrates. The isolated enzyme products were used as standards. Only absorptions at 296 nm are illustrated.

confirmed by time-dependent formation of these products (Figure 4). Figure 4 also proved the double bond migration accompanied by the hydroxylation at the dimethylallyl moiety as the main reaction and the α-hydroxylation at C14 as a side reaction of EAW25734.
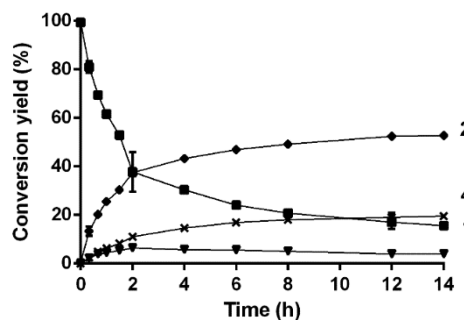
Figure 4. Time-dependent conversion of **1** to **2**, **3**, and **4** catalyzed by EAW25734

LC-MS Analysis of a *N. fischeri* Culture for the Presence of EAW25734 Products. To prove the production of **2**, **3**, and **4** by *N. fischeri* NRRL181, we cultivated the fungus in the mCDY medium at 37 °C for 7 days. The fungal extract was analyzed on LC-MS and is shown in Figure 20 (Supporting Information). Compound **2**, but not **3** or **4** was clearly identified by using the enzyme products as standards and by comparison of their physiochemical properties such as retention times, $[M-H]^-$ ions and fragmentation patterns in MS^2 (Supplementary Figure 21). Also in the fungal culture, the accumulation of **2** was higher compared with **3** and **4**. Obviously, **1** was hijacked by EAW25734 from the fumitremorgin pathway. Of course, it cannot be excluded that other oxidative enzymes are also involved in these conversions.

Postulated Mechanism of EAW25734-Mediated Double Bond Migration Accompanied by Hydroxylation. As aforementioned, a conversion of dimethylallyl to a 3-hydroxy-3-methyl-1-butenyl moiety has not been reported for nonheme Fe^{II}/2-oxoglutarate-dependent oxygenases. Recently, one such enzyme, PrhA, was reported to catalyze a double bond

Scheme 2. Postulated Mechanism of EAW25734-Mediated Double Bond Migration Accompanied by Hydroxylation

tryprostatin B (**1**)

22-hydroxyisotryprostatin B (**2**)
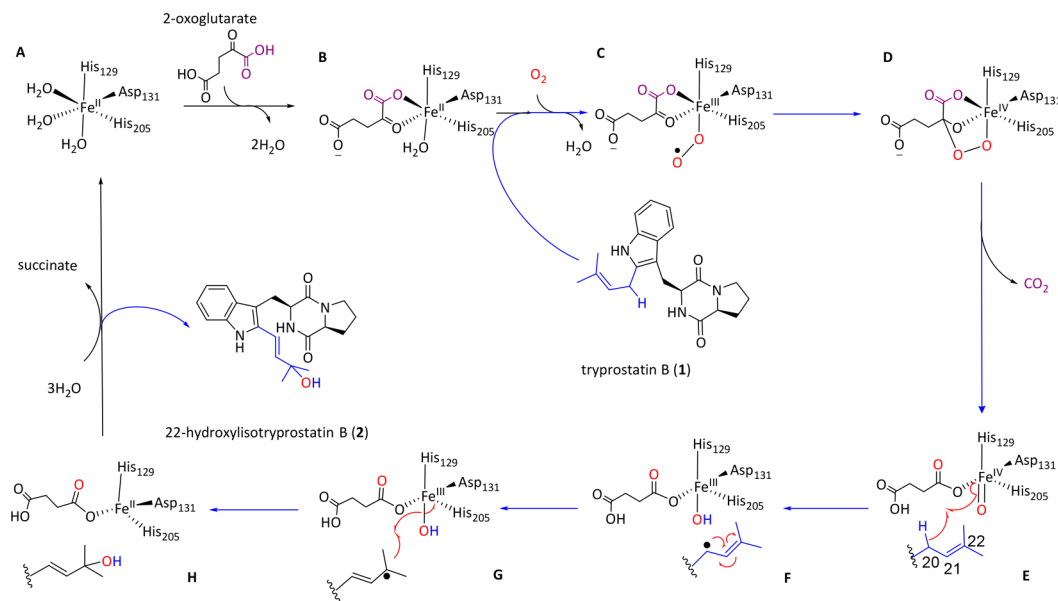
isomerization in a ring system.[34] To understand the double bond migration accompanied by a hydroxylation at the dimethylallyl moiety in **1**, we postulated a reaction mechanism as depicted in Scheme 2. As for all nonheme Fe^{II}/2-oxoglutarate-dependent oxygenases, the catalysis is initiated by coordination of Fe^{II} to the 2-His-1-Asp facial triad[35,36] (Supplementary Figure 1) and three water molecules (intermediate A in Scheme 2), followed by displacement of two metal-bound water molecules with the keto and carboxyl groups of 2-oxoglutarate in the Fe^{II} center (B in Scheme 2). Substrate **1** binds then to the active site of the enzyme, which triggers an available site for O_2 binding, forming a Fe^{III}-superoxo and Fe^{IV} peroxohemiketal bicyclic intermediates (C and D in Scheme 2). After releasing one molecule of CO_2 and the abstraction of a hydrogen at C20 of **1**, the iron was reduced to Fe^{III}, and a radical at C20 of **1** is formed (E and F in Scheme 2). The key intermediate G for the formation of **2** is then formed by electron migration from C20 to C22. Transfer of the hydroxyl radical to C22 would result in the formation of **2** and reduction of Fe^{III} to Fe^{II} (H in Scheme 2). Succinate release under attachment of three water molecules will regenerate the initial state A. Product **3** will be formed via a mechanism for usual nonheme Fe^{II}/2-oxoglutarate-dependent oxygenase-catalyzed hydroxylations by using **1** as substrate.[25] Compound **4** is expected to be the product of **3** via an analogous mechanism as for **2** or the product of **2** by a hydroxylation at C14 (Scheme 2).

To elucidate the origin of the oxygen atoms in the installed hydroxyl groups and to confirm our hypothesis in Scheme 2, EAW25734 assays were carried out under $^{16}O_2$, $^{18}O_2$-enriched atmosphere or in ^{18}O-enriched water (97% purity for both $^{18}O_2$ and $H_2^{18}O$). The reaction mixtures were then analyzed on LC-MS. As shown in Supplementary Figure 22, conversion of **1** to **2**, **3**, and **4** was clearly observed in all reaction mixtures with UV detection. In the incubation mixture under $^{18}O_2$-enriched atmosphere, incorporation of one oxygen-18 atom each in **2** and **3** and up to two in **4** was confirmed by detection of the isotope peaks of their [M−H]⁻ ions. In addition to the [M−H]⁻ ions at m/z 366.18 with the highest percentage of natural abundance, strongly enhanced isotope peaks at m/z

368.19 were detected for **2** and **3**. In the case of **4**, [M−H]⁻ ions at m/z 382.18, 384.18, and 386.19 were detected, proving the incorporation of none, one, and two ^{18}O atoms, respectively. Interestingly, different ratios of the isotope peaks were determined for the [M−H]⁻ ions of **2**, **3**, and **4**. Lower incorporation of ^{18}O into the hydroxyl group at C22 than that of C14 was calculated (35% versus 95%). In contrast, incorporation of one ^{18}O atom into the hydroxyl group at C22, but not into that at 14α, was detected in the incubation mixture in ^{18}O-enriched water. This indicates a solvent exchange in the intermediates proceeding **2** and **4**.[19] These results prove unequivocally that O_2 supplies the majority of the installed hydroxyl groups. However, solvent exchange also contributes to the hydroxylation at C22. The results were confirmed by two independent experiments with lower $^{18}O_2$ contents of the $^{18}O_2$-enriched atmosphere (Supplementary Table 5).

■ CONCLUSIONS

In conclusion, we identified an unusual Fe^{II}/2-oxoglutarate oxygenase EAW25734 catalyzing two chemical reaction steps (i.e. an exceptional double bond migration and hydroxylation at a dimethylallyl moiety). This could be explained by the electron migration in the radial intermediates (F and G in Scheme 2). In our example presented in this study, it seems like EAW25734 in *N. fischeri* NRRL181 just uses intermediates of other biosynthetic pathways, here from the fumitremorgin pathway, as substrates. This could also be considered as a branch-pathway of the tryprostatin metabolism, as in the cases for cyclotryptostatins,[32] which were also isolated from *N. fischeri* NRRL 181 (Scheme 1).[37] Moreover, it would be interesting to find more examples for the conversion of dimethylallyl to a 3-hydroxy-3-methyl-1-butenyl moiety. Some potential candidate substances are shown in Figure 1.

■ METHODS

Materials. Tryprostatin B was isolated as reported previously.[38] Reagents with highest available quality were supplied by Sigma-Aldrich and Carl Roth. Oxygen-18 ($^{18}O_2$, 97%) and ^{18}O-enriched water ($H_2^{18}O$, 97%) were obtained from Eurisotop.

Bacteria, Plasmids, and Cultivation Conditions. pGEM-T Easy (Promega), pQE-70 (Qiagen) were used as cloning and expression vectors. *XL1 Blue* MRF' cells of *Escherichia coli* (Agilent Technologies) were used for both cloning and overexpression. The bacteria were cultivated in Luria−Bertani broth with 5 g L^{-1} yeast extract, 10 g L^{-1} tryptone, and 10 g L^{-1} NaCl or Terrific broth containing 4.5 g L^{-1} glycerol, 12 g L^{-1} tryptone, 24 g L^{-1} yeast extract, 0.017 M KH$_2$PO$_4$, and 0.072 M K$_2$HPO$_4$. The bacteria were also grown on solid LB medium containing 1.5% agar at 37 °C. 50 μg mL^{-1} of carbenicillin were supplemented for recombinant strain selection.

Cultivation of *N. fischeri* NRRL181 for Secondary Metabolite Production. For detection of fungal metabolites, the strain was cultivated in a 250 mL of flask, which contains 100 mL of mCDY medium (30 g L^{-1} sucrose, 5.1 g L^{-1} yeast extract, 2.0 g L^{-1} NaNO$_3$, 1.0 g L^{-1} KH$_2$PO$_4$, 0.3 g L^{-1} MgSO$_4$ 7H$_2$O, and 0.01g L^{-1} FeSO$_4$ 7H$_2$O),[33] at 25 °C and 150 rpm in darkness for 7 days. The filtrates of the culture were extracted twice with EtOAc. The mycelia were thoroughly crushed in a mortar and extracted with methanol/acetone (1:1). Both fractions were combined, and the solvents were evaporated under reduced presure at 30 °C, The residue was taken in methanol and analyzed via LC-MS as described below.

DNA Isolation, Gene Amplification, and Cloning. DNA manipulation and propagation in *E. coli* were performed as reported previously.[39] Genomic DNA was isolated from *N. fischeri* NRRL181 according to a method described previously.[40] *NFIA_045530* containing merely one exon was PCR amplified by using genomic DNA as a template and vwFtmOx1f-2-fw_5 (5′-CC**G**CATGC**C**CC-GTCGACTCCAAGCC-3′) and vwFtmOx1f-2-rev_5 (5′-CC**GGATCC**AGCAGGCAAATCAGTAGCCT-3′) as primers. The underlined letters represent the introduced restriction site SphI in the first and *Bam*HI in the second primer for cloning in pQE-70. For cloning in pQE-70 at the SphI site, the original genomic sequence was mutated by change the base pair labeled as a bold letter in vwFtmOx1f-2-fw_5. The generated PCR fragment containing the entire coding region was inserted into pGEM-T Easy and subsequently sequenced to verify the putative gene sequence (Seqlab Sequence Laboratories). The insert was then cut by the restriction enzymes SphI and *Bam*HI and cloned subsequently into the pQE-70 vector. The resulted construct pVW53 was introduced to the expression host.

Gene Expression and Purification of EAW25734 and FtmOx1$_{Af}$. *XL1 Blue* MRF' cells harboring pVW53 were grown in 500 mL TB media supplemented with 50 μg mL^{-1} carbenicillin at 37 °C and 230 rpm. When absorption at 600 nm reached approximately 0.60, gene expression was induced by 1 mM of isopropyl thiogalactoside. The bacteria were cultivated for additional 16 h at 37 °C. Protein purification was done on Ni-NTA agarose resin (Qiagen) as described in the manufacturer's protocol. The protein fraction was subsequently passed through a Sephadex G25 column (PD-10, GE Healthcare) using 50 mM Tris-HCl, pH 7.5, 15% glycerol as eluent to afford the recombinant protein, which was then stored at −80 °C. Protein yield was calculated to be 7.6 mg L^{-1}. The purity of the obtained protein was proven on SDS-PAGE, showing a major protein band at approximate 33 kDa (Supplementary Figure 2, i). FtmOx1$_{Af}$ was overproduced as described previously.[30]

LC-ESI-TOF Analysis of the Purified His$_6$-EAW25734. To confirm the molecular weight of His$_6$-EAW25734, the purified protein was desalted online using a Waters ACQUITY H-Class HPLC-system equipped with a MassPrep column (Waters). Desalted protein was eluted into the ESI source of a Synapt G2Si mass spectrometer (Waters) under the condition as described previously.[41] Positive ions within the mass range of m/z 500−5000 were detected. Glu-Fibrinopeptide B was measured every 45s for automatic mass drift correction. Averaged spectra were deconvoluted after baseline subtraction and eventually smoothing using MassLynx instrument software with MaxEnt1 extension. The determined value of 33520 Da corresponds to the molecular weight of His$_6$-EAW25734 after removal of the methionine residue at the N-terminus by *E. coli* methionyl aminopeptidase.[42,43]

Enzyme Assays of EAW25734 and FtmOx1$_{Af}$. To determine the enzyme activity toward tryprostatin B and fumitremorgin B, the enzyme assays (100 μL) contained Tris-HCl (50 mM, pH 7.5), ascorbic acid (1 mM), tryprostatin B or fumitremorgin B (1 mM), Fe[(NH$_4$)$_2$(SO$_4$)$_2$] (1 mM), 2-oxoglutarate (1 mM), glycerol (0.5−5%), DMSO (2.5%), and the purified recombinant EAW25734 (50 μg, 15.6 μM) or FtmOx1$_{Af}$ (14 μg, 4.7 μM). The enzyme assays were incubated at 37 °C for 16 h and treated twice with EtOAc. The solvent was removed on a rotary evaporator at 30 °C. The residues were taken in 100 μL of CH$_3$OH and analyzed via LC-MS (see below).

To determine the cofactor dependency of the EAW25734 reaction, the 100 μL reaction mixtures containing 50 μg of EAW25734, 1 mM of tryprostatin B, and different cofactor combinations were incubated at 37 °C for 16 h. For time dependence of EAW25734 toward tryprostatin B, the standard reaction mixtures were incubated at 37 °C for 0−14 h.

Enzyme Assays in the Presence of ^{18}O$_2$-Enriched Atmosphere and ^{18}O-Enriched Water. For incubation with EAW25734 under ^{18}O$_2$-enriched atmosphere, a 500 μL assay contained the same components as in the standard reaction mixture. ^{16}O$_2$ in the reaction mixture was removed by application of vacuum followed by flushing with argon for three times. Argon was then removed by vacuum and finally ^{18}O$_2$ was allowed to enter the reaction mixture. The reaction was terminated by addition of 500 μL methanol after incubation at 37 °C for 30 min. LC-MS was used for monitoring the incorporation.

For incubation with EAW25734 in ^{18}O-enriched water, a 50 μL reaction mixture contained the same components as in the standard assay in a mixture of H$_2^{18}$O and H$_2^{16}$O with a ratio of 4:1.

Preparation and Isolation of Enzyme Products for Structure Elucidation. Assays (50 mL) were done for enzyme product isolation. They contained Tris-HCl (50 mM, pH 7.5), ascorbic acid (1 mM), tryprostatin B (1 mM), Fe[(NH$_4$)$_2$(SO$_4$)$_2$] (1 mM), 2-oxoglutarate (1 mM), and recombinant EAW25734 (25 mg) and were incubated at 37 °C for 16 h. The products were extracted with EtOAc and purified on a preparative HPLC column.

HPLC and LC-MS Conditions. The enzyme assays were analyzed on an Agilent HPLC series 1200 (Agilent Technologies) with an Agilent Eclipse XDB-C18 column (4.6 × 150 mm, 5 μm) by using H$_2$O (solvent A) and CH$_3$CN (B) as solvents at 0.5 mL min^{-1}. The procedure was initiated with a linear gradient from 20−30% B over 5 min, followed by linear gradients from 30−33% B in 30 min, and from 33−40% B in 5 min. After each run, the column was holding with 100% B for 5 min and equilibrated with 20% B for 5 min. Detection was carried out with a photodiode array detector and absorptions at 296 nm are given in this study.

The enzyme products were isolated on the same equipment by using an Agilent Eclipse XDB-C18 column (9.4 × 250 mm, 5 μm) with an isocratic elution at 30% B in 40 min and a flow rate at 2.0 mL min^{-1}.

Analysis of the enzyme products on LC-MS was carried out on an Agilent 1260 series with Eclipse XDB-C18 column (4.6 × 150 mm, 5 μm) and micrOTOF-Q III Mass spectrometer. Analysis of the enzyme products was performed by using the same solvents and elution profile as for HPLC analysis mentioned above. HR-ESI-MS data of the reported compounds are given in Supplementary Table 1.

Analysis of the fungal extract on LC-MS was carried out on the same equipment by using a CS Multosher 120 RP 18 column (2 × 250 mm, 5 μm) with a linear gradient of 5−100% B in 50 min, both containing 0.1% formic acid, and a flow rate at 0.25 mL min^{-1}. After each run, the column was holding with 100% B for 5 min and equilibrated with 5% B for 10 min.

NMR Analysis. For structural elucidation, the samples were dissolved in DMSO-d_6 or CDCl$_3$ and subjected for taking NMR spectra including ^{1}H NMR, ^{13}C NMR, ^{1}H−^{1}H COSY, HSQC, HMBC, and NOESY spectra. The spectra were recorded at RT on a Bruker Avance III 500 MHz (^{1}H) or 125 MHz (^{13}C) spectrometer installed with a cryo probe 5 mm Prodigy for Broad Band Observation. All spectra were processed with MestReNova 6.0.2 (Metrelab Research) and the chemical shifts were referenced to those

of the solvents. The NMR data are given in Supplementary Tables 2−4 and spectra as Supplementary Tables 2−19.

■ ASSOCIATED CONTENT

Ⓢ Supporting Information

The Supporting Information is available free of charge on the ACS Publications website at DOI: 10.1021/acschembio.8b00588.

> Detailed experimental procedures including SDS-PAGE, sequence alignments data, fungal extract analysis, MS and NMR data, NMR spectra as well as ^{18}O-labeling experiment results (PDF)

■ AUTHOR INFORMATION

Corresponding Author

*Tel.: +49 6421 28 22461. E-mail: shuming.li@staff.uni-marburg.de.

ORCID Ⓞ

Shu-Ming Li: 0000-0003-4583-2655

Notes

The authors declare no competing financial interest.

■ ACKNOWLEDGMENTS

■ REFERENCES

(1) Winkelblech, J., Fan, A., and Li, S.-M. (2015) Prenyltransferases as key enzymes in primary and secondary metabolism. *Appl. Microbiol. Biotechnol.* 99, 7379−7397.

(2) Li, S.-M. (2010) Prenylated indole derivatives from fungi: structure diversity, biological activities, biosynthesis and chemo-enzymatic synthesis. *Nat. Prod. Rep.* 27, 57−78.

(3) Li, Y.-F., Wu, X.-B., Niaz, S.-I., Zhang, L.-H., Huang, Z.-J., Lin, Y.-C., Li, J., and Liu, L. (2017) Effect of culture conditions on metabolites produced by the crinoid-derived fungus *Aspergillus ruber* 1017. *Nat. Prod. Res.* 31, 1299−1304.

(4) Wong, K. W., Ee, G. C. L., Ismail, I. S., Karunakaran, T., and Jong, V. Y. M. (2017) A new pyranoxanthone from *Garcinia nervosa*. *Nat. Prod. Res.* 31, 2513−2519.

(5) Ding, G.-Z., Liu, J., Wang, J.-M., Fang, L., and Yu, S.-S. (2013) Secondary metabolites from the endophytic fungi *Penicillium polonicum* and *Aspergillus fumigatus*. *J. Asian Nat. Prod. Res.* 15, 446−452.

(6) Sriyatep, T., Andersen, R. J., Patrick, B. O., Pyne, S. G., Muanprasat, C., Seemakhan, S., Borwornpinyo, S., and Laphookhieo, S. (2017) Scalemic caged xanthones isolated from the stem bark extract of *Garcinia propinqua*. *J. Nat. Prod.* 80, 1658−1667.

(7) Tan, N., Yazıcı-Tütüniş, S., Bilgin, M., Tan, E., and Miski, M. (2017) Antibacterial activities of pyrenylated coumarins from the roots of *Prangos hulusii*. *Molecules* 22, 1098−1105.

(8) Iinuma, M., Tanaka, T., Mizuno, M., and Lang, F. A. (1992) Two flavanones from roots of *Sophora leachiana*. *Phytochemistry* 31, 721−723.

(9) Xiao, Q., Zeng, Y.-B., Mei, W.-L., Zhao, Y.-X., Deng, Y.-Y., and Dai, H.-F. (2008) Cytotoxic prenylated xanthones from *Calophyllum inophyllum*. *J. Asian Nat. Prod. Res.* 10, 993−997.

(10) Liao, Y., Yang, S.-Y., Li, X.-N., Yang, X.-W., and Xu, G. (2016) Polyprenylated acylphloroglucinols from the fruits of *Hypericum henryi*. *Sci. China: Chem.* 59, 1216−1223.

(11) Ryan, K. L., Akhmedov, N. G., and Panaccione, D. G. (2015) Identification and structural elucidation of ergotryptamine, a new ergot alkaloid produced by genetically modified *Aspergillus nidulans* and natural isolates of *Epichloë* species. *J. Agric. Food Chem.* 63, 61−67.

(12) Bohlmann, F., and Suwita, A. (1978) Neue Phloroglucin-Derivate aus *Leontonyx*-Arten sowie weitere Verbindungen aus Vertretern der Tribus *Inuleae*. *Phytochemistry* 17, 1929−1934.

(13) Liu, C., Tagami, K., Minami, A., Matsumoto, T., Frisvad, J. C., Suzuki, H., Ishikawa, J., Gomi, K., and Oikawa, H. (2015) Reconstitution of biosynthetic machinery for the synthesis of the highly elaborated indole diterpene penitrem. *Angew. Chem., Int. Ed.* 54, 5748−5752.

(14) Eriksson, M., Myllyharju, J., Tu, H., Hellman, M., and Kivirikko, K. I. (1999) Evidence for 4-hydroxyproline in viral proteins. Characterization of a viral prolyl 4-hydroxylase and its peptide substrates. *J. Biol. Chem.* 274, 22131−22134.

(15) Vedler, E., Kõiv, V., and Heinaru, A. (2000) Analysis of the 2,4-dichlorophenoxyacetic acid-degradative plasmid pEST4011 of *Achromobacter xylosoxidans* subsp. *denitrificans* strain EST4002. *Gene* 255, 281−288.

(16) Hibi, M., Mori, R., Miyake, R., Kawabata, H., Kozono, S., Takahashi, S., and Ogawa, J. (2016) Novel enzyme family found in filamentous fungi catalyzing *trans*-4-hydroxylation of L-pipecolic acid. *Appl. Environ. Microbiol.* 82, 2070−2077.

(17) Farrow, S. C., and Facchini, P. J. (2013) Dioxygenases catalyze *O*-demethylation and *O,O*-demethylenation with widespread roles in benzylisoquinoline alkaloid metabolism in opium poppy. *J. Biol. Chem.* 288, 28997−29012.

(18) Akahori, H., Guindon, S., Yoshizaki, S., and Muto, Y. (2015) Molecular evolution of the TET gene family in mammals. *Int. J. Mol. Sci.* 16, 28472−28485.

(19) Hausinger, R. P. (2004) Fe (II)/α-ketoglutarate-dependent hydroxylases and related enzymes. *Crit. Rev. Biochem. Mol. Biol.* 39, 21−68.

(20) Hausinger, R. P. (2015) Biochemical diversity of 2-oxoglutarate-dependent oxygenases, in 2-Oxoglutarate-Dependent Oxygenases (Schofield, C. J., and Hausinger, R. P., Eds.) 1st ed., pp 1−58, The Royal Society of Chemistry, Cambridge, UK.

(21) Gao, S.-S., Naowarojna, N., Cheng, R., Liu, X., and Liu, P. (2018) Recent examples of α-ketoglutarate-dependent mononuclear non-haem iron enzymes in natural product biosyntheses. *Nat. Prod. Rep.* 35, 792−837.

(22) Islam, M. S., Leissing, T. M., Chowdhury, R., Hopkinson, R. J., and Schofield, C. J. (2018) 2-Oxoglutarate-Dependent Oxygenases. *Annu. Rev. Biochem.* 87, 585−620.

(23) Herr, C. Q., and Hausinger, R. P. (2018) Amazing diversity in biochemical roles of Fe(II)/2-oxoglutarate oxygenases. *Trends Biochem. Sci.* 43, 517−532.

(24) Hagel, J. M., and Facchini, P. J. (2018) Expanding the roles for 2-oxoglutarate-dependent oxygenases in plant metabolism. *Nat. Prod. Rep.* 35, 721−734.

(25) Martinez, S., and Hausinger, R. P. (2015) Catalytic mechanisms of Fe(II)- and 2-oxoglutarate-dependent oxygenases. *J. Biol. Chem.* 290, 20702−20711.

(26) Baldwin, J. E., and Abraham, E. (1988) The biosynthesis of penicillins and cephalosporins. *Nat. Prod. Rep.* 5, 129−145.

(27) Baldwin, J. E., Adlington, R. M., Aplin, R. T., Crouch, N. P., Knight, G., and Schofield, C. J. (1987) Cephalosporin C biosynthesis; a branched pathway sensitive to a kinetic isotope effect. *J. Chem. Soc., Chem. Commun.*, 1651−1654.

(28) Schofield, C. J., and Zhang, Z. (1999) Structural and mechanistic studies on 2-oxoglutarate-dependent oxygenases and related enzymes. *Curr. Opin. Struct. Biol.* 9, 722−731.

(29) Li, S.-M. (2011) Genome mining and biosynthesis of fumitremorgin-type alkaloids in ascomycetes. *J. Antibiot.* 64, 45−49.

(30) Steffan, N., Grundmann, A., Afiyatullov, A., Ruan, H., and Li, S.-M. (2009) FtmOx1, a non heme Fe(II) and alpha-ketoglutarate-dependent dioxygenase, catalyses the endoperoxide formation of verruculogen in *Aspergillus fumigatus*. *Org. Biomol. Chem. 7*, 4082−4087.

(31) Yan, W., Song, H., Song, F., Guo, Y., Wu, C.-H., Sae Her, A., Pu, Y., Wang, S., Naowarojna, N., Weitz, A., Hendrich, M. P., Costello, C. E., Zhang, L., Liu, P., and Zhang, Y. J. (2015) Endoperoxide formation by an α-ketoglutarate-dependent mononuclear non-haem iron enzyme. *Nature 527*, 539−543.

(32) Tsunematsu, Y., Ishikawa, N., Wakana, D., Goda, Y., Noguchi, H., Moriya, H., Hotta, K., and Watanabe, K. (2013) Distinct mechanisms for spiro-carbon formation reveal biosynthetic pathway crosstalk. *Nat. Chem. Biol. 9*, 818−825.

(33) Mundt, K., Wollinsky, B., Ruan, H.-L., Zhu, T., and Li, S.-M. (2012) Identification of the verruculogen prenyltransferase FtmPT3 by a combination of chemical, bioinformatic and biochemical approaches. *ChemBioChem 13*, 2583−2592.

(34) Matsuda, Y., Iwabuchi, T., Fujimoto, T., Awakawa, T., Nakashima, Y., Mori, T., Zhang, H., Hayashi, F., and Abe, I. (2016) Discovery of key dioxygenases that diverged the paraherquonin and acetoxydehydroaustin pathways in *Penicillium brasilianum*. *J. Am. Chem. Soc. 138*, 12671−12677.

(35) Hegg, E. L., and Que, L., Jr. (1997) The 2-His-1-carboxylate facial triad — an emerging structural motif in mononuclear non-heme iron(II) enzymes. *Eur. J. Biochem. 250*, 625−629.

(36) Aik, W. S., Chowdhury, R., Clifton, I. J., Hopkinson, R. J., Leissing, T., McDonough, M. A., Nowak, R., Schofield, C. J., and Walport, L. J. (2015) Introduction to structural studies on 2-oxoglutarate-dependent oxygenases and related enzymes, in *2-Oxoglutarate-Dependent Oxygenases* (Schofield, C. J., and Hausinger, R. P., Eds.) 1st ed., pp 59−94, The Royal Society of Chemistry, Cambridge, UK.

(37) Wollinsky, B. (2014) *Chemische, molekularbiologische und biochemische Untersuchungen zur Biosynthese von Mykotoxinen aus Ascomyceten*, Ph.D. thesis, University of Marburg, Marburg, Germany.

(38) Maiya, S., Grundmann, A., Li, S.-M., and Turner, G. (2009) Improved tryprostatin B production by heterologous gene expression in *Aspergillus nidulans*. *Fungal Genet. Biol. 46*, 436−440.

(39) Sambrook, J., and Russell, D. W. (2001) *Molecular cloning: a laboratory manual*, 3rd ed., Cold Spring Harbor Laboratory Press, Cold Spring Harbor, New York.

(40) Yu, X., and Li, S.-M. (2012) Prenyltransferases of the dimethylallyltryptophan synthase superfamily. *Methods Enzymol. 516*, 259−278.

(41) Miethke, M., Hou, J., and Marahiel, M. A. (2011) The siderophore-interacting protein YqjH acts as a ferric reductase in different iron assimilation pathways of *Escherichia coli*. *Biochemistry 50*, 10951−10964.

(42) Ben-Bassat, A., Bauer, K., Chang, S.-Y., Myambo, K., Boosman, A., and Chang, S. (1987) Processing of the initiation methionine from proteins: properties of the *Escherichia coli* methionine aminopeptidase and its gene structure. *J. Bacteriol. 169*, 751−757.

(43) Meinnel, T., Mechulam, Y., and Blanquet, S. (1993) Methionine as translation start signal: a review of the enzymes of the pathway in *Escherichia coli*. *Biochimie 75*, 1061−1075.

Supporting Information

A non-heme Fe^{II}/2-oxoglutarate-dependent oxygenase catalyzes a double bond migration within a dimethylallyl moiety accompanied by hydroxylation

Huomiao Ran,[†] Viola Wohlgemuth,[†] Xiulan Xie,[‡] Shu-Ming Li[†]*

[†]Institut für Pharmazeutische Biologie und Biotechnologie, Philipps-Universität Marburg, Robert-Koch-Straße 4, 35037 Marburg, Germany.

[‡]Fachbereich Chemie, Philipps-Universität Marburg, Hans-Meerwein-Straße, 35032 Marburg, Germany

Corresponding Author

*Tel +49 6421 28 22461. shuming.li@staff.uni-marburg.de

ORCID Shu-Ming Li: 0000-0003-4583-2655

Content

1 TABLES

Table S1. HR-ESI-MS data of the reported compounds

Compound	Chemical Formula	[M-H] Calculated	Measured	Deviation (ppm)
1	$C_{21}H_{25}N_3O_2$	350.1874	350.1876	-0.6
2	$C_{21}H_{25}N_3O_3$	366.1823	366.1830	-1.9
3	$C_{21}H_{25}N_3O_3$	366.1823	366.1835	-3.2
4	$C_{21}H_{25}N_3O_4$	382.1772	382.1773	-0.3

Table S2. NMR Data of **2** in DMSO-d_6 (500 MHz for ^{1}H NMR and 125 MHz for ^{13}C NMR)
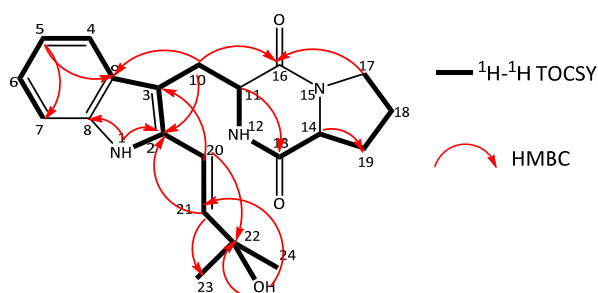
Position	δ$_C$, multi	δ$_H$, multi., J in Hz	HMBC correlation	COSY correlation	TOCSY correlation
1	-	11.03, s	C-2, 3, 8, 9	-	H-4, 5,20, 21
2	134.2	-	-	-	-
3	108.1	-	-	-	-
4	118.7	7.53, d, 8.0	C-3, 6, 8	H-5	H-1, 5, 6, 7, 10α
5	118.5	6.93, dd, 8.0, 7.0	C-7, 9	H-4, 6	H-1, 4, 6, 7, 10α
6	121.8	7.05, dd, 8.0, 7.0	C-4, 8	H-5, 7	H-1, 4, 5, 7, 10α
7	110.6	7.26, d, 8.0	C-5, 9	H-6	H-1, 4, 5, 6, 10α
8	136.4	-	-	-	-
9	128.3	-	-	-	-
10α	25.7	3.35^a, dd, 14.7, 5.2	C-2, 9, 16	H-10β, 11	H-11
10β		3.06, dd, 14.7, 6.5	C-2, 9, 16	H-10α, 11	H-11, 12
11	55.5	4.27, dd, 6.5, 5.2	C-3, 13, 16	H-10α, 10β	H-10α, 10β, 12, 14, 19β
12	-	7.06, br s	C-10, 14, 16	H-11	H-10α, 10β, 11, 14
13	168.5	-	-	-	-
14	58.4	4.02, dd, 9.0, 7.2	C-13, 19	H-19α, 19β	H-11, 12, 18α, 18β, 19α, 19β
16	165.3	-	-	-	-
17α	44.6	3.43, dt, 11.4, 7.9	C-14, 16, 19	H-17β, 18α, 18β	H-14, 18α, 18β, 19α, 19β
17β		3.20, ddd, 11.4, 9.0, 4.2	C-19	H-17α, 18α, 18β	H-14, 18α, 18β, 19α, 19β
18α	21.8	1.65, m	C-17, 19	H-17α, 17β, 18β, 19α, 19β	H-14, 17α, 17β, 19α, 19β
18β		1.55, m	-.	H-17α, 17β, 18α, 19α, 19β	H-14, 17α, 17β, 19α, 19β
19α	27.6	1.93 dtd, 12.1, 7.0, 2.9	C-18, 17	H-14, 18α, 18β, 19β	H-14, 17α, 17β, 18α, 18β
19β		1.28, m	C-13, 14, 17, 18	H-14, 18α, 18β, 19α	H-14, 17α, 17β, 19α, 19β
20	114.6	6.69, d, 16.2	C-2, 3, 22	H-21	H-10α, 10β, 11, 23, 24, 22-OH
21	138.4	6.40, d, 16.2	C-2, 22, 23, 24	H-20	H-10α, 10β, 11, 23, 24, 22-OH
22	69.5	-	-	-	-
22-OH	-	4.70, s	C-21, 22, 23, 24	-	H-20, H-21, H-23, H-24
23	30.2	1.34, s	C-21, 22, 24	-	-
24	30.1	1.35, s	C-21, 22, 23	-	-

^{a} Overlapped with solvent signal at 3.33 ppm; - not observed

S3

55

Table S3. NMR Data of **3** in DMSO-d_6 and CDCl$_3$ (500 MHz for ^{1}H NMR and 125 MHz for ^{13}C NMR)
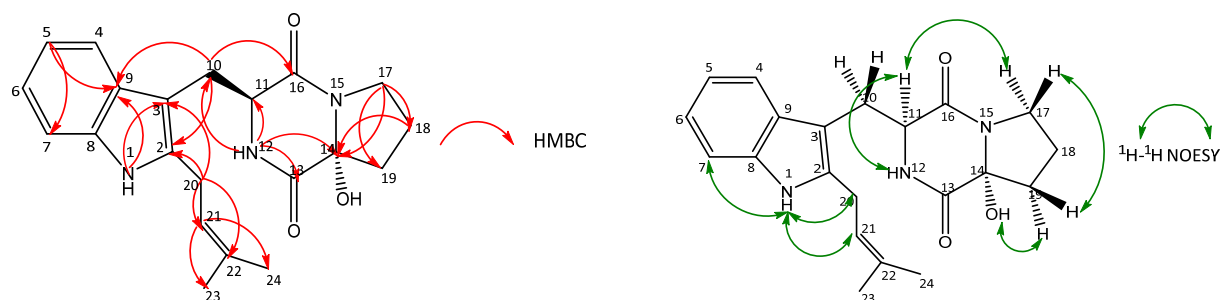
Position	δ_C, multi		δ_H, multi., J in Hz		HMBC correlation		NOESY
	CDCl$_3$	DMSO-d_6	CDCl$_3$	DMSO-d_6	CDCl$_3$	DMSO-d_6	CDCl$_3$
1	-	-	7.93, s	10.74, s	C-3, 8, 9	C-2, 3, 8, 9	H-7, 20, 21, 23
2	136.5	137.4	-	-	-	-	-
3	104.6	104.4	-	-	-	-	-
4	118.0	117.9	7.48, d, 7.2	7.44, d, 7.9	C-3, 6, 8,	C-6, 8,	H-5, 10α, 10β, 11, 12
5	120.1.	120.0	7.10, dd. 8.1, 7.2	6.92, t, 7.9	C-7, 9	C-7, 9	H-7
6	122.0	118.0	7.16, dd, 8.1, 7.1	6.99, t, 7.9	C-4, 8	C-4, 8	H-4
7	110.7	110.4	7.31, d, 7.1	7.25, d, 7.9	C-5, 9	C-5, 9	H-1, 5
8	136.0	135.3	-	-	-	-	-
9	128.1	127. 8	-	-	-	-	-
10α	25.8	25.9	3.69, dd, 15.1, 3.9	3.27, dd, 14.6, 5.2	C-2, 3, 9, 11	C-2, 3, 9, 11, 16	H-10β, 11, 4
10β			2.91, dd, 15.1, 11.6	2.96, dd, 14.6, 6.6	C-2, 3, 9, 11, 16	C-2, 3, 9, 11, 16	H-10α, 20, 12, 11, 4
11	54.3	55.1	4.52, dd, 11.6, 3.9	4.35, t, 6.0	C-3, 10	C-3, 10, 16	H-4, 10α, 10β, 12, 20
12	-	-	5.62, s	7.08, s	C-11, 14	C-10, 11, 13, 14	H-11, 20, 21
13	-	166.8	-	-	-	-	-
14	87.7	86.5	-	-	-	-	-
14-OH	-	-	3.11, s	6.50, s	-	-	H-19α
16	167.0	166.2	-	-	-	-	-
17α	45.5	44.3	3.79, m	3.38^a, m	-	C-18, 19	H-11α, 17β, 18α, 19α
17β			3.62, m	3.33^a, m	-	C-14, 18, 19	H-17α, 18β, 19β
18α	19.9	19.1	2.17, m	1.85, m	C-14	C-14, 17, 19	H-17α, 18β
18β			1.98, m	1.53, m	C-14	C-14, 17, 19	H-18α
19α	37.0	35.1	2.22, m	1.88, m	C-14, 17	C-14, 17, 18	14-OH
19β			2.19, m	1.52, m		C-13, 14, 17, 18	H-17β
20	25.2	24.7	3.49, dd, 16.2, 7.1	3.54, dd, 16.4, 7.8	C-2, 3, 21	C-2, 3, 21, 22	H-1, 10β, 11, 12, 21, 23
			3.44, dd, 16.2, 7.3	3.41, dd, 16.4, 6.6	C-2, 3, 21	C-2, 3, 21, 22	H-1, 10β, 11, 12, 21, 23
21	119.8	121.4	5.31, tdt, 7.2, 2.8,	5.31, t, 7.2	C-23, 24	C-2, 23, 24	H-12, 20, 24
22	136.0	131.9	-	-	-	-	
23	18.1	17.7	1.75, s	1.72, s	C-21, 22, 24	C-21, 22, 24	H-20
24	25.8	25.3	1.78, s	1.69, s	C-21, 22, 23	C-21, 22, 23	H-21
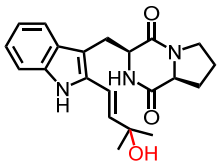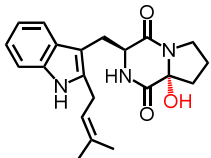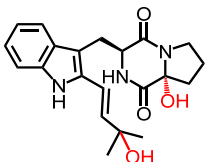
^{a} Overlapped with solvent signal at 3.33 ppm; - not observed

Table S4. NMR Data of **4** in DMSO-d_6 (500 MHz for ^{1}H NMR and 125 MHz for ^{13}C NMR)
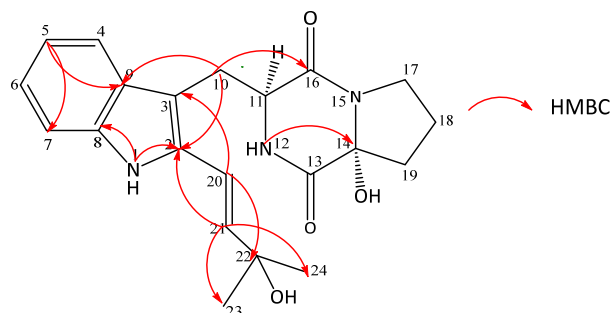
Position	δ$_C$, multi	δ$_H$, multi., *J* in Hz	HMBC correlation
1	-	11.06, s	C-2, 3, 8, 9
2	134.4	-	-
3	108.1	-	-
4	118.3	7.52 d, 8.1	C-6, 8,
5	121.5	6.92, dd, 8.1, 7.3	C-7, 9
6	118.3	7.05, dd, 8.0, 7.3	C-4, 8
7	110.4	7.26 d, 8.0	C-5, 9
8	136.4	-	-
9	128. 6	-	-
10α	25.5	3.38^a, m	C-2, 3, 9, 11, 16
10β		3.03, dd, 14.7, 7.0	C-2, 3, 9, 11, 16
11	55.2	4.37, dd, 7.0, 5.0	C-3, 10, 16
12	-	6.95, s	C-11, 13, 14
13	166.5	-	-
14	86.9	-	-
14-OH	-	6.54, s	-
16	166.4	-	-
17α	44.3	3.42, m	-
17β		3.37^a, m	-
18α	19.6	1.90, m	-
18β		1.65, m	-
19α	35.3	1.90, m	-
19β		1.66, m	-
20	114.2	6.69, d, 16.1	C-2, 3, 22
21	138.2	6.41, d, 16.1	C-2, 22, 23, 24
22	69.8	-	-
22-OH	-	4.75, s	C-23, 24
23	30.6	1.15, s	C-21, 22, 24
24	30.6	1.16, s	C-21, 22, 23

^{a} Overlapped with solvent signal at 3.33 ppm; - not observed.

S5

Table S5. Results of the ^{18}O-labeling experiments

m/z 366.18: [M-H]⁻ without [18]O
m/z 368.19: [M-H]⁻ with 1x [18]O

22-hydroxyl-isotryprostatin B (**2**)

Intensity ratios of m/z 366.18 to m/z 368.19			
experiments	1st	2nd	3rd
control	96:4	97:3	97:3
[18]O$_2$-enriched atmosphere	65:35	86:14	81:9
[18]O-enriched water (97 %)	77:23	80:20	77:23

m/z 366.18: [M-H]⁻ without [18]O
m/z 368.19: [M-H]⁻ with 1x [18]O

14α-hydroxylisotryprostatin B (**3**)

Intensity ratios of m/z 366.18 to m/z 368.19			
experiments	1st	2nd	3rd
control	97:3	96:4	97:3
[18]O$_2$-enriched atmosphere	5:95	62:38	73:27
[18]O-enriched water (97 %)	96:4	97:3	97:3

m/z 382.18: [M-H]⁻ without [18]O
m/z 384.18: [M-H]⁻ with 1x [18]O
m/z 386.19: [M-H]⁻ with 2x [18]O

14α,22-dihydroxylisotryprostatin B (**4**)

Intensity ratios of m/z 382.18: m/z 384.18: m/z 386.19			
experiments	1st	2nd	3rd
control	89.2:10:0.8	95.7:4.0:0.3	95.8:4.0:0.2
[18]O$_2$-enriched atmosphere	5:70:25	57:31:12	77:19:4
[18]O-enriched water (97 %)	72.2:27:0.8	73.8:26:0.2	73.8:26:0.2

The percentages of the supplied [18]O$_2$ for the three experiments with [18]O$_2$-enriched atmosphere are calculated to be 95, 37, and 26 %, respectively.

2   Figures
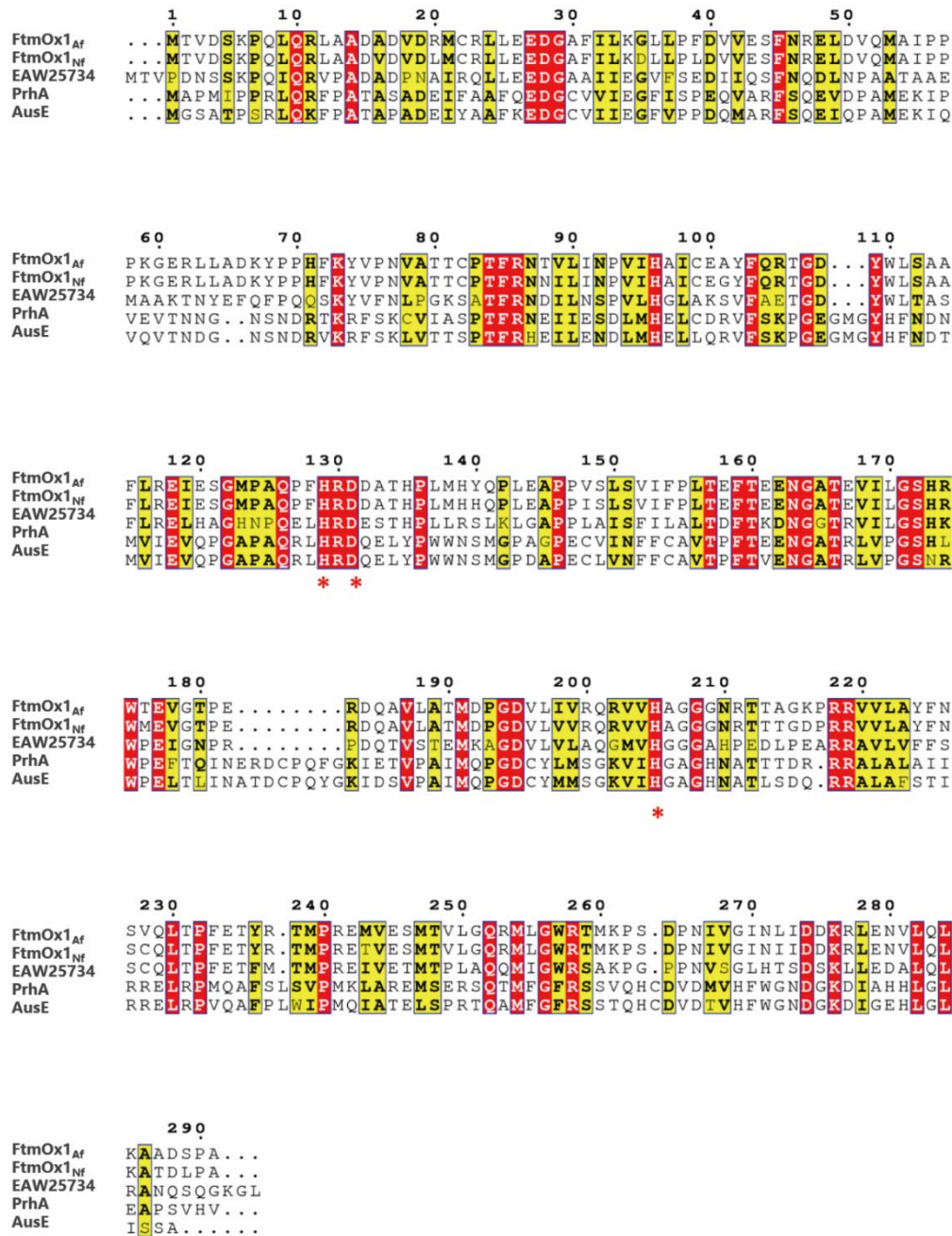
Figure S1. Sequence alignments of FtmOx1$_{Af}$ (XP_747181.1, *A. fumigatus* Af293), FtmOx1$_{Nf}$ (XP_001261651.1, *N. fischeri* NRRL181), EAW25734 (XP_001267631.1, *N. fischeri* NRRL181), PrhA (5YBM_A, *Penicillium brasilianum* NBRC 6234), and AusE (5YBL_A, *A. nidulans* FGSC A4). Red asterisks indicate the conserved two-His-one-Asp iron-binding triad. The alignments were created by using Clustal Omega[1] (https://www.ebi.ac.uk/Tools/msa/clustalo/) and visualized by using EsPript 3.0[2] (http://endscript.ibcp.fr/ESPript/cgi-bin/ESPript.cgi)
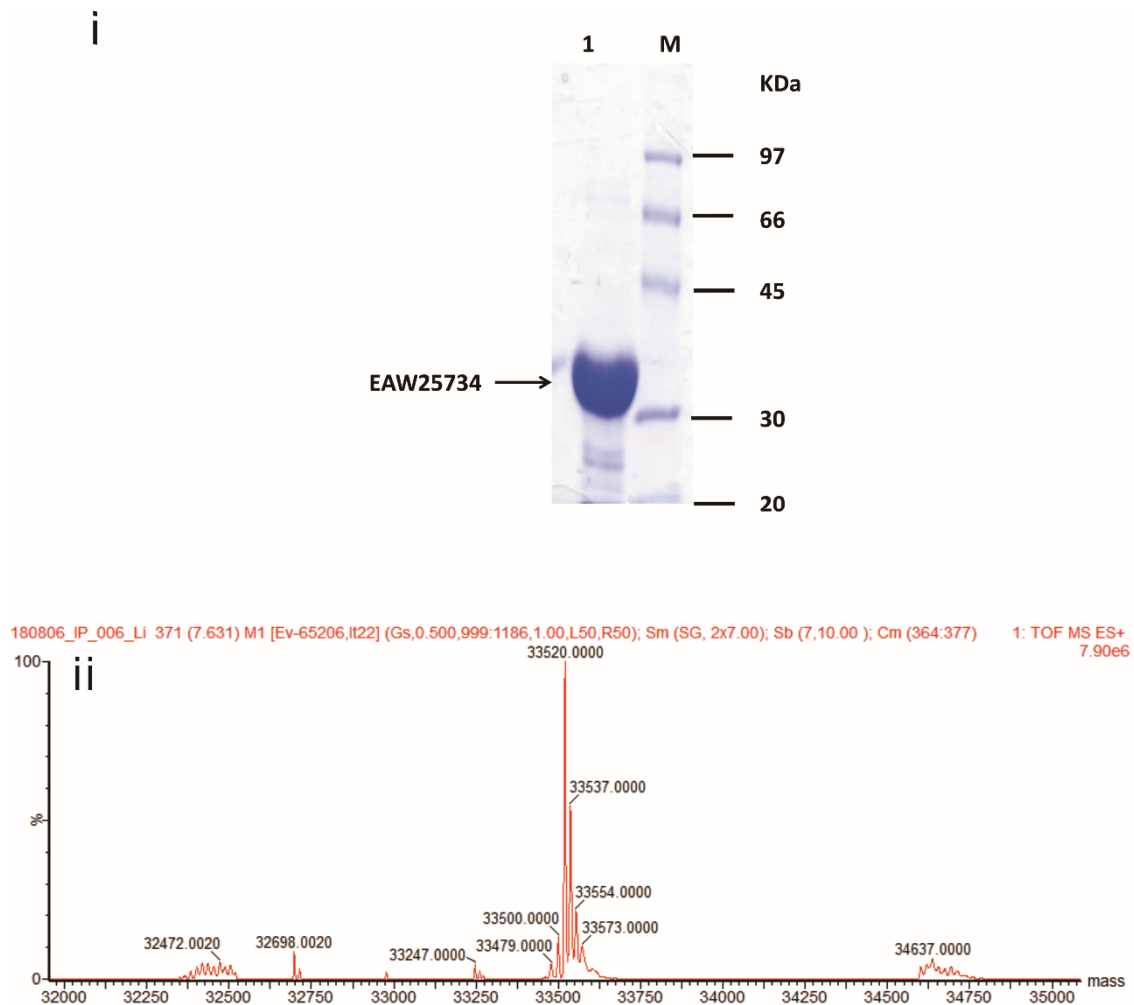
Figure S2. Analysis of the purified His6-EAW25734 on SDS-PAGE (i) and by LC-ESI-TOF-MS (ii). For SDS-PAGE analysis, the proteins were separated on a 12% polyacrylamide gel and stained with Coomassie brilliant blue R-250. The measured molecular weight of 33520 Da corresponds very well to that of His6-EAW25734 after removal of the methionine residue at the N-terminus by *E. coli* methionyl aminopeptidase

S8
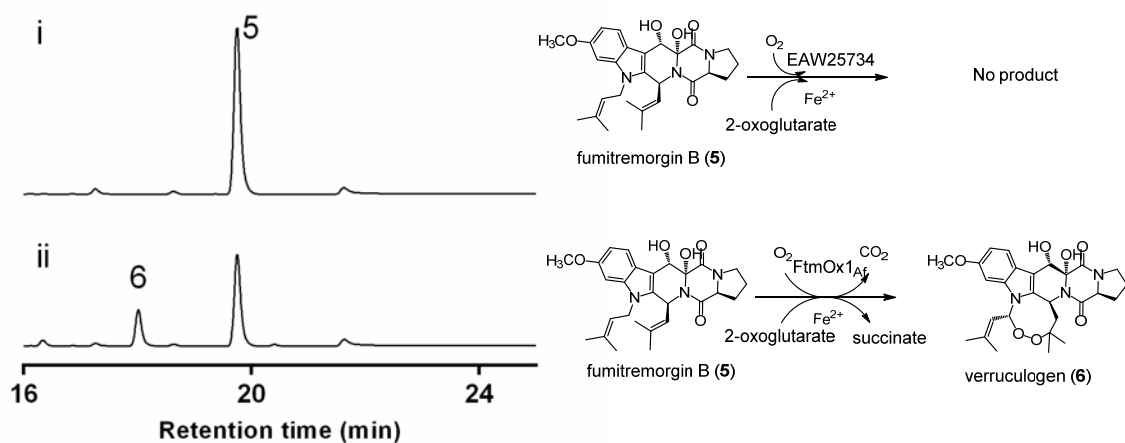
Figure S3. HPLC analysis of the incubation mixtures of fumitremorgin B (**5**) with EAW25734 (i) and FtmOx1$_{Af}$ (ii), which catalyzed **5** to verruculogen (**6**). The enzyme assays were carried out as described previously.[3]
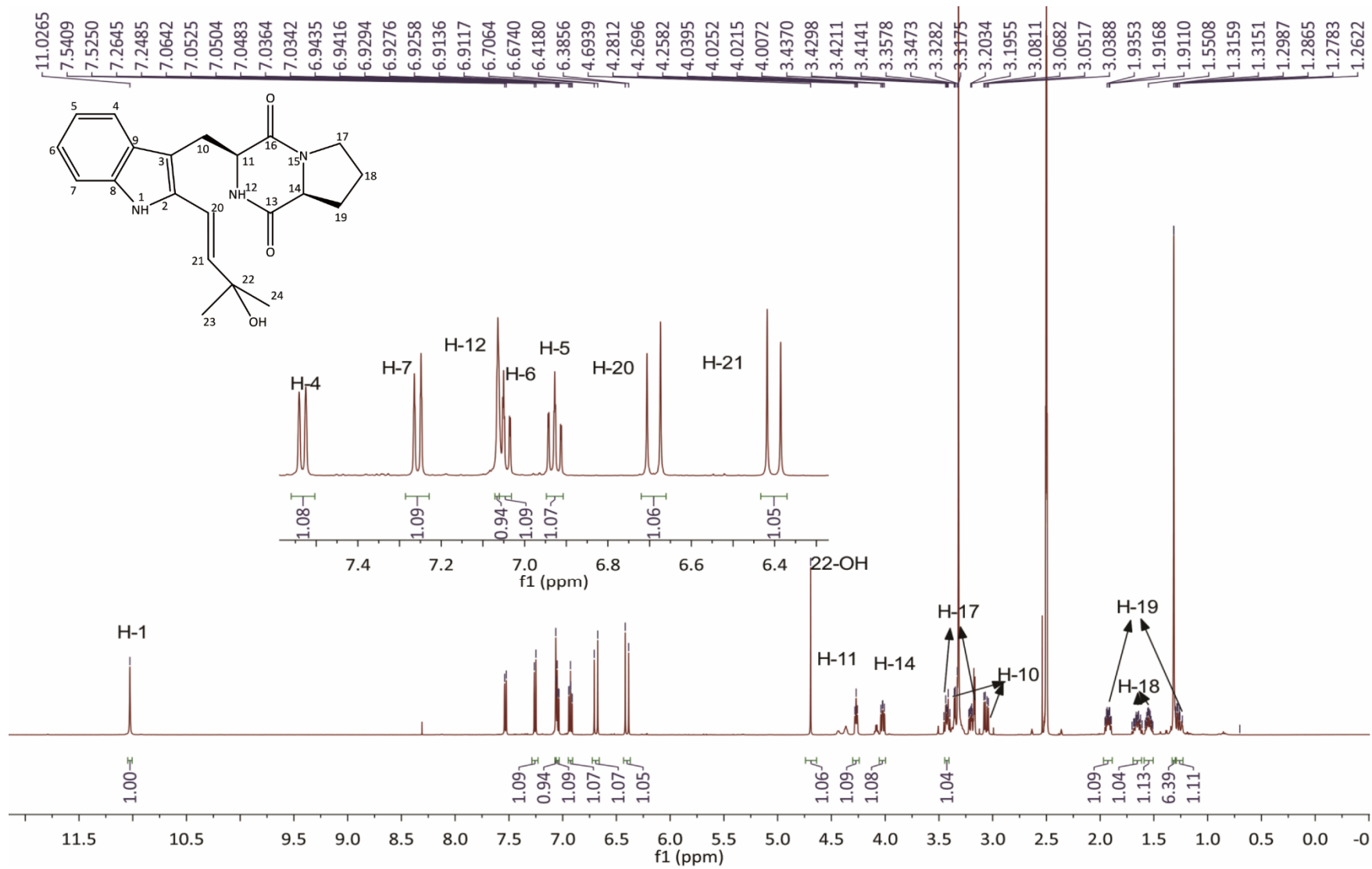
Figure S4. ^{1}H NMR spectrum of 22-hydroxylisotryprostatin B (**2**) in DMSO-d_6 (500 MHz)
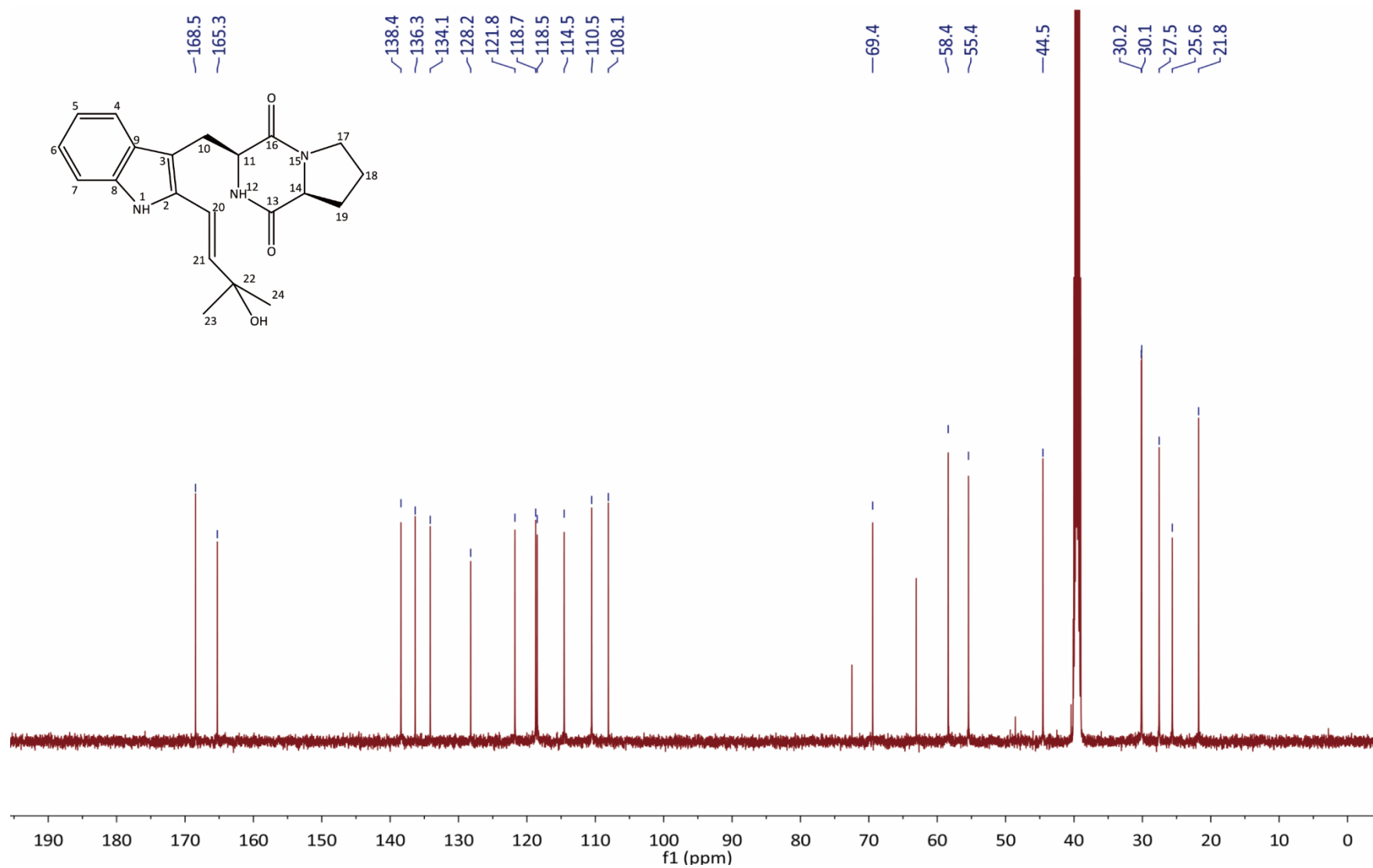
Figure S5. ^{13}C NMR spectrum of 22-hydroxylisotryprostatin B (**2**) in DMSO-d_6 (125 MHz)
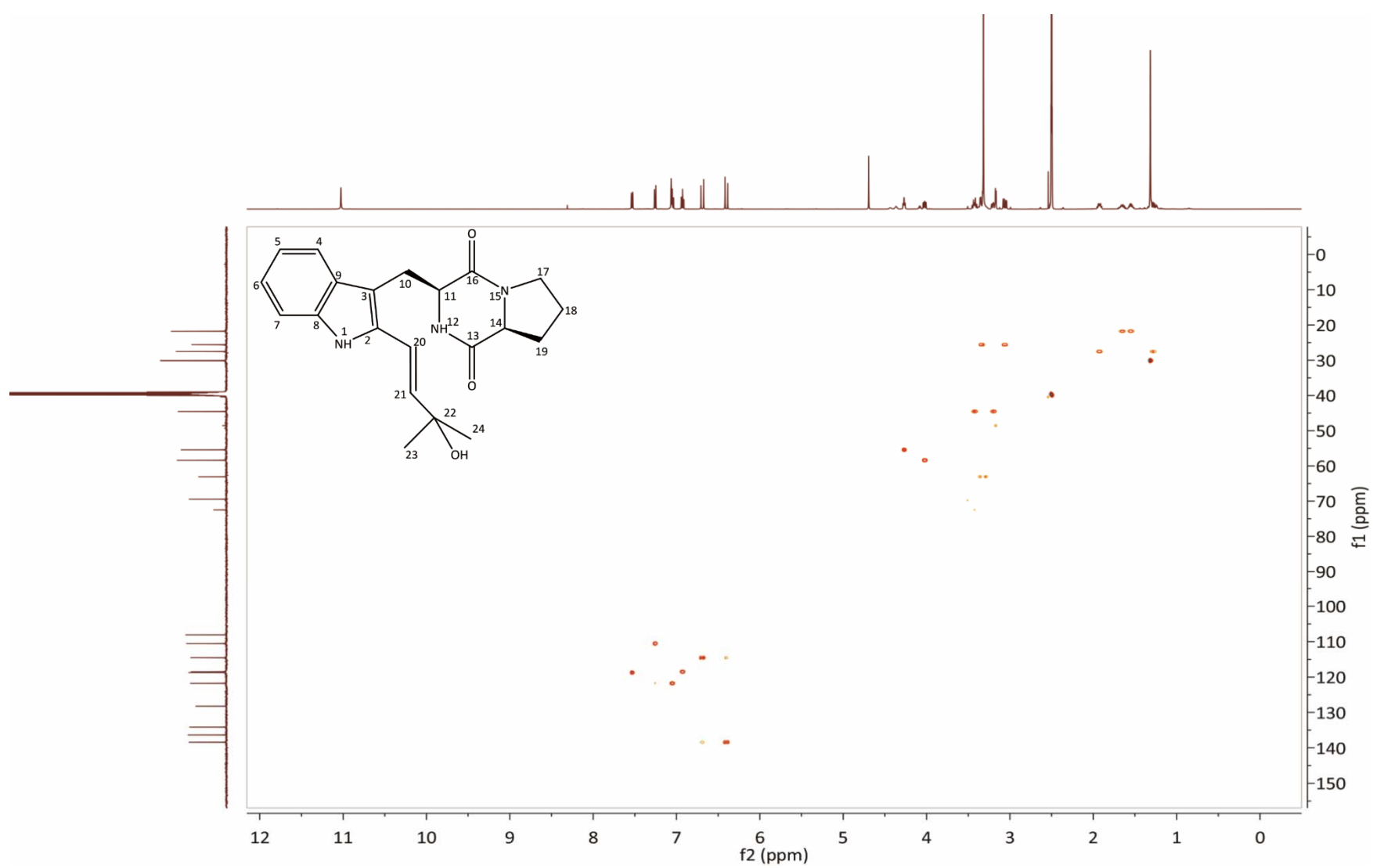
Figure S6. HSQC spectrum of 22-hydroxylisotryprostatin B (**2**) in DMSO-d_6
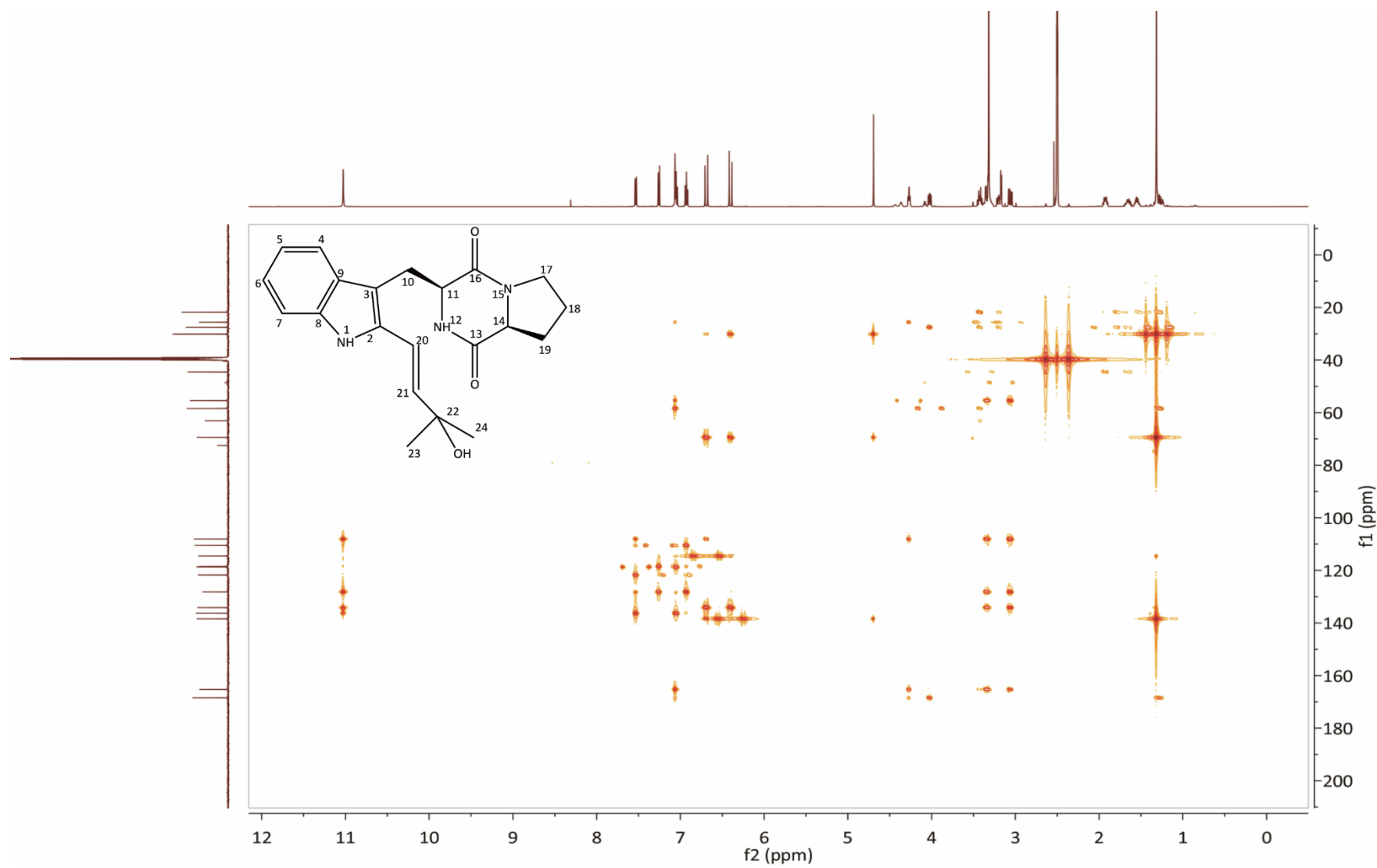
Figure S7. HMBC spectrum of 22-hydroxylisotryprostatin B (**2**) in DMSO-*d₆*
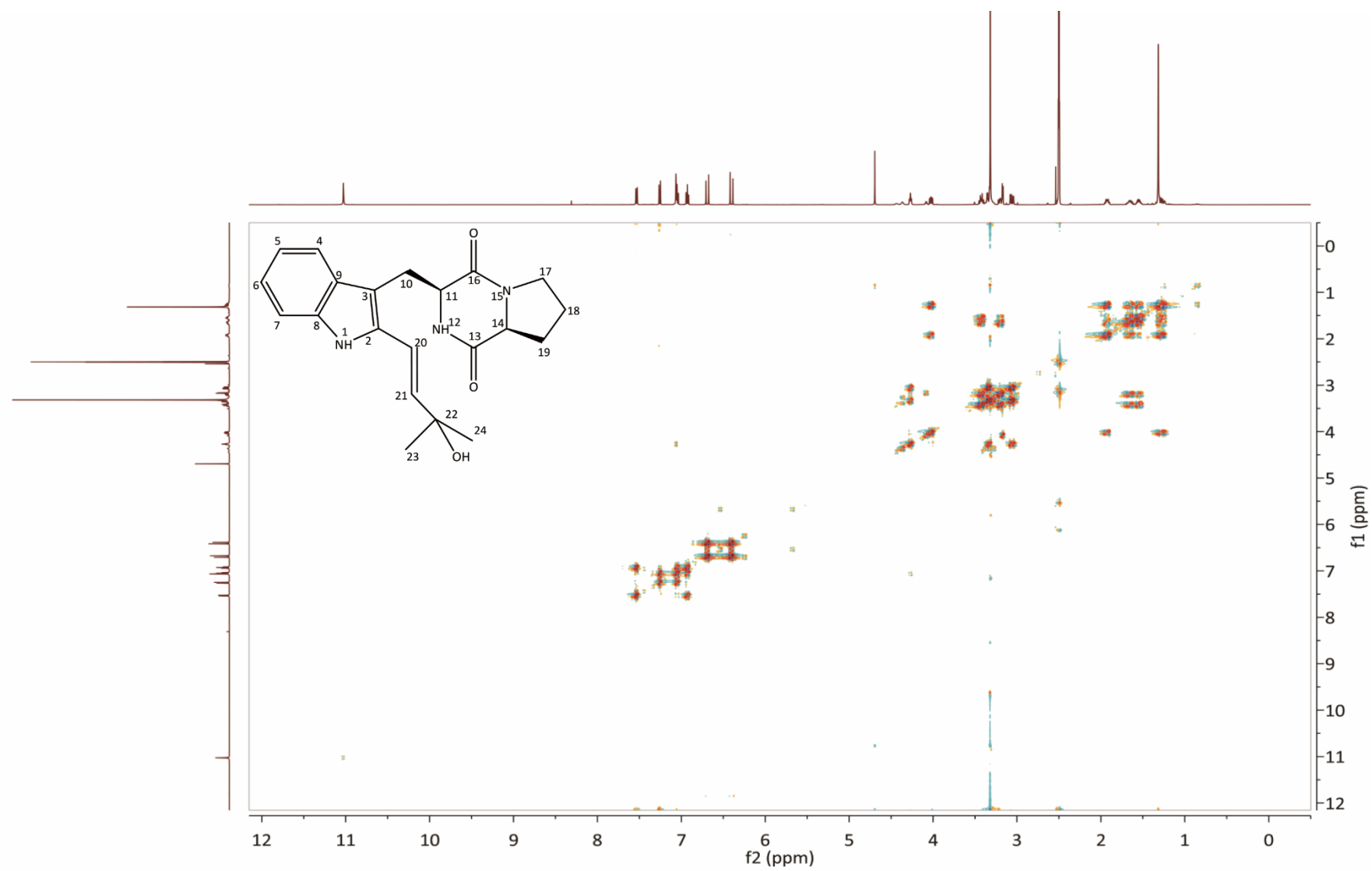
Figure S8. ^{1}H-^{1}H COSY spectrum of 22-hydroxylisotryprostatin B (**2**) in DMSO-d_6
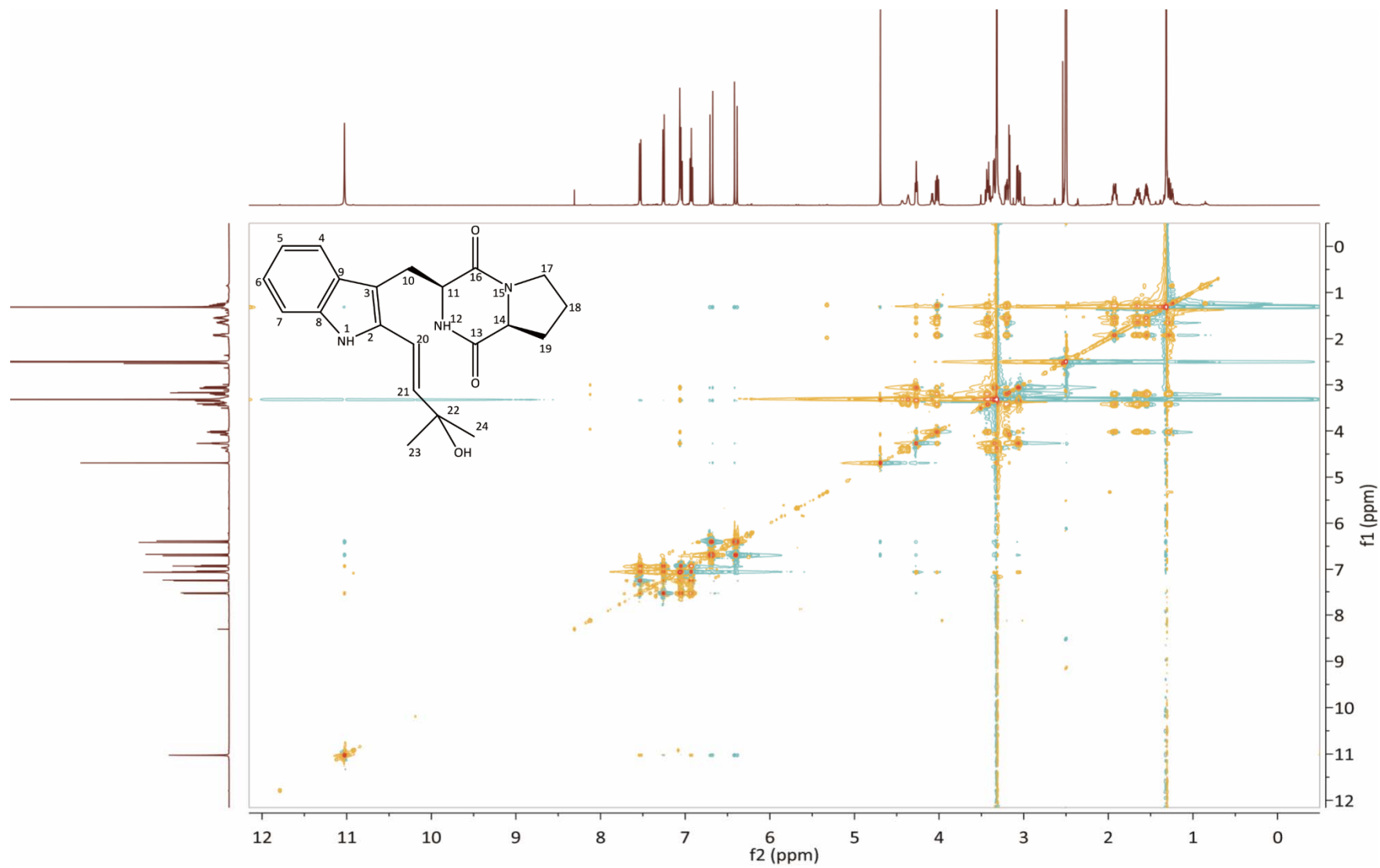
Figure S9. ^{1}H-^{1}H TOCSY spectrum of 22-hydroxylisotryprostatin B (**2**) in DMSO-d_6

S15
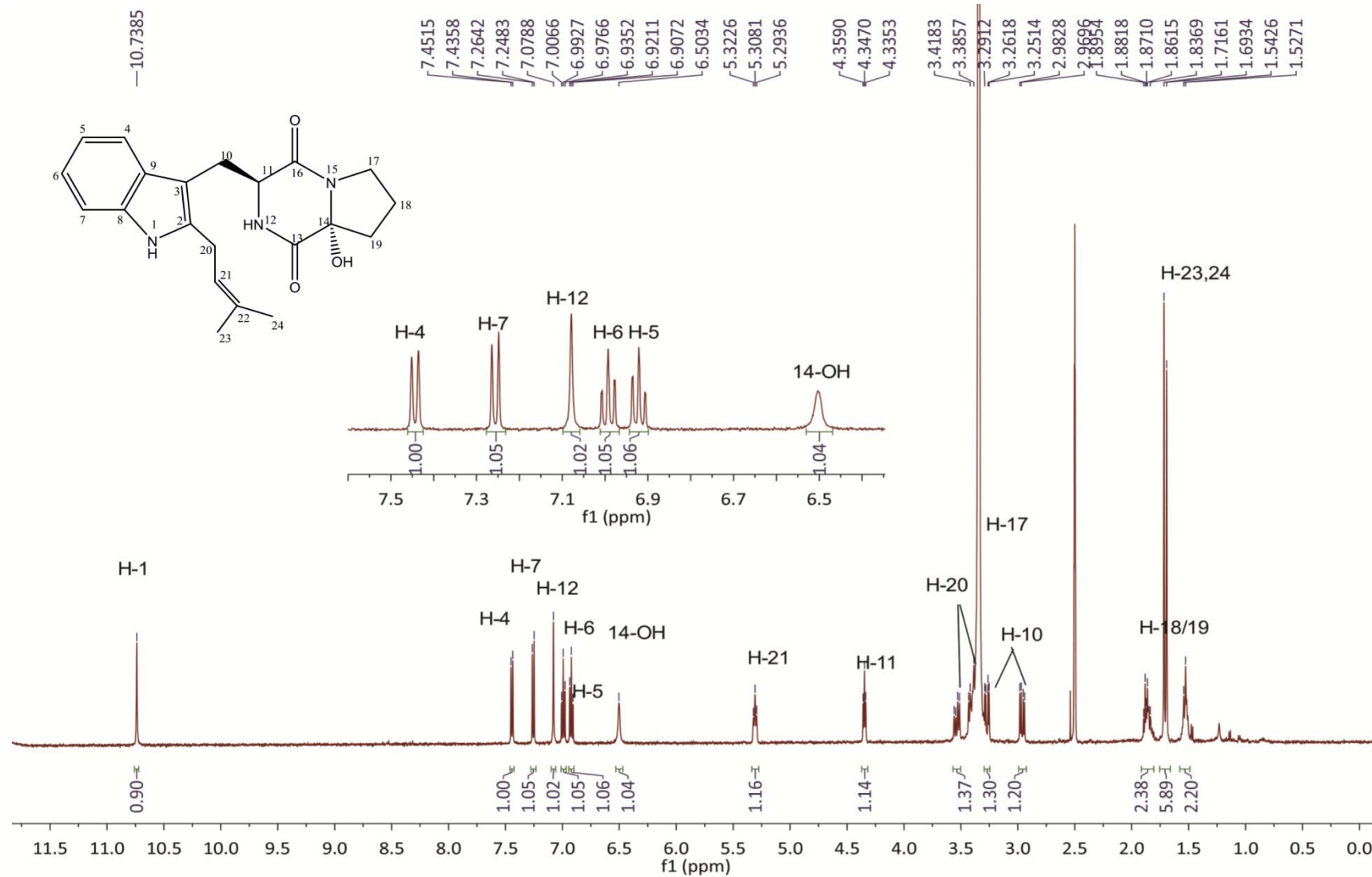
Figure S10. ^{1}H NMR spectrum of 14α-hydroxylisotryprostatin B (**3**) in DMSO-d_6 (500 MHz)

S16
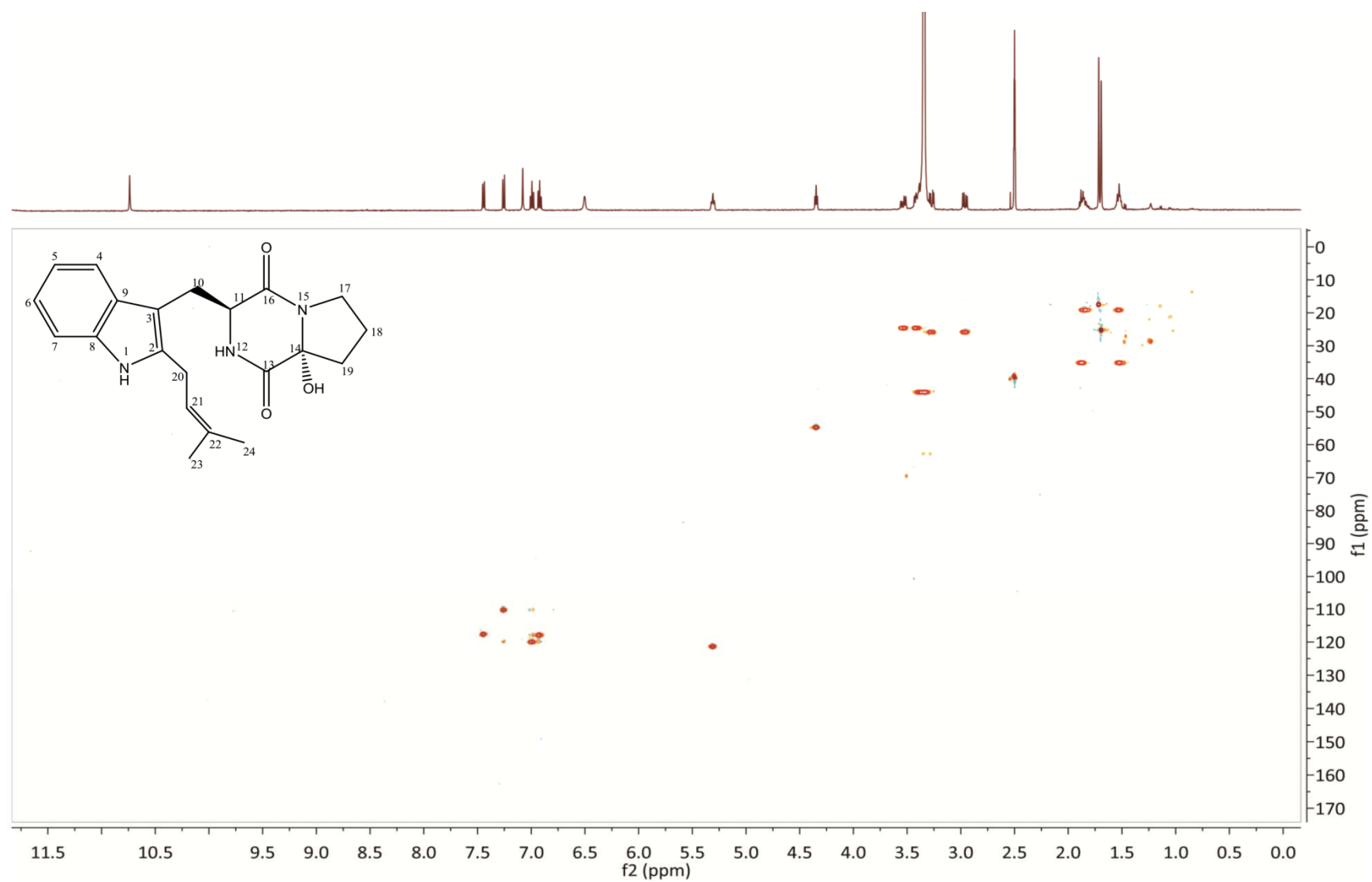
Figure S11. HSQC spectrum of 14α-hydroxylisotryprostatin B (**3**) in DMSO-d_6

S17
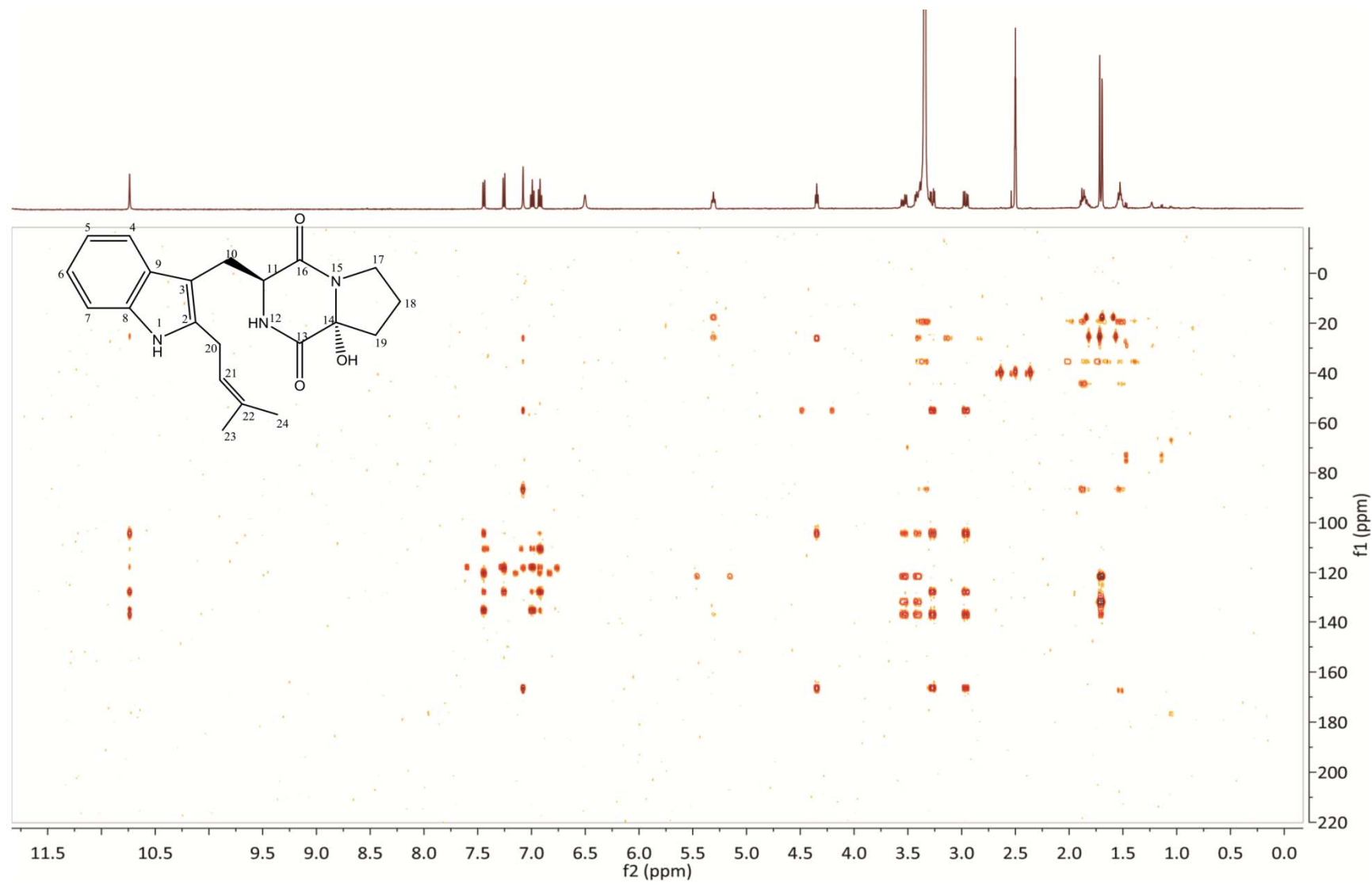
Figure S12. HMBC spectrum of 14α-hydroxylisotryprostatin B (**3**) in DMSO-d_6
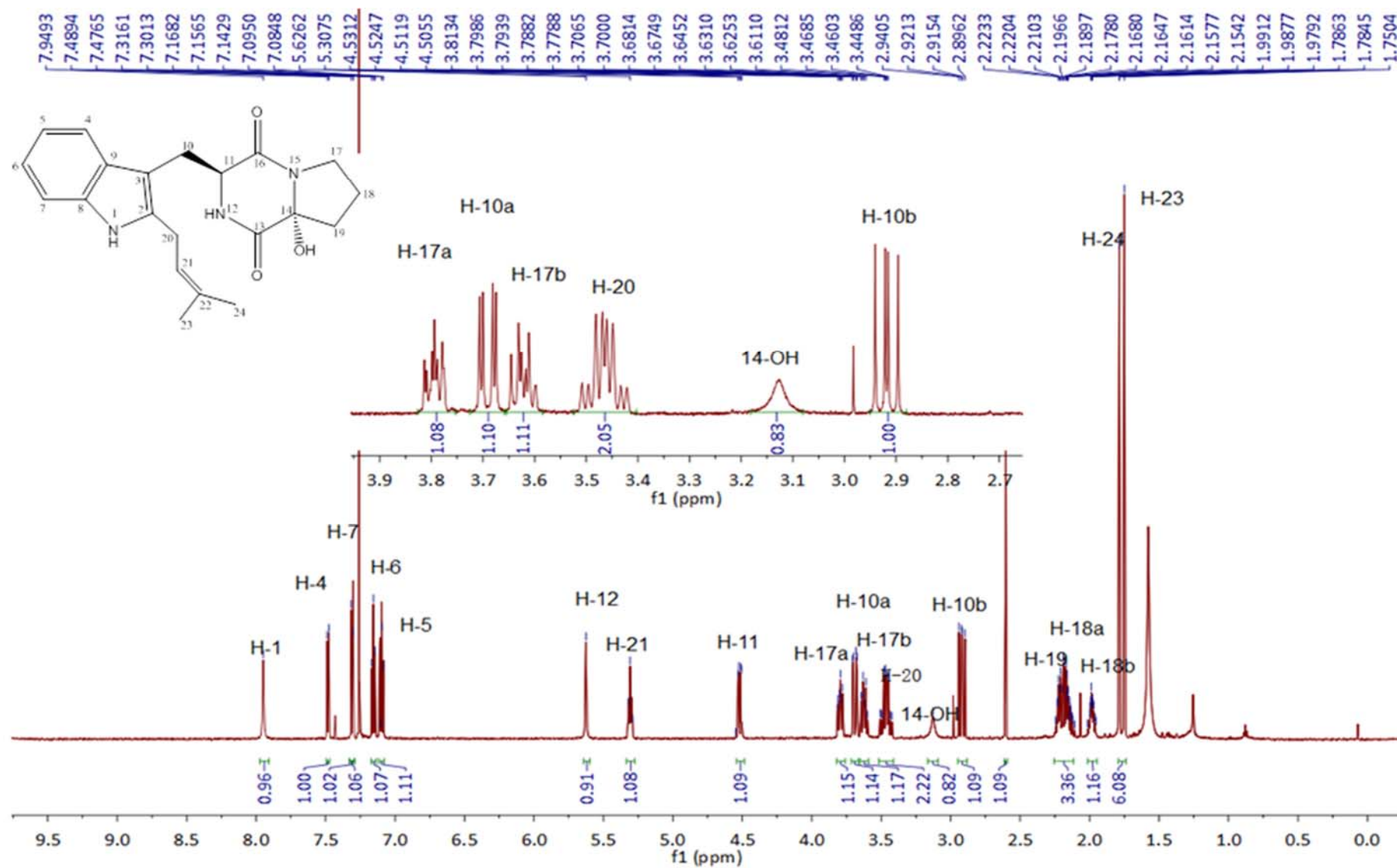
Figure S13. ^1H NMR spectrum of 14α-hydroxylisotryprostatin B (**3**) in CDCl$_3$ (500 MHz)

S19
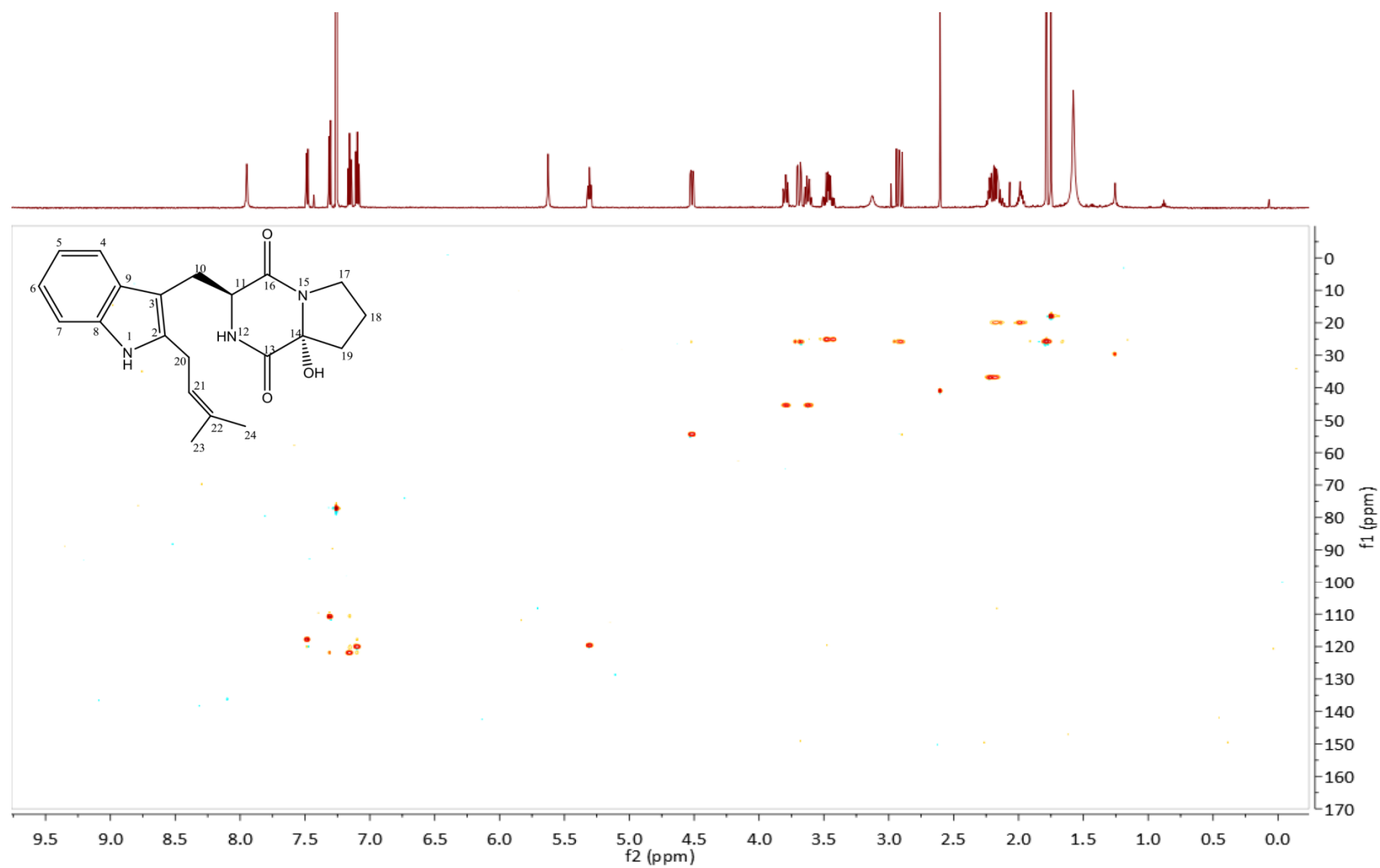
Figure S14. HSQC spectrum of 14α-hydroxylisotryprostatin B (**3**) in CDCl₃
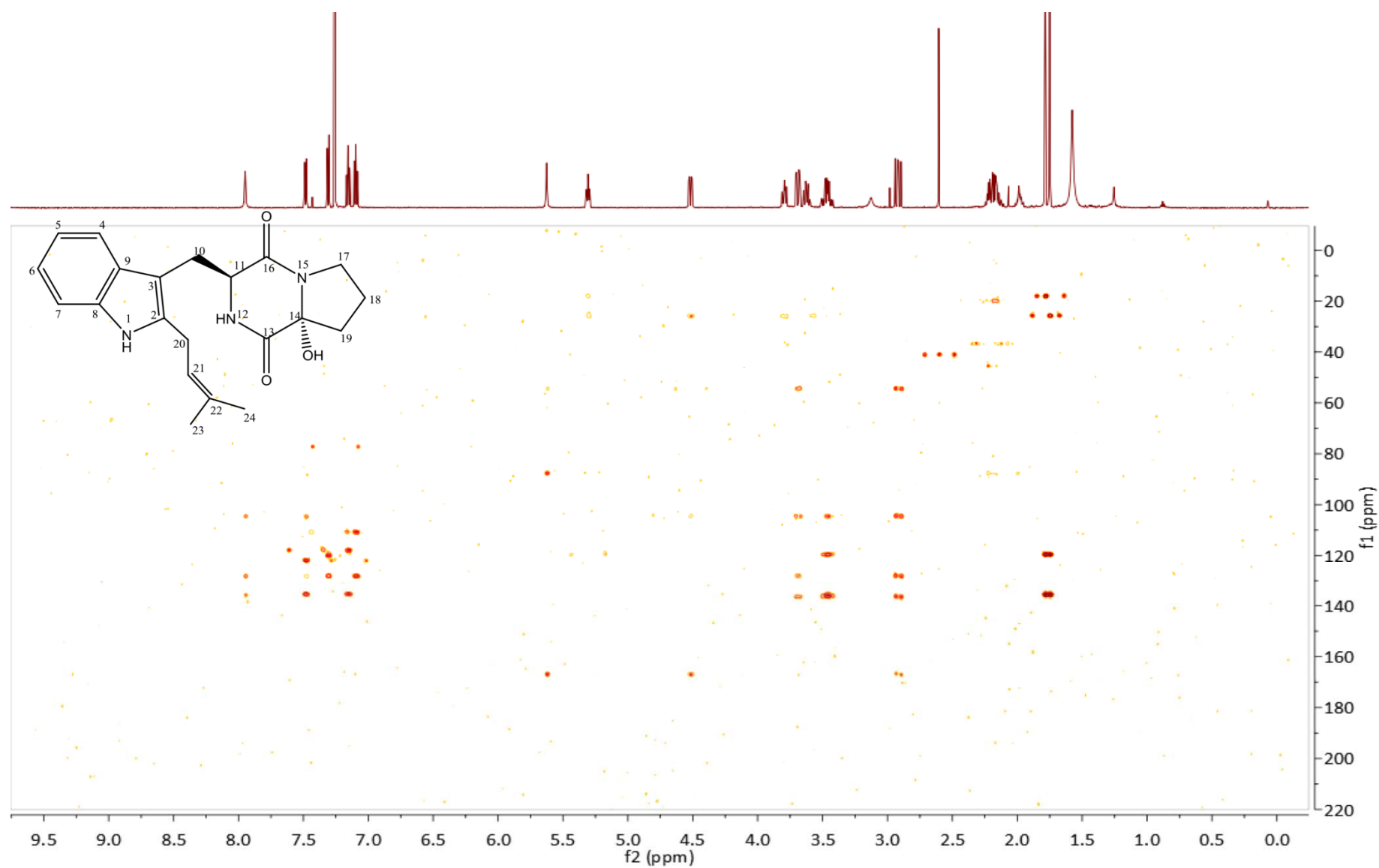
Figure S15. HMBC spectrum of 14α-hydroxylisotryprostatin B (**3**) in CDCl$_3$
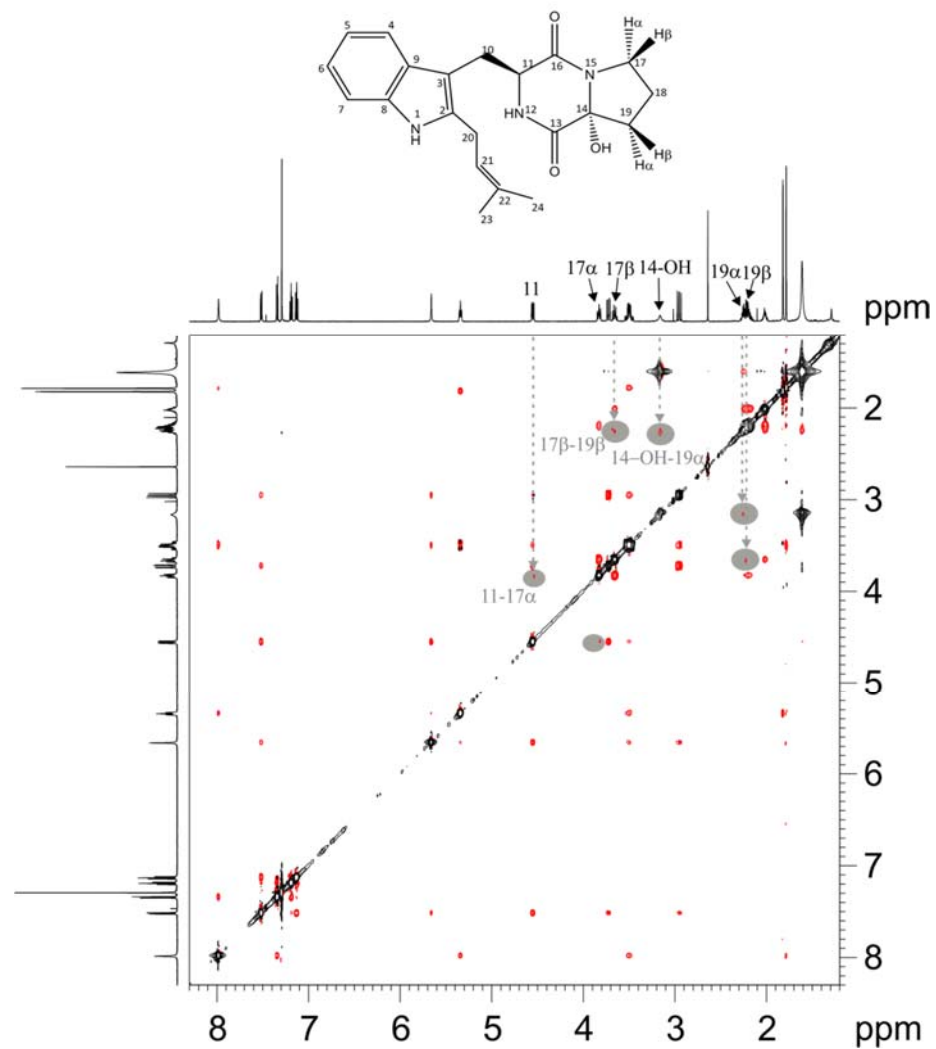
Figure S16. ¹H-¹H NOESY spectrum of 14α-hydroxylisotryprostatin B (**3**) in CDCl₃
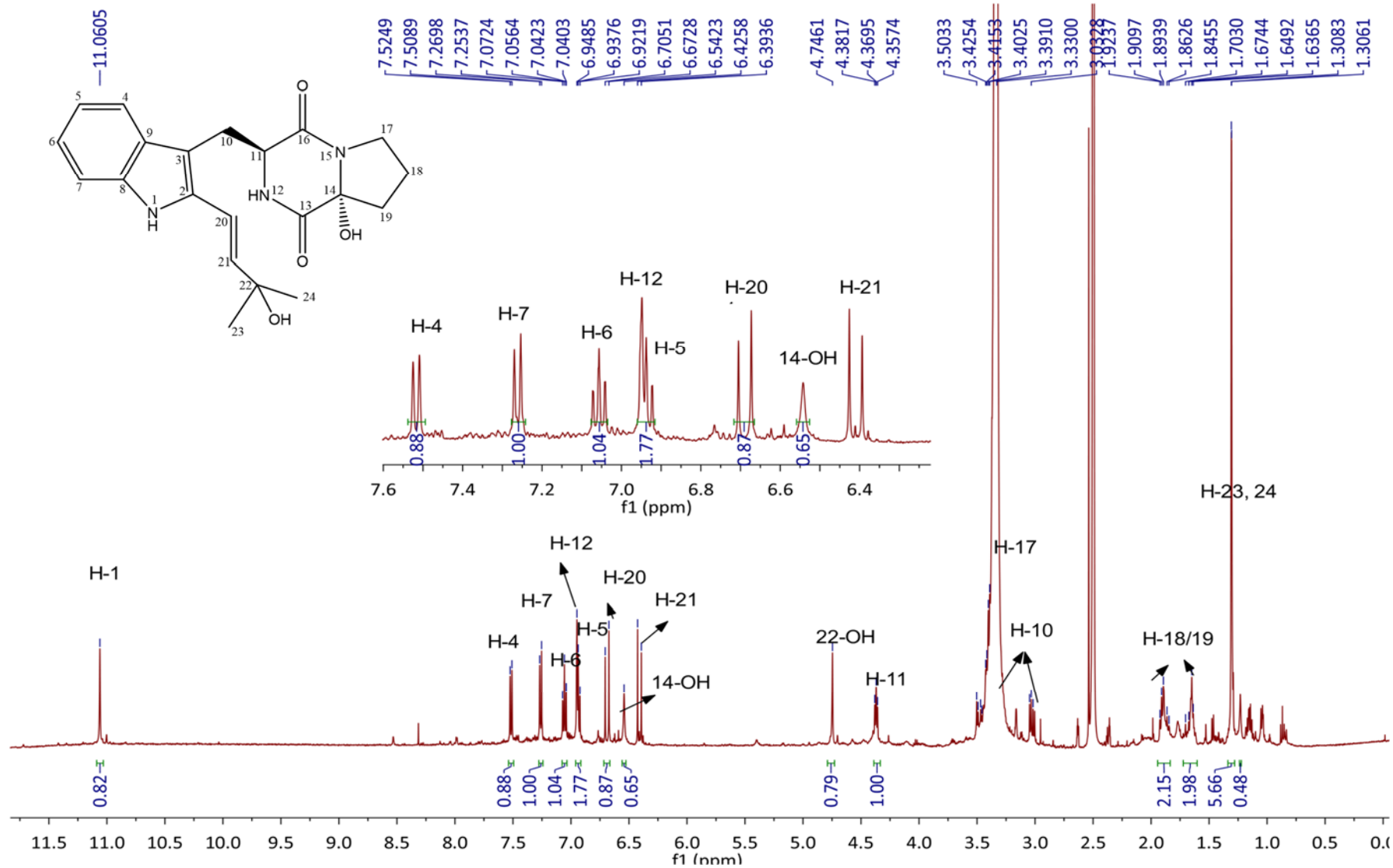
Figure S17. ¹H NMR spectrum of 14α,22-dihydroxylisotryprostatin B (**4**) in DMSO-*d₆* (500 MHz)
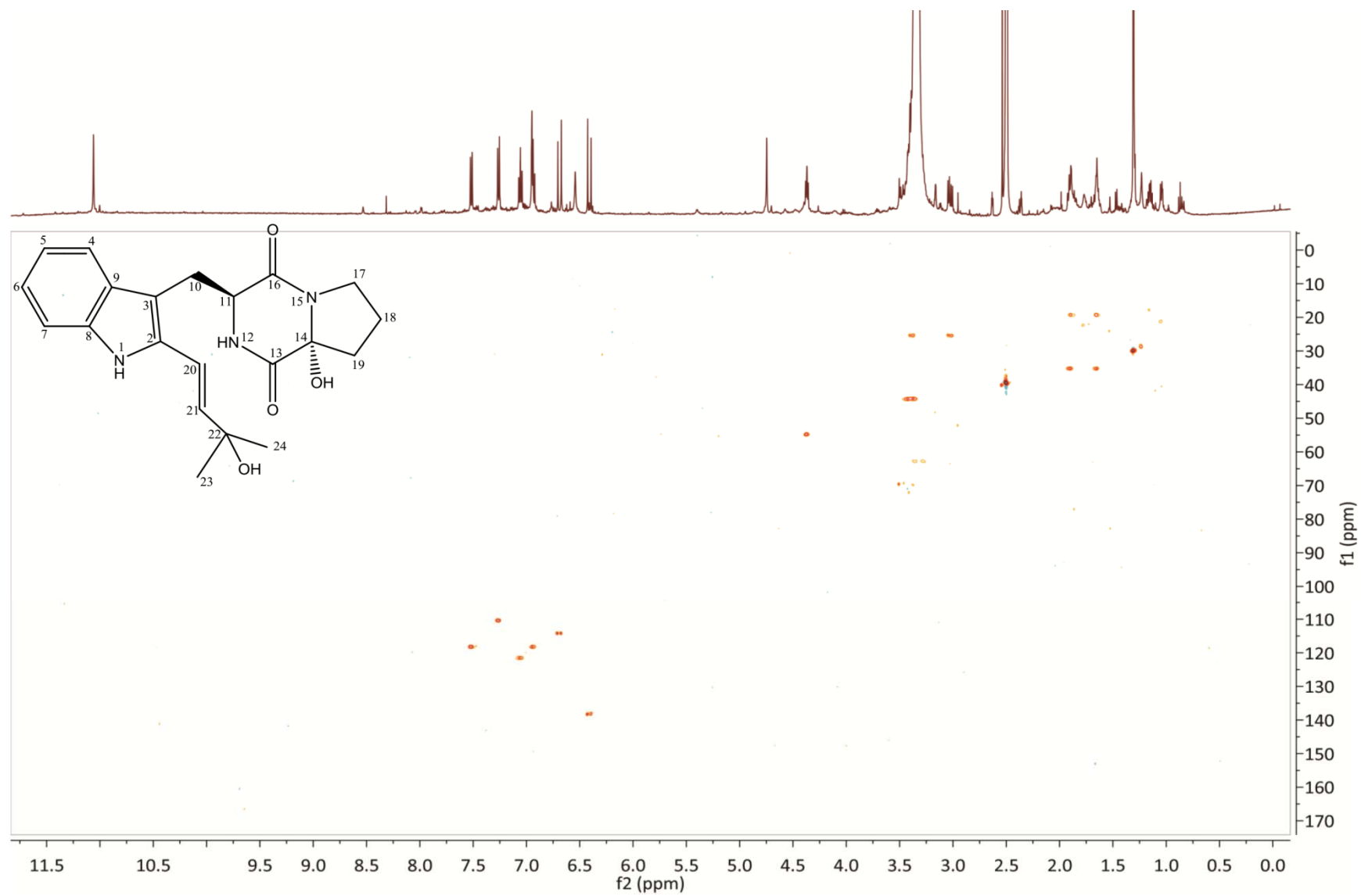
Figure S18. HSQC NMR spectrum of 14α,22-dihydroxylisotryprostatin B (**4**) in DMSO-d_6

S24
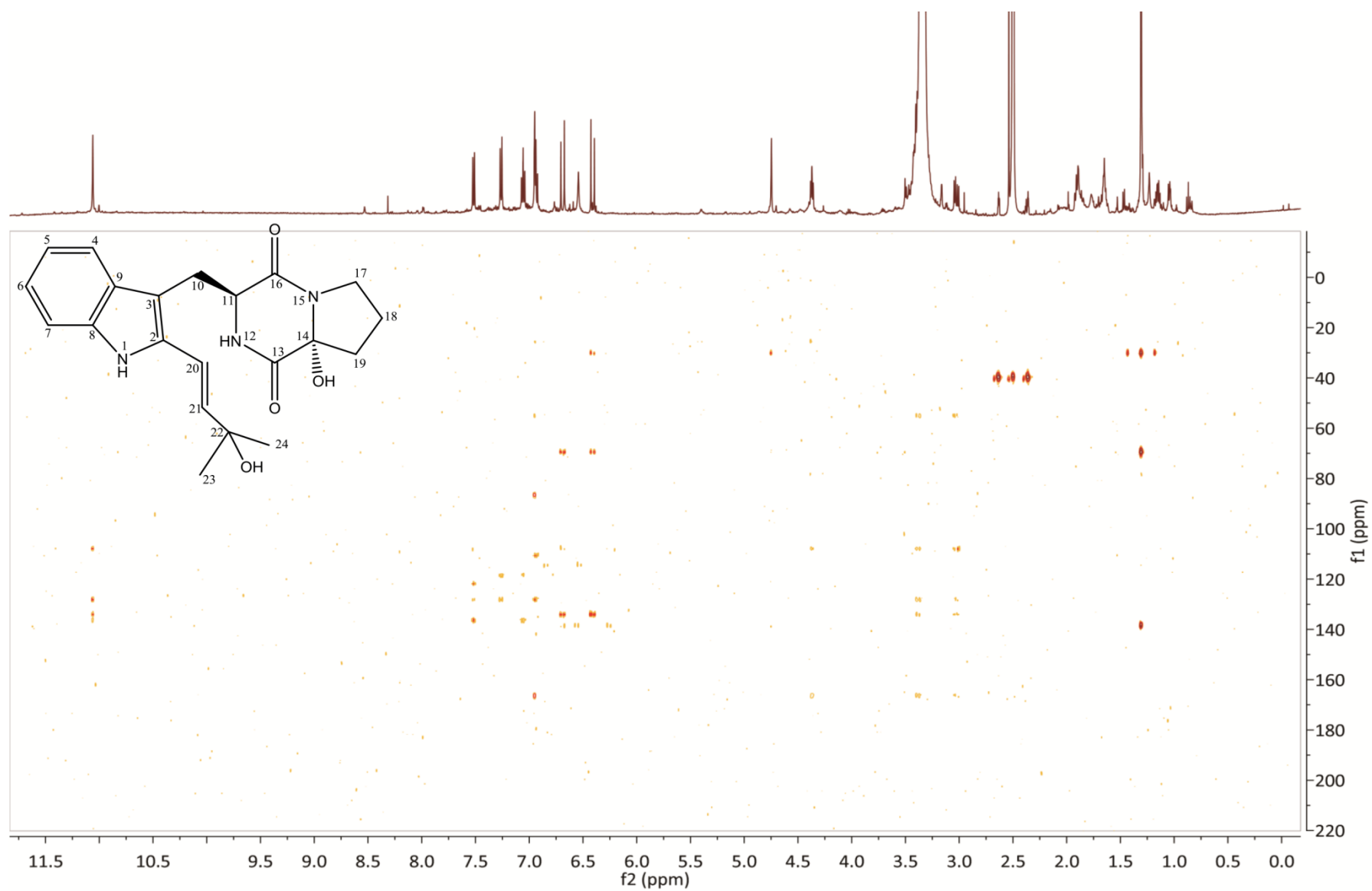
Figure S19. HMBC spectrum of 14α,22-dihydroxylisotryprostatin B (**4**) in DMSO-d_6

S25
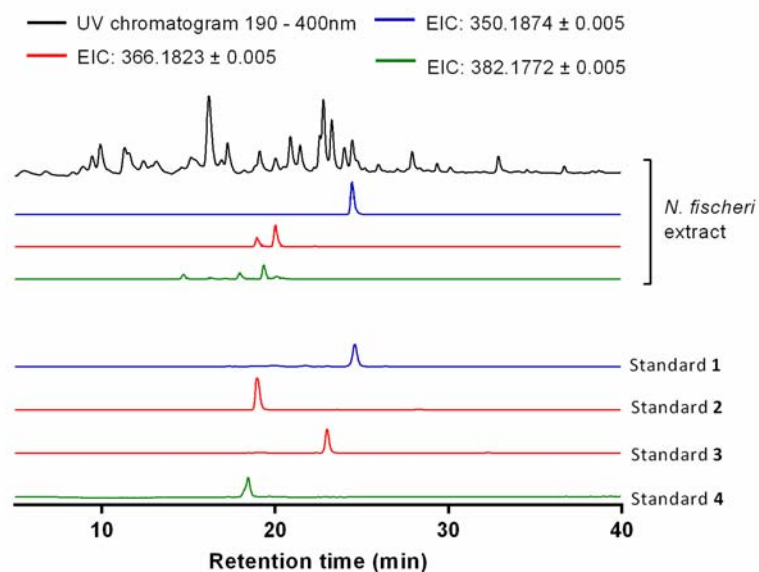
Figure S20. LC-MS analysis of the fungal extract of *N. fischeri*. Detection was carried out at UV 190−400 nm and EIC for [M-H]⁻ ions of **1**, **2**, **3**, and **4**. The isolated enzyme products were used as standards.

1 and **2** were clearly detected in the extract by comparison of their retention times, [M-H]⁻ ions and fragmentation patterns in MS² with those of standards (Figure S21). An additional peak in EIC of 366.1823 was found with a larger retention time than that of **2**. The identity of this peak cannot be proven in this study. No peak in EIC of 382.1772 shares a same retention time with **4**.

S26
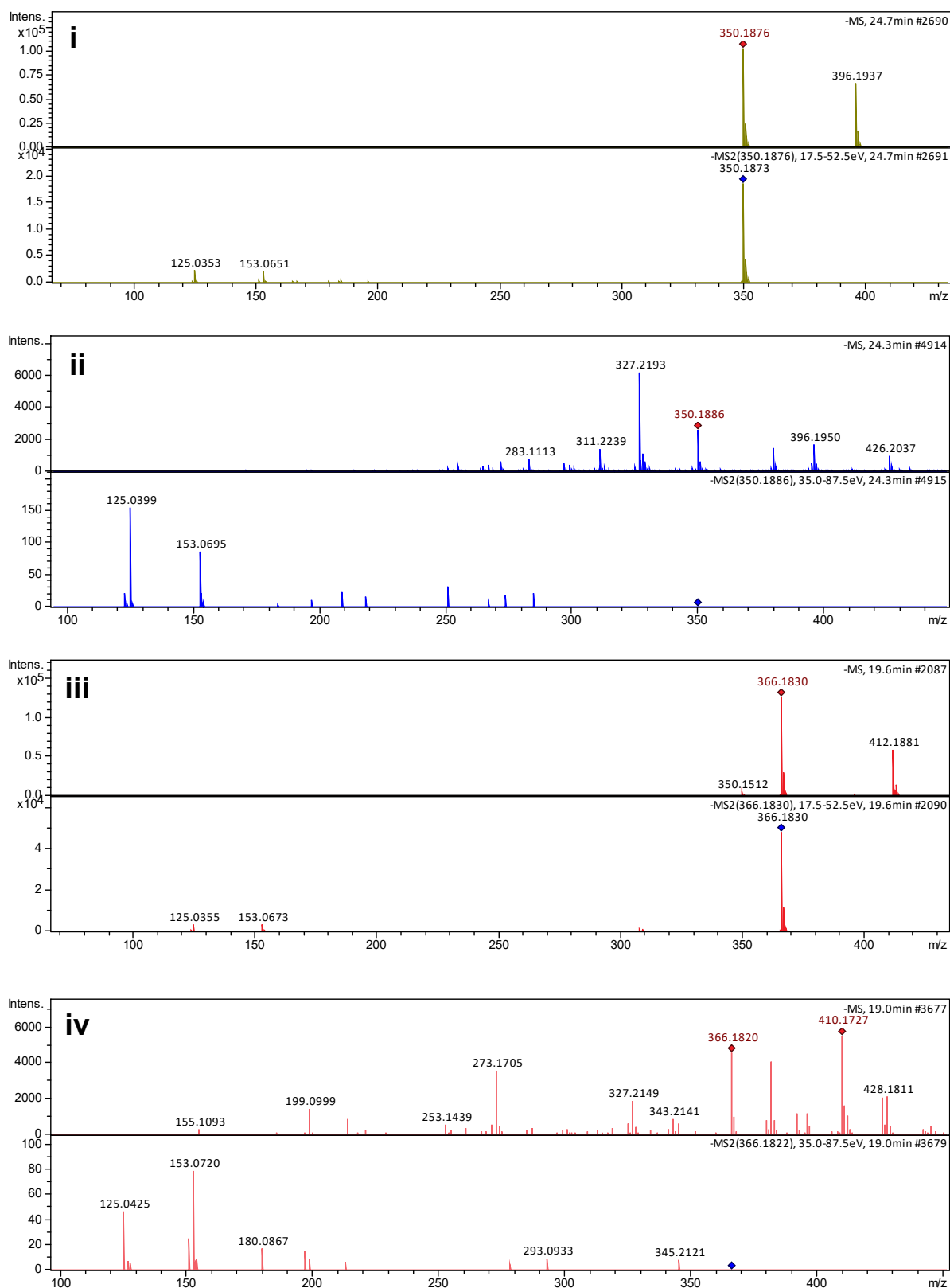
Figure S21. MS and MS^2 spectra of standard **1** (i), compound **1** in extract (ii), standard **2** (iii), and compound **2** in extract (iv). The isolated enzyme products were used as standards.
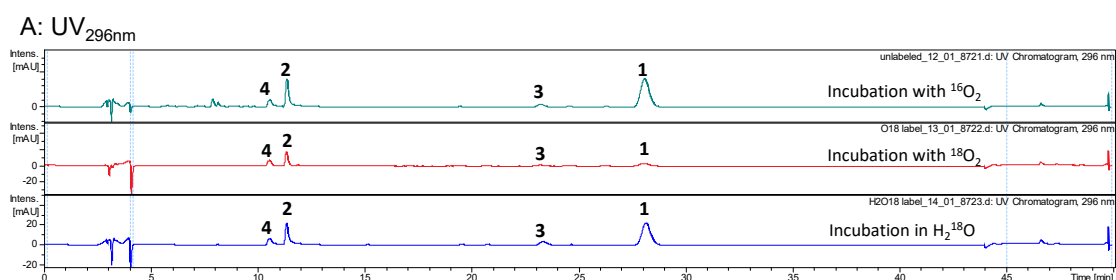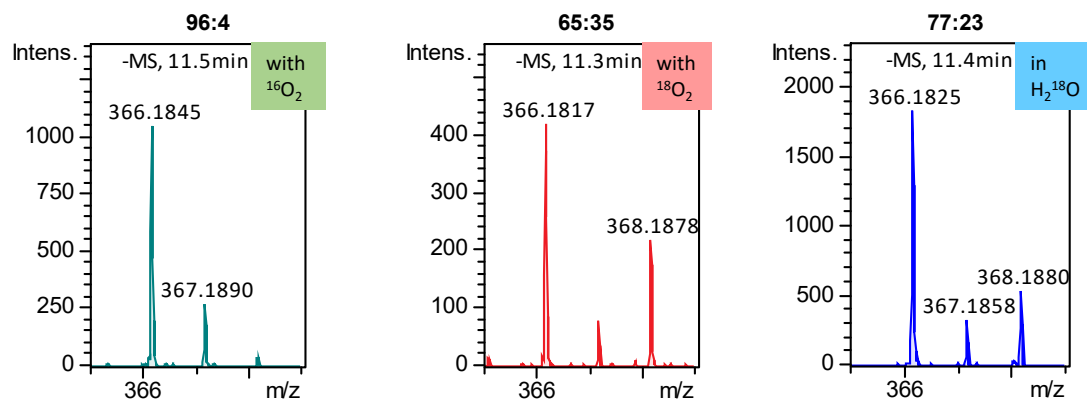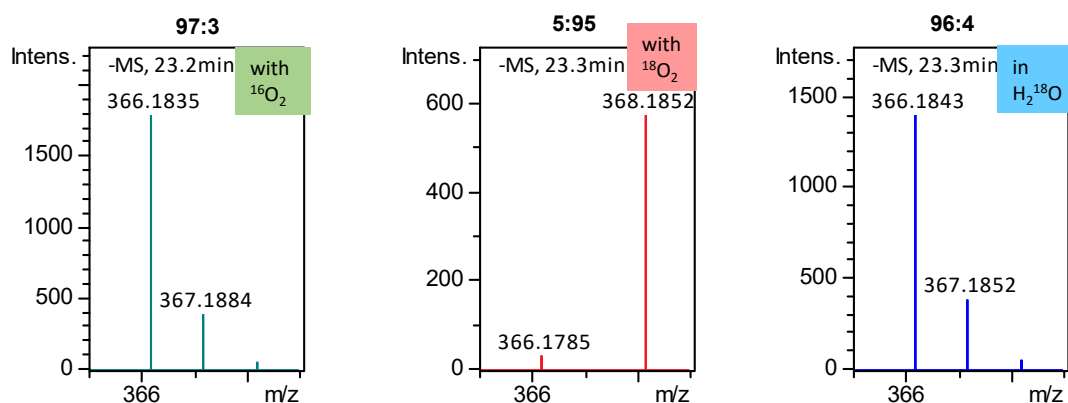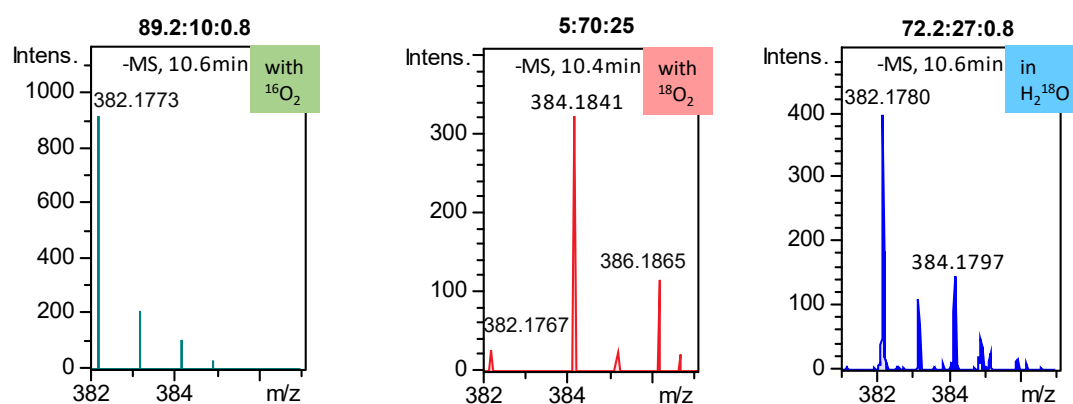
Figure S22. LC-MS analysis of the incubation mixtures of **1** in the presence of $^{16}O_2$, $^{18}O_2$-enriched atmosphere, and ^{18}O-enriched water. A) UV absorptions at 296 nm; C–D) Compared mass spectra of **2−4**.

References

(1) Goujon, M., McWilliam, H., Li, W.Z., Valentin, F., Squizzato, S., Paern, J., and Lopez, R. (2010) A new bioinformatics analysis tools framework at EMBL-EBI, *Nucleic Acids Res. 38*, W695-W699.

(2) Robert, X., and Gouet, P. (2014) Deciphering key features in protein structures with the new ENDscript server, *Nucleic Acids Res. 42*, W320-W324.

(3) Steffan, N., Grundmann, A., Afiyatullov, A., Ruan, H., and Li, S.-M. (2009) FtmOx1, a non heme Fe(II) and alpha-ketoglutarate-dependent dioxygenase, catalyses the endoperoxide formation of verruculogen in *Aspergillus fumigatus*, *Org. Biomol. Chem. 7*, 4082-4087.

4.2 Spontaneous oxidative cyclisations of 1,3-dihydroxy-4-dimethylallylnaphthalene to tricyclic derivatives

COMMUNICATION

Check for updates

Spontaneous oxidative cyclisations of 1,3-dihydroxy-4-dimethylallylnaphthalene to tricyclic derivatives†

Jinglin Wang,‡[a,b] Huomiao Ran,‡[a] Xiulan Xie,[c] Kaiping Wang [d] and Shu-Ming Li [a]*[a]

The attachment of a dimethylallyl moiety to C4 of 1,3-dihydroxynaphthalene led to spontaneous oxidative cyclisations, resulting in the formation of two tetrahydrobenzofuran and one bicyclo[3.3.1] nonane derivatives. Incubation under an ^{18}O-rich atmosphere proved that both the incorporated oxygen atoms originated from O_2. A radical-involved mechanism is proposed for these cyclisations.

Prenylated natural products are hybrid molecules with an aliphatic or aromatic skeleton, with one or more prenyl moieties of different chain lengths derived from dimethylallyl, geranyl or farnesyl diphosphate. The formation of these compounds is usually initialised by prenyl transfer reactions and further modified by oxidation, hydroxylation, cyclisation and even rearrangement.[1–3] Prenylated naphthalene derivatives, especially those of 1,3,6,8-tetrahydroxynaphthalene (THN), have been reported to show intriguing biological and pharmacological activities.[4–6] Cyclisation reactions between the prenyl moieties and hydroxyl groups in THN often led to the formation of a five- or six-numbered ring system.[4,7–10] As shown in Fig. 1, derivatives of both C2- and C4-prenylated THN are identified in nature. Furanonaphthoquinone I,[11] furaquinocins[12] and adenaflorin D[10] belong to the first group. In the formation of these compounds, the nucleophilic attack of one of the *ortho*-hydroxyl groups on the prenyl residue, at C1 or C3, leads to cyclisation and formation of a 2*H*-furan or 2*H*-pyran

ring. Some of the metabolites like adenaflorin C[10] are the cyclisation products of C4-prenylated THNs. Naphterpin[13,14] and marinone analogues[6,9] carrying a modified C3-prenyl moiety originate from a C4-prenylated intermediate, which is formed by oxidative dearomatization and α-hydroxyketone rearrangement.[15] Enzymatic and nonenzymatic reactions are involved in the formation of these prenylated natural products. It seems that complex rearrangement takes place easily in C4-prenylated THNs. Therefore, we were curious to know the behaviour of a C4-prenylated naphthalene with merely two *meta*-hydroxyl groups. In a previous study,[16] we demonstrated prenylations of 12 hydroxynaphthalenes by eight fungal prenyltransferases. In this study, we prepared C4-prenylated 1,3-dihydroxynaphthalene and investigated its stability under mild conditions.

For this purpose, the tryptophan prenyltransferase FgaPT2 was produced in *E. coli* and purified to near homogeneity as reported previously.[17] The recombinant protein was then incubated with 1,3-dihydroxynaphthalene (**1**) in the presence of dimethylallyl diphosphate (DMAPP) at 37 °C for 30 min. The reaction mixture was analysed by HPLC. As shown in Fig. 2A, a peak was detected for product **2** at 33.6 min. LC-HRMS analysis showed the presence of an $[M + H]^+$ ion at m/z 229.1224, corresponding to a mono-prenylated product with the mole-

[a]*Institut für Pharmazeutische Biologie und Biotechnologie,*
Philipps-Universität Marburg, Robert-Koch-Straße 4, 35037 Marburg, Germany.
E-mail: shuming.li@staff.uni-marburg.de
[b]*Union Hospital of Huazhong University of Science and Technology,*
Department of Pharmacy, No. 1227, Jiefang Road, 430030 Wuhan, China
[c]*Fachbereich Chemie, Philipps-Universit-t Marburg, Hans-Meerwein-Straße 4,*
35032 Marburg, Germany
[d]*Hubei Key Laboratory of Nature Medicinal Chemistry and Resource Evaluation,*
Tongji Medical College of Pharmacy, Huazhong University of Science and
Technology, 430030 Wuhan, China
†Electronic supplementary information (ESI) available: MS and NMR data and
spectra. See DOI: 10.1039/d0ob00354a
‡These authors contributed equally to this work.
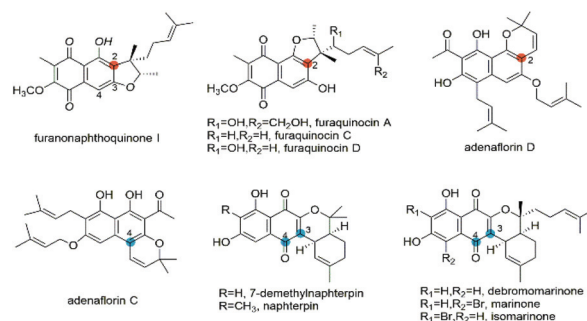
Fig. 1 Representative examples of prenylated THN derivatives.

2646 | *Org. Biomol. Chem.*, 2020, **18**, 2646–2649

85

This journal is © The Royal Society of Chemistry 2020
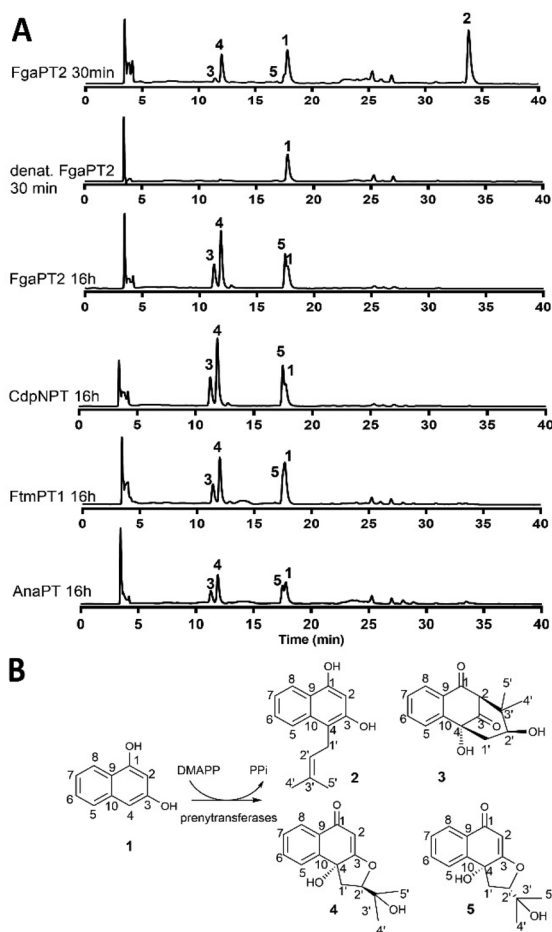
Fig. 2 HPLC chromatograms of the incubation mixtures of 1,3-dihydroxynaphthalene (**1**) with 20 µg purified recombinant FgaPT2, CdpNPT, FtmPT1 and AnaPT in the presence of DMAPP (A) and structures of **1–5** (B). Detection was carried out on a photo diode.

cular formula $C_{15}H_{16}O_2$ (see Table S1 in the ESI†). Interpretation of the HMBC spectrum of **2** confirmed the attachment of the dimethylallyl moiety to C4 of the naphthalene ring. Key correlations of H-1′ of the prenyl residue with C-3, C-4 and C-10 were clearly detected (Table S2 and Fig. S1–S4†). Interestingly, three additional products **3**, **4** and **5** were also observed at 11.2, 11.8 and 17.5 min, respectively. No peaks for **2–5** were detected in the negative control with denatured FgaPT2, indicating the necessity of the active enzyme for their formation. Upon extending the incubation time to 16 h, products **3**, **4** and **5** were detected, but not **2**.

From their $[M + H]^+$ ions at m/z 261.1126 (**3**), 261.1129 (**4**) and 261.1127 (**5**) (Table S1†), it can be deduced that they shared the same molecular formula of $C_{15}H_{16}O_4$, indicating the incorporation of two oxygen atoms into **2**. In the ^1H NMR spectra of **3**, **4** and **5** (NMR data of **3**, **4** and **5** are given in Tables S2–S5† and their spectra are shown in Fig. S5–S23†), the signals of the four coupling protons at C5–C8 are still present, indicating that no changes have taken place on this ring. In contrast, signals of two alcoholic hydroxyl groups at δ_H

4.7–7.0, instead of those of two phenolic protons at δ_H 9.3 and 9.9 in **2**, were detected. The signals at δ_C 124.5 and 129.7 for the olefinic carbons C2′ and C3′ of the dimethylallyl moiety of **2** also disappeared in the ^{13}C NMR spectra of **3**, **4** and **5**. Instead, signals of two ketone carbons at δ_C 194 and δ_C 205 were observed in the ^{13}C NMR spectrum of **3**. A comprehensive analysis of the HSQC and HMBC data confirmed that **3** is a bicyclo[3.3.1]nonane derivative (Fig. 2B). Similarly, signals of two oxygenated carbons in the range of δ_C 65 to 92 were found in the ^{13}C spectra of **4** and **5** and can be assigned to those of C2′ and C3′ of the original dimethylallyl moiety in **2**. Inspection of the HSQC and HMBC data suggested that **4** and **5** are tetrahydrobenzofuran derivatives, which differ from each other only in their stereochemistry. Analysis of the NOESY data and relevant coupling constants confirmed the relative configurations of **3**, **4** and **5**, as given in Fig. 2B.

We wondered whether the formation of **3**, **4** and **5** is specific for the FgaPT2 reaction. **1** was then incubated at 37 °C with DMAPP and three additional prenyltransferases CdpNPT, FtmPT1 and AnaPT[18–20] for 16 h. **3**, **4** and **5**, but not **2**, were detected in all the reaction mixtures (Fig. 2A).

To investigate whether **3**, **4** and **5** are the enzyme products of the prenyltransferases or just nonenzymatic rearrangement
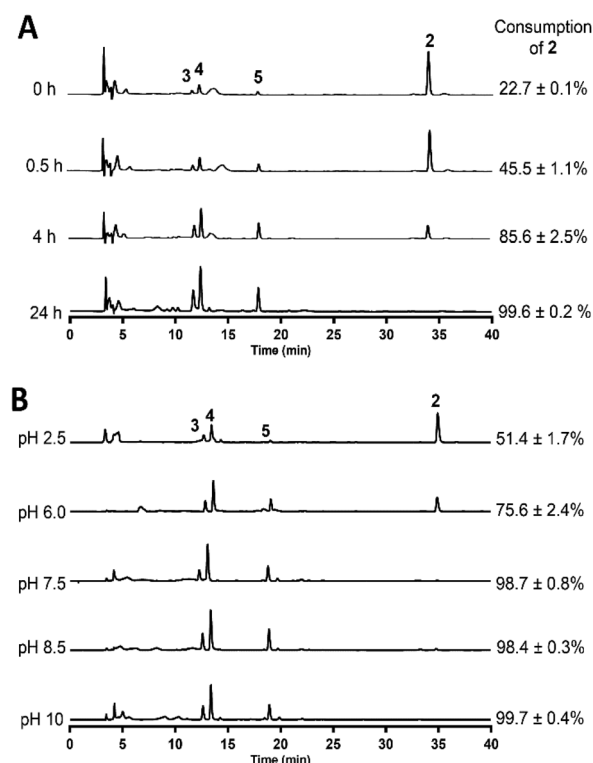
Fig. 3 HPLC chromatograms of the incubation mixtures of **2** and the denatured enzyme. The reaction mixtures were incubated in Tris buffer (pH 7.5) at 37 °C for 0, 0.5, 4 and 24 h (A) or in phosphate buffer at pH 2.5, 6.0, 7.5, 8.5 and 10.0 for 1 h (B). Detection was carried out with a photo diode array detector and absorption at 254 nm is shown. The data were obtained from three independent experiments.

This journal is © The Royal Society of Chemistry 2020

86

Org. Biomol. Chem., 2020, **18**, 2646–2649 | **2647**

events of **2**, the isolated **2** was incubated with denatured recombinant FgaPT2 at 37 °C.

The reaction mixture was monitored using LC-HRMS after 0, 0.5, 4 and 24 h. As shown in Fig. 3A, 22.7 ± 0.1% of **2** was already converted to **3**, **4** and **5** after isolation from enzyme assay and sample dissolving for analysis (at 0 h). No trace of **2** was detected after incubation for 24 h, unequivocally proving

the nonenzymatic spontaneous oxidative cyclisations of **2** to **3**, **4** and **5**. Incubation of **2** in phosphate buffer at pH 2.5, 6.0, 7.5, 8.5 and 10.0 (Fig. 3B) revealed the pH dependence of this conversion. The conversions of **2** to **3**, **4** and **5** under acidic conditions were clearly slower than those under neutral and basic conditions. 51.4 ± 1.7% and 75.6 ± 2.4% of **2** were converted at pH 2.5 and 6.0, respectively, after incubation at 37 °C
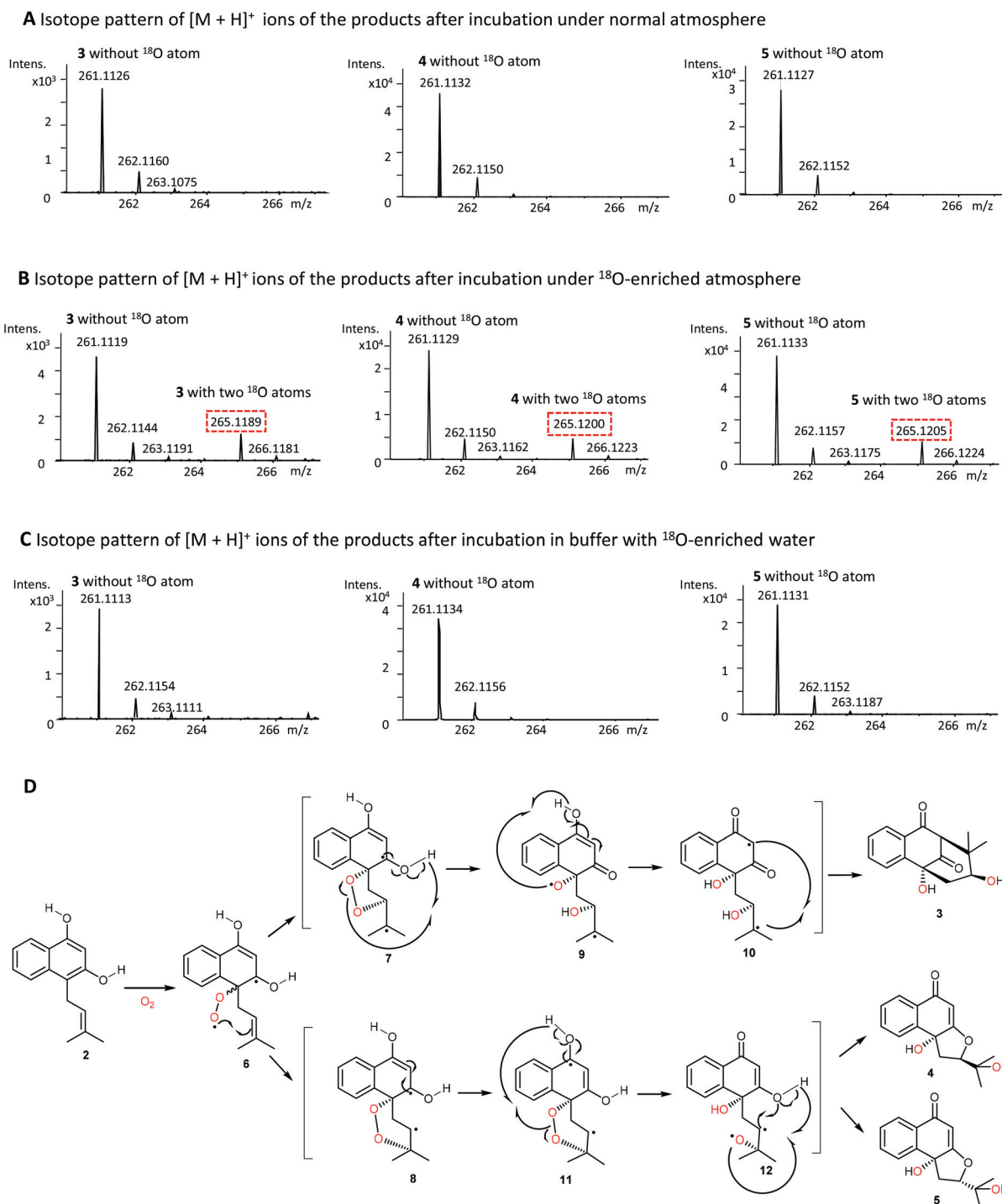
Fig. 4   Mass spectra of **3**, **4** and **5** from different incubation mixtures (A–C) and the proposed cyclisation mechanism (D).

for 1 h. In comparison, approx. 99% of **2** was consumed at pH 7.5 and higher pH values (Fig. 3B).

To clarify the origin of the two incorporated oxygen atoms, FgaPT2 assays with 1,3-dihydroxynaphthalene (**1**) and DMAPP were carried out under an $^{18}O_2$-rich atmosphere and in a buffer with ^{18}O-rich water, as reported previously.[21,22] Incubation of FgaPT2 without isotope labelled components was used as a control. LC-HRMS analysis revealed complete conversion of **1** to **3**, **4** and **5** in all the three assays (Fig. S24†). As mentioned above, $[M + H]^+$ ions at m/z 261.112 ± 0.002 were detected for **3**, **4** and **5** in the control assay and in the incubation mixture with $H_2^{18}O$ (Fig. 4A and C). In the incubation mixture under an ^{18}O-rich atmosphere, incorporation of two oxygen-18 atoms each was confirmed in **3**, **4** and **5** by detection of the isotope peaks of their $[M + H]^+$ ions at m/z 265.120 ± 0.002, in addition to the ions at m/z 261.112 ± 0.002. Incorporation rates of approximately 15% were calculated (Fig. 4B). These results undoubtedly proved that the two oxygen atoms originated from molecular O_2 without any involvement of water.

It can be proposed that the attachment of one O_2 molecule to C4 of the C4-prenylated 1,3-dihydroxynaphthalene initialises the cyclisation process (Fig. 4D). The reactive peroxyl radical **6** can undergo radical addition at both the olefinic positions of the dimethylally moiety, leading to the formation of two different bi-radicals **7** and **8** with endoperoxide features. Cleavage of the endoperoxide structure and radical shift in **7** and **9** as well as subsequent intramolecular cyclisation in **10** would result in the formation of **3**. The fate of radical **8** begins with an electron shift. Cleavage of the endoperoxide bond in **11** would be followed by furan ring formation in **12**, resulting in two diastereomers **4** and **5**. From the postulated mechanism, products of intermolecular coupling could also be expected. However, no such compounds were detected under the conditions used in this study.

In summary, in this study, we isolated three new compounds **3**, **4** and **5** with tetrahydrobenzofuran and a bicyclo[3.3.1]nonane core using prenyltransferase assays. Detailed investigations including isotope labelling experiments proved that they are spontaneous oxidative cyclisation products of 1,3-dihydroxy-4-dimethylallylnaphthalene **2**. This study provides one additional example of natural product formation by contributions from enzymatic and nonenzymatic spontaneous reactions.

Conflicts of interest

The authors declare no competing financial interest.

Acknowledgements

Notes and references

1 S.-M. Li, *Appl. Microbiol. Biotechnol.*, 2009, **84**, 631–639.
2 J. Winkelblech, A. Fan and S.-M. Li, *Appl. Microbiol. Biotechnol.*, 2015, **99**, 7379–7397.
3 L. Heide, *Curr. Opin. Chem. Biol.*, 2009, **13**, 171–179.
4 K. Shin-Ya, S. Imai, K. Furihata, Y. Hayakawa, Y. Kato, G. D. Vanduyne, J. Clardy and H. Seto, *J. Antibiot.*, 1990, **43**, 444–447.
5 K. Shiomi, H. Nakamura, H. Iinuma, H. Naganawa, K. Isshiki, T. Takeuchi, H. Umezawa and Y. Iitaka, *J. Antibiot.*, 1986, **39**, 494–501.
6 C. Pathirana, P. R. Jensen and W. Fenical, *Tetrahedron Lett.*, 1992, **33**, 7663–7666.
7 P. Wessels, A. Göhrt, A. Zeeck, H. Drautz and H. Zähner, *J. Antibiot.*, 1991, **44**, 1013–1018.
8 T. Kumano, T. Tomita, M. Nishiyama and T. Kuzuyama, *J. Biol. Chem.*, 2010, **285**, 39663–39671.
9 I. H. Hardt, P. R. Jensen and W. Fenical, *Tetrahedron Lett.*, 2000, **41**, 2073–2076.
10 A. A. Hussein, I. Barberena, T. L. Capson, T. A. Kursar, P. D. Coley, P. N. Solis and M. P. Gupta, *J. Nat. Prod.*, 2004, **67**, 451–453.
11 Y. Haagen, K. Glück, K. Fay, B. Kammerer, B. Gust and L. Heide, *ChemBioChem*, 2006, **7**, 2016–2027.
12 T. Kawasaki, Y. Hayashi, T. Kuzuyama, K. Furihata, N. Itoh, H. Seto and T. Dairi, *J. Bacteriol.*, 2006, **188**, 1236–1244.
13 T. Kumano, S. B. Richard, J. P. Noel, M. Nishiyama and T. Kuzuyama, *Bioorg. Med. Chem.*, 2008, **16**, 8117–8126.
14 K. Shindo, A. Tachibana, A. Tanaka, S. Toba, E. Yuki, T. Ozaki, T. Kumano, M. Nishiyama, N. Misawa and T. Kuzuyama, *Biosci. Biotechnol. Biochem.*, 2011, **75**, 505–510.
15 L. A. M. Murray, S. M. K. McKinnie, H. P. Pepper, R. Erni, Z. D. Miles, M. C. Cruickshank, B. López-Pérez, B. S. Moore and J. H. George, *Angew. Chem., Int. Ed.*, 2018, **57**, 11009–11014.
16 X. Yu, X. Xie and S.-M. Li, *Appl. Microbiol. Biotechnol.*, 2011, **92**, 737–748.
17 N. Steffan, I. A. Unsöld and S.-M. Li, *ChemBioChem*, 2007, **8**, 1298–1307.
18 W.-B. Yin, A. Grundmann, J. Cheng and S.-M. Li, *J. Biol. Chem.*, 2009, **284**, 100–109.
19 A. Grundmann and S.-M. Li, *Microbiology*, 2005, **151**, 2199–2207.
20 J. M. Schuller, G. Zocher, M. Liebhold, X. Xie, M. Stahl, S.-M. Li and T. Stehle, *J. Mol. Biol.*, 2012, **422**, 87–99.
21 H. Ran, V. Wohlgemuth, X. Xie and S.-M. Li, *ACS Chem. Biol.*, 2018, **13**, 2949–2955.
22 N. Steffan, A. Grundmann, A. Afiyatullov, H. Ruan and S.-M. Li, *Org. Biomol. Chem.*, 2009, **7**, 4082–4087.

This journal is © The Royal Society of Chemistry 2020

88

Org. Biomol. Chem., 2020, **18**, 2646–2649 | **2649**

Electronic Supplementary Information (ESI) to

Spontaneous oxidative cyclisations of 1,3-dihydroxy-4-dimethylallylnaphthalene to tricyclic derivatives

Jinglin Wang, [‡a,b] Huomiao Ran, [‡a] Xiulan Xie, [c] Kaiping Wang [d] and Shu-Ming Li [*a]

[a] Institut für Pharmazeutische Biologie und Biotechnologie, Philipps-Universität Marburg, Robert-Koch-Straße 4, 35037 Marburg, Germany. E-Mail: shuming.li@staff.uni-marburg.de.

[b] Union Hospital of Huazhong University of Science and Technology, Department of Pharmacy, No. 1227, Jiefang Road, 430030 Wuhan, China

[c] Fachbereich Chemie, Philipps-Universität Marburg, Hans-Meerwein-Straße 4, 35032 Marburg, Germany

[d] Hubei Key Laboratory of Nature Medicinal Chemistry and Resource Evaluation, Tongji Medical College of Pharmacy, Huazhong University of Science and Technology, 430030 Wuhan, China

Corresponding to Shu-Ming Li, Telephone: +49-6421-28-22461; FAX: +49-6421-28-26678; E-mail: shuming.li@staff.uni-marburg.de

Table of Contents

S3

Experimental Procedures

1. Chemicals

Dimethylallyl diphosphate (DMAPP) was synthesized according to the method reported previously.[1] 1,3-dihydroxynaphthalene (**1**) was obtained from Fluka. Oxygen-18 ($^{18}O_2$, 97 %) and ^{18}O-enriched water ($H_2^{18}O$, 97 %) were purchased from Eurisotop. All other chemicals used in this study were of analytical grade.

2. Overproduction and purification of recombinant proteins

Overproduction and purification of FgaPT2,[2] CdpNPT,[3] FtmPT1,[4] and AnaPT[5] were carried out as described in the literature.

3. Enzyme assays with different prenyltransferases

The enzymatic reaction mixtures (50 µl) contained 50 mM Tris-HCl (pH 7.5), 10 mM $CaCl_2$, 1 mM 1,3-dihydroxynaphthalene (**1**), 2 mM DMAPP, 0.15–1.5% (*v/v*) glycerol, 5% (*v/v*) dimethyl sulfoxide (DMSO) and 20 µg of the purified recombinant proteins. These mixtures were incubated at 37°C for 30 min or 16 h and terminated by addition of one volume acetonitrile (CH_3CN) and subsequently centrifuged at $17,000 \times g$ for 30 min before further analysis on HPLC. For structure elucidation, products were isolated from large-scale incubations of 10 ml with 4 mg protein.

4. Time and pH dependent assays with 1

To determine the nonenzymatic formation, a time dependent assay was performed. 1 mM 1,3-dihydroxynaphthalene (**1**) was incubated with 10 mM $CaCl_2$, 2 mM DMAPP, 0.15–1.5% (*v/v*) glycerol, 5% (*v/v*) DMSO and 20 µg of denatured FgaPT2 in 50 mM Tris-HCl (pH 7.5) at 37°C for 0, 0.5, 4 and 24h. pH dependence assays were carried out by incubation in phosphate buffer at pH 2.5, 6.0, 7.5, 8.5 and 10 for 1 h. The products were monitored on LC-HRMS.

5. Enzyme assays under $^{18}O_2$-enriched atmosphere and in buffer with ^{18}O-enriched water

For incubation with FgaPT2 and 1,3-dihydroxynaphthalene (**1**) under $^{18}O_2$-enriched atmosphere, a 500 µL assay contained the same components as in the standard reaction mixture. $^{16}O_2$ in the reaction mixture was removed by application of vacuum followed by flushing with argon for three times. Argon was then removed by vacuum and finally $^{18}O_2$ was allowed to enter the reaction mixture, as reported previously.[6,7] After incubation at 37 °C for 3 h, the reaction was terminated by addition of 500 µL CH_3CN, and subjected to LC-HRMS analysis as described below. One assay was carried out under normal condition as a control. For incubation with FgaPT2 and 1,3-dihydroxynaphthalene (**1**) in buffer with ^{18}O-enriched

water, a 50 μL reaction mixture contained the same components as in the standard assay in a mixture of $H_2^{18}O$ and $H_2^{16}O$ with a ratio of 4:1.

6. HPLC and LC-HRMS conditions for analysis and isolation of products

Separation was performed on an Agilent series 1200 HPLC (Agilent Technologies, Böblingen, Germany) with an Agilent Eclipse XDB-C18 column (150 × 4.6 mm, 5 μm). H_2O (A) and CH_3CN (B), both with 0.1 % (*v/v*) trifluoroacetic acid, were used as solvents at a flow rate of 0.5 mL/min. The substances were eluted with a linear gradient from 15–80 % B in 50 min. The column was then washed with 100 % (*v/v*) solvent B for 10 min and equilibrated with 5 % (*v/v*) solvent B for 10 min. Product isolation was performed on the same equipment with an Agilent Eclipse XDB-C18 column (9.4 × 250 mm, 5 μm) column, and a linear gradient from 35–80 % B in 20 min at a flow rate of 2.5 ml/min.

LC-HRMS analysis was performed on an Agilent 1260 HPLC system equipped with a microTOF-Q III spectrometer (Bruker, Bremen, Germany) by using a Multospher 120 RP18-5μ column (250 × 2 mm, 5 μm) (CS-Chromatographie Service GmbH, Langerwehe, Germany). H_2O (A) and CH_3CN (B), both with 0.1% (*v/v*) formic acid, were used as solvents at a flow rate of 0.25 mL/min and the same gradient for separation. Electrospray positive or negative ionization mode was selected for determination of the exact masses. The capillary voltage was set to 4.5 kV and a collision energy of 8.0 eV. Sodium formate was used in each run for mass calibration. The masses were scanned in the range of *m/z* 100–1500. Data were evaluated with the Compass DataAnalysis 4.2 software (Bruker Daltonik, Bremen, Germany).

7. NMR analysis

For structural elucidation, the isolated products were dissolved in DMSO-*d6* or CD_3CN and subjected to NMR analysis. The spectra were recorded at room temperature on a Bruker Avance III 500 MHz (^{1}H) or 125 MHz (^{13}C) spectrometer installed with a cryo probe 5 mm Prodigy for Broad Band Observation. All spectra were processed with MestReNova 6.0.2 (Metrelab Research) and the chemical shifts were referenced to those of the solvents. The NMR data are given in Tables S2–S5 and spectra as Figures S1–S23.

8. Structure elucidation

Compound **2** was obtained as beige amorphous solid. The ¹H and ¹³C NMR of **2** showed signals of one methylene, one olefin and two tertiary methyl units. In addition, the HMBC correlations of H-1′/C-3, C-4 and C-10 suggested that a dimethylallyl residue was attached to position C4.

Compound **3** was isolated as creamy white solid. The HMBC correlations of H-5/C-4, H-8/C-1, H-2/C-4, H-2/C-3′, H-2/C-2′, H-1′/C-3, H-1′/C-3′ as well as ¹H-¹H COSY correlations of H-1′/H-2′/2′-OH indicated that a bicyclo[3.3.1]nonane system was fused with an aromatic ring through C-9 and C-10. Two additional hydroxyl groups were confirmed to be at C-4 and C-2′

by the HMBC correlation of 4-OH/C-4, C-1´ and C-10 as well as of 2´-OH/C-1´, C-2´ and C-3´. The relative configuration of **3** was determined by NOESY analysis. Strong correlations of ´H-2´/H-4´ with H-1´/H-5´ as well as weak cross peak between 4-OH and H-2´ suggest that 4-OH and 3´-OH are located with opposite orientations.

Compound **4** and **5** was obtained as creamy white solids. **4** and **5** are two isomers with the same molecular formula, $C_{15}H_{16}O_4$, deduced from HR-ESI-MS data. The ^1H, ^{13}C, and HMBC (Tables S4 and S5) showed the same planar structures for **4** and **5**, namely 4,3´-dihydroxyl tetrahydrofuran derivatives with two chiral centers. The relative configuration of **4** as shown in Figure S18 was confirmed by the NOESY correlations of 4-OH to H-2´. In comparison, the NOESY spectrum of **5** suggested an α-orientated 4-OH and β-orientated 2´-H as shown in Figure S23.

Tables

Table S1 HR-ESI-MS data of the reported compounds
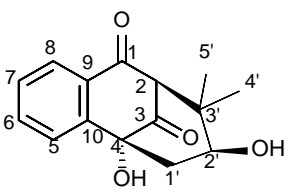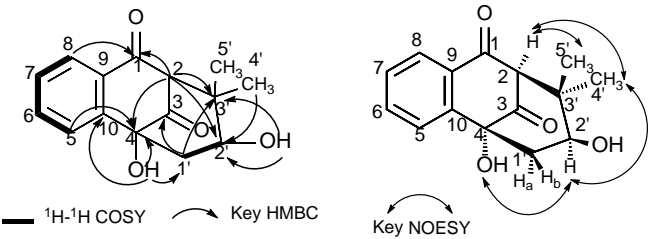
Compound	Formula	[M + H]$^+$		Deviation [ppm]	[M - H]$^-$		Deviation [ppm]
		Calculated	Measured		Calculated	Measured	
2	$C_{15}H_{16}O_2$	229.1223	229.1224	-0.4	227.1078	227.1088	-4.4
3	$C_{15}H_{16}O_4$	261.1121	261.1126	-1.9	259.0976	259.0974	0.8
4	$C_{15}H_{16}O_4$	261.1121	261.1129	-3.1	259.0976	259.0972	1.5
5	$C_{15}H_{16}O_4$	261.1121	261.1127	-2.3	259.0976	259.0983	-2.7

S7

Table S2 NMR data of compound **2** (500 MHz for ^{1}H NMR and 125 MHz for ^{13}C NMR)
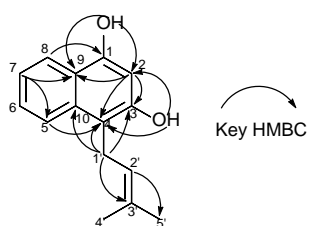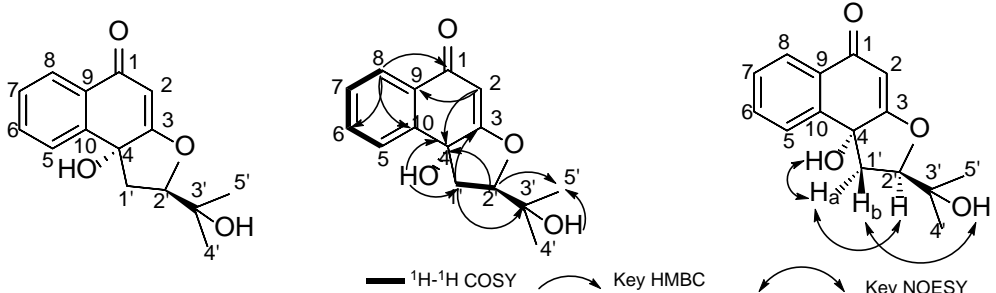
Position	δ_H, multi., *J* in Hz	δ_C, type	HMBC correlations
1	-	152.2, C	-
2	6.62, s	100.6, CH	C-1, 3, 4, 9
3	-	152.2, C	-
4	-	109.5, C	-
5	7.67, dd, 8.5, 1.0	122.6, CH	C-1, 4, 7, 9, 10
6	7.37, ddd, 8.5, 6.7, 1.6	126.3, CH	C-8, 10
7	7.16, ddd, 8.3 6.7, 1.0	120.7, CH	C-5, 6, 9
8	7.98, dd, 8.3, 1.6	122.4, CH	C-1, 6, 10
9	-	120.1, C	-
10	-	133.8, C	-
1´	3.52, d, 6.7	23.1, CH$_2$	C-2´, 3´, 3, 4, 10
2´	5.09, m	124.5, CH	C-4´, 5´
3´	-	129.7, C	-
4´	1.80, s	17.9, CH$_3$	C-2´, 3´, 5´
5´	1.61, s	25.5, CH$_3$	C-2´, 3´, 4´
1-OH	9.88, s	-	C-1, 2, 9
3-OH	9.30, s	-	C-2, 3, 4

Table S3 NMR data of compound **3** (500 MHz for ^{1}H NMR and 125 MHz for ^{13}C NMR)

Position	δ$_H$, multi., *J* in Hz		δ$_C$, type		HMBC correlations		COSY correlations	NOESY correlations (s:strong, w:weak)
solvent	DMSO-*d6*	CD$_3$CN	DMSO-*d6*	CD$_3$CN	DMSO-*d6*	CD$_3$CN	DMSO-*d6*	CD$_3$CN
1	-	-	194.2, C	193.7, C	-	-	-	-
2	3.25, s	3.30, s	73.6, CH	73.1, CH	C-1, 3, 4, 9, 2′, 3′,4′, 5′	C-1, 3, 4, 9, 2′, 3′,4′, 5′	-	H-4′, 5′
3	-	-	205.2, C	204.7, C	-	-	-	-
4	-	-	77.6, C	77.6, C	-	-	-	-
5	7.83, m^a	7.83, ddd, 7.9, 1.3, 0.5	125.5, CH	125.1, CH	C-4, 7, 9	C-4, 7, 9	H-6	-
6	7.82, m^a	7.78, ddd, 7.9, 7.2, 1.4	135.9, CH	135.5, CH	C-10	C-8, 10	H-5, 7	H-7
7	7.55, m	7.51, ddd, 7.9, 7.2, 1.3	128.4, CH	128.1, CH	C-5, 9	C-5, 9	H-6, 8	H-6, 8
8	7.90, d, 7.9	7.94, ddd, 7.9, 1.4, 0.5	125.2, CH	124.8, CH	C-1, 6, 10	C-1, 6, 10	H-7	H-7
9	-	-	131.2, C	129.8, C	-	-	-	-
10	-	-	146.8, C	146.1, C	-	-	-	-
1′a	1.98, dd, 12.8, 5.2	2.17, dd, 12.7, 5.4	46.8, CH$_2$	46.5, CH$_2$	C-3, 4, 10, 2′, 3′	C-3, 4, 10, 2′, 3′	H-2′	H-2′, 2′-OH, H-5′(s), H-4′(w)
1′b	2.11, dd, 12.8, 11.3	2.21, dd, 12.7, 11.3			C-3, 4, 10, 2′, 3′	C-3, 4, 10, 2′, 3′	H-2′	H-2′, 2′-OH
2′	3.09, ddd, 11.3, 5.5, 5.2	3.25, ddd, 11.3, 5.6, 5.4	69.6, CH	69.5, CH	C-3′, 4′, 5′	C-1′, 4′, 5′	H-1′a, 1′b, 2′-OH	H-4′, 1′a, 1′b
3′	-	-	44.8, C	44.7, C	-	-	-	-
4′	1.01, s	1.08, s	18.8, CH$_3$	18.5, CH$_3$	C-2, 2′, 3′, 5′	C-2, 2′, 3′, 5′	-	H-2′, 1′a(w)
5′	0.91, s	0.91, s	24.8, CH$_3$	24.5, CH$_3$	C-2, 2′, 3′, 4′	C-2, 2′, 3′, 4′	-	H-2, 1′a(s)
4-OH	6.37, s	4.37, s	-	-	C-4, 1′, 10	C-4, 1′, 10	-	H-2′
2′-OH	4.94, d, 5.5	2.98, d, 5.6	-	-	C-2′, 3′	C-1′, 2′, 3′	H-2′	H-1′a, 1′b

^{a} Signals are overlapping with each other.

S9

Table S4 NMR data of compound **4** (500 MHz for ^{1}H NMR and 125 MHz for ^{13}C NMR)

Position	δ_H, multi., *J* in Hz	δ_C, type	HMBC	COSY correlations	NOESY correlations
1	-	185.1, C	-	-	-
2	5.55, s	98.5, CH	C-1, 3, 4, 9	-	H-2´, 4-OH
3	-	179.6, C	-	-	-
4	-	73.2, C	-	-	-
5	7.62, m[a]	126.6, CH	C-1, 4, 7, 9	H-6	H-1´a, 1´b, 4-OH, 7
6	7.61, m[a]	132.1, CH	C-8, 10	H-5, 7	H-7
7	7.49, ddd, 7.7, 6.2, 2.4	128.3, CH	C-5, 9, 10	H-6, 8	H-5, 6, 8
8	7.89, d, 7.7	125.4, CH	C-1, 6, 10	H-7	H-7
9	-	130.6, C	-	-	-
10	-	141.2, C	-	-	-
1´a	2.70, dd, 12.6, 4.6		C-3, 4, 2´	H-1´a, 2´	H-5, 2´, 4-OH, 1´b, 5´
1´b	2.05, ddd, 12.6, 10.1, 1.1	35.9, CH₂	C-10, 2´, 3´	H-1´b, 2´	H-5, 3´-OH, 1´a, 4´, 5´
2´	4.77, dd, 10.1, 4.6	91.5, CH	C-1´, 4´, 5´	H-1´a, 1´b	H-1´a, 4´, 5´, 4-OH
3´	-	69.2, C	-	-	-
4´	1.22, s	26.1, CH₃	C-2´, 3´, 5´	-	H-5´,1´a, 1´b, 3´-OH, 2´, 4-OH
5´	1.11, s	25.6, CH₃	C-2´, 3´, 4´	-	H-4´, 1´a, 3´-OH, 2´, 4-OH
4-OH	6.27, d, 1.1	-	C-1´, 3, 4	-	H-4´, 5´, 1´a, 2´, 2, 5
3´-OH	4.68, s	-	C-2´, 3´, 4´, 5´	-	H-4´, 5´, 1´b, 5

[a] Signals are overlapping with each other.

Table S5 NMR data of compound **5** (500 MHz for ^{1}H NMR and 125 MHz for ^{13}C NMR)
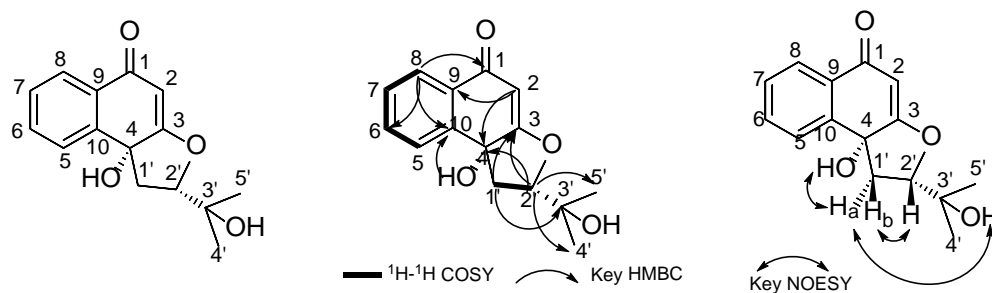
Position	δ$_H$, multi., J in Hz	δ$_C$, type	HMBC correlations	NOESY correlations
1	-	185.2, C	-	-
2	5.60, s	98.5, CH	C-3, 4, 9	H-2´
3	-	180.1, C	-	-
4	-	72.1, C	-	-
5	7.65, m^a	126.8, CH	C-4, 7, 9	H-1´a, 1´b, 6
6	7.64, m^a	132.1, CH	C-8	H-5, 7
7	7.50, ddd, 7.6, 6.2, 2.5	128.3, CH	C-5, 9	H-6, 8
8	7.90, d, 7.6	125.3, CH	C-1, 6, 10	H-7
9	-	130.6, C	-	-
10	-	141.2, C	-	-
1´a	2.91, dd, 13.9, 1.1	34.7, CH$_2$	C-3, 4, 3´	H-1´b, 5, 5´, 3´-OH, 4-OH
1´b	2.54, dd, 13.9, 10.0		C-2´, 10, 4, 3´	H-1´a, 5, 2´
2´	4.71, dd, 10.0, 1.1	91.7, CH	C-1´, 4´, 5´, 3, 4	H-1´b, 4´, 5´, 2
3´	-	70.0, C	-	-
4´	1.35, s	26.4, CH$_3$	C-2´, 3´, 5´	H-2´, 5´, 3´-OH, 4-OH
5´	1.26, s	27.0, CH$_3$	C-2´, 3´, 4´	H-2´, 4´, 1´a, 3´-OH, 4-OH
4-OH	6.98, br s	-	C-1´, 4, 10	1´a, 4´, 5´
3´-OH	6.11, br s	-	C-2´	1´a, 4´, 5´

^{a} Signals are overlapping with each other.

Figures
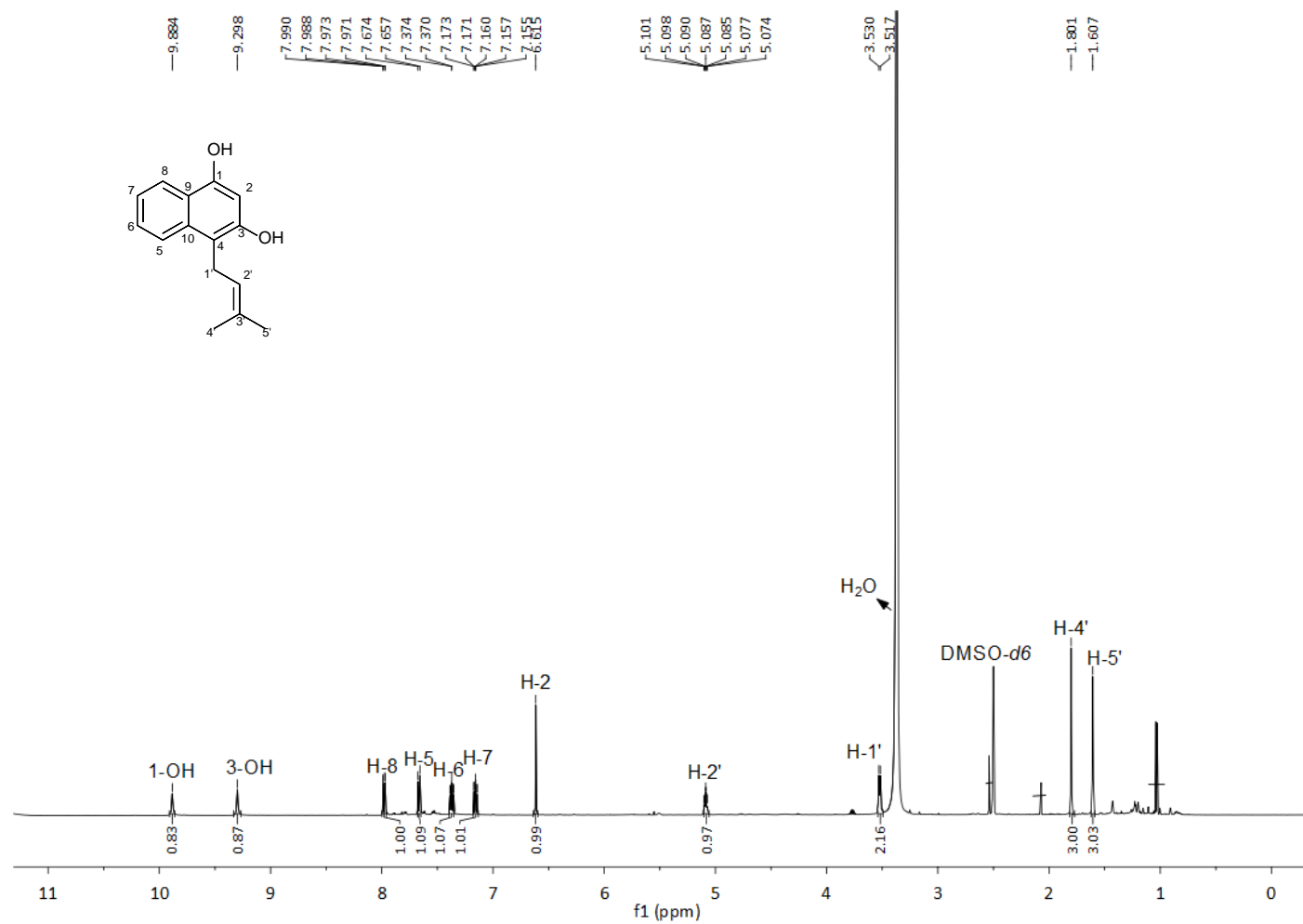
Figure S1. ^{1}H NMR spectrum of compound **2** in DMSO-*d6* (500 MHz)
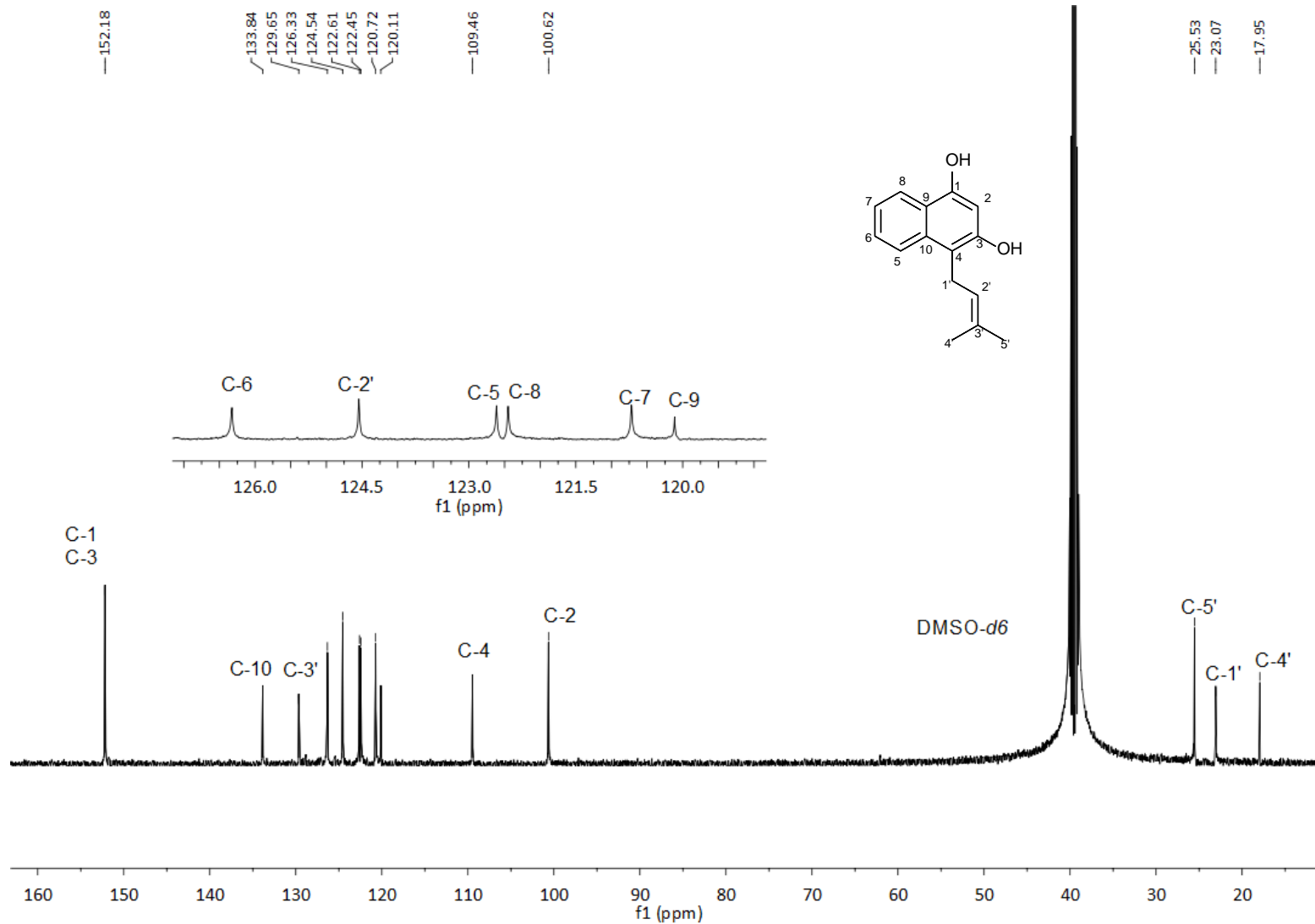
Figure S2. ^{13}C NMR spectrum of compound **2** in DMSO-*d6* (125 MHz)

S13
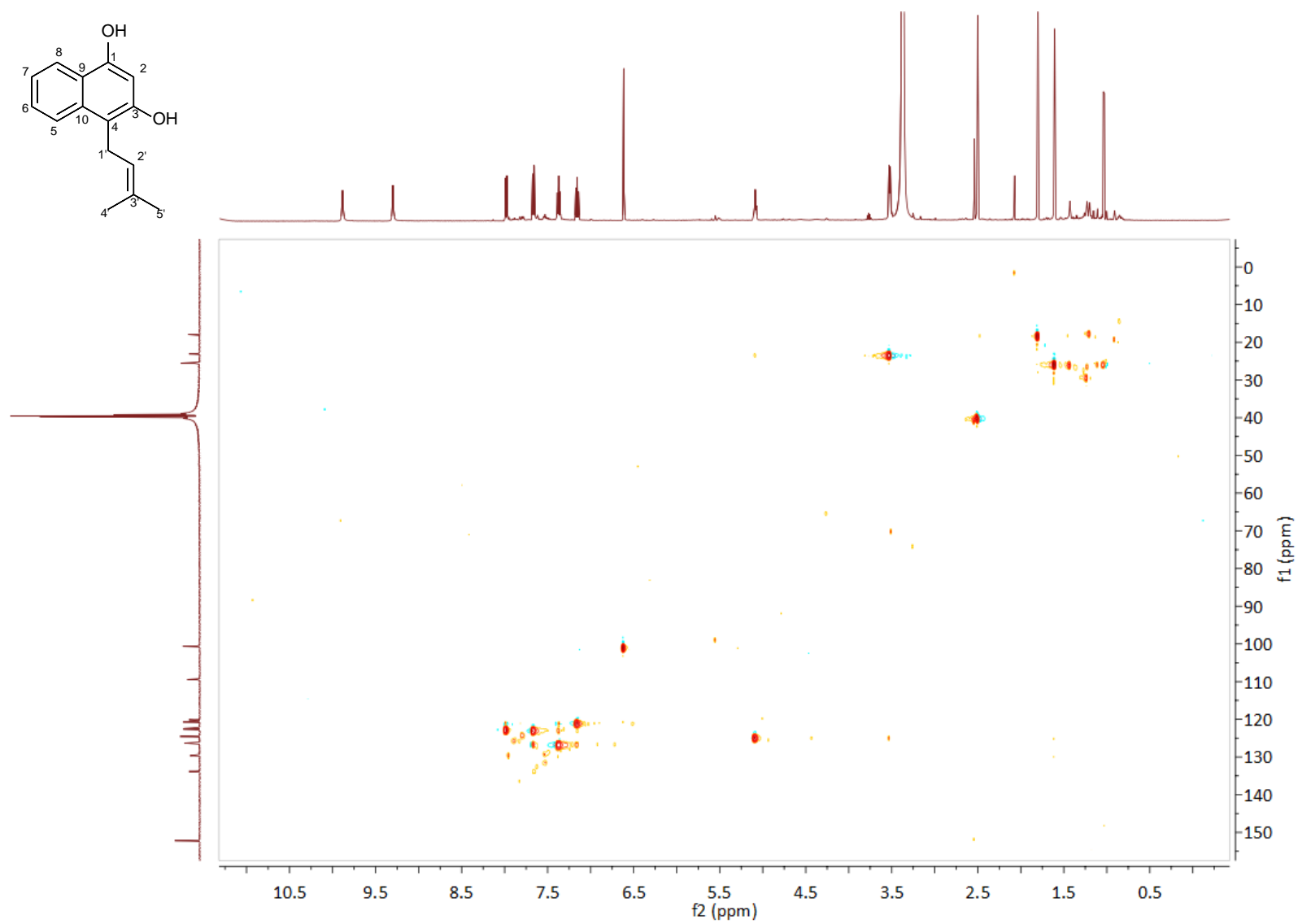
Figure S3. HSQC NMR spectrum of compound **2** in DMSO-*d6*

S14
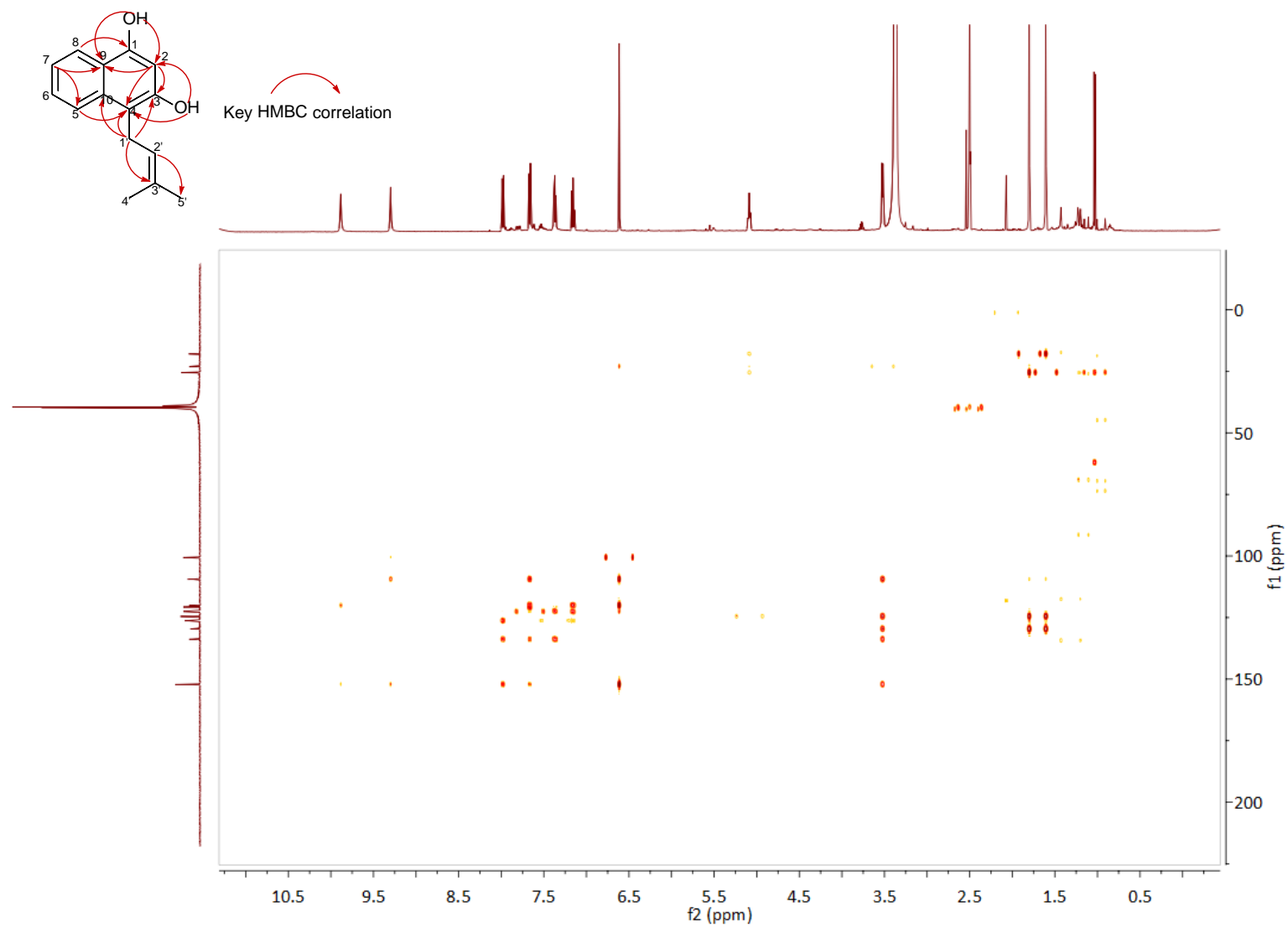
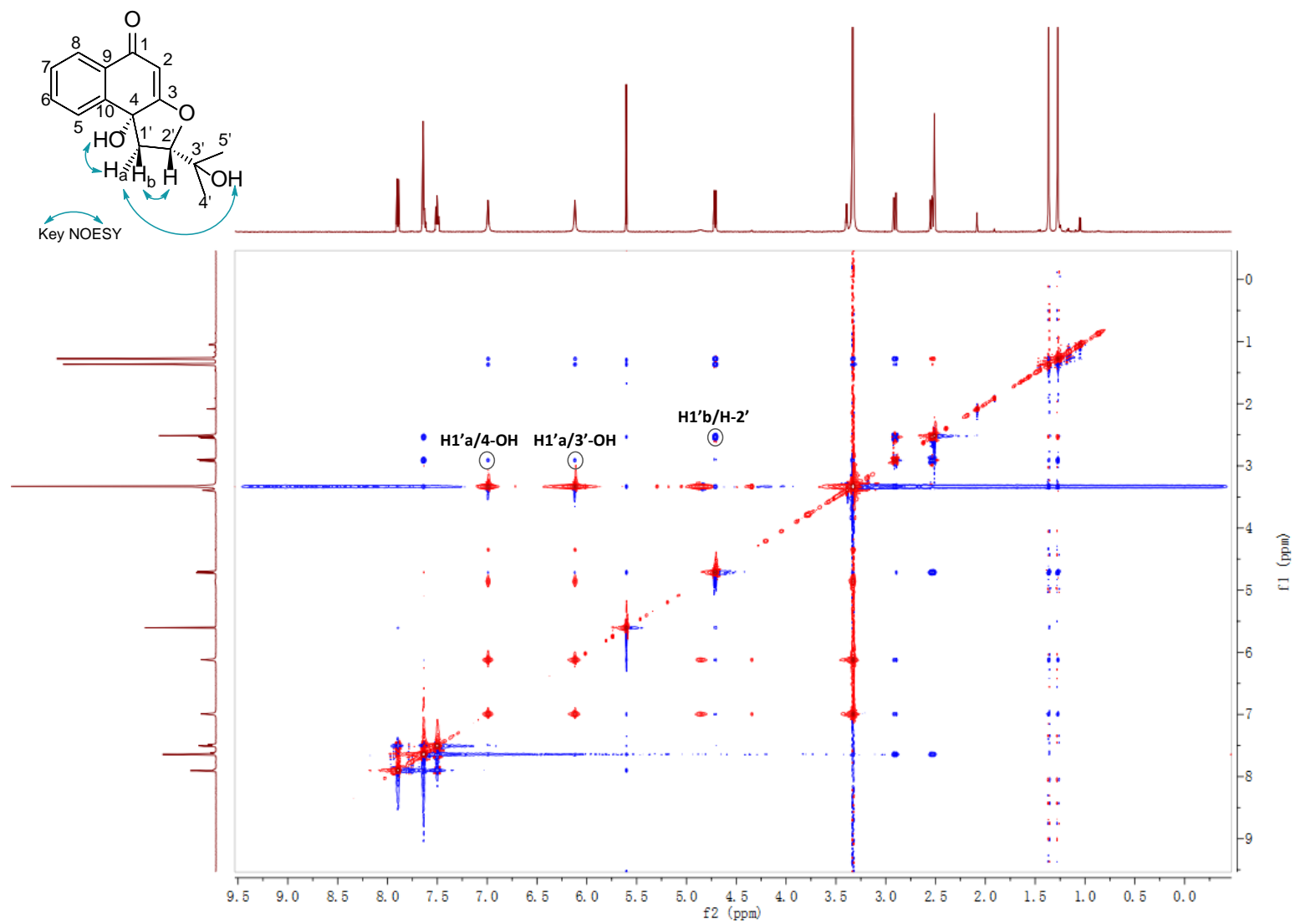**Figure S4.** HMBC NMR spectrum of compound **2** in DMSO-*d6*
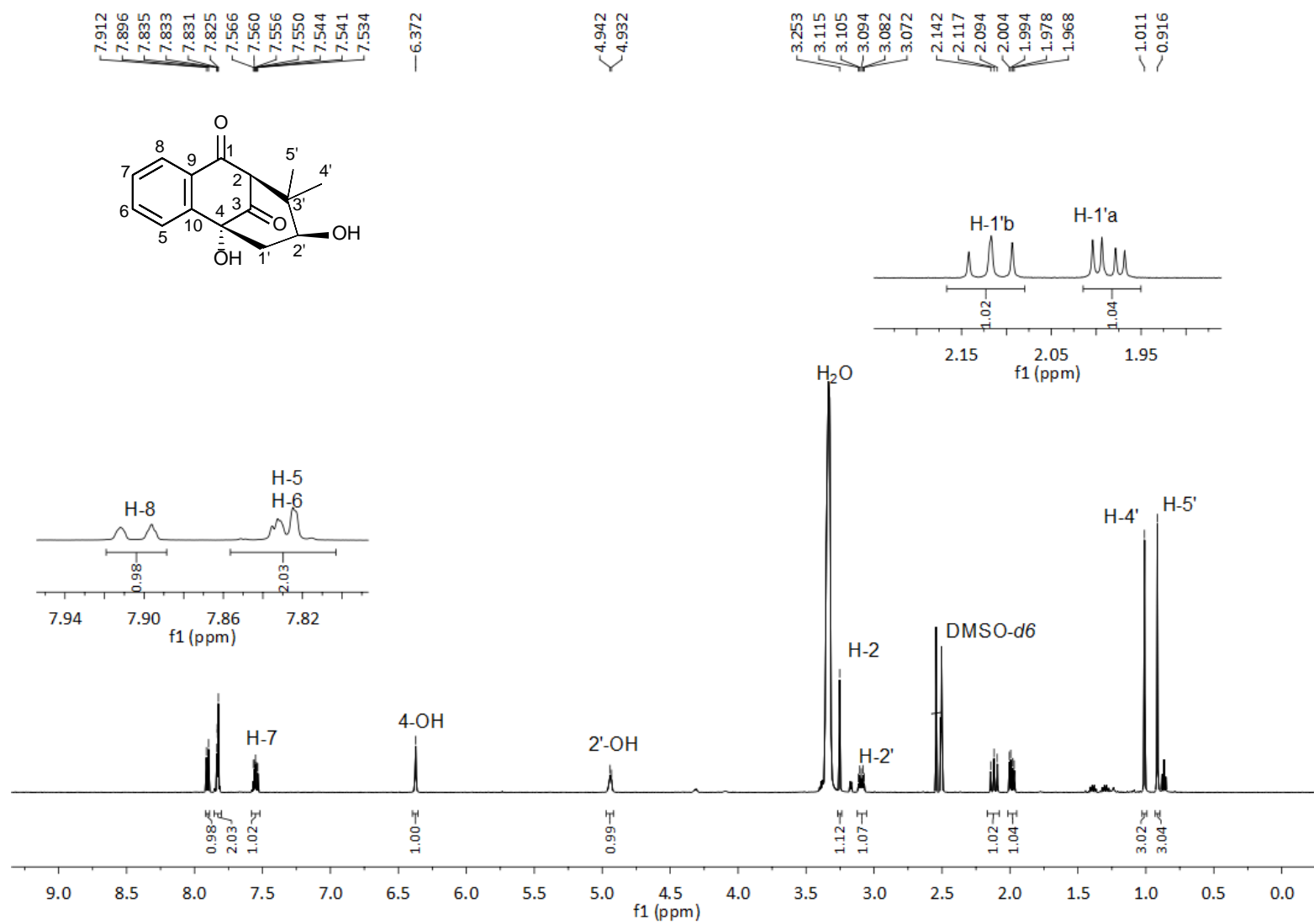
Figure S5. ^{1}H NMR spectrum of compound **3** in DMSO-$d6$ (500 MHz)
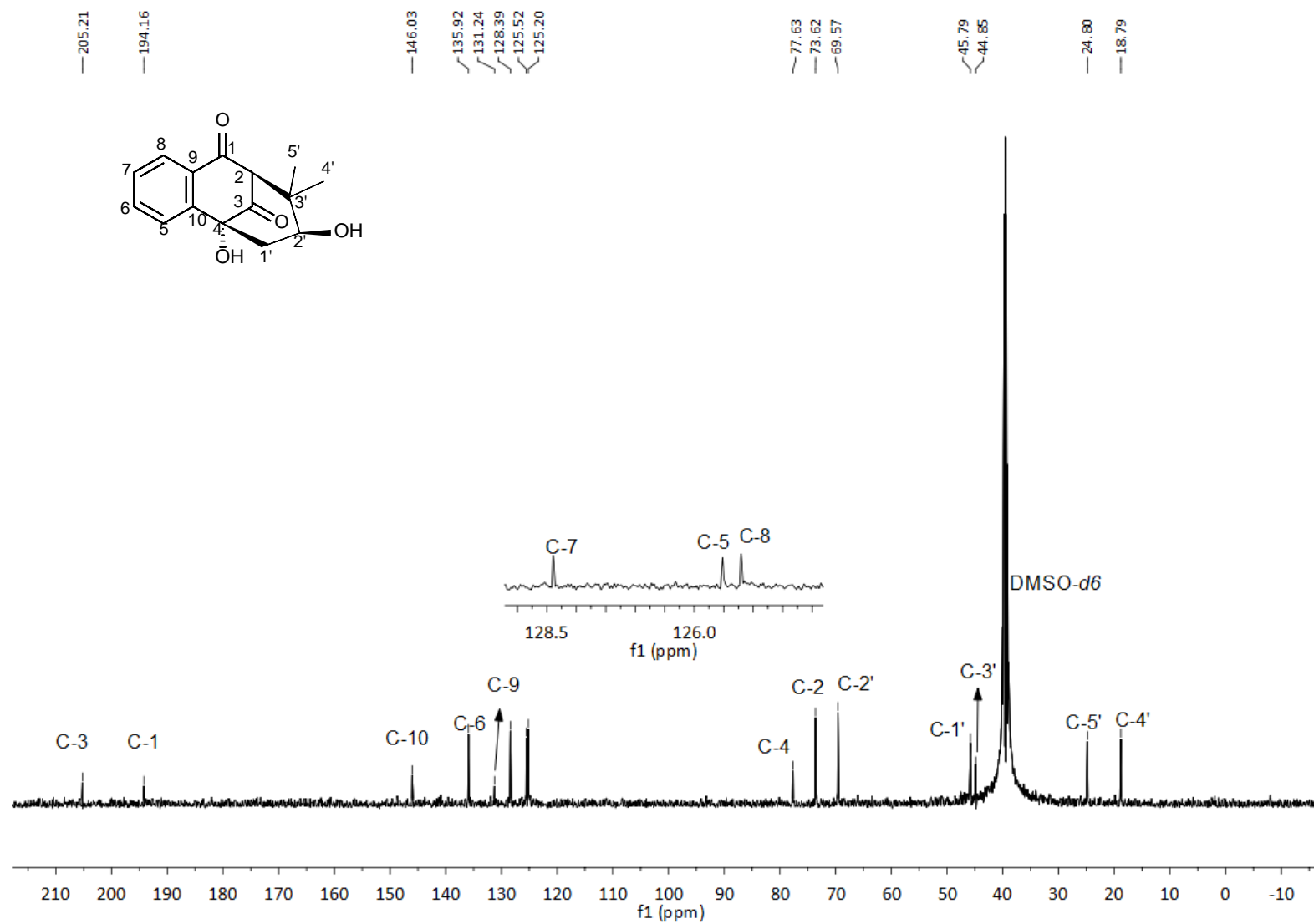
Figure S6. ^{13}C NMR spectrum of compound **3** in DMSO-*d6* (125 MHz)

S17
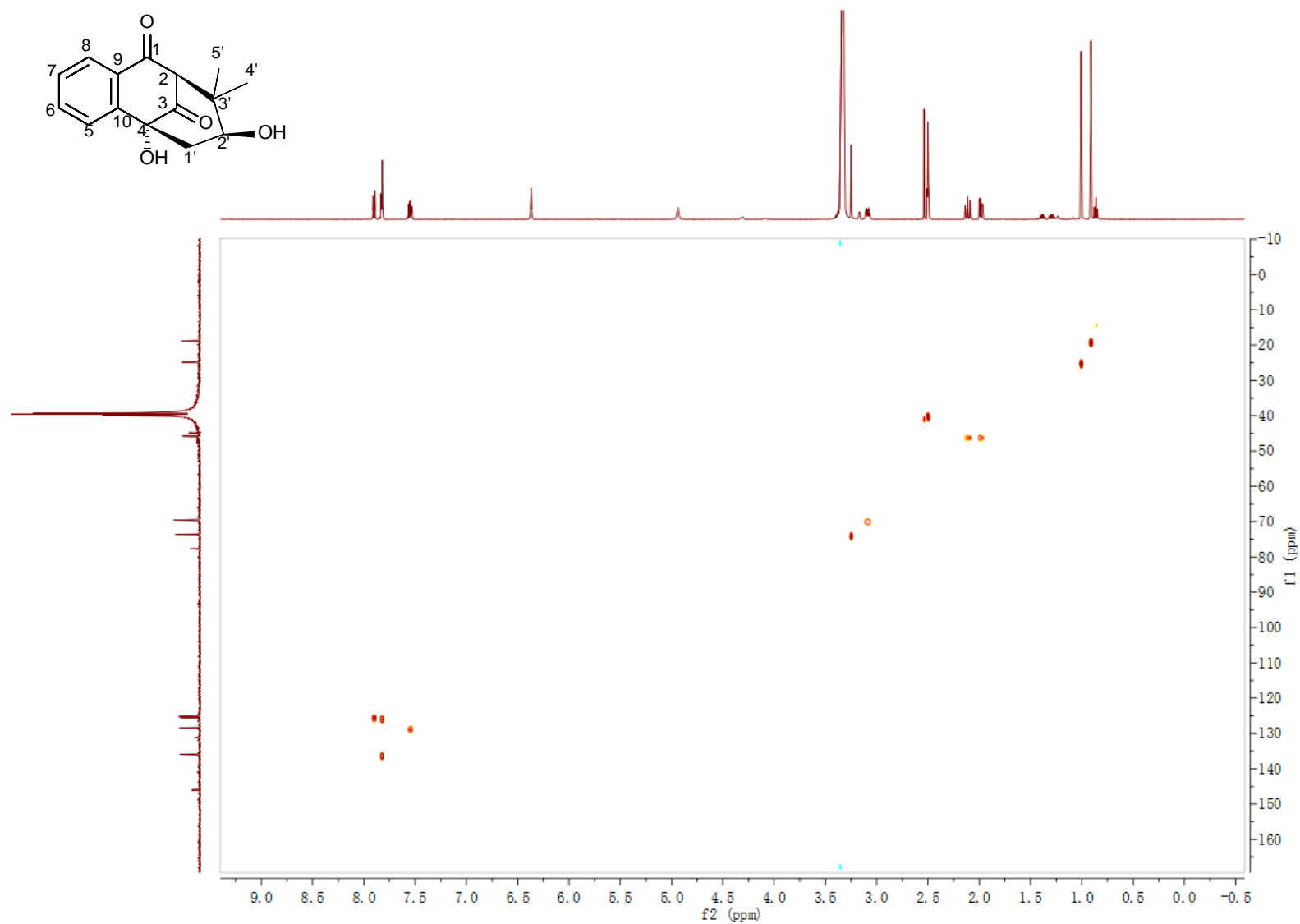
Figure S7. HSQC NMR spectrum of compound **3** in DMSO-*d6*
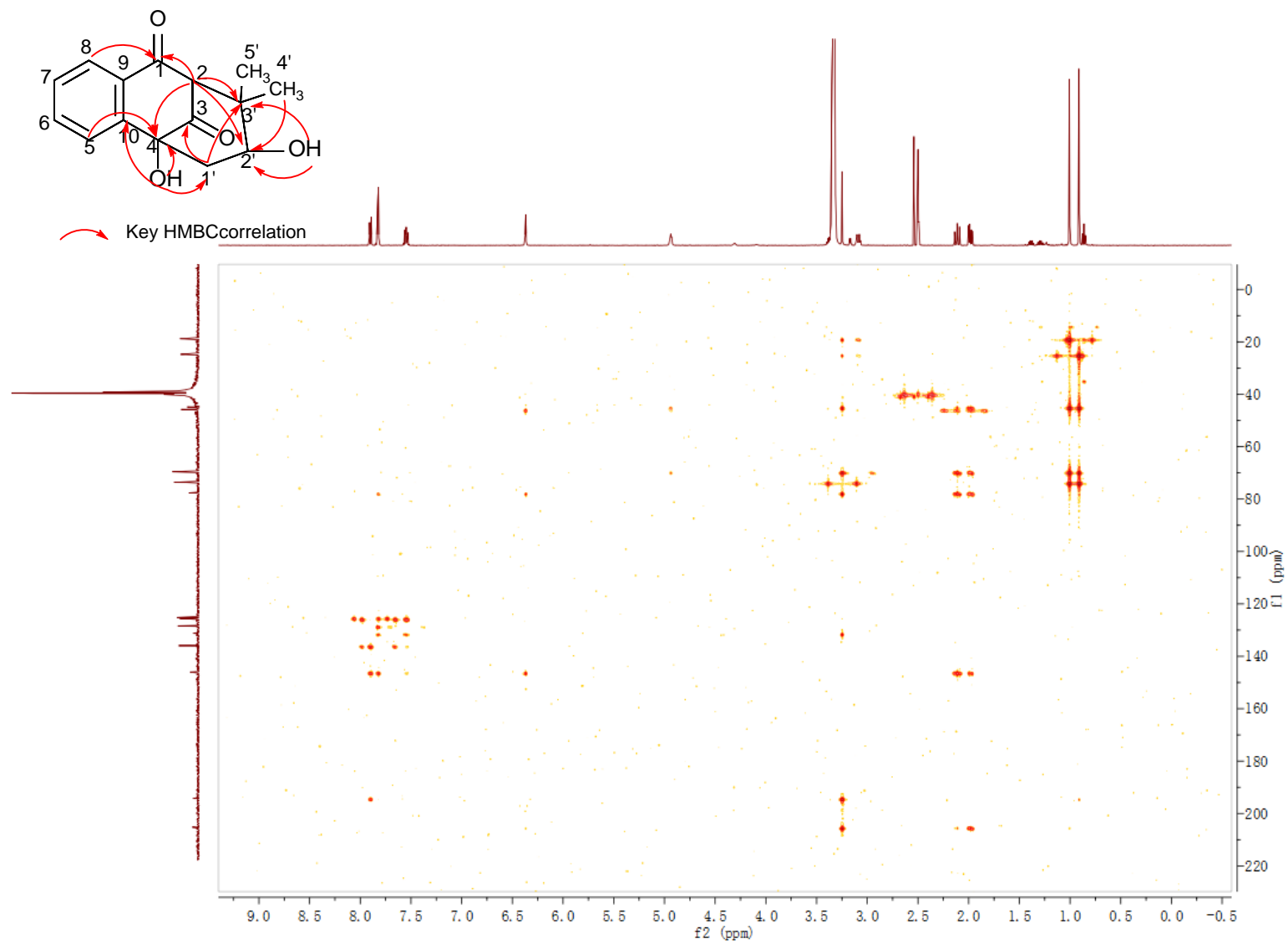
Figure S8. HMBC NMR spectrum of compound **3** in DMSO-*d6*
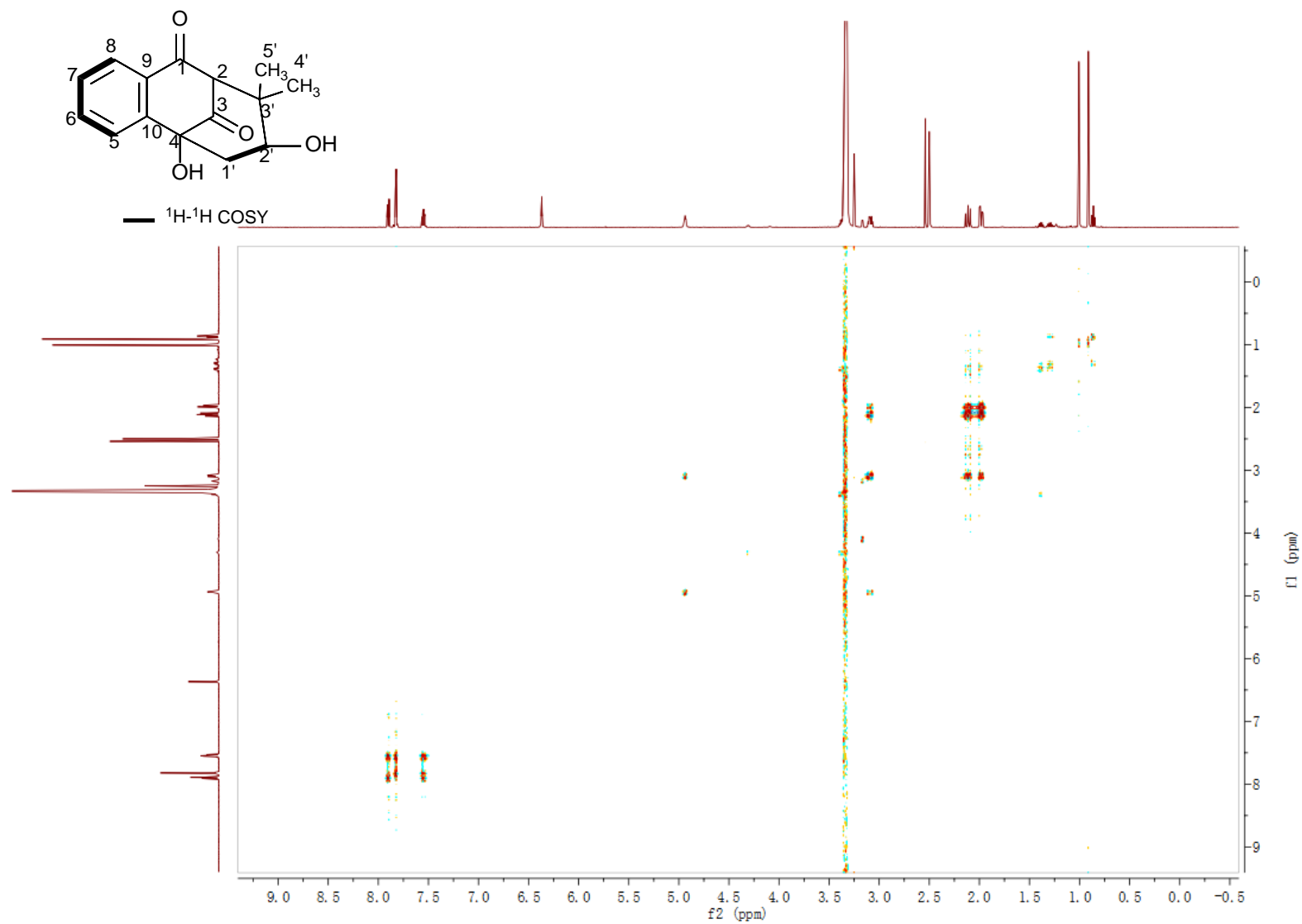
Figure S9. ^{1}H-^{1}H COSY NMR spectrum of compound **3** in DMSO-*d6*
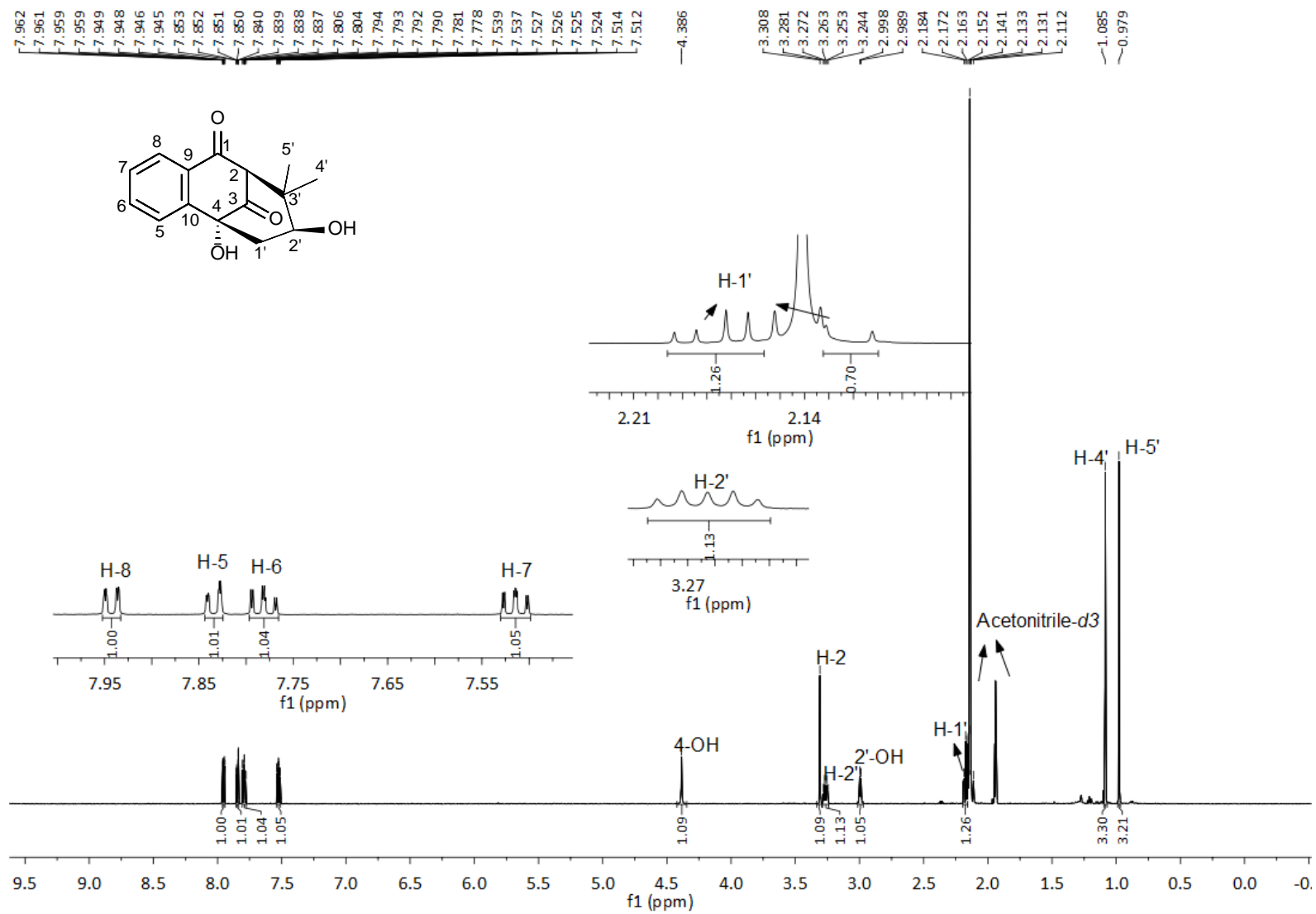
Figure S10. ^{1}H NMR spectrum of compound **3** in CD$_3$CN (500 MHz)
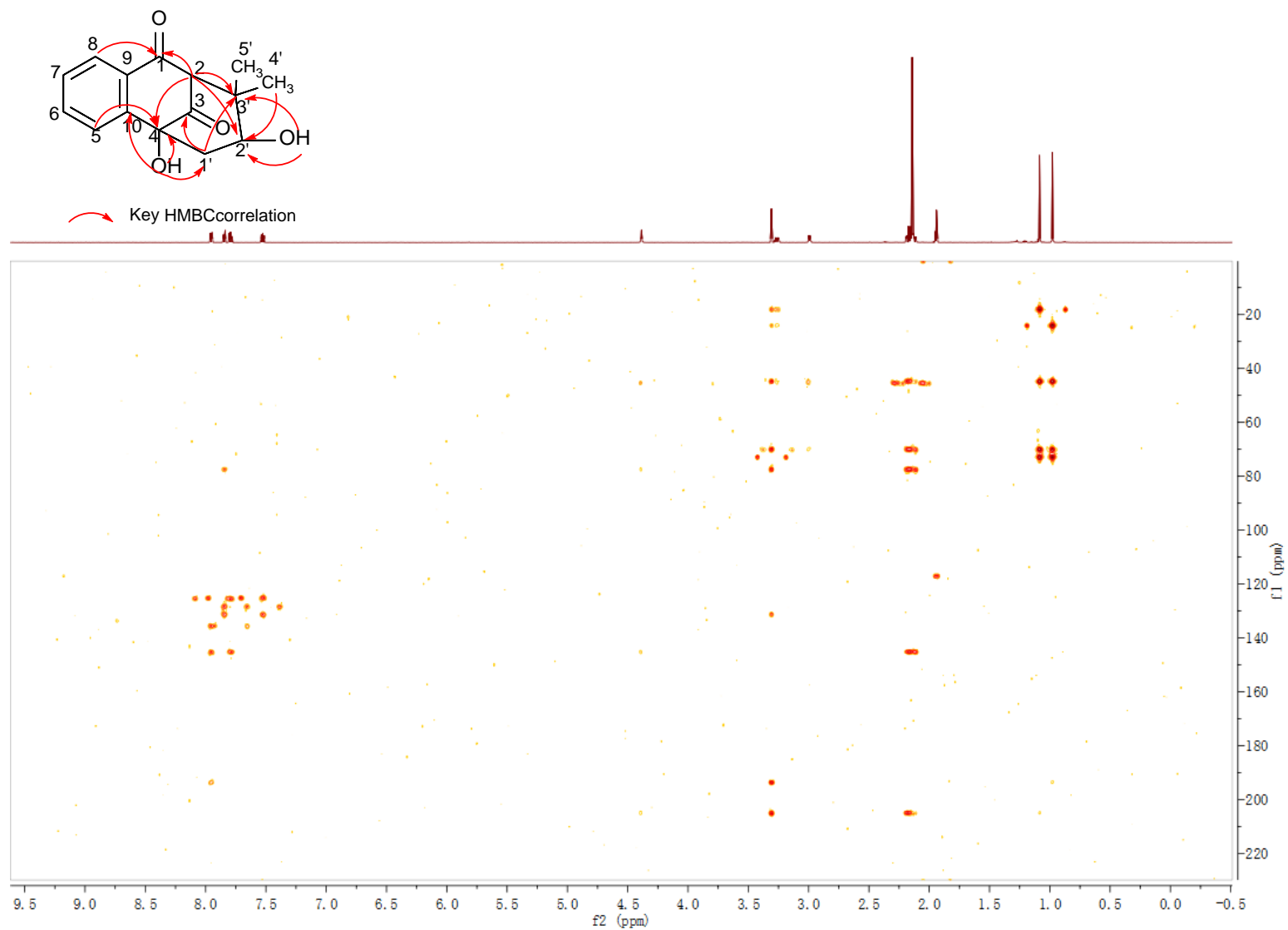
Figure S11. HMBC NMR spectrum of compound **3** in CD₃CN

S22
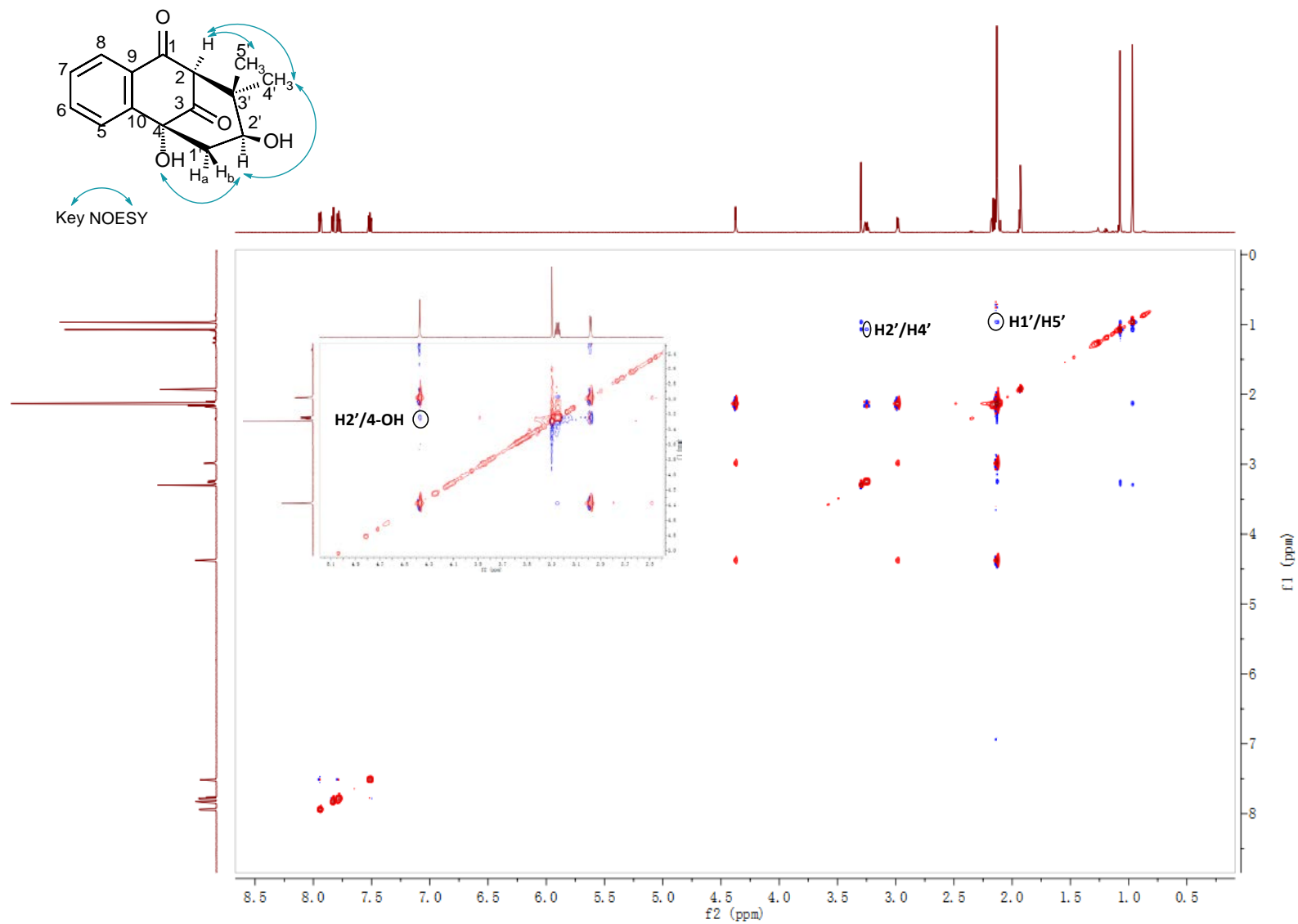
Figure S12. NOESY NMR spectrum of compound **3** in CD₃CN

S23
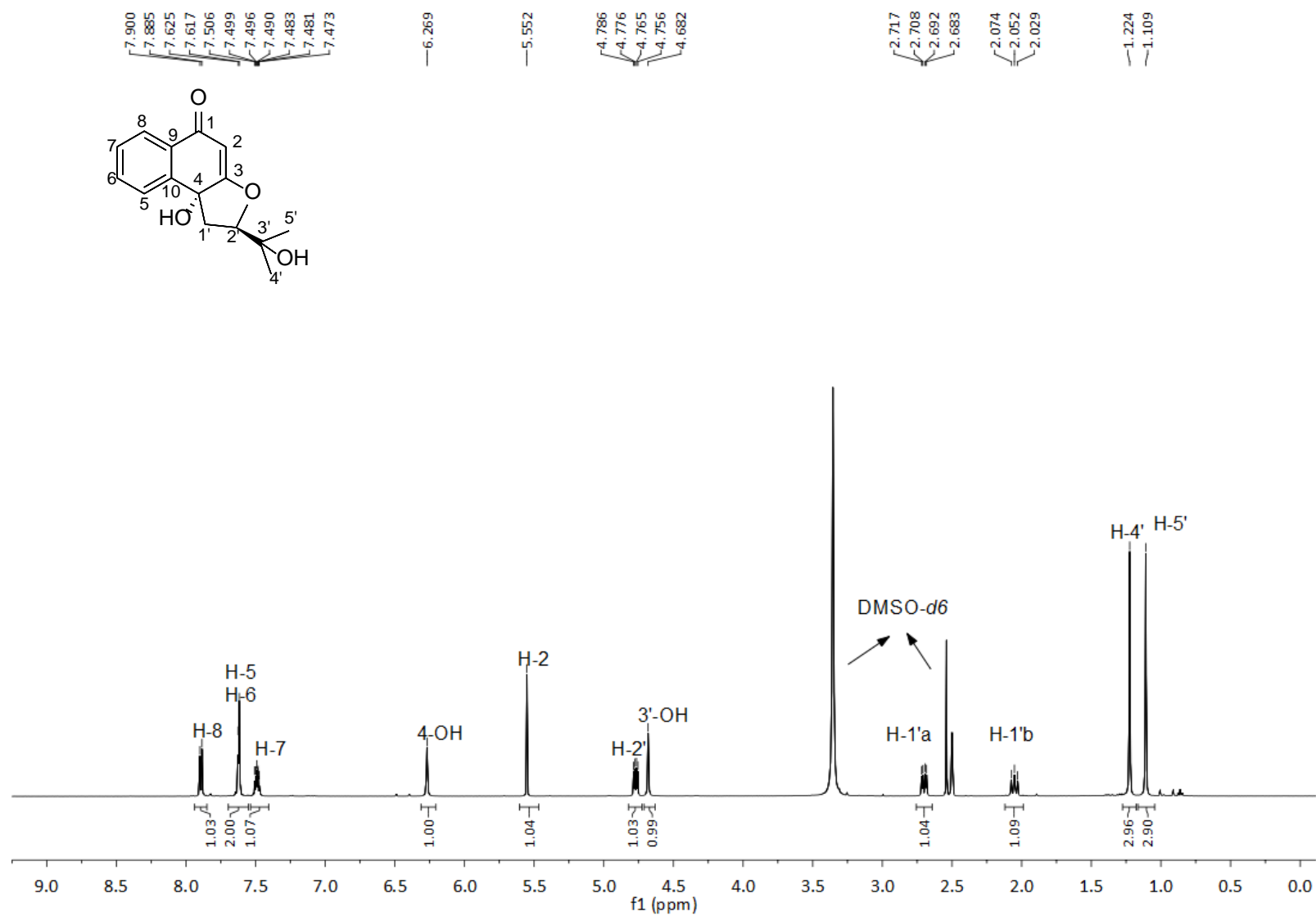
Figure S13. ^{1}H NMR spectrum of compound **4** in DMSO-*d6* (500 MHz)
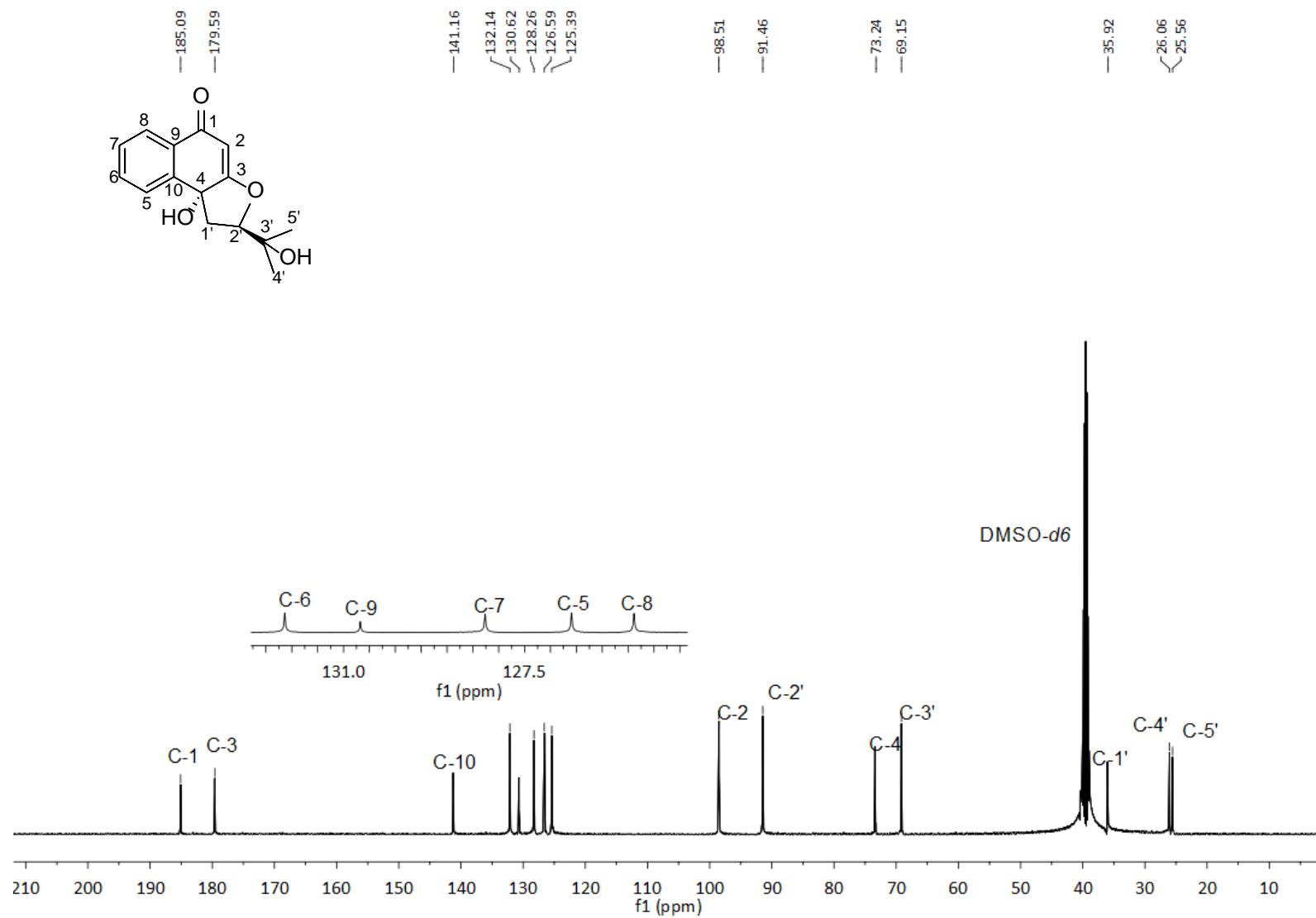
Figure S14. ^{13}C NMR spectrum of compound **4** in DMSO-*d6* (125 MHz)

S25

113
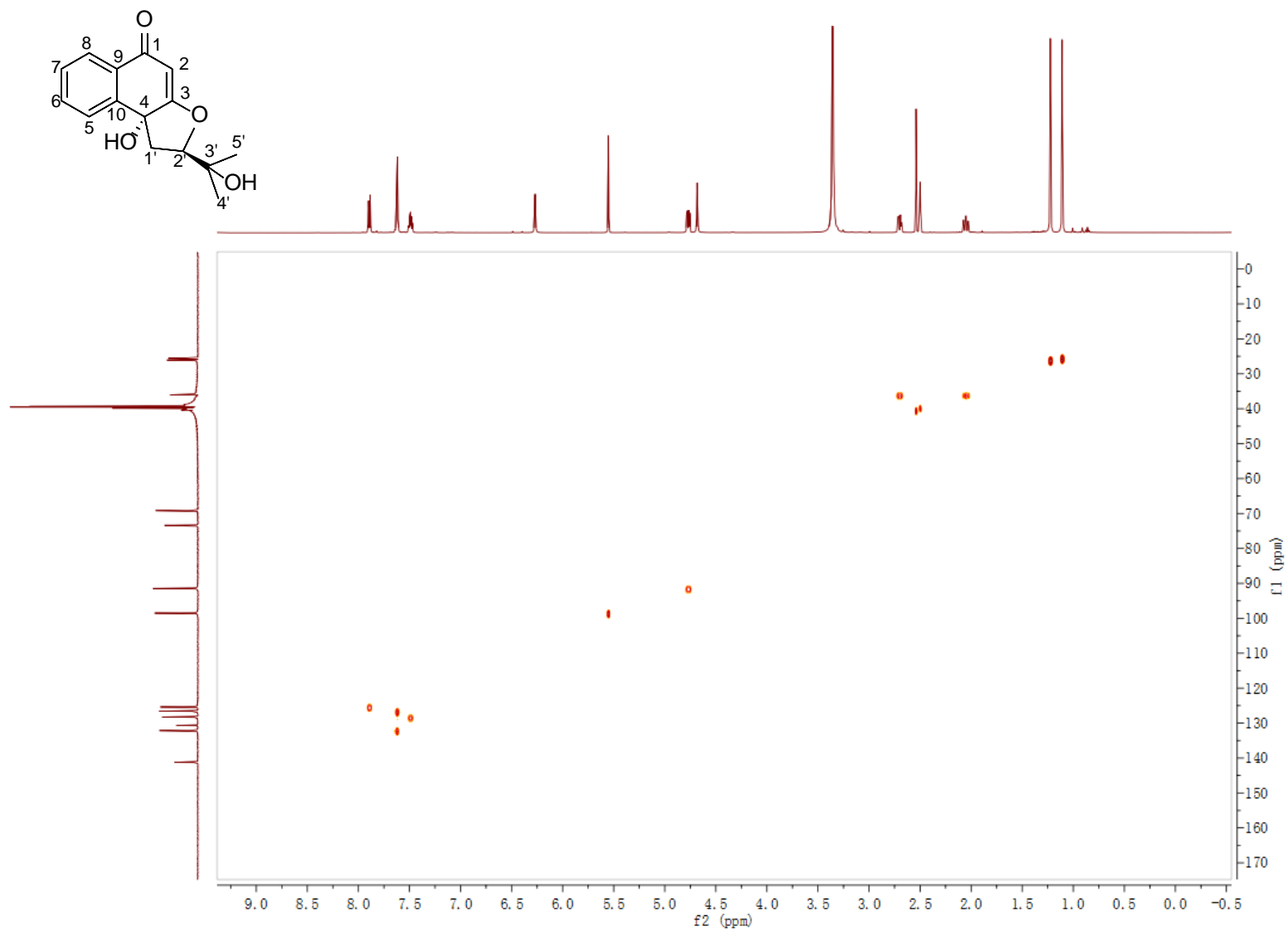
Figure S15. HSQC NMR spectrum of compound **4** in DMSO-*d6*

S26

114
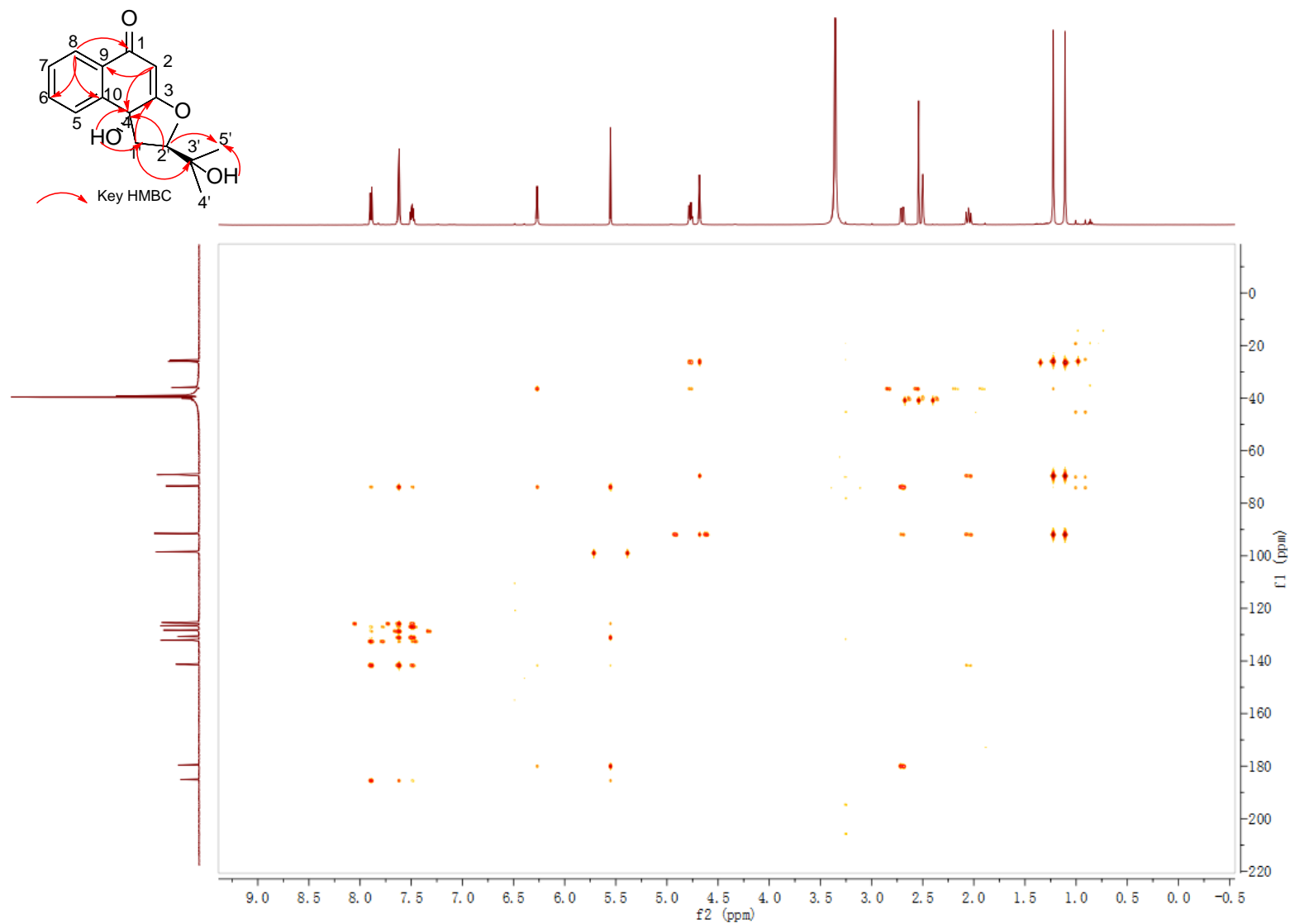
Figure S16. HMBC NMR spectrum of compound **4** in DMSO-*d6*

S27

Figure S17. ^{1}H-^{1}H COSY NMR spectrum of compound **4** in DMSO-*d6*

S28
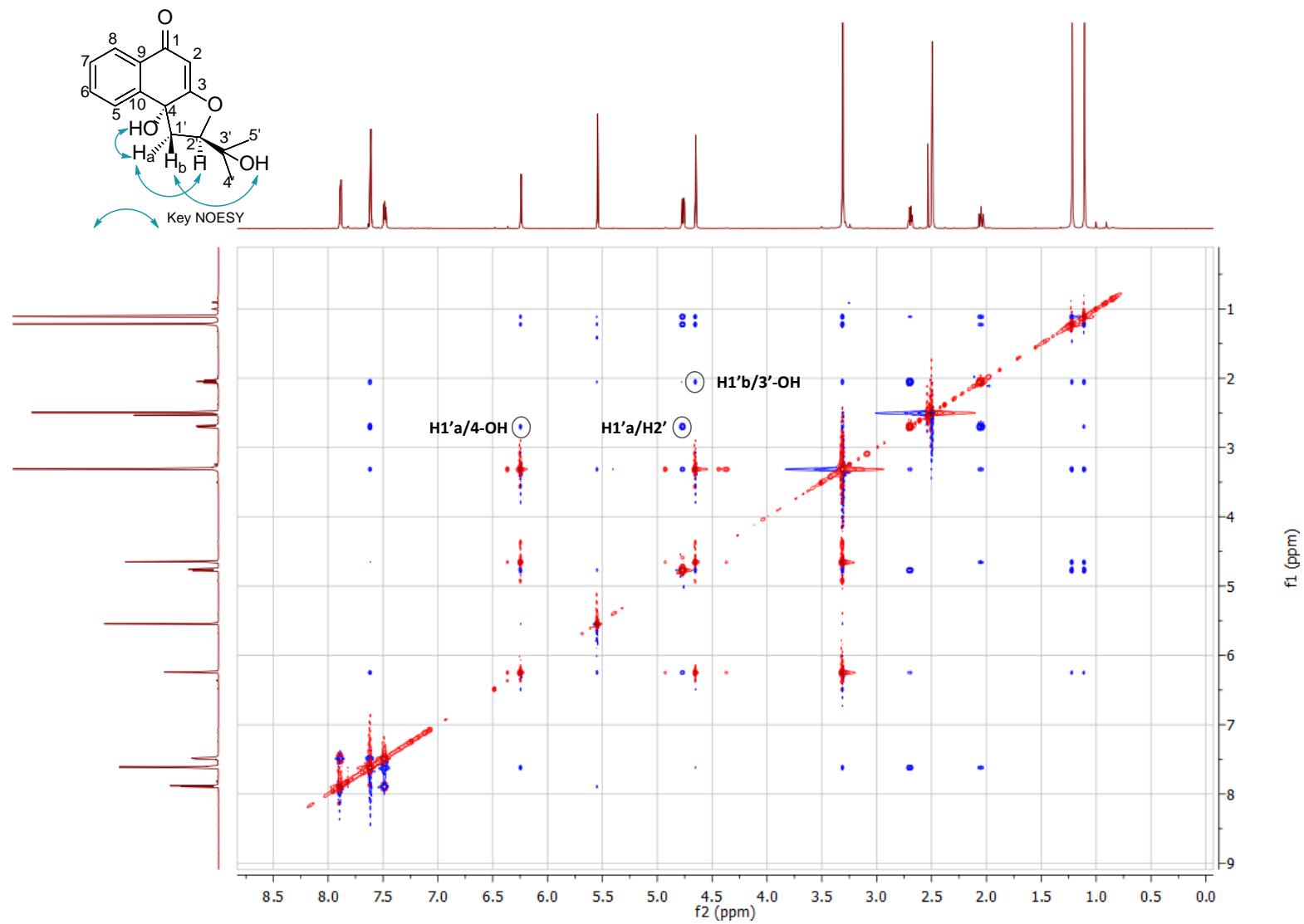
Figure S18. NOESY NMR spectrum of compound **4** in DMSO-*d6*
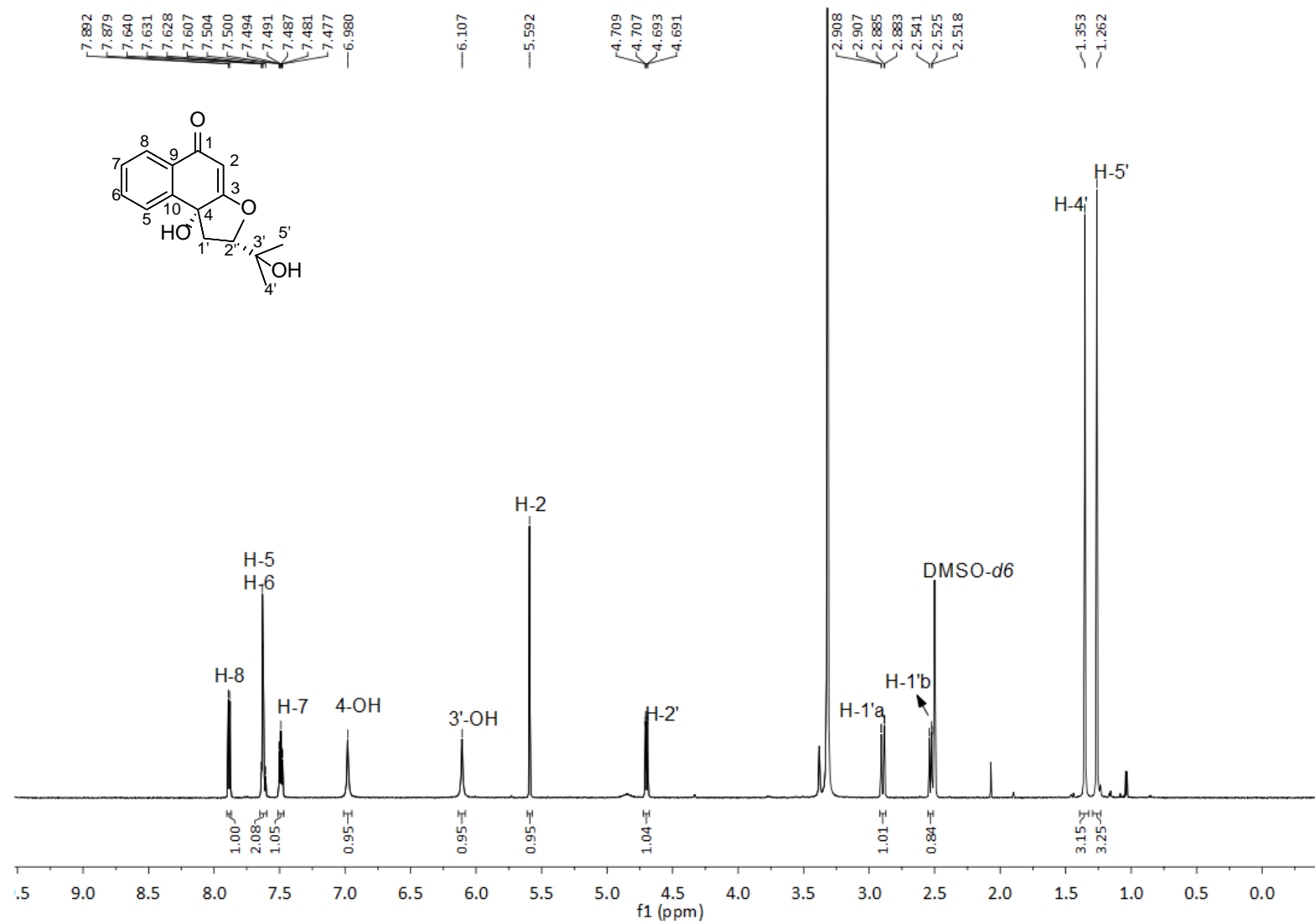
Figure S19. ^{1}H NMR spectrum of compound **5** in DMSO-*d6* (500 MHz)
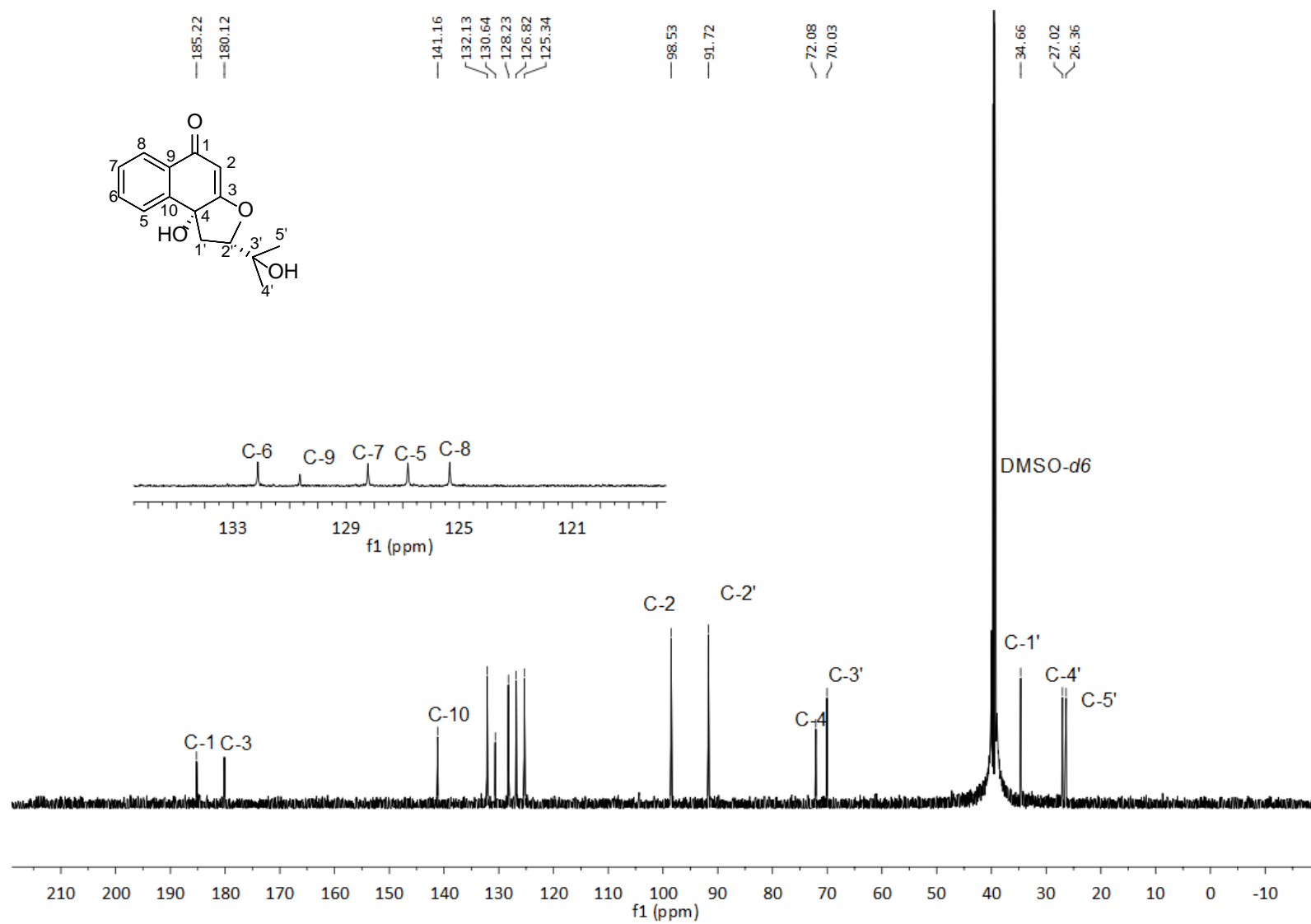
Figure S20. ^{13}C NMR spectrum of compound **5** in DMSO-*d6* (125 MHz)

S31
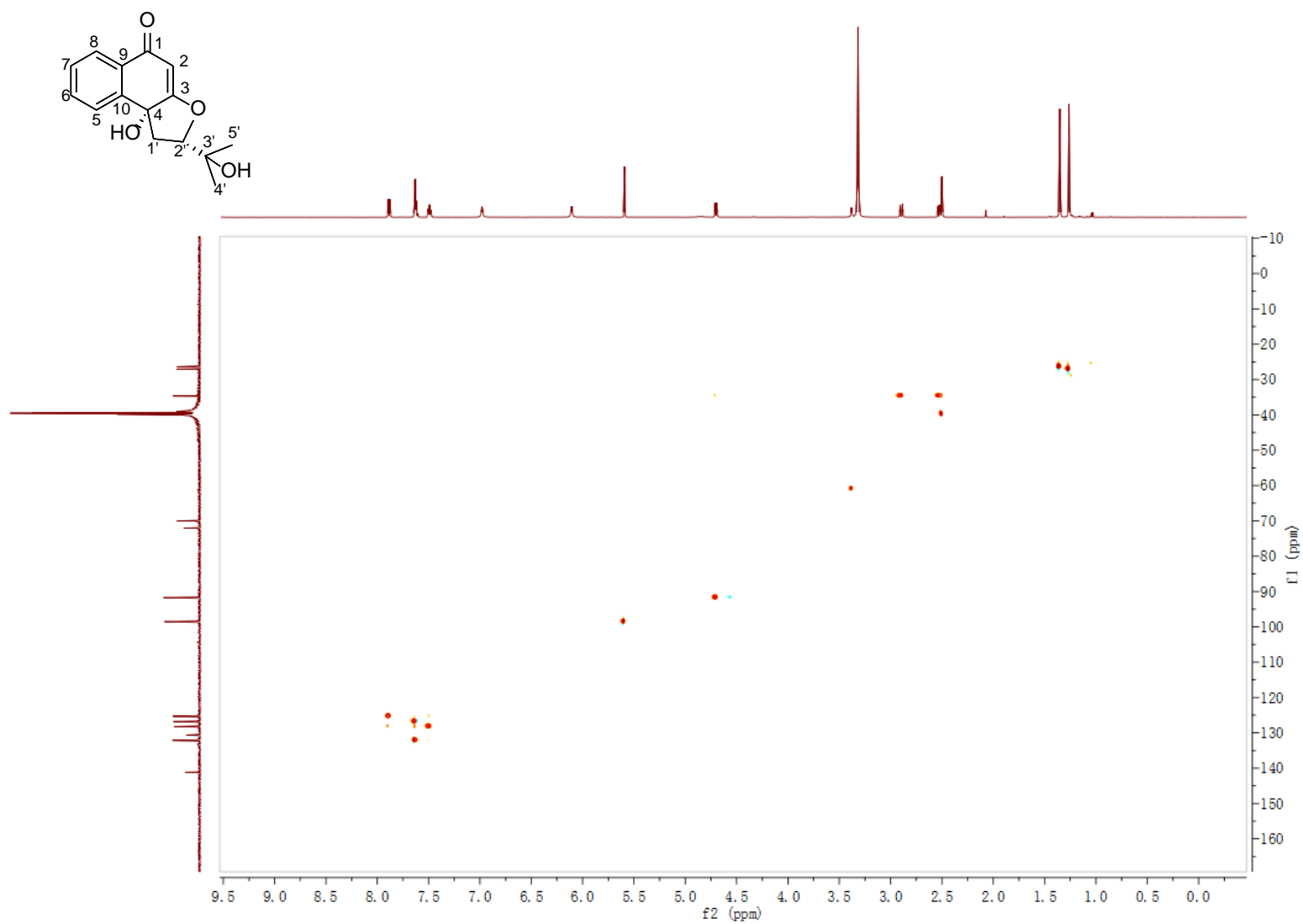
Figure S21. HSQC NMR spectrum of compound **5** in DMSO-*d6*

S32

120
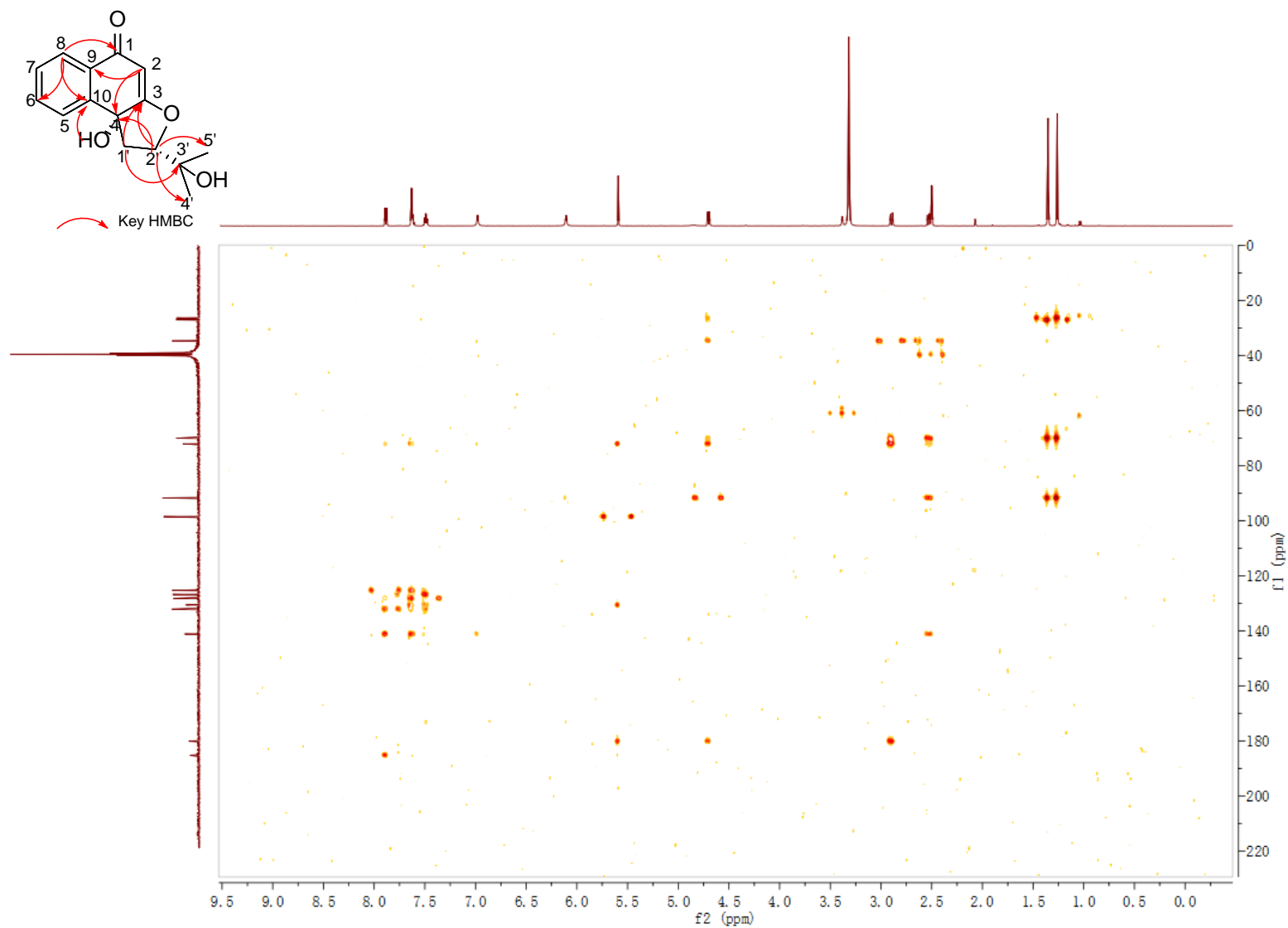
Figure S22. HMBC NMR spectrum of compound **5** in DMSO-*d6*

S33

Figure S23. NOESY NMR spectrum of compound **5** in DMSO-*d6*
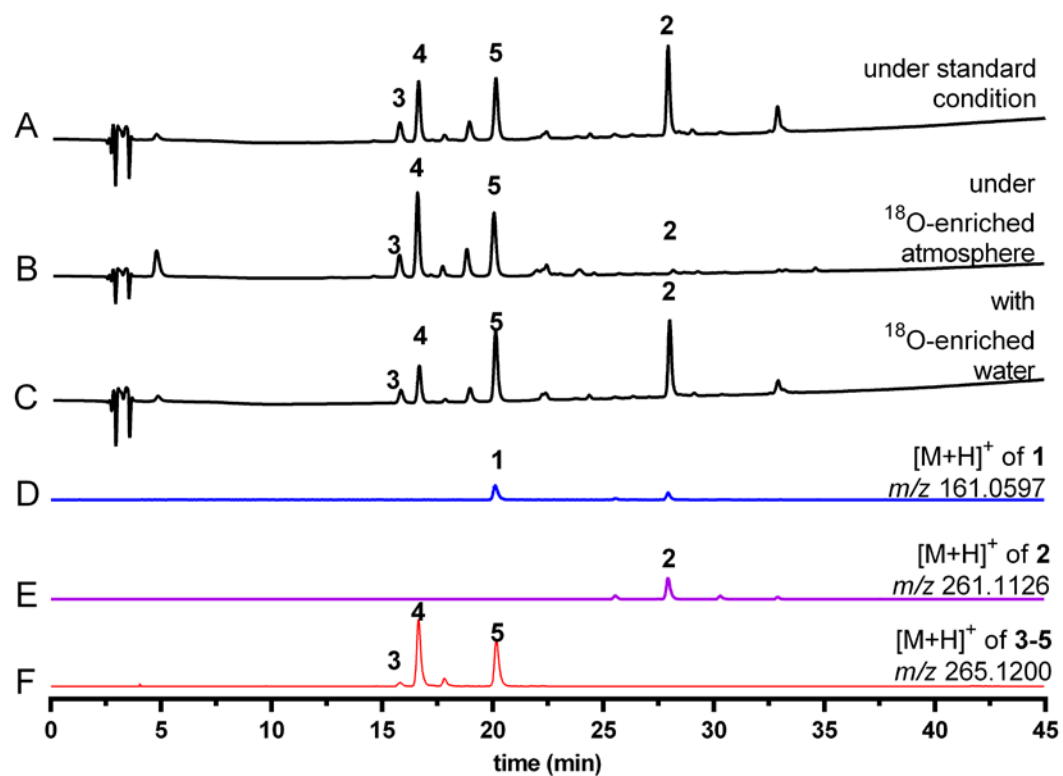
Figure S24. LC-HRMS analysis of the incubation mixtures with FgaPT2

The enzyme assays were incubated under standard condition (A), under ^{18}O-enriched atmosphere (B) or in buffer with ^{18}O-enriched water (C) at room temperature for 3h. Extracted Ion Chromatograms (EICs) refer [M + H]$^+$ ions of **1** (D), **2** (E) and **3−5** (F) with a tolerance range of ±0.005.

Referece list

1   A. B. Woodside, Z. Huang, and C. D. Poulter, *Org. Synth.*, 1988, **66**, 211-215.

2   N. Steffan, I. A. Unsöld, and S.-M. Li, *Chembiochem*, 2007, **8**, 1298-1307.

3   W.-B. Yin, H.-L. Ruan, L. Westrich, A. Grundmann, and S.-M. Li, *Chembiochem*, 2007, **8**, 1154-1161.

4   A. Grundmann and S.-M. Li, *Microbiology*, 2005, **151**, 2199-2207.

5   W.-B. Yin, A. Grundmann, J. Cheng, and S.-M. Li, *J. Biol. Chem.*, 2009, **284**, 100-109.

6   H. Ran, V. Wohlgemuth, X. Xie, and S.-M. Li, *ACS Chem. Biol.*, 2018, **13**, 2949-2955.

7   N. Steffan, A. Grundmann, A. Afiyatullov, H. Ruan, and S.-M. Li, *Org. Biomol. Chem.*, 2009, **7**, 4082-4087.

4.3 Biosynthesis of the prenylated salicylaldehyde flavoglaucin requires temporary reduction to salicyl alcohol for decoration before reoxidation to the final product

Letter

Biosynthesis of the Prenylated Salicylaldehyde Flavoglaucin Requires Temporary Reduction to Salicyl Alcohol for Decoration before Reoxidation to the Final Product

Jonas Nies,[§] Huomiao Ran,[§] Viola Wohlgemuth, Wen-Bing Yin, and Shu-Ming Li*

Read Online

ACCESS | Metrics & More | Article Recommendations | SI Supporting Information

ABSTRACT: The biosynthetic pathway of the prenylated salicylaldehyde flavoglaucin and congeners in *Aspergillus ruber* was elucidated by genome mining, heterologous expression, precursor feeding, and biochemical characterization. The polyketide skeleton was released as alkylated salicyl alcohols, which is a prerequisite for consecutive hydroxylation and prenylation, before reoxidation to the final aldehyde products. Our results provide an excellent example for a highly programmed machinery in natural product biosynthesis.
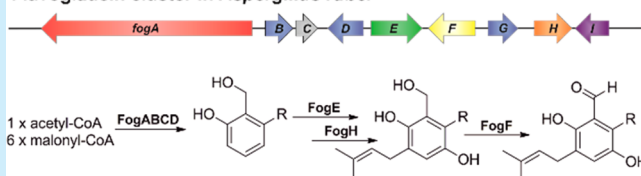
Flavoglaucin (**1a**) and congeners **1b−1h** are prenylated salicylaldehyde derivatives carrying a saturated or an unsaturated C$_7$ side chain (Figure 1). They were isolated from
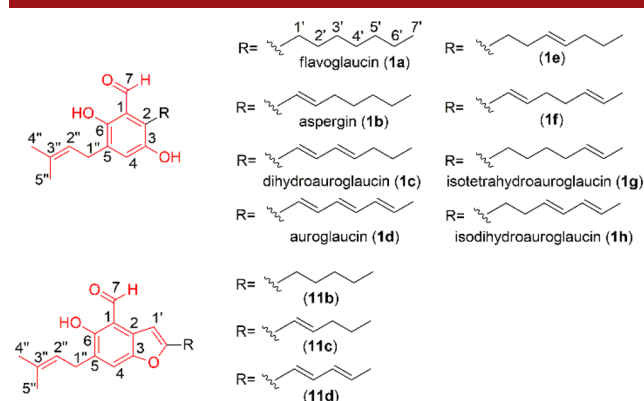
Figure 1. Flavoglaucin and congeners isolated from *A. ruber*.

various microorganisms including *Aspergillus ruber*[1−6] and show interesting biological activities.[2,6−11] Moreover, they are also proposed to be precursors of complex molecules like cryptoechinulin D and effusin A.[12,13] However, little is known about their biosynthesis and the involved enzymes.

Involvement of a highly reducing polyketide synthase (HR-PKS) was reported in the biosynthesis of the alkylated salicylaldehyde pyriculol in *Magnaporthe oryzae*.[14] A homologous (*srd*) cluster from *Neurospora crassa* was later identified for the biosynthesis of sordarial (Figure 2). Four genes coding for a HR-PKS SrdA, a cupin-domain-containing protein SrdD, and two short-chain dehydrogenases/reductases (SDRs) SrdC and SrdE are essential for the formation of sordarial, which was

likely reduced by a reductase from the host *Aspergillus nidulans* A1145.[15] Recently, the *vir* cluster was discovered for the trichoxide biosynthesis in *Trichoderma virens* (Figure 2) by expression in the same host A1145.[16] Three homologous genes of the sordarial cluster, VirA (SrdA homologue), VirB (SrdC), and VirD (SrdE), were proposed to be responsible for alkylated salicylaldehyde formation, which was then reduced by a third SDR VirG.[16]

Genome mining[17] revealed the presence of a nine-gene (*fog*) cluster in *A. ruber* with four homologues of more than 40% identity to that of the *srd* and six of the *vir* cluster (Figure 2). These include a HR-PKS FogA (homologue of SrdA and VirA), SDRs FogB (SrdC, VirB), FogD (SrdE, VirD), and FogG (VirG), a cupin protein FogC (SrdD, VirC), and a cytochrome P450 (CYP) FogE (VirE). This suggests the involvement of the *fog* cluster in the flavoglaucin biosynthesis, which was strongly supported by the presence of a prenyltransferase (PT) gene *fogH*. Furthermore, genes for an oxidoreductase FogF and a transcription factor (TF) FogI are also present. Orthologous clusters sharing sequence identities between 87.5 and 95.6% were found in the *A. glaucus* and *A. cristatus* genomes (Table S1 in Supporting Information (SI)). Cultivation of the three fungi and LC-MS analysis confirmed their capability to produce **1a** and congeners **1b−1f** (Figures 1 and SI, see below for identification).
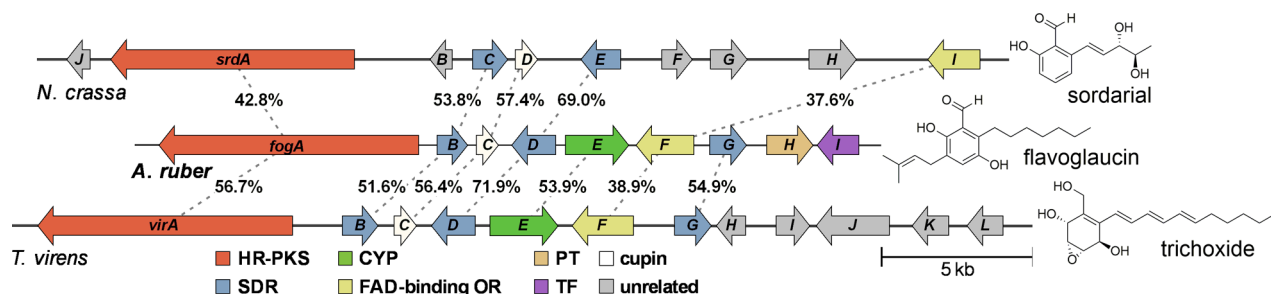
Figure 2. Comparison of *fog* cluster in *A. ruber* with *srd* cluster in *N. crassa* and *vir* cluster in *T. virens*. The sequence identities on the amino acid level are given as percent.

To provide evidence that the identified *fog* cluster is responsible for **1a** biosynthesis, the whole cluster *fogA-I* was assembled in *Saccharomyces cerevisiae* and integrated into the *A. nidulans* LO8030 genome[18] under control of their native promoters (see SI, Tables S2−S4 and Figures S2−S5 for details). LC-MS analysis of the resulting transformant *A. nidulans* JN004 led to detection of **1a**−**1f** (Figures 3ii and S6), in comparison to that of the control (Figure 3i). Isolation and structural elucidation (see SI for details; NMR data are given in SI and spectra as Figures S23−S73) confirmed **1a**, **1b**, **1c**, and **1d** as flavoglaucin,[7] aspergin,[7] dihydroauroglaucin,[1] and auroglaucin,[7] respectively. **1e** and **1f** were also reported previously.[2,19] Deletion of *fogI* led to complete abolishment of the cluster products (Figures 3iii), proving its importance as a positive regulator for gene expression, as reported for other TF genes.[20,21]

Having identified the *fog* cluster, we intended to elucidate the gene function. *fogA*, coding for a HR-PKS with the domain structure KS-AT-ACP-DH-ER-KR, was integrated into the LO8030 genome. LC-MS analysis of the *fogA* expression strain JN001 showed one major product peak **2d** and three minor peaks **3d**−**5d** (Figures 4Ai and S7). **2d** with a $[M(C_{14}H_{22}O_5) - H]^-$ ion at m/z 269.1387 (calcd 269.1389) was instable during isolation and converted in water easily to **3d**, **4d**, and **5d**, sharing a molecular formula of $C_{14}H_{20}O_4$ (Figures 4Aii and S7). Obviously, **2d** was converted to **3d**−**5d** by water elimination. Indeed, structural elucidation confirmed that **3d**, **4d**, and **5d** are lactone and tetrahydropyran derivatives of (8E,10E,12E)-3,5,7-trihydroxytetradeca-8,10,12-trienoic acid (**2d**) (Figure 4B). This result is consistent with that of VirA being responsible for assembling the polyketide chain but requiring additional enzymes for modification and cyclization. In contrast to VirA probably reducing acyl thioesters to aldehydes, FogA released a carboxylic acid **2d** as its product. Moreover, masses for its derivatives with one and two double bonds were also detected (Figure S7). This indicates that FogA is able to reduce the initial triketide, thus being at least partially responsible for the differently saturated heptyl side chains of **1a** congeners.

To find enzymes involved in the aromatic core formation, we deleted single genes in JN004. Deletion of *fogA* resulted in complete abolishment of product formation (Figure 3iv). Neither **1a** and congeners nor **2d** and its rearrangement products **3d**−**5d** could be observed by UV detection after removing *fogB*, *fogC*, or *fogD* from the cluster (Figure 3v−vii). This is in agreement with the expression results of *srdACD*.[15] However, inspection of the extracted ion chromatograms (EICs) of the Δ*fogB*, Δ*fogC*, and Δ*fogD* strains revealed the presence of **2d** (Figure S8). In comparison, no trace of **2d** was

detected in the EIC of the Δ*fogA* mutant. Conserved domain analysis revealed similarities between FogB and enoyl-(ACP) reductases, which catalyze double bond reduction in fatty acid biosynthesis and 3-oxoacyl-(ACP) reductases involved in the conversion between β-ketoacyl-ACP and β-hydroxyacyl-ACP.[22−24] Therefore, FogB was speculated to be responsible for oxidation of a hydroxyl group or reduction of remaining double bond(s) at the C_7 residue (Scheme 1). FogD shares a sequence identity of 71.9% with VirD (Figure 2), catalyzing both alcohol oxidation and aldehyde reduction.[16] The very low accumulation of **2d** in the Δ*fogD* mutant (Figure S8v) could indicate its role for the reductive release of the modified PKS products. In conclusion, this implies that the nascent polyketide is modified in FogA-bound form by FogBCD (Scheme 1).

Four products **6a**−**6d** were detected in the expression strains of *fogABCDI*, i.e., Δ*fogEFGH* from JN004 (Figures 3xi and S9), *fogABCDGI* (Δ*fogEFH*, Figures 3x and S10), and *fogABCDF-GHI* (Δ*fogE*, Figures 3ix and S11). Structural elucidation confirmed **6a**, **6b**, **6c**, and **6d** to be 2-alkyl salicyl alcohols with none, one, two, and three double bonds on the side chain, respectively (Scheme 1). This proved that FogABCD is necessary for the formation of the aromatic core and that the cyclized PKS products were released as salicyl alcohols. The cytochrome P450 FogE is responsible for the hydroxylation at C3 of the benzene ring afterward. FogG, however, seems to have no function because no difference between Δ*fogEFGH* and Δ*fogEFH* transformants (Figures 3x and xi) was observed, which was also confirmed by deletion of *fogG* from JN004 (Figures 3viii and S12). The same products **1a**−**1f** were detected from the *fog* cluster with and without *fogG* (Figures 3ii and viii). These results differ clearly from those observed for its homologue VirG (54.9% sequence identity), which catalyzes the reduction of salicylaldehydes to salicyl alcohols.[16] It can not be excluded that a FogG homologue from *A. nidulans* complements its function. However, the best hit AN5653.2 was found only to share a sequence identity of 37.0% with FogG.

Deletion of *fogE* alone resulted also in the accumulation of **1a** and **1b** as minor products (Figure 3ix). It seems that **6a** and **6b** were used by an endogenous enzyme from *A. nidulans* as substrates and converted to 2-heptyl-3,6-dihydroxybenzyl alcohols violaceoid C (**7a**) and A (**7b**),[25] which were subsequently metabolized by the enzymes of the flavoglaucin pathway. Hydroxylation of **6a** and **6b** by an *A. nidulans* enzyme was also observed in deletion mutants Δ*fogEFH* and Δ*fogEFGH* (Figures 3x and xi). However, the hydroxylated products **7a** and **7b** could not be further consumed in these strains. Blast search revealed indeed the presence of a
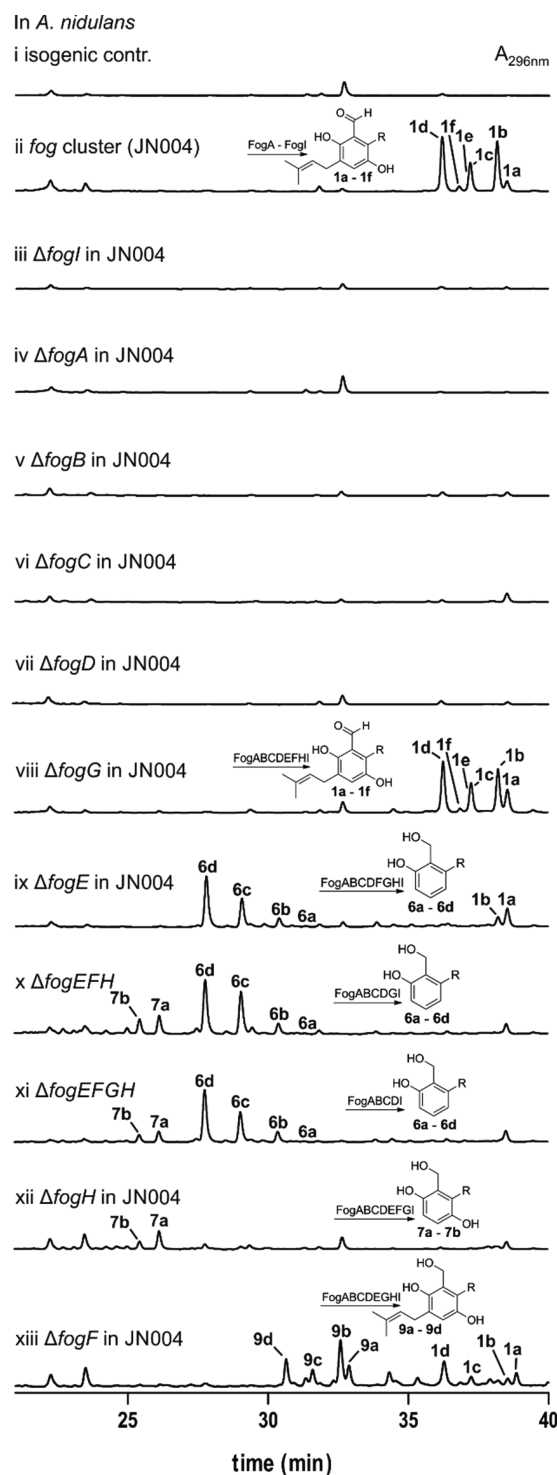
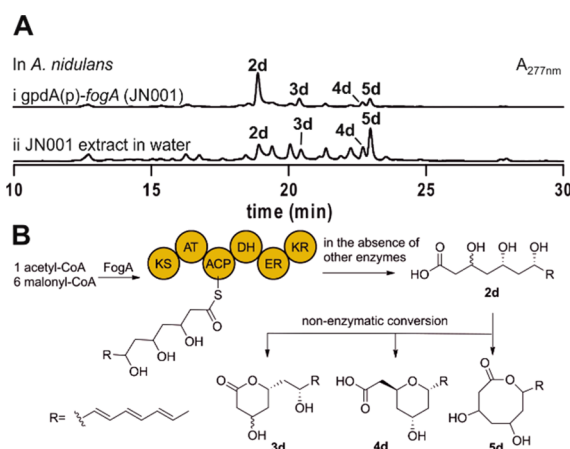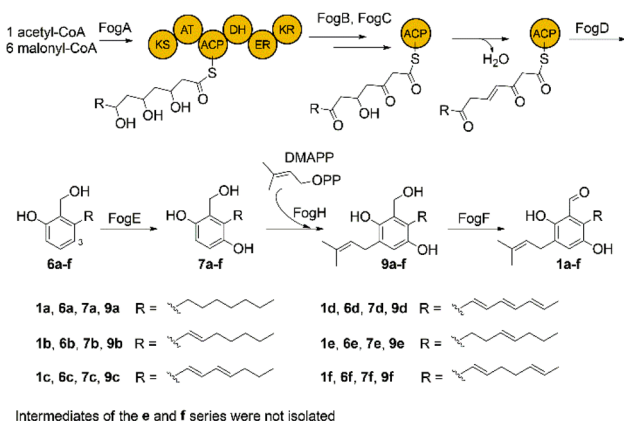**Figure 3.** LC-MS analysis of the extracts of *A. nidulans* strains.

Figure 4. HPLC analysis of the extract of *A. nidulans* JN001 harboring *fogA* and nonenzymatic conversion of **2d** to **3d**−**5d** (A). Schematic presentation of their relationships (B).
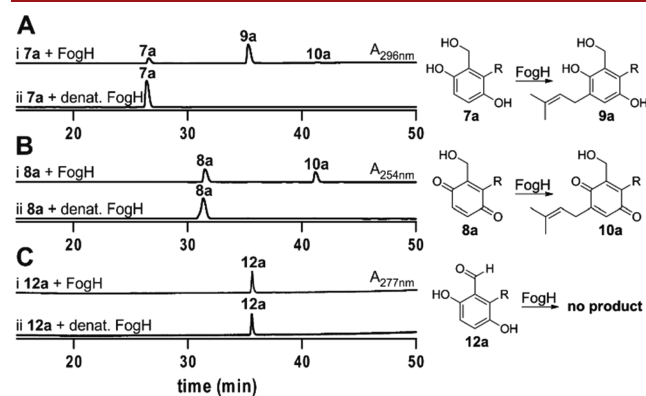
Scheme 1. Proposed Biosynthetic Pathway of Flavoglaucin and Congeners

Figure 5. *In vitro* assays of FogH with its natural substrate **7a** (A) and the corresponding quinone **8a** (B) as well as aldehyde **12a** (C).

candidate cytochrome P450 AN8358.4 in *A. nidulans*, sharing a sequence identity of 49% with FogE.

Accumulation of unprenylated derivatives **7a** and **7b** in the transformants with *fogH* deletion, i.e., Δ*fogEFH*, Δ*fogEFGH*, and Δ*fogH* (Figures 3x−xii, S9, S10, and S13), indicated that the FogE products are substrates of the prenyltransferase FogH (Scheme 1). This hypothesis was proven by biochemical characterization with recombinant FogH from *E. coli* (Figure S15). As shown in Figure 5Ai, 77.7% of **7a** was converted to **9a** by FogH after incubation with dimethylallyl diphosphate

(DMAPP) at 37 °C for 10 min. Structural elucidation confirmed **9a** as the expected prenylated product. During the isolation, it was observed that **9a** was unstable and can be easily oxidized to its quinone **10a**, which was also detected in the FogH assay with a yield of 2.3% (Figure 5Ai). Spontaneous conversion between **7a**, its quinone **8a**, and aldehyde **12a** as well as between **9a** and its quinone **10a** was proven by incubation in aqueous solution at 25 °C (Figures S16 and S17).

To provide evidence that the benzyl alcohol feature is really essential for the prenylation, we synthesized the corresponding aldehyde **12a** (Figure S18) and used it for FogH incubation. The benzoquinone alcohol **8a** was also tested. As shown in Figure 5, **8a** was well accepted by FogH and converted to **10a** with a yield of 41.0%. However, **12a** was not consumed by FogH at all, proving the alcohol group is a prerequisite for acceptance by FogH. Therefore, it makes sense that the aromatic core was released as alcohols rather than aldehydes, although the prenylated benzyl alcohols have to be finally oxidized back to aldehydes. This differs clearly from other known pathways. PTs utilize substituted benzoic acids, lactones, or aldehydes as substrates.[26−28] In the case of ilicicolin B, a metabolite closely related to flavoglaucin, orsellinic acid is first prenylated and subsequently reduced to the aldehyde.[29,30] Determination of kinetic parameters proved the dihydroquinone **7a** and congeners as natural substrates of FogH (Figure S19), being in consistence with **7a** and **7b** as products of the Δ*fogH* mutants (Figures 3x−xii).

The prenylation product **9a** has to be oxidized to **1a** subsequently. We therefore deleted the oxidoreductase gene *fogF* from the cluster, leading indeed to the accumulation of **9a** and congeners **9b−9d** (Figures 3xiii and S14). As observed for **7a**, compounds **9a−9d** were instable and rapidly oxidized to their quinone form, so that **9a** was isolated as its quinone **10a** and **9b** as a benzofuran derivative **13b** after oxidation and intramolecular cyclization (Figure S20). This phenomenon could explain the isolation of flavoglaucin congeners with a benzofuran ring from fungi like *A. ruber*.[1] The prenylated dihydroquinone alcohols **9a−9d** differ from the final cluster products only in the oxidation stage of the hydroxymethyl group. Accumulation of **9a−9d** as major products in the Δ*fogF* mutant indicates its role for the oxidation of the benzyl alcohols to final aryl aldehydes, i.e., the last step in the biosynthesis of flavoglaucin and congeners (Scheme 1). The presence of **1a−1d** in the mutant is very likely caused by direct nonenzymatic oxidation of the alcohol to the aldehyde, which was confirmed by detection of **1a** as the minor product after incubation of **9a** in PDB medium (Figure 6Aiii).
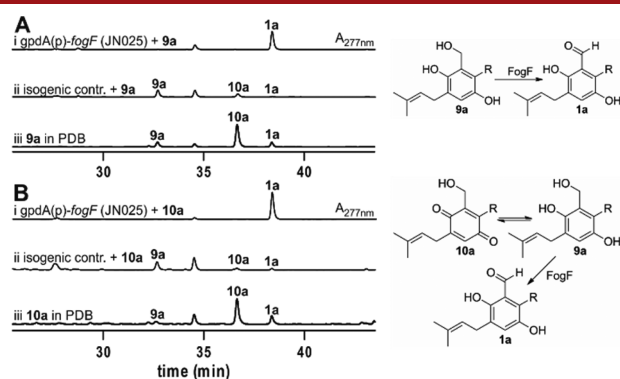
Figure 6. Feeding of **9a** (A) and its quinone **10a** (B) to *A. nidulans* JN025 harboring *fogF*.

Attempts to produce recombinant FogF for biochemical investigation failed (data not shown). We therefore verified its function by expressing *fogF* in *A. nidulans*. The overexpression strain JN025 was cultivated in PDB medium and fed with **9a** and the corresponding quinone **10a** for 4 days at final concentrations of 50 μM. In PDB medium, 66.5% of **9a** was

oxidized to **10a** (Figure 6Aiii). 95% of **9a** was converted to **1a** in JN025 (Figure 6Ai), significantly higher than the 2.8% conversion in the isogenic control (Figure 6Aii). In this culture, **9a** was still the major product (77%), and only 20% was oxidized to quinone **10a**. It seems that the *A. nidulans* culture condition is more suitable to keep the reduced form of dihydroquinone/benzoquinone, being in consistence not only with the detected products **9a−9d** in the Δ*fogF* mutant (Figure 3xiii) but also with the results obtained by feeding **10a** in JN025. As shown in Figure 6B, 98.7% of the fed **10a** was converted to **1a** in JN025, while only 1.4% was transformed to **1a** and 87% to **9a** in the isogenic control. It is plausible that the fed **10a** was first converted to **9a** and then oxidized to **1a** by FogF. Furthermore, reactions between two quinone molecules as shown in Figure S17 also contribute to the presence of **9a**, **10a**, and **1a** in isogenic controls (Figure 6).

Additionally, the unprenylated **7a** and the benzofuran derivative **13b** were fed into the *fogF* overexpression mutant JN025. Neither **7a** nor **13b** was converted to their expected aldehydes **12a** and **11b**, proving the importance of the prenyl moiety and the noncyclized C₇ side chain (Figures S21 and S22). The furan ring of the related flavoglaucin derivatives is very likely formed after oxidation of the benzyl alcohol to aldehyde via nonenzymatic rearrangements as demonstrated above.

In summary, we elucidated the biosynthetic pathway for flavoglaucin and congeners. As reported previously,[15,16] several enzymes are necessary for the formation of the aromatic core structure. Differing from the trichoxide biosynthesis,[16] the backbone of flavoglaucin was released as salicyl alcohol, which is critical for the subsequent hydroxylation and prenylation. After decoration, the alcohol was oxidized to the final aldehyde products by an oxidase, which only accepted prenylated derivatives as substrates. Therefore, this study demonstrated a highly programmed biosynthetic pathway.

■ ASSOCIATED CONTENT

ⓢ Supporting Information

The Supporting Information is available free of charge at https://pubs.acs.org/doi/10.1021/acs.orglett.0c00440.

Materials, experimental procedures, physiochemical properties, and spectroscopic data (PDF)

■ AUTHOR INFORMATION

Corresponding Author

Shu-Ming Li − *Institut für Pharmazeutische Biologie und Biotechnologie, Philipps-Universität Marburg, 35037 Marburg, Germany;* ⓞ orcid.org/0000-0003-4583-2655; Email: shuming.li@staff.uni-marburg.de

Authors

Jonas Nies − *Institut für Pharmazeutische Biologie und Biotechnologie, Philipps-Universität Marburg, 35037 Marburg, Germany*

Huomiao Ran − *Institut für Pharmazeutische Biologie und Biotechnologie, Philipps-Universität Marburg, 35037 Marburg, Germany*

Viola Wohlgemuth − *Institut für Pharmazeutische Biologie und Biotechnologie, Philipps-Universität Marburg, 35037 Marburg, Germany*

Wen-Bing Yin − *State Key Laboratory of Mycology and CAS Key Laboratory of Microbial Physiological and Metabolic*

Engineering, Institute of Microbiology, Chinese Academy of Sciences, Beijing 100101, China; ● orcid.org/0000-0002-9184-3198

Complete contact information is available at:
https://pubs.acs.org/10.1021/acs.orglett.0c00440

Author Contributions

§J.N. and H.R. contributed equally.

Notes

The authors declare no competing financial interest.

■ ACKNOWLEDGMENTS

■ REFERENCES

(1) Li, D.-L.; Li, X.-M.; Li, T.-G.; Dang, H.-Y.; Proksch, P.; Wang, B.-G. *Chem. Pharm. Bull.* **2008**, *56*, 1282.

(2) Cho, J. Y.; Kim, M. S. *Fish. Sci.* **2012**, *78*, 1065.

(3) Gould, B. S.; Raistrick, H. *Biochem. J.* **1934**, *28*, 1640.

(4) Yoshihira, K.; Takahashi, C.; Sekita, S.; Natori, S. *Chem. Pharm. Bull.* **1972**, *20*, 2727.

(5) Ishikawa, Y.; Morimoto, K.; Hamasaki, T. *J. Am. Oil Chem. Soc.* **1984**, *61*, 1864.

(6) Gao, J.; León, F.; Radwan, M. M.; Dale, O. R.; Husni, A. S.; Manly, S. P.; Lupien, S.; Wang, X.; Hill, R. A.; Dugan, F. M.; Cutler, H. G.; Cutler, S. J. *J. Nat. Prod.* **2011**, *74*, 1636.

(7) Miyake, Y.; Ito, C.; Itoigawa, M.; Osawa, T. *Biosci., Biotechnol., Biochem.* **2009**, *73*, 1323.

(8) Kim, K. S.; Cui, X.; Lee, D. S.; Ko, W.; Sohn, J. H.; Yim, J. H.; An, R. B.; Kim, Y. C.; Oh, H. *Int. J. Mol. Sci.* **2014**, *15*, 23749.

(9) Shi, J.; Liu, J.; Kang, D.; Huang, Y.; Kong, W.; Xiang, Y.; Zhu, X.; Duan, Y.; Huang, Y. *ACS Omega* **2019**, *4*, 6630.

(10) Miyake, Y.; Ito, C.; Tokuda, H.; Osawa, T.; Itoigawa, M. *Biosci., Biotechnol., Biochem.* **2010**, *74*, 1120.

(11) Liang, T. M.; Fang, Y. W.; Zheng, J. Y.; Shao, C. L. *Chem. Nat. Compd.* **2018**, *54*, 559.

(12) Gao, H.; Liu, W.; Zhu, T.; Mo, X.; Mandi, A.; Kurtan, T.; Li, J.; Ai, J.; Gu, Q.; Li, D. *Org. Biomol. Chem.* **2012**, *10*, 9501.

(13) Li, D.-L.; Li, X.-M.; Li, T.-G.; Dang, H.-Y.; Wang, B.-G. *Helv. Chim. Acta* **2008**, *91*, 1888.

(14) Jacob, S.; Grötsch, T.; Foster, A. J.; Schüffler, A.; Rieger, P. H.; Sandjo, L. P.; Liermann, J. C.; Opatz, T.; Thines, E. *Microbiology* **2017**, *163*, 541.

(15) Zhao, Z.; Ying, Y.; Hung, Y. S.; Tang, Y. *J. Nat. Prod.* **2019**, *82*, 1029.

(16) Liu, L.; Tang, M. C.; Tang, Y. *J. Am. Chem. Soc.* **2019**, *141*, 19538.

(17) Weber, T.; Blin, K.; Duddela, S.; Krug, D.; Kim, H. U.; Bruccoleri, R.; Lee, S. Y.; Fischbach, M. A.; Müller, R.; Wohlleben, W.; Breitling, R.; Takano, E.; Medema, M. H. *Nucleic Acids Res.* **2015**, *43*, W237.

(18) Chiang, Y. M.; Ahuja, M.; Oakley, C. E.; Entwistle, R.; Asokan, A.; Zutz, C.; Wang, C. C.; Oakley, B. R. *Angew. Chem., Int. Ed.* **2016**, *55*, 1662.

(19) Huang, Y.; Ma, L.; Rong, X.; Liu, D.; Liu, S.; Liu, W. *Chin. Tradit. Herbal Drugs* **2012**, *43*, 837.

(20) Bok, J. W.; Chung, D.; Balajee, S. A.; Marr, K. A.; Andes, D.; Nielsen, K. F.; Frisvad, J. C.; Kirby, K. A.; Keller, N. P. *Infect. Immun.* **2006**, *74*, 6761.

(21) Chiang, Y. M.; Szewczyk, E.; Davidson, A. D.; Keller, N.; Oakley, B. R.; Wang, C. C. *J. Am. Chem. Soc.* **2009**, *131*, 2965.

(22) Massengo-Tiassé, R. P.; Cronan, J. E. *Cell. Mol. Life Sci.* **2009**, *66*, 1507.

(23) Marchler-Bauer, A.; Bo, Y.; Han, L.; He, J.; Lanczycki, C. J.; Lu, S.; Chitsaz, F.; Derbyshire, M. K.; Geer, R. C.; Gonzales, N. R.; Gwadz, M.; Hurwitz, D. I.; Lu, F.; Marchler, G. H.; Song, J. S.; Thanki, N.; Wang, Z.; Yamashita, R. A.; Zhang, D.; Zheng, C.; Geer, L. Y.; Bryant, S. H. *Nucleic Acids Res.* **2017**, *45*, D200.

(24) Shimakata, T.; Stumpf, P. K. *Arch. Biochem. Biophys.* **1982**, *218*, 77.

(25) Myobatake, Y.; Takemoto, K.; Kamisuki, S.; Inoue, N.; Takasaki, A.; Takeuchi, T.; Mizushina, Y.; Sugawara, F. *J. Nat. Prod.* **2014**, *77*, 1236.

(26) Matsuda, Y.; Abe, I. *Nat. Prod. Rep.* **2016**, *33*, 26.

(27) Saeki, H.; Hara, R.; Takahashi, H.; Iijima, M.; Munakata, R.; Kenmoku, H.; Fuku, K.; Sekihara, A.; Yasuno, Y.; Shinada, T.; Ueda, D.; Nishi, T.; Sato, T.; Asakawa, Y.; Kurosaki, F.; Yazaki, K.; Taura, F. *Plant Physiol.* **2018**, *178*, 535.

(28) Zhang, W.; Du, L.; Qu, Z.; Zhang, X.; Li, F.; Li, Z.; Qi, F.; Wang, X.; Jiang, Y.; Men, P.; Sun, J.; Cao, S.; Geng, C.; Qi, F.; Wan, X.; Liu, C.; Li, S. *Proc. Natl. Acad. Sci. U. S. A.* **2019**, *116*, 13305.

(29) Araki, Y.; Awakawa, T.; Matsuzaki, M.; Cho, R.; Matsuda, Y.; Hoshino, S.; Shinohara, Y.; Yamamoto, M.; Kido, Y.; Inaoka, D. K.; Nagamune, K.; Ito, K.; Abe, I.; Kita, K. *Proc. Natl. Acad. Sci. U. S. A.* **2019**, *116*, 8269.

(30) Li, C.; Matsuda, Y.; Gao, H.; Hu, D.; Yao, X. S.; Abe, I. *ChemBioChem* **2016**, *17*, 904.

SUPPORTING INFORMATION

Biosynthesis of the prenylated salicylaldehyde flavoglaucin requires temporary reduction to salicyl alcohol for decoration before reoxidation to final product

Jonas Nies[a,‡], Huomiao Ran[a,‡], Viola Wohlgemuth[a], Wen-Bing Yin,[b] and Shu-Ming Li*[,a]

[a] Institut für Pharmazeutische Biologie und Biotechnologie, Philipps-Universität Marburg, Robert-Koch-Straße 4, Marburg 35037, Germany

[b] State Key Laboratory of Mycology and CAS Key Laboratory of Microbial Physiological and Metabolic Engineering, Institute of Microbiology, Chinese Academy of Sciences, Beijing 100101, China

[‡]These authors contributed equally to this work.

Table content

S3

134

S4

Experimental Procedures

1. Strain cultivation

Escherichia coli DH5α was used for DNA propagation. The bacteria were cultivated at 37°C on Lysogeny Broth medium (LB) supplemented with carbenicillin (50 µg/ml) for selection.

Saccharomyces cerevisiae HOD114-2B was used for cloning by homologous recombination.[1] Generally, yeast was grown at 30°C in YPD medium [1% yeast extract, 2% peptone and 2% glucose]. Selection was performed with synthetic complete (SC) medium without uracil (SC-Ura) [6.7 g/L yeast nitrogen base with ammonium sulfate, 650 mg/L CSM-His-Leu-Ura (MP Biomedicals), histidine and leucine].[2]

Aspergillus nidulans strains were cultured at 37°C on Glucose Minimal Medium (GMM)[3] supplemented with 1 mg/ml uracil, 2.442 mg/ml uridine, 2.5 µg/ml riboflavin and 0.5 mg/ml pyridoxine depending on used selective marker genes. Small-scale fermentation in order to prove new metabolites in the created strains was carried out on 10 g Alnatura long-grain rice with 15 ml distilled H_2O (total volume assumed: 25 ml) supplemented with uracil, uridine, riboflavin or 5 g/L yeast extract for pyridoxine-auxotrophy depending on the selective marker used. These cultures were incubated at 25°C for 10 days.

Aspergillus ruber, *Aspergillus cristatus* and *Aspergillus glaucus* were cultivated at 25°C on Potato Dextrose medium [24 g/L potato dextrose broth (Sigma Aldrich)] either in a standing culture or shaking at 200 rpm for 14–28 days.

2. Isolation of DNA from fungi

For genomic DNA (gDNA) isolation, *A. ruber* QEN-0407-G2 was grown in Potato Dextrose Broth at 25°C and shaking at 230 rpm for 14 days. The mycelium was collected, washed with distilled H_2O, frozen with liquid nitrogen and powdered with mortar and pestle. 1.2 ml Digestion Buffer [100 mM NaCl, 10 mM Tris, 25 mM EDTA, 0,5% (w/v) SDS; pH 8] with 0.1 mg/ml proteinase K were added to 100 mg powdered mycelium. The mixture was incubated at 50°C for 2 h with shaking at 160 rpm. The gDNA was extracted by addition of one volume phenol/chloroform/isoamyl alcohol (25:24:1). After inversion of the mixture for 2 min and centrifugation at 13000 rpm for 5 min the aqueous phase was taken and the DNA was precipitated by addition of 0.1 volume 3 M sodium acetate and 1 volume 2-propanol before centrifugation of the mixture at 13000 rpm at 4°C for 30 min. The DNA was washed once with 600 µl 70% (v/v) ethanol and dissolved in distilled H_2O after drying at 55°C.

For quick gDNA isolation from *A. nidulans*, the fungus was grown in 0.5 ml GMM at 37°C overnight. The lightly dried mycelium was transferred into 400 µl LETS solution [20 mM EDTA, 0.5% (w/v) SDS, 0.1 M LiCl, 10 mM Tris-HCl; pH 8] and crushed with glass beads in a Minilys Homogenizer (Bertin Technologies, Montigny-le-Bretonneux. France) for 200 seconds at full speed. 300 µl LETS solution were added and the further gDNA extraction was carried out as described above.

3. Isolation of RNA and cDNA synthesis

A. ruber QEN-0407-G2 was grown as a shaking culture in PDB at 25°C and 230 rpm for two

S5

weeks. The mycelium was separated from the medium by filtration. Total mRNA was extracted with the E.Z.N.A® Fungal RNA Kit (Omega bio-tek, Norcross, USA) according to the manual. The mRNA was used for cDNA synthesis with the help of the ProtoScript® First Strand cDNA Synthesis Kit (New England BioLabs, Ipswich, USA) using oligo-dT primers.

4. Cloning of flavoglaucin cluster for heterologous expression in *A. nidulans* LO8030

The flavoglaucin cluster (EURHEDRAFT_499888 - _402538 + 500 bp upstream of the first and downstream of the last gene; bp 222263-244370; unplaced genomic scaffold00012; *A. ruber* CBS135680 genome GenBank: KK088422) was amplified from gDNA of *A. ruber* QEN-0407-G2 in 5 fragments with primers listed in Table S2. The fragments were designed with a 300–322 bp overlap to each other, the outmost fragments carried a 25 bp overlap to the linearized pYWB2 which in turn had an overlap to the outmost fragments of 24 bp (Table S2). pYWB2 was linearized via PCR with the primers prJN081 & prJN091 (Table S2). The reconstruction of the cluster and cloning into the plasmid was carried out by yeast homologous recombination as described[4], leading to pJN014 (Table S3). In analogy, pJN041 for triple deletion mutant JN020 Δ*fogEFH* was created similarly. The cluster fragments ended before the first or started after the last base of the genes to be deleted and shared 25 bp overlap to each other.

5. Cloning of the deletion vectors

For the deletion of the single genes of the flavoglaucin gene cluster, 1.2 kb upstream and downstream of the respective gene were amplified with primers listed in Table S2 introducing complementary overhangs of 30-35 bp to the backbone of pYWB2 and the *pyrG*-gene cassette of *A. fumigatus,* which served as selection marker. The cloning of *AfpyrG* between the 5'- and 3'-regions into pYWB2 to form the deletion vector was performed via yeast homologous recombination.

6. Cloning of pVW84 for heterologous expression of *fogH* in *E. coli*

The open reading frame for *fogH* without any introns was amplified from *A. ruber* QEN-0407-G2 cDNA with primers vwRbPT3-f' and vwRbPT3-r introducing recognition sites for SphI (5') and BamHI (3'). The commercially available vector pQE-70 (Qiagen, Venlo, Netherlands) and the *fogH* fragment were digested with SphI and BamHI and purified *via* ethanol precipitation. The purified vector and DNA fragment were ligated with T4 DNA ligase (Jena Bioscience, Jena, Germany) according to the manual before transformation of *E. coli* DH5α with the ligation mixture.

7. Cloning of pJN052 for heterologous expression of *fogF* in *A. nidulans* LO8030

The whole gene *fogF* with 500 bp 3' of the stop codon were amplified from *A. ruber* QEN-0407-G2 gDNA using primers prJN277 and prJN278 (Table S2) exhibiting 30 bp overhang to SfoI-linearized pJN017. The linearized plasmid and the DNA-fragment were cloned together via homologous recombination in yeast to give pJN052.

8. Transformation of *A. nidulans* LO8030

The transformation of *A. nidulans* LO8030 was performed through PEG-mediated protoplast transformation as described[5] with one alteration. Cell wall degradation of the germlings was achieved by digestion with 20 mg yatalase (Takara Bio Inc., Japan) and 50 mg lysing enzymes from *Trichoderma harzianum* (Sigma-Aldrich, St. Louis, USA) in 10 ml osmotic medium (1.2 M

MgSO$_4$, 10 mM sodium phosphate buffer, adjusted to pH 5.8) for 2 - 3 h at 37°C and shaking at 100 rpm.

9. Confirmation of positive *A. nidulans* transformants

gDNA of the transformants was isolated and checked by PCR. Since the correct integration into the waPKS gene locus could be observed by a color change of the conidia from green to white, the presence of the integrated cluster/gene was verified by a single PCR with primers amplifying parts of the inserted gene(s) (Table S2, Figure S1). Primers for the control of gene deletion mutants were binding upstream or downstream of the homologous parts used for integration with counterparts binding in the marker gene. Additionally, a PCR with primers binding in the deleted gene was performed to ensure its absence (Figure S2).

10. Feeding experiments in the *fogF* expression strain *A. nidulans* JN025

In order to test the function of the FAD-dependent oxidoreductase FogF, heterologous expression strain JN025 was created with *fogF* under control of the constitutive gpdA-promoter. 5 ml PDB with 1 mg/ml (8.9 mM) uracil, 2.442 mg/ml (10 mM) uridine, 0.5 mg/ml pyridoxine and 50 μg/ml carbenicillin in a 25 ml Erlenmeyer flask were inoculated with 4x10^5 spores. As substrates the compounds **7a**, **9a**, **10a**, and **13a** were dissolved in DMSO and added to the culture for a final concentration of 50 μM directly after inoculation. In addition to the expression strain JN025, the isogenic control JN002 and a culture without any fungus were also tested to monitor stability of the substrates in the medium. The standing cultures were incubated at 25°C for 4 days. Mycelium and the remaining liquid were transferred into a 50 ml reaction tube. 30 ml EtOAc were added and the mixture was homogenized with a T 18 digital ULTRA-TURRAX (IKA, Staufen, Germany) for 30 sec at 10000 rpm. To achieve better phase separation, the mixture was centrifuged for 5 min at 5000 rpm. The organic phase was filtered and dried via evaporation. The extracts were dissolved in acetonitrile (ACN) and analyzed via LCMS.

11. Large-scale fermentation, extraction and isolation of secondary metabolites

To isolate flavoglaucin (**1a**) and its derivatives (**1b−1f**), *A. nidulans* JN004 spores were inoculated into 10 x 2 L-Fernbach flasks containing 100 g Alnatura long-grain rice and 150 mL H$_2$O supplemented with 500 mg/L uracil + uridine and 5 g/L yeast extract in a total volume of 250 ml each and cultivated at 25°C for 14 days. The cultures were extracted with equal volume of EtOAc for three times, which was then concentrated and evaporated under reduced pressure to obtain a crude extract (9.8 g). The crude extract was subjected to silica gel column chromatography, eluted with petroleum ether (PE) / EtOAc (50:1 to 10:1, gradient), to give nine fractions (1–9). Fraction 3, eluted with PE / EtOAc (30:1), was further purified on semi-preparative HPLC (ACN/H$_2$O (85:15)) to yield flavoglaucin (**1a**) (5 mg) and aspergin (**1b**) (8 mg). While **1e** (3 mg), **1c** (2 mg), and **1f** (1.5 mg) were obtained from fraction 4 (PE / EtOAc 25:1) by using Sephadex LH-20 column eluting with methanol (MeOH) and subsequent semi-preparative HPLC (ACN/H$_2$O (80:20)). Fraction 6 (PE / EtOAc 20:1) was separated on semi-preparative HPLC (ACN/H$_2$O (80:20)) to yield **1d** (3 mg).

To isolate **2d** rearrangement products **3d–5d**, *A. nidulans* JN001 was cultivated in 15 x 2 L-Fernbach flasks each containing 100 g rice and 150 mL H$_2$O supplemented with 500 mg/L uracil + uridine and 5 g/L yeast extract (for an assumed total volume of 250 ml per flask) at 25°C for

7 days. The cultures were extracted with EtOAc as mentioned above to obtain a crude extract (6.3 g). The crude extract was fractionated on a silica gel column and eluted with a gradient PE / acetone (5:1, 4:1, 3:1, 2:1, 1:1, 1:2, and 1:3), yielding seven fractions (1–7). Further purification of fraction 5 on a silica gel column with dichloromethane (CH_2Cl_2) / MeOH (30:1) as solvents afforded three subfractions. Subfraction 1 was subjected to semi-preparative HPLC (ACN/H_2O (35:65)) to give **3d** (10 mg). Fraction 4 (PE / acetone 2:1) was separated on Sephadex LH-20 column eluting with MeOH to yield pure **4d** (5 mg). **5d** (3 mg) was obtained from fraction 3 by semi-preparative HPLC (ACN/H_2O (40:60)).

To isolate **1a−1d**, *A. nidulans* JN007 was cultivated in 10 x 2 L-Fernbach flasks each containing 100 g rice and 150 mL H_2O supplemented with 5 g/L yeast extract in a total volume of 250 ml per flask at 25°C for 10 days. The cultures were extracted with EtOAc as mentioned above to obtain a crude extract (4.9 g). The crude extract was separated on a silica gel column and eluted with a gradient of PE / EtOAc (20:1 to 1:1) to give 5 fractions (1–5). **6a** (3 mg) and **6b** (5 mg) were obtained by semi-preparative HPLC (ACN/H_2O (70:30)) from fraction 3 (PE / EtOAc 5:1), while **6c** (2 mg) was purified by semi-preparative HPLC (ACN/H_2O (65:35)) from fraction 4 (PE / EtOAc 3:1). Compound **6d** (2 mg) was obtained by semi-preparative HPLC (ACN/H_2O (70:30)) from fraction 5 (PE / EtOAc 3:1).

To isolate **7a** and **7b**, *A. nidulans* JN006 was cultivated in 30 x 2 L-Fernbach flasks each containing 100 g rice and 150 mL H_2O supplemented with 5 g/L yeast extract in a total volume of 250 ml per flask) at 25°C for 10 days. The cultures were extracted with EtOAc as mentioned above to obtain a crude extract (5.9 g). The crude extract was subjected to silica gel column chromatography and eluted with a gradient PE / acetone (4:1, 3:1, and 2:1) to give 3 fractions (1–3). **7b** (15 mg) and **7a** (6 mg) were isolated by semi-preparative HPLC (ACN/H_2O (50:50)) from fraction 2 (PE / acetone 3:1).

To isolate **9a** and **9b**, which converted to **10a** and **13b** during isolation, *A. nidulans* JN010 was cultivated in 10 x 2 L-Fernbach flasks each containing 100 g rice and 150 mL H_2O supplemented with 5 g/L yeast extract in a total volume of 250 ml per flask at 25°C for 10 days. The cultures were extracted with EtOAc as mentioned above to obtain a crude extract (2.6 g). The crude extract was fractionated on a silica gel column and eluted with a gradient PE / EtOAc (30:1 to 5:1) to give 6 fractions (1–6). **10a** (8 mg) and **13b** (6 mg) were obtained by semi-preparative HPLC (ACN/H_2O (80:20)) from fraction 3 and 4 (PE / EtOAc 15:1 and 10:1), respectively.

12. Overproduction and purification of FogH

The *fogH* expression plasmid pVW84 was used to transform *E. coli* XL1-Blue. An overnight preculture was used to inoculate 20 x 100 ml LB in 250 ml Erlenmeyer flasks to an OD_{600} of 0.6. These cultures were incubated at 30°C with shaking at 230 rpm for 16–24 h without any induction. The recombinant 6xHis-tagged protein was purified via NiNTA-agarose column (Qiagen, Hilden, Germany) and further subjected to preparative gel filtration chromatography using a Superdex 200 16/60 pg column connected to a ÄKTAprime plus (GE Healthcare, Chalfont St Giles, Great Britain) with storage buffer [50 mM Tris-HCl, 150 mM NaCl, 20 % (w/v) glycerol, pH 7.5] at a flow rate of 0.5 ml/min. The purified protein was analyzed via SDS-PAGE

(Figure S17).

13. *In vitro* assays of FogH

To determine the enzyme activity toward **7a**, **8a**, or **12a** (see below for synthesis), the enzyme assays (50 µL) contained Tris-HCl buffer (50 mM, pH 7.5), CaCl$_2$ (10 mM), dimethylallyl diphosphate (DMAPP) (2 mM), **7a** (0.1 mM), **8a** (0.1 mM, immediately after isolation) or **12a** (0.1 mM), glycerol (0.5−5%), DMSO (up to 5%), and the purified recombinant FogH (0.1 µM). The enzyme assays were incubated at 37°C for 10 min and terminated with one volume of ACN. The reaction mixtures were centrifuged at 17000 $\times g$ for 30 min before further analysis on HPLC.

To isolate **8a** as a non-enzymatic conversion product of **7a**, 5 mg **7a** was incubated in 10 ml Tris-HCl buffer (50 mM, pH 7.5), CaCl$_2$ (10 mM), DMAPP (2 mM) at 37°C for 16 h. The reaction mixture was extracted subsequently with double volume of EtOAc for three times and then subjected to semi-preparative HPLC (ACN/H$_2$O (60:40)) to give **8a** (4 mg).

To isolate **9a** (enzymatic product) and **10a** (non-enzymatic conversion product), 8 mg of **7a** was incubated in 10 ml Tris-HCl buffer (50 mM, pH 7.5), CaCl$_2$ (10 mM), DMAPP (2 mM) and FogH (5 µM) at 37°C for 16 h. The reaction mixture was extracted subsequently with double volume of EtOAc for three times and then subjected on semi-preparative HPLC (ACN/H$_2$O (85:15)) to give **9a** (3 mg) and **10a** (4 mg).

14. Spontaneous conversion between dihydroquinones, quinones and aldehyde

For testing the dihydroquinone derivative stability, **7a** was incubated in aqueous solution at 25°C for up to 4 h. Its oxidized form **8a** was observed already after 30 minutes (Figure S20). Interestingly, **8a** in turn could be spontaneously reduced again to **7a** and converted to the salicylaldehyde **12a** in a ratio of approximately 1:1 after incubation at 25°C for 4 h (Figure S20). The same behavior was also shown for their prenylated counterparts **9a** and **10a** (Figure S20). Therefore, it can be proposed that the benzoquinone alcohol **8a** or **10a** can act as both oxidant and reductant to form dihydroquinone alcohol and aldehyde products with involvement of an instable benzoquinone aldehyde intermediate (Figure S21).

15. Determination of kinetic parameters of FogH

For determination of kinetic parameters of FogH toward **7a** and **8a** (Figure S18), the enzyme assays were performed in 50 µL reaction mixture containing Tris-HCl buffer (50 mM, pH 7.5), CaCl$_2$ (10 mM), DMAPP (2 mM), glycerol (0.5 %), DMSO (2 %), and the purified recombinant FogH (0.1 µM). The concentrations of substrates **7a** and **8a** were 0.01, 0.02, 0.05, 0.1, 0.2, 0.5, 1 mM. The reactions were carried out at 37°C for 10 min, terminated with one volume ACN, and centrifuged at 17,000 $\times g$ for 30 min before further analysis on LC-MS. The kinetic parameters K_M and k_{cat} were determined using non-linear regression analysis of Michaelis-Menten equation by GraphPad Prism 6. All reactions were carried out in triplicate and values reported were taken as the average of these data. **7a** is a slightly better substrate, with a K_M at 0.07 ± 0.01 mM and a k_{cat} at 2.02 ± 0.08 s^{-1}, than **8a** with a K_M at 0.09 ± 0.01 mM and a k_{cat} of 1.15 ± 0.04 s^{-1} (Figure S18).

16. Chemical synthesis of the salicylaldehyde 12a

For *in vitro* assays of FogH, the salicylaldehyde derivative **12a** was synthesized chemically according to the published methods (Figure S19).[6,7] The intermediate 1,4-benzenediol was obtained under microwave irradiation by using KF–Al$_2$O$_3$ as catalyst and then formylated with hexamethylenetetramine (HMTA) to give **12a**.

17. HPLC and LC-HRMS analysis of secondary metabolites

Analysis of secondary metabolites was performed on an Agilent series 1200 HPLC (Agilent Technologies, Böblingen, Germany) with an Agilent Eclipse XDB-C18 column (150 × 4.6 mm, 5 μm). Water (A) and ACN (B), both with 0.1% (*v/v*) trifluoroacetic acid, were used as solvents at a flow rate of 0.5 mL/min. The substances were eluted with a linear gradient from 5–100% B in 40 min, then washed with 100% (*v/v*) solvent B for 5 min and equilibrated with 5% (*v/v*) solvent B for 10 min. Semi-preparative HPLC was performed on the same equipment with an Agilent Eclipse XDB-C18 column (9.4 × 250 mm, 5 μm) column and a flow rate of 2.5 ml/min.

LC-HRMS analysis was performed on an Agilent 1260 HPLC system equipped with a microTOF-Q III spectrometer (quadrupole time-of-flight type mass analyzer) (Bruker, Bremen, Germany) by using a Multospher 120 RP18-5μ column (250 × 2 mm, 5 μm) (CS-Chromatographie Service GmbH, Langerwehe, Germany). Water (A) and ACN (B), both with 0.1% (*v/v*) formic acid, were used as solvents at a flow rate of 0.25 mL/min and the same method for separation. Electrospray positive or negative ionization mode was selected for determination of the exact masses. The capillary voltage was set to 4.5 kV and a collision energy of 8.0 eV. Sodium formate was used in each run for mass calibration. The masses were scanned in the range of m/z 100 - 1500. Data were evaluated with the Compass DataAnalysis 4.2 software (Bruker Daltonik, Bremen, Germany).

18. NMR analysis

NMR spectra were recorded on a JOEL ECA-400 MHz or ECA-500 MHz spectrometer (JEOL, Tokyo, Japan). All spectra were processed with MestReNova 6.1.0 (Mestrelab, Santiago de Compostela, Spain). Chemical shifts are referenced to those of the solvent signals.

19. Physiochemical properties of the compounds described in this study

Flavoglaucin (**1a**): The product was isolated as yellow amorphous solid. ^{1}H NMR (500 MHz, CDCl$_3$) δ 11.92 (s, 1H, 6-OH), 10.25 (s, 1H, H-7), 6.88 (s, 1H, H-4), 5.27 (tq, *J* = 7.3, 1.4 Hz, 1H, H-2′′), 4.31 (br s, 1H, 3-OH), 3.28 (d, *J* = 7.3 Hz, 2H, H-1′′), 2.87 (t, *J* = 7.9 Hz, 2H, H-1′), 1.75 (d, *J* = 1.4 Hz, 3H, H-5′′), 1.69 (d, J = 1.4 Hz, 3H, H-4′′), 1.63 (quintet, *J* = 7.9 Hz, 2H, H-2′), 1.40 (quintet, *J* = 7.9 Hz, 2H, H-3′), 1.35–1.20 (m, 6H, H-4′, H-5′, and H-6′), 0.87 (t, *J* = 7.0 Hz, 3H, H-7′). The NMR data of **1a** correspond well to those of flavoglaucin.[8] HRMS (ESI-TOF) *m/z*: [M + H]$^+$ Calcd for C$_{19}$H$_{29}$O$_3$, 305.2111; Found 305.2112.

Aspergin (**1b**): The product was isolated as yellow amorphous solid. ^{1}H NMR (500 MHz, CDCl$_3$) δ 11.73 (s, 1H, 6-OH), 10.09 (s, 1H, H-7), 7.02 (s, 1H, H-4), 6.48 (d, *J* = 16.2 Hz, 1H, H-1′), 5.99 (dt, *J* = 16.2, 6.8 Hz, 1H, H-2′), 5.31–5.27 (m, 1H, H-2′′), 4.99 (br s, 1H, 3-OH), 3.31 (d, *J* = 7.3 Hz, 2H, H-1′′), 2.30 -2.34 (m, 2H, H-3′), 1.76 (br s, 3H, H-5′′), 1.70 (br s, 3H, H-4′′), 1.52 (quintet, *J* = 7.3 Hz, 2H, H-4′), 1.36–1.33 (m, 4H, H-5′ and H-6′), 0.91 (t, *J* = 7.0 Hz, 3H, H-7′).

S10

The NMR data of **1b** correspond well to those of aspergin.[8] HRMS (ESI-TOF) *m/z*: [M + H]⁺ Calcd for $C_{19}H_{27}O_3$, 303.1955; Found 303.1950.

Dihydroauroglaucin (**1c**): The product was isolated as yellow amorphous solid. ¹H NMR (500 MHz, CDCl₃) δ 11.78 (s, 1H, 6-OH), 10.09 (s, 1H, H-7), 7.00 (s, 1H, H-4), 6.56 (d, *J* = 15.7 Hz, 1H, H-1′), 6.44 (dd, *J* = 15.7, 10.3 Hz, 1H, H-2′), 6.27 (dd, *J* = 15.0, 10.3 Hz, 1H, H-3′), 5.89 (dt, *J* = 15.0, 7.3 Hz, 1H, H-4′), 5.30–5.28 (m, 1H, H-2″), 3.32 (d, *J* = 7.3 Hz, 2H, H-1″), 2.15 (q, *J* = 7.3 Hz, 2H, H-5′), 1.75 (br s, 3H, H-5″), 1.70 (br s, 3H, H-4″), 1.47 (sextet, *J* = 7.3 Hz, 2H, H-6′), 0.94 (t, *J* = 7.3 Hz, 3H, H-7′). The NMR data of **1c** correspond well to those of dihydroauroglaucin.[9] HRMS (ESI-TOF) *m/z*: [M + H]⁺ Calcd for $C_{19}H_{25}O_3$, 301.1798; Found 301.1799.

Auroglaucin (**1d**): The product was isolated as orange amorphous solid. ¹H NMR (500 MHz, CDCl₃) δ 11.80 (s, 1H, 6-OH), 10.09 (s, 1H, H-7), 7.00 (s, 1H, H-4), 6.65 (d, *J* = 15.8 Hz, 1H, H-1′), 6.49 (dd, *J* = 15.8, 9.7 Hz, 1H, H-2′), 6.36–6.31 (m, 2H, H-3′ and H-4′), 6.16 (dd, *J* = 15.0, 9.8 Hz, 1H, H-5′), 5.86 (dq, *J* = 15.0, 6.8 Hz, 1H, H-6′), 5.32–5.27 (m, 1H, H-2″), 3.32 (d, *J* = 7.3 Hz, 2H, H-1″), 1.83 (d, *J* = 6.8 Hz, 3H, H-7′), 1.76 (br s, 3H, H-5″), 1.70 (br s, 3H, H-4″),. The NMR data of **1d** correspond well to those of auroglaucin.[8] HRMS (ESI-TOF) *m/z*: [M + H]⁺ Calcd for $C_{19}H_{23}O_3$, 299.1642; Found 299.1643.

(*E*)-2-(hept-3'-en-1-yl)-3,6-dihydroxy-5-(3"-methylbut-2"-en-1-yl)benzaldehyde (**1e**): The product was isolated as yellow amorphous solid. ¹H NMR (500 MHz, CDCl₃) δ 11.93 (s, 1H, 6-OH), 10.24 (s, 1H, H-7), 6.88 (s, 1H, H-4), 5.46–5.34 (m, 2H, H-3′ and H-4′), 5.28 (t, *J* = 7.3 Hz, 1H, H-2″), 4.34 (br s, 1H, 3-OH), 3.29 (d, *J* = 7.3 Hz, 2H, H-1″), 2.88 (t, *J* = 7.4 Hz, 2H, H-1′), 2.42–2.30 (m, 2H, H-2′), 2.05–1.96 (m, 2H, H-5′), 1.76 (br s, 3H, H-5″), 1.69 (br s, 3H, H-4″), 1.45 (sextet, *J* = 7.4 Hz, 2H, H-6′), 0.87 (t, *J* = 7.4 Hz, 3H, H-7′). The NMR data of **1e** correspond well to those of (*E*)-2-(hept-3'-en-1-yl)-3,6- dihydroxy-5-(3′′-methylbut-2′′-en-1-yl)benzaldehyde.[10] HRMS (ESI-TOF) *m/z*: [M + H]⁺ Calcd for $C_{19}H_{27}O_3$, 303.1955; Found 303.1960.

2-(1′,5′-heptadienyl)-3,6-dihydroxy-5-(3′′-methyl-2′′-butenyl)benzaldehyde (**1f**): The product was isolated as yellow amorphous solid. ¹H NMR (500 MHz, CDCl₃) δ 11.71 (s, 1H, 6-OH), 10.08 (s, 1H, H-7), 7.02 (s, 1H, H-4), 6.44 (d, *J* = 16.2 Hz, 1H, H-1′), 5.91 (dd, *J* = 16.2, 7.0 Hz, 1H, H-2′), 5.55–5.47 (m, 1H, H-6′), 5.46–5.40 (m, 1H, H-5′), 5.29 (br t, *J* = 7.3 Hz, 1H, H-2″), 5.09 (br s, 1H, 3-OH), 3.31 (d, *J* = 7.3 Hz, 2H, H-1″), 2.40 (q, *J* = 6.9 Hz, 2H, H-3′), 2.23 (q, *J* = 6.9 Hz, 2H, H-4′), 1.76 (d, *J* = 1.4 Hz, 3H, H-5″), 1.70 (d, *J* = 1.4 Hz, 3H, H-4″), 1.69 (br d, *J* = 7.0 Hz, 3H, H-7′). The NMR data of **1f** correspond well to those of 2-(1′,5′-heptadienyl)-3,6-dihydroxy-5-(3′′-methyl-2′′-butenyl)benzaldehyde.[8] HRMS (ESI-TOF) *m/z*: [M + H]⁺ Calcd for $C_{19}H_{25}O_3$, 301.1798; Found 301.1795.

5-3-hydroxy-5-(8*E*,10*E*,12*E*)-7-hydroxynona-8,10,12-trien-1-yl)tetrahydro-2*H*-pyran-2-one (**3d**): The product was isolated as yellowish amorphous solid. ¹H NMR (500 MHz, acetone-*d₆*) δ 6.26 (dd, *J* = 15.1, 10.5 Hz, 1H, H-9), 6.21 (dd, *J* = 15.1, 10.5 Hz, 1H, H-10), 6.10 (ddd, *J* = 14.8, 10.4, 1.5 Hz, 1H, H-12), 6.09 (dd, *J* = 15.1, 10.4 Hz, 1H, H-11), 5.72 (dd, *J* = 14.8, 7.0 Hz, 1H,

H-13), 5.71 (dd, *J* = 15.1, 6.8 Hz, 1H, H-8), 4.79 (dddd, *J* = 11.0, 7.6, 5.7, 3.2 Hz, 1H, H-5), 4.37–4.33 (m, 1H, H-7), 4.33–4.30 (m, 1H, H-3), 3.95 (br s, 1H, 7-OH), 2.66 (dd, *J* = 17.3, 4.6 Hz, 1H, H-2a), 2.48 (ddd, *J* = 17.3, 3.5, 1.9 Hz, 1H, H-2b), 2.04–1.99 (m, 1H, H-4b), 1.96 (ddd, *J* = 13.8, 7.3, 7.3 Hz, 1H, H-6a), 1.82 (ddd, *J* = 13.8, 11.5, 3.0 Hz, 1H, H-4a), 1.73 (dd, *J* = 7.0, 1.5 Hz, 3H, H-14), 1.72 (ddd, *J* = 13.8, 6.5, 5.7 Hz, 1H, H-6b). $^{13}C\{^1H\}$ NMR (125 MHz, acetone-d_6) δ 170.2 (C-1), 136.8 (C-8), 133.9 (C-10), 132.7 (C-12), 131.3 (C-9), 130.9 (C-11), 130.4 (C-13), 74.2 (C-5), 69.3 (C-7), 63.2 (C-3), 44.4 (C-6), 39.5 (C-2), 36.6 (C-4), 18.4 (C-14). HRMS (ESI-TOF) *m/z*: [M +HCOOH - H]$^-$ Calcd for $C_{15}H_{21}O_6$, 297.1344; Found 297.1353.

3-(7-((8*E*,10*E*,12*E*)-hepta-8,10,12-trien-1-yl)-5-hydroxytetrahydro-2*H*-pyran-2-yl)acetic   acid (**4d**): The product was isolated as yellowish oil. ^1H NMR (500 MHz, acetone-d_6) δ 6.23 (dd, *J* = 15.0, 10.5 Hz, 1H, H-9), 6.19 (dd, *J* = 15.2, 10.5 Hz, 1H, H-10), 6.10 (dd, *J* = 15.2, 10.3 Hz, 1H, H-11), 6.09 (dd, *J* = 15.2, 10.3 Hz, 1H, H-12), 5.75 (dd, *J* = 15.0, 5.9 Hz, 1H, H-8), 5.71 (dd, *J* = 15.2, 6.9 Hz, 1H, H-13), 4.54–4.48 (m, 1H, H-3), 4.28–4.23 (m, 1H, H-7), 4.06–4.00 (m, 1H, H-5), 2.68 (dd, *J* = 14.9, 8.5 Hz, 1H, H-2b), 2.52 (dd, *J* = 14.9, 6.2 Hz, 1H, H-2a), 1.98–1.93 (m, 1H, H-6a), 1.82 (ddd, *J* = 13.0, 4.0, 1.6 Hz, 1H, H-4a), 1.73 (dd, *J* = 7.0, 1.5 Hz, 3H, H-14), 1.59 (ddd, *J* = 13.0, 9.8, 5.3 Hz, 1H, H-4b), 1.30 (ddd, *J* = 12.7, 9.8, 9.8 Hz, 1H, H-6b). $^{13}C\{^1H\}$ NMR (125 MHz, acetone-d_6) δ 172.3 (C-1), 134.8 (C-8), 133.5 (C-10), 132.7 (C-12), 130.9 (C-11), 130.7 (C-9), 130.0 (C-13), 70.7 (C-5), 69.4 (C-3), 63.8 (C-7), 41.5 (C-4), 38.5 (C-2), 38.3 (C-6), 18.3 (C-14). HRMS (ESI-TOF) *m/z*: [M - H]$^-$ Calcd for $C_{14}H_{19}O_4$, 251.1289; Found 251.1295.

7-((8*E*,10*E*,12*E*)-hepta-8,10,12-trien-1-yl)-3,5-dihydroxyoxocan-2-one (**5d**): The product was isolated as brownish oil. ^1H NMR (500 MHz, acetone-d_6) δ 6.22 (dd, *J* = 15.1, 10.7 Hz, 1H, H-9), 6.19 (dd, *J* = 15.1, 10.7 Hz, 1H, H-10), 6.10 (dd, *J* = 15.5, 10.7 Hz, 1H, H-11), 6.09 (dd, *J* = 15.1, 10.7 Hz, 1H, H-12), 5.71 (dd, *J* = 15.1, 5.9 Hz, 1H, H-13), 5.62 (dd, *J* = 15.1, 5.8 Hz, 1H, H-8), 4.40–4.36 (m, 1H, H-7), 4.35–4.27 (m, 1H, H-3), 4.21–4.18 (m, 1H, H-5), 2.43 (dd, *J* = 15.2, 7.8 Hz, 1H, H-2b), 2.36 (dd, *J* = 15.2, 5.2 Hz, 1H, H-2a), 1.72–1.66 (m, 2H, H-4), 1.73 (dd, *J* = 6.9, 1.0 Hz, 3H, H-14), 1.46 (dddd, *J* = 13.5, 11.7, 5.6, 2.8 Hz, 1H, H-6b), 1.43 (dddd, *J* = 13.5, 11.7, 5.6, 2.8 Hz, 1H, H-6a). HRMS (ESI-TOF) *m/z*: [M - H]$^-$ Calcd for $C_{14}H_{19}O_4$, 251.1289; Found 251.1303.

2-heptyl-1-(hydroxymethyl) phenol (**6a**): The product was isolated as colorless oil. ^1H NMR (500 MHz, CDCl$_3$) δ 7.43 (s, 1H, 6-OH), 7.11 (t, *J* = 7.8 Hz, 1H, H-4), 6.75 (d, *J* = 7.8 Hz, 1H, H-3), 6.71 (d, *J* = 7.8 Hz, 1H, H-5), 4.95 (s, 2H, H-7), 2.59–2.53 (m, 2H, H-1′), 2.08 (s, 1H, 7-OH), 1.50–1.44 (m, 2H, H-2′), 1.33–1.24 (m, 8H, H-3′ - H-6′), 0.89 (t, *J* = 7.1 Hz, 3H, H-7′). $^{13}C\{^1H\}$ NMR (125 MHz, CDCl$_3$) δ 156.9 (C-6), 141.4 (C-2), 129.2 (C-4), 122.6 (C-1), 121.6 (C-5), 114.7 (C-3), 60.6 (C-7), 33.5 (C-1′), 32.0 (C-2′ and C-4′), 29.7 (C-5′), 29.3 (C-3′), 22.8 (C-6′), 14.3 (C-7′). HRMS (ESI-TOF) *m/z*: [M - H]$^-$ Calcd for $C_{14}H_{21}O_2$, 221.1547; Found 221.1549.

(*E*)-2-(hept-1′-en-1-yl)-1-(hydroxymethyl) phenol (**6b**): The product was isolated as yellowish oil. ^1H NMR (500 MHz, CDCl$_3$) δ 7.62 (s, 1H, 6-OH), 7.13 (t, *J* = 7.9 Hz, 1H, H-4), 6.92 (d, *J* = 7.9 Hz, 1H, H-3), 6.77 (d, *J* = 7.9 Hz, 1H, H-5), 6.50 (d, *J* = 15.5 Hz, 1H, H-1′), 6.00 (dt, *J* = 15.5, 6.9 Hz, 1H, H-2′), 4.99 (s, 2H, H-7), 2.29 (s, 1H, 7-OH), 2.20 (ddd, *J* = 15.5, 6.9, 1.5 Hz, 2H, H-3′), 1.48–1.43 (m, 2H, H-4′), 1.34–1.31 (m, 4H, H-5′ and H-6′), 0.90 (t, *J* = 7.1 Hz, 3H, H-7′).

$^{13}C\{^1H\}$ NMR (125 MHz, CDCl₃) δ 156.7 (C-6), 137.7 (C-2), 135.2 (C-2′), 129.0 (C-4), 126.5 (C-1′),121.6 (C-1), 118.9 (C-3), 115.2 (C-5), 60.4 (C-7), 33.4 (C-3′), 31.4 (C-5′), 29.0 (C-4′), 22.6 (C-6′), 14.1 (C-7′). HRMS (ESI-TOF) *m/z*: [M - H]⁻ Calcd for C₁₄H₁₉O₂, 219.1391; Found 219.1399.

2-((1′*E*,3′*E*)-hepta-1′,3′-dien-1-yl)-1-(hydroxymethyl) phenol (**6c**): The product was isolated as yellowish amorphous solid. ^1H NMR (500 MHz, CDCl₃) δ 7.50 (s, 1H, 6-OH), 7.15 (t, *J* = 7.9 Hz, 1H, H-4), 7.01 (d, *J* = 7.9, Hz, 1H, H-3), 6.78 (d, *J* = 7.9 Hz, 1H, H-5), 6.58–6.56 (m, 2H, H-1′ and H-2′), 6.24–6.17 (m, 1H, H-3′), 5.84 (dt, *J* = 14.8, 7.0 Hz, 1H, H-4′), 5.01 (s, 2H, H-7), 2.12 (dd, *J* = 14.4, 7.2 Hz, 2H, H-5′), 1.48–1.43 (m, 2H, H-6′), 0.93 (t, *J* = 7.1 Hz, 3H, H-7′). $^{13}C\{^1H\}$ NMR (125 MHz, CDCl₃) δ 156.7 (C-6), 137.2 (C-2), 136.8 (C-4′), 133.1 (C-2′), 130.6 (C-3′), 129.1 (C-4), 126.3 (C-1′),121.7 (C-1), 118.4 (C-3), 115.7 (C-5), 60.4 (C-7), 35.1 (C-5′), 22.6 (C-6′), 13.9 (C-7′). HRMS (ESI-TOF) *m/z*: [M - H]⁻ Calcd for C₁₄H₁₇O₂, 217.1234; Found 217.1232.

2-((1′*E*,3′*E*,5′*E*)-hepta-1′,3′,5′-trien-1-yl)-1-(hydroxymethyl) phenol (**6d**): The product was isolated as white amorphous solid. ^1H NMR (500 MHz, CDCl₃) δ 7.49 (s, 1H, 6-OH), 7.15 (t, *J* = 7.9 Hz, 1H, H-4), 7.03 (dd, *J* = 7.9, 1.0 Hz, 1H, H-3), 6.78 (dd, *J* = 7.9, 1.0 Hz, 1H, H-5), 6.61 - 6.68 (m, 2H, H-1′ and H-2′), 6.32 (dd, *J* = 15.3, 10.1 Hz, 1H, H-4′), 6.26 (dd, *J* = 15.3, 8.4 Hz, 1H, H-3′), 6.14 (ddq, *J* = 15.0, 10.1, 1.5 Hz, 1H, H-5′), 5.79 (dq, *J* = 15.0, 6.9 Hz, 1H, H-6′), 5.01 (s, 2H, H-7), 2.11 (br s, 1H, 7-OH), 1.81 (dd, *J* = 6.9, 1.5 Hz, 3H, H-7′). $^{13}C\{^1H\}$ NMR (125 MHz, CDCl₃) δ 156.7 (C-6), 137.0 (C-2), 134.5 (C-4′), 132.8 (C-2′), 131.8 (C-5′), 131.2 (C-6′), 130.4 (C-3′), 129.2 (C-4), 127.7 (C-1′), 121.7 (C-1), 118.3 (C-3), 115.8 (C-5), 60.3 (C-7), 18.5 (C-7′). HRMS (ESI-TOF) *m/z*: [M - H]⁻ Calcd for C₁₄H₁₅O₂, 215.1078; Found 215.1075.

Violaceoid C (**7a**): The product was isolated as brown oil. ^1H NMR (500 MHz, methanol-*d₄*) δ 6.53 (d, *J* = 8.6 Hz, 1H, H-4), 6.45 (d, *J* = 8.6 Hz, 1H, H-5), 4.65 (s, 2H, H-7), 2.65–2.61 (m, 2H, H-1′), 1.49–1.48 (m, 2H, H-2′), 1.35–1.30 (m, 4H, H-3′ and H-4′), 1.31–1.25 (m, 4H, H-5′ and H-6′), 0.87 (t, *J* = 6.9 Hz, 3H, H-7′). The NMR data of **7a** correspond well to those of violaceoid C.[11] HRMS (ESI-TOF) *m/z*: [M - H]⁻ Calcd for C₁₄H₂₁O₃, 237.1496; Found 237.1483.

Violaceoid A (**7b**): The product was isolated as white amorphous solid. ^1H NMR (500 MHz, methanol-*d₄*) δ 6.59 (d, *J* = 8.6 Hz, 1H, H-4), 6.53 (d, *J* = 8.6 Hz, 1H, H-5), 6.45 (dt, *J* = 16.0, 1.7 Hz, 1H, H-1′), 6.06 (dt, *J* = 16.0, 6.9 Hz, 1H, H-2′), 4.71 (s, 2H, H-7), 2.25 (tdd, *J* = 6.9, 6.9, 1.5 Hz, 2H, H-3′), 1.54–1.48 (m, 2H, H-4′), 1.42–1.35 (m, 4H, H-5′ and H-6′), 0.94 (t, *J* = 7.1 Hz, 3H, H-7′). The NMR data of **7a** correspond well to those of violaceoid A.[11] HRMS (ESI-TOF) *m/z*: [M - H]⁻ Calcd for C₁₄H₁₉O₃, 235.1340; Found 235.1333.

2-heptyl-1-(hydroxymethyl)cyclohexa-2,5-diene-3,6-dione (**8a**): The product was isolated as brown oil. ^1H NMR (500 MHz, acetone-*d₆*) δ 6.81 (d, *J* = 10.1 Hz, 1H, H-4), 6.78 (d, *J* = 10.1 Hz, 1H, H-5), 4.49 (s, 2H, H-7), 2.60–2.57 (m, 2H, H-1′), 1.54–1.45 (m, 2H, H-2′), 1.36–1.28 (m, 8H, H-3′ - H-6′), 0.88 (t, *J* = 7.0 Hz, 3H, H-7′). $^{13}C\{^1H\}$ NMR (125 MHz, acetone-*d₆*) δ 188.9 (C-3), 188.3 (C-6), 147.2 (C-2), 142.2 (C-1), 137.5 (C-4), 137.2 (C-5), 55.6 (C-7), 32.6 (C-5′), 30.8 (C-2′), 30.7 (C-3′), 30.5 (C-4′), 26.8 (C-1′), 23.4 (C-6′), 14.4 (C-7′). HRMS (ESI-TOF) *m/z*: [M - H]⁻ Calcd for C₁₄H₂₀O₃, 236.1412; Found 236.1414.

S13

2-heptyl-1-(hydroxymethyl)-5-(3´´-methylbut-2´´-en-1-yl)benzene-3,6-diol (**9a**): The product was isolated as white amorphous solid. ^{1}H NMR (500 MHz, acetone-d_6) δ 8.16 (s, 1H, 6-OH), 7.42 (s, 1H, 3-OH), 6.54 (s, 1H, H-4), 5.28 (tq, J = 7.3, 1.3 Hz, 1H, H-2´´), 4.88 (s, 2H, H-7), 3.21 (d, J = 7.3 Hz, 2H, H-1´´), 2.60–2.56 (m, 2H, H-1´), 1.70 (d, J = 1.3 Hz, 3H, H-5´´), 1.68 (d, J = 1.3 Hz, 3H, H-4´´), 1.46–1.40 (m, 2H, H-2´), 1.37–1.26 (m, 8H, H-3´ - H-6´), 0.87 (t, J = 7.0 Hz, 3H, H-7´). ^{13}C{^{1}H} NMR (125 MHz, acetone-d_6) δ 148.8 (C-6), 148.4 (C-3), 132.1 (C-3´´), 126.9 (C-5), 125.2 (C-1), 124.8 (C-2), 124.1 (C-2´´), 115.7 (C-4), 60.7 (C-7), 32.6 (C-5´), 31.3 (C-2´), 29.8 (C-3´ and C-4´), 28.6 (C-1´´), 26.2 (C-5´´), 25.9 (C-1´), 23.3 (C-6´), 17.8 (C-4´´), 14.4 (C-7´). HRMS (ESI-TOF) *m/z*: [M - H]$^-$ Calcd for $C_{19}H_{29}O_3$, 305.2122; Found 305.2136.

2-heptyl-1-(hydroxymethyl)-5-(3´´-methylbut-2´´-en-1-yl)cyclohexa-2,5-diene-3,6-dione (**10a**): The product was isolated as brown oil. ^{1}H NMR (500 MHz, acetone-d_6) δ 6.47 (s, 1H, H-4), 5.28 (tq, J = 7.3, 1.4 Hz, 1H, H-2´´), 4.50 (s, 2H, H-7), 3.12 (d, J = 7.4 Hz, 2H, H-1´´), 2.59–2.54 (m, 2H, H-1´), 1.75 (d, J = 1.4 Hz, 3H, H-5´´), 1.65 (d, J = 1.4 Hz, 3H, H-4´´), 1.48–1.43 (m, 2H, H-2´), 1.37–1.26 (m, 8H, H-3´ - H-6´), 0.87 (t, J = 7.0 Hz, 3H, H-7´). ^{13}C{^{1}H} NMR (125 MHz, acetone-d_6) δ 188.9 (C-3), 188.3 (C-6), 148.8 (C-4), 146.9 (C-2), 142.4 (C-1), 136.3 (C-3´´), 132.9 (C-5), 119.8 (C-2´´), 55.8 (C-7), 32.5 (C-5´), 30.8 (C-1´), 30.7 (C-2´), 30.1 (C-4´), 26.6 (C-3´), 28.2 (C-1´´), 25.9 (C-5´´), 23.4 (C-6´), 17.9 (C-4´´), 14.4 (C-7´). HRMS (ESI-TOF) *m/z*: [M]$^-$ Calcd for $C_{19}H_{28}O_3$, 304.2038; Found 304.2034.

2-heptyl-3,6-dihydroxybenzaldehyde (**12a**): The product was isolated as orange amorphous solid. ^{1}H NMR (400 MHz, CDCl$_3$) δ 11.59 (s, 1H, 6-OH), 10.28 (s, 1H, H-7), 7.00 (d, J = 8.9 Hz, 1H, H-4), 6.72 (d, J = 8.9 Hz, 1H, H-5), 4.42 (s, 1H, 3-OH), 2.95–2.89 (m, 2H, H-1´), 1.64–1.56 (m, 2H, H-2´), 1.42–1.37 (m, 2H, H-3´), 1.35–1.25 (m, 6H, H-4´, H-5´, and H-6´), 0.88 (t, J = 7.0 Hz, 3H, H-7´). ^{13}C{^{1}H} NMR (100 MHz, CDCl$_3$) δ 195.6 (C-7), 157.7 (C-6), 145.5 (C-3), 131.7 (C-2), 126.0 (C-4), 118.0 (C-5), 115.8 (C-1), 32.0 (C-2´), 31.9 (C-5´), 29.8 (C-3´), 29.2 (C-4´), 24.4 (C-1´), 22.9 (C-6´), 14.2 (C-7´). HRMS (ESI-TOF) *m/z*: [M - H]$^-$ Calcd for $C_{14}H_{19}O_3$, 235.1340; Found 235.1343.

1-(hydroxymethyl)-5-(3´´-methylbut-2´´-en-1-yl)-3-pentylbenzofuran-5-ol (**13b**): The product was isolated as brown oil. ^{1}H NMR (500 MHz, acetone-d_6) δ 8.42 (br s , 1H, 6-OH), 7.06 (s, 1H, H-4), 6.43 (s, 1H, H-1´), 5.28 (tq, J = 7.5, 1.0 Hz, 1H, H-2´´), 5.23 (br s, 1H, 7-OH), 5.04 (s, 2H, H-7), 3.37 (d, J = 7.5 Hz, 2H, H-1´´), 2.71 (td, J = 7.5, 0.9 Hz, 2H, H-3´), 1.73 (d, J = 1.0 Hz, 3H, H-4´´), 1.72 (d, J = 1.0 Hz, 3H, H-5´´), 1.69–1.72 (m, 2H, H-4´),1.39–1.34 (m, 4H, H-5´ and H-6´), 0.89 (t, J = 7.3 Hz, 3H, H-7´). ^{13}C{^{1}H} NMR (125 MHz, acetone-d_6) δ 159.9 (C-2´), 151.1 (C-3), 149.6 (C-6), 132.6 (C-3´´), 126.1 (C-1), 126.0 (C-5), 123.9 (C-2´´), 120.8 (C-2), 110.3 (C-1´), 100.7 (C-4), 61.8 (C-7), 32.1 (C-5´), 28.9 (C-3´), 28.6 (C-1´´), 28.2 (C-4´), 25.8 (C-5´´), 23.0 (C-6´), 17.7 (C-4´´), 14.3 (C-7´). HRMS (ESI-TOF) *m/z*: [M - H]$^-$ Calcd for $C_{19}H_{25}O_3$, 301.1809; Found 301.1802.

20. Structural elucidation

The structures of the isolated products were elucidated by comprehensive interpretation of their UV and MS (Figure S23) as well as NMR data (Figures S24−S73). All known compounds were identified by comparison of these data with those described in the literature.

The triene system of **3d−5d**, the rearrangement products of **2d** obtained from the *fogA* expression stain JN001, was determined as all trans-(8*E*,10*E*,12*E*) geometry by determination of the ^{1}H-^{1}H coupling constants for the olefinic protons, *i.e.* 15Hz for $J_{8,9}$, $J_{10,11}$, and $J_{12,13}$ as well as 10Hz for $J_{9,10}$, $J_{11,12}$, and $J_{11,12}$. The relative configuration in **3d** and **4d** were determined by interpretation of the NOESY correlations.

Characterized signals of the methylene groups (C7) in alkylated salicyl alcohols are the singlets for two protons at 4.49 - 5.04 ppm in ^{1}H NMR spectra and 55.6 - 61.8 ppm in ^{13}C{^{1}H} NMR spectra. The signals for the corresponding aldehyde group were observed at δ_H 10.09–10.28 ppm and δ_C 195.6 ppm in their NMR spectra. The chemical shift of C3 of the benzoquinone **10a** at δ_C 188.9 ppm differs clearly from that of the same carbon of dihydroquinone **9a** at 148.4 ppm.

21. Gene and protein sequence of FogH

Genomic sequence of *fogH*

ATGGCTTTACAAACGACCAATACATGGGAGACACTGGCGCAACTGTTGCCCTCGCGCAATCATGATCAGGACTTTTGGTGGAAGGTGACA
GGGCGCCAGCTGGCTGTGTTGTTGGAGGCGGCCGGCTATCCTATTGAGAGACAGTACAACACTCTCTTGTTTCACTATCACTGGGCGGTA
TGAAGCTTCTTTTTTTTTTTTTTCCTTTCTTTCTTTTTTCTTTCTGCCCCTCATAATTTAGGCTAATTGCGTGCTGTTGCCAGATTCCATACCTG
GGACCAGCTCCTGCAAGTGGTGTAGCCAAATGGCCGTCGCAGCTATCTGTTGACGGGTCTCCAATTGAGTATTCGTGGAAATGGAACACA
AAGTCAAAGGCGCCTGATGTGCGGTATACCATGGAGCCTATGAGCGAGTTTACGGGCACAAAGTTGGACCCGCTTAACCAGCGCGCGTT
CCGCGAGCTGCTGCACAAGCTTAGCCAGTTCGTGCCTGACGTCGATTTAGCACCGACTGATTACTTTATGTCTACCCTGTTCGATCATGAC
AGGTCAGTGCTGATGAAGGCGGTTGACGATGGCGTGCCGTTGCAGTTTTCTAGCACTGCTCTTGCATTCGAGTTTCTAGACAAGGGCCTT
TTGCTCAAGACGTATTACGCGCCCCGCAAACTGGAGACAGGTCACTTTGTCCTGAAGGACTGGGACACGGCTATTCGCGGCTATTACCCC
GAGAGCAAGGCGCTGGATATCGTGTATGAGTTCCTGAAGACAAGCCCCGAGGGCGAACTTATGAACCCGTACCATCTCGCCGTCGACAA
CGTCAAAGACGGACGGCTCAAATTCTATTTCCAGTCGCCTCACCGCACCTTTACTTCGGTCCGCGAGATCTTGACCATCGGCGGGGCGTGT
ACAGCGCGAGGGCTTAGAAGAGCAACTCCTCTCCCTGCGCGATCTCCTCAACGCACTGACCGGCCAGTCTCCCGACTTCCCCGAAGAC
GGCGAGCCCCCGATCGTCGAGGAAGACGTCACCGCCGACTTAGACACAGACGGCCACCCGGAACTCATGTCCGGATATCTATACTACTTC
GACATCGCCCCCGGCGCGGCCCTACCCGAGATCCGCTTCTACGTCCCCATCCGCCGGTACTGCAAGAGCGATCTGGACCTGGCGCAATC
GCTCACGGCCTGGATGGCAGCGAACGGCCGTGGCACGTACTGCCAGCAGTACTTGGACCTAGTCCACAGTCTGGCCGAGCACCGTGAG
ATATCAAAGGATCGGGGGCTGCAGCGGTACATCGCTTGCCTGTTGGCAAAGAATGGGGAGATTGAGGTGACGACGTATTTGGCACCAGA
GACGTATGAGCAGGTCAGGCGTTCGCAGAAAACTGCGGTATAAATATGGATTATGGGAAATGTGATGTG

Coding region of *fogH*

ATGCCTTTACAAACGACCAATACATGGGAGACACTGGCGCAACTGTTGCCCTCGCGCAATCATGATCAGGACTTTTGGTGGAAGGTGACA
GGGCGCCAGCTGGCTGTGTTGTTGGAGGCGGCCGGCTATCCTATTGAGAGACAGTACAACACTCTCTTGTTTCACTATCACTGGGCGATT
CCATACCTGGGACCAGCTCCTGCAAGTGGTGTAGCCAAATGGCCGTCGCAGCTATCTGTTGACGGGTCTCCAATTGAGTATTCGTGGAAA
TGGAACACAAAGTCAAAGGCGCCTGATGTGCGGTATACCATGGAGCCTATGAGCGAGTTTACGGGCACAAAGTTGGACCCGCTTAACCAG
CGCGCGTTCCGCGAGCTGCTGCACAAGCTTAGCCAGTTCGTGCCTGACGTCGATTTAGCACCGACTGATTACTTTATGTCTACCCTGTTC
GATCATGACAGGTCAGTGCTGATGAAGGCGGTTGACGATGGCGTGCCGTTGCAGTTTTCTAGCACTGCTCTTGCATTCGAGTTTCTAGAC
AAGGGCCTTTTGCTCAAGACGTATTACGCGCCCCGCAAACTGGAGACAGGTCACTTTGTCCTGAAGGACTGGGACACGGCTATTCGCGG
CTATTACCCCGAGAGCAAGGCGCTGGATATCGTGTATGAGTTCCTGAAGACAAGCCCCGAGGGCGAACTTATGAACCCGTACCATCTCGC
CGTCGACAACGTCAAAGACGGACGGCTCAAATTCTATTTCCAGTCGCCTCACCGCACCTTTACTTCGGTCCGCGAGATCTTGACCATCGG
CGGGGCGTGTACAGCGCGAGGGCTTAGAAGAGCAACTCCTCTCCCTGCGCGATCTCCTCAACGCACTGACCGGCCAGTCTCCCGACTTC
CCCGAAGACGGCGAGCCCCCGATCGTCGAGGAAGACGTCACCGCCGACTTAGACACAGACGGCCACCCGGAACTCATGTCCGGATATC
TATACTACTTCGACATCGCCCCCGGCGCGGCCCTACCCGAGATCCGCTTCTACGTCCCCATCCGCCGGTACTGCAAGAGCGATCTGGACC
TGGCGCAATCGCTCACGGCCTGGATGGCAGCGAACGGCCGTGGCACGTACTGCCAGCAGTACTTGGACCTAGTCCACAGTCTGGCCGA
GCACCGTGAGATATCAAAGGATCGGGGGCTGCAGCGGTACATCGCTTGCCTGTTGGCAAAGAATGGGGAGATTGAGGTGACGACGTATTT
GGCACCAGAGACGTATGAGCAGGTCAGGCGTTCGCAGAAAACTGCGGTA

Protein sequence of FogH

MALQTTNTWETLAQLLPSRNHDQDFWWKVTGRQLAVLLEAAGYPIERQYNTLLFHYHWAIPYLGPAPASGVAKWPSQLSVDGSPIEYSWKWN
TKSKAPDVRYTMEPMSEFTGTKLDPLNQRAFRELLHKLSQFVPDVDLAPTDYFMSTLFDHDRSVLMKAVDDGVPLQFSSTALAFEFLDKGLLLK
TYYAPRKLETGHFVLKDWDTAIRGYYPESKALDIVYEFLKTSPEGELMNPYHLAVDNVKDGRLKFYFQSPHRTFTSVREILTIGGRVQREGLEEQ
LLSLRDLLNALTGQSPDFPEDGEPPIVEEDVTADLDTDGHPELMSGYLYYFDIAPGAALPEIRFYVPIRRYCKSDLDLAQSLTAWMAANGRGTYC
QQYLDLVHSLAEHREISKDRGLQRYIACLLAKNGEIEVTTYLAPETYEQVRRSQKTAV

Supplementary Tables

Table S1. Similarities and putative functions of proteins encoded by the *fog* clusters in *A. ruber*, *A. cristatus* & *A. glaucus*

A.ruber		*A. cristatus*		*A. glaucus*		Putative function
Protein (Acc. Nr.)	length in aa	**Acc. Nr** (length in aa)	**Identity** (similarity)	**Acc. Nr** (length in aa)	**Identity** (similarity)	
FogA (EYE95336; EURHEDRAFT_499888)	2403	ODM22003 (2443)	92.0% (95.7%)	XP_022400332 (2442)	94.0% (96.2%)	highly-reducing polyketide synthase
FogB (5' partial annotation; EYE95337; EURHEDRAFT_377419)	273	ODM22004 (273)	91.6% (94.9%)	XP_022400333 (5' partial) (273)	94.1% (97.4%)	short-chain dehydrogenase / reductase
FogC (3' partial annotation; EYE95337; EURHEDRAFT_377419)	203	ODM22005 (203)	93.1% (97.0%)	XP_022400333 (3' partial) (203)	95.6% (97.5)	cupin domain-containing protein
-	-	-	-	XP_022400334 (304)	-	transposon
FogD (EYE95338; EURHEDRAFT_455854)	286	ODM22006 (286)	93.0% (96.9%)	XP_022400335 (282)	92.7% (96.9%)	short-chain dehydrogenase / reductase
FogE (EYE95339; EURHEDRAFT_455792)	538	ODM22007 (498)	86.8% (89.8%)	XP_022400336 (539)	95.2% (97.4%)	cytochrome P450
FogF (EYE95340; EURHEDRAFT_412154)	497	ODM22008 (498)	91.8% (96.0%)	XP_022400337 (498)	91.4% (95.8%)	FAD-binding oxidoreductase
FogG (EYE95341; EURHEDRAFT_515220)	348	ODM22009 (348)	92.0% (96.3%)	XP_022400338 (348)	92.2% (95.4%)	short-chain dehydrogenase / reductase
FogH (EYE95342; EURHEDRAFT_530727)	434	ODM22010 (435)	90.6% (94.9%)	XP_022400339 (434)	94.2% (97.2%)	prenyltransferase
FogI (EYE95343; EURHEDRAFT_402538)	415	ODM22011 (414)	87.5% (92.3%)	XP_022400340 (411)	88.6% (91.5%)	transcription factor

Table S2. Strains used in this study

Strain	Genotype	Created with Plasmid	Reference
E. coli DH5α	F⁻ *endA1 glnV44 thi-1 recA1 relA1 gyrA96 deoR nupG purB20* φ80d*lacZ*ΔM15 Δ(*lacZYA-argF*)U169, hsdR17(r$_K^-$ m$_K^+$), λ⁻	-	2
E. coli XL1-Blue	endA1 gyrA96(nal^R) thi-1 recA1 relA1 lac glnV44 F'[::Tn10 proAB⁺ lacI^q Δ(lacZ)M15] hsdR17(r$_K^-$ m$_K^+$)	-	Stratagene
S. cerevisiae HOD114-2B	*MATα ura3-52 his3Δ1 leu2-3112*	-	1
A. ruber QEN-0407-G2	wt	-	12
A. cristatus CGMCC 3.6083	wt	-	Chinese General Microbiological Culture Collection (China)
A. glaucus NRRL116	wt	-	ARS Culture Collection (USA)
A. nidulans:			
LO8030	*pyroA4*, *riboB2*, *AfpyrG89*, *nkuA*::*argB*, deletion of secondary metabolite clusters: (AN7804-AN7825)Δ, (AN2545-AN2549)Δ, (AN1039-AN1029)Δ, (AN10023-AN10021)Δ, (AN8512-AN8520)Δ, (AN8379-AN8384)Δ, (AN9246-AN9259)Δ, (AN7906-AN7915)Δ, (AN6000-AN6002)Δ.	-	13
JN001	*wA-PKS*::gpdA(p)-*fogA* + 500bp 3'UTR-*Afribo* in LO8030	pJN012	This study
JN002	*wA-PKS*::*Afribo* in LO8030 (isogenic control strain)	pYWB2	This study
JN004	*wA-PKS*::flavoglaucin cluster (500 bp 5'UTR-EURHEDRAFT_402538-EURHEDRAFT_499888–500 bp 3'UTR)-*Afribo* in LO8030	pJN014	This study
JN006	*fogH*::*AfpyrG* in JN004.3	pJN019	This study
JN007	*fogE*::*AfpyrG* in JN004.3	pJN020	This study
JN009	*fogD*::*AfpyrG* in JN004.3	pJN022	This study
JN010	*fogF*::*AfpyrG* in JN004.3	pJN023	This study
JN013	*fogG*::*AfpyrG* in JN004.3	pJN025	This study
JN015	*fogA*::*AfpyrG* in JN004.3	pJN031	This study
JN020	*wA-PKS*::flavoglaucin cluster (500 bp 5'UTR-EURHEDRAFT_402538-EURHEDRAFT_499888–500 bp 3'UTR)-*Afribo* without *fogEFH* in LO8030	pJN041	This study
JN025	*wA-PKS*::gpdA(p)-*fogF* + 500bp 3'UTR-*Afribo* in LO8030	pJN052	This study
JN029	*fogG*::*AfpyrG* in JN020.3	pJN051	This study
JN033	*fogI*::*AfpyrG* in JN004.3	pJN053	This study
JN034	*fogB*::*AfpyrG* in JN004.3	pJN060	This study
JN035	*fogC*::*AfpyrG* in JN004.3	pJN061	This study

Table S3. Oliogonucleotide primers used in this study

Primer	Sequence	Description
499888_f	ctaccccgcttgagcagacatcaccatgaatgatgacccgccatgcatcg	for cloning of pJN012: amplification of *fogA* in 2 fragments and recombination with pJN017
499888_r2	acaacagggacaccgtgggg	
499888_f2	cttccctagcaacgagcccc	
499888_r	caacaccatattttaatcccatgtggacccaacagccattctcgacatca	
499888_contr_f	ggccacgtactcgactgg	Control for integration of *fogA*
pJN017_499888_or	cgatgcatggcgggtcatcattcatggtgatgtctgctcaagcggggtag	Linearization of pJN017
prJN059	tgatgtcgagaatggctgttgggtccacatgggattaaaatatggtgttg	
prJN080	gatgtcgagaatggctgttgggtcgatcccacatgggattaaaatatgg	for cloning of pJN014: flavoglaucin cluster (in 5 fragments) to clone into pYWB2
prJN081	caccatattttaatcccatgtgggatcgacccaacagccattctcgaca	
prJN082	aggaagacgcagatgaatgcc	
prJN083	catggcatctccttagggcg	
prJN084	cctcgatgacgacaccgtag	
prJN085	tgattcggagggtcgatccg	
prJN086	tttgactggttggaatcgcttgg	
prJN087	tgctcttgcctcgcaaagc	
prJN088	agataactgcttacgagctgagc	
prJN089	gggctacgcatcttcatctggg	
prJN090	cggacttgactctccttctcctgatcggatccagggaggggggtccggtg	
prJN091	ctcgcctcaccggaccccctccctggatccgatcaggagaaggagagtc	
prJN104	aactcaattgcctgatc	Verification of 5'-region of *fogI*; binds in *waPKS*-down
prJN115	gagagttattctgtgtctg	Amplification of *AfpyrG*
prJN116	attctgtctgagaggag	
prJN117	caggggataacgcagg	Amplification of general *E.coli* ori/ampR + ScURA-CEN/ARS-backbone from pYWB2
prJN118	acacaggaaacagctatgac	
prJN119	tttgctcacatgttctttcctgcgttatcccctggaccggaaacactcc	for cloning of pJN19: 5'-region of *fogH*
prJN120	catatttcgtcagacacagaataactctctttgacagataactgcttac	
prJN121	cacgcatcagtgcctcctctcagacagaatatatggattatgggaaatg	for cloning of pJN19: 3'-region of *fogH*
prJN122	attcgtaatcatggtcatagctgtttcctgtgtgcattcacattcgcac	
prJN123	ctcacatgttctttcctgcgttatcccctgagaacgttcacatcgaatg	for cloning of pJN20: 5'-region of *fogE*
prJN124	aacatatttcgtcagacacagaataactctctgtgataattgaagtttg	
prJN125	cacgcatcagtgcctcctctcagacagaatatttgtcattctcatatgg	for cloning of pJN20: 3'-region of *fogE*
prJN126	cgtaatcatggtcatagctgtttcctgtgtggattcaactttggcattg	
prJN127	ttgctcacatgttctttcctgcgttatcccctggttgaaaacatggctg	for cloning of pJN60: 5'-region of *fogB*
prJN128	acatatttcgtcagacacagaataactctctttagtagatgtctttggc	
prJN129	tcacgcatcagtgcctcctctcagacagaattaaaactagtgcattgtac	for cloning of pJN61: 3'-region of *fogC*
prJN130	attcgtaatcatggtcatagctgtttcctgtgtattggttcgatcggag	
prJN131	tcacatgttctttcctgcgttatcccctgaagtagtgatcccgaaatag	for cloning of pJN22: 5'-region of *fogD*
prJN132	cacaacatatttcgtcagacacagaataactctctttgacggccgtagg	
prJN133	acgcatcagtgcctcctctcagacagaatattaccatggaaatataggg	for cloning of pJN22: 3'-region of *fogD*
prJN134	tcgtaatcatggtcatagctgtttcctgtgtttcgggcatgcatggttg	
prJN135	gctcacatgttctttcctgcgttatcccctgcgtgacgaggacggcatc	for cloning of pJN23: 5'-region of *fogF*
prJN136	aacatatttcgtcagacacagaataactctctgcggttcgtctgtcccg	
prJN137	tcacgcatcagtgcctcctctcagacagaattgttacgtatatagcttg	for cloning of pJN23: 3'-region of *fogF*

prJN138	attcgtaatcatggtcatagctgtttcctgtgtacccggagaaaattac	for cloning of pJN23: 3'-region of *fogF*
prJN139	ctcacatgttctttcctgcgttatcccctgattcggcattctccgtttc	for cloning of pJN25: 5'-region of *fogG*
prJN140	catatttcgtcagacacagaataactctcattgaaattacaagtagaag	
prJN141	cacgcatcagtgcctcctctcagacagaatctctattttctttagcgc	for cloning of pJN25: 3'-region of *fogG*
prJN170	gtaatcatggtcatagctgtttcctgtgttcgacgtcaggcacgaactg	
prJN143	tatcactctgctagcgcc	Verification of 5'-region of *fogH*
prJN144	actcacaaagacgcgcc	Verification of 3'-region of *fogH*
prJN145	atggctttacaaacgacc	Partial fragment of *fogH*
prJN146	tcttcctcgacgatcgg	
prJN147	ggaaattctccgcaagagg	Verification of 5'-region of *fogE*
prJN148	atgccgaattattctggggg	Verification of 3'-region of *fogE*
prJN149	atgataacggcctcatcag	Partial fragment of *fogE*
prJN150	agtttcataaggtcgacg	
prJN151	tgaagctgtaatccggtg	Verification of 5'-region of *fogB/C*
prJN152	ccaccggagcaattgtg	Verification of 3'-region of *fogB/C*
prJN153	atggacattaccggaaacg	Partial fragment of *fogB*
prJN154	gaaagtcttcgggactctaac	
prJN155	gtcctgtaattttctccggg	Verification of 5'-region of *fogD*
prJN156	tcccgagaatctcaagag	Verification of 3'-region of *fogD*
prJN157	atgtctacgaaatttgctc	Partial fragment of *fogD*
prJN158	tgttttttagtttcaatacccag	
prJN159	acacaaaccgcagttgg	Verification of 5'-region of *fogF*
prJN160	tttcgggatcactacttcg	Verification of 3'-region of *fogF*
prJN161	atgcgcaggaacatcttg	Partial fragment of *fogF*
prJN162	gtttgctccgatttggcc	
prJN163	cagcaccacgaacacc	Verification of 5'-region of *fogG*
prJN164	gaaactcgaatgcaagagc	Verification of 3'-region of *fogG*
prJN165	atggccgttacttttgacatc	Partial fragment of *fogG*
prJN166	ttacttggtgaggctatcaataatctc	
prJN167	cactggtaactccacgg	Binding in *AfpyrG* facing outwards as complementary primer for up- and downstream verification
prJN168	atcagtgcctcctctcag	
prJN171	atggctttacaaacgaccaatacatg	Verification of 3'-region of *fogI*
prJN202	ctcacatgttctttcctgcgttatcccctgccccgtctaggcgactcg	for cloning of pJN31: 5'-region of *fogA*
prJN203	acatatttcgtcagacacagaataactctccgactccaagccgacaacgc	
prJN204	cacgcatcagtgcctcctctcagacagaattattttttttccttgtagactctagtg	for cloning of pJN31: 3'-region of *fogA*
prJN205	cgtaatcatggtcatagctgtttcctgtgtttgcgcttagctgaaatg	
prJN216	gggagtgtcgacccatgaaggac	Verification of 3'-region of *fogA*
prJN249	gcactctggaaacgaactcc	Verification of 5'-region of *fogA*
prJN250	tactatacgggacagacgaaccgcatgtgataattgaagtttgaacatagatggaagg	for cloning of pJN041: amplification of cluster fragments 3 -5 leaving out *fogEFH*
prJN251	ctatgttcaaacttcaattatcacatgcggttcgtctgtcccg	
prJN252	acatcacatttcccataatccatattttgacagataactgcttacgagctg	

Table S3. (continued)

prJN253	agctcgtaagcagttatctgtcaaaatatggattatgggaaatgtgatgtgg	for cloning of pJN041: amplification of cluster fragments 3 -5 leaving out *fogEFH*
prJN273	ctcacatgttctttcctgcgttatcccctggacgttgaacatgcgctg	for cloning of pJN051: 5'-region of *fogG* in *A. nidulans* JN020; used with prJN140
prJN274	cgtaatcatggtcatagctgtttcctgtgtatagcctctgaagcgtc	for cloning of pJN051: 3'-region of *fogG* in *A. nidulans* JN020; used with prJN141
prJN277	agctaccccgcttgagcagacatcaccggcatgcgcaggaacatcttgac	for cloning of pJN052: amplification of *fogF* to clone into pJN017
prJN278	ctcaacaccatattttaatcccatgtgggcagcatttctcgtctgctgtg	
prJN280	ctcacatgttctttcctgcgttatcccctgaccgagtagttacggtgtacag	for cloning of pJN53: 5'-region of *fogI*
prJN281	acatatttcgtcagacacagaataactctcttcttcgttggctgtcaggaag	
prJN282	tcacgcatcagtgcctcctctcagacagaatatttaaaacaggggacacggg	for cloning of pJN53: 3'-region of *fogI*
prJN283	cgtaatcatggtcatagctgtttcctgtgtgcagctatctgttgacgggtc	
prJN287	gtgatggtgatggtgatgagatctggatctactactacgtccttcatagtccttg	Amplification of *fogC*
prJN291	tgtgagcggataacaatttcacacagaattatggccgaacaaaccgag	
prJN292	cacgcatcagtgcctcctctcagacagaataacaattacctcaattctatgcacg	for cloning of pJN60: 3'-region of *fogB*
prJN293	cgtaatcatggtcatagctgtttcctgtgtcacaagaagctagacatggg	
prJN294	ctcacatgttctttcctgcgttatcccctggccaaagacatctactaaaatggac	for cloning of pJN61: 5'-region of *fogC*
prJN295	acatatttcgtcagacacagaataactctctttgcttgtgtgtcacgtc	
prJN296	tgtgagcggataacaatttcacacagaattatggatggaaaaacatacaaattac	Amplification of *fogI*
prJN297	agtgatggtgatggtgatgagatctggatctactagggatcctgcctg	
vwRbPT3-f'	cgcatgcctttacaaacgaccaa	for cloning of pVW84: amplification of _530727 without introns from cDNA
vwRbPT3-r	cggatcctaccgcagttttctgc	

Table S4. Plasmids used in this study

Plasmid	Genotype	Description	Reference
pYWB2	*URA3, wA flanking, AfRiboB, Amp*	Basic integration vector for *A. nidulans*	[14]
pQE-70	*Amp,* 6xHis	Protein expression in *E. coli*	Qiagen
pYH-*wA-AfpyrG*	*URA3, wA flanking, AfpyrG, Amp*	Basic integration vector for *A. nidulans*	[5]
pJN012	gpdA(p)-*fogA* in pYWB2	Heterologous expression of *fogA* in *A. nidulans*	This study
pJN014	flavoglaucin-cluster + 500 bp 5' of first and 3`of last gene in pYWB2	Heterologous expression of flavoglaucin cluster in *A. nidulans* LO8030	This study
pJN017	*URA3, wA flanking, AfRiboB, Amp, gpdA(p)*	standard-vector for heterologous expression in *A. nidulans* LO8030	[15]
pJN019	*URA3, Amp, AfpyrG* flanked by 1.2 kb 5' and 3' of *fogH*	Deletion of *fogH* (PT) in *A. nidulans* JN004	This study
pJN020	*URA3, Amp, AfpyrG* flanked by 1.2 kb 5' and 3' of *fogE*	Deletion of *fogE* (CYP) in *A. nidulans* JN004	This study
pJN022	*URA3, Amp, AfpyrG* flanked by 1.2 kb 5' and 3' of *fogD*	Deletion of *fogD* (SDR) in *A. nidulans* JN004	This study
pJN023	*URA3, Amp, AfpyrG* flanked by 1.2 kb 5' and 3' of *fogF*	Deletion of *fogF* (OR) in *A. nidulans* JN004	This study
pJN025	*URA3, Amp, AfpyrG* flanked by 1.1 kb 5' and 3' of *fogG*	Deletion of *fogG* (SDR) in *A. nidulans* JN004	This study
pJN031	*URA3, Amp, AfpyrG* flanked by 1.2 kb 5' and 3' of *fogA*	Deletion of *fogA* (PKS) in *A. nidulans* JN004	This study
pJN041	flavoglaucin-cluster + 500 bp 5' of first and 3`of last gene without coding sequences of *fogEFH* in pYWB2	Heterologous expression of flavoglaucin cluster without genes for CYP, OR3 & PT in *A. nidulans* LO8030	This study
pJN051	*URA3, Amp, AfpyrG* flanked by 1.2 kb 5' and 3' of *fogG* especially for JN020	Deletion of *fogG* (SDR) in *A. nidulans* JN020	This study
pJN052	*fogF* in pJN017	Heterologous expression of *fogF* (OR) in *A. nidulans*	This study
pJN053	*URA3, Amp, AfpyrG* flanked by 1.2 kb 5' and 3' of *fogI*	Deletion of *fogI* (TF) in *A. nidulans* JN004	This study
pJN060	*URA3, Amp, AfpyrG* flanked by 1.2 kb 5' and 3' of *fogB*	Deletion of *fogB* (SDR) in *A. nidulans* JN004	This study
pJN061	*URA3, Amp, AfpyrG* flanked by 1.2 kb 5' and 3' of *fogC*	Deletion of *fogC* (Cupin) in *A. nidulans* JN004	This study
pVW84	*fogH* (without introns) in pQE-70	Heterologous Expression of *fogH* (PT) in *E. coli*	This study

S22

Supplementary Figures
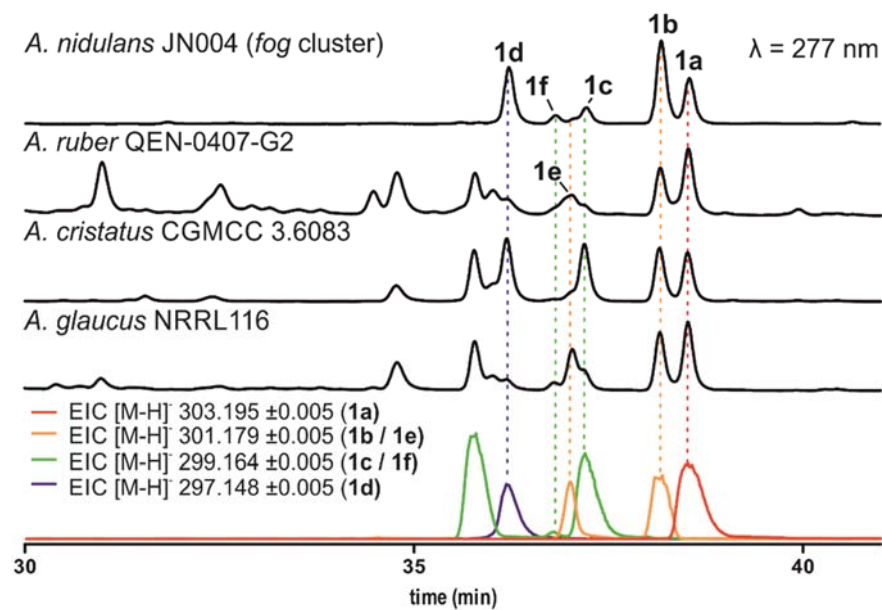
Figure S1. LC-MS analysis of *A. nidulans* with *fog* cluster, *A. ruber*, *A. cristatus*, and *A. glaucus* extracts.

The strains were cultivated in PDB medium for 28 days at 25°C. Flavoglaucin (**1a**) and its congeners **1b**−**1f** were detected in all the extracts.
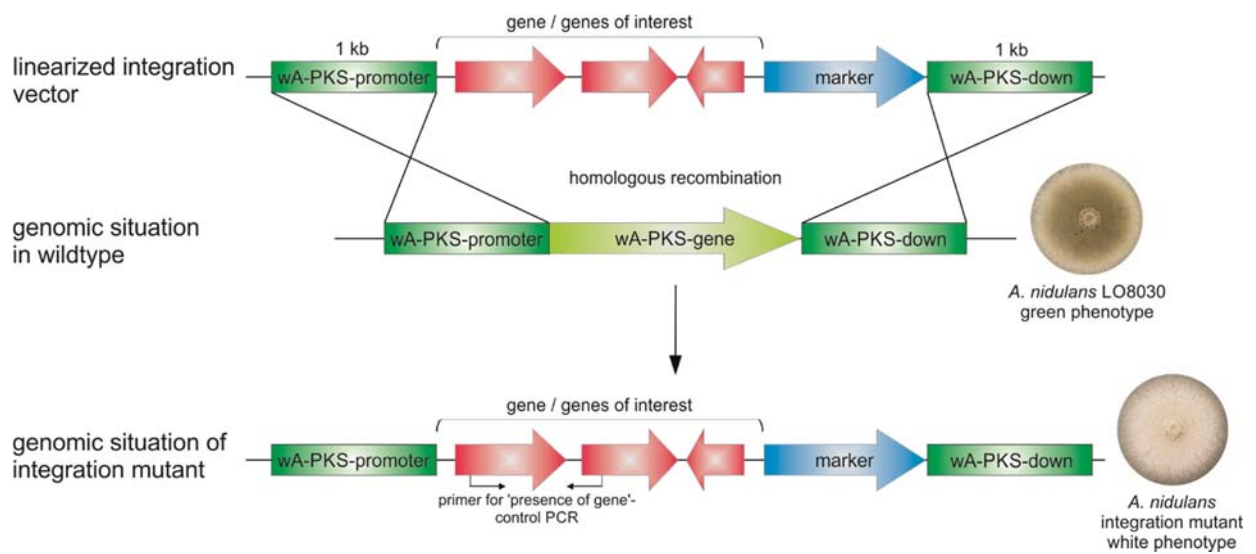
Figure S2. Schematic representation of gene integration into the wA-PKS locus of *A. nidulans* LO8030.

Verification of the integration mutants was performed via detection of the white phenotype indicating the integration into the wA-PKS-locus and a PCR with primers binding in the integrated gene(s) proving their presence.
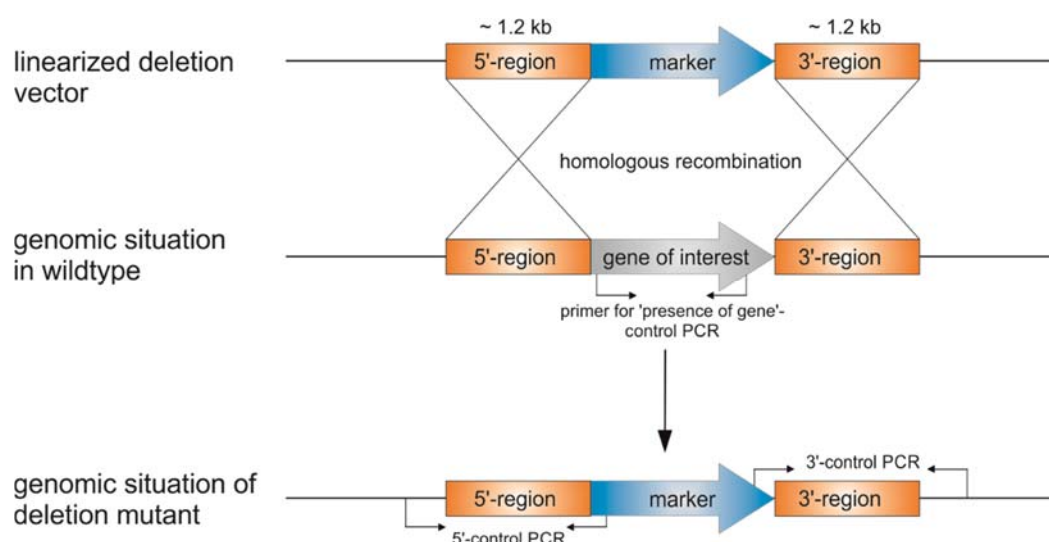
Figure S3. Schematic representation of gene deletion from *fog* cluster in *A. nidulans* strains. Verification of deletion mutants was carried out by proving the absence of the gene(s) of interest with primers binding in the region which should be deleted. Additionally, the correct integration of the 5'- and 3'-regions were checked by PCR with primers binding in the marker and the unmodified DNA 5' or 3' of the up- or downstream region. Control PCRs were performed with gDNA of *A. nidulans* LO8030 and gDNA of the strain in which the deletion should be done.
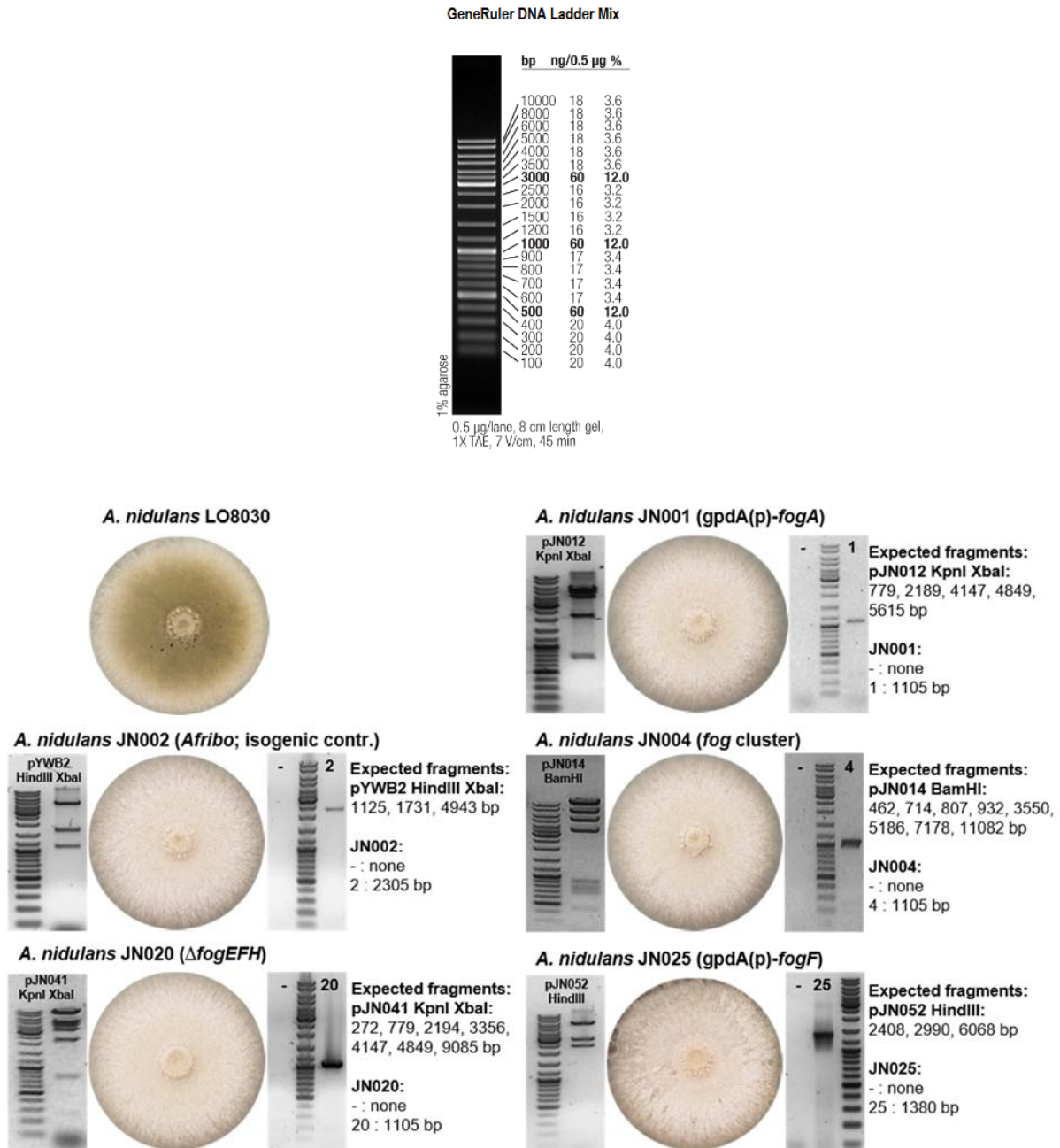
Figure S4. Fragment sizes of the used DNA-marker, mutant verification *via* PCR amplification and phenotypes of integration mutants.

As size standard for DNA fragments the GeneRuler DNA Ladder Mix by Thermo Fisher (Waltham, USA) was used. The verification of the correct plasmid in combination with the white phenotype of the mutant and control PCR for presence of the inserted gene/cluster confirmed the correct integration into the wA-PKS locus of the *A. nidulans* LO8030 genome.
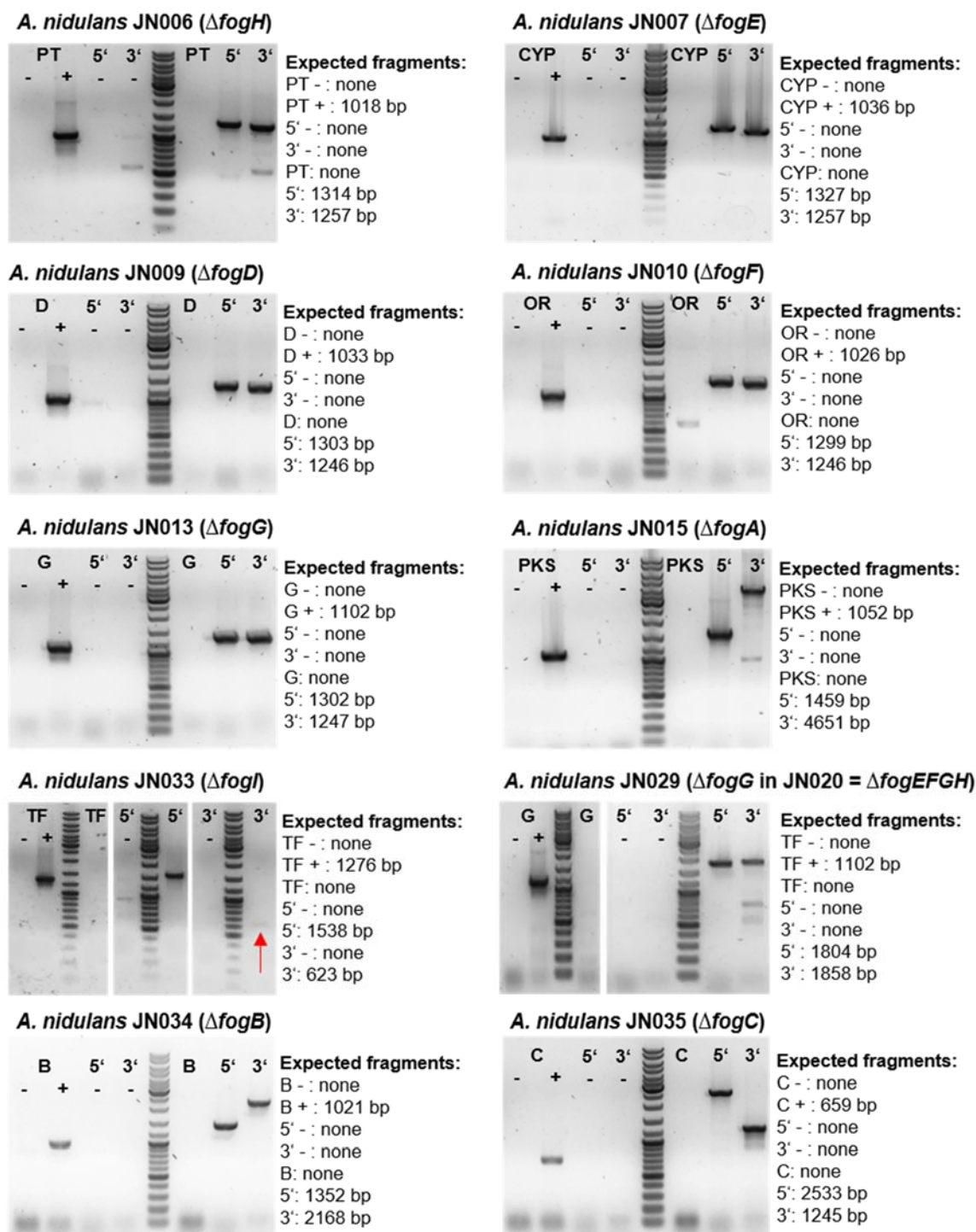
Figure S5. PCR verification of single gene deletions from the *fog* cluster in *A. nidulans* JN004. Three control PCRs have been carried out to verify the absence of the gene of interest together with the correct site specific integration via amplification of the corresponding 5'- and 3'-regions. Genomic DNA of *A. nidulans* LO8030 was used for negative control PCR & genomic DNA of *A. nidulans* JN004 was used as template for the positive control PCR.
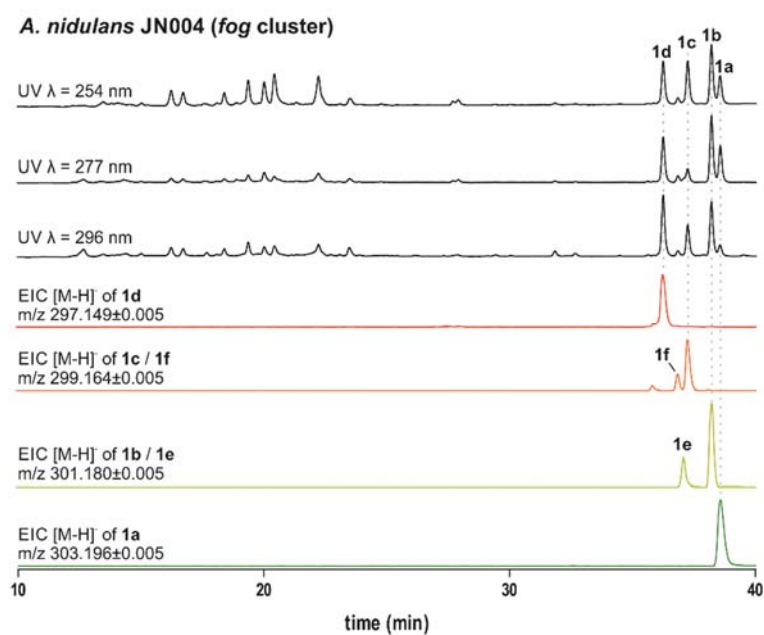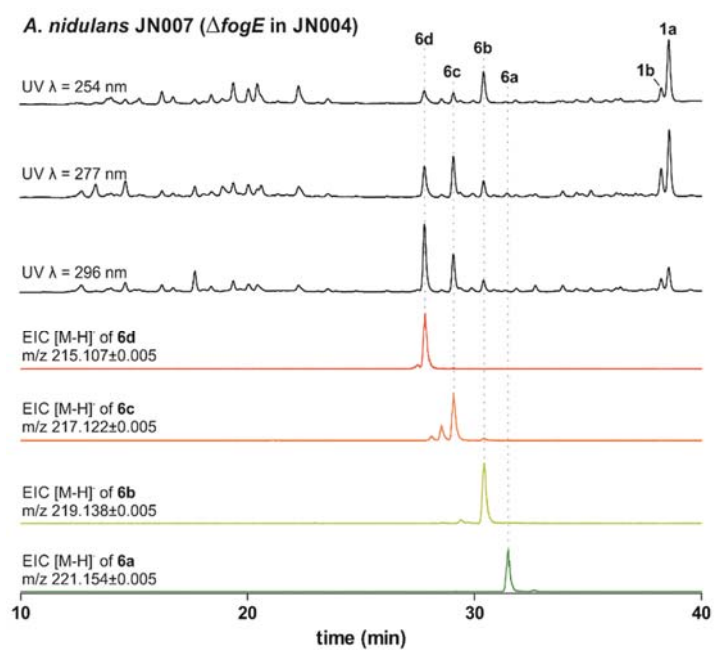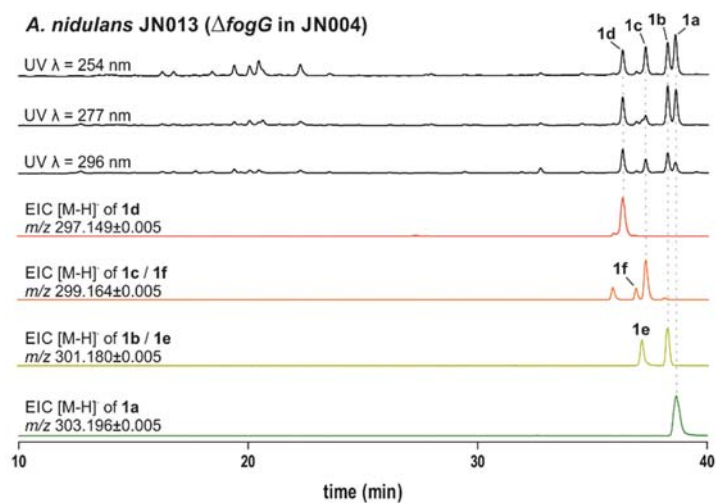
Figure S6. LC-MS analysis of the *fog* cluster expression strain *A. nidulans* JN004. The chromatograms depicted in color are EICs for the cluster end products with different number of double bonds.
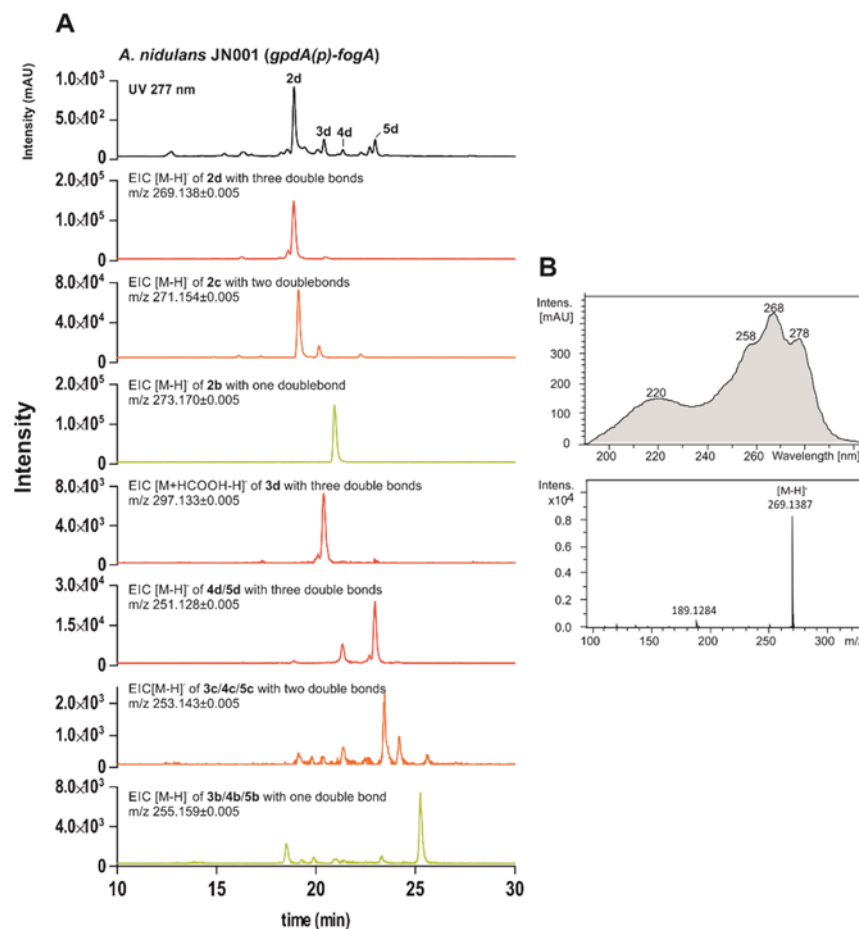
Figure S7. LC-MS analysis of *fogA* heterologous expression in *A. nidulans* JN001
UV chromatogram of the extract and EICs of the PKS products (A). Compound **2d** is the original product but can cyclize to **3d**, **4d** or **5d**. [M-H]⁻ for products with two (orange) and one (yellow) double bond could also be detected, proving FogA is also able to reduce at least two of the initial three ketide units completely. UV and mass spectrum of **2d** (B).
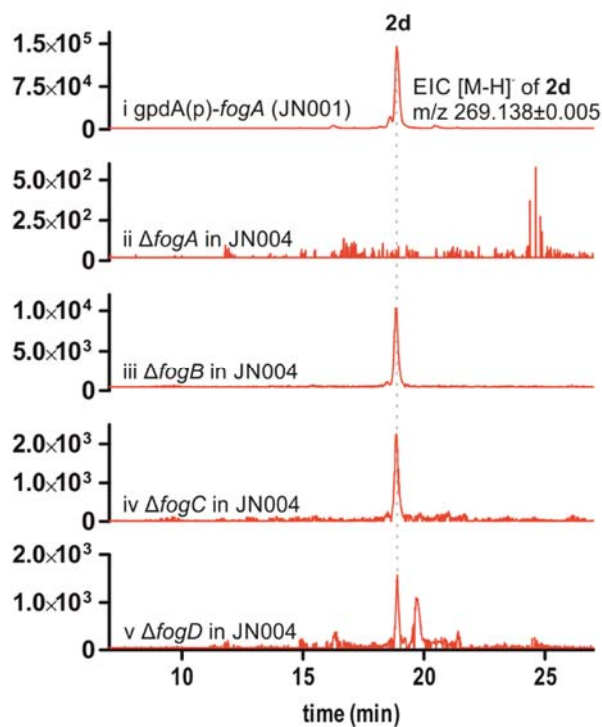
Figure S8. EICs of **2d** in the PKS expression strain and in the *fogA*, *fogB*, *fogC,* and *fogD* deletion strains

2d was clearly detected in the Δ*fogB* and Δ*fogC* mutants. Small amounts of this compound were also present in the Δ*fogD* strain but not in the Δ*fogA* mutant. The high accumulation of **2d** in *fogA* overexpression strain JN001 (Figures 4i and S8i) and low accumulation in the Δ*fogB*, Δ*fogC*, and Δ*fogD* mutants (Figures 3v–vii and S8iii–v) could be due to the different expression level of *fogA* alone under a strong and in other strains under its native promotor. A higher abundance of the PKS would result in an increased amount of hydrolytic product, when it was not further converted by FogBCD.
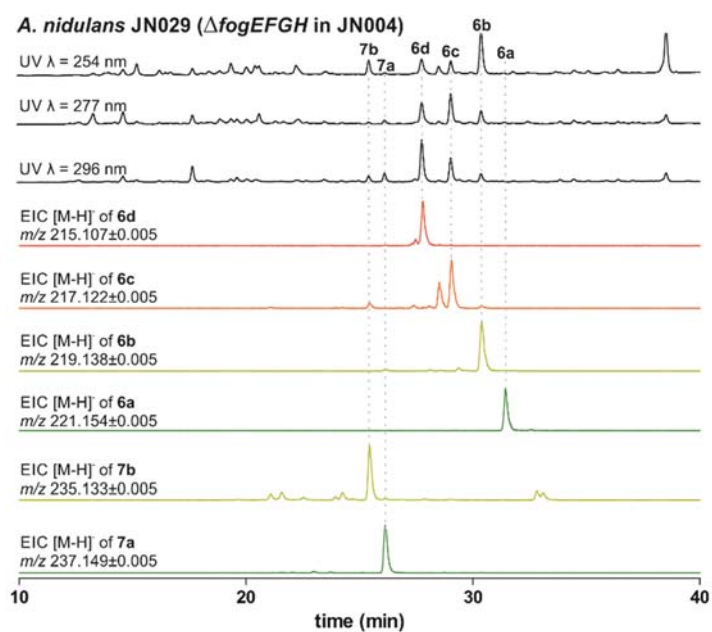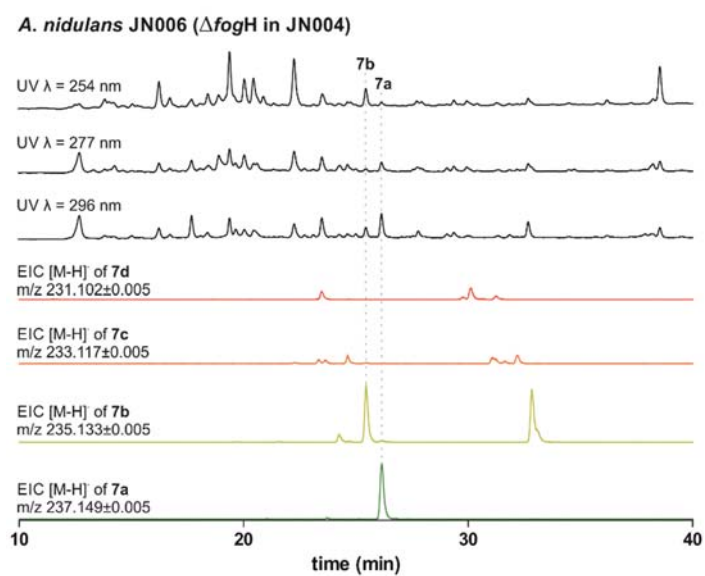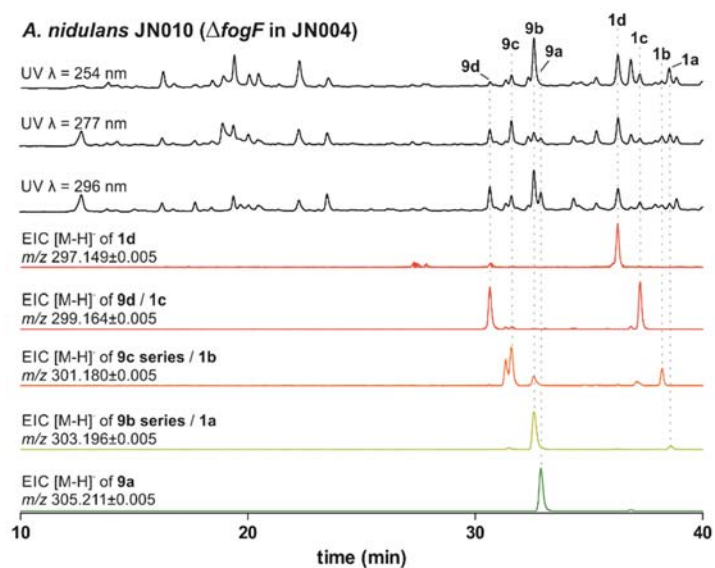
Figure S9. LC-MS analysis of the *fogEFGH* deletion strain *A. nidulans* JN029
The chromatograms depicted in color are EICs for the accumulated intermediates **6a−6d**.
Hydroxylation by *A. nidulans* enzymes resulted in slight conversion to **7a** and **7b**.

S31
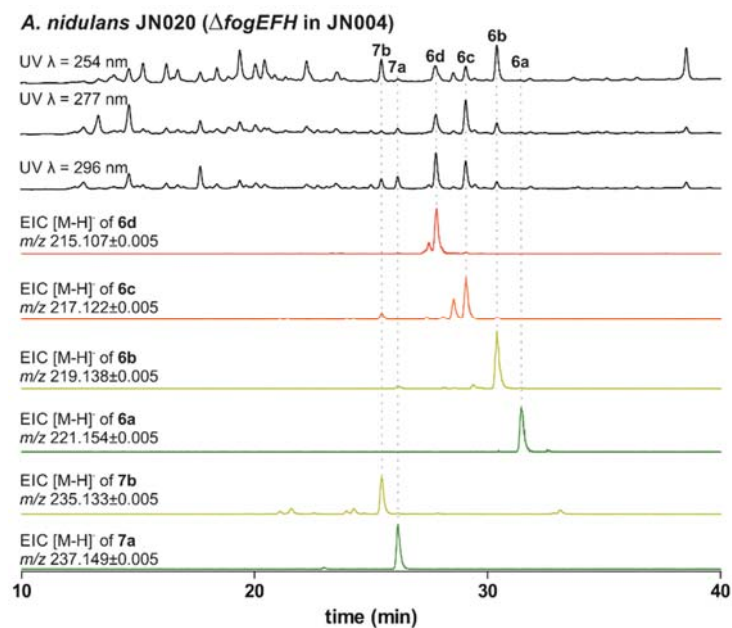
Figure S10. LC-MS analysis of the *fogEFH* deletion strain *A. nidulans* JN020
The chromatograms depicted in color are EICs for the accumulated intermediates **6a−6d**, and **6d**.
Hydroxylation by *A. nidulans* enzymes resulted in slight conversion to **7a** and **7b**.

Figure S11. LC-MS analysis of the *fogE* deletion strain *A. nidulans* JN007.
The chromatograms depicted in color are EICs for the accumulated intermediates **6a**−**6d**, and **6d**.
Hydroxylation by *A. nidulans* enzymes resulted in slight accumulation of **1a** and **1b**.

Figure S12. LC-MS analysis of the *fogG* deletion strain *A. nidulans* JN013.

The chromatograms depicted in color are EICs for the accumulated end products with different numbers of double bonds.

Figure S13. LC-MS analysis of the *fogH* deletion strain *A. nidulans* JN006.

The chromatograms depicted in color are EICs for the accumulated or expected intermediates **7a**–**7d** series.

Figure S14. LC-MS analysis of the *fogF* deletion strain *A. nidulans* JN010
The chromatograms depicted in color are EICs for the accumulated intermediates **9a−9d**. Chemical conversion via the benzoquinones **10a** is proposed to be responsible for moderate amounts of the end products **1a−1d** (see Figure S17 for details).
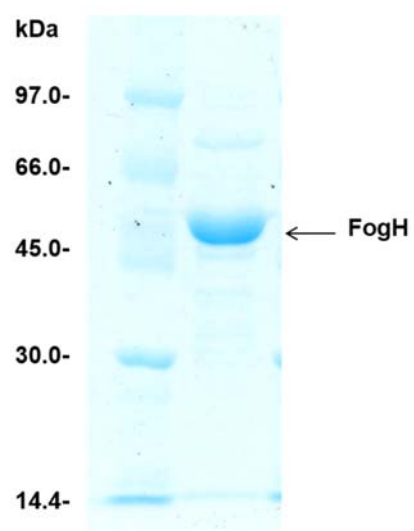
Figure S15. SDS-PAGE of the purified FogH

FogH with a C-terminal 6xHis-tag (~50 kDa) was purified from *E. coli* XLI-Blue cultures via Ni-NTA-agarose with subsequent preparative gel filtration.

S37
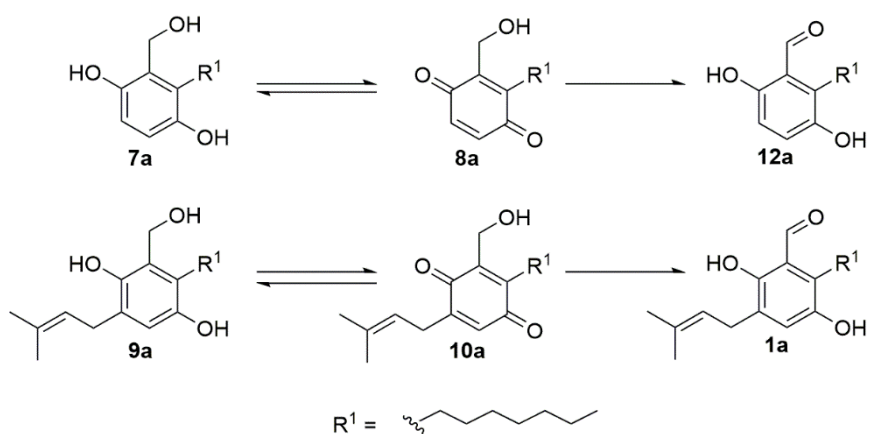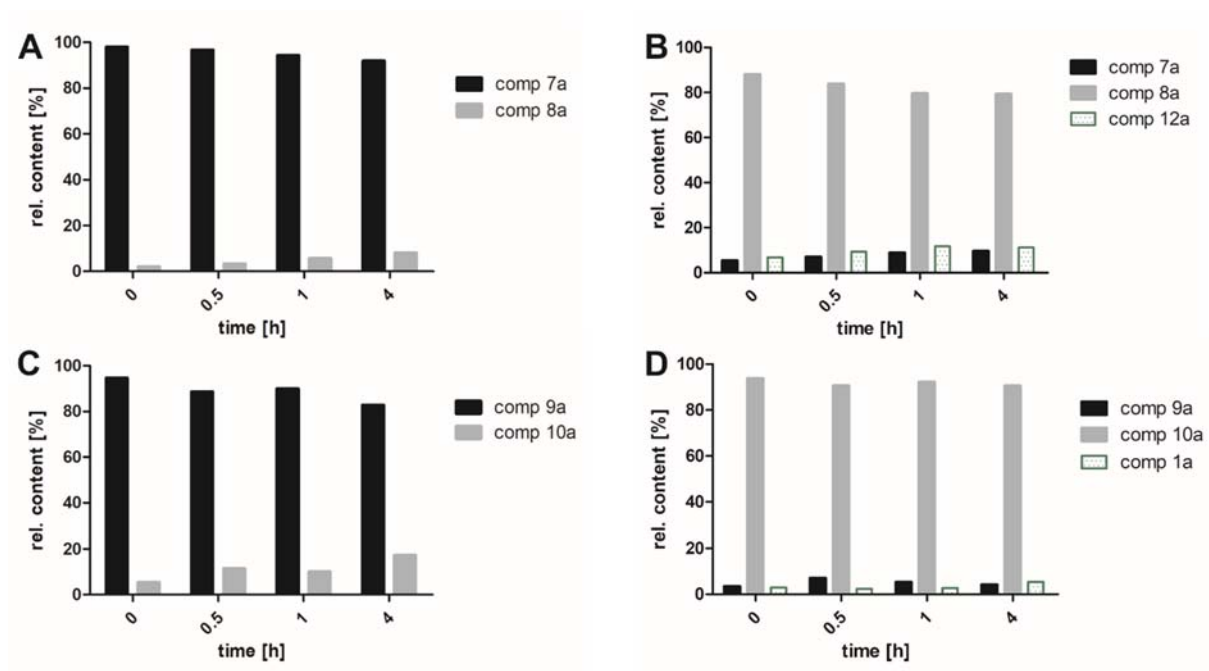
Figure S16. Stability test of **7a** (A), **8a** (B), **9a** (C), and **10a** (D) in water at 25°C.

Slow oxidation of **7a** to **8a** and **9a** to **10a** was observed. The benzoquinone alcohols **8a**/**10a** were converted in approximately equal amounts to the dihydroquinone alcohols **7a**/**9a** and the dihydroquinone aldehydes **12a**/**1a**.
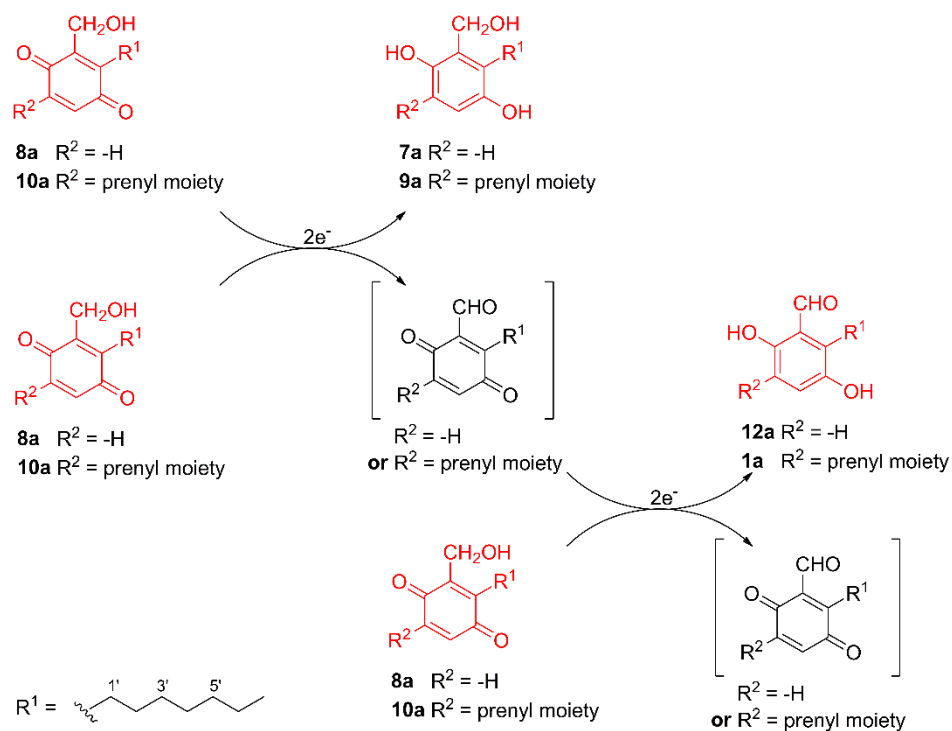
Figure S17. Proposed mechanism of benzoquinone alcohol conversion to dihydroquinone alcohol and dihydroquinone aldehyde.
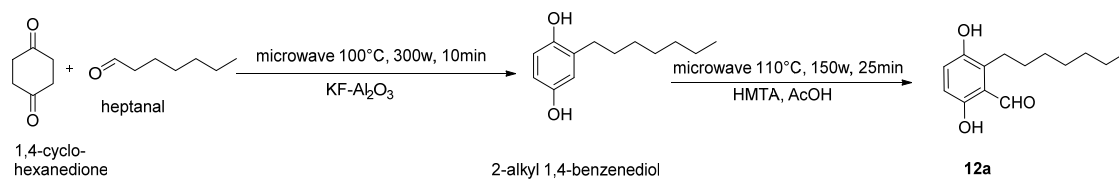
Figure S18. Chemical synthesis of the salicylaldehyde **12a**
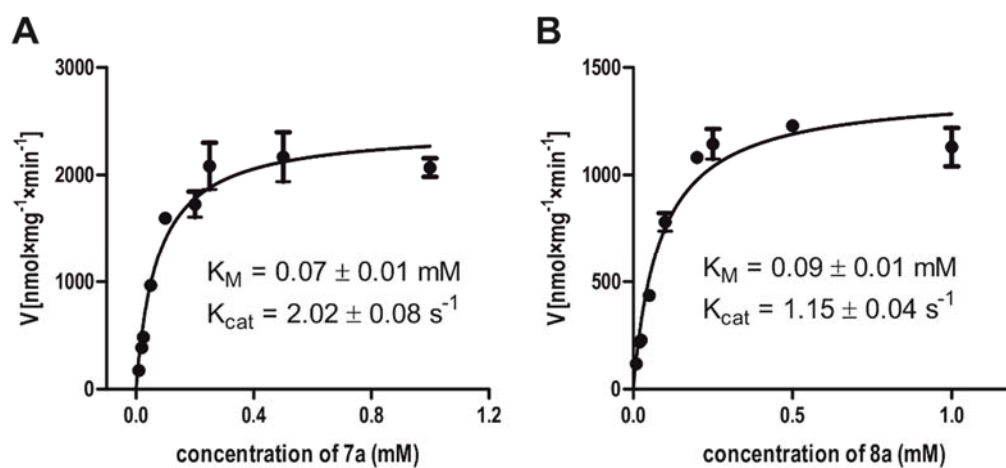
Figure S19. Determination of the kinetic parameters of FogH with the substrates **7a** (A) and **8a** (B)
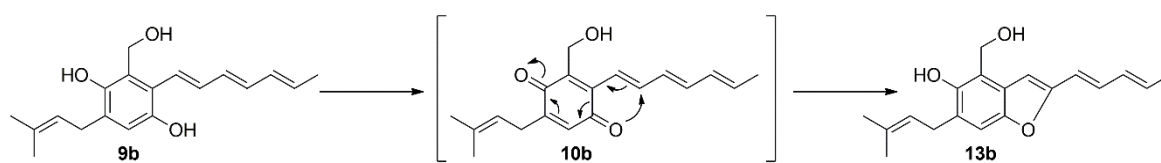
Figure S20. Intramolecular cyclization of **9b** to the benzofuran derivative **13b**
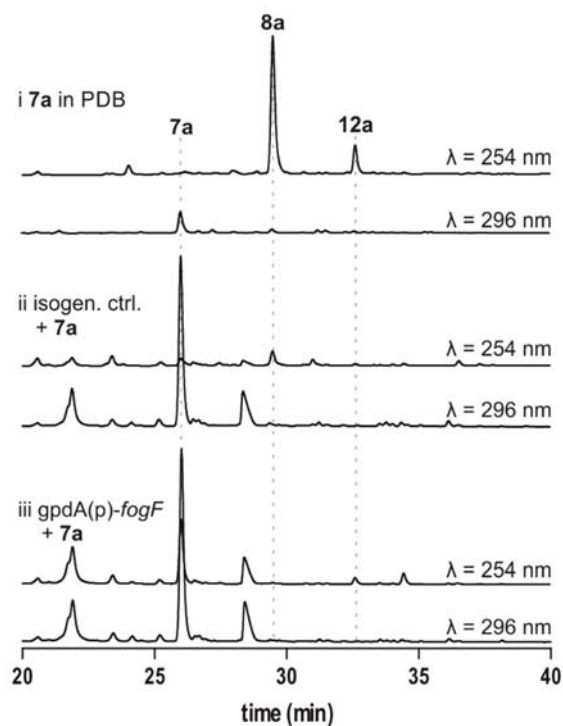
Figure S21. Feeding of **7a** to *fogF*-expression strain *A. nidulans* JN025

The majority of **7a** was oxidized to **8a** in PDB and further converted to a low amount of **12a** (i). No consumption of **7a** was observed in the presence of the isogenic control (ii) and in the *fogF* expression strain (iii).
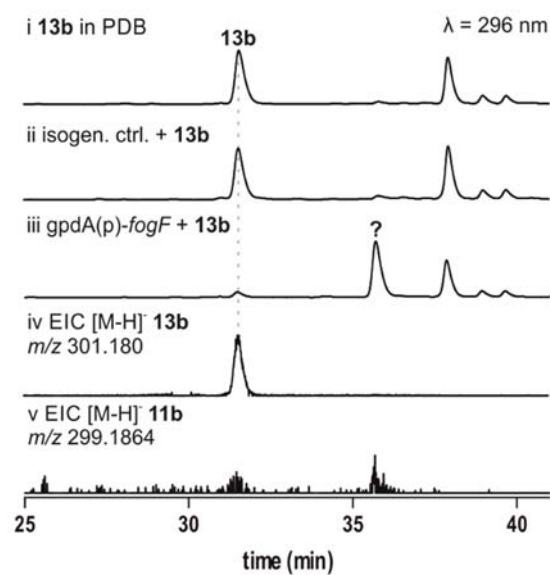
Figure S22. Feeding of **13b** into *fogF* expression strain *A. nidulans* JN025
13b was not converted in PDB (i) and in the isogenic control strain *A. nidulans* JN002 (ii). Conversion of **13b** is detected in the *fogF* expression strain (iii). The product is not the expected aldehyde **11b** and was not further identified yet.
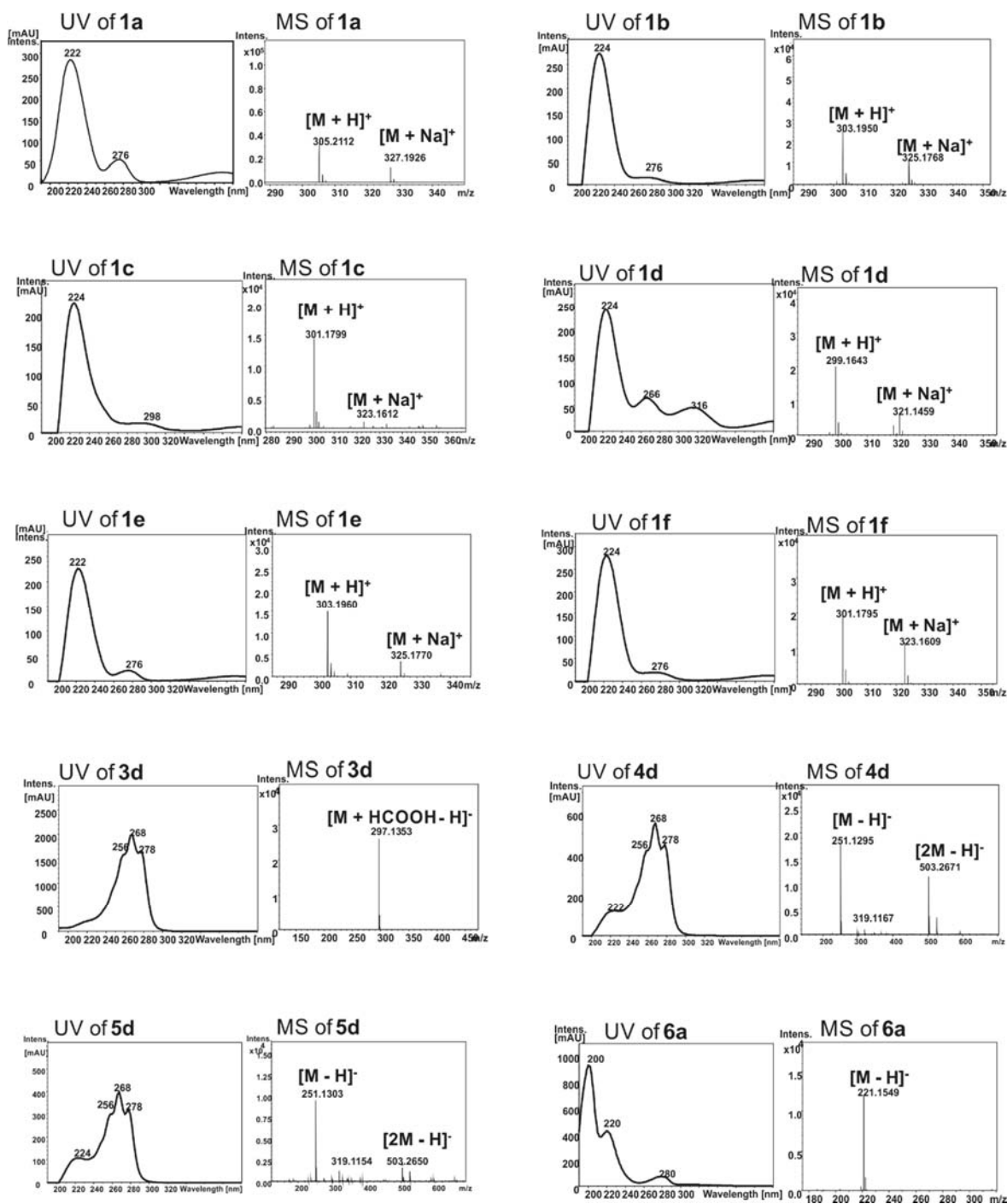
Figure S23. UV and MS spectra of the identified compounds in this study
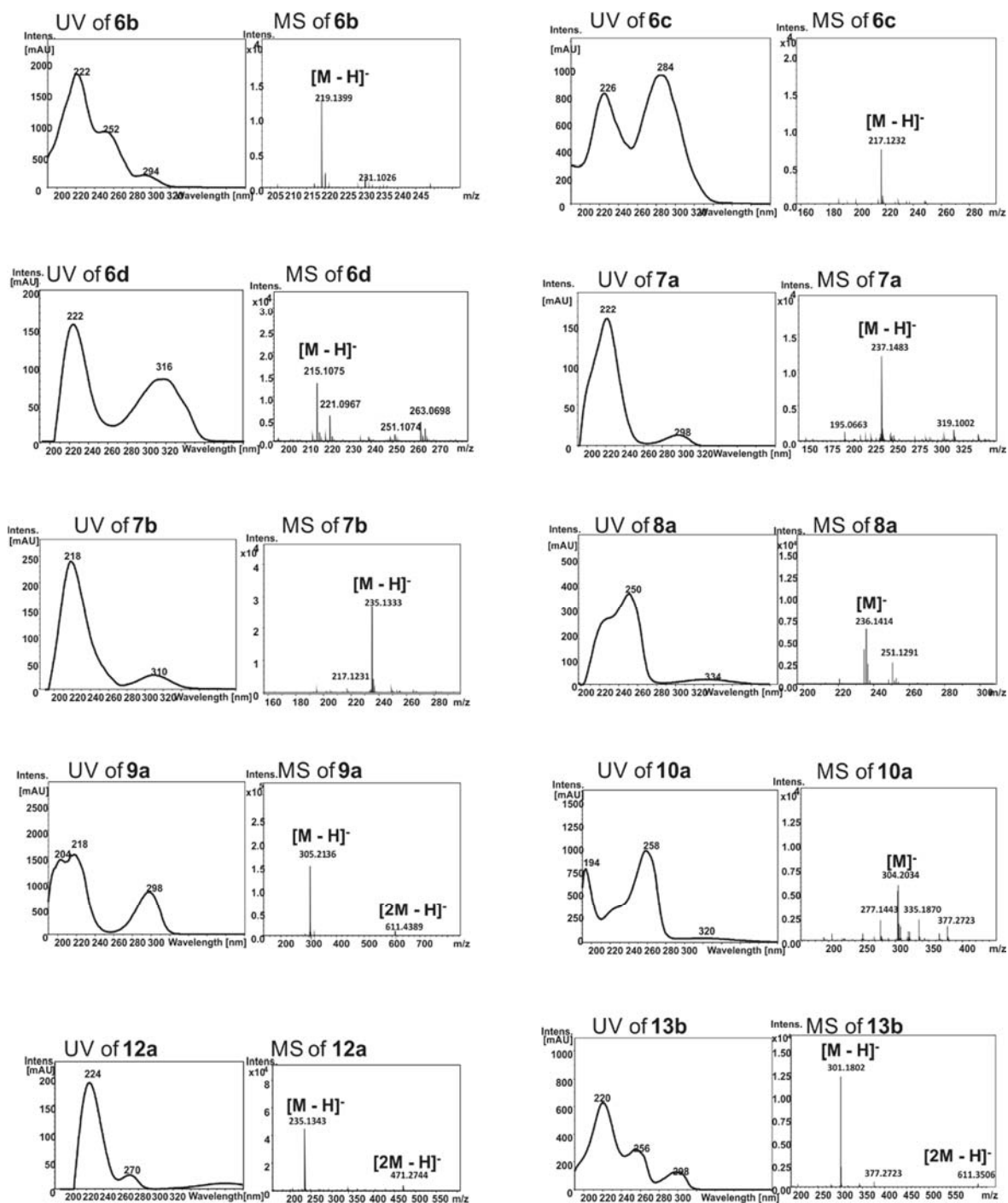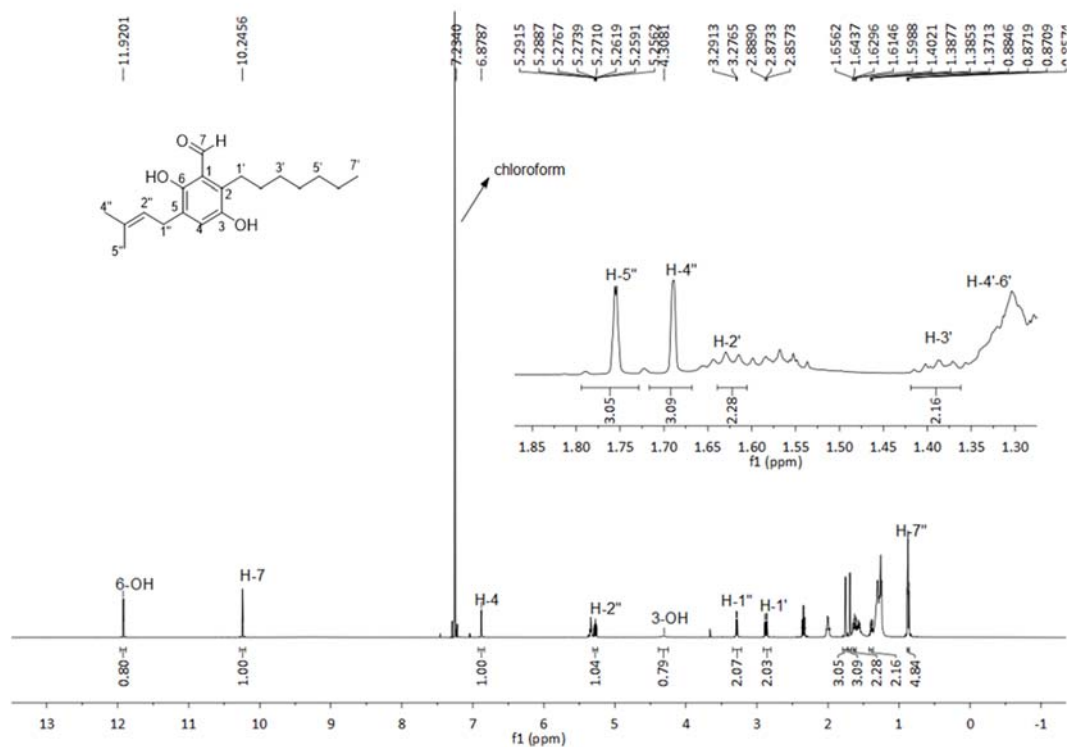
Figure S23. (continued)

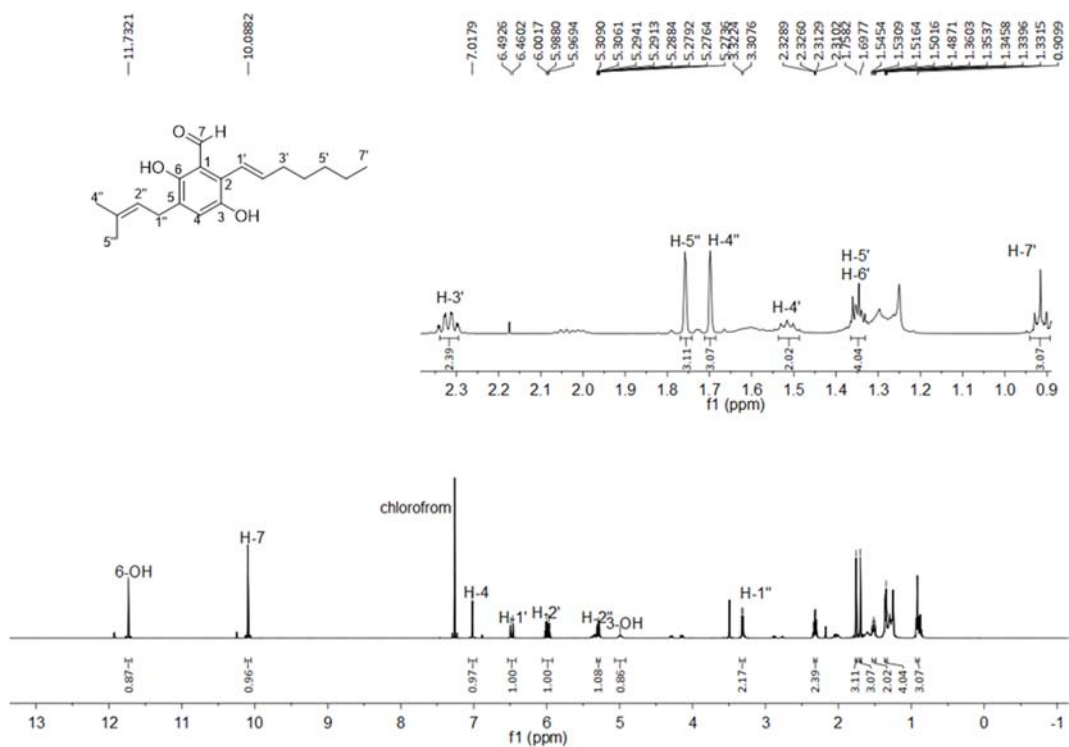**Figure S24.** ^{1}H NMR spectrum of compound **1a** in CDCl$_3$ (500 MHz)

Figure S25. ^{1}H NMR spectrum of compound **1b** in CDCl$_3$ (500 MHz)

Figure S26. ^{1}H NMR spectrum of compound **1c** in CDCl$_3$ (500 MHz)

Figure S27. ^{1}H NMR spectrum of compound **1d** in CDCl$_3$ (500 MHz)
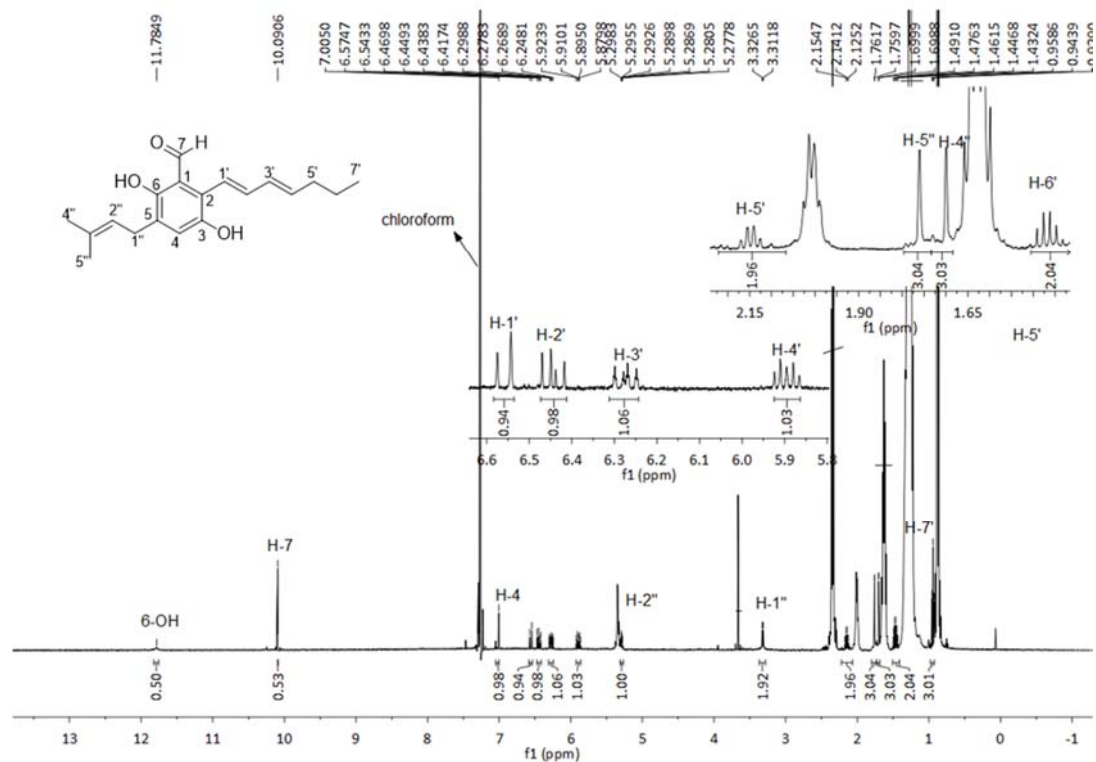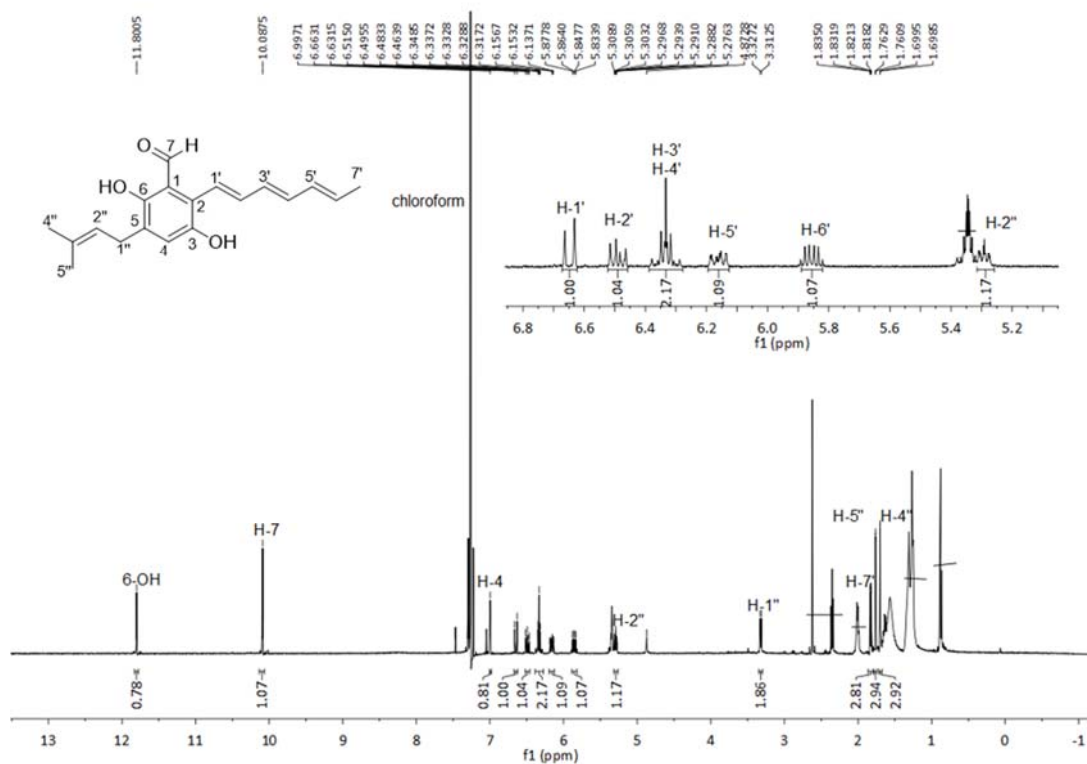
S48
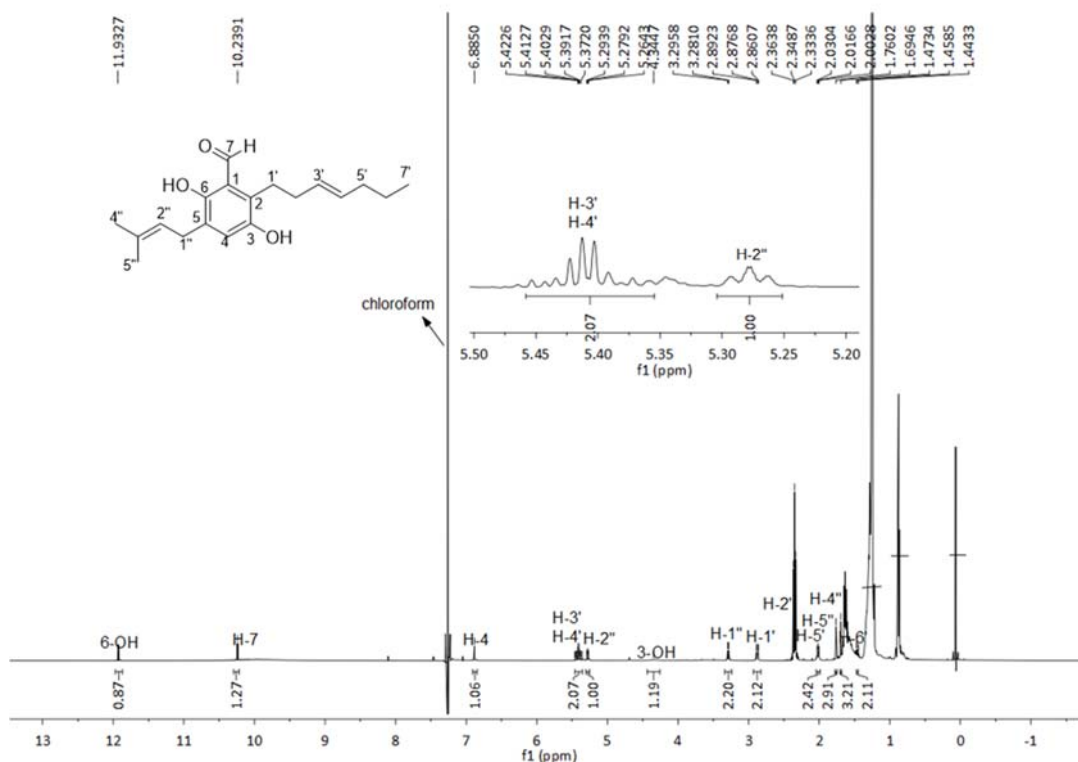
Figure S28. ^{1}H NMR spectrum of compound **1e** in CDCl$_3$ (500 MHz)
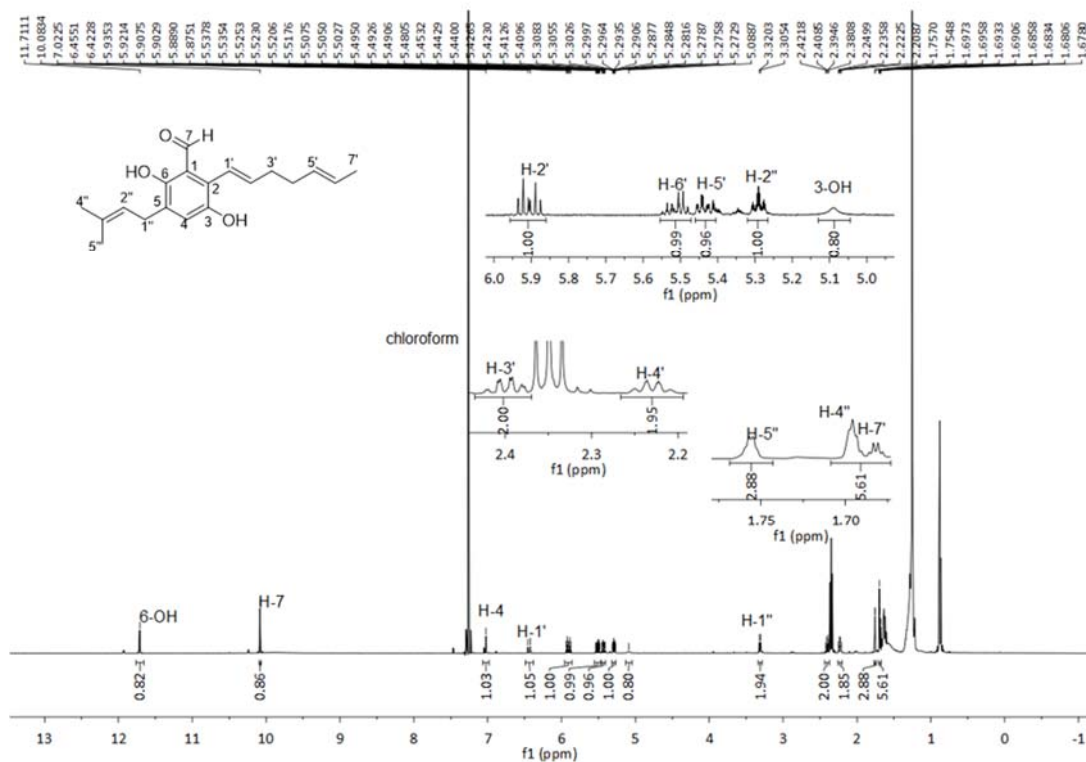
Figure S29. ^{1}H NMR spectrum of compound **1f** in CDCl$_3$ (500 MHz)
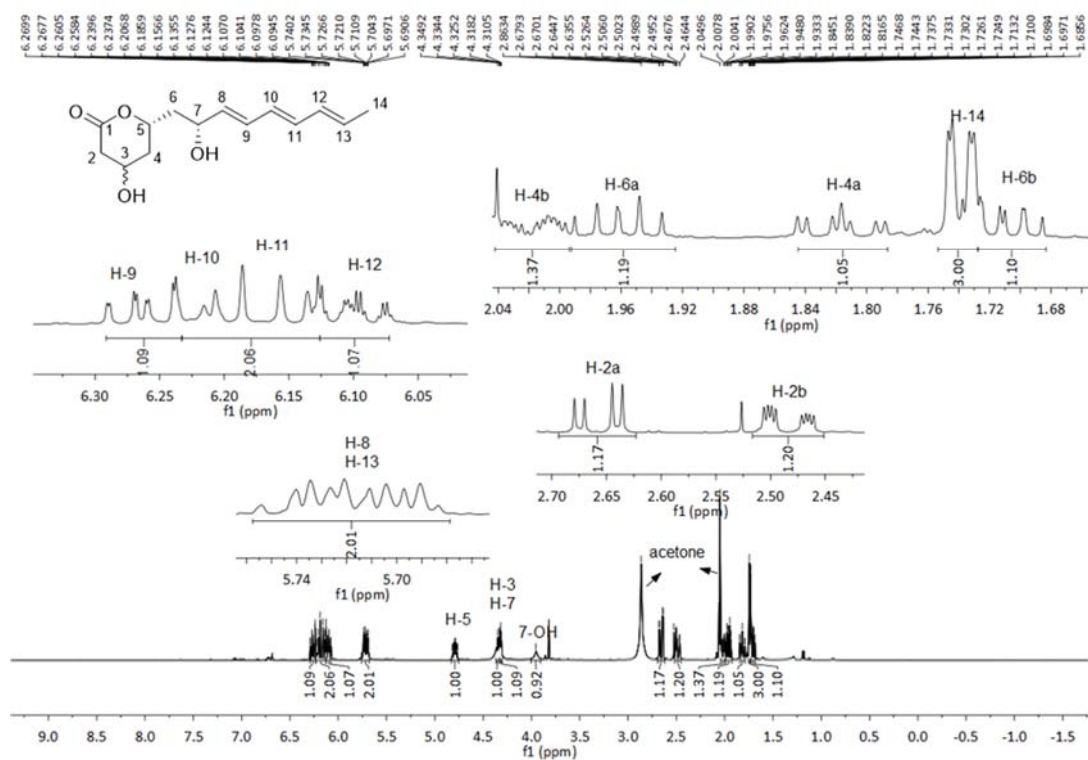
Figure S30. ^{1}H NMR spectrum of compound **3d** in CD$_3$COCD$_3$ (500 MHz)
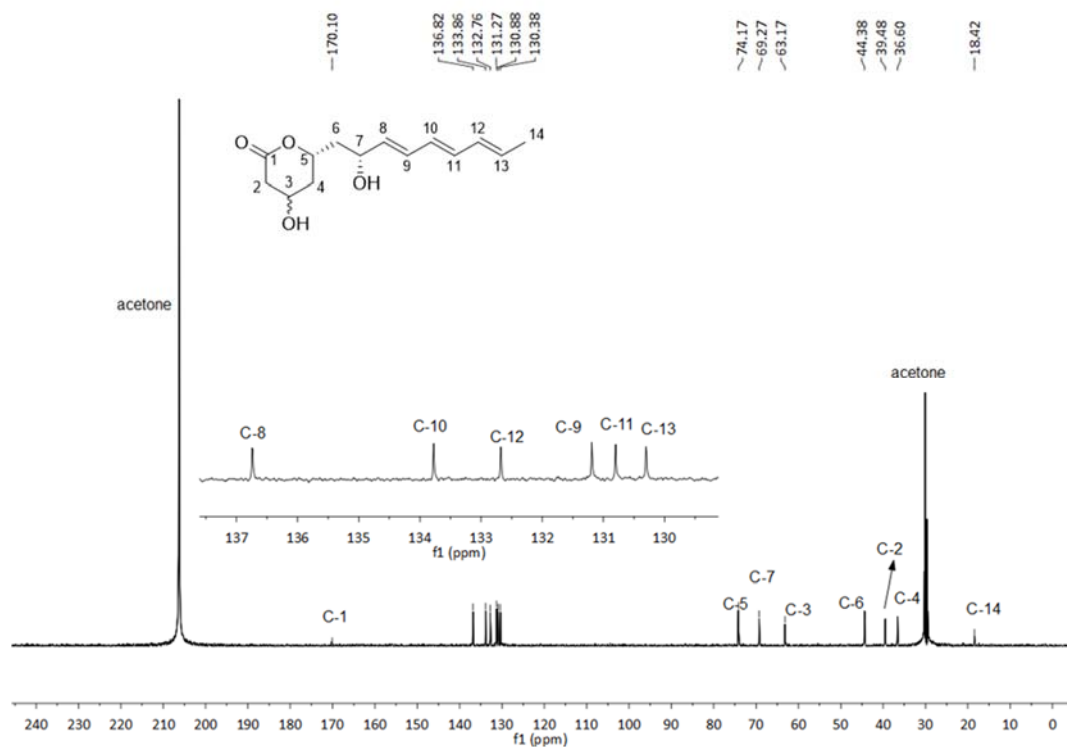
Figure S31. ^{13}C{^{1}H} NMR spectrum of compound **3d** in CD$_3$COCD$_3$ (125 MHz)

S50

Figure S32. HSQC NMR spectrum of compound **3d** in CD$_3$COCD$_3$
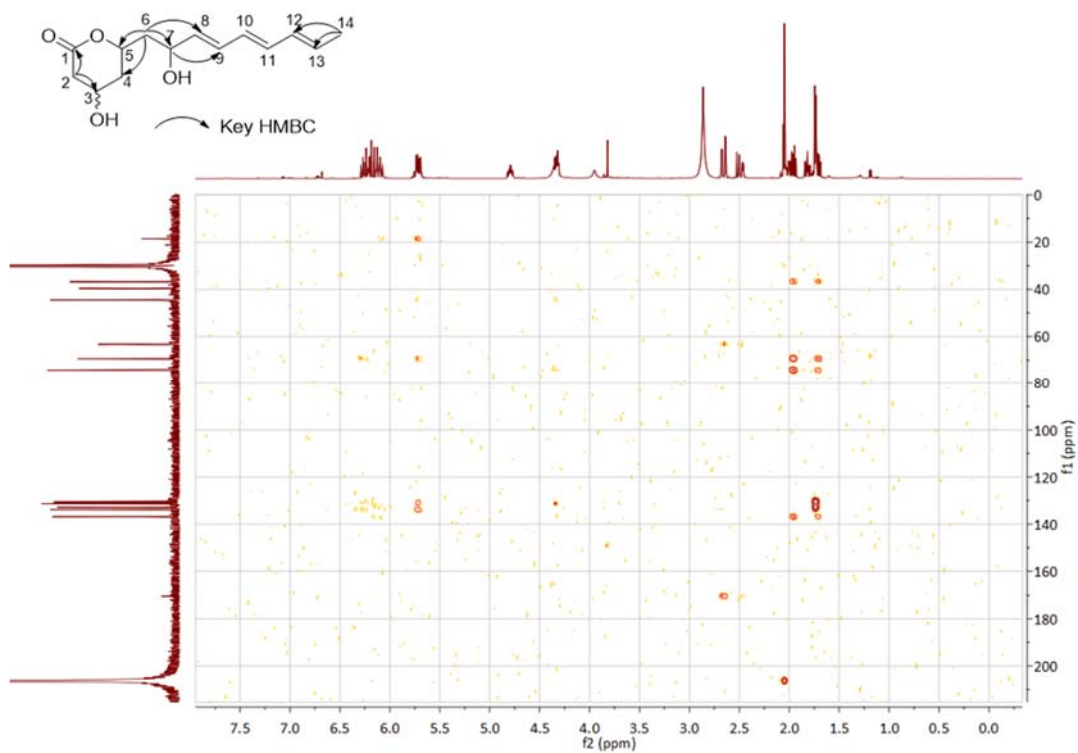
Figure S33. HMBC spectrum of compound **3d** in CD$_3$COCD$_3$
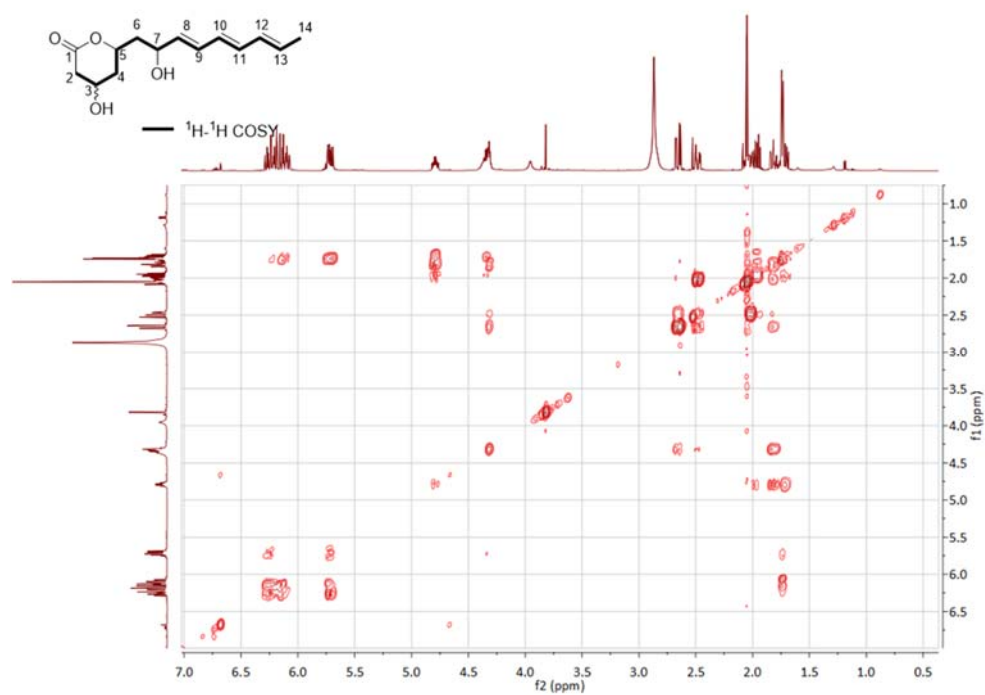
Figure S34. ^1H-^1H COSY spectrum of compound **3d** in CD_3COCD_3
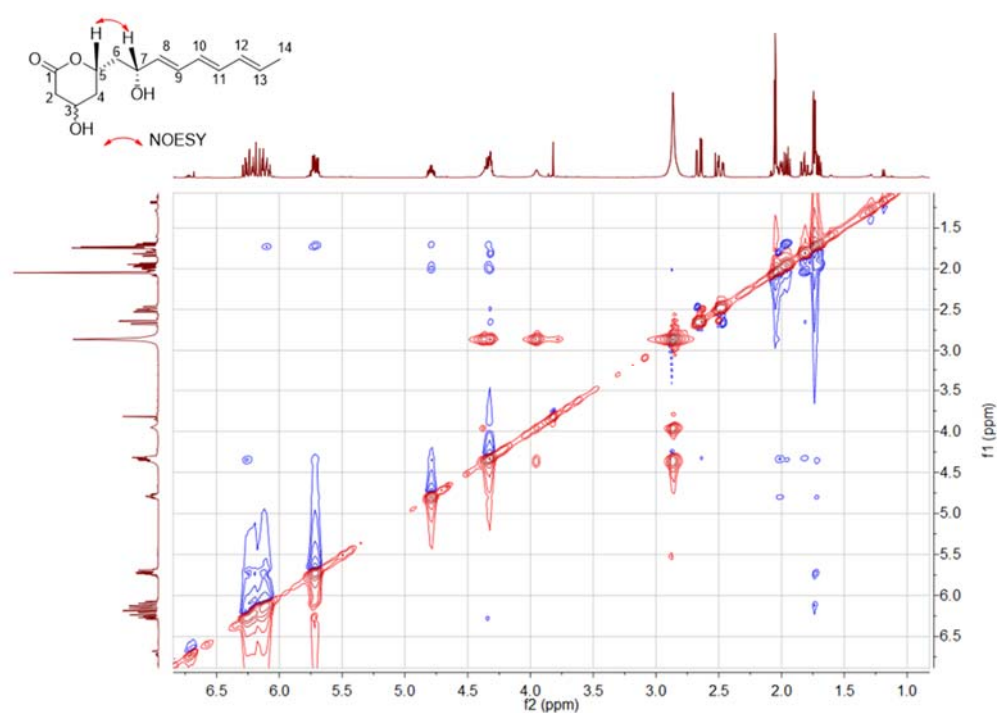
Figure S35. ^1H-^1H NOESY spectrum of compound **3d** in CD_3COCD_3

S52

183

Figure S36. ^{1}H NMR spectrum of compound **4d** in CD$_3$COCD$_3$ (500 MHz)

Figure S37. ^{13}C{^{1}H} NMR spectrum of compound **4d** in CD$_3$COCD$_3$ (125 MHz)

Figure S38. HMBC spectrum of compound **4d** in CD₃COCD₃

Figure S39. ¹H-¹H COSY spectrum of compound **4d** in CD₃COCD₃

S54

185
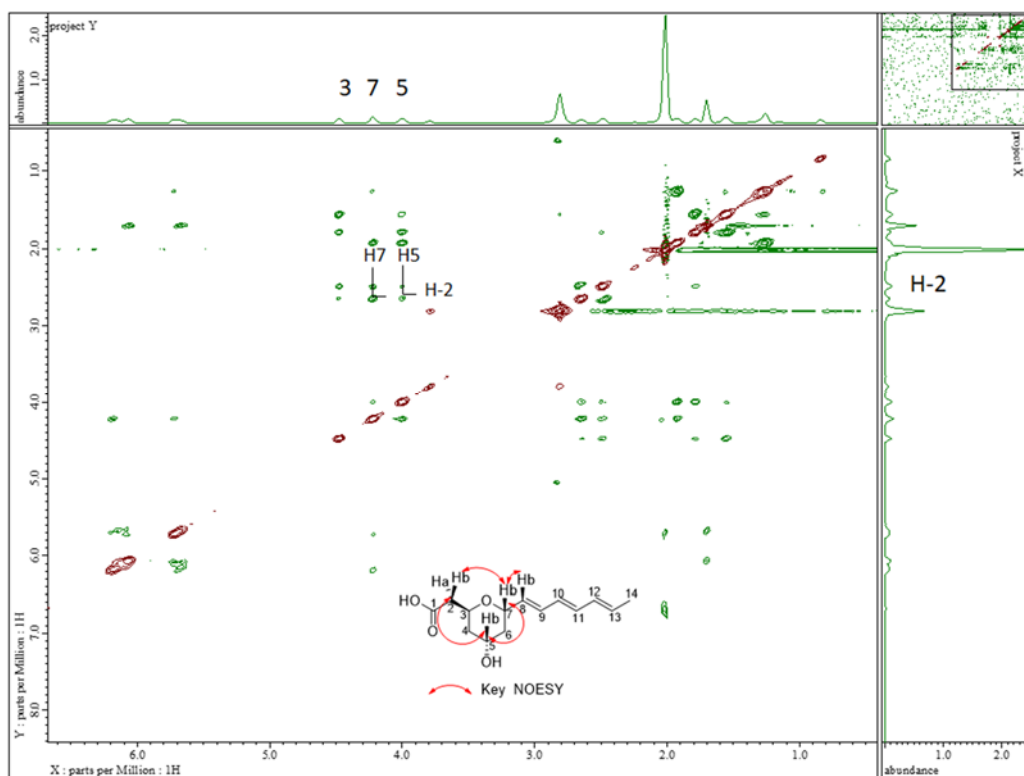
Figure S40. ^{1}H-^{1}H NOESY spectrum of compound **4d** in CD$_3$COCD$_3$
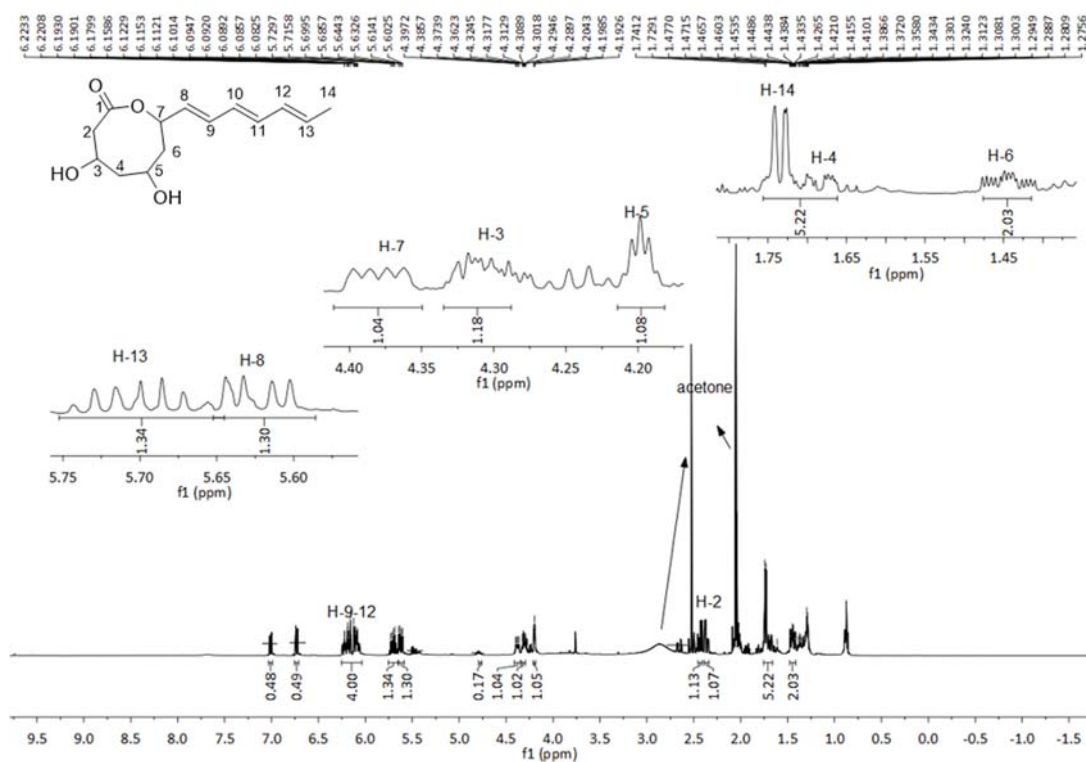
Figure S41. ^{1}H NMR spectrum of compound **5d** in CD$_3$COCD$_3$ (500 MHz)
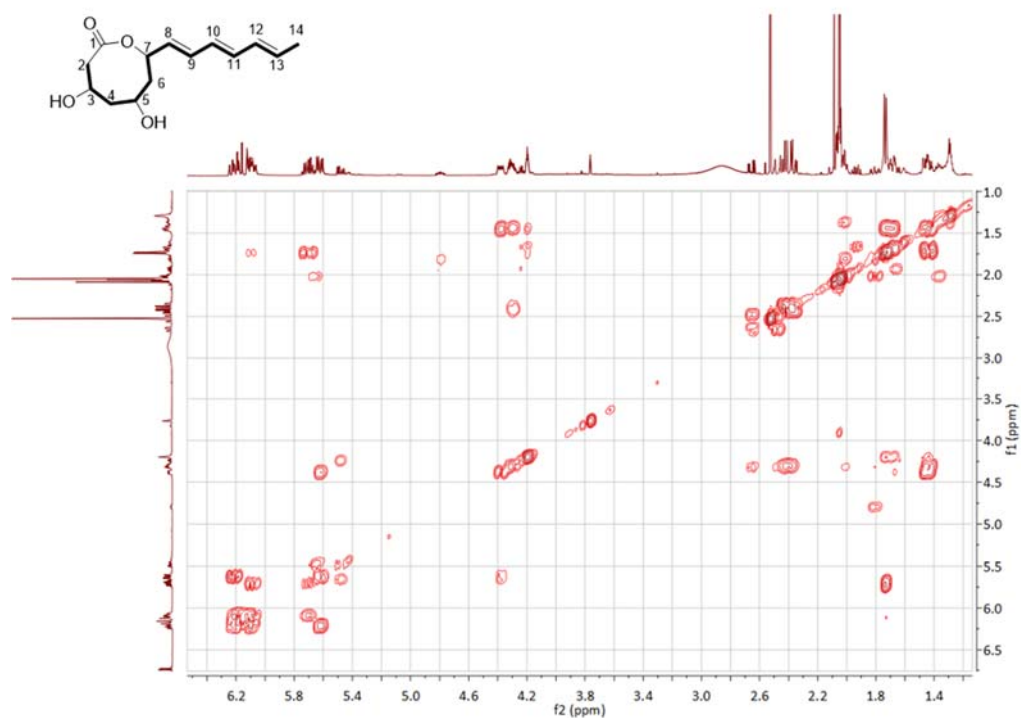
Figure S42. ^{1}H-^{1}H COSY spectrum of compound **5d** in CD$_3$COCD$_3$
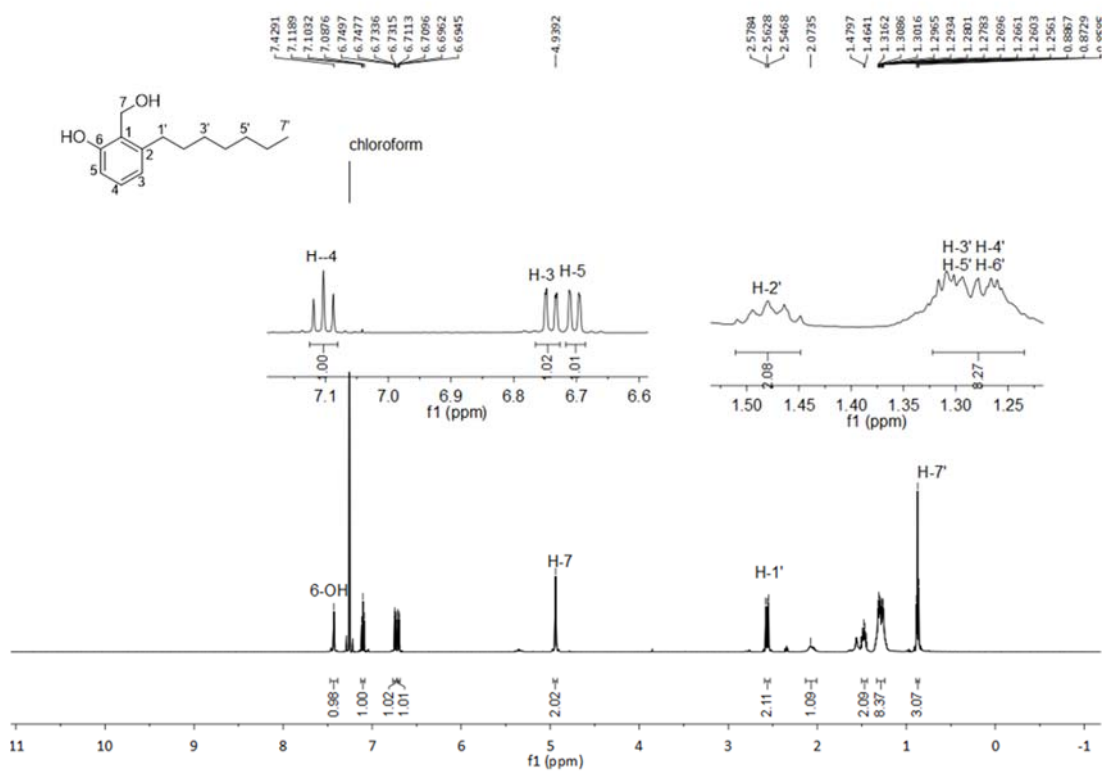
Figure S43. ^{1}H NMR spectrum of compound **6a** in CDCl$_3$ (500 MHz)
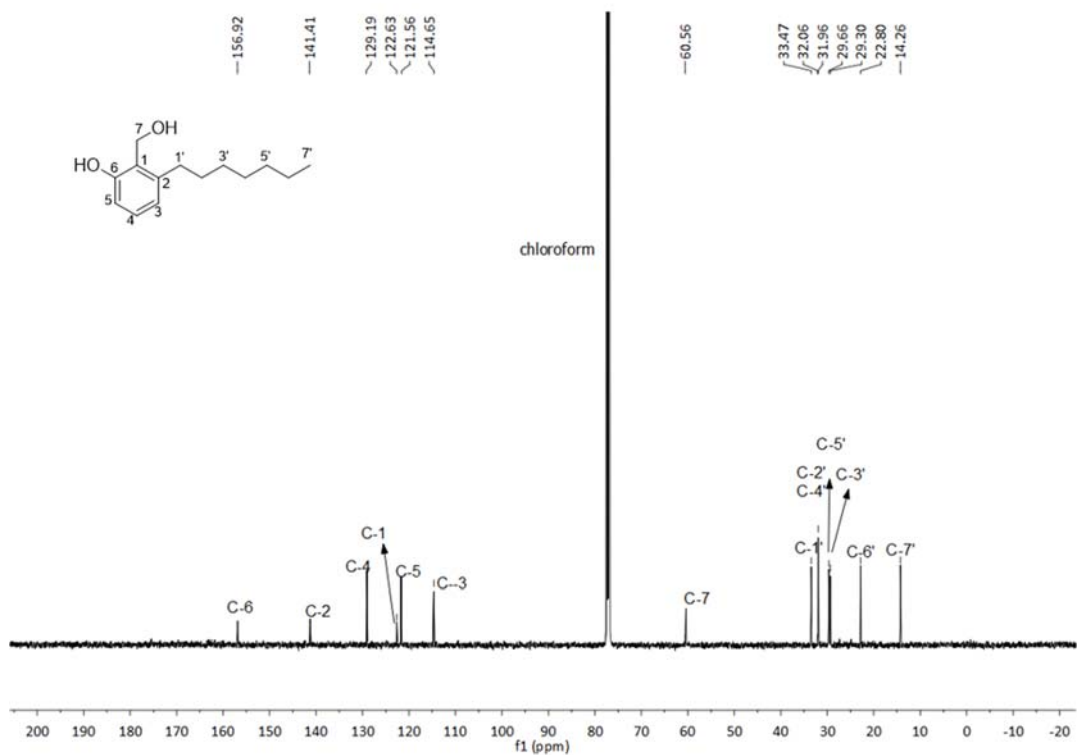
Figure S44. $^{13}C\{^1H\}$ NMR spectrum of compound **6a** in CDCl₃ (125 MHz)
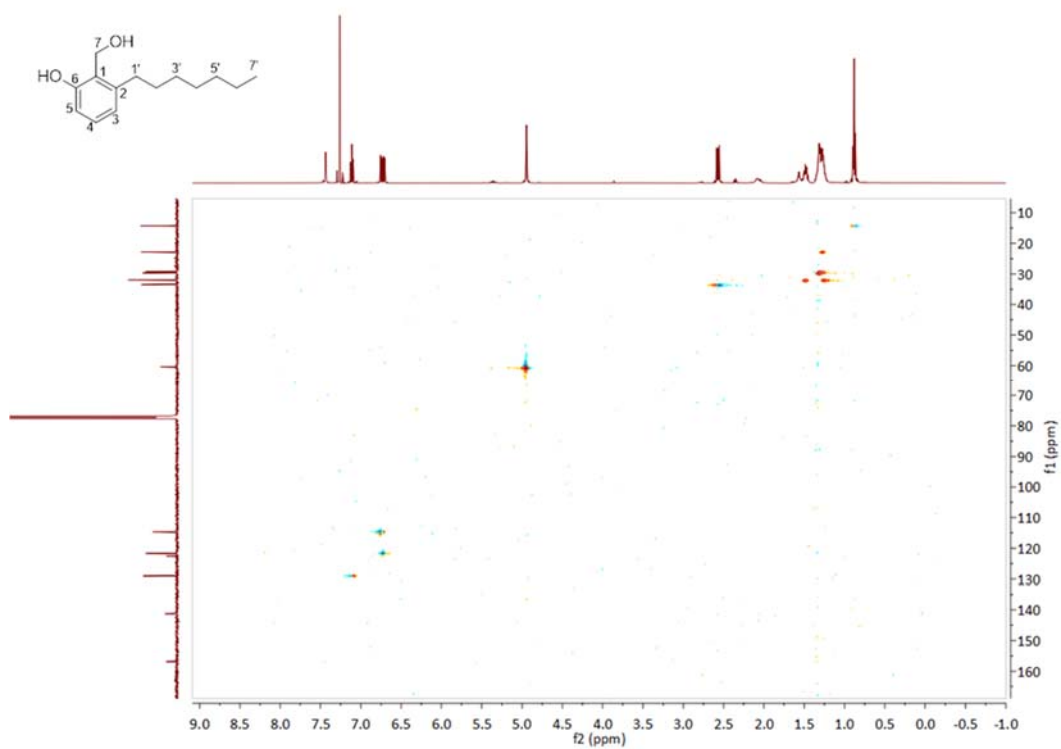
Figure S45. HSQC spectrum of compound **6a** in CDCl₃

S57

188
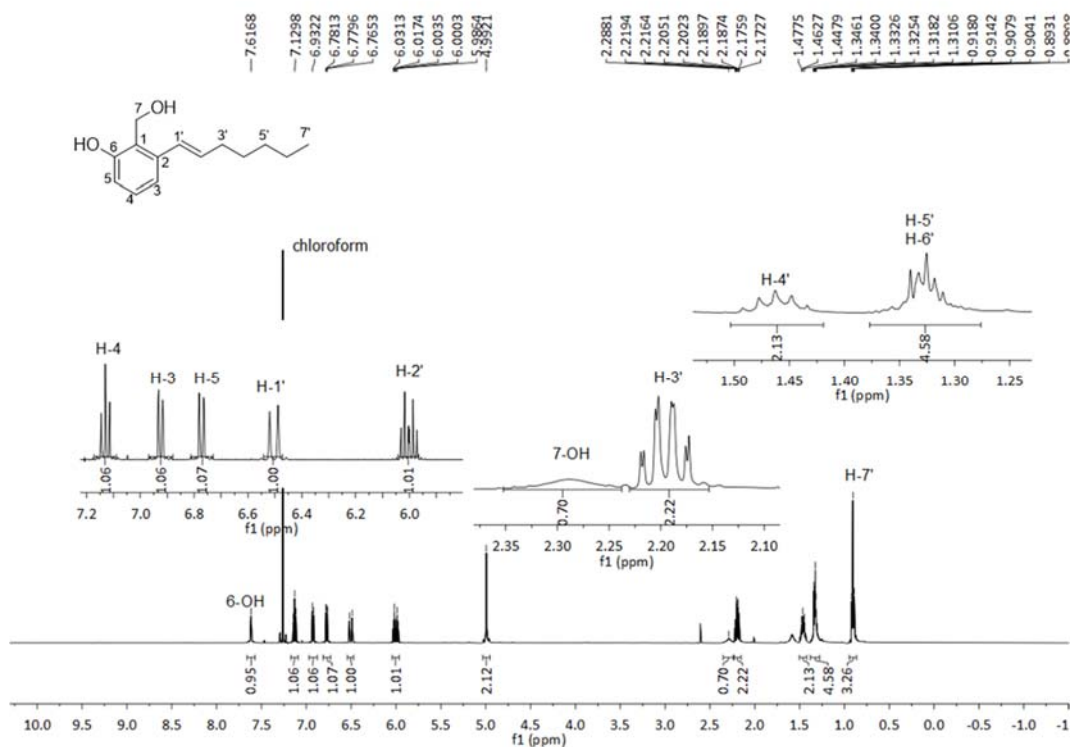
Figure S46. ^{1}H NMR spectrum of compound **6b** in CDCl₃ (500 MHz)
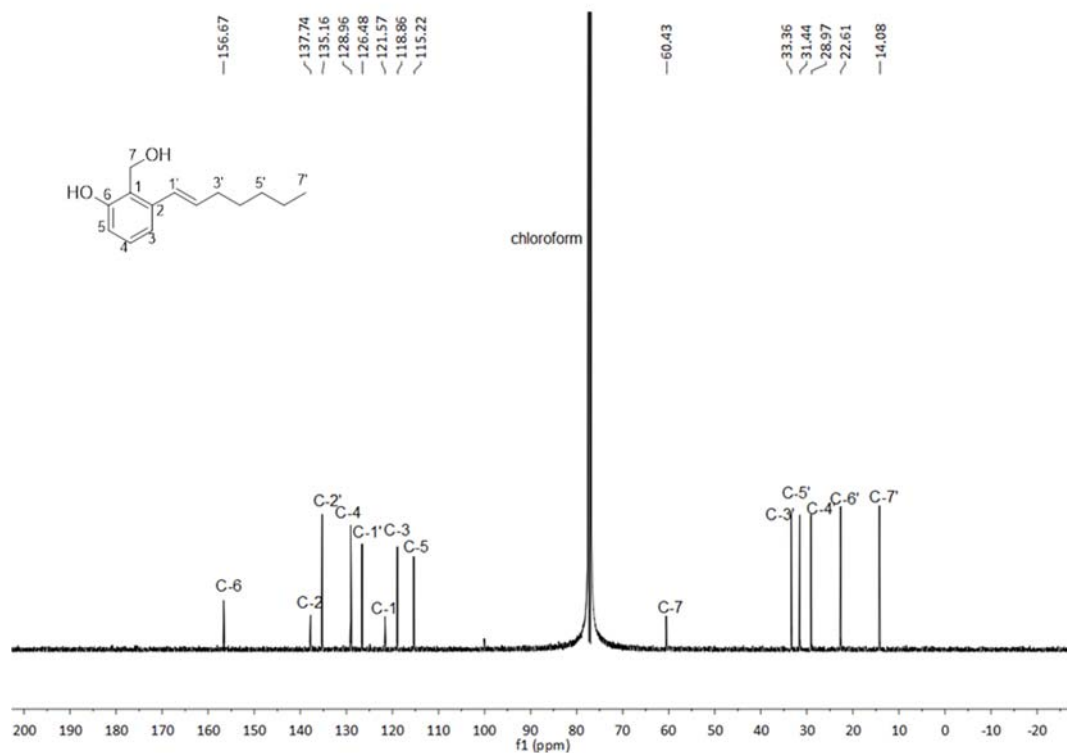
Figure S47. ^{13}C{^{1}H} NMR pectrum of compound **6b** in CDCl₃ (125 MHz)

S58

189
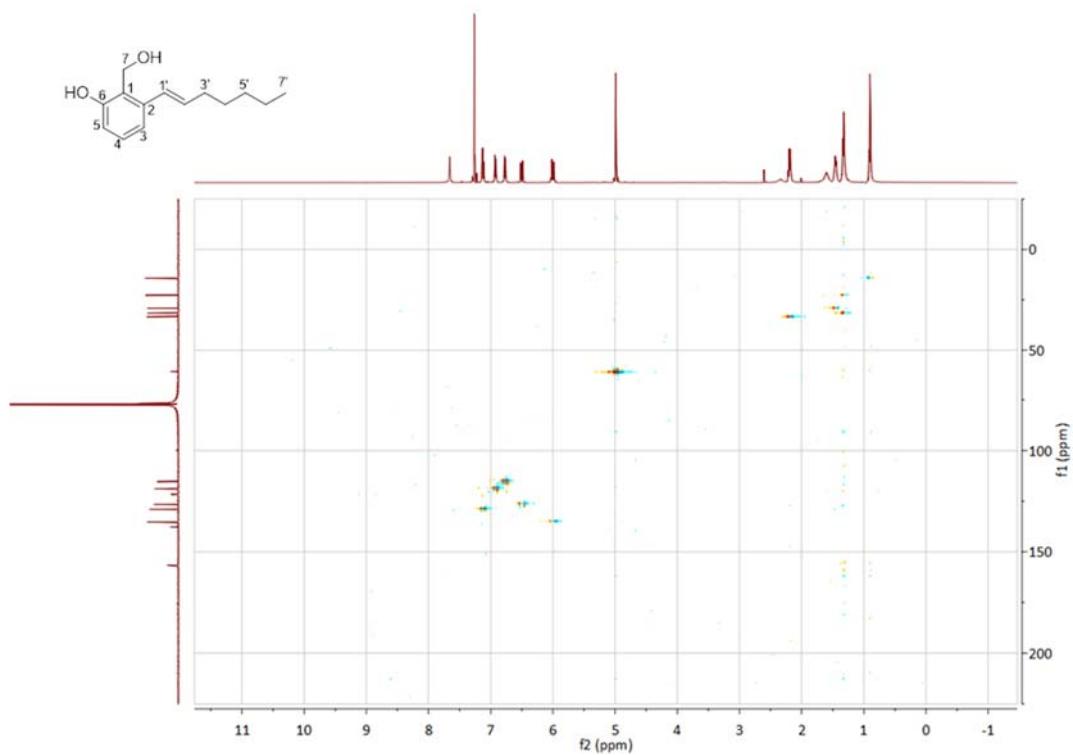
Figure S48. HMQC spectrum of compound **6b** in CDCl$_3$
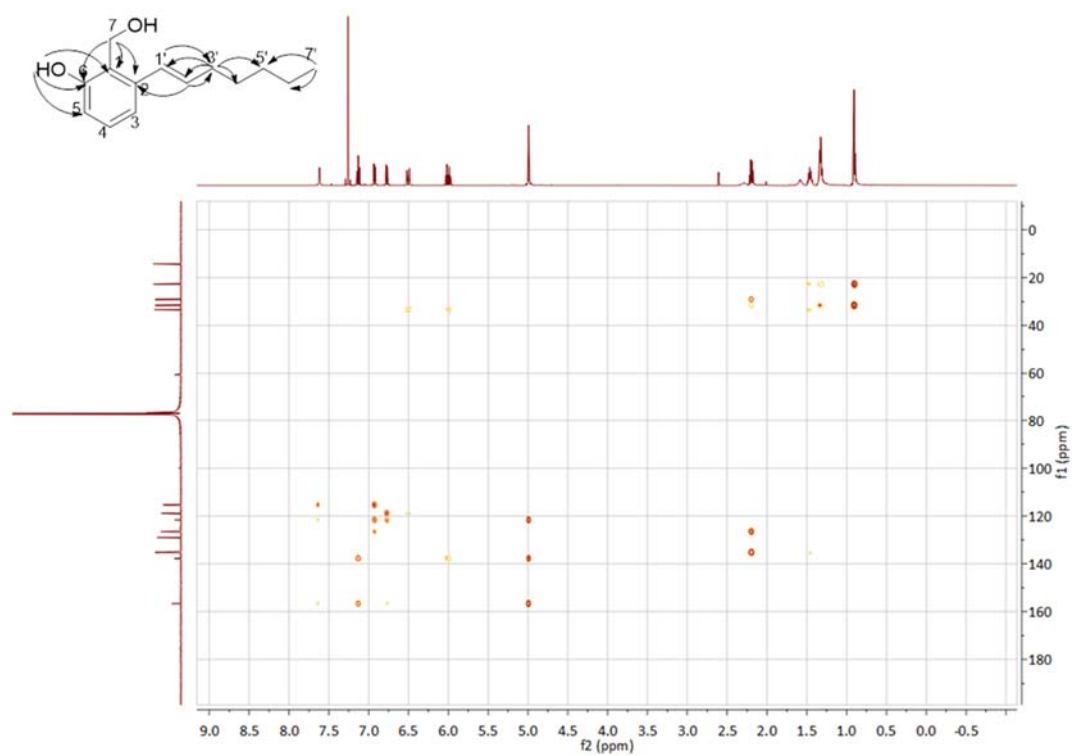
Figure S49. HMBC spectrum of compound **6b** in CDCl$_3$
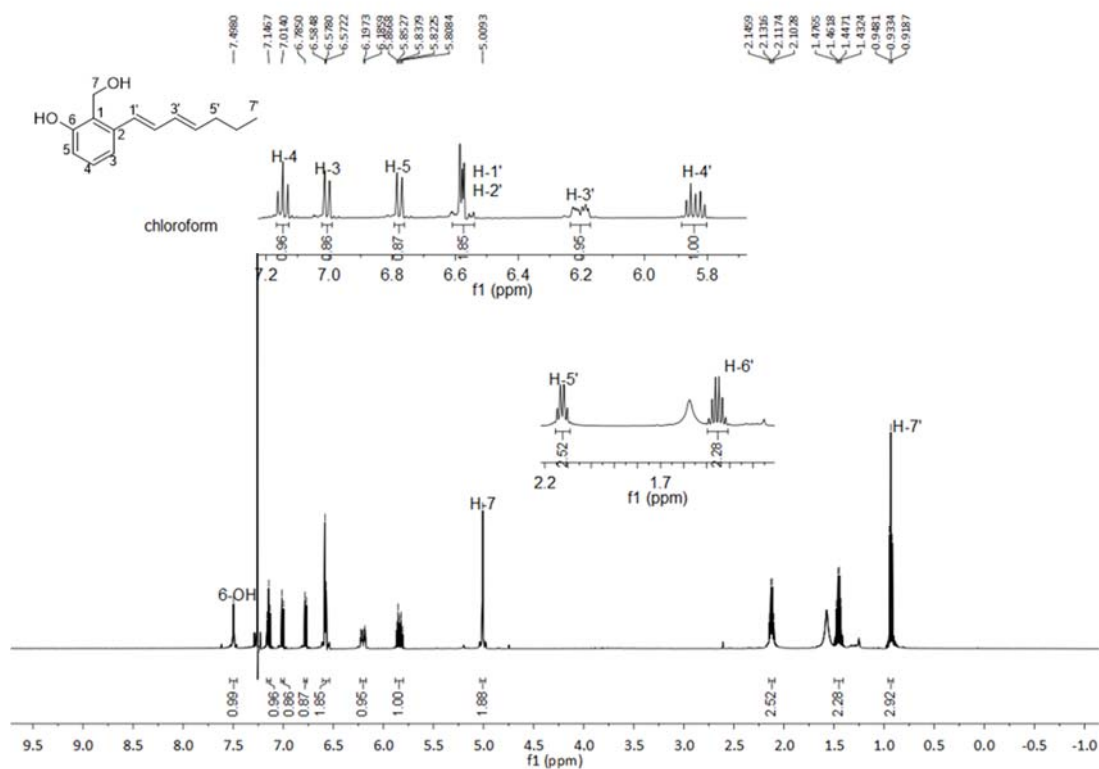
Figure S50. ¹H NMR spectrum of compound **6c** in CDCl₃ (500 MHz)
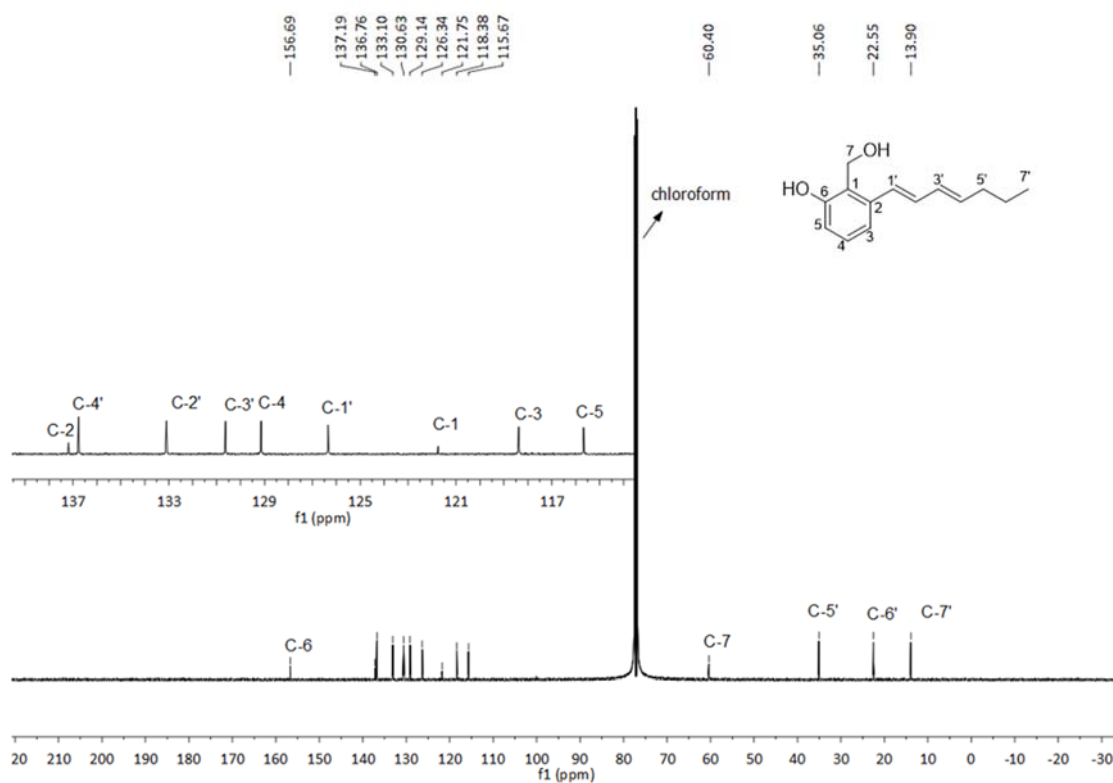
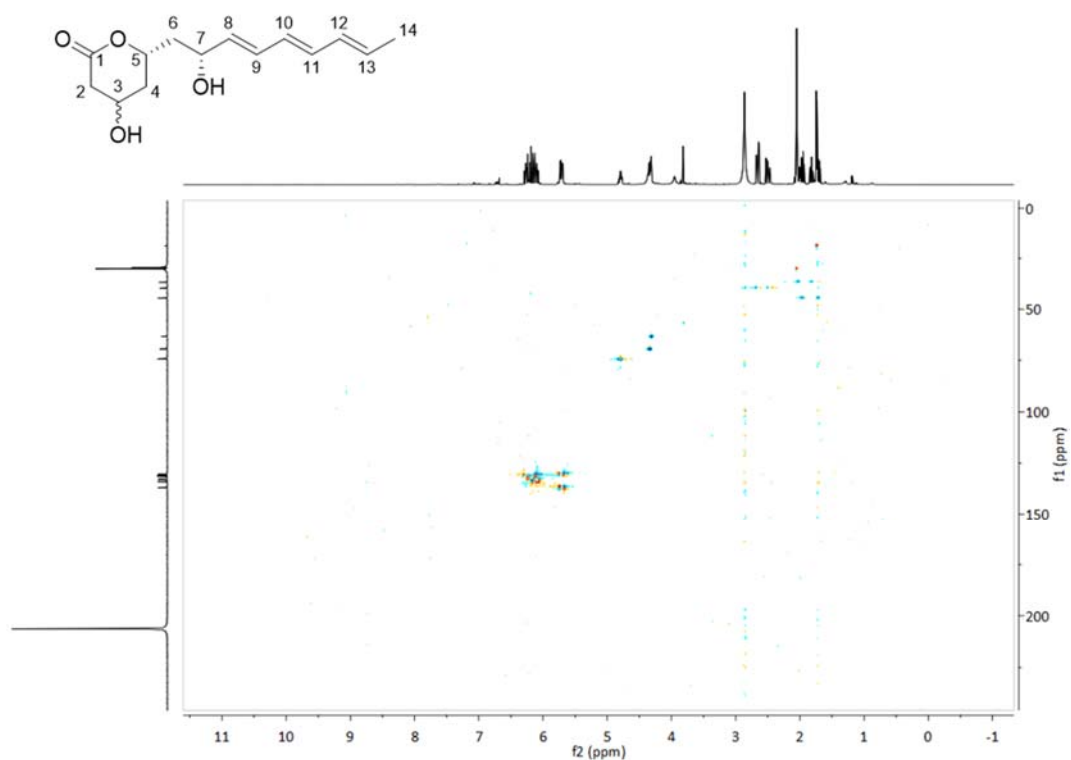**Figure S51.** ¹³C{¹H} NMR spectrum of compound **6c** in CDCl₃ (125 MHz)

S60
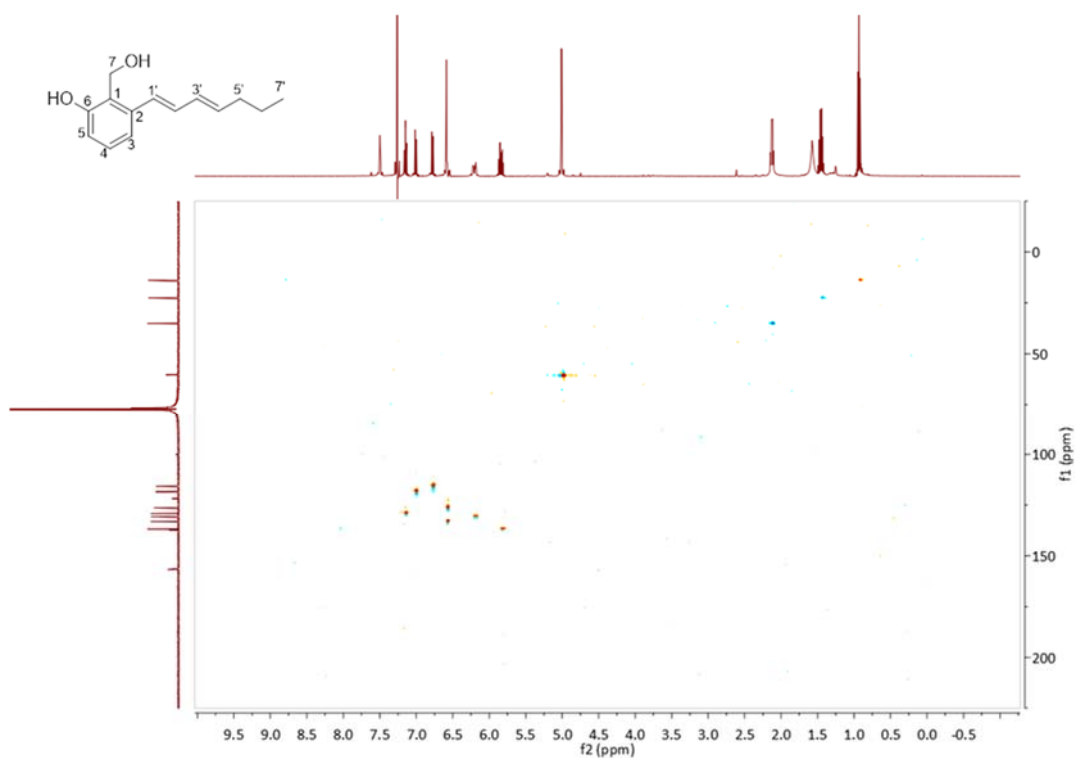
Figure S52. HSQC spectrum of compound **6c** in CDCl$_3$

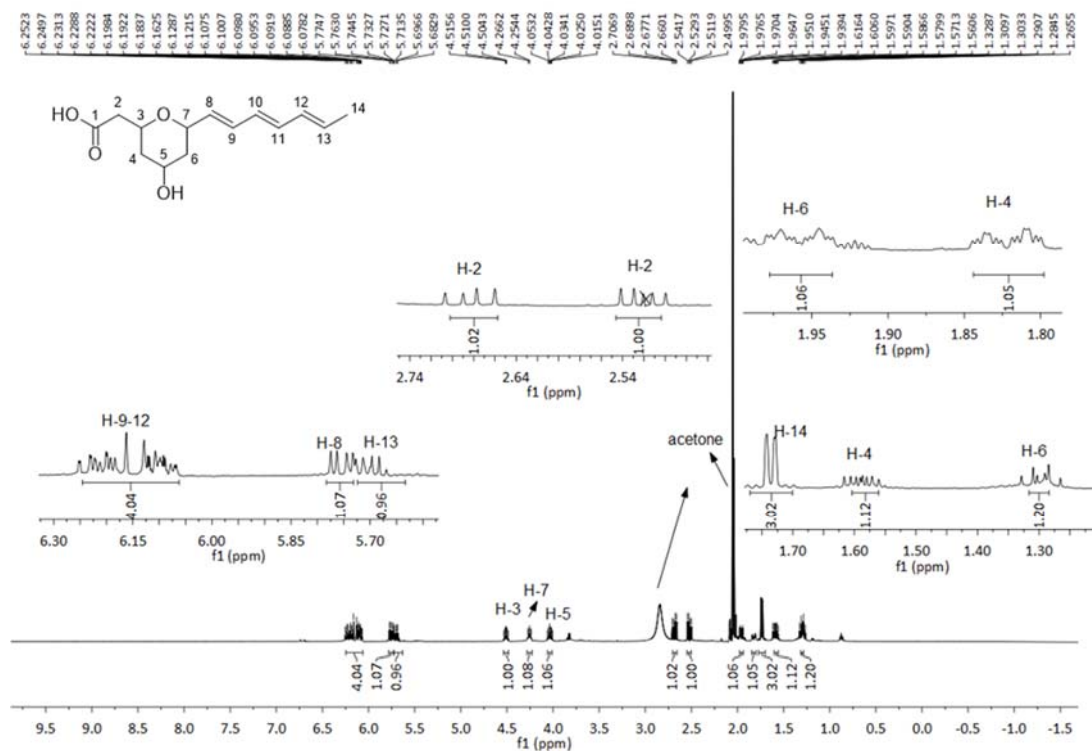**Figure S53.** ^{1}H NMR spectrum of compound **6d** in CDCl$_3$ (500 MHz)
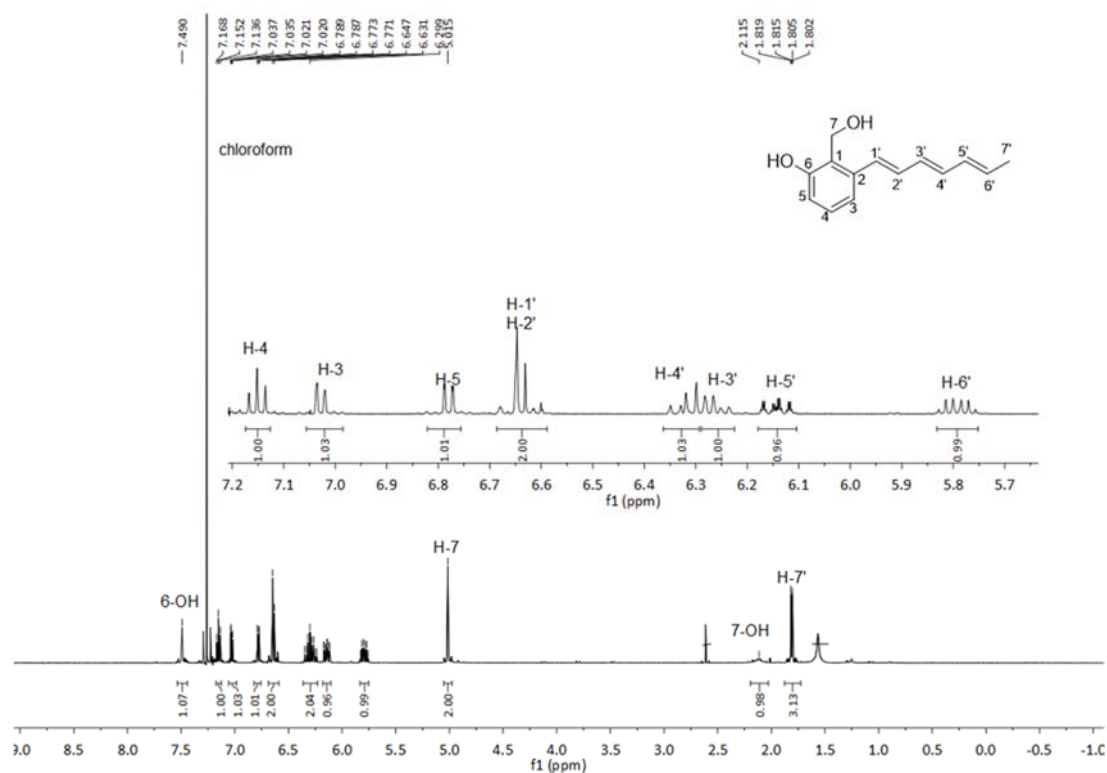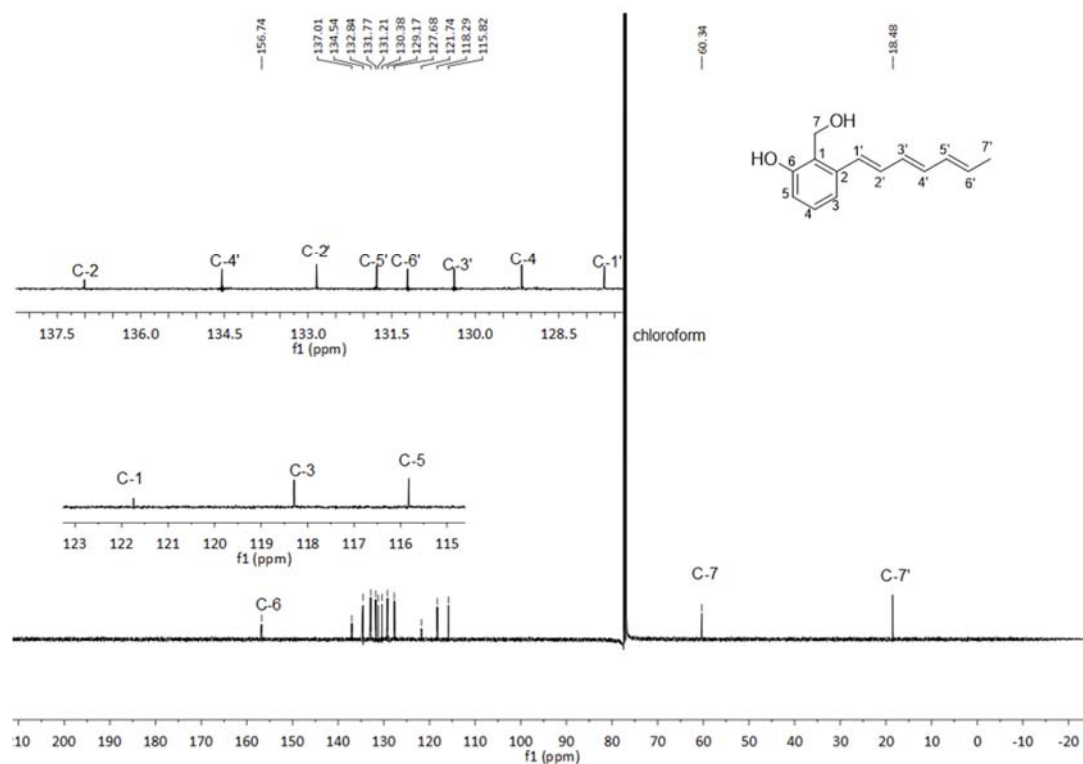
Figure S54. $^{13}C\{^1H\}$ NMR spectrum of compound **6d** in CDCl$_3$ (125 MHz)
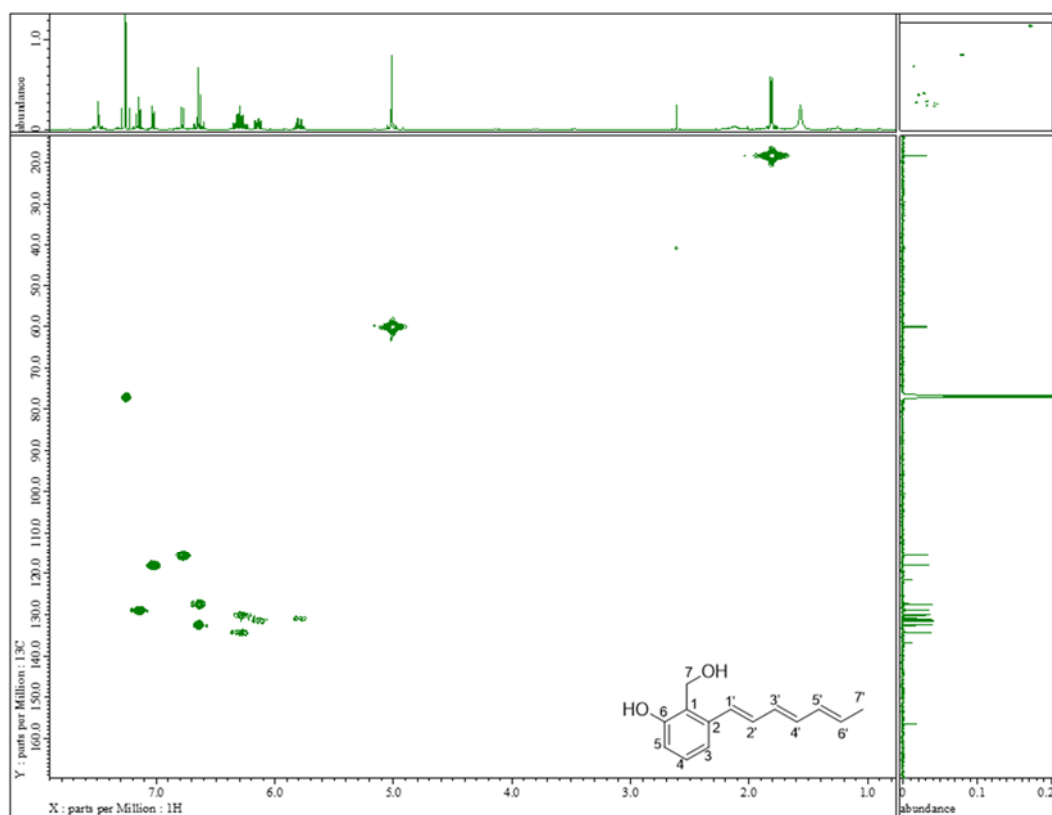
Figure S55. HSQC spectrum of compound **6d** in CDCl$_3$
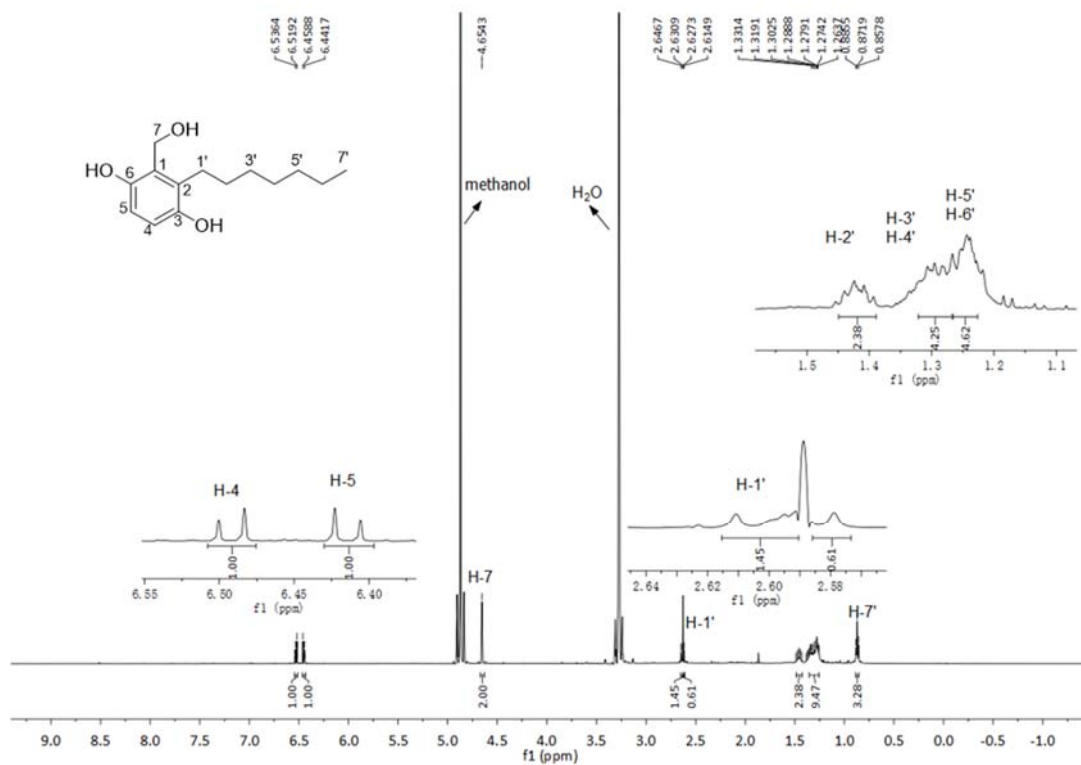
Figure S56. ^{1}H NMR spectrum of compound **7a** in CD$_3$OD (500 MHz)
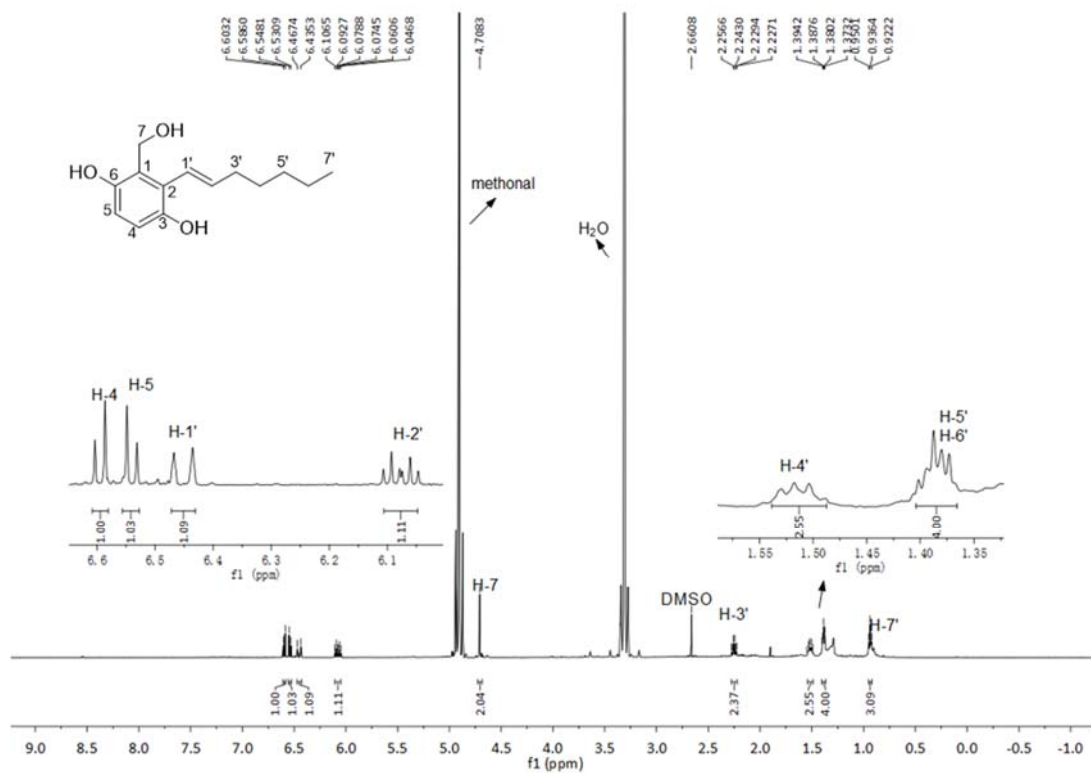
Figure S57. ^{1}H NMR spectrum of compound **7b** in CD$_3$OD (500 MHz)
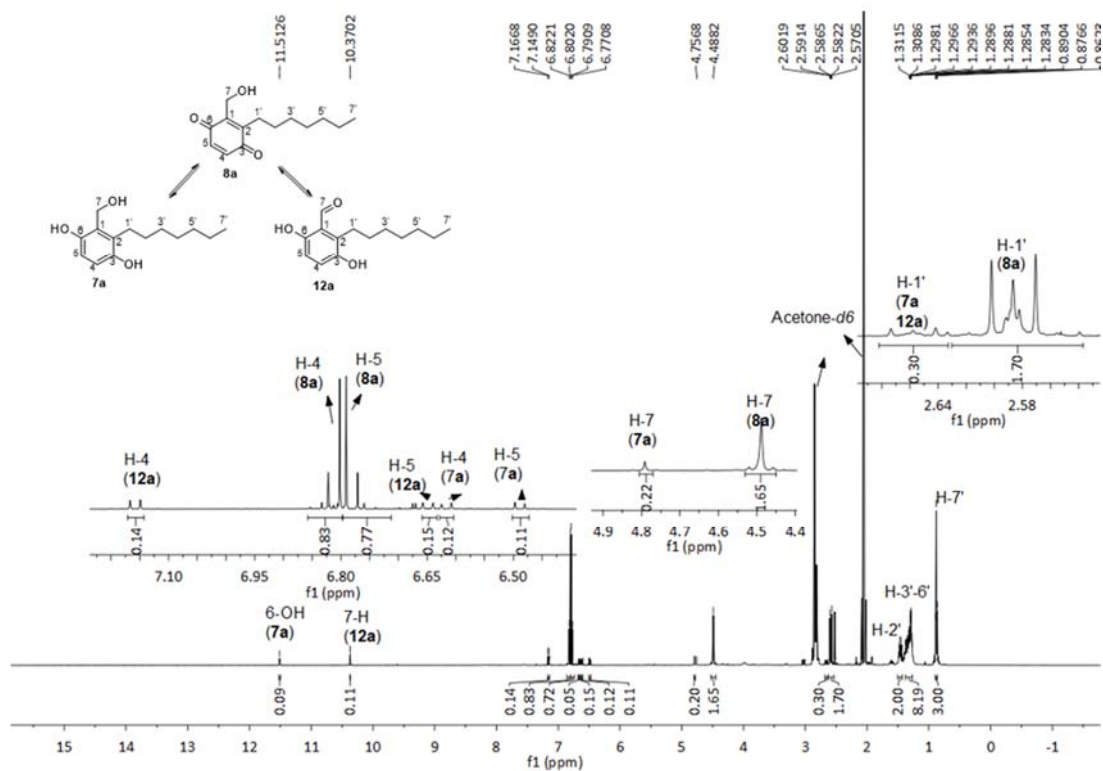
Figure S58. ^{1}H NMR spectrum of compound **8a** in CD$_3$COCD$_3$ (500 MHz)
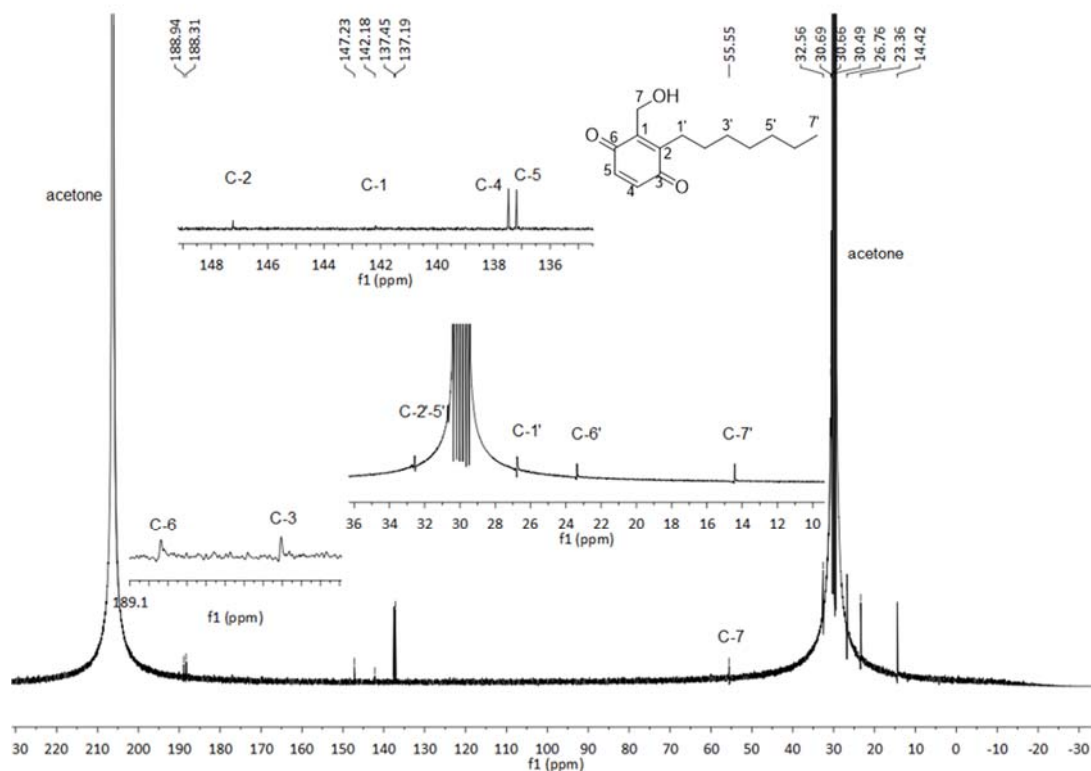
Figure S59. ^{13}C{^{1}H} NMR spectrum of compound **8a** in CD$_3$COCD$_3$ (125 MHz)

S64
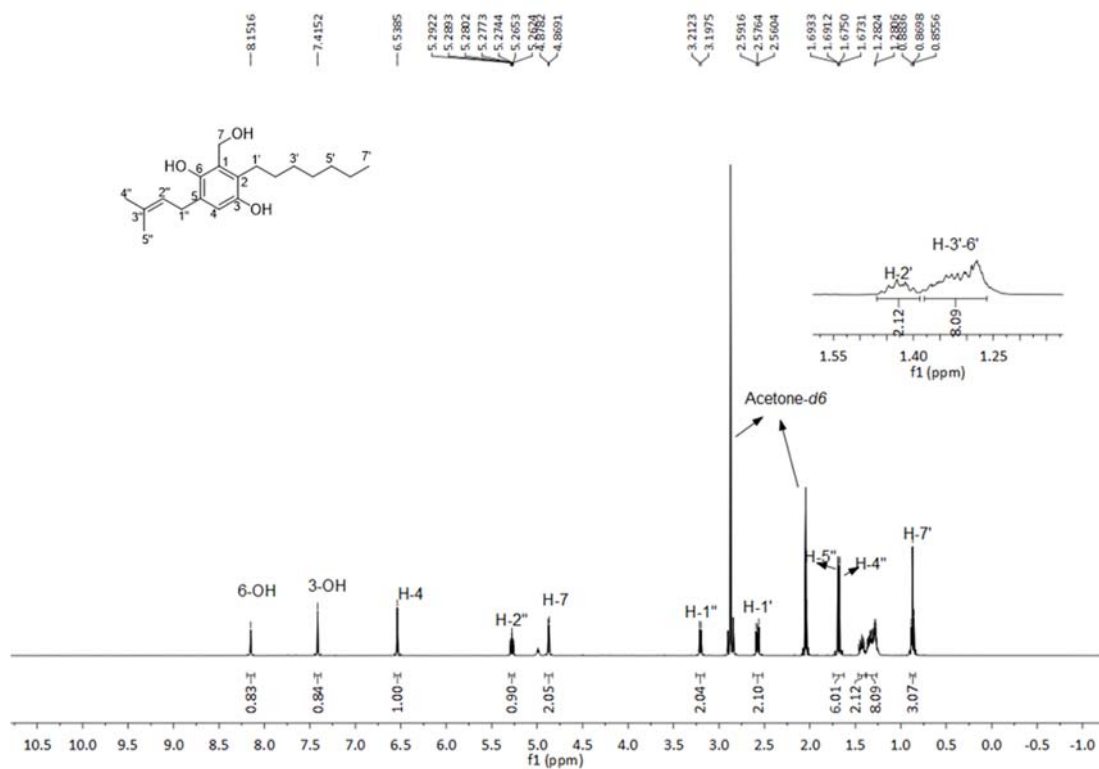
Figure S60. ¹H NMR spectrum of compound **9a** in CD₃COCD₃ (500 MHz)
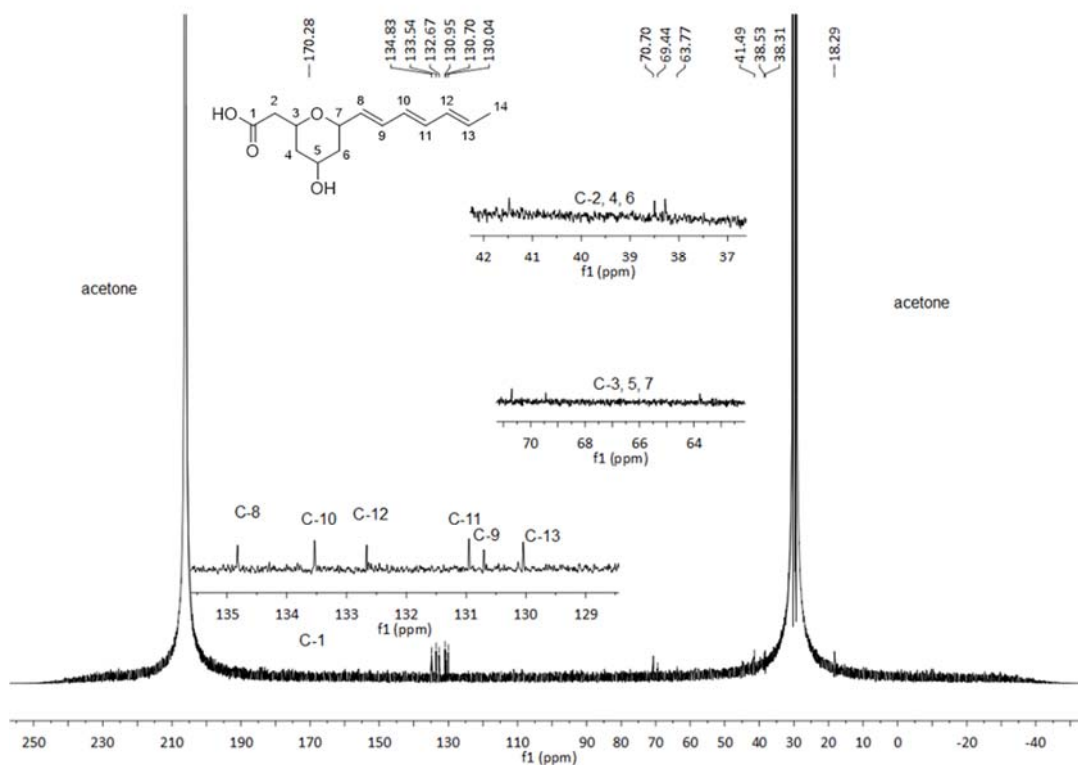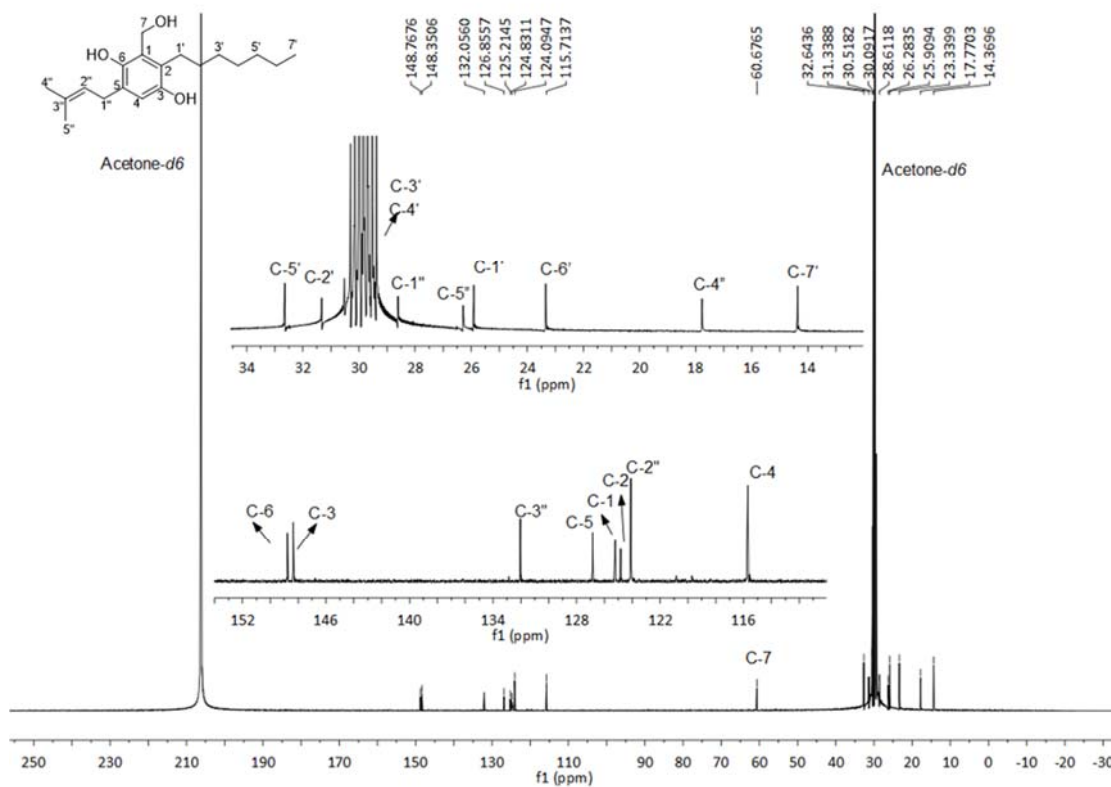

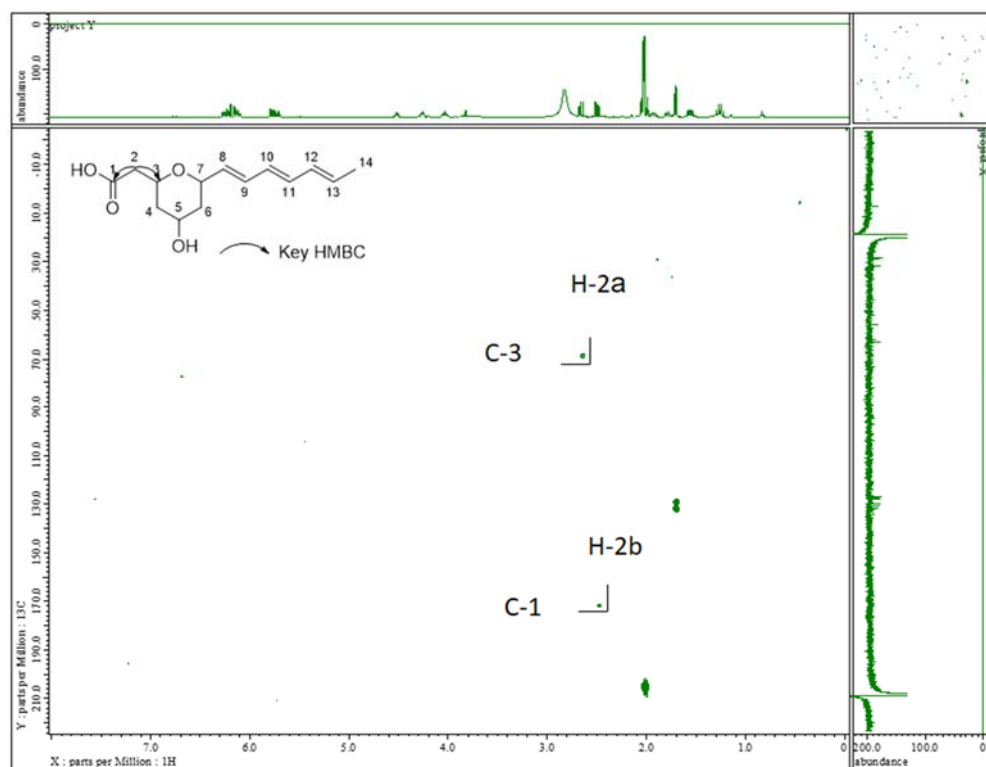**Figure S61.** ¹³C{¹H} NMR spectrum of compound **9a** in CD₃COCD₃ (125 MHz)

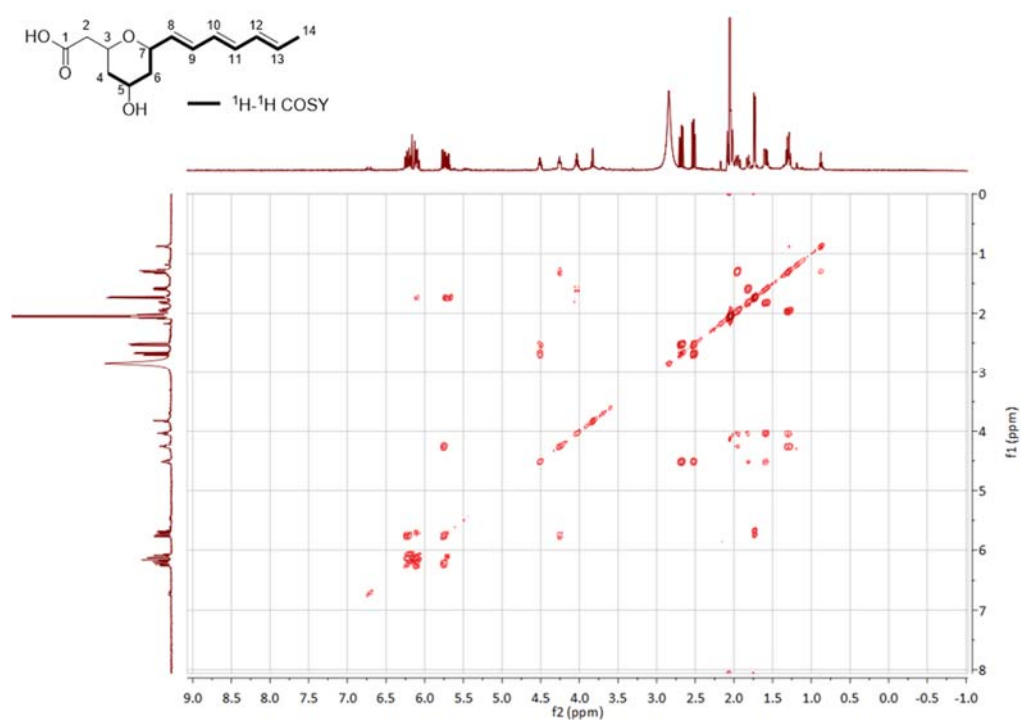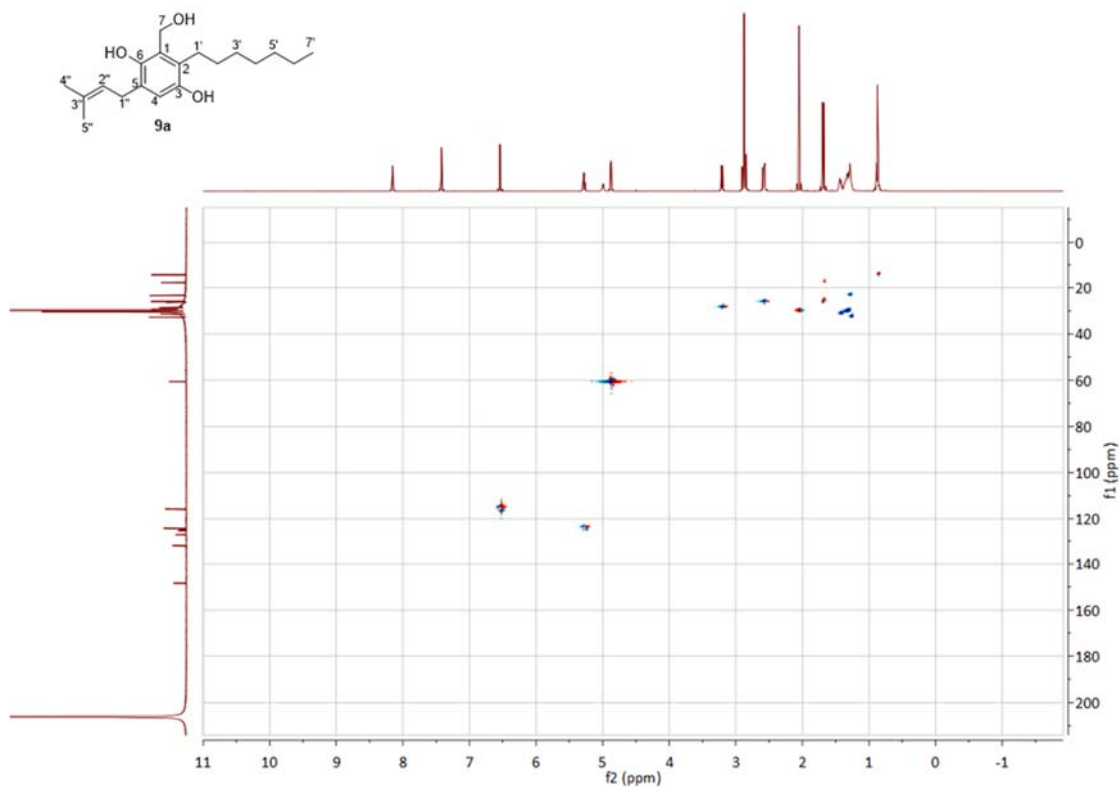**Figure S62.** HSQC spectrum of compound **9a** in CD$_3$COCD$_3$
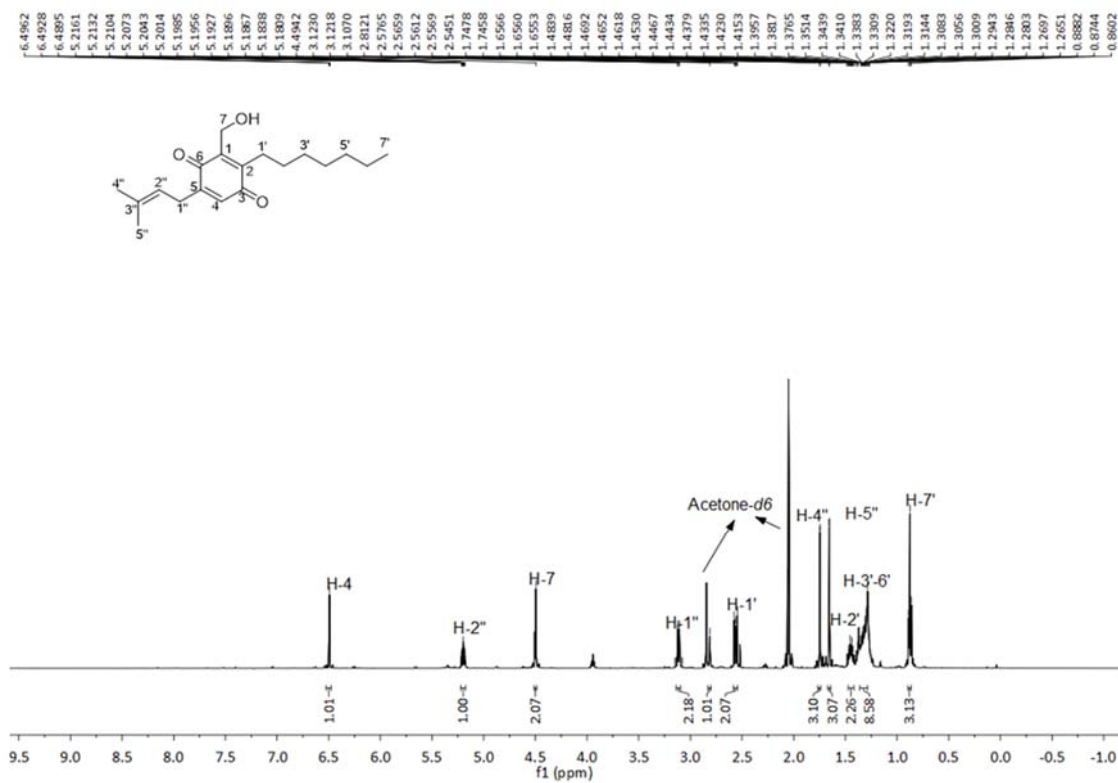
Figure S63. ^{1}H NMR spectrum of compound **10a** in CD$_3$COCD$_3$ (500 MHz)

S66
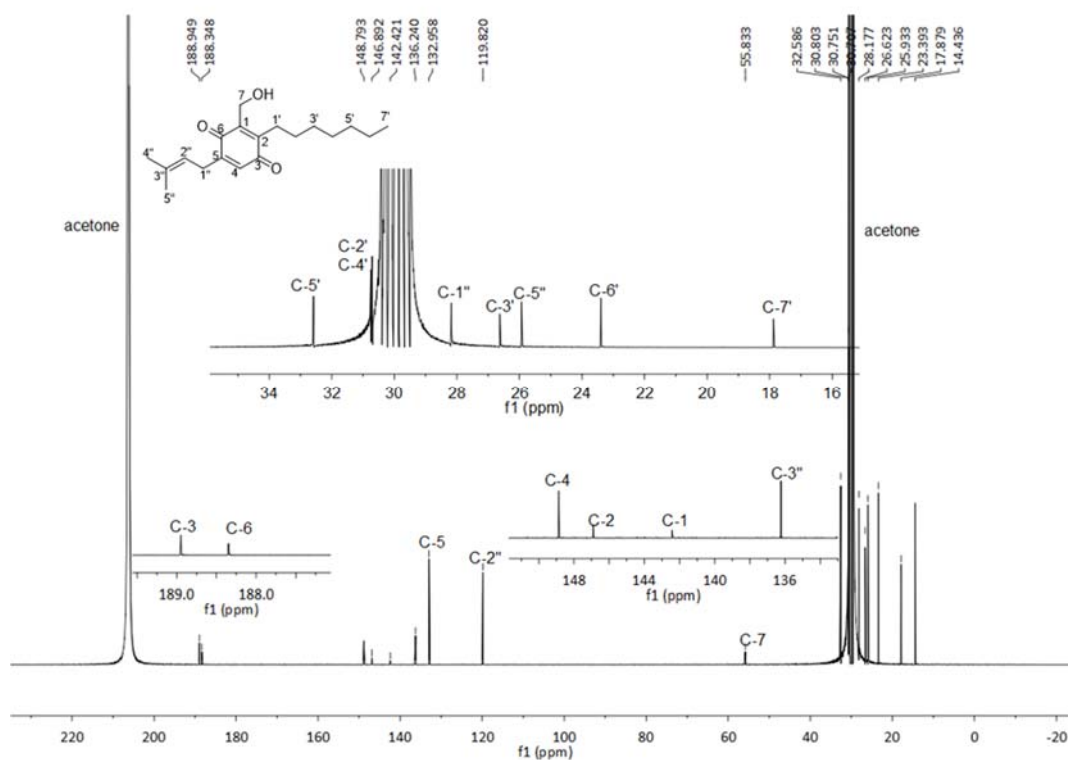
Figure S64. $^{13}C\{^1H\}$ NMR spectrum of compound **10a** in CD$_3$COCD$_3$ (125 MHz)
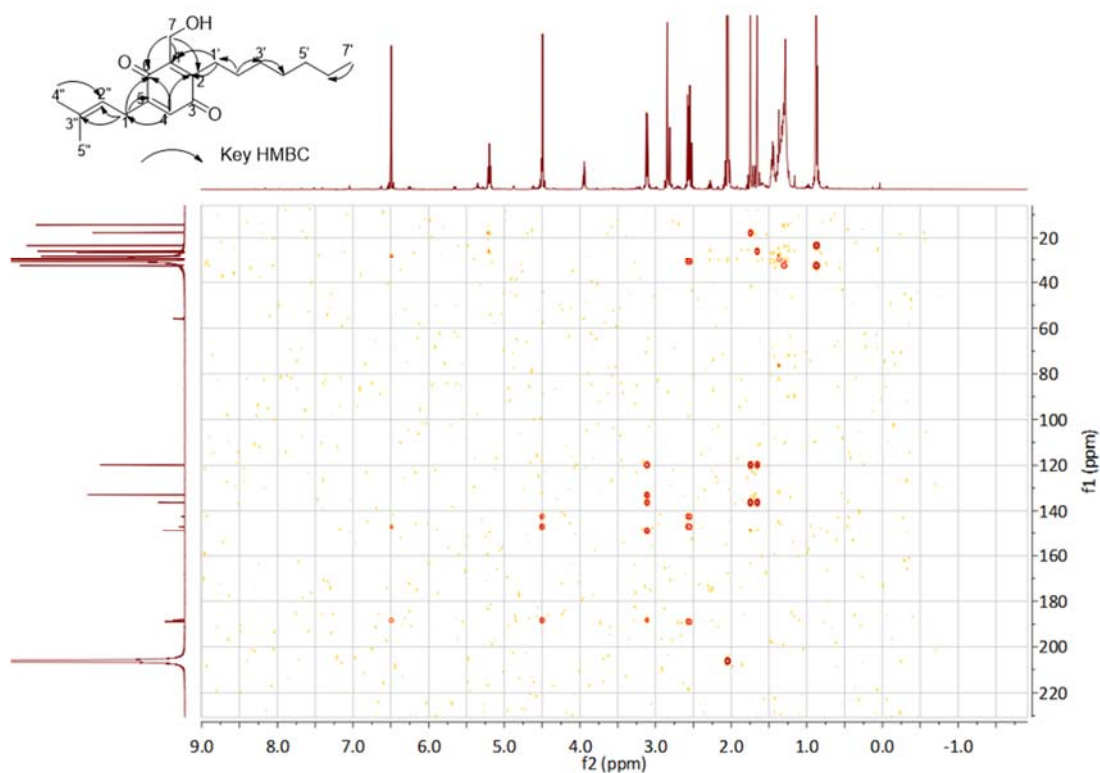
Figure S65. HMBC spectrum of compound **10a** in CD$_3$COCD$_3$

S67
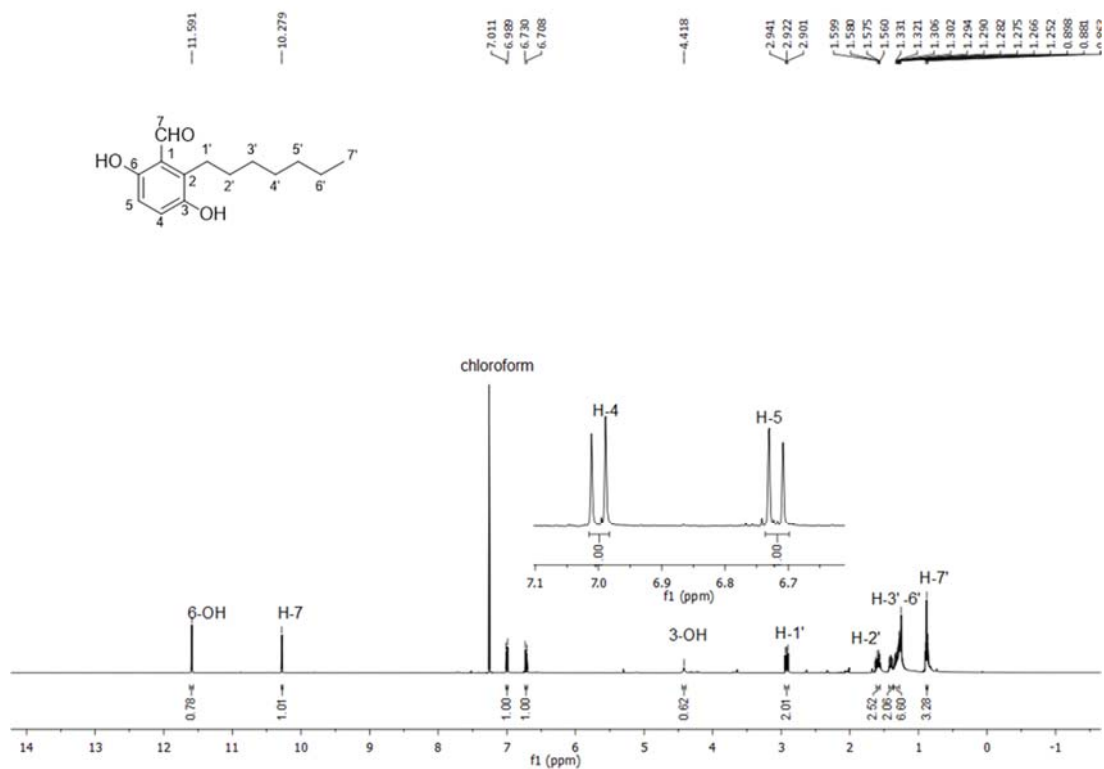
Figure S66. ^{1}H NMR spectrum of compound **12a** in CDCl$_3$ (400 MHz)
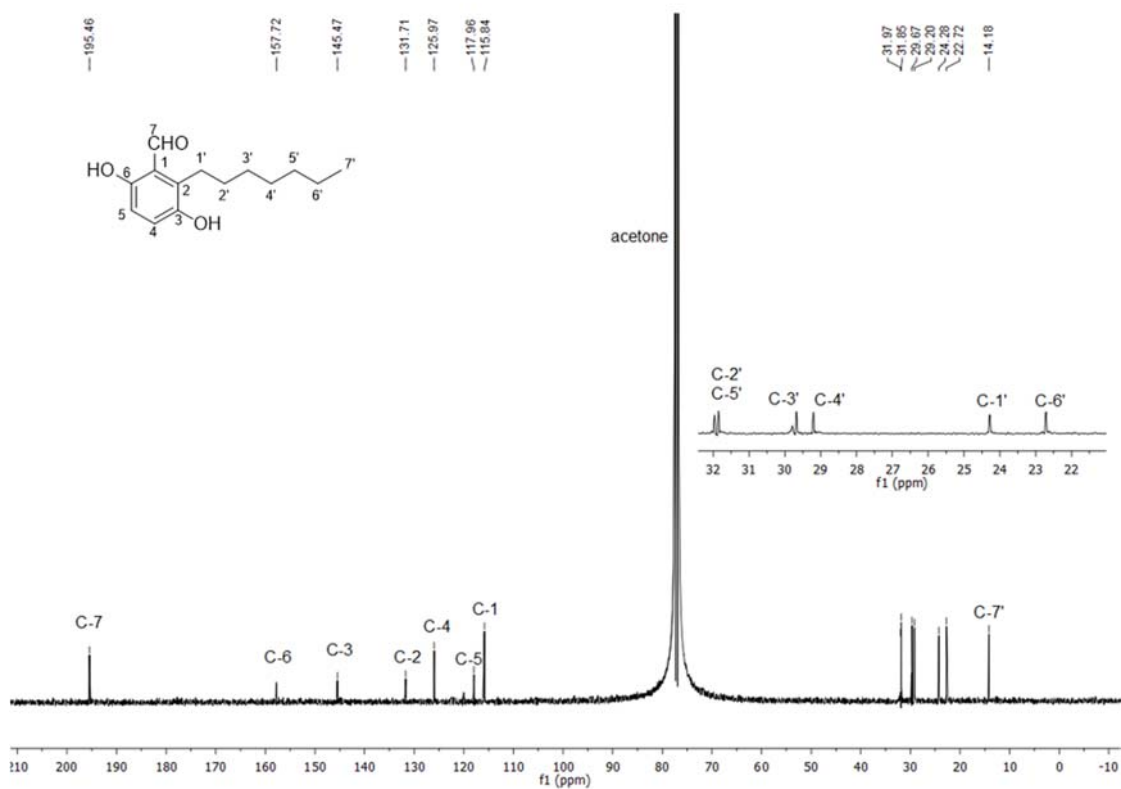
Figure S67. ^{13}C{^{1}H} NMR spectrum of compound **12a** in CDCl$_3$ (100 MHz)

S68

199
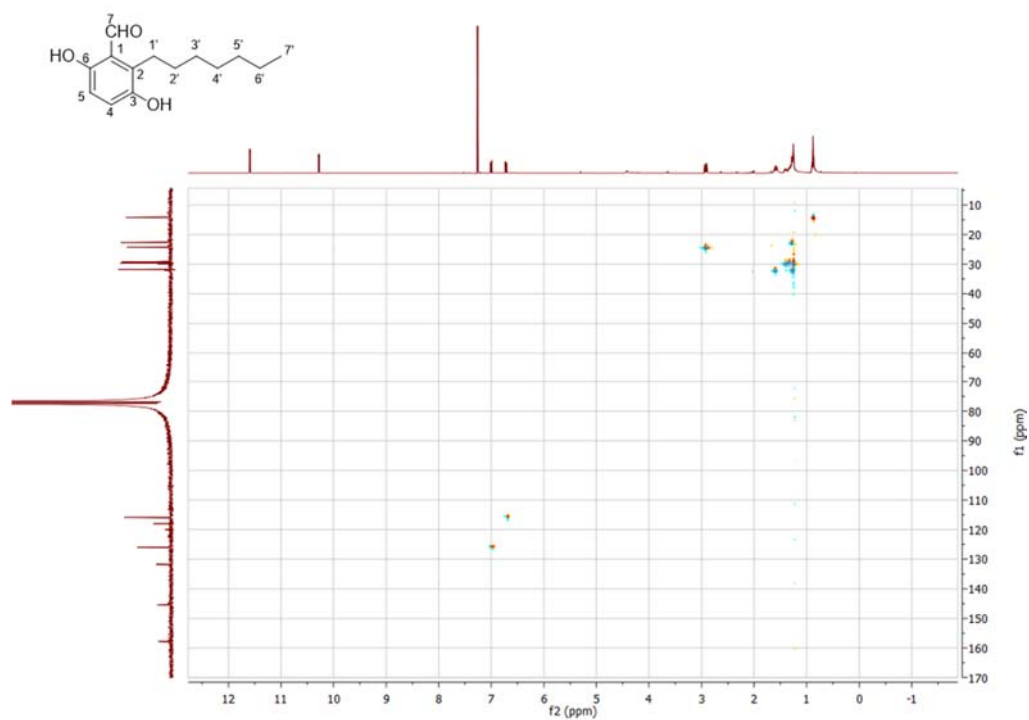
Figure S68. HSQC NMR spectrum of compound **12a** in CDCl₃
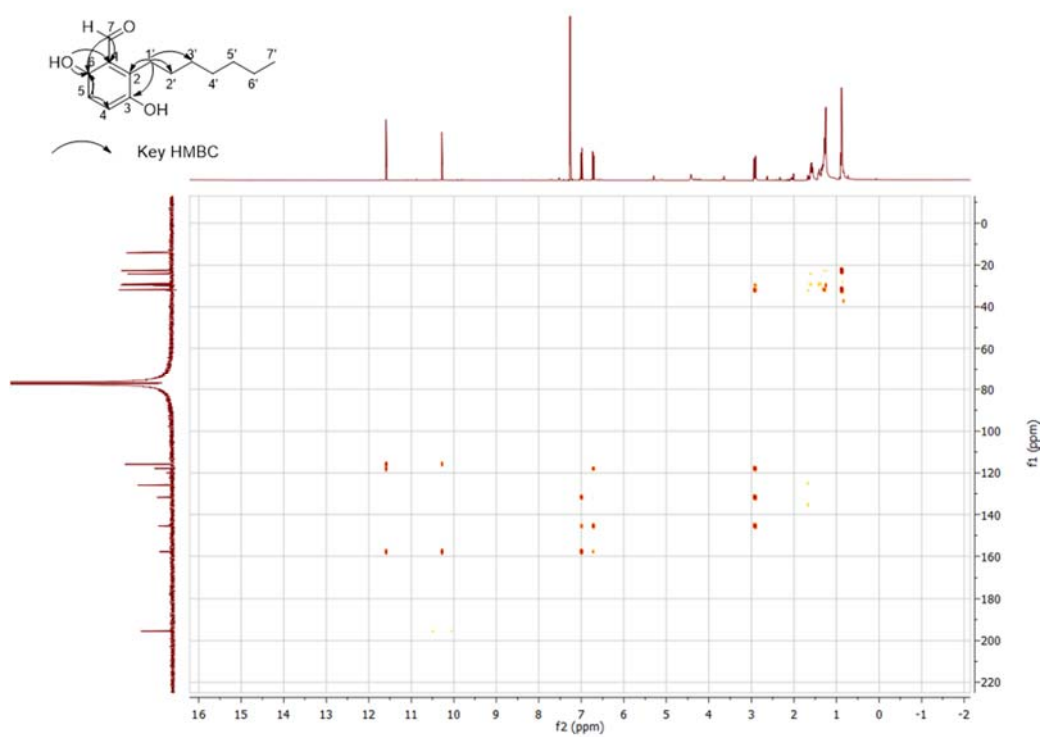
Figure S69. HMBC spectrum of compound **12a** in CDCl₃
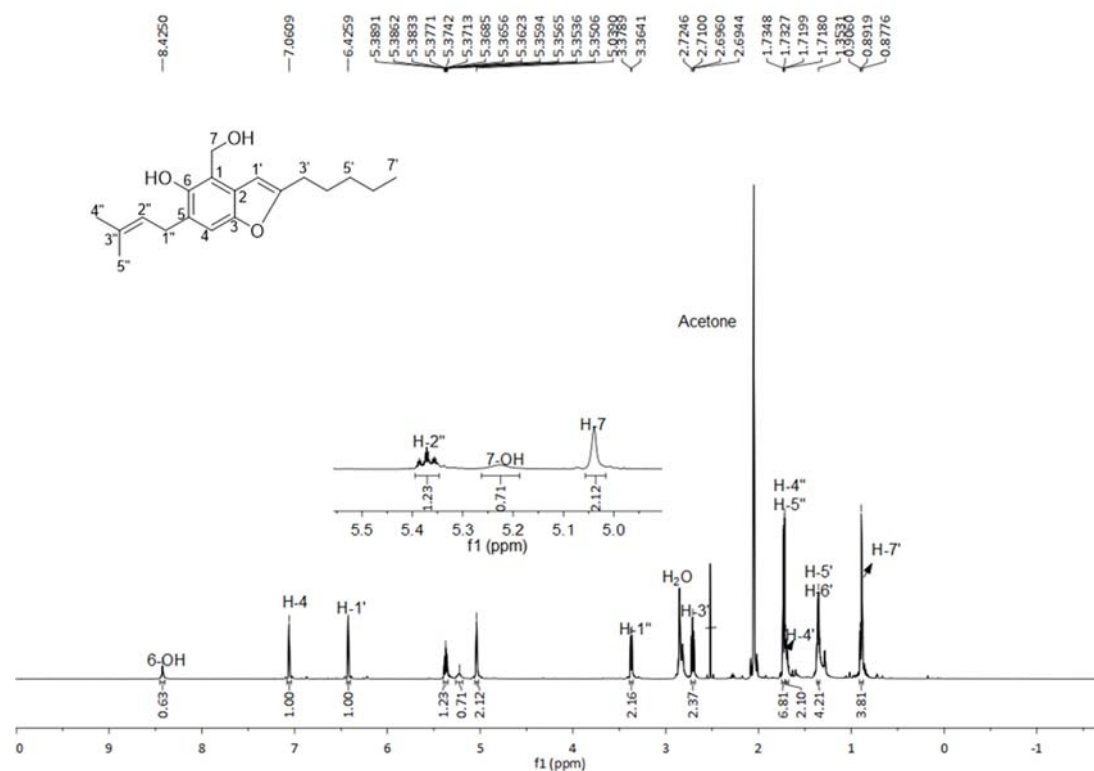
Figure S70. ^{1}H NMR spectrum of compound **13b** in CD$_3$COCD$_3$ (500 MHz)
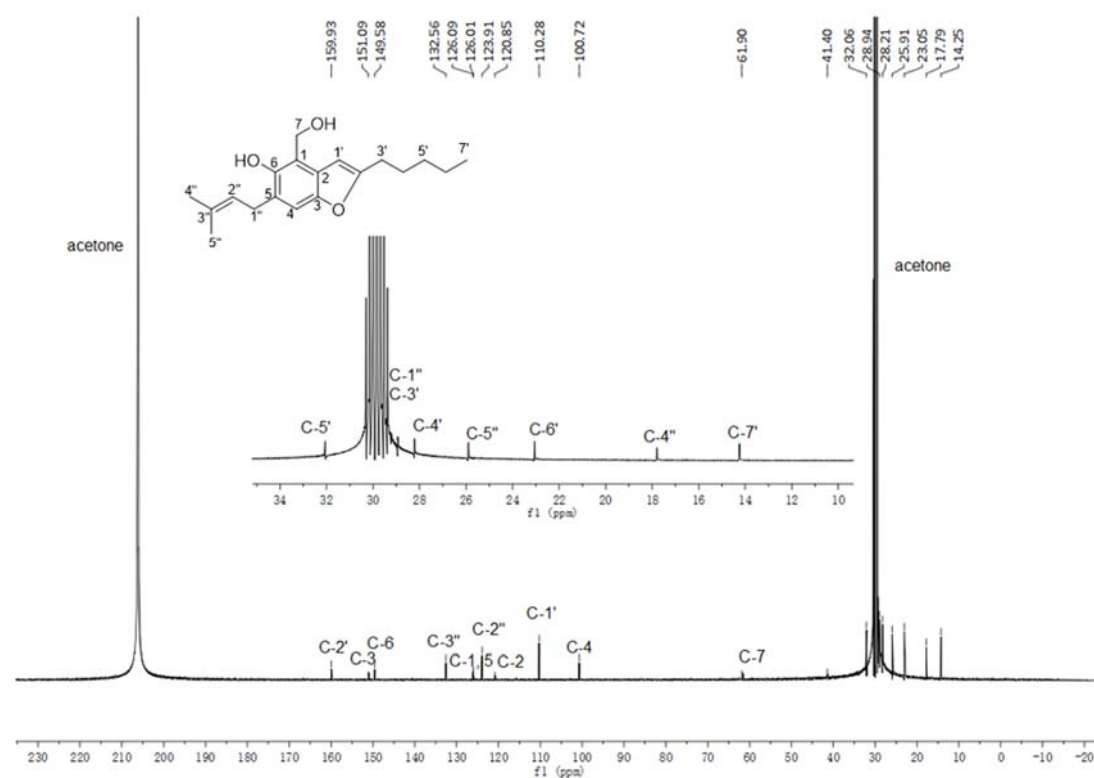
Figure S71. ^{13}C{^{1}H} NMR spectrum of compound **13b** in CD$_3$COCD$_3$ (125 MHz)
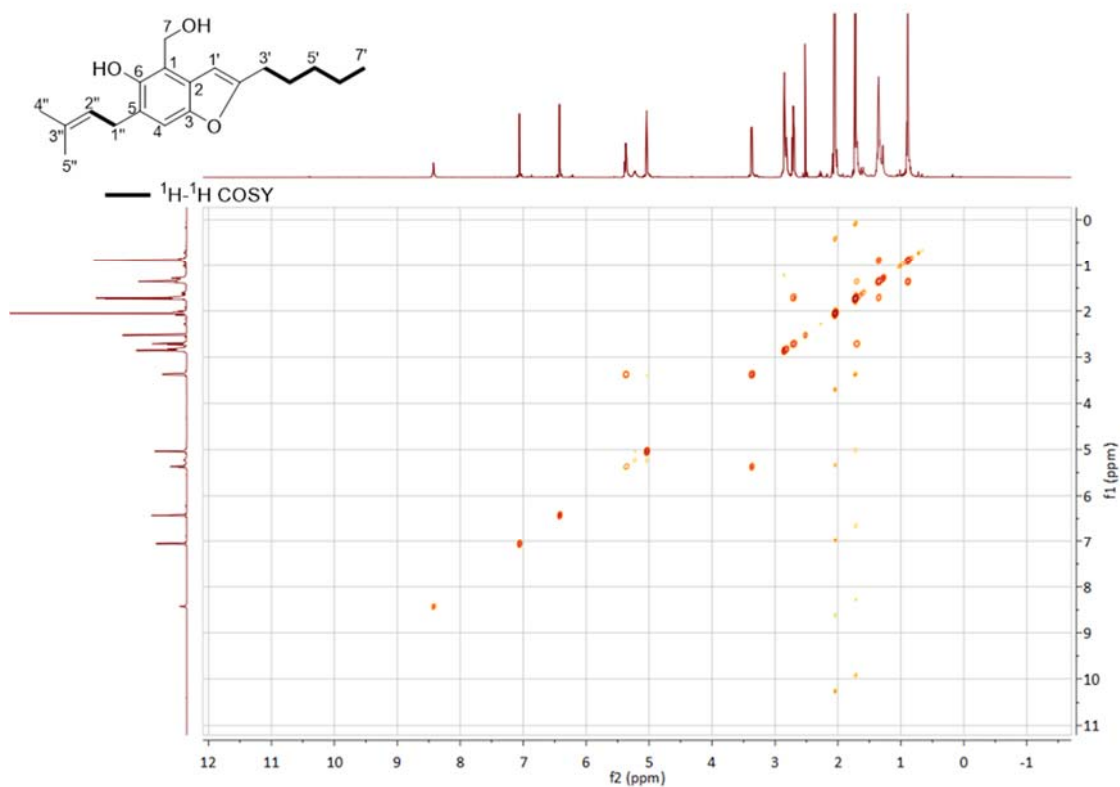
Figure S72. ^{1}H-^{1}H COSY spectrum of compound **13b** in CD$_3$COCD$_3$
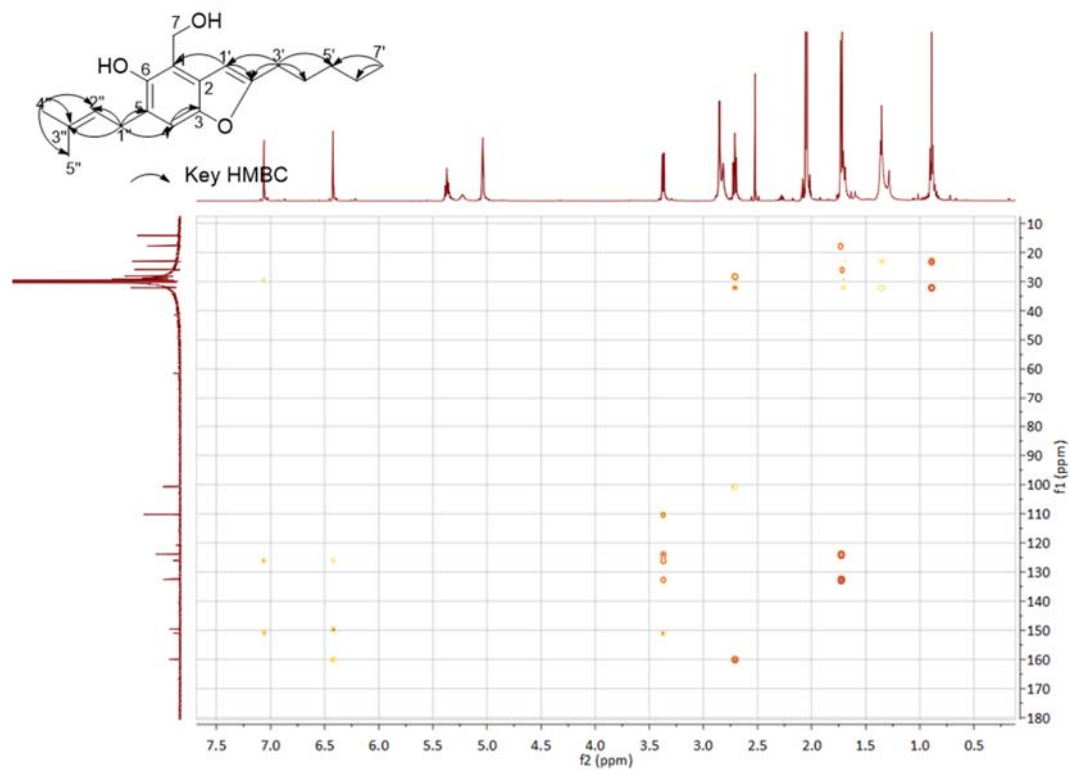
Figure S73. HMBC spectrum of compound **13b** in CD$_3$COCD$_3$

Supplementary References

(1) Mojardín, L.; Vega, M.; Moreno, F.; Schmitz, H. P.; Heinisch, J. J.; Rodicio, R. Lack of the NAD$^+$-dependent glycerol 3-phosphate dehydrogenase impairs the function of transcription factors Sip4 and Cat8 required for ethanol utilization in *Kluyveromyces lactis*. *Fungal. Genet. Biol.* **2018**, *111,* 16.

(2) Green, M. R.; Sambrook, J. *Molecular cloning: a laboratory manual;* 5th ed.; Cold Spring Harbor Laboratory Press, Cold Spring Harbor: New York, 2012.

(3) Shimizu, K. and Keller, N. P. Genetic involvement of a cAMP-dependent protein kinase in a G protein signaling pathway regulating morphological and chemical transitions in *Aspergillus nidulans*. *Genetics* **2001**, *157,* 591.

(4) Oldenburg, K. R.; Vo, K. T.; Michaelis, S.; Paddon, C. Recombination-mediated PCR-directed plasmid construction *in vivo* in yeast. *Nucleic Acids Res.* **1997**, *25,* 451.

(5) Yin, W. B.; Chooi, Y. H.; Smith, A. R.; Cacho, R. A.; Hu, Y.; White, T. C.; Tang, Y. Discovery of cryptic polyketide metabolites from dermatophytes using heterologous expression in *Aspergillus nidulans*. *ACS Synth. Biol.* **2013**, *2,* 629.

(6) Chavan, O. S.; Chavan, S. B.; Baseer, M. A. An efficient synthesis of formyl coumarins by microwave irradiation method-duff formylation. *Pharm. Chem.* **2015**, *7,* 197.

(7) Kumar, H. M. S.; Reddy, B. V. S.; Reddy, E. J.; Yadav, J. S. Microwave-assisted eco-friendly synthesis of 2-alkylated hydroquinones in dry media. *Green Chem.* **1999**, *1,* 141.

(8) Miyake, Y.; Ito, C.; Itoigawa, M.; Osawa, T. Antioxidants produced by *Eurotium herbariorum* of filamentous fungi used for the manufacture of karebushi, dried bonito (Katsuobushi). *Biosci. Biotechnol. Biochem.* **2009**, *73,* 1323.

(9) Li, D. L.; Li, X. M.; Li, T. G.; Dang, H. Y.; Proksch, P.; Wang, B. G. Benzaldehyde derivatives from *Eurotium rubrum*, an endophytic fungus derived from the mangrove plant *Hibiscus tiliaceus*. *Chem Pharm. Bull. (Tokyo)* **2008**, *56,* 1282.

(10) Huang, Y.; Ma, L.; Rong, X.; Liu, D.; Liu, S.; Liu, W.-Z. Benzaldehyde derivatives from a marine-derived fungus *Aspergillus* sp. *Chin. Tradit. Herbal Drugs* **2012**, *43,* 837.

(11) Myobatake, Y.; Takemoto, K.; Kamisuki, S.; Inoue, N.; Takasaki, A.; Takeuchi, T.; Mizushina, Y.; Sugawara, F. Cytotoxic alkylated hydroquinone, phenol, and cyclohexenone derivatives from *Aspergillus violaceofuscus* Gasperini. *J. Nat. Prod.* **2014**, *77,* 1236.

(12) Li, D.-L.; Li, X.-M.; Li, T.-G.; Dang, H.-Y.; Wang, B.-G. Dioxopiperazine alkaloids produced by the marine mangrove derived endophytic fungus *Eurotium rubrum*. *Helv. Chim. Acta* **2008**, *91,* 1888.

(13) Chiang, Y. M.; Ahuja, M.; Oakley, C. E.; Entwistle, R.; Asokan, A.; Zutz, C.; Wang, C. C.; Oakley, B. R. Development of genetic dereplication strains in *Aspergillus nidulans* results in the discovery of aspercryptin. *Angew. Chem. Int. Ed. Engl.* **2016**, *55,* 1662.

(14) Zhang, P.; Wang, X.; Fan, A.; Zheng, Y.; Liu, X.; Wang, S.; Zou, H.; Oakley, B. R.; Keller, N. P.; Yin, W. B. A cryptic pigment biosynthetic pathway uncovered by heterologous expression is essential for conidial development in *Pestalotiopsis fici*. *Mol. Microbiol.* **2017**, *105,* 469.

(15) Kindinger, F.; Nies, J.; Becker, A.; Zhu, T.; Li, S.-M. Genomic locus of a *Penicillium crustosum* pigment as an integration site for secondary metabolite gene expression. *ACS Chem. Biol.* **2019**, *14,* 1227.

4.4 Fungal benzene carbaldehydes: occurrence, structural diversity, activities and biosynthesis

REVIEW

Fungal benzene carbaldehydes: occurrence, structural diversity, activities and biosynthesis

Huomiao Ran and Shu-Ming Li ID *

Covering: up to April 2020

Fungal benzene carbaldehydes with salicylaldehydes as predominant representatives carry usually hydroxyl groups, prenyl moieties and alkyl side chains. They are found in both basidiomycetes and ascomycetes as key intermediates or end products of various biosynthetic pathways and exhibit diverse biological and pharmacological activities. The skeletons of the benzene carbaldehydes are usually derived from polyketide pathways catalysed by iterative fungal polyketide synthases. The aldehyde groups are formed by direct PKS releasing, reduction of benzoic acids or oxidation of benzyl alcohols.

Institut für Pharmazeutische Biologie und Biotechnologie, Fachbereich Pharmazie, Philipps-Universität Marburg, Robert-Koch-Straße 4, 35037 Marburg, Germany. E-mail: shuming.li@staff.uni-marburg.de

1. Introduction

Benzene carbaldehydes, from the simplest benzaldehyde to structural features in relatively complex molecules, are widely distributed in ascomycetes and also found in basidiomycetes (Table 1 and Fig. 1). Their producers include terrestrial, sponge-associated, marine- and mangrove-derived, plant endophytic and pathogenic fungi. The compounds from this family exhibit diverse biological and pharmacological properties. Cytotoxic, antibacterial and antifungal activities have been detected for a large number of benzene carbaldehydes, followed by anti-inflammatory and antioxidant activities (Table 2 and Fig. 2). Since the first report on flavoglaucin and auroglaucin in the fungus *Aspergillus glaucus* in 1934,[1] at least 185 structures including 36 alkylated, 59 prenylated (meroterpenoids) and 30 both alkylated and prenylated derivatives have been described in the literature. 146 of them were isolated from ascomycetes, 32 from basidiomycetes and only three from both ascomycetes and basidiomycetes (Fig. 1). *Aspergillus* strains with 49 metabolites are clearly the dominant producers of benzene carbaldehydes, followed by *Pestalotiopsis*, *Stachybotrys* and *Penicillium* with 14, 13 and 13 metabolites, respectively (Table 1). Reports on the elucidation of their biosynthetic pathways in fungi have accumulated tremendously in recent years, especially on the backbone assembly by iterative polyketide synthases and the formation of the aldehyde group *via* different routes. The benzene carbaldehydes act as critical intermediates or end products of various biosynthetic pathways. Furthermore, key pathway-specific enzymes have also been characterized. Up to April 2020, more than 140 publications deal with the producers,

isolation and structural elucidation, biological activities and applications as well as biosynthetic origin and pathways of benzene carbaldehydes. However, no systematic review on this natural product family is available in the literature. Therefore, we summarize these data in the present review to fill this gap.

2. Occurrence, biological and pharmacological activities

2.1. Simple benzene carbaldehydes

In this review, merely slightly modified like hydroxylated, halogenated, methylated and/or ethylated benzaldehydes are classified as simple benzene carbaldehydes accounting for 23 members (Fig. 3). Despite their simple structures, these compounds also exhibit broad biological and pharmacological activities such as antifungal (eight compounds), antibacterial and cytotoxic activities (Table 2). Hydroxylated and methoxylated simple benzaldehydes are also natural products of plant origin.[2] Eleven simple fungal benzene carbaldehydes were isolated from ascomycetes and eight from basidiomycetes (Fig. 1). The main producers are members of the genera *Aspergillus*, *Penicillium* and *Bjerkandera* (Table 1).

The simplest member of this family is benzaldehyde **1** without other additional substituents. It is one of the most industrial used chemicals and can be found as a preservative in cosmetics and food as well as in personal care and select car detailing products. Its 4-hydroxylated derivative **2** was identified in plants[2] and a wide range of fungi such as the plant pathogens *Botryosphaeria obtusa*[3] and *Phaeoacremonium chlamydosporum*,[4] the endophytic fungi *Aspergillus* sp. YL-6[5] and *Penicillium thiomii*[6] as well as the brown-rot fungi *Tyromyces palustris* and *Gloeophyllum trabeum*.[7] In addition to phytotoxicity,[3] **2** also possesses anti-angiogenic,[8] anti-inflammatory[8] and anti-nociceptive[8] activities.

Compounds **3–8** are hydroxylated, methoxylated or chlorinated benzaldehyde derivatives. The dihydroxylated benzaldehyde, protocatechuic aldehyde **3**, was identified in the aforementioned brown-rot basidiomycetes *T. palustris* and *G. trabeum*.[7] 2,5-Dihydroxylated benzaldehyde **4** and 6-formylsalicylic acid **15** were metabolites of *Penicillium patulum*.[9] Biosynthetic study on the white-rot fungus *Bjerkandera adusta* led to the identification of compounds **1**, **5**, **7** and **8**.[10] Another congener syringaldehyde **6** was obtained from the plant endophytic fungus *Phoma* sp. YN02-P-3.[11]

To understand the preventive mechanism of the root rot biocontrol fungus *Phlebiopsis gigantea*, its chemical constituents were investigated, leading to identification of *o*-orsellinaldehyde **9** with inhibitory activity against the pathogenic fungi *Heterobasidion occidentale* and *Fusarium oxysporum*, and the saprotrophic fungus *Penicillium canescens*[12] as well as cytotoxic activity against the human carcinoma cell line Hep 3B and the lung fibroblast cell line MRC-5.[13] The highly decorated and cytotoxic 2,4-dihydroxy-3,5,6-trimethylbenzaldehyde **10** was obtained from the deep sea-derived fungus *Aspergillus sydowi*.[14] *o*-Orsellinaldehyde derivatives **11–14** were identified as biosynthetic precursors in genetically manipulated fungal strains.[15,16] The dialdehyde flavipin **16** from *Aspergillus*,[17] *Chaetomium*[18,19] and *Epicoccum*[20,21] species was well documented for its antibacterial,[17] antifungal,[22] antiproliferative[18] and antioxidant[19] activities as well as inhibitory effect on α-glucosidase, even more potential than the clinically used drug acarbose.[19]

Benzene carbaldehydes **17** and **18** carrying ethyl groups were isolated from a marine mangrove endophytic fungus.[23] Gladiolic acid **19** from *Penicillium gladioli*[24,25] and cyclopaldic acid **20** from *Seiridium cupressi*[26] are hemiacetal lactones and differ from each other just in a hydroxyl group. Chemical investigation on a co-culture broth extract of two marine mangrove pathogenic fungi led to the isolation of the hydroxylated benzaldehyde **21** with both ethyl ether and ester bonds.[27] The two antifungal benzene carbaldehydes **22** and **23** with *O*-prenyl moieties have been isolated from *Peniophora polygonia* and were demonstrated to strongly inhibit the growth of the aspen decay fungus *Phellinus tremulae*.[28]

2.2. Alkylated benzene carbaldehydes

Alkylated derivatives with 66 structures, *i.e.* more than one-third of the known benzene carbaldehydes, constitute one of the

Huomiao Ran received her Bachelor's degree in 2013 from Hainan University and obtained her Master's degree in 2016 from Nanjing Agricultural University. She is currently a PhD student at the Philipps-Universität Marburg. Her research focuses on pathway elucidation of fungal secondary metabolites and characterisation of the involved enzymes under the supervision of Prof. Shu-Ming Li.

Shu-Ming Li is full professor of Pharmaceutical Biology and Biotechnology at the Philipps-University in Marburg, Germany. He studied pharmacy and received his Bachelor's and Master's degrees from Beijing University, China. Shu-Ming Li was awarded in 1992 his PhD in natural product chemistry by the Rheinische Friedrich-Wilhelms-University in Bonn, Germany. He has served as an associate professor of Pharmaceutical Biology at the Heinrich-Heine-University in Düsseldorf. Li's group is interested in the biosynthesis of secondary metabolites in bacteria and fungi.

Table 1 Taxonomic distribution of fungal benzene carbaldehydes

Fungal genera	Simple derivatives	Alkylated derivatives	Meroterpenoid derivatives	Benzophenone derivatives	Spirocyclic derivatives	Miscellaneous derivatives	Total
Ascomycetes							
Aspergillus	6	29	4	1	7	2	**49**
Pestalotiopsis	—	10	1	—	—	3	**14**
Stachybotrys	—	—	13	—	—	—	**13**
Penicillium	4	5		1	3	—	**13**
Acremonium	—	—	8	—	—	—	**8**
Fusarium	—	—	7	—	—	—	**7**
Torrubiella	—	—	7	—	—	—	**7**
Colletotrichum	—	—	6	—	—	—	**6**
Paraphaeosphaeria	—	6	—	—	—	—	**6**
Pyricularia	—	5	—	—	—	1	**6**
Trichoderma	—	5	—	—	—	—	**5**
Diaporthe	—	—	—	—	—	4	**4**
Epicoccum	1	—	—	—	—	2	**3**
Neonectria	—	—	3	—	—	—	**3**
Chaetomium	1	2	—	—	—	—	**3**
Ascochyta	—	1	—	—	1	1	**3**
Daldinia	—	—	—	2	—	—	**2**
Hymenoscyphus	—	2	—	—	—	—	**2**
Lasiodiplodia	—	—	—	—	—	2	**2**
Pestalotia	—	—	—	2	—	—	**2**
Pyrenula	—	2	—	—	—	—	**2**
Nalanthamala	—	—	2	—	—	—	**2**
Zopfiella	—	2	—	—	—	—	**2**
Amniculicola	—	1	—	—	—	—	**1**
Cordyceps	—	1	—	—	—	—	**1**
Diplodia	1	—	—	—	—	—	**1**
Gelasinospora	—	1	—	—	—	—	**1**
Phaeomoniella	1	—	—	—	—	—	**1**
Phoma	1	—	—	—	—	—	**1**
Sordaria	—	1	—	—	—	—	**1**
Seiridium	1	—	—	—	—	—	**1**
Talaromyces	1	—	—	—	—	—	**1**
Basidiomycestes							
Hericium	—	—	7	—	—	—	**7**
Heterobasidion	—	—	4	—	—	—	**4**
Albatrellus	—	—	3	—	—	—	**3**
Bjerkandera	3	—	—	—	—	—	**3**
Stereum	—	—	3	—	—	—	**3**
Bondarzewia	—	1	1	—	—	—	**2**
Clitocybe	—	—	—	—	—	2	**2**
Gloeophyllum	2	—	—	—	—	—	**2**
Peniophora	2	—	—	—	—	—	**2**
Sarcodontia	—	—	—	—	—	2	**2**
Tyromyces	2	—	—	—	—	—	**2**
Russula	—	—	2	—	—	—	**2**
Agrocybe	1	—	—	—	—	—	**1**
Fomitiporia	—	—	—	—	—	1	**1**
Phlebiopsis	1	—	—	—	—	—	**1**

largest classes. In comparison to the simple benzene carbaldehydes, members from this class contain an additional unmodified or modified alkyl chain, which is attached in most cases (94%) to the *ortho*-position of the formyl group. With the exception for **35** from the basidiomycete *Bondarzewia montana*, all these fungal products are salicylaldehyde derivatives from ascomycetes (Fig. 1). Their main producers belong to the genera *Aspergillus* and *Pestalotiopsis* with 29 and 10 metabolites, respectively (Table 1 and Fig. 1). In addition to their main

activities like antibacterial, antifungal and cytotoxic activities, most group members also exhibit anti-inflammatory and antioxidant effects, which were observed only for few members from other classes (Table 2).

Biosynthetically, alkylated benzene carbaldehydes are derivatives of aromatic polyketides with different numbers of malonyl-CoA as extension units.[29,30] Their alkyl chains differ consequently from each other by numbers of C_2 units. Thus, the members of this class can be conveniently subdivided
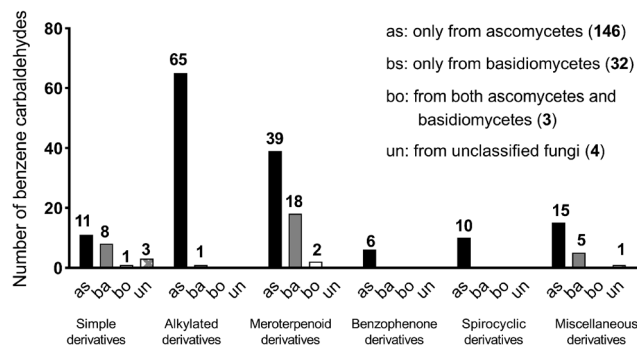
Fig. 1 Taxonomic distribution of different fungal benzene carbaldehyde classes.

according to the length of the side chains, *i.e.* C_3-, C_5-, C_7-, C_9- and C_{11}-alkylated benzene carbaldehydes.

2.2.1. C_3-alkylated benzene carbaldehydes. 12 benzaldehyde derivatives **24–35** bear modified C_3-alkyl chains (Fig. 4). Six of them, sporulosaldeins A–F **24–29**, were identified in the endophytic fungus *Paraphaeosphaeria* sp. F03.[31] **24–26** carry an acetonyl group at C6 with different oxidative levels on the C3 substituents. It was proposed that cyclisation between the acetal group on the benzene ring and the ketal group of the side chain in the dialdehyde **26** leads to the formation of two chromene aldehydes **27** and **28** as well as one chromane aldehyde **29**. The structurally similar redoxcitrinin **30** with two additional methyl groups at C5 and C1′, was obtained from a marine-derived *Penicillium* strain and acts as a precursor in citrinin biosynthesis.[32,33] Investigation on the secondary metabolites of two *Pestalotiopsis* species resulted in the isolation of the salicylaldehyde derivative **31** carrying a propanic acid residue and its methyl ester **32**, respectively.[34,35] The two prenylated chromene-5-carbaldehydes, **33** from the marine-derived fungi *Eurotium cristatum*[36] and **34** from *Aspergillus* sp. SF-5976,[37] display significant anti-inflammatory effect.

The only basidiomycete-derived metabolite in this group is the dihydroxylated aldehyde **35** from the rare white-rot fungus *Bondarzewia montana*.[38] An alkenyl substitution at the *meta*-position to the formyl group differs clearly from the *ortho*-position of other members **24–34** from ascomycetes.

2.2.2. C_5-alkylated benzene carbaldehydes. Compounds **36–46** are C_5-alkylated metabolites with a formyl group at the *ortho*-position (Fig. 5). Two 2,4-dihydroxy-3-methylbenzaldehydes **36** and **37** with a modified C_5-alkyl chain were obtained from the deep sea-derived fungus *Aspergillus versicolor* SCSIO 41502.[39] Chemical investigation of another marine fungus *Zopfiella marina* BCC 18240 resulted in the isolation of salicylaldehyde derivative **38** with a pentandiene carboxylic acid residue.[40] Its derivative **39** with a 1,3-pentan-diene moiety has also been isolated as a key biosynthetic intermediate of sordarial.[41] A set of oxidation products of **39** with 3′,4′-dihydroxyl group (**40–44**) were identified in several ascomycetes. Sordariol **40** with an immunosuppressive activity was isolated from *Sordariol macrospora*,[42] *Gelasinospora heterospora*[43] and *G. longispora*[43] and then identified in the same

biosynthetic pathway with **39**.[41] Its isomer, agropyrenol **41**, was isolated as a phytotoxin from the plant pathogen *Ascochyta agropyrina* var. nana.[44] Its absolute configuration was determined as 3′R and 4′R by the Mosher ester method. Three additional 3′R,4′R-dihydroxylated polyketide analogues with adjunct prenyl unit or saturated alkyl chain, vaccinol G **42**, heterocornols A **43** and F **44**, were obtained from the marine sponge-associated fungus *Pestalotiopsis heterocornis*.[35] Bioactivity tests with **41–44** showed their cytotoxic and antibacterial potentials against human cancer cell lines and Gram-positive bacteria, respectively. The benzofuran aldehyde **45** with a saturated C_5-alkyl residue was isolated from the entomopathogen *Cordyceps annullata*.[45] It exhibits potent agonistic activity towards the cannabinoid receptors CB1 and CB2. Moreover, the antifungal and antibacterial metabolite anguillosporal **46** with an ethyl and a branched C_6-alkyl chain was isolated from the freshwater fungus *Anguillospora* (also known as *Amniculicola*) *longissima* CS-869-1A.[46]

2.2.3. C_7-alkylated benzene carbaldehydes. This benzene carbaldehyde class includes more than 30 structures (**47–78**) and shares a salicylaldehyde scaffold mostly with a modified C_7-alkyl chains. The majority (**56–78**) bears an additional dimethylallyl (C_5) moiety or structural feature derived thereof. Various modifications on the alkyl chains are found for derivatives without a prenyl moiety (**47–55**, Fig. 6).

Four salicylaldehydes with a dihydroxyheptyl moiety **47–50** and their oxidised dicarbonyl derivative **51** were obtained from the rice pathogen *Magnaporthe grisea*.[47,48] Two similar metabolites, heterocornol B **52** and pestalol D **53**, were isolated from *Pestalotiopsis heterocornis* and *Pestalotiopsis* sp. AcBC2, respectively.[35,49] Ginsenocin **54** with a substituted 2H-pyran ring resulted from cyclisation on the C_7-alkylatd chain was identified as an anti-tumour metabolite in the endophytic fungus *Penicillium melinii* Yuan-25.[50] It shows potent cytotoxicity with IC$_{50}$ values ranging from 0.49 to 5.03 μg mL^{-1} to six cell lines including MKN45, LOVO, A549, MDA-MB-435, HepG2 and HL-60. Pyrenulafuran **55**, a 2H-benzofuran derivative, was isolated from the cultured lichen mycobionts of *Pyrenula* sp.[51]

The majority of the C_7-alkylated benzene carbaldehydes are 3,6-dihydroxybenzaldehydes with a dimethylallyl moiety at C3 (**56–78**, Fig. 7). These compounds belong to the groups of flavoglaucins and auroglaucins and were obtained from different *Aspergillus/Eurotium* species including several mangrove-derived strains. One of the notable features is the presence of a complete saturated (**56**) or unsaturated (**57–63**) C_7-alkyl chains at C6 of the benzene ring. This set of compounds show broad bioactivities *e.g.* antioxidant,[52–54] antibacterial[55,56] and anti-inflammatory activities[56,57] as well as binding affinity to human opioid or cannabinoid receptors.[58]

In the cases of **64** and **65**, the alkyl residues are further modified by hydroxylation. Compound **64** with a 3′,6′-dihydroxyhepta-1′,4′-dienyl moiety was identified in the fruit-associated fungus *Aspergillus amstelodami*.[55] The C3′-hydroxylated analogue **65** was isolated from the gorgonian-derived fungus *Eurotium* sp.[59]

The alkyl chain has cyclised with the C5-hydroxyl group to a 2H-benzopyran in **66–69**, to a dihydrobenzopyran in **70–73**,

Table 2 Biological activities of benzene carbaldehydes

Substance class	Biological activities	Compounds
Simple derivatives	Antiviral activity	—
	Antifungal activity	1,[155] 4,[156] 9,[12] 16,[22] 19,[25] 21,[27] 22,[28] 23 [28]
	Antibacterial activity	1,[155] 4,[157] 16,[17] 19 [25]
	Antioxidant activity	1,[155] 2,[158] 16 [19]
	Anti-inflammatory activity	2 [8] and 3 [159]
	Anti-insect activity	1,[155] 4,[160] 20 [26]
	Phytotoxic activity	2 [3]
	Cytotoxic activity	4,[161] 9,[13] 10,[14] 16 [18]
	Enzyme inhibitors, activators and receptors	2,[162] 3,[163] 16 [19]
	Anti-nociceptive activity	2 [8]
	Anti-angiogenic activity	2 [8]
	Positive modulation of GABAergic neuromodulation	2 [158]
Alkylated derivatives	Antiviral activity	53,[49] 79,[49] 80 [49]
	Antifungal activity	24–29,[31] 41,[35] 42,[35] 46,[46] 82 [64]
	Antibacterial activity	32,[35] 41–44,[35] 46,[46] 56,[56] 57,[56] 60,[55,56] 62,[56] 79,[49] 81,[64] 82,[64] 89 [40]
	Antioxidant activity	30,[32] 56,[53,54] 57,[53,54] 58,[53] 60,[53] 62,[53,54] 73,[53] 75,[52] 76 [52]
	Anti-inflammatory activity	33,[36] 34,[37] 56,[36,56,57] 57,[56,57] 60,[56] 62,[56] 70,[37] 71,[37] 75 [36,56]
	Anti-insect activity	47–50 [47]
	Phytotoxic activity	41,[44] 49,[164] 51 [48]
	Cytotoxic activity	28,[31] 32,[35] 41–44,[35] 52,[35] 54,[50] 73,[62] 78,[63] 79,[49] 80,[49] 81,[64] 82,[64] 84–86,[69] 89 [40]
	Enzyme inhibitors, activators and receptors	45,[45] 56,[58] 63 [58]
	Immunomodulatory activity	40 [43]
	Antifouling activity	36 [39]
	Antimalarial activity	85,[69] 86 [69]
Meroterpenoid derivatives	Antiviral activity	119,[87] 134,[92] 135,[92] 137,[93] 138 [93]
	Antifungal activity	98,[79] 99,[79] 112,[79] 126 [79]
	Antibacterial activity	98,[79] 99,[79] 112,[91] 113,[91] 126,[91] 127,[78,79,91] 131,[91] 132,[91] 133,[78] 136,[91] 146 [95]
	Antioxidant activity	—
	Anti-inflammatory activity	126,[87] 127,[87] 132,[87] 136 [87] and 141 [87]
	Anti-insect activity	—
	Phytotoxic activity	90,[76] 95,[77] 97,[38] 98,[79] 99 [79]
	Cytotoxic activity	97,[38] 99,[78] 127,[78] 129,[92] 131–134,[92] 136 [92]
	Enzyme inhibitors, activators and receptors	98,[78] 99,[78] 114,[85] 127,[78] 134,[78] 133 [78]
	Neuritogenic activity	106–111,[83,84] 116 [86]
Benzophenone	Antibacterial activity	153 [100]
	Enzyme inhibitors, activators and receptors	154 [101]
	Anti-inflammatory activity	149 [97] and 150 [97]
	Cytotoxic activity	153 [100]
Spirocyclic derivatives	Antioxidant activity	155,[104] 157–160 [105]
	Cytotoxic activity	160,[106] 162–164 [107]
Miscellaneous derivatives	Antiviral activity	169 [49] and 171 [34]
	Antifungal activity	165,[108] 166,[108] 179,[113] 180,[113] 182,[21] 183 [21]
	Antibacterial activity	167,[109] 182,[21] 183 [21]
	Anti-inflammatory activity	171,[34] 175–178 [112]
	Anti-insect activity	168 [47]
	Phytotoxic activity	168 [48] and 170 [4]
	Cytotoxic activity	179,[113] 180,[113] 181 [114]

and to a benzofuran ring in **74–76**, respectively. A spontaneous intramolecular cyclisation of **65** to an enantiomer pair **66/67** with a 2*H*-chromene skeleton was observed when it was dissolved in CDCl₃.[60] Their derivatives **68** and **69** with an additional C4′ hydroxylated group were identified in a gorgonian-derived fungus *Eurotium* sp. as well.[60] Two chromane-5-carbaldehyde isomers, **70** and **71**, with opposite configurations of the C4′

hydroxyl group, were characterized from the Antarctic marine-derived fungus *Aspergillus* sp. SF-5976 and proven to have anti-inflammatory activity.[37] Investigation on the chemical constituents of the mangrove endophytic fungus *Eurotium rubrum* led to the identification of compounds **72–76** and eurotirumin **77** with a cyclopentabenzopyran ring system.[61] Among them, chaetopyranin **73** exhibits cytotoxic activity
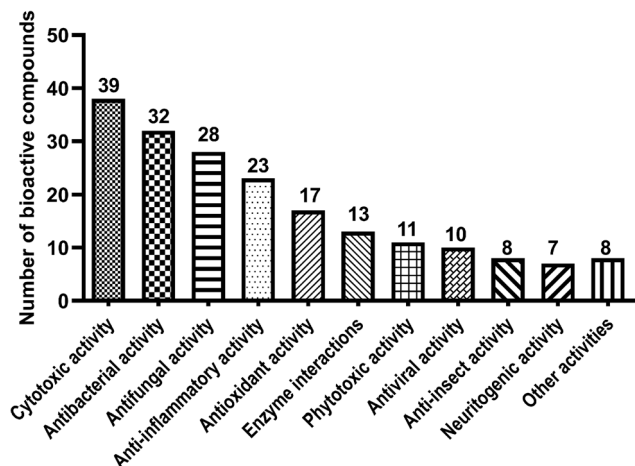
Fig. 2 Bioactivity distribution of fungal benzene carbaldehydes.

toward several tumour cell lines,[62] while compounds **75** and **76** show antioxidant activity.[52] The anti-proliferative prenylated benzene carbaldehyde **78** with a rare endo peroxide bond was isolated from the mangrove-derived fungus *Aspergillus* sp. AV-2.[63]

Two rare examples of C5-prenylated and C₇-alkylated salicylaldehydes, pestalols B **79** and C **80** (Fig. 8), were obtained from the mangrove endophytic fungus *Pestalotiopsis* sp. AcBC2 and show stronger anti-influenza virus activity than the non-prenylated precursor **53**.[49] The dimethylallyl moiety in **79** was further modified by adjunction of two hydroxyl groups in **80**.

2.2.4. C_9- and C_{11}-alkylated benzene carbaldehydes. Only three C_9- and six C_{11}-alkylated benzene carbaldehydes are until now reported (Fig. 9). All of the known members from these classes are salicylaldehyde derivatives from ascomycetes. The two antibiotics albiducins B **81** and A **82** were isolated from the ash tree-associated saprotrophic fungus *Hymenoscyphus albidus*.[64] Hydroxylation at C5, **82** *versus* **81**, enhances the
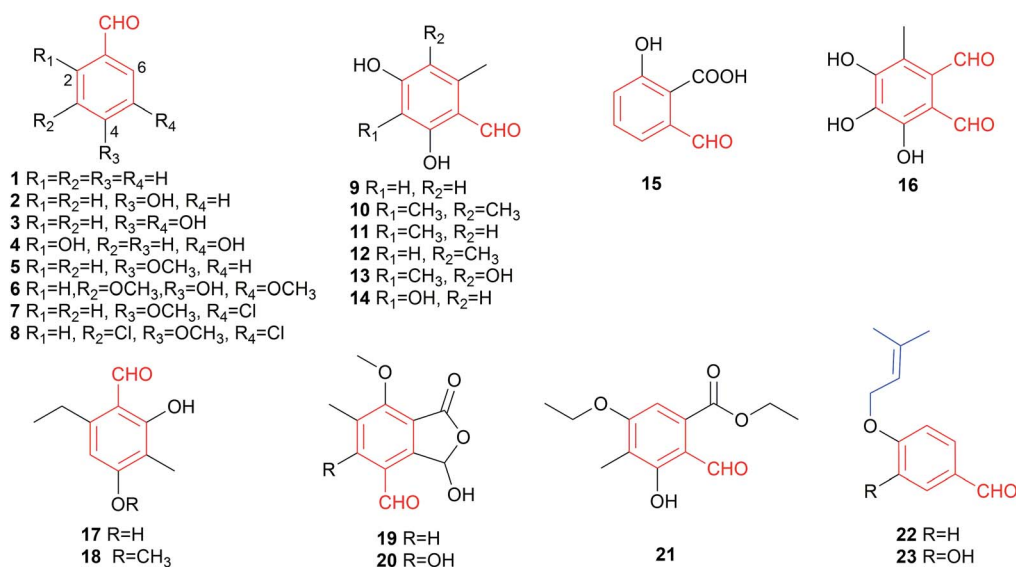
Fig. 3 Structures of simple aldehydes **1–23**.
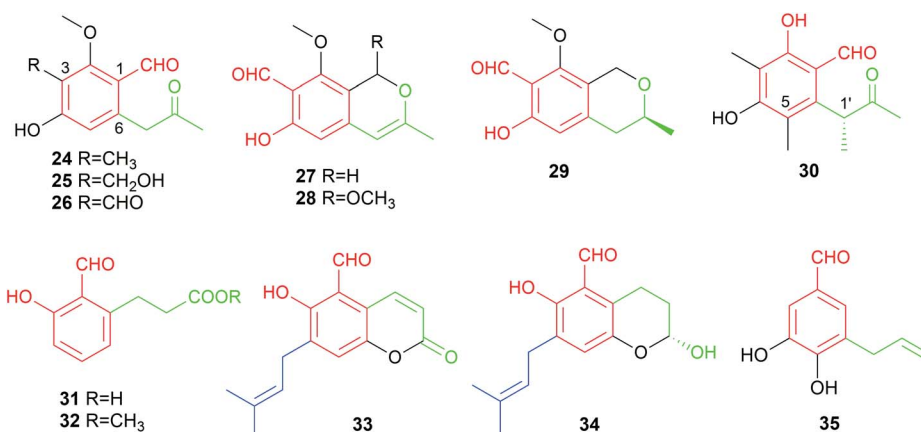
Fig. 4 Structures of C₃-alkylated aldehydes **24–35**.

212
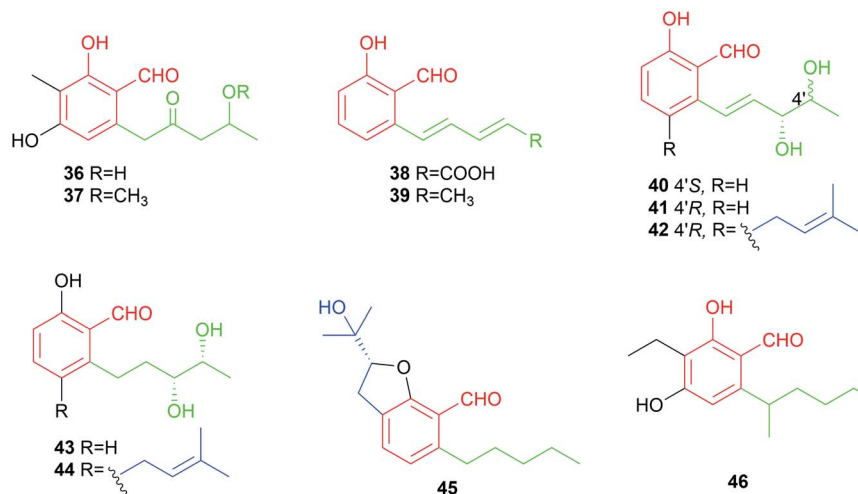
Fig. 5 Structures of C$_5$-alkylated aldehydes 36–46.
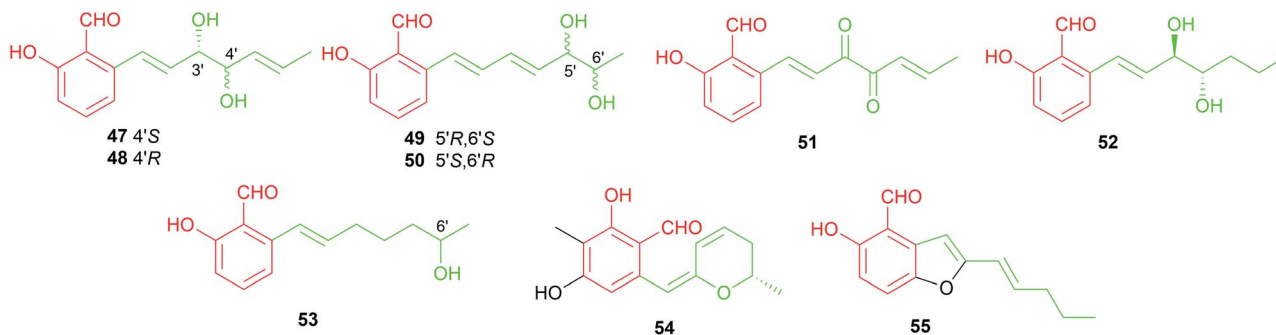
Fig. 6 Structures of C$_7$-alkylated aldehydes 47–55.
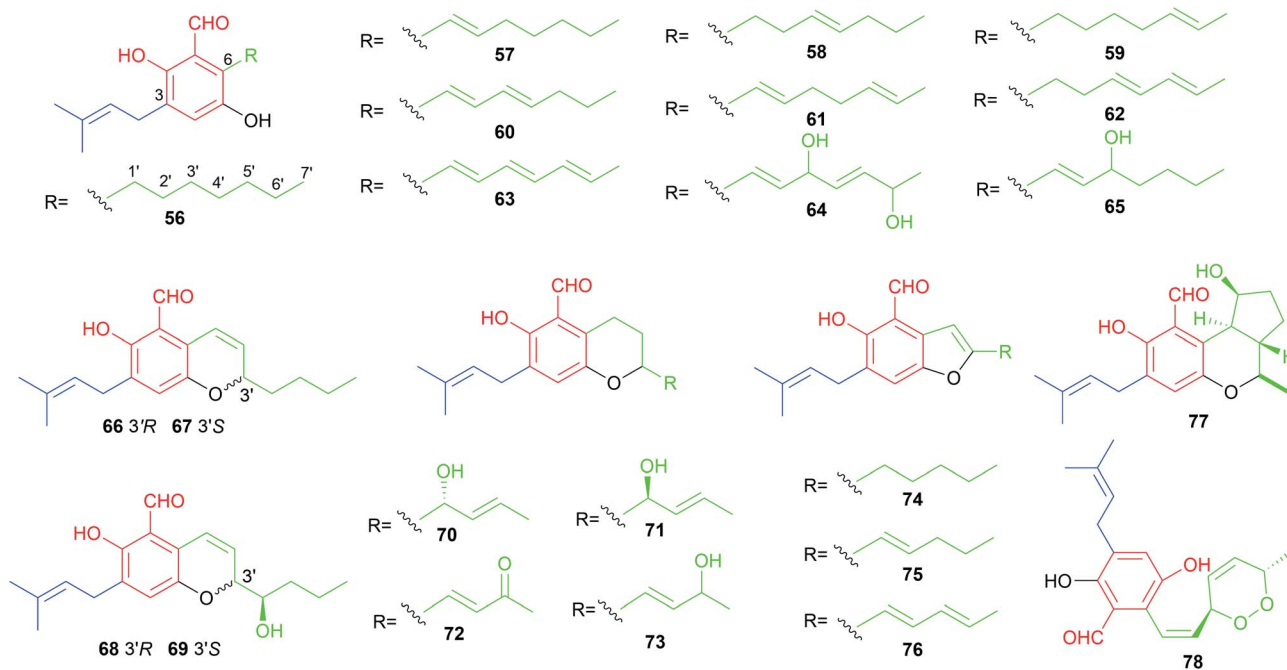
Fig. 7 Structures of C$_7$-alkylated and at C3 prenylated aldehydes 56–78.
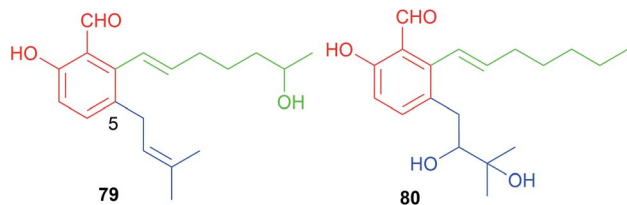
Fig. 8 Structures of C_7-alkylated at C5 prenylated aldehydes **79** and **80**.

antimicrobial and cytotoxic activities. Another C_9-alkylated salicylaldehyde **83** with modifications of the alkyl chain by one keto and two methyl groups was found to be one of the common secondary metabolites in *Penicillium* species and as a key precursor in the asperfuranone biosynthetic pathway (see Section 3.1.2 for details).[65–68]

Two reports described the identification of C_{11}-alkylated benzene carbaldehydes. Bioassay-guided constituent investigation of the wood-decay fungus, *Hypocrea* (syn. *Trichoderma*) sp. BCC 14122, resulted in the isolation of the C_{11}-alkylated salicylaldehyde **84**, gentisaldehyde **85**, its isomer **86** with a *cis*-configured double bond and two benzofuran derivatives **87** and **88**.[69] **85** with an additional phenolic hydroxyl group shows stronger cytotoxicity against tumour cell lines KB, BC and NCI-H187 than its non-hydroxylated analogue **84**. In 2018, a C7'-hydroxylated congener **89** was obtained from the marine-derived fungus *Zopfiella marina*. It shows antibacterial activities against *Mycobacterium tuberculosis* and *Bacillus cereus*.[40]

In summary, alkylated benzene carbaldehydes with 66 members contribute not only significantly to the structural diversity, but also to the broad biological activities. They exhibit all the described activities for benzene carbaldehydes with antibacterial, antioxidant, anti-inflammatory and cytotoxic activities as their remarkable features (Table 2).

2.3. Meroterpenoids

Meroterpenoids are hybrid natural products of terpene and other pathways.[70] They generally contain a start molecule from the polyketide, alkaloid or shikimate pathway, which is connected with a prenyl moiety of various chain lengths. The attachment of the prenyl moiety to different core structures is usually catalysed by prenyltransferases.[71] Several related reviews on meroterpenoids have been published previously.[70–74]

Since the first report on benzaldehyde-containing meroterpenoids by Ellestad *et al.* in 1969,[75] at least 86 metabolites from this class have been isolated from fungal strains. These include structures carrying a dimethylallyl moiety already discussed above, *e.g.* the simple aldehydes **22** and **23** (2.1), the C_3-alkylated benzene carbaldehydes **34** and **35** (2.2.1) and the C_7-alkylated derivatives **56–80** (2.2.3).

Therefore, meroterpenoids belong to one of the major benzene carbaldehyde classes and contribute significantly to the structural diversity of these natural products. More than 30% of the mentioned products were isolated from basidiomycetes and 66% from ascomycetes (Fig. 1). The majority of the fungal meroterpenoids have a C_5, C_{10} or C_{15} terpenoid chain, which is usually connected to *meta*-position of the formyl group and *ortho*-position of at least one hydroxyl group or structural feature derived thereof.

2.3.1. Meroterpenoids derived from C_5- and C_{10}-prenylated precursors. Meroterpenoids **90–111** are benzaldehyde derivatives with a C_5- or C_{10}-terpenoid chain (Fig. 10). Fomannoxin **90**, a benzene carbaldehyde from the shikimate pathway with a fused isoprenyl dihydrofuran, was suggested to be involved in the pathogenicity of the root rotting fungus *Heterobasidion annosum sensu lato*.[76] Compounds **91–93** were isolated and characterized as key intermediates in the fomannoxin biosynthesis.[76] It was proposed that the prenylated precursor **93** was oxidatively cyclised to benzofuran **92** and subsequently reduced to **91** and **90**. Grapevine disease-guided study led to the isolation of three rare acetylenic benzene carbaldehydes **94–96** from the plant pathogenic strain *Stereum hirsutum*.[77] Sterehirsutinal **95** exhibits a high phytotoxicity and inhibits 100% of the plant callus growth at 500 μM. Another dimethylallyl-carrying benzene carbaldehyde, montadial A **97**, was isolated from the polypore *Bondarzewia montana* and shows strong cytotoxic activities against tumour cells L1210 with MIC of 10 μg mL^{-1} and HL60 with MIC of 5 μg mL^{-1}.[38]

Representatives of the geranylated (C_{10}) meroterpenoids are colletorin B **98** and its chlorinated derivative colletochlorin B **99**. They were obtained from several fungi like *Nectria galligena*,[78] *Fusarium* sp.[79] and *Cephalosporium diospyri*.[80] **98** and **99**
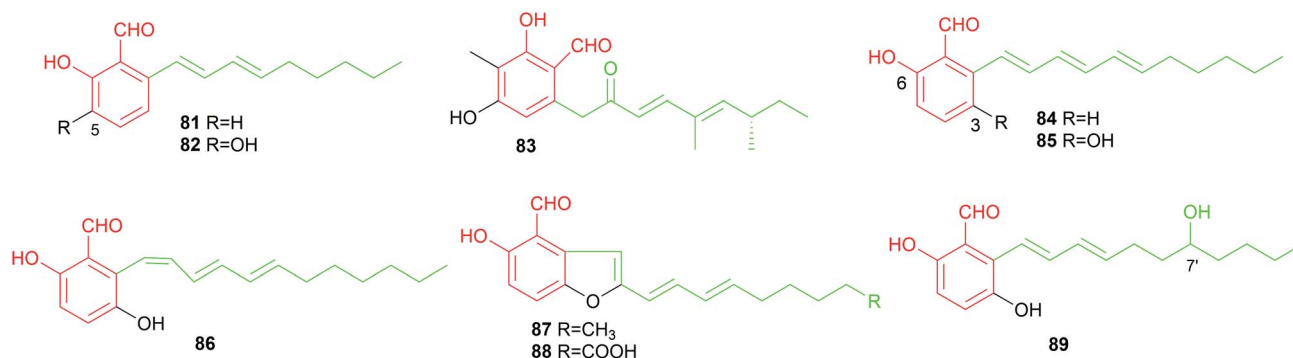
Fig. 9 Structures of C_9- and C_{11}-alkylated aldehydes **71–89**.
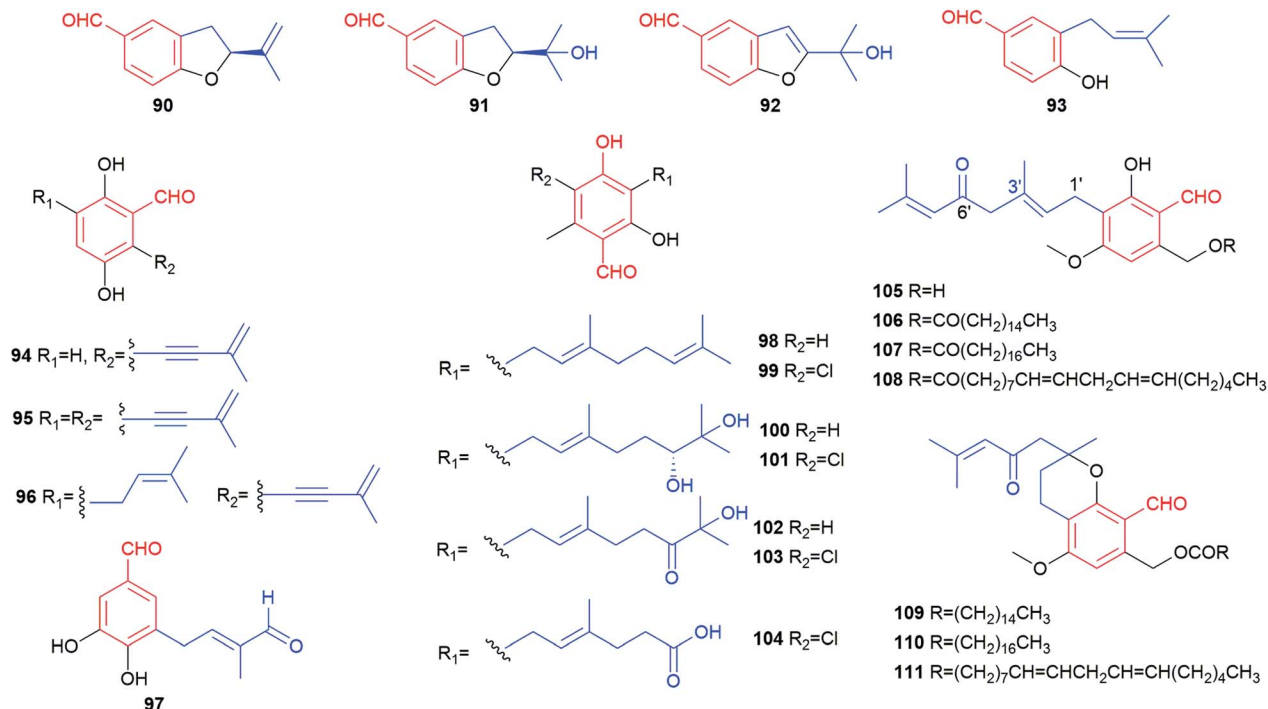
Fig. 10 Structures of meroterpenoids 90–111.

display moderate herbicidal, antifungal and antibacterial activities against *Chlorella fusca*, *Ustilago violacea* and *Fusarium oxysporum* as well as *Bacillus megaterium*, respectively.[79] They are also regarded as potential drugs for the treatment of Alzheimer's disease due to the inhibitory activities towards β-glucuronidase and acetylcholinesterase (AChE).[78] Five structurally-related metabolites with a modified geranyl residue (100–104) were isolated from *Colletotrichum nicotianae*. Colletochlorins A 101 and C 103 are chlorinated derivatives of colletorins A 100 and C 102, respectively.[81] Phytotoxicity tests against *Ambrosia artemisifolia* and *Sonchus arvensis* with 100 and 101 as well as their analogues indicated the importance of the stereochemistry at the hydroxylated geranyl chain and the enhancing effect of chlorination.[82] Six fatty acid esters hericenones C–H 106–111 bearing a 6′-carbonyl geranyl moiety, were isolated, together with their proposed precursor 105, from the edible mushroom *Hericium erinaceum*.[83,84] 109–111 can be considered as cyclisation products of 106–108, respectively.

2.3.2. Meroterpenoids derived from C₁₅-prenylated precursors. Benzene carbaldehydes carrying an unmodified or modified farnesyl (C₁₅) moiety with 35 members build the largest group within meroterpenoids (Fig. 11). Compound 112, a C3-farnesylated *o*-orsellinaldehyde 9, can be considered as prototype of these metabolites.

During a screening programme for interacting agents with mammalian CNS receptors, three farnesylated benzene carbaldehydes, LL-Z1272 β 112, ovinal 114 and scutigeral 115, were isolated from an extract of the edible mushroom *Albatrellus ovinus* by bioassay-guided fractionation of the crude extracts.[85]

The antibiotic LL-Z1272 α 113, a chlorinated derivative of 112, was isolated from the ascomycete *Fusarium* sp.[75]

Three benzene carbaldehydes 116–118 bear a hydroxylated farnesyl moiety. Parvisporin 116 was isolated from the culture broth of *Stachybotrys parvispora* F4708 and demonstrated to have a weak neuritogenic activity.[86] Its analogues chlorocylindrocarpol 117 and cylindrocarpol 118 were later obtained from the sponge-derived fungus *Acremonium* sp.[87] Recently, stachybonoids A–C 119–121, with a benzopyran ring after cyclisation of the farnesyl chain with the salicylic hydroxyl group, were isolated from the crinoid-derived fungus *Stachybotrys chartarum* 952.[88] Compound 119 exhibits an inhibitory activity against the replication of dengue virus.

Asperugin B 122 and A 123, two phthalaldehydes, carrying an intact *O*-farnesyl moiety were identified as metabolites of a mutated strain of *Aspergillus rugulosus*.[89] Their derivatives 124 and 125 were obtained from a genetically engineered *A. nidulans* strain as biosynthetic intermediates of aspernidine A 186 (see 3.1.1. for details).[90]

Structurally, 126–134 are meroterpenoids with a substituted cyclohexone ring by cyclisation within a modified farnesyl chain. To counter antibiotic-resistance bacteria, Mogi *et al.* screened hundreds of natural products and identified a unique set of active natural products LL-Z1272 β 112, ε 126, δ 127, γ 132, ζ 133, which were isolated originally from *Fusarium* sp.[75,91] Chlorination determines the biological activities. The non-chlorinated derivatives 112 and 126 are active against cytochrome bd, while the chlorinated derivatives 127, 132 and 133 are potent inhibitors of cytochrome bo and trypanosome alternative oxidase.[91] 126 shows very strong antifungal activity
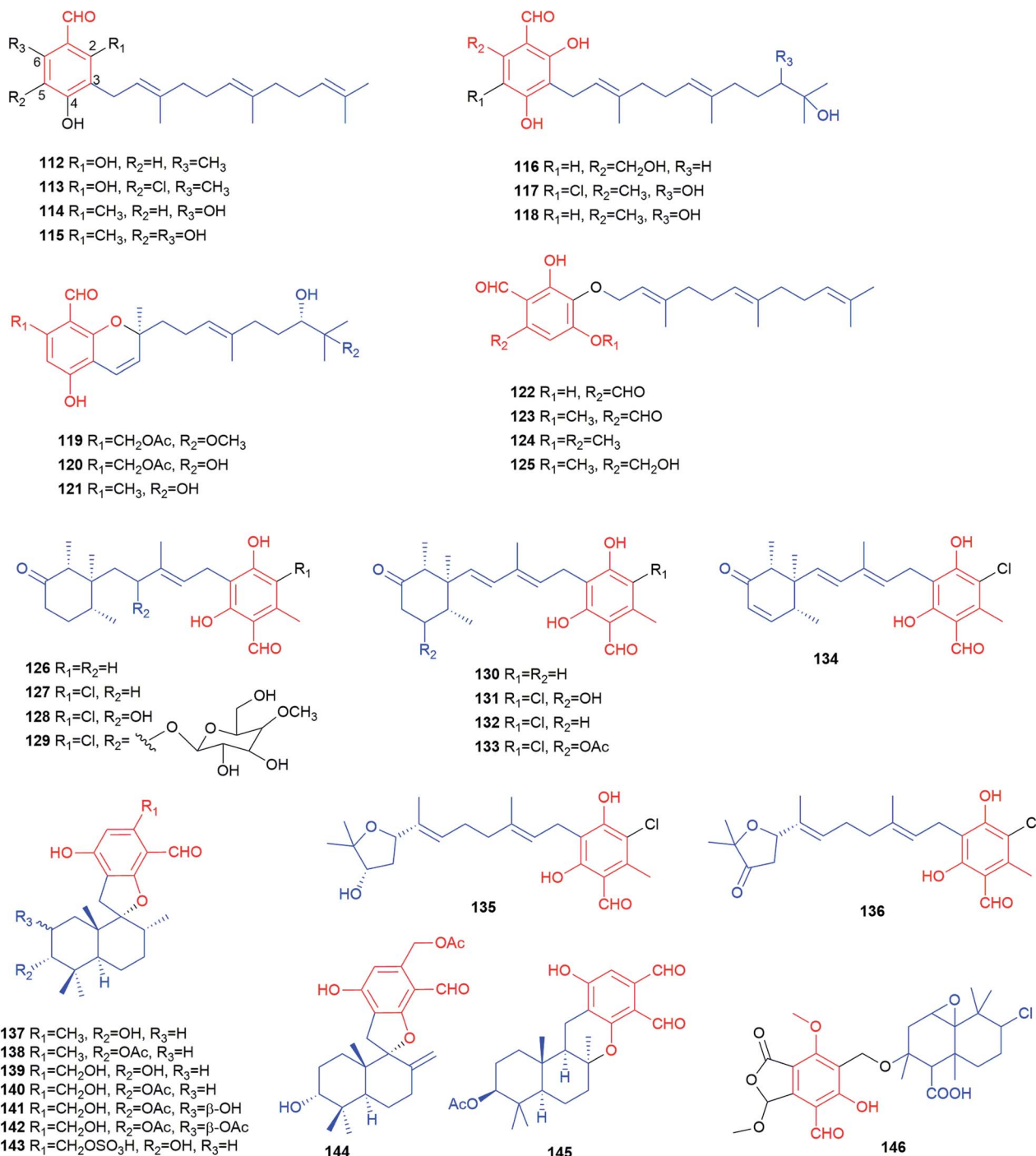
Fig. 11 Structures of meroterpenoids 112–146.

against *Eurotium repens*.[79] Compounds **127** and **133** display moderate inhibitory activity towards the enzymes AChE and β-glucuronidase as well as toxicity towards human lung fibroblasts.[78]

Chemical investigation of the bioactive metabolites in the pathogenic fungus *Verticillium hemipterigenum* and the sponge-derived fungus *Acremonium* sp. led to the isolation of deacetylchloronectrin **128**,[87,92] the glycoside vertihemipterin A **129**,[92] cylindrol B **130**,[87] 8′-hydroxyascochlorin **131**,[92]

compounds **132** and **133** [87,92] as well as ilicicolin E **134**.[92] Compounds **129** and **131–134** possess remarkable cytotoxicity to several cell lines such as KB, BC-1, NCI-H187 and vero with IC$_{50}$ values ranging from 0.36 to 19 μg mL^{-1}.[92] Two meroterpenoids with a tetrahydrofuran ring at the modified farnesyl chain, ascofuranol **135** and ascofuranone **136**, were obtained also from the fungi *Verticillium hemipterigenum* and *Acremonium* sp.[87,92] **135** has antiviral potential and

216
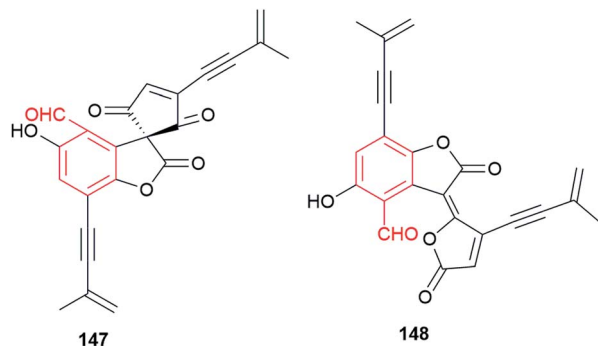
Fig. 12 Structures of meroterpenoids 147 and 148.

cytotoxicity,[91] while 136 shows significant anti-inflammatory activity.[87]

Eight phenylspirodrimane derivatives 137–144 were identified in the fungus *Stachybotrys chartarum*.[88,93] In their structures, a decahydronaphthalene ring system and a fused spiroketal feature are formed within the farnesyl chain. Stachybonoid A 141 exhibits moderate anti-inflammatory activity by inhibiting the production of nitric oxide in lipopolysaccharide-activated RAW264.7 cells with an IC_{50} value of 27.2 μM.[88] Stachybotrysins A 137 and B 138 display antiviral activity.[93] Kampanol C 145, a pentacyclic meroterpenoid, was obtained from *Stachybotrys kampalensis* Hansf.[94] Dicarbaldehyde backbone makes it extremely unstable in CD_2Cl_2, but reasonable stable in acetone. Pestalotiopen A 146 was isolated from the Chinese mangrove-endophytic fungus *Pestalotiopsis* sp. as an ether of altiloxin A derived from a farnesyl moiety and a highly substituted benzene carbaldehyde (cyclopaldic acid). It shows moderate antibacterial activity against *Enterococcus faecalis*.[95] The rare acetylenic spirodioxolactone ochroleucin A_1 147 was obtained from the mushrooms *Russula ochroleuca* and *R. viscida* after treatment with aqueous KOH. The labile chromogen undergoes easily rearrangement into the isomeric dilactone ochroleucin A_2 148 (Fig. 12).[96]

Taking together, meroterpenoid benzene carbaldehydes contain usually C_5-, C_{10}-, C_{15}-prenyl moiety or structures derived thereof. Antiviral, antifungal, antibacterial, phytotoxic and cytotoxic activities were determined for many members of this substance class. Furthermore, six compounds act as enzyme inhibitors, activators or receptors (Table 2).

2.4. Benzophenones

Natural products of this class share a diarylketone skeleton, which can be further modified by hydroxylation, methylation, methoxylation, halogenation or prenylation (Fig. 13). Six such substances were identified in fungi. They are usually oxidative ring opening products of anthrones (see Section 3.2.3 for details).

Daldinals A 149 and B 150, benzophenones with two bilateral methoxyl groups, differ from each other by just a hydroxyl or methoxyl group and were isolated from the fungus *Daldinia childiae* with anti-inflammatory activity.[97] The diversity of this group is increased by prenylation on the benzene ring, like the metabolites 151–154. Arugosins I 151 and H 152 with a dimethylallyl moiety at C2 are key intermediates in the shamixanthone biosynthesis and were isolated from the endophytic fungi *Penicillum* sp. JP-1 and *Emericella nidulans* var. *acristata*, respectively.[98,99] Co-cultivation of a marine-derived fungus *Pestalotia* sp. with a unicellular antibiotic-resistant bacterium led to the identification of a chlorinated benzophenone derivative, pestalone 153.[100] It shows antibiotic activity against resistant bacteria and moderate cytotoxicity. Its demethylated analogue 154 has been reported for *Chrysosporium* sp. with inhibitory activity against testosterone-5α-reductase.[101]

2.5. Spirocyclic benzene carbaldehydes

10 spirocyclic benzene carbaldehydes have been found in different *Aspergillus*, *Eurotium* and *Penicillum* species (Fig. 14). The spirocyclic derivatives 155–160 are presumably head-to-tail [4 + 2] Diels–Alder reaction products between the diene feature of a prenylated C_7-alkyl benzene carbaldehyde and an enone group of a prenylated diketopiperazine derived from *cyclo*-Trp-Ala. 155 and 156 have an olefinic bond at C1′ and 156 carries an additional dimethylallyl chain at C6.

Cryptoechinuline D 155 and 7-isopentenylcryptoechinuline D 156 were first reported in 1976 from *Aspergillus amstelodami* and isolated later from the mangrove endophytic fungus *Eurotium rubrum*.[102–104] Eurotinoids A–C 157–159 and dihydrocryptoechinulin D 160 were recently identified as enantiomeric pairs in the marine-derived fungus *Eurotium* sp. SCSIO F452.[105] Compounds 157 and 158 represent two "*meta*", while 159 and 160 "*ortho*" structures, regarding the relative position of the aryl-alkyl substitute to the spiro centre. With the exception for 156, all of the
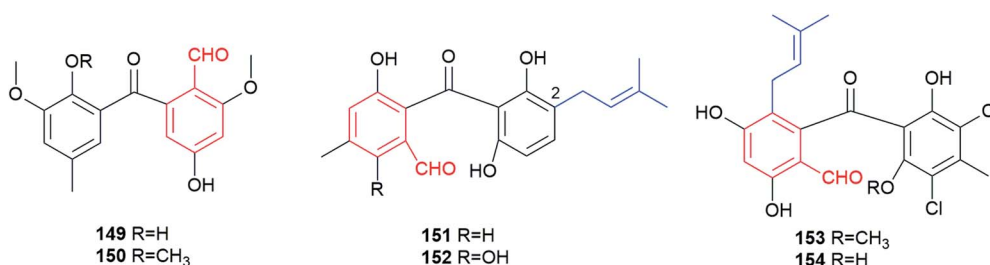
Fig. 13 Structures of benzophenones 149–154.
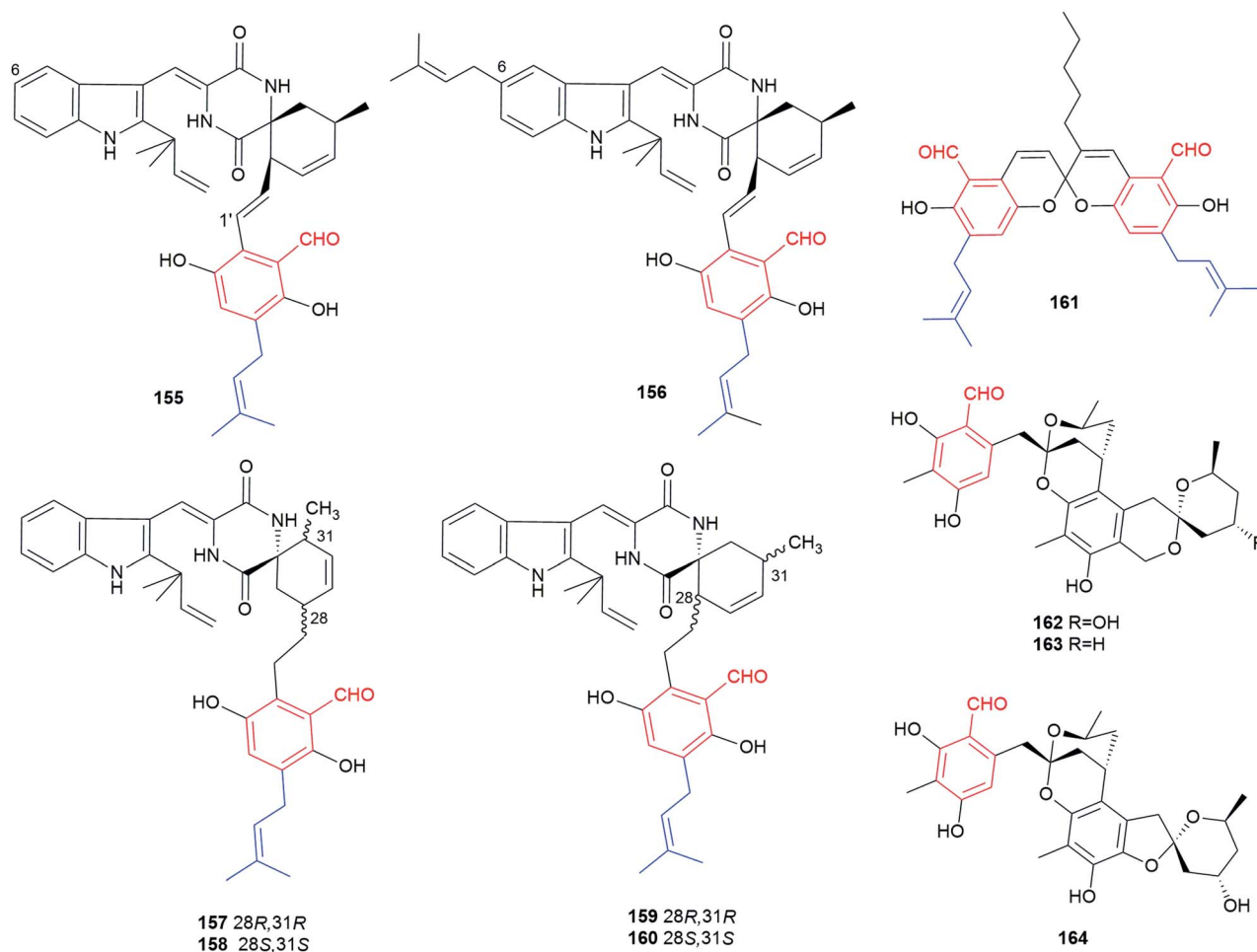
Fig. 14 Structures of spirocyclic benzene carbaldehydes **155–164**.

spirocyclic compounds exhibit antioxidant activity.[105] Compound **160** also displays cytotoxic activity against two tumour cell lines.[106]

Four spiroketal benzene carbaldehydes have been until now reported. Cristaldehyde B **161**, a spiro dichromene derivative, was isolated from the crinoid-associated fungus *Eurotium cristatum*.[36] Peniciketals A–C **162–164** with two spiroketal features were isolated from the saline soil-derived fungus *Penicillium raistrichii* and show a selective cytotoxity against HL-60 cell line.[107]

2.6. Miscellaneous benzene carbaldehydes

More than 20 fungal benzene carbaldehydes with naphthalene, chromanone or other skeletons cannot be grouped in the classes described above and are listed in this section (Fig. 15). They are usually events of strong rearrangements.

Bioactivity-guided fractionation led to isolation of two volatile benzaldehyde derivatives **165** and **166** from an extract of the basidiomycete *Sarcodontia crosea* (syn. *S. setosa*).[108] They exhibit weak activity against several phytopathogenic fungi including *Leptosphaeria maculans* and *Botrytis cinerea*. A biphenyl carbaldehyde **167** with

antibacterial activity was obtained from the endophytic fungus *Pestalotiopsis zonata*.[109]

Two C_6-alkylated salicylaldehydes, pyricuol **168** and pestalol E **169**, were obtained from *Magnaporthe grisea* and *Pestalotiopsis* sp., respectively.[47,49,110] Pyricuol **168** shows a strong nematicidal activity and killed 94.5% of *Caenorhabditis elegans* at 400 ppm over 24 h. Obviously, the hydroxymethyl group at C3′ in **168** enhances the nematicidal activity, compared to its C_7-alkylated analogues **47–50**.[47] Compound **169** carrying a sulfonic group at C4′ shows inhibitory activity against influenza A and swine flu viruses.

Agropyrenal **170** and vaccinal A **171**, two naphthalene carbaldehydes, were isolated from the phytopathogen *Ascochyta agropyrina* var. *nana* and the endogenic fungus *Pestalotiopsis vaccinii*, respectively.[34,44] Compound **171** displays anti-enterovirus and anti-inflammatory activities. Three 4/2-chromanone carbaldehydes **172–174** were obtained from the basidiomycetes *Fomitiporia punctata* and *Clitocybe illudens*.[4,111] Four unusual 2,3-dihydro-1*H*-indene benzaldehydes bearing a 1,4-benzodioxan moiety, diaporindenes A–D **175–178**, were identified in the endophytic fungus *Diaporthe* sp. SYSU-HQ3.[112] They possess significant anti-inflammatory activity against nitric oxide production.
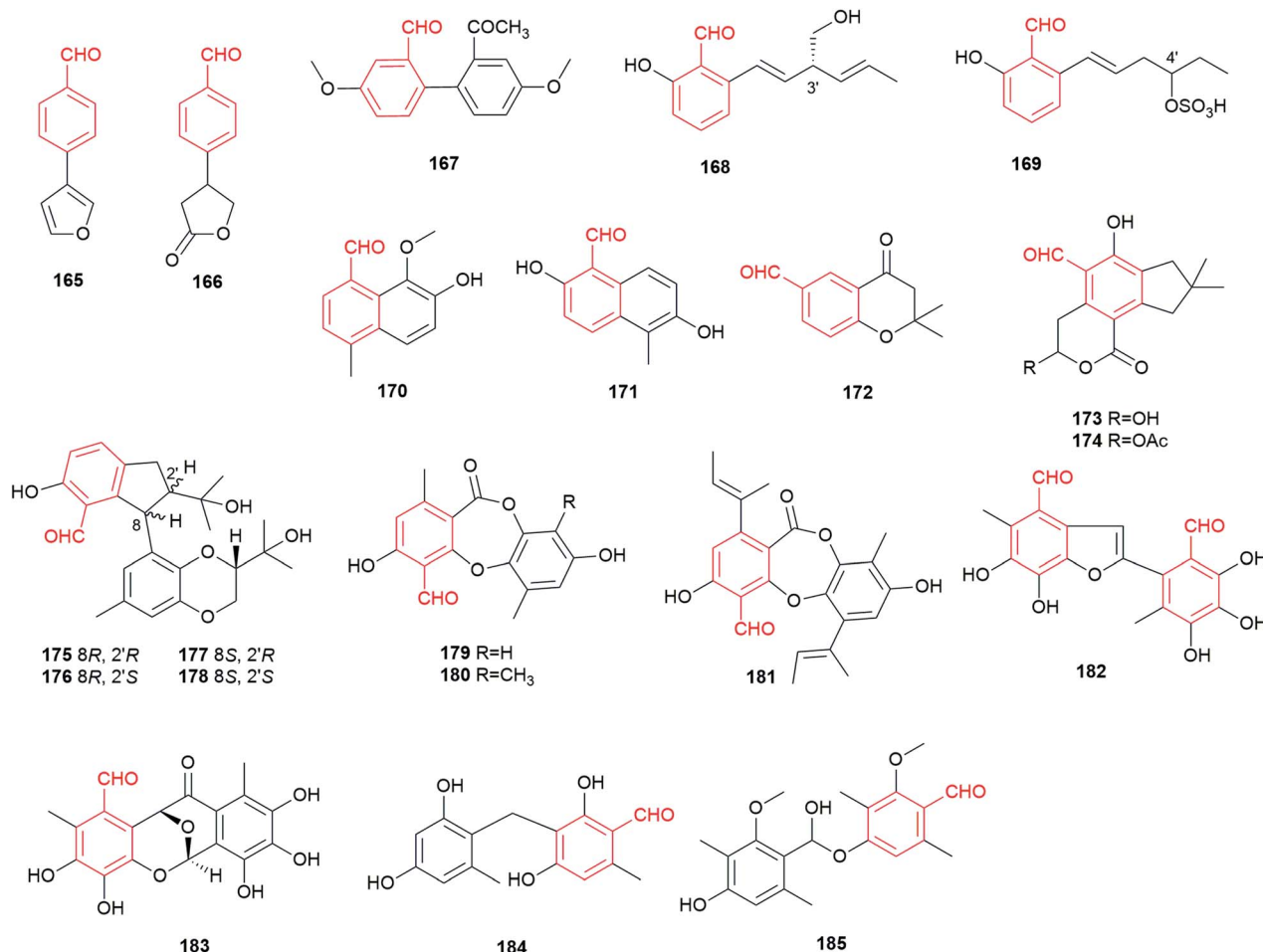
Fig. 15 Structures of miscellaneous aldehydes 165–185.

Depsidones 179–181 share a characteristic seven-member ring formed by ester and ether bonds between two benzene rings. They were isolated from the endophyte *Botryosphaeria rhodina* and the endophytic fungus BCC 8616.[113,114] Botryorhodines A 179 and B 180 show cytotoxic and antifungal activities, while compound 181 exhibits only cytotoxic activity.

Secondary metabolite investigation of the endophytic fungus *Epicoccum* sp. resulted in the isolation of a tetracyclic aromatic benzene carbaldehyde 182 and a 2-phenylbenzofuran carbaldehyde 183, which show potent antibacterial and significant anti-phytopathogenic activities.[21] It was proposed that epicoccolides A 182 and B 183 are presumably formed from two molecules of flavipin 16 *via* an unsymmetrical benzoin condensation, which undergoes further modification.[21] Two benzene carbaldehydes were identified in the genetically manipulated strains. Compound 184 with a diphenylmethane skeleton, probably derived from *o*-osellinaldehyde 9, was isolated from a non-reducing polyketide (NR-PKS) heterologous expression host.[115] Moreover, deletion of the down-regulator in *Aspergillus nidulans* led to the discovery of compound 185, a hemiacetal ether from two 3-methylosellinaldehyde 11 molecules.[116]

3. Formation of benzene carbaldehydes and their involvement in the biosynthesis of fungal metabolites

In the last years, significant progress has been achieved for the understanding of the formation of fungal benzene carbaldehydes. While some of them are formed by direct releasing from non-reducing polyketide synthases (NR-PKSs) with a terminal reductive domain or from highly reducing PKSs (HR-PKSs) by involvement of additional enzymes, other derivatives are formed *via* modification by tailoring enzymes, *e.g.* oxidoreductases and NRPS-like enzymes.

3.1. Direct releasing from backbone enzymes

Fungal benzene carbaldehydes are often generated by NR-PKSs with acetyl-CoA as the start and malonyl-CoA as the extender unit. The start unit initiates precursor for polyketide synthesis, while the extender units elongate the polyketide backbone to completion.[117] The number of extender units determines the length of the polyketide size. A set of grouped catalytic domains control the incorporation of changed or unchanged C_2-units into the polyketide backbone. A minimal fungal PKS consists of

Fig. 16 Genetic organisation of the *pkf* gene cluster in *A. nidulans* and the simplified postulated biosynthetic pathway of aspernidine A **186** (modified after Yaegashi *et al.*[90]). SAT: starter unit, ACP transacylase, CYP: cytochrome P450, SDR: short-chain dehydrogenase, PT: prenyltransferase, DH: dehydrogenase, NR-PKS: non-reducing polyketide synthase.

a ketosynthase (KS), an acyltransferase (AT), and an acyl carrier protein (ACP). Most PKSs also contain accessory domains, such as β-ketoacyl reductase (KR), dehydratase (DH), enoyl reductase (ER), product template (PT), C-methyltransferase (CMeT) and terminal reductase (R).[29,118]

3.1.1. Releasing from non-reducing polyketide synthases. The R domain in NR-PKSs is often used as chain releasing mechanism to form an aldehyde by NAD(P)H-dependent reduction. In the case of aspernidine A **186** biosynthesis, the responsible *pkf* cluster was identified in the genome of

Aspergillus nidulans.[90] Gene deletion experiments confirmed the function of the involved genes. The simple *o*-osellinaldehyde **9** is released from the NR-PKS PkfA by its C-terminal R domain (Fig. 16) and further converted to aspernidine D **124** with a farnesyl moiety by the UbiA-like prenyltransferase PkfE. Additional tailoring enzymes catalyse hydroxylation, reduction and methylation steps to form the final meroterpenoid **186**.

Similarly, 3-methylosellinaldehyde **11** and redoxcitrinin **30** were detected as the direct releasing products of the NR-PKSs TropA and CitS with R domains (Fig. 17 and 18). In
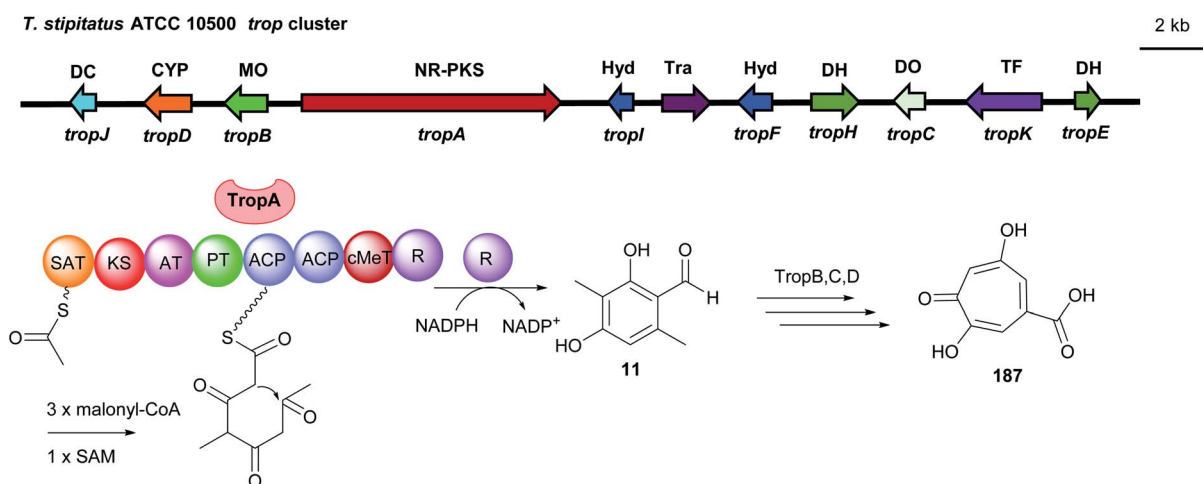
Fig. 17 Genetic organisation of the *trop* gene cluster in *T. stipitatus* and the simplified postulated biosynthetic pathway of stipitatic acid **187** (modified after Davison *et al.*[16]). SAT: starter unit, ACP transacylase, DC: decarboxylase, CYP: cytochrome P450, MO: monooxygenase. Hyd: hydrolase, Tra: transport, DH: dehydrogenase, DO: dioxygenase, TF: transcription factor, NR-PKS: non-reducing polyketide synthase.
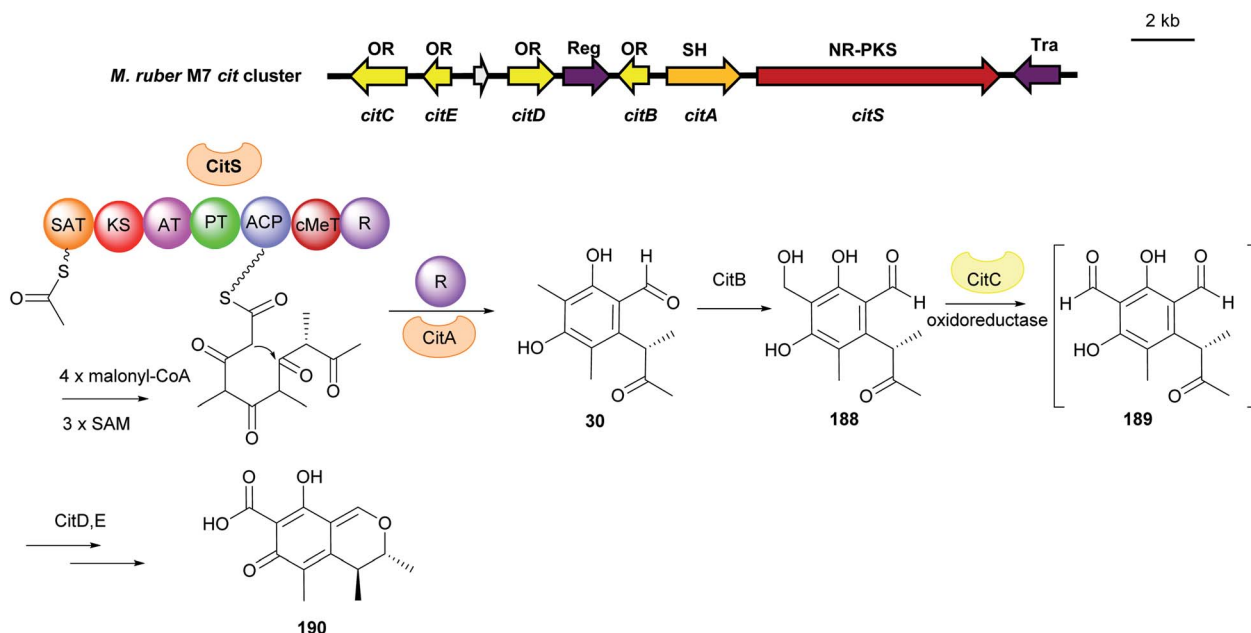
Fig. 18 Genetic organisation of the *cit* gene cluster in *M. ruber* and the simplified biosynthetic pathway of citrinin **190** (modified after He and Cox[33]). SAT: starter unit, ACP transacylase, OR: oxidoreductase, Reg: regulator, SH: serine hydrolase, Tra: transporter, NR-PKS non-reducing polyketide synthase.

comparison to PkfA, TropA (also known as Tspks1) and CitS (also known as PksCT) contain an additional CMeT domain for methylation during the polyketide chain elongation leading to the formation of the dimethylated benzene carbaldehydes **11** and **30**. Heterologous expression of the intronless *tropA* in the fungal host *Aspergillus oryzae* led to the identification of the benzaldehyde **11**.[16] Gene deletion and heterologous expression experiments demonstrated stipitatic acid **187** as the final product of the *trop* cluster (Fig. 17). Cox and He reported the reconstruction of the biosynthetic gene cluster (BGC) for citrinin **190** from *Monascus ruber* in *A. oryzae*.[33] The iterative NR-PKS gene *citS* codes for a redoxcitrinin
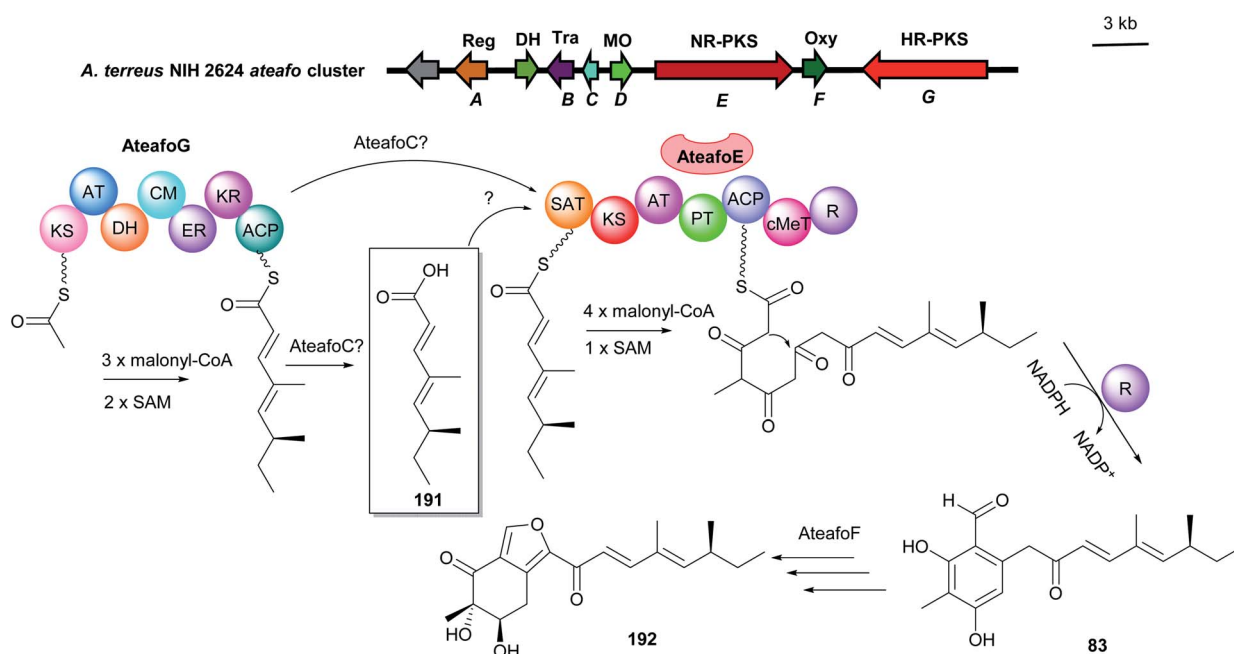
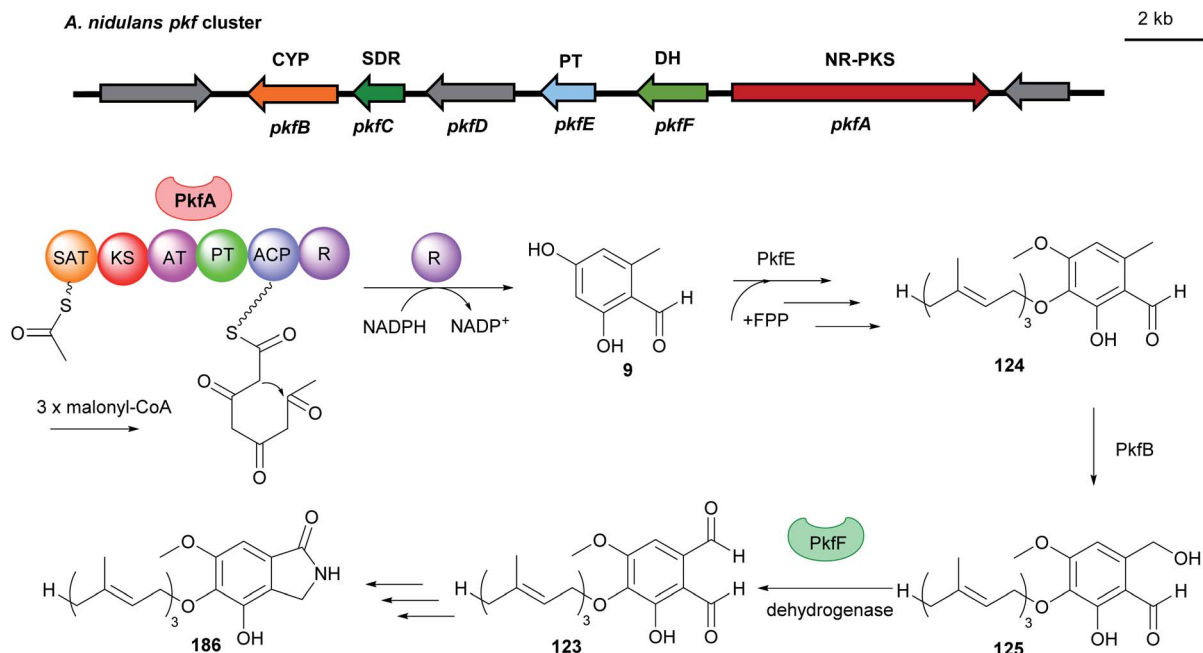**Fig. 19** Genetic organisation of the *ateafo* gene cluster in *A. terreus* and the simplified postulated biosynthetic pathway of asperfuranone **192** (modified after Chiang et al.[120]). SAT: starter unit, ACP transacylase, Reg: regulator, DH: dehydrogenasem Tra: transporter, OR: oxidoreductase, MO: monooxygenase, Oxy: oxygenase, NR-PKS: non-reducing polyketide synthase, HR-PKS: highly reducing polyketide synthase.

synthase. Expression of *citS* alone led to low production of the ketoaldehyde **30** evidently released from the PKS by its terminal reductive R domain. Coexpression of *citA* coding for a serine hydrolase with *citS* resulted in a much higher titre of **30**. This indicates that cooperation of CitA with the R domain of CitS serves as the release machinery in the native strain (Fig. 18).

3.1.2. Releasing from dual polyketide synthases. The majority of fungal PKS-derived metabolites uses only one PKS for assembling the skeleton as exemplified above. However, there are also numerous biosynthetic pathways, in which two PKSs contribute to the complex fungal products.[29,119] It was reported that the BGC of asperfuranone **192** in *A. terreus* contains one HR-PKS gene *ateafoG* and one NR-PKS gene *ateafoE*. Co-expression of the two PKS genes under control of a strong promoter each resulted in the formation of a shunt product **191** and the C_9-alkylated salicylaldehyde **83**.[120] The HR-PKS AteafoG was demonstrated to synthesize a dimethylated C_8-chain start moiety, which is transferred to the NR-PKS AteafoE for further extension with the facilitation of AteafoC (Fig. 19).

Yi Tang and coworkers reported a convergent model of dual PKS-containing BGC from *A. niger* by activation of the silent gene cluster.[121] The two PKSs can function independently in parallel to form precursors which can be ultimately connected *via* accessory enzymes. The NR-PKS AzaA released a C_5-alkylated salicylaldehyde **193** by its R domain, which is further reduced to the intermediate **36**. The precursor **194** with a pyran ring was then afforded by involvement of the monooxygenase AzaH. In parallel, 2′,4′-dimethylhexanoly CoA **195** as another precursor is synthesized by the HR-PKS AzaB and is proposed to be transferred to the C4-hydroxyl group of **194** to form the key intermediate **196**. Further modifications by several tailoring enzymes led to the end product azanigerone C **197** (Fig. 20).

3.1.3. Releasing from highly reducing polyketide synthases by involvement of additional oxidoreductases. All the aforementioned fungal benzene carbaldehyde-forming enzymes belong to NR-PKS.[29] Recently, two examples of HR-PKSs for the involvement in the benzaldehyde biosynthesis were reported for *vir* and *fog* clusters.[122,123] Investigation on *vir* BGC revealed the benzaldehyde releasing mechanism from the HR-
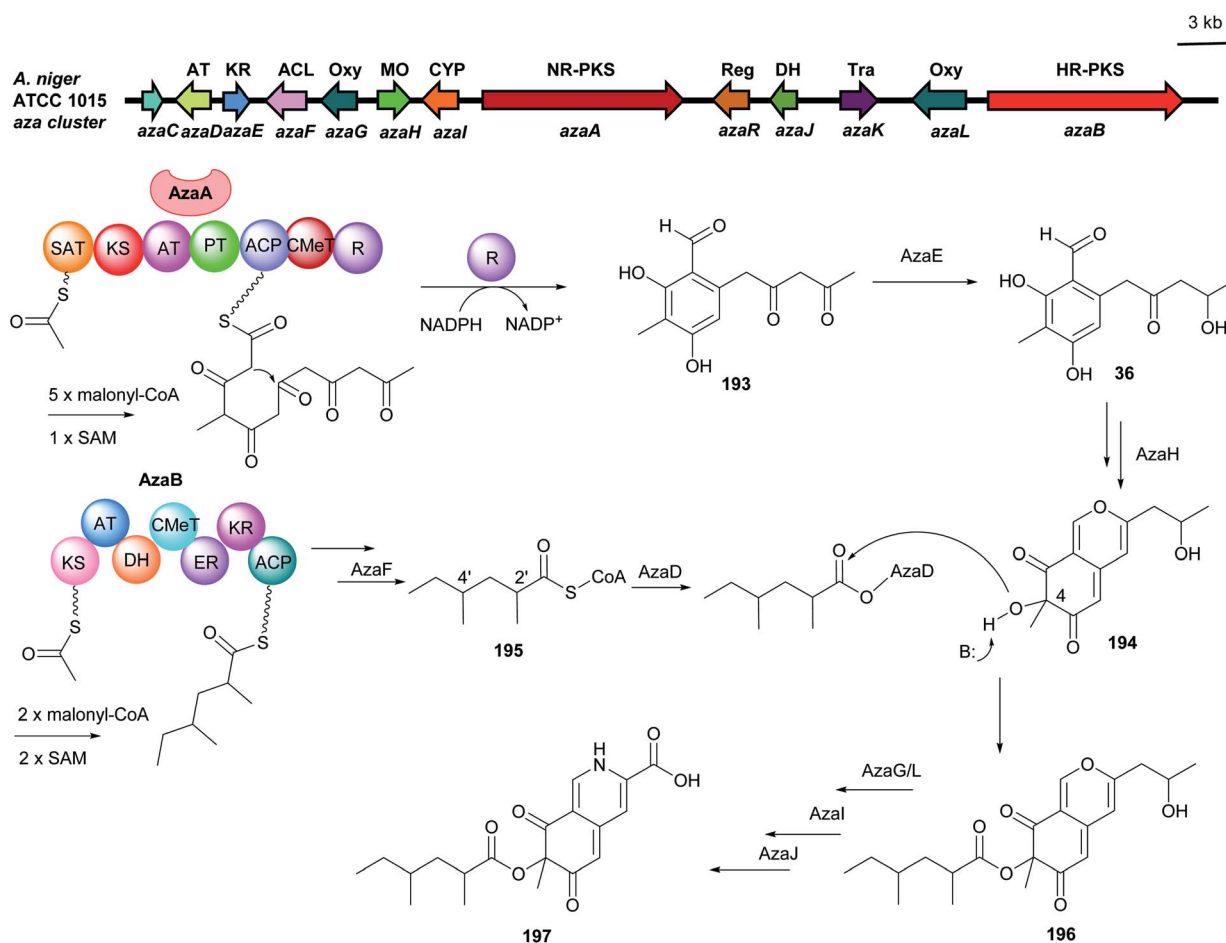
Fig. 20 Genetic organisation of the *aza* gene cluster in *A. niger* and the simplified postulated biosynthetic pathway of azanigerone **197** (modified after Zabala *et al.*[121]). SAT: starter unit, ACP transacylase, AT: acyltransferase, KR: ketoreductase, ACL: acyl:CoA ligase, Oxy: oxygenase, MO: monooxygenase, CYP: cytochrome P450, Reg: regulator, DH: dehydrogenase, Tra: transporter, NR–PKS: non–reducing polyketide synthase, HR–PKS: highly reducing polyketide synthase.

222
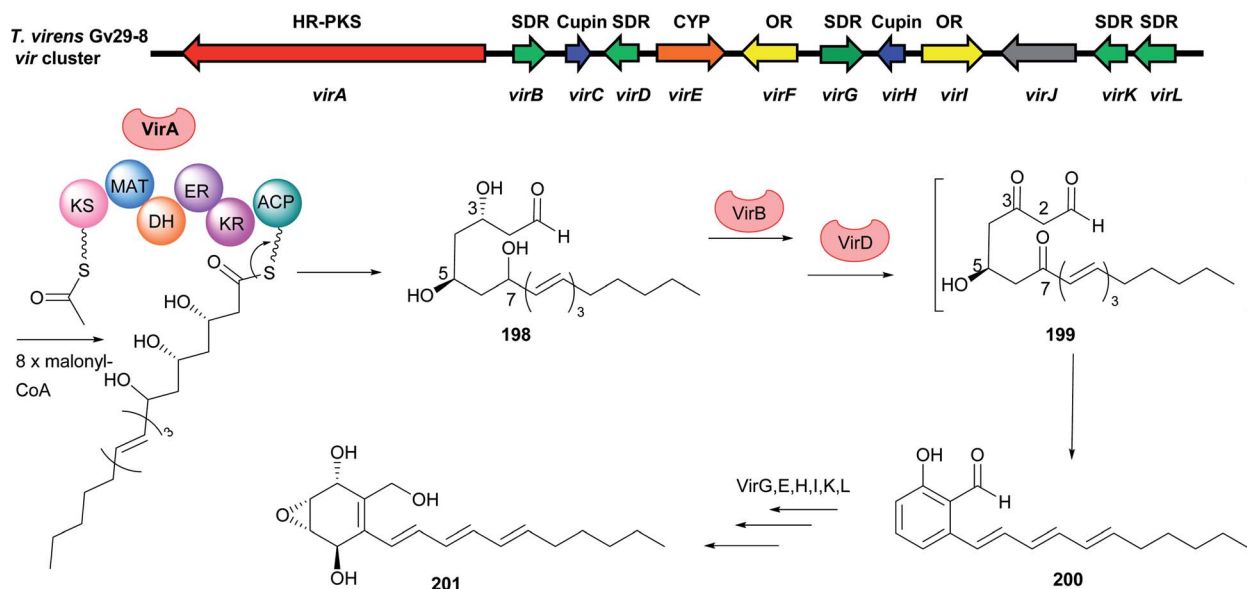
Fig. 21 Genetic organisation of the *vir* gene cluster in *T. virens* and the simplified postulated biosynthetic pathway of trichoxide **202** (modified after Liu *et al.*[122]). SDR: short chain reductase, Cupin: cupin-domain containing protein, CYP: cytochrome P450, OR: oxidoreductase, HR-PKS: highly reducing polyketide synthase.

PKS with involvement of associated tailoring enzymes.[122] Heterologous expression of *virA* alone led merely to an aliphatic C_{18} product virensol C **198**, which exists mostly as a pair of hemiacetals. Two short-chain reductases (SDRs) VirB and VirD catalyse dehydrogenation at C7 and C3 to β-ketone aldehyde **199**. The salicylaldehyde **200** is formed after intramolecular aldol condensation between C2 and C7 and dehydration likely catalysed by VirD. The final pathway product trichoxide **201** was afforded after decoration by different

tailoring enzymes (Fig. 21). The third known HR-PKS for the formation of aromatic compounds is FogA, which releases a salicyl alcohol derivative in the presence of additional oxidoreductases (see 3.2.1. for details).

3.2. Modification by tailoring enzymes

3.2.1. Alcohol oxidation by oxidoreductases. We recently identified a HR-PKS-containing *fog* cluster from *Aspergillus*

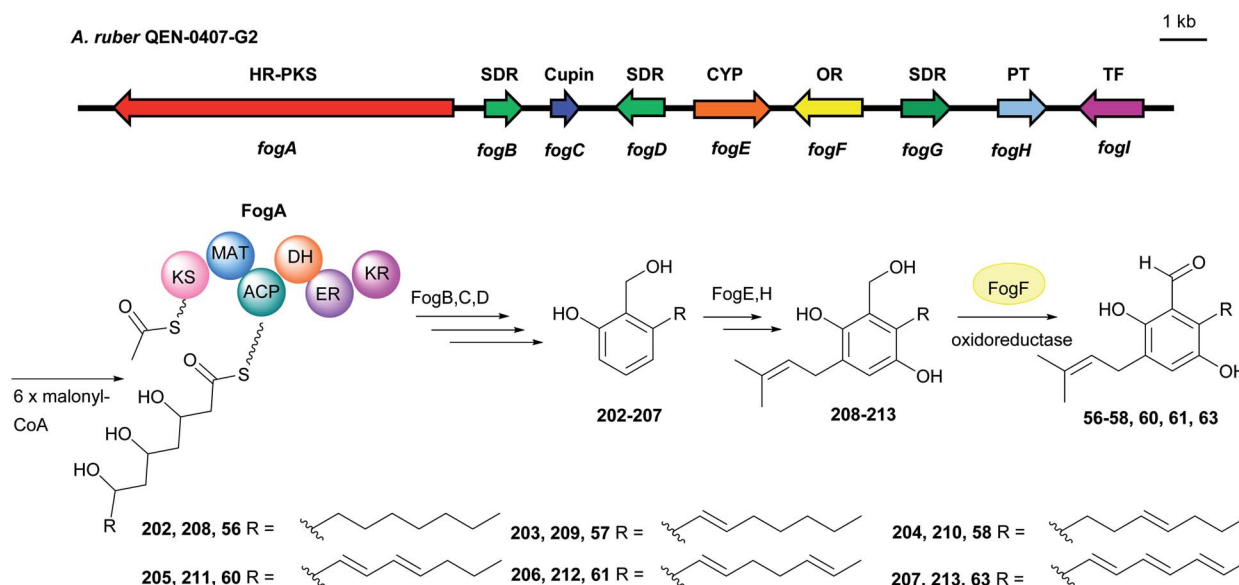Fig. 22 Genetic organisation of the *fog* gene cluster in *A. ruber* and the simplified postulated biosynthetic pathway of flavoglaucin **56** and its congeners (modified after Nies *et al.*[123]). SDR: short chain reductase, Cupin: cupin-domain containing protein, CYP: cytochrome P450, OR: oxidoreductase, PT: prenyltransferase, TF: transcription factor, HR-PKS: highly reducing polyketide synthase.

ruber and proved its responsibility for the biosynthesis of the C$_7$-alkylated salicylaldehyde flavoglaucin **56** and congeners (Fig. 22).[123] Heterologous expression of four genes including *fogA* coding for a HR-PKS, two for SDRs FogB and FogD as well as one for the cupin-domain-containing protein FogC led to the accumulation of the alkylated salicyl alcohols **202–207**, which is a prerequisite for consecutive hydroxylation and prenylation to form alcohol derivatives **208–213**. Feeding experiment confirmed that the FAD-binding oxidoreductase FogF oxidises these alcohols to the final aldehyde products.

In the citrinin biosynthetic pathway, the unstable dialdehyde intermediate **189** was formed *via* alcohol oxidation catalysed by the nicotinamide-dependent oxidoreductase CitC (also known as Mrl7) (Fig. 18).[33] Furthermore, in the biosynthesis of aspernidine A **186**, the P450 PkfB introduces a hydroxyl group on the methyl moiety to yield asoernidine E **125**, which is proposed to be further oxidised by the choline dehydrogenase PkfF to a reactive dialdehyde **123** (Fig. 16).

3.2.2. Acid reduction by NRPS-like enzymes. Zhao and coworkers reported that an aryl-acid produced by a NR-PKS can be activated by a nonribosomal peptide synthase (NRPS)-like protein with an A-ACP-R domain structure and reduced to a benzene carbaldehyde.[15] By cloning and heterologous expression of both cryptic NR-PKS and NRPS-like genes from *Aspergillus terreus* in *Saccharomyces cerevisiae*, they detected 5-methylorsellinic acid **214** and 5-methyl-osellinaldehyde **10** as the accumulated products. The purified ATEG_03630 protein can convert **214** to **10** *in vitro*. Therefore, they proposed that the aryl-acid **214** is activated by the adenylation (A) domain of ATEG_03630 and transferred to its ACP domain. Reduction of the thioester by the R domain led to the releasing of the aldehyde product **10** (Fig. 23). Further investigation of this NRPS-like protein showed that the adenylation (A) domain acts as the first "gate-keeper" to ensure the activation and thioester formation of the correct monomer onto the ACP.[124] Abe and coworkers identified later a NRPS-like enzyme StbB, which can catalyse the reduction of a farnesylated benzoic acid agrifolic acid (also known as ilicicolinic acid B) **216** to the aldehyde LL-Z1272β (also known as ilicicolin B) **112** (Fig. 24).[125]
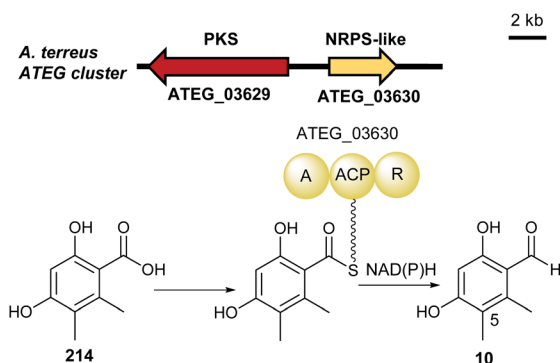
Fig. 23 Genetic organisation of the *ATEG* gene cluster in *A. terrus* and the proposed biosynthetic pathway of 5-methylosellinaldehyde **10** (modified after Wang *et al.*[15]).
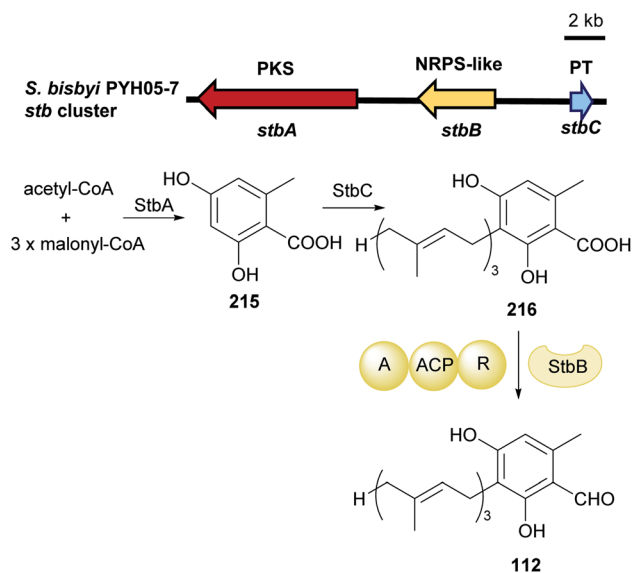
Fig. 24 Genetic organisation of the *stb* gene cluster in *Stachybotrys bisbyi* and the proposed biosynthetic pathway of LL-Z1272β **112** (modified after Li *et al.*[125]).

Investigation on *asc* cluster in *Acremonium egyptiacum* shows the aforementioned reduction of **216** to **112** (3.2.2) can also be catalysed by the NRPS-like enzyme AscB, which shares a 59% identity to StbB. This was observed in the biosynthesis of ascochlorin **132** and ascofuranone **136** in *Acremonium egyptiacum* (Fig. 25).[126] Both pathways share the same key precursor ilicicolin A epoxide **217**. Cyclisation of **218** catalysed by the terpene cyclase AscF and further dehydrogenation by AscG result in the final product of the ascochlorin pathway. Hydroxylation of **217** by AscH, cyclisation by AscI and oxidation by AscJ complete the ascofuranone pathway. All genes for the ascochlorin biosynthesis are located within the *asc-1* cluster, which also contains responsible genes for the common precursors. Additional genes required for the formation of ascofuranone, *i.e. ascHIJ* were found on the second locus *asc-2* (Fig. 25).

3.2.3. Reductive or oxidative cleavage of ring systems. A FAD-binding oxidoreductase CicC was proposed to catalyse a ring opening reaction, leading to the formation of the putative aldehyde intermediate **221** in the postulated cichorine **222** biosynthetic pathway (Fig. 26) in *Aspergillus nidulans*.[127] Analysis of the extracts from deletion strains indicated that the PKS PkbA assembled the precursor 3-methylorsellinic acid **219**, which undergoes hydroxylation, methylation and lactonization to the lactone intermediate **220**. However, no experimental data are till now available to support the definite CicC function and the conversion of the lactone **220** to the final lactam **222** also remains speculative.

Oxidative cleavage of chrysophanol anthrone **223** was observed in the formation of the benzophenone aldehydes **152** and **224** (Scheme 1). Subsequent intramolecular hemiacetal formation or reduction and ether formation give the
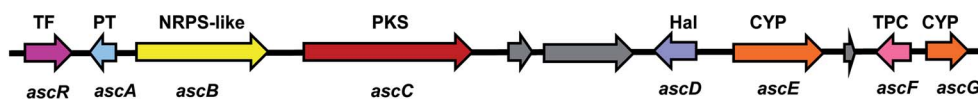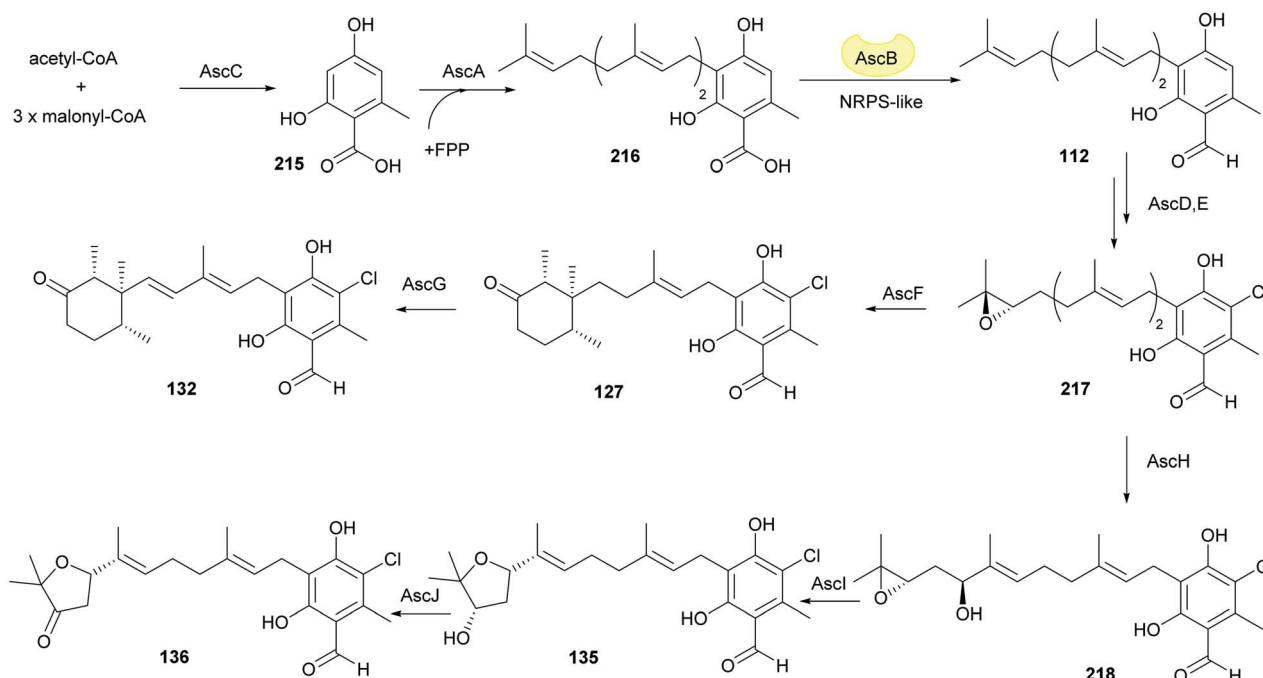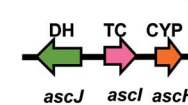
Fig. 25 Genetic organisation of the *asc* gene cluster in *A. egyptiacum* and the simplified biosynthetic pathways of ascochlorin **132** and asco-furanone **136** (modified after Araki *et al.*[126]). TF: transcription factor, PT: prenyltransferase, OR: oxidoreductase, Hal: halogenase, CYP: cyto-chrome P450, TPC: terpene cyclase, DH: dehydrogenase, PKS: polyketide synthase.

dibenzooxepinones **225–228**.[98,128,129] It is unclear whether enzymes are involved in the transformation.

3.3. Spontaneous reactions

In our previous study, we observed the spontaneous oxidor-eduction of the benzoquinone alcohol **229**, leading to the formation of the salicylaldehyde **56**, the benzyl alcohol **230** and the benzoquinone aldehyde **231**.[123] A proposed mechanism is given in Scheme 2. Two **229** molecules can act as both oxidant and reductant to form the hydroquinone alcohol **230** and the instable benzoquinone aldehyde intermediate **231**, which reacts with a third **229** molecule to form the aldehyde **56**. In addition, a set of dimethyl sulfoxide (DMSO) induced oxidations of benzyl alcohol to benzaldehyde were also described in the literature.[130]
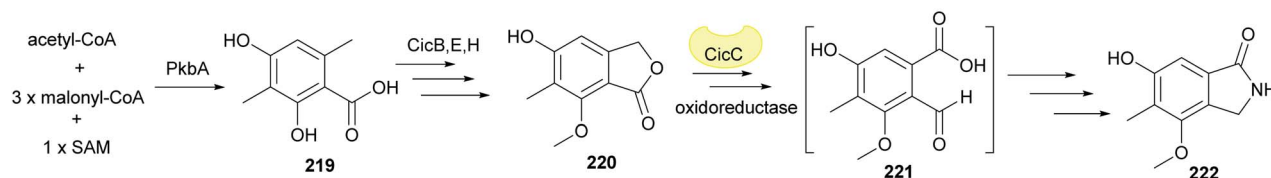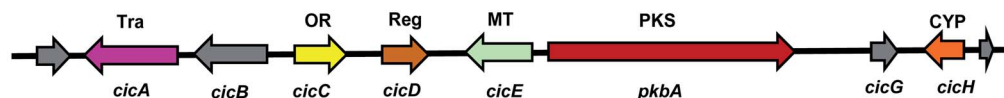
Fig. 26 Genetic organisation of the *cic* gene cluster in *A. nidulans* and the simplified postulated biosynthetic pathway of cichorine **222** (modified after Sanchez *et al.*[127]). Tra: transporter, OR: oxidoreductase, Reg: regulator, MT: methyltransferase, CYP: cytochrome P450, PKS: polyketide synthase.
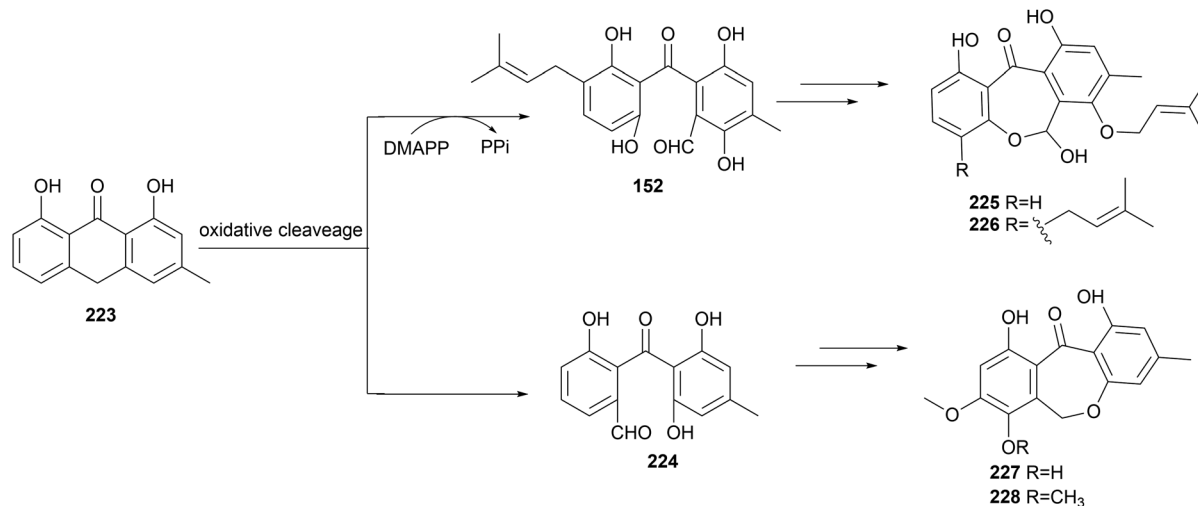
Scheme 1 Proposed biosynthesis of dibenzooxepinones **225–228**.
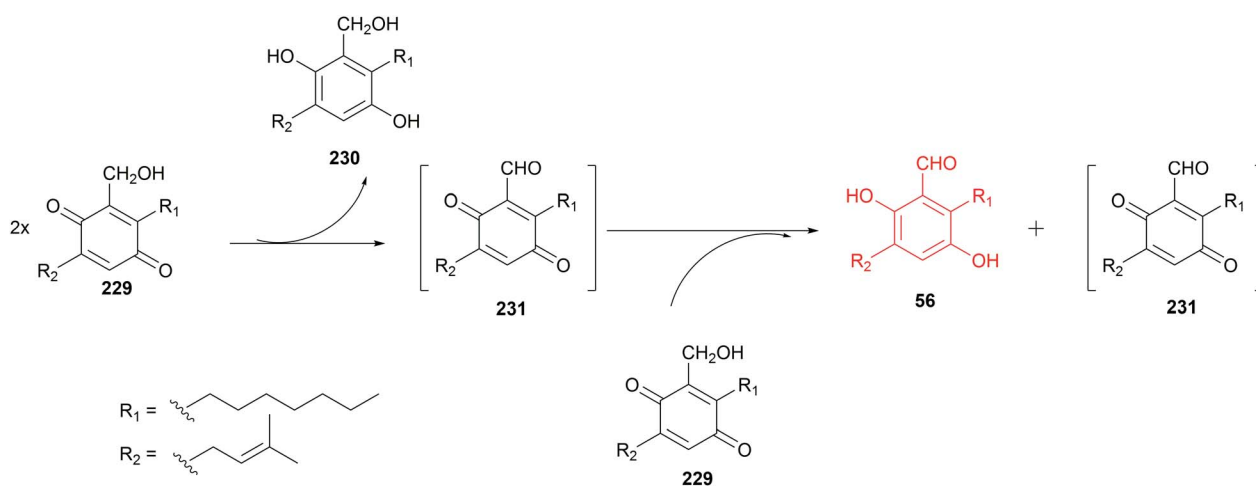
Scheme 2 Proposed mechanism of benzoquinone alcohol **229** conversion to salicylaldehyde **56** (modified after Nies *et al.*[123]).

4. Conclusions and future perspectives

In this review, we summarized the structural features, distribution, biological activities and applications as well as the origin and biosynthesis of benzene carbaldehydes from fungi. The topic compounds are mainly produced by ascomycetes (79%) and occasionally by basidiomycetes (17%) (Fig. 1). Approx. 51% of the ascomycetes-originated benzene carbaldehydes are from the genera of *Aspergillus*, *Stachybotrys*, *Penicillium* and *Pestalotiopsis*. For basidiomycetes, the genus of the edible mushroom *Hericium* contributes to approximate a fifth of benzene carbaldehydes (Table 1). The described biological activities are grouped into eleven categories with cytotoxic, antibacterial and antifungal activities as the top three (Fig. 2).

The backbones of the benzene carbaldehydes are usually originated from polyketides assembled by iterative fungal polyketide synthases, although other biosynthetic routes like shikimate or alkaloid pathways also serve as additional possibilities. The key aldehyde functional group can be formed by direct release from the polyketide chain, reduction of carboxylic acids or oxidation of benzyl alcohols. Other procedures such as oxidative ring opening also deliver aldehyde products. The simplest member of these natural products, *i.e.* benzaldehyde, can be decorated by hydroxylation, alkylation including methylation and ethylation, halogenation, prenylation at the benzene ring. Further modifications include oxidation, reduction and cyclisation. The majority of the compounds mentioned in this review belongs to derivatives of salicylaldehyde from the PKS pathway. Alkylated derivatives with different chain length (C_3, C_5, C_7, C_9 or C_{11}) at the *ortho*-position to the aldehyde group and meroterpenoids containing structural features derived from C_5, C_{10} or C_{15} prenyl moiety constitute the two large classes of benzene carbaldehydes. Benzene carbaldehydes are accumulated as pathway final products or serve as intermediate for more complex natural products.

As aforementioned, a number of fungal benzene carbaldehydes with interesting biological activities have been discovered in the past decades. However, the studies on structure–activity relationship have been few reported. More information on interactions of benzene carbaldehydes with biological targets will enhance the application potential of these compounds. Furthermore, it became a challenge to get new bioactive natural products under conventional laboratory culture conditions. Therefore, screening microorganisms from less explored or untapped sources, *e.g.* fungi from extreme environments[131–134] like saltern,[135] sulfur-rich hydrothermal vents,[136] in deep-sea segments,[137] hot springs[138] and mine area[139] becomes more important for bioactive metabolite finding. Symbiotic systems between fungi and bacteria, plants, insect, animals or invertebrate are also less studied promising sources of secondary metabolites.[140] Metabolite dereplication, *e.g.* by library-based LC-MS analysis[141,142] and comparative mass spectrometry-based metabolomics[143] have been successfully used in the past and will also play an important role in the future to accelerate novel metabolite discovery. Furthermore, the OSMAC (One Strain – Many Compounds) approach[144–146] by cultivation under different conditions and co-cultivation with other organisms has also been developed and successfully applied. However, the most putative genes and gene clusters for natural product biosynthesis still remain silent.[147] It can be therefore expected that reactivation of such genetic potentials by transcriptional regulator manipulation, promoter engineering and heterologous expression would deliver a large number of structures hidden the silent biosynthetic machinery.[148–150] Different new strategies have been published recently for the identification of fungal metabolites and their gene clusters, especially of large clusters. One of such approaches is the fungal artificial chromosomes and metabolic scoring (FAC-MS) strategy, which allows scientists to identify metabolites from complex mixtures after heterologous expression of clusters.[151] Metagenomics of uncultivable microbes and reconstruction of biosynthetic pathways provide other possibilities to get new metabolites.[152–154] Elucidation of biosynthetic pathways and characterisation of key enzymes would provide another way to create designed molecules by synthetic biology.

5. Conflicts of interest

There are no conflicts to declare.

6. Acknowledgements

7. References

1 B. S. Gould and H. Raistrick, *Biochem. J.*, 1934, **28**, 1640–1656.

2 A. Kundu, *Planta*, 2017, **245**, 1069–1078.

3 P. Venkatasubbaiah and W. S. Chilton, *J. Nat. Prod.*, 1990, **53**, 1628–1630.

4 R. Tabacchi, A. Fkyerat, C. Poliart and G. M. Dubin, *Phytopathol. Mediterr.*, 2000, **39**, 156–161.

5 R. Gui, L. Xu, Y. Kuang, M. Chung, J. Qin, L. Liu, S. Yang and L. Zhao, *J. Plant Interact.*, 2015, **10**, 87–92.

6 M. Shoeb, M. Haque and N. Nahar, *J. Nat. Prod. Plant Resour.*, 2014, **4**, 65–70.

7 F. Kamada, S. Abe, N. Hiratsuka, H. Wariishi and H. Tanaka, *Microbiology*, 2002, **148**, 1939–1946.

8 E. J. Lim, H. J. Kang, H. J. Jung, K. H. Kim, C. J. Lim and E. H. Park, *Biomol. Ther.*, 2008, **16**, 231–236.

9 E. W. Bassett and S. W. Tanenbaum, *Experientia*, 1958, **14**, 38–40.

10 H. C. Beck, *FEMS Microbiol. Lett.*, 1997, **149**, 233–238.

11 X. Sang, S. Chen, X. An, G. Chen, H. Wang and Y. Pei, *J. Asian Nat. Prod. Res.*, 2017, **19**, 436–443.

12 D. Kälvö, A. Menkis and A. Broberg, *Molecules*, 2018, **23**, 1417.

13 J. T. Lin and W. H. Liu, *J. Agric. Food Chem.*, 2006, **54**, 7564–7569.

14 L. Tian, S. X. Cai, D. H. Li, Z. J. Lin, T. J. Zhu, Y. C. Fang, P. P. Liu, Q. Q. Gu and W. M. Zhu, *Arch. Pharmacal Res.*, 2007, **30**, 1051–1054.

15 M. Wang, M. Beissner and H. Zhao, *Chem. Biol.*, 2014, **21**, 257–263.

16 J. Davison, F. A. al, M. Cai, Z. Song, S. Y. Yehia, C. M. Lazarus, A. M. Bailey, T. J. Simpson and R. J. Cox, *Proc. Natl. Acad. Sci. U. S. A.*, 2012, **109**, 7642–7647.

17 A. J. Flewelling, A. L. Bishop, J. A. Johnson and C. A. Gray, *Nat. Prod. Commun.*, 2015, **10**, 1661–1662.

18 V. S. Kumar, S. Kumaresan, M. M. Tamizh, M. I. Hairul Islam and K. Thirugnanasambantham, *Phytomedicine*, 2019, **61**, 152830.

19 H. Li, Z. B. Liao, D. Tang, W. B. Han, Q. Zhang and J. M. Gao, *J. Antibiot.*, 2018, **71**, 677–681.

20 W. R. Burge, L. J. Buckley, J. D. Sullivan Jr, C. J. McGrattan and M. Ikawa, *J. Agric. Food Chem.*, 1976, **24**, 555–559.

21 F. M. Talontsi, B. Dittrich, A. Schüffler, H. Sun and H. Laatsch, *Eur. J. Org. Chem.*, 2013, **2013**, 3174–3180.

22 Y. Xiao, H. X. Li, C. Li, J. X. Wang, J. Li, M. H. Wang and Y. H. Ye, *FEMS Microbiol. Lett.*, 2013, **339**, 130–136.

23 C. Shao, C. Wang, M. Wei, Z. Jia, Z. She and Y. Lin, *Chem. Nat. Compd.*, 2009, **45**, 779–781.

24 J. F. Grove, *Biochem. J.*, 1952, **50**, 648–666.

25 J. F. Grove, *Biochem. J.*, 1953, **54**, 664–673.

26 A. Cimmino, A. Andolfi, F. Avolio, A. Ali, N. Tabanca, I. A. Khan and A. Evidente, *Chem. Biodiversity*, 2013, **10**, 1239–1251.

27 J. Wang, W. Ding, C. Li, S. Huang, Z. g. She and Y. Lin, *Chem. Nat. Compd.*, 2013, **49**, 799–802.

28 L. S. Trifonov, P. Chakravarty, Y. Hiratsuka and W. A. Ayer, *Eur. J. For. Pathol.*, 1992, **22**, 441–448.

29 R. J. Cox, *Org. Biomol. Chem.*, 2007, **5**, 2010–2026.

30 J. Staunton and K. J. Weissman, *Nat. Prod. Rep.*, 2001, **18**, 380–416.

31 M. R. de Amorim, F. Hilario, F. M. J. Dos Santos, J. J. Batista, T. M. Bauab, A. R. Araujo, I. Z. Carlos, W. Vilegas and L. C. Dos Santos, *Planta Med.*, 2019, **85**, 957–964.

32 D. Zhang, X. Li, J. S. Kang, H. D. Choi, J. H. Jung and B. W. Son, *J. Microbiol. Biotechnol.*, 2007, **17**, 865–867.

33 Y. He and R. J. Cox, *Chem. Sci.*, 2016, **7**, 2119–2127.

34 J. Wang, X. Wei, X. Lu, F. Xu, J. Wan, X. Lin, X. Zhou, S. Liao, B. Yang, Z. Tu and Y. Liu, *Tetrahedron*, 2014, **70**, 9695–9701.

35 H. Lei, X. Lin, L. Han, J. Ma, K. Dong, X. Wang, J. Zhong, Y. Mu, Y. Liu and X. Huang, *Phytochemistry*, 2017, **142**, 51–59.

36 P. Zhang, C. Jia, Y. Deng, S. Chen, B. Chen, S. Yan, J. Li and L. Liu, *Phytochemistry*, 2019, **158**, 120–125.

37 J. Kwon, H. Lee, W. Ko, D. C. Kim, K.-W. Kim, H. C. Kwon, Y. Guo, J. H. Sohn, J. H. Yim and Y. C. Kim, *Tetrahedron*, 2017, **73**, 3905–3912.

38 B. Sontag, N. Arnold, W. Steglich and T. Anke, *J. Nat. Prod.*, 1999, **62**, 1425–1426.

39 Z. Huang, X. Nong, Z. Ren, J. Wang, X. Zhang and S. Qi, *Bioorg. Med. Chem. Lett.*, 2017, **27**, 787–791.

40 S. Chokpaiboon, P. Unagul, S. Nithithanasilp, S. Komwijit, W. Somyong, T. Ratiarpakul, M. Isaka and T. Bunyapaiboonsri, *Nat. Prod. Res.*, 2018, **32**, 149–153.

41 Z. Zhao, Y. Ying, Y. S. Hung and Y. Tang, *J. Nat. Prod.*, 2019, **82**, 1029–1033.

42 M. L. Bouillant, J. Favre-Bonvin, N. Salin and J. Bernillon, *Phytochemistry*, 1988, **27**, 1517–1519.

43 H. Fujimoto, T. Fujimaki, E. Okuyama and M. Yamazaki, *Chem. Pharm. Bull.*, 1999, **47**, 1426–1432.

44 A. Andolfi, A. Cimmino, M. Vurro, A. Berestetskiy, C. Troise, M. C. Zonno, A. Motta and A. Evidente, *Phytochemistry*, 2012, **79**, 102–108.

45 T. Asai, D. Luo, Y. Obara, T. Taniguchi, K. Monde, K. Yamashita and Y. Oshima, *Tetrahedron Lett.*, 2012, **53**, 2239–2243.

46 G. G. Harrigan, B. L. Aremntrout, J. D. Gloer and C. A. Shearer, *J. Nat. Prod.*, 1995, **58**, 1467–1469.

47 Y. H. Yang, D. S. Yang, H. M. Lei, C. Y. Li, G. H. Li and P. J. Zhao, *Molecules*, 2020, **25**, 72.

48 K. Tanaka, A. Sasaki, H.-Q. Cao, T. Yamada, M. Igarashi, I. Komine, H. Nakahigashi, N. Minami, S. Kuwahara, M. Nukina and H. Kiyota, *Eur. J. Org. Chem.*, 2011, **2011**, 6276–6280.

49 J. Sun, X. Lin, X. Zhou, J. Wan, T. Zhang, B. Yang, X. Yang, Z. Tu and Y. Liu, *J. Antibiot.*, 2014, **67**, 451–457.

50 C. Zheng, L. Xu, Y. Y. Li, T. Han, Q. Zhang, Q. Ming, K. Rahman and L. P. Qin, *Appl. Microbiol. Biotechnol.*, 2013, **97**, 7617–7625.

51 Y. Takenaka, T. Tanahashi, N. Nagakura, A. Itoh and N. Hamada, *Phytochemistry*, 2004, **65**, 3119–3123.

52 S. W. Sun, C. Z. Ji, Q. Q. Gu, D. H. Li and T. J. Zhu, *J. Asian Nat. Prod. Res.*, 2013, **15**, 956–961.

53 Y. Huang, L. Ma, X. Rong, D. Liu, S. Liu and W. Liu, *Chin. Tradit. Herb. Drugs*, 2012, **43**, 837–840.

54 Y. Miyake, C. Ito, T. Kimura, A. Suzuki, Y. Nishida and M. Itoigawa, *Food Sci. Technol. Res.*, 2014, **20**, 139–146.

55 N. Fathallah, M. M. Raafat, M. Y. Issa, M. M. Abdel-Aziz, M. Bishr, M. A. Abdelkawy and O. Salama, *Molecules*, 2019, **24**, 4118.

56 J. Shi, J. Liu, D. Kang, Y. Huang, W. Kong, Y. Xiang, X. Zhu, Y. Duan and Y. Huang, *ACS Omega*, 2019, **4**, 6630–6636.

57 M. D. Wu, M. J. Cheng, S. Y. Hsieh and G. F. Yuan, *Chem. Nat. Compd.*, 2014, **49**, 1175–1176.

58 J. Gao, F. León, M. M. Radwan, O. R. Dale, A. S. Husni, S. P. Manly, S. Lupien, X. Wang, R. A. Hill, F. M. Dugan, H. G. Cutler and S. J. Cutler, *J. Nat. Prod.*, 2011, **74**, 1636–1639.

59 M. Chen, C.-L. Shao, K.-L. Wang, Y. Xu, Z.-G. She and C.-Y. Wang, *Tetrahedron*, 2014, **70**, 9132–9138.

60 M. Chen, Q. Zhao, J. D. Hao and C. Y. Wang, *Nat. Prod. Res.*, 2017, **31**, 268–274.

61 D.-L. Li, X.-M. Li, T.-G. Li, H.-Y. Dang, P. Proksch and B.-G. Wang, *Chem. Pharm. Bull.*, 2008, **56**, 1282–1285.

62 S. Wang, X. M. Li, F. Teuscher, D. L. Li, A. Diesel, R. Ebel, P. Proksch and B.-G. Wang, *J. Nat. Prod.*, 2006, **69**, 1622–1625.

63 A. M. Elissawy, S. S. Ebada, M. L. Ashour, M. El-Neketi, W. Ebrahim and A. B. Singab, *Phytochem. Lett.*, 2019, **29**, 1–5.

64 S. Halecker, F. Surup, H. Solheim and M. Stadler, *J. Antibiot.*, 2018, **71**, 339–341.

65 S. Son, S. K. Ko, J. W. Kim, J. K. Lee, M. Jang, I. J. Ryoo, G. J. Hwang, M. C. Kwon, K. S. Shin, Y. Futamura, Y. S. Hong, H. Oh, B. Y. Kim, M. Ueki, S. Takahashi, H. Osada, J. H. Jang and J. S. Ahn, *Phytochemistry*, 2016, **122**, 154–164.

66 K. Matsuzaki, H. Tahara, J. Inokoshi, H. Tanaka, R. Masuma and S. Omura, *J. Antibiot.*, 1998, **51**, 1004–1011.

67 J. Arunpanichlert, V. Rukachaisirikul, Y. Sukpondma, S. Phongpaichit, S. Tewtrakul, N. Rungjindamai and J. Sakayaroj, *Chem. Pharm. Bull.*, 2010, **58**, 1033–1036.

68 Y. M. Chiang, E. Szewczyk, A. D. Davidson, N. Keller, B. R. Oakley and C. C. Wang, *J. Am. Chem. Soc.*, 2009, **131**, 2965–2970.

69 P. Berkaew, N. Soonthornchareonnon, K. Salasawadee, R. Chanthaket and M. Isaka, *J. Nat. Prod.*, 2008, **71**, 902–904.

70 R. Geris and T. J. Simpson, *Nat. Prod. Rep.*, 2009, **26**, 1063–1094.

71 Y. Matsuda and I. Abe, *Nat. Prod. Rep.*, 2016, **33**, 26–53.

72 J. W. Blunt, B. R. Copp, M. H. Munro, P. T. Northcote and M. R. Prinsep, *Nat. Prod. Rep.*, 2004, **21**, 1–49.

73 S. N. Sunassee and M. T. Davies-Coleman, *Nat. Prod. Rep.*, 2012, **29**, 513–535.

74 L. A. M. Murray, S. M. K. McKinnie, B. S. Moore and J. H. George, *Nat. Prod. Rep.*, 2020, **37**, DOI: 10.1039/d0np00018c.

75 G. A. Ellestad, R. H. Evans and M. P. Kunstmann, *Tetrahedron*, 1969, **25**, 1323–1334.

76 D. Hansson, A. Menkis, Å. Olson, J. Stenlid, A. Broberg and M. Karlsson, *Phytochemistry*, 2012, **84**, 31–39.

77 G. M. Dubin, A. Fkyerat and R. Tabacchi, *Phytochemistry*, 2000, **53**, 571–574.

78 M. Gutiérrez, C. Theoduloz, J. Rodríguez, M. Lolas and G. Schmeda-Hirschmann, *J. Agric. Food Chem.*, 2005, **53**, 7701–7708.

79 H. Hussain, K. H. Drogies, A. Al-Harrasi, Z. Hassan, A. Shah, U. A. Rana, I. R. Green, S. Draeger, B. Schulz and K. Krohn, *Asian Pac. J. Trop. Dis.*, 2015, **5**, 186–189.

80 H. Kawagishi, H. Sato, S. Sakamura, K. Kobayashi and U. Tadao, *Agric. Biol. Chem.*, 1984, **48**, 1903–1904.

81 Y. Kosuge, A. Suzuki and S. Tamura, *Agric. Biol. Chem.*, 1974, **38**, 1265–1267.

82 G. Marsico, B. A. Pignataro, M. Masi, A. Evidente, F. Casella, M. C. Zonno, J. H. Tak, J. R. Bloomquist, S. Superchi and P. Scafato, *Tetrahedron*, 2018, **74**, 3912–3923.

83 H. Kawagishi, M. Ando, K. Shinba, H. Sakamoto, S. Yoshida, F. Ojima, Y. Ishiguro, N. Ukai and S. Furukawa, *Phytochemistry*, 1992, **32**, 175–178.

84 H. Kawagishi, M. Ando, H. Sakamoto, S. Yoshida, F. Ojima, Y. Ishiguro, N. Ukai and S. Furukawa, *Tetrahedron Lett.*, 1991, **32**, 4561–4564.

85 K. Dekermendjian, R. Shan, M. Nielsen, M. Stadler, O. Sterner and M. R. Witt, *Eur. J. Med. Chem.*, 1997, **32**, 351–356.

86 Y. Nozawa, K. Yamamoto, M. Ito, N. Sakai, K. Mizoue, F. Mizobe and K. Hanada, *J. Antibiot.*, 1997, **50**, 635–640.

87 P. Zhang, B. Bao, H. T. Dang, J. Hong, H. J. Lee, E. S. Yoo, K. S. Bae and J. H. Jung, *J. Nat. Prod.*, 2009, **72**, 270–275.

88 P. Zhang, Y. Li, C. Jia, J. Lang, S. I. Niaz, J. Li, J. Yuan, J. Yu, S. Chen and L. Liu, *RSC Adv.*, 2017, **7**, 49910–49916.

89 J. A. Ballantine, V. Ferrito, C. H. Hassall and V. I. P. Jones, *J. Chem. Soc. C*, 1969, 56–61.

90 J. Yaegashi, M. B. Praseuth, S. W. Tyan, J. F. Sanchez, R. Entwistle, Y. M. Chiang, B. R. Oakley and C. C. Wang, *Org. Lett.*, 2013, **15**, 2862–2865.

91 T. Mogi, H. Ui, K. Shiomi, S. Omura, H. Miyoshi and K. Kita, *Biochim. Biophys. Acta*, 2009, **1787**, 129–133.

92 P. Seephonkai, M. Isaka, P. Kittakoop, U. Boonudomlap and Y. Thebtaranonth, *J. Antibiot.*, 2004, **57**, 10–16.

93 J. Zhao, J. Feng, Z. Tan, J. Liu, J. Zhao, R. Chen, K. Xie, D. Zhang, Y. Li, L. Yu, X. Chen and J. Dai, *J. Nat. Prod.*, 2017, **80**, 1819–1826.

94 S. B. Singh, D. L. Zink, M. Williams, J. D. Polishook, M. Sanchez, K. C. Silverman and R. B. Lingham, *Bioorg. Med. Chem. Lett.*, 1998, **8**, 2071–2076.

95 Y. Hemberger, J. Xu, V. Wray, P. Proksch, J. Wu and G. Bringmann, *Chem.–Eur. J.*, 2013, **19**, 15556–15564.

96 B. Sontag, M. Rüth, P. Spiteller, N. Arnold, W. Steglich, M. Reichert and G. Bringmann, *Eur. J. Org. Chem.*, 2006, **2006**, 1023–1033.

97 D. N. Quang, L. Harinantenaina, T. Nishizawa, T. Hashimoto, C. Kohchi, G. I. Soma and Y. Asakawa, *J. Nat. Med.*, 2006, **60**, 303–307.

98 A. Kralj, S. Kehraus, A. Krick, E. Eguereva, G. Kelter, M. Maurer, A. Wortmann, H. H. Fiebig and G. M. König, *J. Nat. Prod.*, 2006, **69**, 995–1000.

99 Z. Lin, T. Zhu, Y. Fang, Q. Gu and W. Zhu, *Phytochemistry*, 2008, **69**, 1273–1278.

100 M. Cueto, P. R. Jensen, C. Kauffman, W. Fenical, E. Lobkovsky and J. Clardy, *J. Nat. Prod.*, 2001, **64**, 1444–1446.

101 Y. Wachi, T. Yamashita, K. Komatsu and S. Yoshida, *New Benzophenone Derivative, Its Production and Its Use*, JP19930207818 19930823[JKXXAF JP 07061950 A2 19950307], 1995.

102 G. Gatti, R. Cardillo, C. Fuganti and D. Ghiringhelli, *J. Chem. Soc., Chem. Commun.*, 1976, 435–436.

103 H.-J. Yan, X.-M. Li, C.-S. Li and B.-G. Wang, *Helv. Chim. Acta*, 2012, **95**, 163–167.

104 D.-L. Li, X.-M. Li, T.-G. Li, H.-Y. Dang and B.-G. Wang, *Helv. Chim. Acta*, 2008, **91**, 1888–1892.

105 W. Zhong, J. Wang, X. Wei, T. Fu, Y. Chen, Q. Zeng, Z. Huang, X. Huang, W. Zhang, S. Zhang, L. Long and F. Wang, *Front. Chem.*, 2019, **7**, 350.

106 H. Gao, W. Liu, T. Zhu, X. Mo, A. Mandi, T. Kurtan, J. Li, J. Ai, Q. Gu and D. Li, *Org. Biomol. Chem.*, 2012, **10**, 9501–9506.

107 W. Z. Liu, L. Y. Ma, D. S. Liu, Y. L. Huang, C. H. Wang, S. S. Shi, X. H. Pan, X. D. Song and R. X. Zhu, *Org. Lett.*, 2014, **16**, 90–93.

108 T. Kokubun, Z. Rozwadowski and H. Duddeck, *J. Nat. Prod.*, 2007, **70**, 1539–1541.

109 X. Yang, S. Zhang, S. Song, Y. Zhang, D. Luo and M. Zhang, *Chin. J. Nat. Med.*, 2011, **9**, 101–104.

110 J. C. Kim, J. Y. Min, H. T. Kim, K. Y. Cho and S. H. Yu, *Biosci., Biotechnol., Biochem.*, 1998, **62**, 173–174.

111 M. S. R. Nair, H. Takeshita, T. C. McMorris and M. Anchel, *J. Org. Chem.*, 1969, **34**, 240–243.

112 H. Cui, Y. Liu, J. Li, X. Huang, T. Yan, W. Cao, H. Liu, Y. Long and Z. She, *J. Org. Chem.*, 2018, **83**, 11804–11813.

113 R. Abdou, K. Scherlach, H. M. Dahse, I. Sattler and C. Hertweck, *Phytochemistry*, 2010, **71**, 110–116.

114 P. Pittayakhajonwut, A. Dramae, S. Madla, N. Lartpornmatulee, N. Boonyuen and M. Tanticharoen, *J. Nat. Prod.*, 2006, **69**, 1361–1363.

115 M. Ahuja, Y. M. Chiang, S. L. Chang, M. B. Praseuth, R. Entwistle, J. F. Sanchez, H. C. Lo, H. H. Yeh, B. R. Oakley and C. C. Wang, *J. Am. Chem. Soc.*, 2012, **134**, 8212–8221.

116 C. E. Oakley, M. Ahuja, W. W. Sun, R. Entwistle, T. Akashi, J. Yaegashi, C. J. Guo, G. C. Cerqueira, W. J. Russo, C. C. Wang, Y. M. Chiang and B. R. Oakley, *Mol. Microbiol.*, 2017, **103**, 347–365.

117 Y. A. Chan, A. M. Podevels, B. M. Kevany and M. G. Thomas, *Nat. Prod. Rep.*, 2009, **26**, 90–114.

118 L. Du and L. Lou, *Nat. Prod. Rep.*, 2010, **27**, 255–278.

119 J. F. Sanchez, A. D. Somoza, N. P. Keller and C. C. Wang, *Nat. Prod. Rep.*, 2012, **29**, 351–371.

120 Y. M. Chiang, C. E. Oakley, M. Ahuja, R. Entwistle, A. Schultz, S. L. Chang, C. T. Sung, C. C. Wang and B. R. Oakley, *J. Am. Chem. Soc.*, 2013, **135**, 7720–7731.

121 A. O. Zabala, W. Xu, Y. H. Chooi and Y. Tang, *Chem. Biol.*, 2012, **19**, 1049–1059.

122 L. Liu, M. C. Tang and Y. Tang, *J. Am. Chem. Soc.*, 2019, **141**, 19538–19541.

123 J. Nies, H. Ran, V. Wohlgemuth, W. B. Yin and S.-M. Li, *Org. Lett.*, 2020, **22**, 2256–2260.

124 M. Wang and H. Zhao, *ACS Catal.*, 2014, **4**, 1219–1225.

125 C. Li, Y. Matsuda, H. Gao, D. Hu, X. S. Yao and I. Abe, *Chembiochem*, 2016, **17**, 904–907.

126 Y. Araki, T. Awakawa, M. Matsuzaki, R. Cho, Y. Matsuda, S. Hoshino, Y. Shinohara, M. Yamamoto, Y. Kido, D. K. Inaoka, K. Nagamune, K. Ito, I. Abe and K. Kita, *Proc. Natl. Acad. Sci. U. S. A.*, 2019, **116**, 8269–8274.

127 J. F. Sanchez, R. Entwistle, D. Corcoran, B. R. Oakley and C. C. C. Wang, *Med. Chem. Commun.*, 2012, **3**, 997–1002.

128 D. Pockrandt, L. Ludwig, A. Fan, G. M. König and S.-M. Li, *Chembiochem*, 2012, **13**, 2764–2771.

129 J. Kornsakulkarn, S. Saepua, P. Laksanacharoen, P. Rachtawee and C. Thongpanchang, *Tetrahedron Lett.*, 2016, **57**, 305–307.

130 W. W. Epstein and F. W. Sweat, *Chem. Rev.*, 1967, **67**, 247–260.

131 R. Chávez, F. Fierro, R. O. Garcia-Rico and I. Vaca, *Front. Microbiol.*, 2015, **6**, 903.

132 Z. E. Wilson and M. A. Brimble, *Nat. Prod. Rep.*, 2020, **37**, DOI: 10.1039/d0np00021c.

133 Z. E. Wilson and M. A. Brimble, *Nat. Prod. Rep.*, 2009, **26**, 44–71.

134 M. Ibrar, M. W. Ullah, S. Manan, U. Farooq, M. Rafiq and F. Hasan, *Appl. Microbiol. Biotechnol.*, 2020, **104**, 2777–2801.

135 D. Chung, H. Kim and H. S. Choi, *J. Microbiol.*, 2019, **57**, 717–724.

136 W. Jiang, P. Ye, C. T. Chen, K. Wang, P. Liu, S. He, X. Wu, L. Gan, Y. Ye and B. Wu, *Mar. Drugs*, 2013, **11**, 4761–4772.

137 Y. T. Wang, Y. R. Xue and C. H. Liu, *Mar. Drugs*, 2015, **13**, 4594–4616.

138 W. Y. Liao, C. N. Shen, L. H. Lin, Y. L. Yang, H. Y. Han, J. W. Chen, S. C. Kuo, S. H. Wu and C. C. Liaw, *J. Nat. Prod.*, 2012, **75**, 630–635.

139 A. A. Stierle and D. B. Stierle, *Nat. Prod. Commun.*, 2014, **9**, 1037–1044.

140 N. Adnani, S. R. Rajski and T. S. Bugni, *Nat. Prod. Rep.*, 2017, **34**, 784–814.

141 H. Mohimani, A. Gurevich, A. Mikheenko, N. Garg, L. F. Nothias, A. Ninomiya, K. Takada, P. C. Dorrestein and P. A. Pevzner, *Nat. Chem. Biol.*, 2017, **13**, 30–37.

142 K. F. Nielsen and T. O. Larsen, *Front. Microbiol.*, 2015, **6**, 71.

143 B. C. Covington, J. A. McLean and B. O. Bachmann, *Nat. Prod. Rep.*, 2017, **34**, 6–24.

144 H. B. Bode, B. Bethe, R. Hofs and A. Zeeck, *Chembiochem*, 2002, **3**, 619–627.

145 N. P. Ariantari, G. Daletos, A. Mándi, T. Kurtán, W. E. G. Müller, W. Lin, E. Ancheeva and P. Proksch, *RSC Adv.*, 2019, **9**, 25119–25132.

146 D. M. Selegato, R. T. Freire, A. C. Pilon, C. R. Biasetto, H. C. de Oliveira, L. M. de Abreu, A. R. Araujo, V. da Silva Bolzani and I. Castro-Gamboa, *Magn. Reson. Chem.*, 2019, **57**, 458–471.

147 A. A. Brakhage, P. Sprote, Q. Al Abdallah, A. Gehrke, H. Plattner and A. Tuncher, *Adv. Biochem. Eng./ Biotechnol.*, 2004, **88**, 45–90.

148 M. Zerikly and G. L. Challis, *Chembiochem*, 2009, **10**, 625–633.

149 H. N. Lyu, H. W. Liu, N. P. Keller and W. B. Yin, *Nat. Prod. Rep.*, 2020, **37**, 6–16.

150 A. A. Brakhage, *Nat. Rev. Microbiol.*, 2013, **11**, 21–32.

151 K. D. Clevenger, J. W. Bok, R. Ye, G. P. Miley, M. H. Verdan, T. Velk, C. Chen, K. Yang, M. T. Robey, P. Gao, M. Lamprecht, P. M. Thomas, M. N. Islam, J. M. Palmer, C. C. Wu, N. P. Keller and N. L. Kelleher, *Nat. Chem. Biol.*, 2017, **13**, 895–901.

152 Y. He, B. Wang, W. Chen, R. J. Cox, J. He and F. Chen, *Biotechnol. Adv.*, 2018, **36**, 739–783.

153 M. Katz, B. M. Hover and S. F. Brady, *J. Ind. Microbiol. Biotechnol.*, 2016, **43**, 129–141.

154 B. K. Singh and C. A. Macdonald, *Drug Discovery Today*, 2010, **15**, 792–799.

155 I. Ullah, A. L. Khan, L. Ali, A. R. Khan, M. Waqas, J. Hussain, I. J. Lee and J. H. Shin, *J. Microbiol.*, 2015, **53**, 127–133.

156 N. C. G. Faria, J. H. Kim, L. A. P. Gonçalves, M. d. Martins, K. L. Chan and B. C. Campbell, *Lett. Appl. Microbiol.*, 2011, **52**, 506–513.

157 S. Y. Y. Wong, I. R. Grant, M. Friedman, C. T. Elliott and C. Situ, *Appl. Environ. Microbiol.*, 2008, **74**, 5986.

158 J. H. Ha, D. U. Lee, J. T. Lee, J. S. Kim, C. S. Yong, J. A. Kim, J. S. Ha and K. Huh, *J. Ethnopharmacol.*, 2000, **73**, 329–333.

159 X. Li, B. Xiang, T. Shen, C. Xiao, R. Dai, F. He and Q. Lin, *Int. Immunopharmacol.*, 2020, **82**, 106353.

160 L. G. Malak, M. A. Ibrahim, D. W. Bishay, A. M. Abdel-baky, A. M. Moharram, B. Tekwani, S. J. Cutler and S. A. Ross, *J. Nat. Prod.*, 2014, **77**, 1987–1991.

161 F. A. R. Rodrigues, A. C. A. Oliveira, B. C. Cavalcanti, M. P. Costa, C. Pessoa, M. V. N. de Souza and A. C. Pinheiro, *Eur. Chem. Bull.*, 2014, **3**, 555–558.

162 Y. H. Tao, Z. Yuan, X. Q. Tang, H. B. Xu and X. L. Yang, *Bioorg. Med. Chem. Lett.*, 2006, **16**, 592–595.

163 B. H. Lee, S. H. Yoon, Y. S. Kim, S. K. Kim, B. J. Moon and Y. S. Bae, *Nat. Prod. Res.*, 2008, **22**, 1441–1450.

164 M. Masi, F. Freda, F. Sangermano, V. Calabro, A. Cimmino, M. Cristofaro, S. Meyer and A. Evidente, *Molecules*, 2019, **24**, E1086.

5 Conclusions and future prospects

This thesis describes multiple approaches to increase the structural diversity of low-molecular molecules by post-modifications on the prenylated moieties. Various chemical transformations on the prenyl groups, such as hydroxylation, cyclisation, oxidation and rearrangement, can occur both enzymatically and nonenzymatically. Studies on chemoenzymatic synthesis, spontaneous reaction mechanisms and chemical logic of entire biosynthetic pathways provide examples for the chemical diversification of natural products.

Inspired by the notable behaviour of the Fe^{II}/2-OG-dependent oxygenase FtmOx1, a homologous protein EAW25734 was identified in *Neosartorya fischeri* NRRL 181. Incubation of EAW25734 with tryprostatin B (**8**) in the presence of ascorbic acid, Fe^{II} and 2-OG led to a two-step reaction, *i.e.* an exceptional double bond migration and hydroxylation, to yield 22-hydroxylisotryprostatin B (**9**). Biochemical characterisation proved EAW25734 to be a nonheme Fe^{II}-2OG-dependent oxygenase. Secondary metabolite analysis in the native strain revealed that EAW25734 indeed hijacked the intermediate **8** from the fumitremorgin biosynthetic pathway to produce **9,** but only with a low yield. This study highlighted the advantage and potential of *in vitro* enzyme characterisation for new biocatalyst finding, even for those of not clustered or low expressed genes in the host.

In addition, a spontaneous oxidative cyclisation was investigated for 1,3-dihydroxy-4-dimethylallylnaphthalene. Isolation and structure elucidation of the nonenzymatic products showed the rearranged tetrahydrobenzofuran and bicyclo[3.3.1]nonane scaffolds. Labelling experiments with an $^{18}O_2$-enriched atmosphere and in $^{18}O_2$-enriched water confirmed that the two additional hydroxyl groups originated from oxygen. This allowed us to propose a radical mediated cyclisation mechanism with the reactive C4-peroxyl intermediate **17** as the "stimulating device" for the following radical rearrangement and intramolecular cyclisation. Here we provide one additional example that products of enzyme reactions could undergo further nonenzymatic rearrangements during the incubation process.

A combination of *in vitro* enzymatic studies and heterologous expression *in vivo*, was used to understand how simple benzaldehyde scaffolds can be further diversified through enzymatic and nonenzymatic reactions. Flavoglaucin (**24a**) and congeners **24b−f** are prenylated salicylaldehyde derivatives from different fungi including *Aspergillus ruber* with impressive biological activities. However, little is known about their biosynthesis and the involved enzymes prior to our study. With the assistance of genome mining, heterologous expression, feeding experiments and biochemical characterization, a nine-gene *fog* cluster was identified as the genetic information for the biosynthesis of flavoglaucin and analogues. The salicyl alcohol derivatives were released from the HR-PKS as the initial aromatic intermediates in cooperation with three oxidoreductases. The alcohol substituent served as an essential functional group for subsequent decorations. The cytochrome P450 FogE

converts the benzyl alcohols to C5-hydroxylated derivatives, which are then prenylated by the prenyltransferase FogH. After prenylation, the alcohol function was oxidized to the final aldehyde by the oxidase FogF. Therefore, this study demonstrated a highly efficient and programmed biosynthetic pathway to assemble a set of prenylated salicylaldehydes.

For future prospects, the following works can be performed:

- ➤ Investigation of the mechanistic details for the notable nonheme Fe^{II}/2-OG-dependent oxygenase EAW25734 by X-ray crystal structure analysis will enrich our knowledge on the structure–reactivity relationship. Further site-directed mutagenesis of this enzyme could expand the catalytic potential for structure modifications.

- ➤ Although the biosynthetic pathway of flavoglaucin has been identified, initial aromatization mechanism is still unclear. Biochemical characterization of the three tailoring enzymes, *i.e.* FogB, FogC and FogD, may provide new insights into the unique aromatization involved in this pathway.

- ➤ The prenyltransferase FogH belongs to the DMATS family and uses a benzyl alcohol as substrate, differing clearly from other members of this family. Therefore, it would be interesting to test its substrate specificity towards other aromatic compounds.

- ➤ Targeted protein engineering of the prenyltransferase FogH can also be performed to expand the substrate specificity and regioselectivity as well as prenyl donor space.

6 References

Abe I, Morita H (2010) Structure and function of the chalcone synthase superfamily of plant type III polyketide synthases. Nat Prod Rep 27:809-838.

Adnani N, Rajski SR, Bugni TS (2017) Symbiosis-inspired approaches to antibiotic discovery. Nat Prod Rep 34:784-814.

Alberts AW, Chen J, Kuron G, Hunt V, Huff J, Hoffman C, Rothrock J, Lopez M, Joshua H, Harris E et al. (1980) Mevinolin: a highly potent competitive inhibitor of hydroxymethylglutaryl-coenzyme A reductase and a cholesterol-lowering agent. Proc Natl Acad Sci USA 77:3957-3961.

Amare MG, Keller NP (2014) Molecular mechanisms of *Aspergillus flavus* secondary metabolism and development. Fungal Genet Biol 66:11-18.

Ariantari NP, Daletos G, Mándi A, Kurtán T, Müller WEG, Lin W, Ancheeva E, Proksch P (2019) Expanding the chemical diversity of an endophytic fungus *Bulgaria inquinans*, an ascomycete associated with mistletoe, through an OSMAC approach. RSC Advances 9:25119-25132.

Asai T, Luo D, Obara Y, Taniguchi T, Monde K, Yamashita K, Oshima Y (2012) Dihydrobenzofurans as cannabinoid receptor ligands from *Cordyceps annullata*, an entomopathogenic fungus cultivated in the presence of an HDAC inhibitor. Tetrahedron Lett 53:2239-2243.

Bérdy J (2012) Thoughts and facts about antibiotics: Where we are now and where we are heading. J Antibiot 65:385-395.

Bernhardt P, Okino T, Winter JM, Miyanaga A, Moore BS (2011) A stereoselective vanadium-dependent chloroperoxidase in bacterial antibiotic biosynthesis. J Am Chem Soc 133:4268-4270.

Birch AJ, Blance GE, David S, Smith H (1961) Studies in relation to biosynthesis. XXIV. Some remarks on the structure of echinuline. J Chem Soc:3128-3131.

Birch AJ, Simpson TJ, Westerman PW (1975) Biosynthesis of ravenelin from [1-^{13}C]-acetate. Tetrahedron Lett 16:4173-4177.

Blackwell M (2011) The Fungi: 1, 2, 3 … 5.1 million species? Am J Bot 98:426-438.

Bloomer JL, Moppett CE, Sutherland JK (1968) The nonadrides. part V. Biosynthesis of glauconic acid. J Chem Soc (C):588-591.

Blunt JW, Copp BR, Munro MH, Northcote PT, Prinsep MR (2004) Marine natural products. Nat Prod Rep 21:1-49.

Bode HB, Bethe B, Hofs R, Zeeck A (2002) Big effects from small changes: possible ways to explore nature's chemical diversity. Chembiochem 3:619-627.

Bok JW, Balajee SA, Marr KA, Andes D, Nielsen KF, Frisvad JC, Keller NP (2005) LaeA, a regulator of morphogenetic fungal virulence factors. Eukaryot Cell 4:1574-1582.

Bok JW, Keller NP (2004) LaeA, a regulator of secondary metabolism in *Aspergillus* spp. Eukaryot Cell 3:527-535.

Bolton C, Borel JF, Cuzner ML, Davison AN, Turner AM (1982) Immunosuppression by cyclosporin a of experimental allergic encephalomyelitis. J Neurol Sci 56:147-153.

REFERENCES

Bomke C, Tudzynski B (2009) Diversity, regulation, and evolution of the gibberellin biosynthetic pathway in fungi compared to plants and bacteria. Phytochemistry 70:1876-1893.

Bonitz T, Alva V, Saleh O, Lupas AN, Heide L (2011) Evolutionary relationships of microbial aromatic prenyltransferases. PloS one 6:e27336.

Borel JF, Wiesinger D (1979) Studies on the mechanism of action of cyclosporin A. Bri J Pharmacol 66:66P-67P.

Brakhage AA (2013) Regulation of fungal secondary metabolism. Nat Rev Microbiol 11:21-32.

Calvo AM, Cary JW (2015) Association of fungal secondary metabolism and sclerotial biology. Front Microbiol 6:1-16.

Capon RJ (2020) Extracting value: mechanistic insights into the formation of natural product artifacts - case studies in marine natural products. Nat Prod Rep 37:55-79.

Cardani C, Casnati G, Piozzi F, Quilico A (1959) The constitution of echinulin. Tetrahedron Lett 1:1-8.

Cardoso AS, Marques MM, Srinivasan N, Prabhakar S, Lobo AM, Rzepa HS (2006) Studies in sigmatropic rearrangements of *N*-prenylindole derivatives - a formal enantiomerically pure synthesis of tryprostatin B. Org Biomol Chem 4:3966-3972.

Chávez R, Fierro F, Garcia-Rico RO, Vaca I (2015) Filamentous fungi from extreme environments as a promising source of novel bioactive secondary metabolites. Front Microbiol 6:903.

Chen KL, Lai CY, Pham MT, Chein RJ, Tang Y, Lin HC (2020) Enzyme-catalyzed azepinoindole formation in clavine alkaloid biosynthesis. Org Lett 22:3302-3306.

Chooi YH, Hong YJ, Cacho RA, Tantillo DJ, Tang Y (2013) A cytochrome P450 serves as an unexpected terpene cyclase during fungal meroterpenoid biosynthesis. J Am Chem Soc 135:16805-16808.

Cole RJ, Dorner JW, Lansden JA, Cox RH, Pape C, Cunfer B, Nicholson SS, Bedell DM (1977) Paspalum staggers: isolation and identification of tremorgenic metabolites from sclerotia of *Claviceps paspali*. J Agric Food Chem 25:1197-1201.

Covington BC, McLean JA, Bachmann BO (2017) Comparative mass spectrometry-based metabolomics strategies for the investigation of microbial secondary metabolites. Nat Prod Rep 34:6-24.

Cox RJ (2007) Polyketides, proteins and genes in fungi: programmed nano-machines begin to reveal their secrets. Org Biomol Chem 5:2010-2026.

Cui CB, Kakeya H, Osada H (1996) Novel mammalian cell cycle inhibitors, spirotryprostatins A and B, produced by *Aspergillus fumigatus*, which inhibit mammalian cell cycle at G2/M phase. Tetrahedron 52:12651-12666.

Dan Q, Newmister SA, Klas KR, Fraley AE, McAfoos TJ, Somoza AD, Sunderhaus JD, Ye Y, Shende VV, Yu F et al. (2019) Fungal indole alkaloid biogenesis through evolution of a bifunctional reductase/Diels–Alderase. Nat Chem 11:972-980.

Develoux M (2001) Griseofulvin. Annu Dermatol Veneréol 128:1317-1325.

Dong X, Fu J, Yin X, Cao S, Li X, Lin L, Huyiligeqi, Ni J (2016) Emodin: a review of its pharmacology, toxicity and pharmacokinetics. Phytother Res 30:1207-1218.

REFERENCES

Du F-Y, Li X-M, Li C-S, Shang Z, Wang B-G (2012) Cristatumins A-D, new indole alkaloids from the marine-derived endophytic fungus *Eurotium cristatum* EN-220. Bioorg Med Chem Lett 22:4650-4653.

Dufour N, Rao RP (2011) Secondary metabolites and other small molecules as intercellular pathogenic signals. FEMS Microbiol Lett 314:10-17.

Fan A, Li S-M (2013) One substrate - seven products with different prenylation positions in one-step reactions: prenyltransferases make it possible. Adv Synth Catal 355:2659-2666.

Fan A, Winkelblech J, Li S-M (2015) Impacts and perspectives of prenyltransferases of the DMATS superfamily for use in biotechnology. Appl Microbiol Biotechnol 99:7399-7415.

Fan J, Liao G, Kindinger F, Ludwig-Radtke L, Yin W-B, Li S-M (2019) Peniphenone and penilactone formation in *Penicillium crustosum via* 1,4-Michael additions of *ortho*-quinone methide from hydroxyclavatol to γ-butyrolactones from crustosic acid. J Am Chem Soc 141:4225-4229.

Fathallah N, Raafat MM, Issa MY, Abdel-Aziz MM, Bishr M, Abdelkawy MA, Salama O (2019) Bio-guided fractionation of prenylated benzaldehyde derivatives as potent antimicrobial and antibiofilm from *Ammi majus* L. fruits-associated *Aspergillus amstelodami*. Molecules 24:4118-4135.

Fleming A (1929) On the antibacterial action of cultures of a *Penicillium,* with special reference to their use in the isolation of *B. influenzae*. Br J Exp Pathol 10:226-236.

Flieger M, Wurst M, Shelby R (1997) Ergot alkaloids - sources, structures and analytical methods. Folia Microbiol (Praha) 42:3-30.

Funa N, Ohnishi Y, Fujii I, Shibuya M, Ebizuka Y, Horinouchi S (1999) A new pathway for polyketide synthesis in microorganisms. Nature 400:897-899.

Funayama S, Ishibashi M, Komiyama K, Omura S (1990) Biosynthesis of furaquinocins A and B. J Org Chem 55:1132-1133.

Gao X, Haynes SW, Ames BD, Wang P, Vien LP, Walsh CT, Tang Y (2012a) Cyclization of fungal nonribosomal peptides by a terminal condensation-like domain. Nat Chem Biol 8:823-830.

Gao Y, Honzatko RB, Peters RJ (2012b) Terpenoid synthase structures: a so far incomplete view of complex catalysis. Nat Prod Rep 29:1153-1175.

Garson MJ, Simpson JS (2004) Marine isocyanides and related natural products – structure, biosynthesis and ecology. Nat Prod Rep 21:164-179.

Gebler JC, Poulter CD (1992) Purification and characterization of dimethylallyl tryptophan synthase from *Claviceps purpurea*. Arch Biochem Biophys 296:308-313.

Geris R, Simpson TJ (2009) Meroterpenoids produced by fungi. Nat Prod Rep 26:1063-1094.

Golomb BA, Evans MA (2008) Statin adverse effects. Am J Cardiovasc Drugs 8:373-418.

Gould BS, Raistrick H (1934) Studies in the biochemistry of micro-organisms: The crystalline pigments of species in the *Aspergillus glaucus* series. Biochem J 28:1640-1656.

Grundmann A, Kuznetsova T, Afiyatullov SS, Li S-M (2008) FtmPT2, an *N*-prenyltransferase from *Aspergillus fumigatus*, catalyses the last step in the biosynthesis of fumitremorgin B. Chembiochem 9:2059-2063.

REFERENCES

Grundmann A, Li S-M (2005) Overproduction, purification and characterization of FtmPT1, a brevianamide F prenyltransferase from *Aspergillus fumigatus*. Microbiology 151:2199-2207.

Haagen Y, Glück K, Fay K, Kammerer B, Gust B, Heide L (2006) A gene cluster for prenylated naphthoquinone and prenylated phenazine biosynthesis in *Streptomyces cinnamonensis* DSM 1042. Chembiochem 7:2016-2027.

Hamasaki T, Fukunaga M, Kimura Y, Hatsuda Y (1980) Isolation and structures of two new metabolites from *Aspergillus ruber*. Agric Biol Chem 44:1685-1687.

Hashimoto M, Nonaka T, Fujii I (2014) Fungal type III polyketide synthases. Nat Prod Rep 31:1306-1317.

He B-B, Zhou T, Bu X-L, Weng J-Y, Xu J, Lin S, Zheng J-T, Zhao Y-L, Xu M-J (2019) Enzymatic pyran formation involved in xiamenmycin biosynthesis. ACS cataly 9:5391-5399.

Heide L (2009) Prenyl transfer to aromatic substrates: genetics and enzymology. Curr Opin Chem Biol 13:171-179.

Heitman J, Howlett BJ, Crous PW, Stukenbrock EH, James TY, Gow NAR, and Gow N (2017) The fungal kingdom. ASM Press,

Hertweck C, Luzhetskyy A, Rebets Y, Bechthold A (2007) Type II polyketide synthases: gaining a deeper insight into enzymatic teamwork. Nat Prod Rep 24:162-190.

Hesseltine CW, Shotwell OL, Ellis JJ, Stubblefield RD (1966) Aflatoxin formation by *Aspergillus flavus*. Bacteriol Rev 30:795-805.

Hibbett DS, Binder M, Bischoff JF, Blackwell M, Cannon PF, Eriksson OE, Huhndorf S, James T, Kirk PM, Lücking R et al. (2007) A higher-level phylogenetic classification of the fungi. Mycol Res 111:509-547.

Hill JG, Nakashima TT, Vederas JC (1982) Fungal xanthone biosynthesis. Distribution of acetate-derived oxygens in ravenelin. J Am Chem Soc 104:1745-1748.

Houbraken J, Frisvad JC, Samson RA (2011) Fleming's penicillin producing strain is not *Penicillium chrysogenum* but *P. rubens*. IMA Fungus 2:87-95.

Huang Y, Ma L, Rong X, Liu D, Liu S, Liu W (2012) Benzaldehyde derivatives from a marine-derived fungus *Aspergillus* sp. Chin Tradit Herbal Drugs 43:837-840.

Hussein AA, Barberena I, Capson TL, Kursar TA, Coley PD, Solis PN, Gupta MP (2004) New cytotoxic naphthopyrane derivatives from *Adenaria floribunda*. J Nat Prod 67:451-453.

Ibrar M, Ullah MW, Manan S, Farooq U, Rafiq M, Hasan F (2020) Fungi from the extremes of life: an untapped treasure for bioactive compounds. App Microbol Biotechnol 104:2777-2801.

Jacobson RA, Adams R (1924) Trihydroxy-methylanthraquinones. III. Synthesis of emodin. J Am Chem Soc 46:1312-1316.

Kato H, Yoshida T, Tokue T, Nojiri Y, Hirota H, Ohta T, Williams RM, Tsukamoto S (2007) Notoamides A-D: prenylated indole alkaloids isolated from a marine-derived fungus, *Aspergillus* sp. Angew Chem Int Ed 46:2254-2256.

Kato N, Suzuki H, Takagi H, Asami Y, Kakeya H, Uramoto M, Usui T, Takahashi S, Sugimoto Y, Osada H (2009) Identification of cytochrome P450s required for fumitremorgin biosynthesis in *Aspergillus fumigatus*. Chembiochem 10:920-928.

REFERENCES

Kavanagh K (2017) Fungi: biology and applications. Wiley,

Kaysser L, Bernhardt P, Nam SJ, Loesgen S, Ruby JG, Skewes-Cox P, Jensen PR, Fenical W, Moore BS (2012) Merochlorins A–D, cyclic meroterpenoid antibiotics biosynthesized in divergent pathways with vanadium-dependent chloroperoxidases. J Am Chem Soc 134:11988-11991.

Keatinge-Clay AT (2012) The structures of type I polyketide synthases. Nat Prod Rep 29:1050-1073.

Keller NP (2019) Fungal secondary metabolism: regulation, function and drug discovery. Nat Rev Microbiol 17:167-180.

Kellogg BA, Poulter CD (1997) Chain elongation in the isoprenoid biosynthetic pathway. Curr Opin Chem Biol 1:570-578.

Komiyama K, Funayama S, Anraku Y, Ishibashi M, Takahashi Y, Omura S (1990) Novel antibiotics, furaquinocins A and B. J Antibiot 43:247-252.

Kozlovsky AG, Vinokurova NG, Adanin VM, Burkhardt G, Dahse HM, Gräfe U (2000) New diketopiperazine alkaloids from *Penicillium fellutanum*. J Nat Prod 63:698-700.

Kumar D, Barad S, Chen Y, Luo X, Tannous J, Dubey A, Glam Matana N, Tian S, Li B, Keller NP et al. (2017) LaeA regulation of secondary metabolism modulates virulence in *Penicillium expansum* and is mediated by sucrose. Mol Plant Pathol 18:1150-1163.

Kuzuyama T, Noel JP, Richard SB (2005) Structural basis for the promiscuous biosynthetic prenylation of aromatic natural products. Nature 435:983-987.

Laphookhieo S, Maneerat W, Koysomboon S (2009) Antimalarial and cytotoxic phenolic compounds from *Cratoxylum maingayi* and *Cratoxylum cochinchinense*. Molecules 14:1389-1395.

Lazarus CM, Williams K, Bailey AM (2014) Reconstructing fungal natural product biosynthetic pathways. Nat Prod Rep 31:1339-1347.

Lesburg CA, Caruthers JM, Paschall CM, Christianson DW (1998) Managing and manipulating carbocations in biology: terpenoid cyclase structure and mechanism. Curr Opin Struct Biol 8:695-703.

Li C-S, Li X-M, An C-Y, Wang B-G (2014) Prenylated indole alkaloid derivatives from marine sediment-derived fungus *Penicillium paneum* SD-44. Helv Chi Acta 97:1440-1444.

Li D-L, Li X-M, Li T-G, Dang H-Y, Proksch P, Wang B-G (2008a) Benzaldehyde derivatives from *Eurotium rubrum*, an endophytic fungus derived from the mangrove plant *Hibiscus tiliaceus*. Chem Pharm Bull 56:1282-1285.

Li D-L, Li X-M, Li T-G, Dang H-Y, Wang B-G (2008b) Dioxopiperazine alkaloids produced by the marine mangrove derived endophytic fungus *Eurotium rubrum*. Helv Chim Acta 91:1888-1892.

Li FQ, Yoshizawa T, Kawamura O, Luo XY, Li YW (2001) Aflatoxins and fumonisins in corn from the high-incidence area for human hepatocellular carcinoma in Guangxi, China. J Agric Food Chem 49:4122-4126.

Li S-M (2009) Applications of dimethylallyltryptophan synthases and other indole prenyltransferases for structural modification of natural products. Appl Microbiol Biotechnol 84:631-639.

Li S-M (2010) Prenylated indole derivatives from fungi: structure diversity, biological activities, biosynthesis and chemoenzymatic synthesis. Nat Prod Rep 27:57-78.

REFERENCES

Li S-M (2011) Genome mining and biosynthesis of fumitremorgin-type alkaloids in ascomycetes. J Antibiot 64:45-49.

Li W (2016) Bringing bioactive compounds into membranes: The UbiA superfamily of intramembrane aromatic prenyltransferases. Trends Biochem Sci 41:356-370.

Liao G, Mai P, Fan J, Zocher G, Stehle T, Li S-M (2018) Complete decoration of the indolyl residue in *cyclo*-L-Trp-L-Trp with geranyl moieties by using engineered dimethylallyl transferases. Org Lett 20:7201-7205.

Lim FY, Won TH, Raffa N, Baccile JA, Wisecaver J, Rokas A, Schroeder FC, Keller NP (2018) Fungal isocyanide synthases and xanthocillin biosynthesis in *Aspergillus fumigatus*. mBio 9:e00785.

Liu AH, Liu DQ, Liang TJ, Yu XQ, Feng MT, Yao LG, Fang Y, Wang B, Feng LH, Zhang MX et al. (2013) Caulerprenylols A and B, two rare antifungal prenylated *para*-xylenes from the green alga *Caulerpa racemosa*. Bioorg Med Chem Lett 23:2491-2494.

Liu C, Tagami K, Minami A, Matsumoto T, Frisvad JC, Suzuki H, Ishikawa J, Gomi K, Oikawa H (2015) Reconstitution of biosynthetic machinery for the synthesis of the highly elaborated indole diterpene penitrem. Angew Chem Int Ed Engl 54:5748-5752.

Liu L, Tang MC, Tang Y (2019) Fungal highly reducing polyketide synthases biosynthesize salicylaldehydes that are precursors to epoxycyclohexenol natural products. J Am Chem Soc 141:19538-19541.

Luk LYP, Qian Q, Tanner ME (2011) A cope rearrangement in the reaction catalyzed by dimethylallyltryptophan synthase? J Am Chem Soc 133:12342-12345.

Lv JM, Gao YH, Zhao H, Awakawa T, Liu L, Chen GD, Yao XS, Hu D, Abe I, Gao H (2020) Biosynthesis of biscognienyne B involving a cytochrome P450-dependent alkynylation. Angew Chem Int Ed doi:org/10.1002/anie.202004364.

Lyu HN, Liu HW, Keller NP, Yin WB (2020) Harnessing diverse transcriptional regulators for natural product discovery in fungi. Nat Prod Rep 37:6-16.

Ma YM, Liang XA, Kong Y, Jia B (2016) Structural diversity and biological activities of indole diketopiperazine alkaloids from fungi. J Agric Food Chem 64:6659-6671.

Mai P, Zocher G, Stehle T, Li S-M (2018) Structure-based protein engineering enables prenyl donor switching of a fungal aromatic prenyltransferase. Org Biomol Chem 16:7461-7469.

Maiya S, Grundmann A, Li S-M, Turner G (2006) The fumitremorgin gene cluster of *Aspergillus fumigatus*: identification of a gene encoding brevianamide F synthetase. Chembiochem 7:1062-1069.

Matsuda Y, Abe I (2016) Biosynthesis of fungal meroterpenoids. Nat Prod Rep 33:26-53.

McIntosh JA, Donia MS, Nair SK, Schmidt EW (2011) Enzymatic basis of ribosomal peptide prenylation in cyanobacteria. J Am Chem Soc 133:13698-13705.

Meganathan R, Kwon O (2009) Biosynthesis of menaquinone (Vitamin K2) and ubiquinone (Coenzyme Q). EcoSal Plus 3:10-47.

Mérillon JM, Ramawat K (2016) Fungal metabolites. Springer,

Metzger U, Schall C, Zocher G, Unsüld I, Stec E, Li S-M, Heide L, Stehle T (2009) The structure of dimethylallyl tryptophan synthase reveals a common architecture of aromatic prenyltransferases in fungi and bacteria. Proc Natl Acad Sci 106:14309-14314.

REFERENCES

Miyake Y, Ito C, Kimura T, Suzuki A, Nishida Y, Itoigawa M (2014) Isolation of aromatic compounds produced by *Eurotium herbariorum* NU-2 from karebushi, a katsuobushi, and their DPPH-radical scavenging activities. Food Sci Technol Res 20:139-146.

Mohimani H, Gurevich A, Mikheenko A, Garg N, Nothias LF, Ninomiya A, Takada K, Dorrestein PC, Pevzner PA (2017) Dereplication of peptidic natural products through database search of mass spectra. Nat Chem Biol 13:30-37.

Moore D, Robson GD, and Trinci APJ (2020) 21st century guidebook to fungi. Cambridge University Press,

Mundt K, Wollinsky B, Ruan HL, Zhu T, Li S-M (2012) Identification of the verruculogen prenyltransferase FtmPT3 by a combination of chemical, bioinformatic and biochemical approaches. Chembiochem 13:2583-2592.

Murray LAM, McKinnie SMK, Moore BS, George JH (2020) Meroterpenoid natural products from Streptomyces bacteria ΓÇô the evolution of chemoenzymatic syntheses. Nat Prod Rep doi.org/10.1039/D0NP00018C.

Murray LAM, McKinnie SMK, Pepper HP, Erni R, Miles ZD, Cruickshank MC, López-Pérez B, Moore BS, George JH (2018) Total synthesis establishes the biosynthetic pathway to the naphterpin and marinone natural products. Angew Chem Int Ed 57:11009-11014.

Nagata K, Hirai KI, Koyama J, Wada Y, Tamura T (1998) Antimicrobial activity of novel furanonaphthoquinone analogs. Antimicrob Agents and Chemother 42:700-702.

Nakashima Y, Mori T, Nakamura H, Awakawa T, Hoshino S, Senda M, Senda T, Abe I (2018) Structure function and engineering of multifunctional non-heme iron dependent oxygenases in fungal meroterpenoid biosynthesis. Nat Commun 9:104-114.

Nielsen KF, Larsen TO (2015) The importance of mass spectrometric dereplication in fungal secondary metabolite analysis. Front Microbiol 6:71.

O'Brien DM, Boggs CL, Fogel ML (2003) Pollen feeding in the butterfly Heliconius charitonia: isotopic evidence for essential amino acid transfer from pollen to eggs. P Roy Soc B-Biol Sci 270:2631-2636.

Oakley CE, Ahuja M, Sun WW, Entwistle R, Akashi T, Yaegashi J, Guo CJ, Cerqueira GC, Russo WJ, Wang CC et al. (2017) Discovery of McrA, a master regulator of *Aspergillus* secondary metabolism. Mol Microbiol 103:347-365.

Overy DP, Nielsen KF, Smedsgaard J (2005) Roquefortine/oxaline biosynthesis pathway metabolites in *Penicillium* ser. *Corymbifera*: in planta production and implications for competitive fitness. J Chem Ecol 31:2373-2390.

Oxford AE, Raistrick H, Simonart P (1939) Studies in the biochemistry of micro-organisms: griseofulvin, $C_{17}H_{17}O_6Cl$, a metabolic product of *Penicillium griseo-fulvum* dierckx. Biochem J 33:240-248.

Oya A, Tanaka N, Kusama T, Kim SY, Hayashi S, Kojoma M, Hishida A, Kawahara N, Sakai K, Gonoi T et al. (2015) Prenylated benzophenones from *Triadenum japonicum*. J Nat Prod 78:258-264.

Parvatkar RR, D'Souza C, Tripathi A, Naik CG (2009) Aspernolides A and B, butenolides from a marine-derived fungus *Aspergillus terreus*. Phytochemistry 70:128-132.

Pathirana C, Jensen PR, Fenical W (1992) Marinone and debromomarinone: antibiotic sesquiterpenoid naphthoquinones of a new structure class from a marine bacterium. Tetrahedron Lett 33:7663-7666.

REFERENCES

Pockrandt D, Ludwig L, Fan A, König GM, Li S-M (2012) New insights into the biosynthesis of prenylated xanthones: XptB from *Aspergillus nidulans* catalyses an *O*-prenylation of xanthones. Chembiochem 13:2764-2771.

Pojer F, Wemakor E, Kammerer B, Chen H, Walsh CT, Li S-M, Heide L (2003) CloQ, a prenyltransferase involved in clorobiocin biosynthesis. Proc Natl Acad Sci U S A 100:2316-2321.

Poulter CD, Rilling HC (1978) The prenyl transfer reaction. Enzymic and mechanistic studies of the 1'-4 coupling reaction in the terpene biosynthetic pathway. Acc Chem Res 11:307-313.

Qian Q, Schultz AW, Moore BS, Tanner ME (2012) Mechanistic studies on CymD: A tryptophan reverse N-prenyltransferase. Biochemistry 51:7733-7739.

Quin MB, Flynn CM, Schmidt-Dannert C (2014) Traversing the fungal terpenome. Nat Prod Rep 31:1449-1473.

Raistrick H, Robinson R, White DE (1936) Studies in the biochemistry of micro-organisms: ravenelin (3-methyl-1,4,8-trihydroxyxanthone), a new metabolic product of *Helminthosporium Ravenelii Curtis* and of *H. turcicum Passerini*. Biochem J 30:1303-1314.

Reshetilova TA, Vinokurova NG, Khmelenina VN, Kozlovskii AG (1995) The role of roquefortine in the synthesis of alkaloids, meleagrine, glandicolines A and B, and oxaline in *Penicillum glandicola* and *P. atramentosum*. Mikrobiology (Moscow) 64:27-29.

Rohlfs M, Churchill ACL (2011) Fungal secondary metabolites as modulators of interactions with insects and other arthropods. Fungal Genet Biol 48:23-34.

Rokas A, Mead ME, Steenwyk JL, Raja HA, Oberlies NH (2020) Biosynthetic gene clusters and the evolution of fungal chemodiversity. Nat Prod Rep:doi:10.1039/c9np00045c.

Rothe W (1954) The new antibiotic xanthocillin. Dtsch Med Wochenschr 79:1080-1081.

Rowan DD (1993) Lolitrems, peramine and paxilline: mycotoxins of the ryegrass/endophyte interaction. Agri Ecosyst Environ 44:103-122.

Saleh O, Haagen Y, Seeger K, Heide L (2009) Prenyl transfer to aromatic substrates in the biosynthesis of aminocoumarins, meroterpenoids and phenazines: The ABBA prenyltransferase family. Phytochemistry 70:1728-1738.

Sanchez JF, Somoza AD, Keller NP, Wang CC (2012a) Advances in *Aspergillus* secondary metabolite research in the post-genomic era. Nat Prod Rep 29:351-371.

Sanchez JF, Somoza AD, Keller NP, Wang CC (2012b) Advances in *Aspergillus* secondary metabolite research in the post-genomic era. Nat Prod Rep 29:351-371.

Sanna C, Scognamiglio M, Fiorentino A, Corona A, Graziani V, Caredda A, Cortis P, Montisci M, Ceresola ER, Canducci F (2018) Prenylated phloroglucinols from *Hypericum scruglii*, an endemic species of Sardinia (Italy), as new dual HIV-1 inhibitors effective on HIV-1 replication. PloS one 13:e0195168.

Sasaki K, Tsurumaru Y, Yamamoto H, Yazaki K (2011) Molecular characterization of a membrane-bound prenyltransferase specific for isoflavone from *Sophora flavescens*. J Biol Chem 286:24125-24134.

Sattely ES, Fischbach MA, Walsh CT (2008) Total biosynthesis: *in vitro* reconstitution of polyketide and nonribosomal peptide pathways. Nat Prod Rep 25:757-793.

REFERENCES

Schardl CL, Panaccione DG, Tudzynski P (2006) Ergot alkaloids - biology and molecular biology. The Alkaloids:Chem Biol 63:45-86.

Schofield CJ, Hausinger RP (2015) 2-Oxoglutarate-dependent oxygenases. Royal Society of Chemistry,

Schor R, Cox R (2018a) Classic fungal natural products in the genomic age: the molecular legacy of Harold Raistrick. Nat Prod Rep 35:230-256.

Schor R, Cox RJ (2018b) Classic fungal natural products in the genomic age: the molecular legacy of Harold Raistrick. Nat Prod Rep 35:230-256.

Schrettl M, Carberry S, Kavanagh K, Haas H, Jones GW, O'Brien J, Nolan A, Stephens J, Fenelon O, Doyle S (2010) Self-protection against gliotoxin - a component of the gliotoxin biosynthetic cluster, GliT, completely protects *Aspergillus fumigatus* against exogenous gliotoxin. PLoS pathog 6:e1000952.

Scott PM, Kennedy BPC (1976) Analysis of blue cheese for roquefortine and other alkaloids from *Penicillium roqueforti*. J Agric Food Chem 24:865-868.

Seephonkai P, Isaka M, Kittakoop P, Boonudomlap U, Thebtaranonth Y (2004) A novel ascochlorin glycoside from the insect pathogenic fungus *Verticillium hemipterigenum* BCC 2370. J Antibiot 57:10-16.

Selegato DM, Freire RT, Pilon AC, Biasetto CR, de Oliveira HC, de Abreu LM, Araujo AR, da Silva Bolzani V, Castro-Gamboa I (2019) Improvement of bioactive metabolite production in microbial cultures – a systems approach by OSMAC and deconvolution-based ^{1}HNMR quantification. Magn Reson Chem 57:458-471.

Shen G, Huhman D, Lei Z, Snyder J, Sumner LW, Dixon RA (2012) Characterization of an isoflavonoid-specific prenyltransferase from *Lupinus albus*. Plant Physiol 159:70-80.

Shi J, Liu J, Kang D, Huang Y, Kong W, Xiang Y, Zhu X, Duan Y, Huang Y (2019) Isolation and characterization of benzaldehyde derivatives with anti-inflammatory activities from *Eurotium cristatum*, the dominant fungi species in Fuzhuan Brick tea. ACS Omega 4:6630-6636.

Shin-ya K, Imai S, Furihata K, Hayakawa Y, Kato Y, Vanduyne GD, Clardy J, Seto H (1990) Isolation and structural elucidation of an antioxidative agent, naphterpin. J Antibiot 43:444-447.

Shin-ya K, Shimazu A, Hayakawa Y, Seto H (1992) 7-Demethylnaphterpin, a new free radical scavenger from *Streptomyces prunicolor*. J Antibiot 45:124-125.

Shiomi K, Nakamura H, Iinuma H, Naganawa H, Isshiki K, Takeuchi T, Umezawa H, Iitaka Y (1986) Structures of new antibiotics napyradiomycins. J Antibiot 39:494-501.

Sieber SA, Marahiel MA (2005) Molecular mechanisms underlying nonribosomal peptide synthesis: approaches to new antibiotics. Chem Rev 105:715-738.

Sika-Paotonu D, Liligeto U (2019) The utility of benzathine penicillin G for Rheumatic Fever prevention in the Solomon Islands. J Immunol 202:229-236.

Silberstein SD (1997) The pharmacology of ergotamine and dihydroergotamine. Headache 37:S15-S25.

Sings H, Singh S (2003) Tremorgenic and nontremorgenic 2,3-fused indole diterpenoids. The Alkaloids:Chem Biol 60:51-163.

Smith DJ, Burnham MKR, Edwards J, Earl AJ, Turner G (1990) Cloning and heterologous expression of the penicillin biosynthetic gene cluster from *Penicillium chrysogenum*. Biotechnology 8:39-41.

REFERENCES

Staunton J, Weissman KJ (2001) Polyketide biosynthesis: a millennium review. Nat Prod Rep 18:380-416.

Steffan N, Grundmann A, Afiyatullov A, Ruan H, Li S-M (2009) FtmOx1, a non heme Fe(II) and alpha-ketoglutarate-dependent dioxygenase, catalyses the endoperoxide formation of verruculogen in *Aspergillus fumigatus*. Org Biomol Chem 7:4082-4087.

Steffan N, Unsöld IA, Li S-M (2007) Chemoenzymatic synthesis of prenylated indole derivatives by using a 4-dimethylallyltryptophan synthase from *Aspergillus fumigatus*. Chembiochem 8:1298-1307.

Steyn PS, Vleggaar R (1983) Roquefortine, an intermediate in the biosynthesis of oxaline in cultures of *Penicillium oxalicum*. J Chem Soc Chem Commun 10:560-561.

Sun SW, Ji CZ, Gu QQ, Li DH, Zhu TJ (2013) Three new polyketides from marine-derived fungus *Aspergillus glaucus* HB1-19. J Asian Nat Prod Res 15:956-961.

Sun Y, Liu J, Li L, Gong C, Wang S, Yang F, Hua H, Lin H (2018) New butenolide derivatives from the marine sponge-derived fungus *Aspergillus terreus*. Bioorg Med Chem Lett 28:315-318.

Sunassee SN, Davies-Coleman MT (2012) Cytotoxic and antioxidant marine prenylated quinones and hydroquinones. Nat Prod Rep 29:513-535.

Süssmuth RD, Mainz A (2017) Nonribosomal peptide synthesis-principles and prospects. Angew Chem Int Ed 56:3770-3821.

Tagami K, Liu C, Minami A, Noike M, Isaka T, Fueki S, Shichijo Y, Toshima H, Gomi K, Dairi T et al. (2013) Reconstitution of biosynthetic machinery for indole-diterpene paxilline in *Aspergillus oryzae*. J Am Chem Soc 135:1260-1263.

Tanner ME (2015) Mechanistic studies on the indole prenyltransferases. Nat Prod Rep 32:88-101.

Tsai HF, Wang H, Gebler JC, Poulter CD, Schardl CL (1995) The *Claviceps purpurea* gene encoding dimethylallyltryptophan synthase, the committed step for ergot alkaloid biosynthesis. Biochem Biophys Res Commun 216:119-125.

Tsitsigiannis DI, Keller NP (2007) Oxylipins as developmental and host - fungal communication signals. Trends Microbiol 15:109-118.

Tsukamoto S, Kato H, Samizo M, Nojiri Y, Onuki H, Hirota H, Ohta T (2008) Notoamides F-K, prenylated indole alkaloids isolated from a marine-derived *Aspergillus* sp. J Nat Prod 71:2064-2067.

Ullah I, Khan AL, Ali L, Khan AR, Waqas M, Hussain J, Lee IJ, Shin JH (2015) Benzaldehyde as an insecticidal, antimicrobial, and antioxidant compound produced by *Photorhabdus temperata* M1021. J Microbiol 53:127-133.

Unsöld IA, Li S-M (2005) Overproduction, purification and characterization of FgaPT2, a dimethylallyltryptophan synthase from *Aspergillus fumigatus*. Microbiology 151:1499-1505.

Walsh CT (2008) The chemical versatility of natural-product assembly lines. Acc Chem Res 41:4-10.

Walsh CT, Tang Y (2017) Natural Product Biosynthesis. Royal Society of Chemistry,

Wang S, Li XM, Teuscher F, Li DL, Diesel A, Ebel R, Proksch P, Wang B-G (2006) Chaetopyranin, a benzaldehyde derivative, and other related metabolites from *Chaetomium globosum*, an endophytic fungus derived from the marine red alga *Polysiphonia urceolata*. J Nat Prod 69:1622-1625.

REFERENCES

Wang Y, Zheng J, Liu P, Wang W, Zhu W (2011) Three new compounds from *Aspergillus terreus* PT06-2 grown in a high salt medium. Mar Drugs 9:1368-1378.

Watkinson SC, Boddy L, and Money NP (2015) The fungi. Academic Press,

Weber T, Charusanti P, Musiol-Kroll EM, Jiang X, Tong Y, Kim HU, Lee SY (2015) Metabolic engineering of antibiotic factories: new tools for antibiotic production in actinomycetes. Trends Biotechnol 33:15-26.

Williams RM, Stocking EM, Sanz-Cervera JF (2000) Biosynthesis of prenylated alkaloids derived from tryptophan. Topics Curr Chem 209:97-173.

Wilson BAP, Thornburg CC, Henrich CJ, Grkovic T, O'Keefe BR (2020) Creating and screening natural product libraries. Nat Prod Rep:doi:10.1039/c9np00068b.

Wilson RM, Stockdill JL, Wu X, Li X, Vadola PA, Park PK, Wang P, Danishefsky SJ (2012) A fascinating journey into history: exploration of the world of isonitriles en route to complex amides. Angew Chem Int Ed 51:2834-2848.

Wilson ZE, Brimble MA (2009) Molecules derived from the extremes of life. Nat Prod Rep 26:44-71.

Wilson ZE, Brimble MA (2020) Molecules derived from the extremes of life: a decade later. Nat Prod Rep 37:doi:10.1039/D0NP00021C.

Winkelblech J, Fan A, Li S-M (2015) Prenyltransferases as key enzymes in primary and secondary metabolism. Appl Microbiol Biotechnol 99:7379-7397.

Wohlgemuth V, Kindinger F, Xie X, Wang BG, Li S-M (2017) Two prenyltransferases govern a consecutive prenylation cascade in the biosynthesis of echinulin and neoechinulin. Org Lett 19:5928-5931.

Wu MD, Cheng MJ, Hsieh SY, Yuan GF (2014a) Chemical constituents of the fungus of *Eurotium chevalieri* BCRC 07F0022. Chemi Nat Comp 49:1175-1176.

Wu MD, Cheng MJ, Hsieh SY, Yuan GF (2014b) Chemical constituents of the fungus of *Eurotium chevalieri* BCRC 07F0022. Chem Nat Comp 49:1175-1176.

Yan W, Song H, Song F, Guo Y, Wu CH, Sae HA, Pu Y, Wang S, Naowarojna N, Weitz A et al. (2015) Endoperoxide formation by an alpha-ketoglutarate-dependent mononuclear non-haem iron enzyme. Nature 527:539-543.

Yao Y, An C, Evans D, Liu W, Wang W, Wei G, Ding N, Houk KN, Gao SS (2019) Catalase involved in oxidative cyclization of the tetracyclic ergoline of fungal ergot alkaloids. J Am Chem Soc 141:17517-17521.

Young IG, Leppik RA, Hamilton JA, Gibson F (1972) Biochemical and genetic studies on ubiquinone biosynthesis in *Escherichia coli* K-12: 4-hydroxybenzoate octaprenyltransferase. J Bacteriol 110:18-25.

Yu X, Yang A, Lin W, Li S-M (2012) Friedel-Crafts alkylation on indolocarbazoles catalyzed by two dimethylallyltryptophan synthases from *Aspergillus*. Tetrahedron Lett 53:6861-6864.

Yu X, Li S-M (2011) Prenylation of flavonoids by using a dimethylallyltryptophan synthase 7-DMATS from *Aspergillus fumigatus*. Chembiochem 12:2280-2283.

Yu X, Xie X, Li S-M (2011) Substrate promiscuity of secondary metabolite enzymes: prenylation of hydroxynaphthalenes by fungal indole prenyltransferases. Appl Microbiol Biotechnol 92:737-748.

REFERENCES

Zhang JJ, Tang X, Moore BS (2019a) Genetic platforms for heterologous expression of microbial natural products. Nat Prod Rep 36:1313-1332.

Zhang P, Jia C, Deng Y, Chen S, Chen B, Yan S, Li J, Liu L (2019b) Anti-inflammatory prenylbenzaldehyde derivatives isolated from *Eurotium cristatum*. Phytochemistry 158:120-125.

Zhou K, Ludwig L, Li S-M (2015) Friedel-Crafts alkylation of acylphloroglucinols catalyzed by a fungal indole prenyltransferase. J Nat Prod 78:929-933.

Zou Y, Garcia-Borràs M, Tang MC, Hirayama Y, Li DH, Li L, Watanabe K, Houk KN, Tang Y (2017) Enzyme-catalyzed cationic epoxide rearrangements in quinolone alkaloid biosynthesis. Nat Chem Biol 13:325-332.

Zou Y, Zhan Z, Li D, Tang M, Cacho RA, Watanabe K, Tang Y (2015) Tandem prenyltransferases catalyze isoprenoid elongation and complexity generation in biosynthesis of quinolone alkaloids. J Am Chem Soc 137:4980-4983.

Statutory Declaration

Ich, Huomiao Ran, versichere, dass ich meine Dissertation

„Increasing structural diversity by prenylation-based modifications"

selbständig ohne unerlaubte Hilfe angefertigt und mich dabei keiner anderen als der von mir ausdrücklich bezeichneten Quellen bedient habe. Alle vollständig oder sinngemäß übernommenen Zitate sind als solche gekennzeichnet.

Die Dissertation wurde in der jetzigen oder einer ähnlichen Form noch bei keiner anderen Hochschule eingereicht und hat noch keinen sonstigen Prüfungszwecken gedient.

Marburg, den..........................

....

Huomiao Ran

Acknowledgements

Curriculum Vitae

Personal Information

Name: Huomiao Ran

Gender: Female

Birthday: 07.07.1991

Place of Birth: Jiyuan, He'nan Province, P. R. China

Address: Geschwister-Scholl-Str. 9, 35039, Marburg

Email: ran@staff.uni-marburg.de

Scientific Education ＆Research

PhD candidate: 10.2016—now

Philipps-University Marburg, Germany

Institute for Pharmaceutical Biology and Biotechnology

Thesis title: "Increasing structural diversity by prenylation-based modifications"

Supervisor: Prof. Dr. Shu-Ming Li

Master of Science: 09.2013 ─ 05.2016

Nanjing Agricultural University, China

Fermentation Engineering

Thesis title: "Isolation and characterization of endophytic microorganisms from Jufeng grape as well as their secondary metabolite identification"

Supervisor: Prof. Dr. Zhihong Xin

Bachelor of Science: 09.2009 ─ 06.2013

Hainan University, China

College of Food Science

Thesis title: "Optimization of the preparation process for polypeptides from Black Leaf Ginseng"

Supervisor: Prof. Dr. Yongcheng Li

Education:

09.2006 ─ 05.2009   Jiyuan No.1 Middle School